2020

NHICE 02

Conference Proceedings

Department of Civil Engineering, University of Victoria

02nd International Conference on New Horizons in Green Civil Engineering

August 24 – 26, 2020, Victoria, British Columbia, Canada

Editor: Phalguni Mukhopadhyaya

University of Victoria

BC HOUSING

Foreword

This compilation of papers contains papers from the *2nd International Conference on New Horizons in Green Civil Engineering* (http://nhice.engr.uvic.ca), held on August 24 – 26, 2020, Victoria, British Columbia, Canada. The conference was organized by the University of Victoria (www.uvic.ca) and sponsored by BC Housing (www.bchousing.org).

This conference, originally planned to be held on April 29 – May 01, 2020, was organized during COVID-19 pandemic and kudos to all authors, presenters, reviewers, participants, members of the scientific & local advisory committee, and support staffs for their sincerity, endurance and passion during those extremely difficult days. I do not have enough words to express my gratitude to all of you.

Conference Chair and Editor:

Phalguni Mukhopadhyaya
University of Victoria
Victoria, BC, Canada

ISBN-13: 978-1-55058-672-5

Scientific Committee

Andrew Rowe	University of Victoria	Canada
Ashutosh Bagchi	Concordia University	Canada
Atsushi Iwamae	Kindai University	Japan
Bijan Adl-Zarrabi	Chalmers University of Technology	Sweden
Brahim Benmokrane	University of Sherbrooke	Canada
Caterina Valeo	University of Victoria	Canada
Christopher Kennedy	University of Victoria	Canada
Daisuke Ogura	Kyoto University	Japan
Daniel Hoornweg	University of Ontario Institute of Technology	Canada
Denisa Ionescu	BC Housing	Canada
Dominique Derome	Swiss Federal Lab for Materials Science and Technology	Switzerland
Ferenc Kalmár	University of Debrecen	Hungary
Fitsum Tariku	British Columbia Institute of Technology	Canada
Guido Wimmers	University of Northern British Columbia	Canada
Harjit Singh	Brunel University London	UK
Hua Ge	Concordia University	Canada
Jieying Wang	FPInnovations	Canada
Jun-Tae Kim	Kongju National University	Korea
Kasun Hewage	UBC	Canada
Mario A. Medina	The University of Kansas	USA
Murray R. Metcalfe	University of Toronto	Canada
Nemkumar Banthia	University of British Columbia	Canada
Phalguni Mukhopadhyaya (Chair)	University of Victoria	Canada
Ping Fan	Hunan University	China
Rajasekar Elangovan	Indian Institute of Technology – Roorkee	India
Richard Laing	Robert Gordon University	UK
Rishi Gupta	University of Victoria	Canada
Samuel Brunner	Swiss Federal Lab for Materials Science and Technology	Switzerland
Samuel V. Glass	Forest Products Laboratory	USA
Shauna Mallory-Hill	University of Manitoba	Canada
Sigrid M. Adriaenssens	Princeton University	USA
Thomas Froese	University of Victoria	Canada
Wahid Maref	École de technologie supérieure (ÉTS)	Canada
Wilma Leung	BC Housing	Canada
Y. H. Chui	University of Alberta	Canada
Zhaofeng Chen	Nanjing University of Aeronautics and Astronautics	China

Local Advisory Committee

Andrew Pape-Salmon	Executive Director, Building and Safety Standards Branch at BC Public Service
Andy Chong	Principal, Integral Group
Cecile Lacombe	Director, Research and Knowledge Development at BC Provincial Government
Graham Finch	Principal, RDH Building Science Inc.
Jonathan Reiter	Principal, Skyline Engineering
Patrick Roppel	Principal, Morrison Hershfield
Rob Bernhardt	Chief Executive Officer, Passive House Canada
Terry Bergen	Managing Principal, Read Jones Christoffersen Ltd.

Contents

Paper ID	Title	Authors	Page #
03	Optimizing building form for energy-efficient school design	M. Rahmani, K. Al-Sallal	1
05	Economic and energy impacts of adaptive reuse building construction	J. Chan, C. Bachmann, C. Haas	7
06	Canada's Green Construction through Wood Program	M. Mohammad, D. Pothier, J. Tourrilhes, R. Coxford, and M. Williamson	11
07	Application Research of Integration Vacuum Insulation Panel (IVIP) in New Building	Z. Chen, M. Li, S. Asim, Y. Li, D. Zhang, Q. Zhou	15
08	Seismic performance of timber connections for sustainable tallwood building	G. Vojtila, C. MacDougall	19
09	Northern Ontario air transportation: infrastructure resilience and community well-being	P. Dimayuga, E. Ohlrogge, M. Widener, T. Galloway, S. Saxe	24
11	Influence of Steam Curing Parameters on Concrete Strength and Optimization at 28 Days	R. A. E. Elnour	29
13	Cost and limiting efficiency of silicon solar panels past and future	T. Tiedje	34
14	In-situ Envelope Performance and Actual vs Modeled Energy Consumption of a Passive House Certified Research and Testing Facility in Northern BC	A. Conroy, G. Wimmers	37
15	Hygrothermal Performance and the Effect of an Exterior Air Barrier on High-Performance Building Envelope Assemblies	A. Conroy, G. Wimmers	41
16	Pros and Cons of Different Strategies and Levels of Prefabrication and the Influence of the BC Energy Step Code on the Manufacturing of Buildings	G. Wimmers, L.Wimmers	45
17	Fiber Holder to Assist in Sputter Deposition of Optical Fibers	C.A. Vail, G. Burton, P.M. Wild, H.L. Buckley	49
20	Simulation of wind-driven rain exposure of a heritage façade using future climate weather data	J. Bourcet, A. Kubilay, D. Derome, J. Carmeliet	53
21	Why Wood – Building the case for more wood education	R. Kelterborn	58
22	Morphing Weather Data for Climate Resilient Building Design: A Study on Lifetime Thermal Comfort, Energy Demand and Energy Consumption	M. Fakoor	62
23	Future Context for Retrofitting Existing Buildings: Impacts of A Changing Climate on Energy Conservation Measures	M. Fakoor	66
24	Towards Net-Zero Energy Ready: Where Passive House Lies on the High Performance Staircase of the BC Energy Step Code	M. Kennedy-Parrott, M. Fakoor	70
25	Towards Net-Zero Carbon Buildings:	L. Polovina, M. Fakoor	74

	A Comparative Study Between Operational and Embodied Carbon Emissions		
26	Designing Buildings for a Warming Climate	L. Westerhoff, S. MacDougall, C. Dedels, S. Shepherd	78
27	Experimental Study on the Thermal Performance of Green Roof Substrates as a Function of Temperature and Moisture Content	B. Shao, C. Valeo, P. Mukhopadhyaya, J. He	83
29	Identification of model pioneer bacteria used to test biofouling on reverse osmosis water treatment membranes and related protocol	A. Curtin, M. Thibodeau, A. Piper-Arroliga, H.L. Buckley	87
30	In-Situ Temperature and Moisture Monitoring of a High-Performance Tiny House with Vacuum Insulation Panels	C. Campbell, S. Bucking, C.A. Cruickshank	96
34	Feasibility study of integrating carbon capturing and utilization in building level natural gas heating systems	D. R. Liyanage, K. Hewage, H. Karunathilake, R. Sadiq,	100
36	The physics of the outdoor urban climate	J. Carmeliet, A. Kubilay, A. Ferrari, D. Derome	105
37	Modeling wood performance? The challenge of using natural materials.	D. Derome, M. Chen, C. Zhang, A. Shomali, B. Coasne, J. Carmeliet	109
38	Impact of Climate Change on Energy Demand of a Mid-Rise Office Building	C. Jha, S. Lall, E. Rajasekar	113
39	Parametric Design of Balconies in Multi--Unit Residential Buildings	T. Peters, T. Kesik	117
41	Optimizing mass timber-concrete composite floor systems with respect to embodied carbon	T. Joyce, H. Daneshvar, Y.H. Chui, L. Zhang	122
45	Recent developments in engineered wood products for green building constructions	M. Oudjene	126
49	Coastal resiliency of Canadian low-rise light wood frame buildings against climate change	H. Daneshvar, T. Joyce, Y.H. Chui	130
50	Mapping of the Renewable Energy Generation Potential in India	N. S. Manna , B. K. Choudhury	134
51	Microscale Characteristics of New Bitumen-Based Carbon Fibers (BBCF)	M. Monazami, R. Gupta	140
52	Smart Buildings – A Road Map: Where we are, where we are going, and how we get there	N. Hodge, A. Crosson	146
53	A Comparison of carbon capturing technologies for community energy systems: A techno-economic assessment	R. K. Hetti, H. Karunathilake, K. Hewage, R. Sadiq	150
58	Critical road network recovery in the District of North Vancouver	A. Deelstra, D. Bristow	155
60	What are the extent and opportunities of Sustainable Development in the Construction Industry?	S. Espindola, T. Froese	160
61	A neural network metamodel for predicting hygrothermal performance of wood framed envelopes under future climatic loads	L. Wang, Hua Ge	165

65	A New Sensing System to Detect Liquid Water Penetration through Water Resistant Barriers	W. Qi, C. Valeo, P. Mukhopadhyaya	169
66	Impact of Insulating the Rough Opening Gap on the Total Heat Flow at the Window to Wall Interface	E. Lau, F. Tariku	173
67	Quantifying overheating in highly glazed buildings and evaluating glazing films as a mitigation strategy	S. Zhang, J. Fine, M. Touchie, W. O'Brien	178
68	Insulation and energy performance of metal exterior curtain wall including thermal bridges	J. Song, D. Lee, B. Choi, S. Song	182
72	Development of assessment criteria for overheating risk analysis in buildings	A. Laouadi, M. Bartko, M. Lacasse	186
73	On the implementation of thermal bridge calculations in the Belgian building code	N. Bossche, L. Landuyt, A. Janssens	190
76	A Review of Definition and Classification of Heritage Buildings and Framework for their Evaluation	A. Al-Sakkaf, T. Zayed, and A. Bagchi	194
77	Operational energy use versus LCA: case study The Mobble for the Solar Decathlon Europe 2019 competition	L. Landuyt, S. Turck ,S. Lauwerys, N. Bossche	199
78	Effect of render properties on moisture risk in internally insulated masonry walls	X. Zhou, J. Carmeliet, D. Derome	203
80	Hygrothermal performance of mass timber wall assembly with External Insulation Finish System	V. Kukka, J. Kers, T. Kalamees	207
83	Hygrothermal response of tallwood building enclosures to climate change in different climate zones in Canada	M. Defo, M. Lacasse	212
86	Assessment of summertime overheating conditions in vulnerable buildings in Montréal	L. Wang, C. Shu, H. Ge, R. Zmeureanu, M. Lacasse, S. Leroyer, S. Belair, L. Ji, X. Bai, L. Wang, M. Mortezazadeh, A. Katal	217
90	Cold Thermal Energy Storage for Buildings: A Feasibility Study	M. Ghobadi, A. Laouadi, A. Galasiu	221
92	Basic Case Study on Development of Decision Support System for Evacuation Instructions	K. Kawano, K. Tsukahara, Y. Mitani, H. Taniguchi, T. Sato	225
93	Thermal Bridging: Methodologies, Tools, and Advancements in Mitigation	V. Gretka, P. Roppel	227
97	National Energy Code of Canada reference thermal resistance calculation methods compared to a validated 3D heat transfer simulation for framed walls containing thermal bridges	H. Schreiber, T. Moore, M. Ghobadi	237
98	The Thermal Effects of Adding a window to a Wood Stud Wall Assembly	M. Ghobadi, J. Cingel, K. Kadzadej	241
99	Research for Detecting Relationship Information Between Point Cloud Data and Plan of Completion Drawing	Y. Umehara, K. Nakamura, Y. Tsukada, S. Tanaka, K. Nakahata	246
100	Identify the common challenges in the green building practices	Zahra Alaghehmandan, Christiane Papineau, Gabriel Lefebvre	250
101	Research on Improvement of Road Maintenance Using Point Cloud Data with Feature Information	Y. Tsukada, K. Nakamura, R. Imai, S. Tanaka, Y. Umehara	256

102	Research for Detection and Positional Analysis of People in Construction Fields using Multiple Cameras from a Single Viewpoint	W. Jiang, Y. Yamamoto, S. Tanaka, K. Nakamura, C. Tanaka	260
103	Fundamental Research concerning Personal Identification for Safety Management of Construction Sites Using Deep Learning	R. Imai, D. Kamiya, H. Inoue, S. Tanaka	264
104	Survey Research on Mobile Recognition Technologies using Deep Learning for Application to Traffic Census	R. Imai, D. Kamiya, Y. Yamamoto, S. Tanaka, M. Nakahara, K. Nakahata	268
106	Field Survey on Indoor Overheating in School and Hospital Buildings in Montréal	C. Shu, L. Ji, L. Wang, X. Bai, M. Lacasse, H. Ge, R. Zmeureanu, L. Wang	272
107	Performance of dynamic shading systems based on non-deterministic algorithm	V. Charpentier, F. Meggers, S. Adriaenssens, O. Baverel	276
108	Mechanical behavior of a new type of flexible, pressurized storm surge barrier under hydrostatic loading	J. Goodglass, A. Niewiarowski, S. Adriaenssens	280
109	Global bioretention cell guidelines: a review and recommendations to meet hydrological performance targets	M. Bacys, U. T. Khan, J. Sharma, T. R. Bentzen	284
110	The Low Impact Development Demand Index: a geospatial framework to identify LID demand for three Canadian cities	S. Kaykhosravi, K. Abogadil, U. T. Khan, A. Jadidi	287
112	Assessment of Feasibility of Hollow Core Slabs in Building Construction Considering Cost, Energy, and Carbon Imprint	A. Noman, A. Bagchi, A. Athienitis	290
113	Post Occupancy Evaluation in Canada: Challenges, Potential Improvements and New Frontiers	I. Tripathi, T. Froese	295
114	Stormwater Management by Bioretention Mesocosms – the Dynamic Role of Vegetation and Media in the Performance	A. Skorobogatov, J. He, A. Chu, C. Valeo, and B. Duin	299
115	Thermal behaviour of an extensive green roof in a cold and semi-arid climate	M. Akther, J. He, A. Chu, B. Duin	303
116	Municipal Natural Asset Management as a Climate Resiliency Strategy	A. Strang, E. Machado	307
117	Metro Vancouver's Application of the Envision Sustainable Infrastructure Framework	A. Strang, M. Pitre, D. McCallum	311
118	Kalman Filtering Applied to Sensor Fused Data to Deliver Accurate and Rapid Environmental Feedback of an Occupied Space	G. Mustapha, D. Vaz, K. Batdorf	315

Optimizing building form for energy-efficient school design

M. Rahmani[a], K. Al-Sallal[b,*]

[a,b] UAE University, Al-Ain, UAE
* Corresponding author, email: k_sallal@yahoo.com

Abstract:
Inappropriate designs of architectural forms lead to high rates of energy consumption in schools. The optimized design of the form's geometry and the spacing between building masses could help improve connection to the outdoor environment such as daylight, air, and outdoor greenery, as well as reduce energy and carbon emissions. It can create educational environments that are more lively and cheerful; which leads to improving students' performance, health, and attitude. Investigating optimum architectural forms that maximize reliance on natural lighting and help reduce carbon emissions through limited use of energy consumption is tackled in this paper. The main focus is performance improvement of the learning community concept adopted in the new school model. The investigation relied on computer simulation based on actual data gathered from school surveying and interviews with officials, architects, engineers in charge of schools' design. The ultimate goal of this research is to find models that express optimum relationships between design and performance variables of form. The graphical representations of the results and discussions can help architects and decision makers achieve sustainable school design.

Keywords:
Low energy, sustainable design, green schools, learning community, building form

1. Introduction

Building designs that rely merely on mechanical and electrical systems to provide needed requirements of heating, cooling, ventilation, and lighting leads to considerable energy. In UK, schools were classified as the third most consuming energy buildings, while in the USA, schools were shown to consume 10.8% of the total electrical energy of buildings [1]. Around 80% of the total consumed energy in UAE is attributed to buildings' sector, with an average of 220-360 kWh/m^2 per year. Governmental and commercial buildings in Abu Dhabi including schools are responsible of about 60% of the consumed energy [2]. Since the recent booming of Abu Dhabi' economy in 2012, new buildings have been built especially schools; which has led to considerable increase in building energy (more than 33% increase between 2012-2016). The problem is not only about the continuously increased levels of energy and cost. As building industry increases with the need to build more settlements, many cities around the globe have expanded and major ones transformed into mega cities that created threatening challenges on how to deal with serious issues such as scarcity of water, damage of natural resources, and increase of pollution and greenhouse gas emissions (GHG). The Environmental Protection Agency (EPA) reported that Americans spend 90% of their time in buildings with 84 million spending almost their entire day in schools; 73.7 million of this figure were children. Their reports also showed that people in one of five of the surveyed schools expressed dissatisfaction about indoor air quality [3].

The high rates of energy consumption by the building sector in UAE is a result of the excessive use of cooling systems due to the harsh climatic conditions. The climate in the UAE can be classified as extremely hot in summer and warm to moderate in winter. July and August are the hottest months of the year with temperatures that can reach up to 50°C in [4]. In such extreme conditions, one should give highest priority to building design that helps conserve energy and natural resources, as well as reduce GHG emissions.

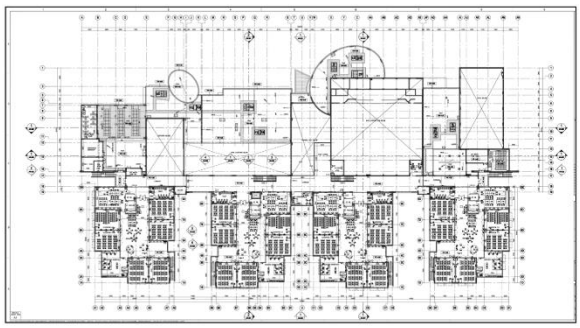

Fig 1: The finger-plan configuration with the learning community concept of ADEK as applied in the design of Al-Sammalia School, Abu Dhabi [5].

Abu Dhabi 2030 vision launched several initiatives to enhance sustainability. Abu Dhabi Department of Education and Knowledge (ADEK) launched the initiative, known as the New School Model (NSM), with the objective to enhance sustainability levels and overall quality of Abu Dhabi schools. The NSM is a student-centered learning approach that employs technology and modern teaching facilities in an integrated sustainable environment. The NSM recommends the reliance on passive design strategies and the integration with other energy-efficient environmental systems. The finger-plan typology was adopted, with each finger representing one or more

learning communities (LC). Fig. 1 shows the finger-plan configuration in the design of Al-Sammalia School, Abu Dhabi [5]. One can notice clearly from the floor plan how the learning community concept was applied by the four fingers of the form design. The LCs known also as pods, families, academies, houses, and schools-within-a-school is a well-known concept that has been researched and applied internationally for decades [6]. The LC is used as an organizational approach to divide the school into units, with each LC including one or multiple grade levels [5].

The finger-plan configuration provides many advantages for educational buildings. It helps improve connection to the outdoor environment such as daylight, air, and outdoor greenery; which creates educational environments that are more lively and cheerful. These advantages lead eventually to improving students' performance, health, and attitude. The purpose of this study is investigate how to optimize this form design with regards to energy performance. The study represents an initial phase of a more comprehensive research project that aims to find models expressing optimum relationships between design and performance variables of the form. The ultimate goal is to create useful tools for school designers and decision makers to achieve sustainable school design.

2. Literature Review

Several studies identified that more than 40% of the total building energy in a school is used for heating and cooling requirements [7, 8]. To tackle effectively the issue of reducing energy consumption in buildings, two studies recommended dividing the energy efficiency strategies into three groups [9, 10]; these are: (1) strategies that should be implemented at the site planning and architectural design stage, (2) strategies that should be implemented when developing the design of the building envelope and selecting equipment and material, and (3) strategies that should be implemented when designing and installing energy technologies. The investigation of this paper focuses mainly on the design of building form during the planning and design stage; hence, it falls under group (1).

In general, compact forms help reduce heat gain in hot dry climates and loss in cold climates due to their limited exposure of external surfaces to the outdoor conditions; while spread-out forms are most effective in hot humid climates since they help maintain passage of cool breezes. The introvert form or the courtyard design have many benefits in hot dry or humid climates such as maximizing form self-shading, promoting nocturnal radiative cooling (in dry climates), promoting evaporative cooling (in dry climates), promoting convective cooling through cross ventilation, promoting stack effect when combined with other systems such as the wind tower or solar chimney [9].

Many researchers have used the relative compactness (RC) of the form to express how form configuration influences building energy [11, 12, 13, 14, 15, 16]. The findings of their research confirmed that an increase of the RC of the form generally leads to a decrease in the energy consumption. The RC can be defined as the ratio of the form's volume to its surface area. It can be a useful approach when compared to the most compact form that has the same volume [17]. Realistically, for the RC method to be useful other important factors that have strong connection to the form design should also be considered with the RC calculations. These are the window to wall ratio (WWR) and the solar heat gain coefficient (SHGC).

3. Method

At the outset, the study carried out a survey to track down the typologies and number of schools used in the Abu Dhabi and Al-Ain regions of Abu Dhabi Emirate. The total number of public and private schools, when the survey was conducted, was 411 in these two regions. Only the public schools were considered in the study because their design typologies were officially approved (and being applied already) by the government and they are much more common than the private ones; which can cause significant impact on the total energy consumption of school buildings. ADEK advised that old schools were no longer authorized and hence the study should give priority for the new generation of public schools. Several tools and resources were used; these included an online database application called School Finder, Google Maps, and School Contacts Excel sheet. The School Finder and School Contacts are databases available in ADEK website. The School Finder database provided full information about schools in the Abu Dhabi Emirate such as their names, school contacts, education level, year of construction, location, and GPS coordinates. The coordinates helped fetch the site layout of each school in Google maps. The School Contacts helped obtain other information such as school's types (public or private), gender, and grades.

The survey was accompanied by analysis of case studies that represented the design models and design guidelines adopted by ADEK [5]. The researchers also met several times with officials and engineers who were in charge of ADEK schools' design. The meetings helped obtain the architectural drawings of model case studies and answer many questions about design specs/data of these school buildings. The case study analysis helped identify design variables of the school form that had potential effect on energy consumption and define the value range of each variable. The survey helped track down the number of schools under the four design models of ADEK (see Fig. 2). The total number of schools were 48: 10 schools followed Model-1, 16 schools followed Model-2, 9 schools followed Model-3, and 13 schools followed Model-4. The four models followed a finger-plan configuration; with each finger having a number of LCs distributed in

2-3 floors. The following points summarize the variables found in the case studies with their value ranges:

- Learning community (LC) width-to-length aspect ratio: ranging from 1:1.38-1:1.5
- Courtyard space width (C): 0-14m
- Number of floors: 2-3; most cases have 2 floors.

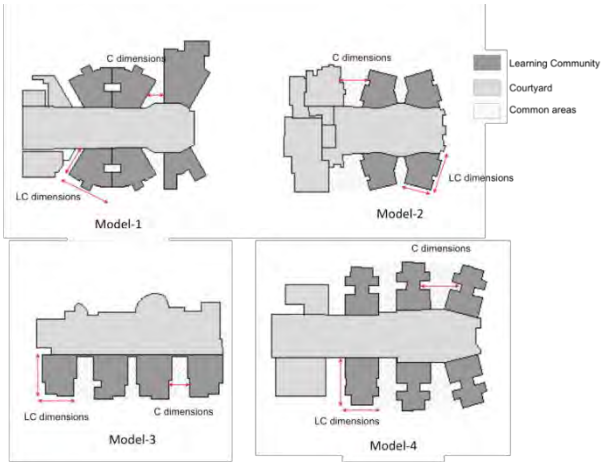

Fig 2: ADEK Design Models [5].

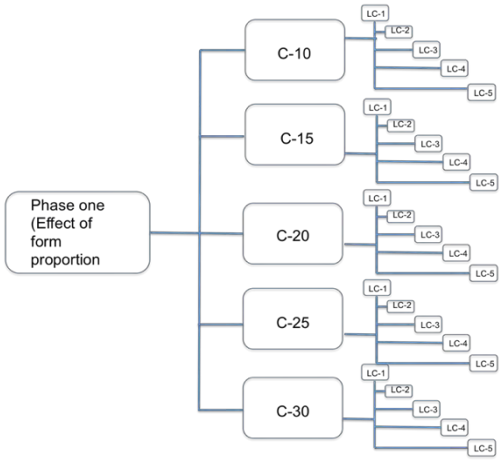

Fig 3: Tree-like structure of the simulation plan.

The simulation process was planned to examine, and compare between, different proportions of LC forms ranging from a square to a rectangle shape with length-to-width proportion = 0.8-1.8, tested under different courtyard widths with the same total floor area, glazing area, and the number of floors. The number of floors in all cases was 2 floors. The window area in all cases was fixed to a specific value of 61.25m^2. This value was calculated based on gross WWR equal to 35%; which was judged to provide cheerful daylit classrooms. During the data input process, the building design parameters were selected to comply with ADEK requirements. In addition to the data mentioned above, other common parameters between all the investigated cases can be outlined as follows:

- Energy efficiency measures following ASHRAE 90.1 2010 version.
- Ceiling height of 3.75 m for each floor as obtained from the case studies.
- HVAC system: VAV w/ parallel FCU (Cent. Chilled Water C.T.)
- Electrical lighting system: Fluorescent.
- Exterior Exposure: Grass area.
- Lighting target lux in classrooms = 500 lux.

Table 1: The simulated cases, combinations of different learning community (LC) and courtyard space (C).

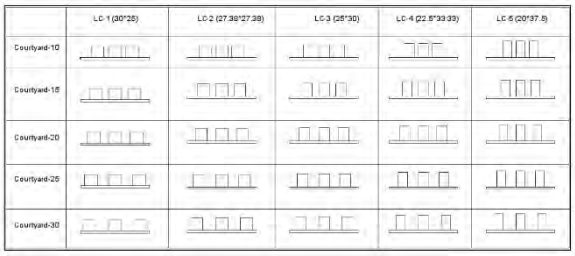

The simulation plan that can be represented by the tree-like structure (Fig. 3) involved a total number of 25 cases, as shown in Table 1. All cases had finger-plan configuration with 6 learning communities (LC) distributed in 2 floors. The simulation plan comprised five subgroups; each one is characterized by a different courtyard space width (C): 10, 15, 20, 25, and 30 metre. The order of cases was planned to help understand how the dynamic behavior of changing the form proportions (in two dimensions: X and Y) influences the building's energy performance.

The main performance variable of this research is energy consumption, expressed in MJ/m^2.y unit. The results reveal the energy breakdown between the different energy uses for the different cases including space cooling, space heating, lighting, water heating, fan and motors, and equipment for all the investigated cases. This investigation helps to easily view those energy uses that cause the most energy consumption for further action. Other investigated performance variables were as follows:

- Energy cost in terms of U.S. Dollars and the equivalent value in UAE currency (AED).
- Environmental impact performance variables expressed in metric tons includes:
  - Carbon dioxide (CO_2) emissions.
  - Sulfur Dioxide (SO_2) emissions.
  - Nitrogen Oxides (NOx) emissions.

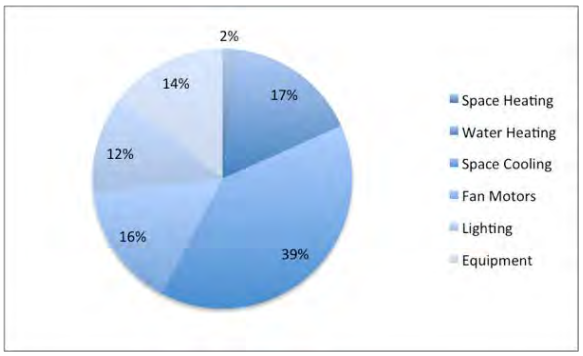

Fig 4: Breakdown of energy uses.

4. Results

The results revealed that cooling consumes the largest part of energy compared to other systems. On average, 39% of the total energy is consumed by cooling requirements, followed by water heating (17%), fan motors (16%) equipment (14%), lighting (12%) and finally, space heating (2%) (See Fig. 4). The cooling load increases slightly with the increase of the courtyard space width. The energy requirements by the other systems are almost constant across all cases. The highest levels of the energy consumption were recorded during July and August for all cases; i.e., when cooling loads were highest.

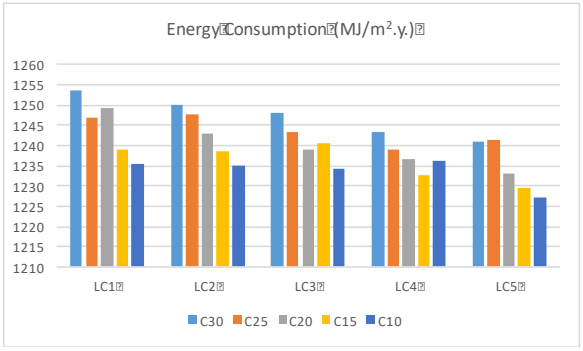

Fig 5: Energy consumption for all cases.

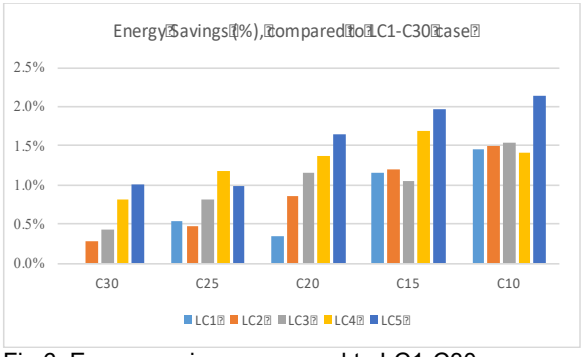

Fig 6: Energy savings compared to LC1-C30 case.

The energy consumption results are shown in Fig. 5, expressed in MJ/m2.y. Fig. 6 shows percentage of energy savings potential of the cases compared to the least performance one, case LC1-C30. These cases represent different combinations of learning community and courtyard designs. From these simulation results, one can observe the following:

- The change of the LC form proportion causes a noticeable change in energy consumption. The LC-5 (the most linear form) generally have a higher potential in achieving energy savings than the other LC forms, followed by the other cases: LC-4, LC-3, LC-2, and lastly LC-1.
- The change of the courtyard proportion also causes a noticeable change in energy consumption. One can observe in the shown figures how the linear courtyards in the carried out simulations such as C10 or C15 performs better than the more squared courtyards such as C30 or C25; C10 achieved the best courtyard performance.

Although the reduction in energy consumption (per metre square), across results from LC-5 to LC-1 or from C30 to C10, does not appear very significant (up to 2.1% energy savings); yet the implication of these figures have a considerable effect on the total energy cost and environmental impact particularly for schools with large built-up areas, as discussed in the following sections.

The difference between LC-1 and LC-5 in energy cost is remarkable. An average of AED 0.83/m^2 per year was noticed, which is equivalent to CAN$ 0.30/m^2 per year; that is a saving of AED 10447.73 (CAN$ 3800) per year in a typical school with 12,600 m^2 total built-up area. The difference between C10 and C30 cases in energy cost is also remarkable. An average of AED 1.1/m^2 per year was noticed, which is equivalent to CAN$ 0.39/m^2 per year; that is a saving of AED 13515 (CAN$ 4888) per year.

Table 2: Average results of the CO_2, SO_2, and NO_X and percentage of improvement between LC-1 and LC-5 and C30 and C-10.

	Average of LC-1 Cases	**Average of LC-5 Cases**	**Difference**	**% of Improvement**
	(Metric Tons)			
CO_2	1441	1429	12	1%
SO_2	7.57	7.52	0.05	1%
NO_x	1.58	1.57	0.01	0.4%
	Average of C-30 Cases	**Average of C-10 Cases**	**Difference**	**% of Improvement**
	(Metric Tons)			
CO_2	1444	1429	15	1%
SO_2	7.6	7.5	0.1	1%
NO_x	1.59	1.56	0.03	2%

The executed simulation runs have also computed the GHG emissions, namely; Carbon Dioxide (CO_2), Sulfur dioxide (SO_2), and Nitrogen Oxides (NOx). Table 2 shows the average results of the CO_2, SO_2, and NO_X

for the courtyard cases when LC-1 and LC-5 are used. One can deduce from the results that these pollutants can be controlled when energy consumption is minimized by proper form design; and the linearity of form can help to make difference in reducing GHG emissions. The results of any particular case is directly dependent on the amount of energy consumption of that case and its capacity to save energy. Hence, the pattern of improvement in environmental impacts (CO_2, SO_2, and NOx) that can be achieved between the cases would look similar to Fig. 5.

5. Conclusions and outlook

The findings with regards to the variables LC form proportion and courtyard space width (C) can be summarized as follows:

- The linearity of the form has a noticeable impact on energy consumption.
- The cases with thin-width of courtyard like C10 (highest aspect ratio, 1:3) proved to achieve more energy savings than cases with more squarely courtyards or having lower aspect ratio. Also, the cases with LC5 (those with the most linear LC form or the highest aspect ratio 1:1.8) proved to achieve more energy savings than the cases with more squarely LC forms or having lower aspect ratio. Overall, the cases that show best performance are those with highest linearity of LC forms and thinnest courtyard spaces.
- The results showed that the change in courtyard space proportion has a higher potential for energy savings than the change in the learning community form proportion. This is evidenced when we compare two cases one having the same LC proportions but different courtyard proportion versus another one having the same courtyard proportion but different LC proportion. For instance, when we compare the difference in energy consumption made between case LC1-C10 and case LC1-C30 against the difference made between case LC1-C10 and case LC5-C10, we find the former produced better savings.
- Although the energy results (as per-m^2) showed limited improvements between different proportions of LC forms and courtyard spaces, the implications on total values of energy cost and environmental impacts (per year) can lead to considerable amounts especially in the case of large schools. One should also take into consideration that when the calculations are done at the national level, governmental schools are built in large number; which eventually leads to considerable amounts of energy costs and environmental threats.
- Future research should cover other variables when combined with different form and space design proportions on energy consumption, such as the following:
    - Effect of vertical form versus horizontal form proportions.
    - Effect of different building orientations.
    - Effect of different window to wall ratios (WWR).

References

[1] L. Pérez-Lombard, J. Ortiz, C. Pout, A review on buildings energy consumption information. Energy and Buildings (2008), 40(3), 394–398. https://doi.org/http://dx.doi.org/10.1016/j.enbuild.2007.03.007

[2] K. Clarke, 80% energy consumed by buildings (2016, Feb. 04). Retrieved December 26, 2017, from https://www.khaleejtimes.com/nation/abu-dhabi/80-energy-consumed-by-buildings

[3] EPA, Buildings and the Environment: A Statistical Summary. U.S. Environmental Protection Agency Green Building Workgroup (2009).

[4] A. Al-Mandoos, Synoptic and atmospheric stability classification for the United Arab Emirates (Doctoral dissertation, The Witwatersrand, johannesburg, (2005, February).

[5] ADEK, Educational Facilities Design Manual, Abu Dhabi, UAE (2013).

[6] Kellough and Jarolimek. (2008). Teaching and Learning K-8: A Guide to Methods and Resources, 9th Edition (2008).

[7] DOE, Advanced energy retrofit guide – K 12 schools. Guide; 2013.

[8] TW Kim, KG Lee, WH Hong, Energy consumption characteristics of the elementary schools in South Korea. Energy and Buildings (2012) 54, 480– 489. https://doi.org/http://dx.doi.org/10.1016/j.enbuild.2012.07.015

[9] K.A. Al-Sallal, Low Energy Low Carbon Architecture: Recent Advances and Future Directions. CRC Taylor and Francis Group (2016). Retrieved from https://www.crcpress.com/Low-Energy-Low-Carbon-Architecture-Recent-Advances--Future-Directions/Al-Sallal/p/book/9781138027480

[10] P.A. Kharecha, C.F. Kutscher, J.E.Hansen, E. Mazria, Options for Near-Term Phaseout of CO_2 Emissions from Coal Use in the United States. Environmental Science and Technology (2012) 44(11), 4050–4062. https://doi.org/10.1021/es903884a

[11] Pessenlehner and Mahdavi, Building morphology, transparency, and energy performance. ResearchGate. Retrieved from transparency_and_energy_performance (2012) https://www.researchgate.net/publication/237581710_Building_morphology_

[12] P. Depecker, C. Menezo, J. Virgone, S. Lepers, Design of buildings shape and energetic consumption. Building and Environment (2001), 36(5), 627–635.https://doi.org/http://dx.doi.org/10.1016/S0360-1323(00)00044-5

[13] A. AlAnzi, D. Seo, M. Krarti, Impact of building shape on thermal performance of office buildings in Kuwait. Energy Conversion and Management (2009) 50(3), 822-828.

https://doi.org/http://dx.doi.org/10.1016/j.enconman.2008.09.033

[14] M. Rahmani M., K.A. Al-Sallal, Abu Dhabi Schools: Optimization of Building Form for Energy Efficiency. In: Sayigh A. (eds) Renewable Energy and Sustainable Buildings. Innovative Renewable Energy. Springer, Cham (2020). DOI: https://doi.org/10.1007/978-3-030-18488-9_49

[15] M. Rahmani M., K.A. Al-Sallal, Energy Savings by Form Design in Schools. ARCC 2019, Ryerson University, Toronto, May 29-June 1 (2019). *ARCC Conference Repository*, *1*(1). https://www.arcc-journal.org/index.php/repository/article/view/645

[16] M. Rahmani M., K.A. Al-Sallal, Impact of Building Form on Energy Performance in New School Models. IBPSA 2019 in Rome, Italy, 2-4 Sep., (2019).

[17] A. Mahdavi, B. Gurtekin, Adventures in the design-performance space. European Meetings on Cybernetics (2002).

Economic and energy impacts of adaptive reuse building construction

J. Chan[a], C. Bachmann[a,*], C. Haas[a]

[a] University of Waterloo, 200 University Avenue West, Waterloo, ON, Canada N2L 3G1
* Corresponding author, 519-888-4567 x31303, chris.bachmann@uwaterloo.ca

Abstract:
The adaptive reuse of buildings is an alternative to a building's end-of-life where the functional life may be extended to serve another purpose. Many studies suggest that adaptive reuse is more sustainable compared to typical demolition and new construction in terms of environmental, social, and economic impacts. However, these claims are qualitative in nature and are limited to analyses at the project scale. This paper quantifies the energy and economic impacts of adaptive reuse building construction in the province of Ontario, Canada. An Input-Output (IO) model for Ontario was developed to study the impacts of adaptive reuse building construction. The building construction industries' intermediate inputs and final demands were altered in the Ontario IO model to reflect changes in the construction industries due to changes in the supply and demand of adaptive reuse buildings. A basic scenario represents the situation where only the building's superstructure and substructure are reused. The basic scenario was then extended to reflect the reuse of internal non-structural components. The Ontario IO model examines impacts to gross domestic product (GDP), industry outputs, employment, and energy use. It was found that adaptive reuse building construction may benefit Ontario's economy and reduce energy consumption under certain combinations of changes in intermediate inputs and final demands. The desirable domain of adaptive reuse construction, where energy use decreases, while GDP and employment increase, is discerned for both residential and non-residential building construction in Ontario.

Keywords:
Adaptive reuse; construction; economic impacts; energy; input-output (IO)

1. Introduction

Adaptive reuse of buildings is an end-of-life alternative that extends the life of functionally obsolete buildings through repurposing the basic structure as well as some non-structural components (NSCs) and satisfies principles of environmental sustainability via encouragement of material reuse. Studies focused on the impacts of building adaptive reuse, as well as deconstruction and material reuse, while foundational, have only been comprised of cost analyses (i.e., project economics rather than the wider economic and environmental impacts).

The overall objective of this research is to quantify the potential energy and economic impacts of adaptive reuse building construction in the Province of Ontario, Canada. In particular, this research seeks to (1) quantify the potential impacts of adaptive reuse construction on gross domestic product ($), total and sectoral output ($), employment (jobs) and energy consumption (terajoules) in Ontario; and (2) identify the domains of potential scenarios that have positive outcomes on both the economy and the environment.

An Input-Output (IO) model for Ontario was developed to study the impacts of adaptive reuse building construction. The building construction industries' intermediate inputs and final demands were altered in the Ontario IO model to reflect changes in the supply and demand of adaptive reuse buildings in the construction industries. A basic scenario represents the situation where only the building's superstructure and substructure are reused. The basic scenario was then extended to reflect the reuse of internal NSCs.

2. Data and Method

The basis of IO modelling stems from the ordinary IO model developed by Wassily Leontief in the 1930's (Miller and Blair, 2009). IO models are developed from IO tables that record interindustry transactions, final demand, value-added, and total industry output. These tables are then converted into matrices and vectors, which are used to construct an IO model. In matrix notation, the ordinary IO model is

$$\mathbf{x} = (\mathbf{I} - \mathbf{A})^{-1}\mathbf{f} \quad (1)$$

where $\mathbf{x}$ is the total industry outputs vector, $\mathbf{I}$ is the identity matrix, $\mathbf{A} = \mathbf{Z}(\hat{\mathbf{x}})^{-1}$ is the matrix of technical coefficients (or direct requirements matrix), $\mathbf{Z}$ is the interindustry transaction matrix, and $\mathbf{f}$ is the industry final demand vector. The elements of the technical coefficients matrix, a_{ij}, represent the value of inputs from industry i to produce one unit of *output* from industry j. The matrix $(\mathbf{I} - \mathbf{A})^{-1}$ is the Leontief inverse (or total requirements matrix). The elements of the Leontief inverse, l_{ij}, represent the value of inputs from industry i to satisfy one unit of *final demand* from industry j.

The Make and Use approach introduces new matrices and vectors that are not present in the ordinary IO model. These are the use matrix, $\mathbf{U}$, the make matrix, $\mathbf{V}$, commodity final demand vector, $\mathbf{e}$, and commodity output vector, $\mathbf{q}$ (Figure 1). There are multiple ways to convert the Make and Use approach to the ordinary IO model depending on whether demand is assumed to be industry or commodity driven, and whether the

structure of the economy is assumed to be under commodity or industry technology. For this study, it is assumed that the Ontario economy is industry demand driven and is under the industry technology assumption - i.e., that industries use commodities in fixed proportions (as opposed to making them in fixed proportions).

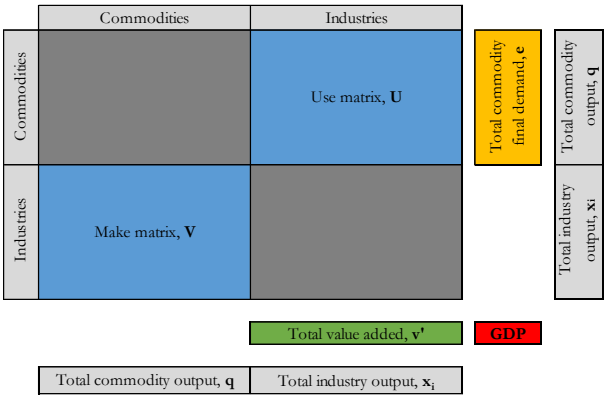

Fig 1: Commodity-by-industry accounting summary

Ontario IO data for 2014 was retrieved from Statistics Canada from Table 36-10-0478-01, providing IO data at the detailed level with 226 industries and 482 commodities. Energy use data by industry for Canada were obtained from Statistics Canada's Table 38-10-0096-01 (formerly CANSIM 153-0113) for the year 2014. The data presented is a vector of total energy use by industries measured in terajoules (TJ). Energy intensity for industry i is calculated by dividing total energy use of industry i, by output of industry i. Employment data by industry for Ontario was retrieved from Statistics Canada's Table 14-10-0098-01 (formerly CANSIM 282-0131) for the year 2014. Employment intensities for industry i were calculated by dividing employment of industry i by its output.

Impacts as a result of changes in the production structure of an industry can be simulated with an IO model by changing u_{ij} values in the **U** matrix. Adaptive reuse adjustments of residential and non-residential buildings were applied separately to represent various scenarios. First, the base case scenario was defined, and then extended to define 15 additional scenarios. Based on Sanchez et al. (2019)'s superstructure and substructure saving estimates, the base case structural steel and concrete savings are 80% for the non-residential building industry, whereas the residential building industry incurs 80% savings in structural wood, concrete and steel (Table 1). Moreover, it was found that, in general, adaptive reuse of buildings results in reduced transportation of construction waste disposal (-20%), and increased labour and engineering/ architectural design (+20%). Finally, the existing market share of buildings (residential and non-residential) that are candidates for adaptive reuse is estimated to be 20% (i.e., 20% of final demand is eligible for this change in production). Note that a portion of the commodities used by industries in the provincial use tables are imported. Thus, it is necessary to reduce imports in the import vector (final demand), to appropriately calculate the gross domestic product (GDP) for these scenarios.

Table 1: Existing and new commodity use in the residential building sector

Commodities	Change (%)	Existing ($)	Basic ($)
Cement	-80	44302	37214
Ready-mixed concrete	-80	553836	465222
Concrete products	-80	189611	159273
Prefabricated metal buildings and components	-80	74692	62741
Fabricated steel plates and other fabricated structural metal	-80	235079	197466
Other architectural metal products	-80	422599	354983
Hardwood lumber	-80	952	800
Softwood lumber	-80	402416	338029
Other sawmill products and treated wood products	-80	218762	183760
Veneer and plywood	-80	216021	181458
Wood trusses and engineered wood members	-80	268569	225598
Reconstituted wood products	-80	165767	139244
Wood windows and doors	-80	316654	265989
Prefabricated wood and manufactured (mobile) buildings and components	-80	426729	358452
Wood products	-80	628115	527617
Truck transportation services for general freight	-20	133386	128051
Truck transportation services for specialized freight	-20	302365	290270
Architectural, engineering and related services	+20	1044609	1086393
Household labour	+20	9212507	9581007

The 16 scenarios of adaptive reuse can be categorized into two sets. One set of scenarios represents the situations where demand for adaptive reuse buildings is fixed, and varying percentages (10%, 45%, and 90%) of NSCs are also adaptively reused (such as cabinetry, furniture, windows, doors, electric wiring, interior finishes, plumbing, HVAC, etc.). The other set represents the situations where demand for adaptive reuse buildings increases ("f2.5", "f5", "f10" represent increases of 2.5%, 5%, and 10% respectively).

3. Results and discussions

Absolute impacts to output, energy consumption, GDP, and jobs for 80% superstructure material savings (detailed in Table 1 for the residential sector) are summarized in Tables 2 and 3 for the residential and non-residential building industries, respectively. Total output, energy consumption, and jobs decrease as the percentage of NSCs reused increase. This is expected as material reuse enabled by adaptive reuse reduces inputs into building construction. Also, output, energy consumption, and jobs increase as the demand for adaptive reuse building increase. GDP increases as NSC increase. Recall that the Use table records industries' uses of domestic and imported commodities. Thus, reducing the commodity recipe reduces imports, and hence GDP increases (since net exports increases). Moreover, increasing demand for adaptive reuse of residential and non-residential building construction increases GDP. On the other hand, as the percent material savings for building material decreases, total output, energy consumption, and jobs increase, while GDP decreases.

Table 2: Total changes to output, energy consumption, GDP, and jobs from *residential* adaptive reuse scenarios – 80% material savings in superstructure

Scenario	Output (x$1000)	Energy (TJ)	GDP (x$1000)	Jobs
Basic	-766684	-3688	340631	-2397
10% NSC	-935591	-4011	414709	-3170
45% NSC	-1526765	-5141	673982	-5874
90% NSC	-2286847	-6595	1007333	-9352
f2.5_basic	-312396	-3091	573471	-47
f2.5_10	-482576	-3416	647675	-826
f2.5_45	-1078208	-4555	907389	-3552
f2.5_90	-1844023	-6019	1241305	-7057
f5_basic	141891	-2493	806311	2304
f5_10	-29562	-2821	880641	1518
f5_45	-629650	-3968	1140796	-1229
f5_90	-1401199	-5443	1475277	-4762
f10_basic	1050466	-1299	1271991	7004
f10_10	876467	-1631	1346574	6206
f10_45	267465	-2795	1607610	3416
f10_90	-515550	-4291	1943221	-172

Table 3: Total changes to output, energy consumption, GDP, and jobs from *non-residential* adaptive reuse scenarios – 80% material savings in superstructure

Scenario	Output (x$1000)	Energy (TJ)	GDP (x$1000)	Jobs
Basic	-183215	-1047	51836	-374
10% NSC	-231039	-1159	77906	-581
45% NSC	-398425	-1548	169151	-1308
90% NSC	-613634	-2050	286466	-2243
f2.5_basic	6242	-810	153361	619
f2.5_10	-41941	-922	179493	409
f2.5_45	-210581	-1315	270956	-323
f2.5_90	-427405	-1820	388551	-1265
f5_basic	195698	-573	281081	1611
f5_10	147157	-686	372761	1400
f5_45	-22738	-1081	490637	662
f5_90	-241175	-1589	254886	-288
f10_basic	574612	-99	457936	3597
f10_10	525353	-213	484255	3382
f10_45	352948	-614	576372	2632
f10_90	131283	-1129	694807	1668

All scenarios and measures of effectiveness for adaptive reuse of building construction were consolidated into two domain plots (Figures 2 and 3). The hatched areas show the desired domain for each adaptive reuse building industry, while the white space represents the undesirable domain. This desired domain is specified where changes in GDP and employment are positive, while changes in energy use are negative. Note that the domain boundary for GDP change is not shown in these Figures because they are positive for all scenarios.

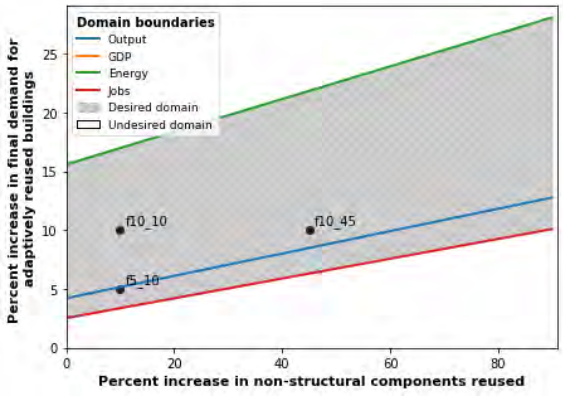

Fig 2: Desired domain for adaptive reuse of *residential* building industry in Ontario

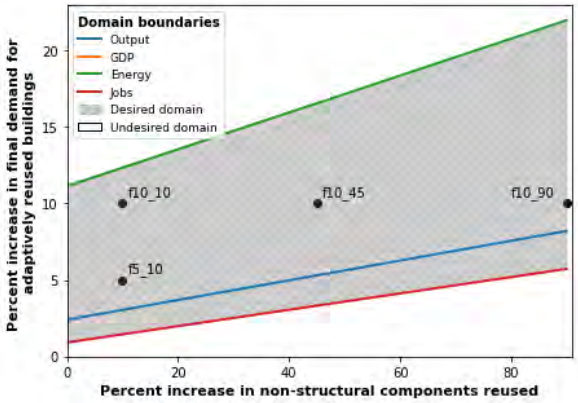

Fig 3: Desired domain for adaptive reuse of *non-residential* building industry in Ontario

Scenarios 'f5_10', 'f10_10', and 'f10_45' in Figure 2 and scenarios 'f5_10', 'f10_10', 'f10_45', and 'f10_90' in Figure 3 are scenarios where GDP and employment changes are positive, but energy use changes are negative. This may be counter intuitive since energy use is linearly proportionate to output (assuming fixed energy intensities). Desirable situations like these arise

because of variations in industrial energy intensities. About 90% of all negative output changes consist of manufacturing, wholesale trade, mining and transportation warehousing, where energy intensities for these industries are 0.1866, 0.0371, 0.0476, and 0.077 TJ per $ output, respectively. On the other hand, about 90% of all positive output changes consist of professional and scientific services; finance, insurance, real estate, rental and leasing, holding companies; owner occupied dwellings; and non-residential or residential buildings, with energy intensities of 0.00273, 0.015, 0.00126, and 0.000142 or 0.000238 TJ per $ output, respectively. Energy intensities of industries experiencing decreases in outputs are substantially larger than energy intensities of industries experiencing increases in output. Thus, certain compositions of negative and positive industry output changes results in scenarios where the total output change is positive, but the total energy use change is negative. In other words, the economy is shifting activity from energy-intense sectors, such as manufacturing, to sectors with lower energy intensity, such as professional and scientific services.

Industry output changes are larger when implementing adaptive reuse in the residential building industry (Table 2 vs Table 3), implying that adapting non-residential buildings into residential buildings has a greater impact on the economy than vice-versa. Notwithstanding large increases in demand, the adaptive reuse of buildings reduces energy consumption and material use (output) (Figures 2 and 3). Only large increases in demand would result in an increase in energy consumption – which is to be expected, since many more buildings are being constructed compared to the base case. The results indicate that adaptive reuse always benefits GDP, since material reuse reduces inputs, a portion of which are imports, and thus increases a region's net exports. In other words, adaptive reuse makes a region more self-sufficient through less reliance on imported construction material. To the extent that extraction-based industries dominate a region, this effect would be lessened (approaching zero).

Figures 2 and 3 illustrate a fundamental tension that currently exists between the economy and the environment. Reducing new production (output) is favourable in view of energy reduction and material scarcity. Hence, the reuse of construction material is environmentally beneficial. On the other hand, reducing new production reduces employment, unless a surplus of new jobs is created by gains in other industries or by increases in economic growth (demand). In the case of adaptive reuse construction in Ontario, gains in the construction-related industries (including architectural, engineering, and related services) do not offset the losses in upstream manufacturing sectors, and hence some increase in demand for adaptive reuse construction is required to remain neutral or create an increase in jobs. Some structural adjustment in the economy is also needed to accommodate the economy's change in job composition. Note however, that adaptive reuse may affect regions differently. This study focused on the Province of Ontario in Canada, which may have a different economic structure compared to other geographic regions in the world.

4. Conclusions and outlook

Adaptive reuse building construction is one method that the construction industry can adopt to help achieve environmental and economic sustainability. This paper quantifies the potential energy and economic impacts of adaptive reuse building construction in the Province of Ontario, Canada using an Input-Output model. Results of the IO model show that adaptive reuse of buildings is often but not always beneficial to the environment and economy.

Future economic impact studies of adaptive reuse may use different economic models to address limitations of IO models and/or compare results found in this research. For example, a Computable General Equilibrium (CGE) model can include price effects and supply constraints, making it a suitable method to study long-term impacts, or for studying large and widespread shifts in construction practices that are likely to require those model features.

Conducting similar studies using the methodology presented here should lead to insights for regional economies that may lead to effective policy and tax structure changes. Effectiveness will depend on the veracity of the model, its use and its interpretation, as well as on price elasticity and behavioural changes related to such policies.

Acknowledgements

We would like to thank Andreas Trau, Senior Economic Analyst from Statistics Canada for answering questions regarding the Input-Output data used in this paper. We would also like to thank Benjamin Sanchez and Mansour Esnaashary Esfahani for providing the BIM model and quantity take-offs for their case study of Region of Waterloo's Courthouse adaptive reuse project.

References

Miller, R.E., Blair, P.D., 2009. Input-Output Analysis - Foundations and Extensions.pdf. Prentice-Hall, Inc., New Jersey, United States.

Sanchez, B., Esfahani, M.E., Haas, C., 2019. A methodology to analyze the net environmental impacts and building ' s cost performance of an adaptive reuse project : a case study of the Waterloo County Courthouse renovations. Environ. Syst. Decis. https://doi.org/10.1007/s10669-019-09734-2

Canada's Green Construction through Wood Program

M. Mohammad[a]*, Dana Pothier[b], Julie Tourrilhes[c], Richard Coxford[d], and Miranda Williamson[e]

[a] Senior Research Advisor, Natural Resources Canada, Canada,
mohammad.mohammad@canada.ca
[b] Co-op Engineering Student, Natural Resources Canada, Canada,
dana.pothier@canada.ca
[c] Junior Program Officer, Natural Resources Canada, Canada,
julie.tourrilhes2@canada.ca
[d] Program Officer, Natural Resources Canada,
richard.coxford@canada.ca
[e] Program Manager, Natural Resources Canada,
miranda.wiliamson@canada.ca
*Corresponding author's e-mail: mohammad.mohammad@canada.ca

Abstract:
With the overall objective to promote economic growth and reduce carbon emissions, the Government of Canada launched the Green Construction through Wood (GCWood) program in the fall of 2017. This four-year initiative (that ends in March, 2022) aims to increase the use of wood as a green building material option across the construction industry through demonstration projects, revisions to the National Building Code of Canada (NBCC), and advancing wood education at Canadian post-secondary institutions. To accelerate market acceptance and facilitate the commercial uptake of wood-based products and building systems in non-traditional construction applications in Canada, three calls for expressions of interest (EOI) were launched for buildings and bridges. For selected projects, the GCWood program provides funding for the incremental activities associated with the design and construction of the wood-based structural components and systems. The three EOI calls for proposals were launched between October 2017 and April 2019 targeting tall wood buildings (minimum of 10 storeys), low-rise non-residential wood and hybrid wood projects including commercial, office, industrial, and institutional buildings and timber bridges. Such efforts are supported by ongoing R&D activities to provide science-based information to encourage acceptance of code provisions allowing for taller and larger wood buildings in the NBCC. Over the past two years, the GCWood program has provided funding to the National Research Council of Canada (NRC) to support key research activities, such as the development of Life Cycle Assessment datasets and guidelines. This research, along with the development of wood design course curriculum for professors at post-secondary institutions, will allow for Canada's future design and construction practitioners to continue building green with wood.

Keywords:
Tall Wood, mass timber, building codes, demonstration buildings.

1. INTRODUCTION

At the turn of the 20th century, buildings as high as nine storeys were constructed with traditional solid sawn timbers across Canada [1]. However, toward the mid-20th century, the construction of such building stopped. It was slowly replaced by reinforced concrete and steel systems due to the introduction of modern building codes and advancements made for the steel and concrete construction technologies. Many of those old wood buildings are still operational after going through seismic and fire upgrades to ensure they conform to the current building codes in Canada. However, with the arrival of modern engineered wood products (EWP) and systems, the development of a new generation of innovative timber connections, and the growing interest in green building materials, taller and larger wood buildings are remerging. Building with this new class of large modern wood members is called "mass timber construction". New generations of advanced engineered mass timber products include glued-laminated timber (glulam), structural composite lumber (SCL), dowelled-laminated timber (DLT) and cross-laminated timber (CLT) among others.

The Government of Canada (Natural Resources Canada (NRCan)) recognized, that in order to support and facilitate acceptance for wood products and systems domestically, it is critical to showcase use of wood in non-traditional applications including high-rise buildings. This led to several initiatives and programs being launched the last 10 years designed to support expanding the use of wood in Canadian construction sector through government funded demonstration projects, advancing wood education and training and revising building codes to allow taller and larger wood buildings in Canada.

2. NRCAN'S TALL WOOD BUILDINGS DEMONSTRATION PROJECTS

NRCan's Tall Wood Building Demonstration Initiative (TWBDI), launched in 2013, led to the construction of two tall wood buildings (Figure 1). The first is an 18-

storey hybrid mass timber student residence located in Vancouver, which was the world's tallest hybrid wood building when completed. The second is a 13-storey residential building in Québec City. NRCan funded the critical incremental R&D activities required to design, approve and construct the two demonstration buildings including fire, structural and acoustics testing [3]. The success of the TWBDI led to new initiatives by the Government of Canada that further encouraged the design and construction of timber structures, not just in the high-rise applications, but in low-rise non-residential and bridge construction sectors given the great interest in expanding use of wood in those applications.

Fig 1: UBC Brock Commons 18-storey residence on the left, and Quebec's 13-storey Origine building

3 GREEN CONSTRUCTION THROUGH WOOD PROGRAM

The Canadian Federal Government's Budget in 2017 provided funding of $39.8 million over 4 years under the Pan-Canadian Framework on Clean Growth and Climate Change. As a result, a new program called Green Construction Through Wood (GCWood) was announced in October, 2017. Starting in April 2018, the program aims to increase the use of timber as a greener construction material in buildings and public infrastructure projects. GCWood has three key components:

- Wood and hybrid wood demonstration projects (e.g., high-rise, low-rise commercial and bridges)
- Building code revisions and supporting research (i.e., targeting 12-storey tall wood buildings by 2020 and performance-based by 2025)
- Technology transfer and advanced wood education (training courses, design and costing tools for architects, engineers and builders, and Life Cycle Assessment (LCA) data and tools)

3.1 GCWood's Demonstration Projects

To expedite market acceptance of mass timber products and systems in Canada, three expression of interest (EOI) calls for proposals were launched for innovative wood-based buildings and bridges. To support these proposed projects, the GCWood program funds up to 100% of eligible incremental project costs. NRCan's funding is intended to support the specific eligible incremental costs associated with the design, construction and post construction of the selected demonstration projects.

3.1.1 Tall Wood Building

The first EOI was for tall wood buildings (minimum of 10 storeys) which targeted innovative use of advanced wood products and systems in high-rise applications. This call was well received with 14 applications submitted from across the country. With the help of an expert evaluation panel, a handful of highly innovative projects that show case the use of advanced wood-based products and systems were selected for funding. One of these short-listed projects was The Arbour, a 10-storey tall wood building located at George Brown College's waterfront campus in downtown Toronto, Ontario (Figure 2). This academic building will serve as a learning space for students and will house a mass timber research facility. The lateral system is composed of large CLT shear walls, mainly located at elevator and stair core areas, which will be anchored to the concrete foundation by discrete steel connections. The building will be a leader in sustainability as Ontario's first tall wood, low-carbon institutional building.

Fig 2: George Brown College 10-storey TWB

3.1.2 Low-Rise Non-Residential

GCWood's second EOI targeted low-rise non-residential wood buildings and was open from September 10 to December 3, 2018. This call for proposals targeted commercial, industrial, office, and institutional buildings of four storeys or less and required the innovative use of wood product or systems that could be easily replicated. Thirty applications were submitted and shortlisted projects are currently going through the due-diligence process.

One of the successful projects was the Toronto and Region Conservation Authority's (TRCA) New Administrative Office Building. This is a 4-storey innovative mass timber office building located in Toronto, Ontario (Figure 3). TRCA's new

administrative office building is also part of the Canada Green Building Council's Zero Carbon Building Pilot Program. When complete, the building will achieve a low-carbon footprint through all lifecycle phases, with model simulations predicting over 50% reduction in operating emissions and over 75% reduction in embodied carbon compared to the average building in Toronto. The structure system is composed of CLT mass timber floor panels supported on glulam beams and columns on a structural grid of approximately 6mx6m. The floor panels will be one and two span systems designed for strength and serviceability. Metal steel strapping would be introduced on the top surface of the CLT floor/diaphragm where drag forces are concentrated to transfer the forces to shear walls. The lateral load resisting system for the office building will utilize stair cores, elevator cores, and individual shear walls comprised of conventionally-reinforced concrete shear walls, in combination with vertical glulam diagonal bracing walls.

Fig 3: TRCA's New Administrative Office

3.1.3 Advanced Timber Bridges

The third EOI was for timber bridges that use advanced wood-based products and systems. The EOI for timber bridges was held from November 18, 2018 to April 8, 2019. Eligible bridge types included traffic (e.g. roadway bridges over rivers or train tracks, highway, etc.) and pedestrian (e.g. skywalks, bridges over rivers, highways, train tracks, etc.). The call was well received with 13 applications submitted for both traffic and pedestrian bridges with minimum of 20m spans. With the guidance of an expert evaluation panel, NRCan shortlisted several mass timber and wood-hybrid bridge demonstration projects to be financially supported. Almost all selected demonstration bridges belong to provinces or municipalities with the majority being a proposed replacement of existing steel or concrete bridges. These bridges have been either closed to traffic or their load carrying capacity reduced as they are showing signs of deterioration and require major maintenance.

It must be noted that both industry and the provincial and federal governments have initiated several market and research efforts over the last 10 years to help promote the use of timber in bridge applications. As a result, several modern innovative timber bridges have been built recently. The majority have been constructed in the provinces of Quebec, Ontario, and British Columbia. The Mistissini Bridge (Figure 4), built in 2014 and located at Uupaachikus Pass in Mistissini, Québec, is 160m long and features four sections of straight beams supported by semi-continuous glulam arches. This is one of the longest modern timber bridges in Canada and was one of the first bridges to use CLT in the country. The GCWood EOI for timber bridges builds on the success of these initiatives and projects and ensure continued market momentum.

Fig 4: Mistissini Bridge (160m), located in Mistissini, Québec (Courtesy of Stantec)

3.1.4 Common Innovative Wood-Based systems adopted in selected demonstration projects

Selected buildings and projects for potential funding by NRCan's GCWood program were those which have demonstrated innovative use of wood-based products and systems in their design. Examples of such innovative features include among many:

- Advanced floor and bridge systems using box beam/girder/floors (i.e., longer spans, shallow girders, etc.)
- Advanced Lateral Load Resisting Systems using CLT shear walls, braced frames, post-tensioning and innovative hold-down systems
- Composite technologies such as carbon and glass fibre reinforced polymers, advanced treatments and coatings, innovative durability by design concepts, etc.
- Hybrid mass timber/concrete or steel systems
- Advanced connections systems

3.2 Education Road Map

GCWood funding will also help develop design and Building information modelling (BIM) and costing tools to assist designers and builders, as well as wood-based curriculum and other education resources to expand wood design education at Canadian universities and colleges. Currently, only a few Canadian universities and colleges provide wood design courses for their engineering and architectural

schools at the undergraduate levels. Often those courses are not mandatory. A national wood education roadmap has been developed and the GCWood program is helping its implementation across Canada. Several workshops and other activities are underway to support its implementation.

3.3 NRC Life Cycle Assessment Data and Tools

GCWood is also funding activities focused on developing Life Cycle Assessment (LCA) tools and Life Cycle Inventory (LCI) data associated with wood-based products and systems to help perform LCA of wooden buildings and demonstrate the environmental benefits of building with wood. GCWood is providing funding to a major initiative led by the National Research Council of Canada (NRC) to support the development of LCI data and LCA guidelines that will be used to facilitate procurement policies at the federal and provincial level and also by the design and construction industry.

3.4 Adoption of Tall Wood Buildings in Canadian Building Codes

The 2015 edition of the National Building Code of Canada (NBCC) includes some significant changes with respect to wood design as it permits 5- and 6-storey tall wood frame buildings [3]. Building on the revolutionary acceptance of 12-storey mass timber buildings as a “pre-approved” Alternative Solution by the province of Québec in 2015 [4], a code change proposal for encapsulated mass timber was submitted to the NBCC Code Committee for their consideration targeting the 2020 edition of NBCC. A Task Group and several Working Groups were established to discuss the proposed code change and identify potential issues and research needs. Several research projects (mainly on the fire performance) have been initiated at the NRC, with funding from NRCan, to support the proposed code change provisions including developing research to support a performance-based code targeting the 2025 and 2030 editions of the NBCC. This included fire testing focused on what would be the allowable percentage of exposed mass timber that should be permitted in encapsulated mass timber construction targeting 12 storeys tall wood buildings and the effectiveness of water mist systems compared to conventional sprinkler systems that are commonly used in tall buildings.

Additional research has been ongoing as well to develop design guidelines for mass shear walls for tall wood buildings applications. A Technical Guide has been developed by NRC which will be used to support the proposed design provisions for tall wood buildings in the building code. NRCan has been funding critical R&D activities and the code change process itself at the NBCC since 2010.

.

4. CONCLUSIONS AND OUTLOOK

Canada has been recognized as a leader with a successfully developed multi-disciplinary research capacity in wood building systems, and possessing a critical mass of design and construction firms, as well as manufacturing capacity. Canada’s Tall Wood Demonstration Initiative has had a huge impact and led to the design and construction of two unique tall wood buildings. The Government of Canada continues to invest in new programs such as GCWood to facilitate broader market and regulatory acceptance of wood in non-traditional construction applications including tall buildings, low-rise non-residential and bridges, through demonstration projects and the adoption of tall wood buildings in the Canadian building codes. The GCWood program is making huge inroads towards achieving the Government of Canada’s goals in reducing GHG emissions through green building materials such as wood-based products.

ACKNOWLEDGEMENTS

NRCan would like to thank their partners, the provinces of British Columbia (Forestry Innovation Investment), Ontario and Québec for providing additional funding to support NRCan’s initiatives and programs. Contributions from NRC, Canadian Wood Council and FPInnovations are much appreciated. Thanks are also extended to the proponents of the demonstration projects and their design teams for their interest and excellent collaboration.

REFERENCES

[1] Koo, Kenneth. A study on Historical Tall-Wood Buildings in Toronto and Vancouver. FPInnovations, Québec, Québec, 2013.

[2] Mohammad, M.; Jones, R.; Maureen Whelan, Richard Coxford. Canada’s Tall Wood Buildings Demonstration Projects. Proceedings of the 2018 World Conference on Timber Engineering (WCTE), Seoul, South Korea, 2018.

[3] National Research Council. National Building Code of Canada (NBCC). National Research Council of Canada, Ottawa, Ontario, 2015

[4] Government of Québec. Mass timber buildings up to 12 Storeys: Directives and Explanatory Guide. Régie du bâtiment du Québec, Québec, 2015.

Application Research of Integration Vacuum Insulation Panel (IVIP) in New Building

Zhaofeng Chen[a*], Min Li[b], Shahzad Asim[a], Yuanhao Li[a], Duanyin Zhang[a], Qianbo Zhou[a]

[a] International Laboratory for Insulation and Energy Efficiency Materials, Nanjing University of Aeronautics and Astronautics, Nanjing, 211106, P.R. China
[b] Suzhou Hongjiu Aviation Thermal Materials Technology Co Ltd., Taicang, 215400, P.R. China
* Corresponding author, Tel: 18952018969, email: czf_msc@nuaa.edu.cn

Abstract:
Integration vacuum Insulation panel (IVIP) is becoming a new thermal insulation structure, which has potential use in the field of construction, and could greatly improve the durability and safety of the insulation structure. In this paper, IVIP was prepared by taking the VIP as the inner layer and the organic/inorganic material as the protective layer. The results showed that the thermal conductivity of IVIP is 50~100% higher than that of VIP. IVIP durability has increased by 50%, and the thermal bridge has reduced by 20%. IVIP could work in the range of temperature from -150℃ to 150℃. IVIP has become a safe, reliable, flame retardant and beautiful new type of high-efficiency insulation structure. As soon as the VIP is broken, it is feared that it is bulging to create a risk of falling off. However, in an IVIP, the VIP is not only well protected, but, once broken, the robust housing will extremely block any change in its size. The IVIP could be used as the external heat insulation of the outer wall and provides the bright, self-cleaning and beautiful appearance of a similar ceramic tile. The IVIP could be used as the heat preservation of the inner wall surface, in particular to the heat preservation of the toilet, and even the floor and the person could walk directly on the upper surface. The IVIP core material could be made of ultra-fine glass wool, nano-inorganic powder. The IVIP envelope could use aluminum plastic film, no longer need glass fiber cloth, which increased the cost. Flame retardant, reflecting agent, and water-resistant agent could be added to the protective layer to further improve the thermal insulation performance of the IVIP, and more properties could be given to the IVIP.

Keywords:
Integration vacuum insulation panels, Protective layer, Insulation structure, Flame retardant.

1. Introduction

Building energy consumption is a major part of China's total energy consumption. Therefore, wall insulation is an essential way to reduce energy consumption in buildings. However, the traditional external wall thermal insulation structure has failed to meet the national thermal insulation technical requirements, which urges the development of high-performance thermal insulation materials to reduce energy consumption[1-2].

In recent years, vacuum insulation panel (VIP) with the features of environmentally friendly and energy-saving is a very efficient thermal insulation material with a thermal conductivity of 1.5mW/(m·K). It has attracted much attention in the building industry resulting from the extremely low thermal coefficient and ultra-thin thickness[3]. However, the unstable thermal conductivity over their useful lifetime of VIP has become one of the main drawbacks[4]. H. Simmler also pointed out the failure issue of the VIPs is that the required service life hardly achieved the expected performance index due to the weak mechanical property especially under specific temperature and humidity conditions, which hindered its application in building thermal insulation[5].

To address this, the integrated board is becoming a novel and hot thermal insulation structure with the functions of decoration, energy-saving, waterproofing, fire and heat preservation, environment-friendly, and wide adaptability. It can significantly improve the durability and safety of the structure as well as solve the fire and the fall of the thermal insulation structure of the external building wall, which plays a vital role in the new building and shows excellent development potential and market prospects[6]. Based on this, the well-protected integration vacuum insulation panel (IVIP) can prevent damage caused by the impact loading on the external or internal wall surface significantly. It is also compatible with the use of floor applications and cannot be damaged by residence feet steps. Ultrafine glass wool, nano-inorganic powders can be used as the core material of the IVIP[7]. The aluminum-plastic film can be applied as the cheap membrane material to replace the traditional glass fiber cloth. Besides, the thermal insulation performance of the IVIP can be further improved by adding flame retardant, reflector, and water retardant.

In this paper, a safe, reliable, flame retardant and beautiful new type of high-efficiency IVIP was prepared by taking the VIP as the inner layer and the organic/inorganic material as the protective layer, which could work in the range of temperature from -150℃ to 150℃. Although the thermal conductivity of the IVIP is 50~100% higher than that of VIP, the durability has increased by 50% while the thermal bridge has reduced by 20%. Besides, the VIP in the IVIP is well protected and blocked by the robust housing once broken. The IVIP could not only be used as the external heat insulation of the outer wall and provides the bright, self-cleaning and beautiful appearance of a similar ceramic tile, but also as the heat preservation of the inner wall surface, in particular to the heat preservation of the toilet, and even the floor.

2. Experiment

2.1. Preparation of the IVIP

In this work, two types of the IVIP core materials including

the ultra-fine glass wool and fumed silica were studied. The aluminum-plastic film was used to reduce the cost of the envelope materials. The additional protective layer was flame retardant, reflector, and water repellent, which further improved the performance of the IVIP. The dimensions of the VIP were 280×280×30mm and the IVIP with dimensions of 300×300×30mm were prepared with the mixture of sand and phenolic resin as the protective layer, which was mixed with a foaming agent, curing agent, and other auxiliaries to obtain the final phenolic foam[8]. The as-prepared IVIP possessed excellent fire resistance as well as excellent insulation performance and exceptional corrosion resistance.

2.2. Thermal conductivity test

The Netzsch HFM 436 thermal conductivity analyzer was used to assess the thermal conductivity of the IVIP at 24℃ and 31% R.H. The working temperature of the hot plate was set to be 38℃, and that of the cold plate was 10℃ with the average temperature of 24℃.

2.3. Aging test

The CZ-A-21600 programmable constant temperature and humidity testing machine was used for the aging test of the samples. The laboratory temperature and humidity were set to be 30℃ and 60% R.H., respectively. Three sets of test programs with different conditions were performed for the accelerated aging experiment: the high temperature and high humidity (+80℃, 90% R.H.), the low temperature (-80℃), and the high and low-temperature alternating experiment (-70℃~50℃, 90% R.H.). The IVIP was placed in the CZ-A-21600 programmable constant temperature and humidity tester, followed by accelerating the aging program and then taken out after every 7 days. For each aging experiment, the Netzsch HFM 436 thermal conductivity analyzer was used to measure the thermal conductivity of the IVIP.

3. Results and discussions

3.1. The thermal conductivity of the IVIP

The life assessment of the IVIP is in accordance with ASTM C 1484 [9]. The $P_{1/2}$ of the panel is maintained below 11.5mW/(m·K) under 24℃ temperature and 50% R.H. The thermal conductivity (λ_e) of the IVIP was integrated by the following equation:

$$\lambda_e = \lambda_{evac} + \frac{\lambda_0}{1 + (CT / \delta P_{gas})} \quad (1)$$

Where

$\lambda_{evac} = \lambda_s + \lambda_r$;

λ_s - the heat conduction of solid skeleton;

λ_r - heat radiation;

λ_0 - the gas thermal conductivity coefficient of free static air at room temperature, 24.2 mW/(m·K);

T - temperature (K);

δ - the characteristic size of the hole;

P_{gas}-the internal gas pressure of the panel (Pa);

Where C can be defined as:

$$C = 2\beta k / \sqrt{2}\pi d_g^2 \quad (2)$$

β - the energy conversion efficiency of the collision between gas molecules and solid structural materials, for air $\beta \approx 2$;

k - Boltzmann constant, 1.38×10^{-23}J/K;

d_g - Diameter of gas molecules, 3.72×10^{-10}m for air;

According to the above equations, the thermal conductivity of the IVIP is mainly affected by the gas pressure in the panel. The internal gas pressure of the panel mainly includes two aspects: The first one is the penetration of external gases through the envelope, and the second is the venting of the internal core material. The nitrogen, oxygen, water vapor, and other gases from the external environment enter the panel during the evacuation process. The small amount of air also penetrates through the edge sealed regions. A small amount of gases permeates into the IVIP during its service life after its application. Besides, the core material also releases moisture and gases due to the aging factor, resulting in increased internal gas pressure. However, the use of inorganic powder as the core material such as fumed silica, which is also a good adsorbent, slows down the rise of the internal gas pressure of the IVIP.

3.2. The thermal conductivity of the IVIP under different aging conditions

Various aging tests were performed on the IVIP and VIP with both glass fiber core, and fumed silica core materials. The thermal performances of the tested panels are shown in Table 1.

Table 1 Thermal conductivity of the IVIP and VIP under different aging conditions.

Panel	Core material	No aging	High temperature and humidity	Low temperature	Alternation of high and low temperature
IVIP	Glass fiber	2.98	4.02	3.25	4.98
	Fumed silica	4.29	4.92	4.39	5.28
VIP	Glass fiber	3.67	4.93	4.22	5.63
	Fumed silica	4.59	5.92	5.35	5.97

Thermal conductivity of the IVIP and VIP with different core materials tested under different aging conditions have been plotted in Fig. 1. The test code "1" in Fig. 1 indicates that no aging test has been carried out, "2" represents aging at high temperature and high humidity (+80℃, and 90% RH), "3" represents aging at low temperature (-80℃), "4" represents aging at high and low temperature (-70℃~50℃, and 90% RH).

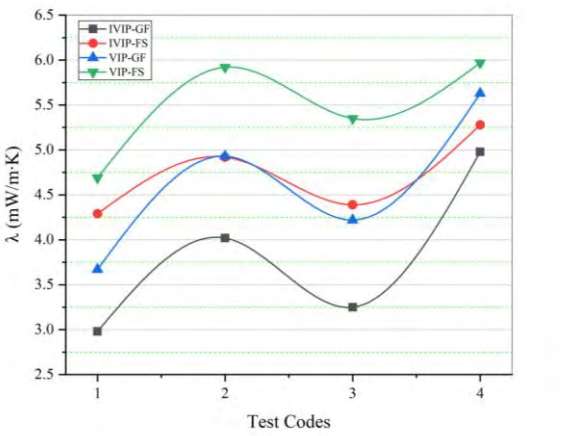

Fig. 1 Thermal conductivities of the IVIP and VIP with glass fiber and fumed silica cores under different aging conditions

From Table 1 and Fig.1, it can be stated that the insulation performance of the IVIP is much better than that of VIP with the same core material. It also should be pointed out that for the same core material, the thermal conductivity of the IVIP, as well as VIP with glass fiber core material, is significantly lower than those with fumed silica core material. Similarly, after various aging tests, a steep rise in the thermal conductivity of glass fiber core-based panels has been observed for both the IVIP and VIP. This steep rise is ascribed to the increase in the internal pressure of the panel above 100Pa.

Mostly, the core materials are highly porous, which absorbs moisture and gas during their service life, resulting in the loss of thermal insulation performance. The adiabatic mechanism of the porous materials is that when the average free path of gas molecules is larger than that of the porous materials, the heat transfer will be inhibited[10]. Achieving the desired performance level of the evacuated panel largely depends on the gas pressure inside the panel as well as the thermal bridging effect. Herein, the glass fiber-based IVIPs have lower thermal conductivity values compared with the fumed silica-based panels due to the better insulation performance of glass fiber at lower internal pressure. However, the fumed silica core panels are less sensitive to the internal gas pressure because of its fine pore structure, resulting in a lower rise in thermal conductivity after aging[11].

3.3. Thermal bridge

The VIP mainly consists of three parts: core material, envelope material, and getter. The thermal conductivity of the surface diaphragm is much higher than that of the internal core material. The thermal conductivity of the core material is within 2~6mW/(m·K) while that of the aluminum foil can be as high as 200W/(m·K). The major heat transfer is caused by the solid conduction process, which mainly flows through the envelope surface, thus enhancing the thermal bridging effect. The service life and performance of the VIP are highly affected by the thermal bridging phenomenon. The IVIP has successfully controlled the heat transfer through the thermal bridging effect by increasing and complicating the heat flow path, as can be seen in Fig. 2.

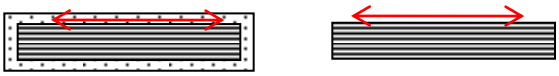

(a) IVIP (b) VIP

Fig. 2 Schematic diagram of the thermal bridge effect

As shown in Fig. 2(a), it can be seen that a very small amount of heat passes the IVIP compared to the VIP in Fig. 2(b). As to the IVIP, the heat flow is initially resisted by the outer protective layer, which is the mixture of phenolic resin and sand. When the small amount of heat reaches the envelope surface, it starts flowing through the interface region due to the face resistance. However, the thermal bridging through envelope material directly takes place in VIP. Thus, the heat flow path reduces, resulting in the rise in the thermal conductivity compared with the IVIP. The application of the IVIP in the building sector can increase the thermal insulation performance as well as the service life. In addition, thermal bridging can further be reduced by developing highly insulating structural columns, frames, beams, and other smart structures.

4. Conclusions

In this paper, the IVIP with organic/inorganic materials as the protective layer was prepared. The results showed that although the thermal conductivity of the material increased by 10~50% compared with that of VIP, its durability was much improved and the thermal bridge was reduced by 20~50%. The working temperature range of the IVIP ranged from -150℃ to +150℃. The flame-retardant and puncture resistance of the material was reduced, making it environmentally friendly. The IVIP can significantly improve the durability and safety of the wall insulation structure and meet the standards of the energy-saving and environmental protection. It has enormous development potential and market prospects in the new construction market.

References

1.Kwon, J. S.; Jang, C. H.; Jung, H.; Song, T. H., Effective thermal conductivity of various filling materials for vacuum insulation panels. *International Journal of Heat & Mass Transfer 52* (23-24), 5525-5532.

2.Hua, X.; An, X. In *The Economic Evaluation of the External Wall Insulation Structure Based on the Life-cycle*, 2016 4th International Conference on Mechanical Materials and Manufacturing Engineering, 2016/10; Atlantis Press: 2016.

3.Li, C. D.; Saeed, M. U.; Pan, N.; Chen, Z. F.; Xu, T. Z., Fabrication and characterization of low-cost and green vacuum insulation panels with fumed silica/rice husk ash hybrid core material. *Mater Des* **2016,** *107*, 440-449.

4.Chen, Z.; Chen, Z.; Yang, Z.; Hu, J.; Yang, Y.; Chang, L.; Lee, L. J.; Xu, T., Preparation and characterization of

vacuum insulation panels with super-stratified glass fiber core material. *Energy* **2015,** *93*, 945-954.
5.Simmler; Brunner, Vacuum insulation panels for building application Basic properties, aging mechanisms and service life. **2005,** *37* (11), 1122-1131.
6.Ascione, F.; De Masi, R. F.; Mastrullo, R. M.; Ruggiero, S.; Vanoli, G. P., Experimental investigation and numerical evaluation of adoption of multi- layered wall with vacuum insulation panel for typical Mediterranean climate. *Energy Buildings* **2017,** *152*, 108-123.
7.Farooq, A.; Abd El-Aty, A., Centre of panel thermal conductivity performance analysis of aerocor-centrifugal hybrid ultrafine glass fiber VIP core materials. *Advanced Materials Research 1120-1121*, 1511-1515.
8.Yang, H.; Jiang, Y.; Liu, H.; Xie, D.; Wan, C.; Pan, H.; Jiang, S., Mechanical, thermal and fire performance of an inorganic-organic insulation material composed of hollow glass microspheres and phenolic resin. *Journal of Colloid and Interface Science* **2018,** *530*, 163-170.
9.Wakili, K. G.; Bundi, R.; Binder, B., Effective thermal conductivity of vacuum insulation panels. *Building Research & Information* **2004,** *32* (4), 293-299.
10.Di, X.; Gao, Y.; Bao, C.; Ma, S., Thermal insulation property and service life of vacuum insulation panels with glass fiber chopped strand as core materials. *Energy Buildings* **2014,** *73*, 176-183.
11.Li, C.; Li, B.; Pan, N.; Chen, Z.; Saeed, M. U.; Xu, T.; Yang, Y., Thermo-physical properties of polyester fiber reinforced fumed silica/hollow glass microsphere composite core and resulted vacuum insulation panel. *Energy Buildings* **2016,** *125*, 298-309.

Seismic performance of timber connections for sustainable tallwood building

G. Vojtila[a,*], C. MacDougall[b]

[a] Gabriella Vojtila, M.A.Sc. Civil Engineering, Queen's University, Kingston, Ontario, Canada, gabriella.vojtila@queensu.ca
[b] Colin MacDougall, Professor, Queen's University, Kingston, Ontario, Canada, macdougc@queensu.ca
* Gabriella Vojtila, (905)808-0148, gabriella.vojtila@queensu.ca

Abstract:
Concrete and steel are currently the leading materials used among most building applications, significantly contributing to the release of global carbon emissions. Sustainable alternatives are now needed to address climate change. Wood has arguably one of the lowest carbon footprints of any building material and can in fact sequester carbon. Improvements in engineered wood products, also known as mass timber, and connection systems have made tallwood buildings feasible and economical. Tallwood buildings are defined as buildings over six-storeys comprised of mass timber for its structural system. The demand for such structures has recently increased. Higher tallwood structures will have increased lateral and seismic demands and the performance and design of the connections is critical. Thus, research is needed to understand engineered connections in mass timber buildings and their functionality under lateral and seismic loads.
This paper presents the evaluation of several beam-column timber connections under seismic loading and provides a literature review on previous research that has been conducted on generic beam-column timber connections. From this literature review, it is evident that there is a lack of research conducted on pre-engineered timber connections, which are very common in tallwood buildings today. The second portion of this paper examines recent experiments on several pre-engineered timber connections. The performance of these connections was investigated using the Consortium of Universities for Research in Earthquake Engineering (CUREE) seismic loading protocol, used to simulate an earthquake. Typical failure modes will be evaluated and a comparison of the cumulative energy dissipations of these pre-engineered beam-hanger connections with other moment-resisting connections will be made.

Keywords:
Timber connections, tallwood buildings, seismic response, energy dissipation, sustainable building.

1. Introduction

For the last century, there has been no need to challenge steel or concrete as the primary building material for large buildings. However, due to an increasing pressure to reduce the world's carbon footprint, and the building sector contributing largely to global greenhouse gas (GHG) emissions, the way society builds its buildings must be addressed [1].
The world is experiencing a rapid migration of people to urban areas, whereby in 2050, 2 out of 3 people in the world will be living in cities. Therefore, the future will need meaningful, sustainable and taller buildings to live and work in [2]. Mid-rise and high-rise buildings have predominantly been built using concrete and steel [3]. The manufacturing of steel and concrete contribute significant amounts of GHG emissions to the atmosphere. Although these materials have proven to be exceptional structural choices and are important to the construction of buildings for the future, climate change, urbanization, sustainable development and housing needs are creating a demand for wood as a structural material for tall buildings [4].
The demand for tallwood buildings has been particularly acute on the west coast of North America, however this is also a region with high seismic demands. Higher tallwood structures will have increased lateral and seismic demands and the performance and design of the connections will be crucial for acceptable seismic performance.
Beam-hanger connectors (Fig. 1), are typically designed as shear connectors. An example of this application can be seen in the First Tech Credit Union building in Portland, Oregon which uses fully concealed beam-hanger connections at the beam-column interfaces [5]. These connections are not intended to resist loads other than shear loads and are not part of the lateral-load resisting system of the building. However, the connection's behaviour and performance under cyclic deformations caused by earthquakes is critical for the overall resiliency of the structure. A variety of 'off-the-shelf,' pre-engineered beam-hanger connection systems are readily available for mass timber construction. However, there is a lack of experimental research conducted on the seismic performance of these timber beam-hanger connection systems.
This paper will present a brief review of the behaviour of timber connections under cyclic loading. Then, it will outline an experimental study conducted on pre-engineered beam-hanger timber connectors to evaluate their seismic performance. Their ability to

dissipate energy during cyclic loading will be compared with other timber connection systems.

2. Literature review

The characteristics of the connections (type, mechanical properties, geometry, etc.) will strongly influence the stiffness, strength, ductility and energy dissipation of the whole structure [5]. Previous cyclic testing conducted on moment-resisting connections and beam-hanger connections will be briefly reviewed.

2.1 Cyclic loading tests of moment-resisting connections

Research conducted on the seismic performance of timber connections has focused primarily on moment-resisting connections intended to be part of the lateral-load resisting system. Lam et al. (2010) and Wang et al. (2014) investigated the performance of bolted beam-column connections under reversed cyclic loading while using self-tapping screws perpendicular-to-grain as reinforcement to avoid brittle failure and to obtain a ductile connection. The loading scheme was in accordance with the Consortium of Universities for Research in Earthquake Engineering (CUREE) loading protocol. Zhang et al. (2017) experimentally investigated a hybrid lateral-load resisting system as the main energy dissipator that combined steel beams connected to a cross-laminated timber core. Lastly, Gohlich (2015) observed the seismic performance of a new hybrid timber-steel moment-resisting connection that consisted of a steel link between the timber column and beam.

2.2 Cyclic loading tests of beam-hanger connections

Leach (2018) studied the performance of seven various beam-hanger connections under reversed cyclic loading using a modified version of the CUREE loading protocol. These beam-hanger connectors included a variety of different sized Megant and Ricon connection systems manufactured by KNAPP. These connections are not intended to resist moments and lateral loads, however the results indicate that these connections have measurable moment capacity and ductility.

3. Materials

An experimental study on the reversed cyclic performance of four 'off-the-shelf' 430x150 (tradename Megant) pre-engineered beam-hanger connectors was conducted. The connection system consists of two identical aluminum plates that are attached to a glulam beam and column (Spruce-Pine-Fir with a stress grade of 20f-E and 12c-E for the beam and column, respectively) using self-tapping screws oriented parallel and at 45° to the grain. The Megant connector is shown in Fig. 1.

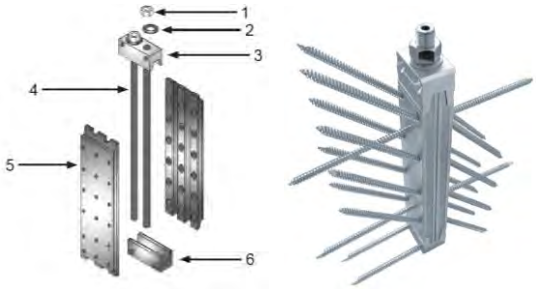

Fig. 1: Megant connector system (courtesy of MTC Solutions).

4. Test set-up and procedure

The glulam column was clamped to a stiff steel reaction frame and connected to the beam using the Megant connector. On the opposite end of the beam is a swivel attachment through which a 2000-kN capacity servo-hydraulic actuator applies reversed cyclic loading through controlled deflections. In addition, a hydraulic ram was used to apply a static shear load to the glulam beam to simulate gravity loads. This set-up can be seen in Fig. 2.

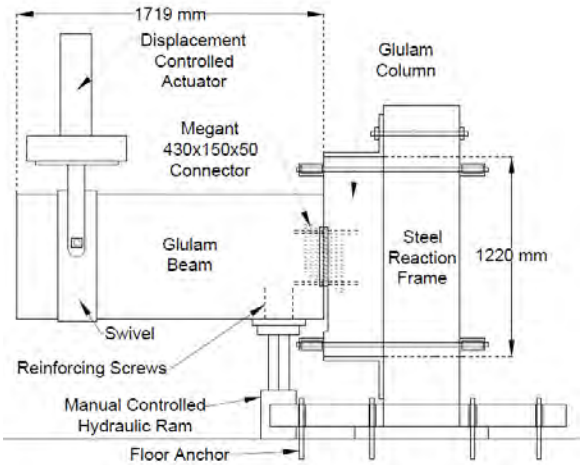

Fig. 2: Test set-up for reversed cyclic loading of Megant 430x150 beam-hanger connector.

4.1 Loading Protocol

The connectors underwent controlled deflections, which are used to simulate similar interstorey dirfts caused by seismic vibrations. A modified version of the standard loading scheme proposed by CUREE for reversed cyclic loading for timber structures, seen in Fig. 3, was employed.

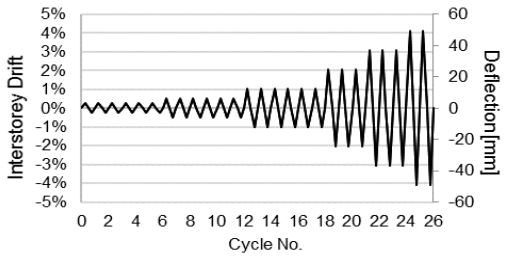

Fig. 3 : Modified reversed cyclic loading scheme.

The loading protocol is defined by variations of deformation amplitudes that begin with a sequence of small amplitude cycles followed by larger amplitude cycles. Up to 26 cycles were applied to the connectors until final failure was observed.

5. Results and discussions

The following section will outline the failure modes and the energy dissipated by the Megant 430x150 connector under reversed cyclic loading, applied on the basis of the CUREE loading protocol.

5.1 Failure modes

Fig. 4 depicts the typical failure behaviour of the Megant connector. Common failure mechanisms include pull-out failure due to tension in the self-tapping screws, and permanent deformation in the aluminum connector plate and self-tapping screws.

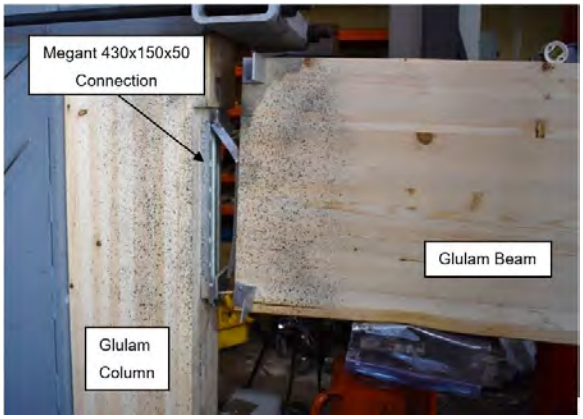

Fig. 4: Typical failure mode of Megant 430x150 beam-hanger connection.

Fig. 5 shows the ultimate failures of Tests #1 - #4. Tests #1-#3 underwent the same failure mechanism where ultimate failure was reached due to excessive bending of the aluminum plate, whereas Test #4 failed due to screws pulling out of the glulam beam.

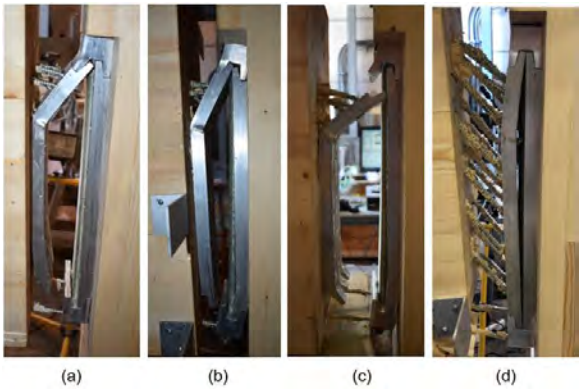

Fig. 5: Failure modes for (a) Test #1, (b) Test #2, (c) Test #3, (d) Test #4.

The connectors exhibited ductile behaviour indicating that they are capable of dissipating energy, even if not intended to. This behaviour is in contrast to the brittle failure commonly seen in bolted connections (e.g. Lam et al. 2010) under reversed cyclic loading.

5.2 Energy dissipation

The energy dissipated by the Megant connector provides valuable information on how these connections perform when subjected to seismic vibrations. The more energy dissipated by a connector, the more effective the connection type for seismic resistance. The energy dissipated during the modified CUREE cyclic loading protocol is equivalent to the enclosed area of the connection's moment-rotation envelopes (moment-rotation graphs not presented in this paper) at each cycle, where the cumulative energy dissipated can be determined by summing these enclosed areas. The energy dissipated by the Megant 430x150 connector is shown by the black line in Fig. 6 and its cumulative energy dissipated in Fig. 7. This is compared to the energy dissipation observed by Leach (2018) for other sizes of similar connections.

It is evident that the Megant 430x150 connector out-performs the two larger Megant connector sizes, which have higher design capacity on shear. From Fig. 7, the Megant 430x150 connector dissipated the most energy of 22.7 kJ (kNm), whereas the largest Megant connector dissipated a maximum of 6 kJ of energy. It should be noted that these differences were likely heavily influenced by the shear load applied. The Megant 430x150 had an applied shear load of 90 kN (approximately service load), whereas the Megant 520x100 and 550x150 had an applied shear load of 240 kN (approximately ultimate shear load).

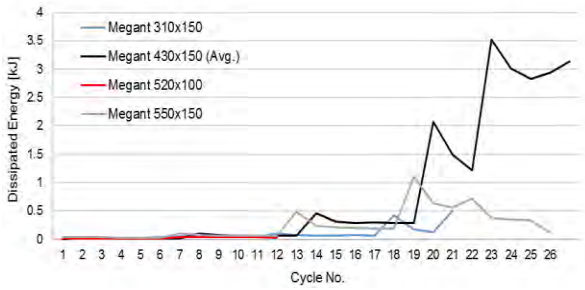

Figure 6 : Energy dissipated at each cycle till failure.

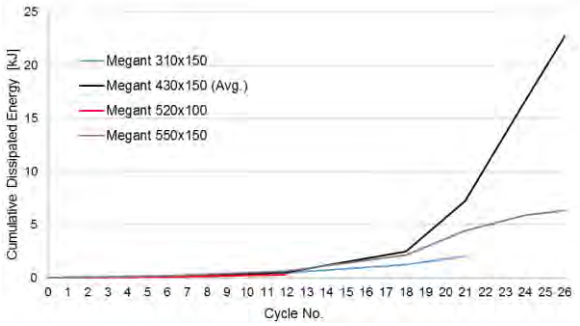

Fig. 7: Cumulative energy dissipated at failure.

It should be noted, that although these beam-hanger connection systems are not intended to partake in resisting lateral loads, these tests indicate that beam-hanger connections could make a contribution to the seismic resistance of the building.

5.3 Comparison of Megant connectors to literature

Gohlich (2015) conducted a cyclic loading test on a hybrid steel-timber moment-resisting connection, under interstorey drifts applied on the basis of the CUREE loading protocol. The cumulative energy dissipated by these hybrid moment-resisting connections, seen in Fig. 8, absorb much higher values of energy than the Megant connectors, reaching a maximum cumulative energy dissipation of between 60 kJ to 115 kJ, whereas the Megant connector dissipated a cumulative energy of 22.7 kJ.

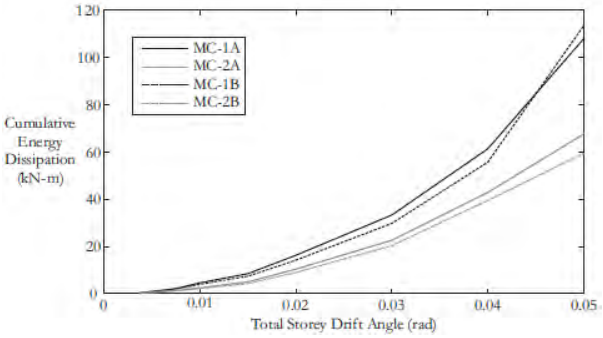

Fig. 8: Cumulative energy dissipated by hybrid steel-timber moment-resisting connection [9].

Popovski et. al (2002) investigated the seismic performance on braced timber frames of riveted connections in timber construction. Braced frames are structural systems used to resist lateral loads. The riveted connections showed superior seismic performance and large displacements were possible before failure. The dissipated energy values for the system are seen in Fig. 9. Note that these are assumed to be the energy values dissipated *per cycle*, rather than the cumulative energy dissipated, although this was not explicitly described by the authors. These connections had a maximum per cycle energy dissipation of just under 15 kJ, while the Megant 430x150 connector had a maximum cyclic energy dissipation of only 3.5 kJ.

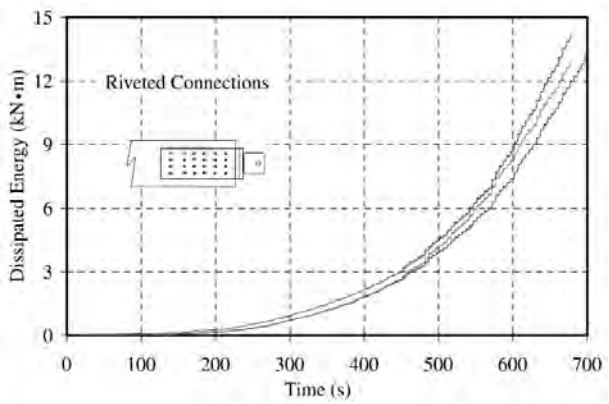

Fig. 9: Dissipated energy of glulam rivet connections under cyclic loading.

6. Conclusions and outlook

Beam-hanger connections are not considered part of the lateral-load resisting system which is why they they dissipate much lower energy than moment-resisting connectors found in literature. However, the Megant beam-hanger connectors showed ductile behavior and notable energy dissipation values that could help the overall seismic resiliency of a timber building.

References

[1] mgh Architecture + Design, Equilibrium Consulting, LMDG Ltd., BTY Group, "The Case For Tall Wood Buildings: How Mass Timber Offers a Safe, Economical, and Environmentally Friendly Alternative for Tall Building Structures," Michael C. Green, Vancouver, 2012.

[2] Perkins+Will, "Mass Timber Influencers: Understanding mass timber perceptions among key industry influencers," Forestry Innovation Investment Ltd., 2018.

[3] R. H. Crawford and X. Cadorel, "A framework for assessing the environmental benefits of mass

timber construction," *Procedia Engineering,* no. 196, pp. 838-846, 2018.

[4] "The Environmental Case for Tall Wood Buildings," *Canadian Journal of Green Building & Design,* pp. 46-49.

[5] Structurlam Mass Timber Corporation: Intelligence in Wood, "First Tech Federal Credit Union," Structulam. [Online]. [Accessed 30 November 2019].

[6] M. Wang, X. Song, X. Gu, Y. Zhang and L. Luo, "Rotation behavior of bolted beam-to-column connections with locally cross-laminated glulam," *American Society of Civil Engineers,* pp. 04014121-1 to 04014121-7, 2014.

[7] M. C. Porcu, "Ductile behavior of timber structures under strong dynamic loads," InTech, 2017.

[8] X. Zhang, R. Axim, P. Bhat, M. Popovski and T. Tannert, "Seismic performance of embedded steel beam connection in cross-laminated timber panels for tall-wood hybrid system," *Canadian Journal of Civil Engineering,* pp. 1-31, 2017.

[9] R. J. Gohlich, "Development of an Innovative Hybrid Timber-Steel Moment-Resisting Frame for Seismic-Resistant Heavy Timber Structures," Carleton University, Ottawa, 2015.

[10] MyTiCon Timber Connectors, "Inter-storey drift testing of KNAPP RICON S VS connectors," MyTiCon Timber Connectors, Surrey, Canada, 2016.

[11] F. Lam, M. Gehloff and M. Closen, "Moment-resisting bolted timber connections," *Institution of Civil Engineers,* pp. **163(4):** 267-274, 2010.

[12] H. Leach, "Interstorey drift performance of timber beam-hanger connections," Queen's University, Kingston, Ontario, Canada, 2018.

[13] M. Popovski, H. G. Prion and E. Karacabeyli, "Seismic performance of connections in heavy timber construction," *Canadian Journal of Civil Engineering,* pp. **29**: 389-399, 2002.

Northern Ontario air transportation: infrastructure resilience and community well-being

P. Dimayuga[a,*], E. Ohlrogge[b], M. Widener[c], T. Galloway[d], S. Saxe[a]

[a] Civil and Mineral Engineering, University of Toronto, 35 St George St, Toronto, ON M5S 1A4, Canada

[b] Global Health, Vrje Universitait Amsterdam, De Boelelaan 1105, 1081 HV Amsterdam, Netherlands
[c] Geography and Planning, University of Toronto, 100 St. George St., Toronto, Ontario M5S 3G3
[c] Anthropology, University of Toronto, 3359 Mississauga Rd N, Mississauga ON Canada L5L 1C6

* Corresponding author, email: pia.dimayuga@mail.utoronto.ca

Abstract:
In this research, we assess air transportation infrastructure in northern Ontario through a resilience lens to understand its interdependencies with other infrastructure (e.g. power) and its vulnerabilities to external hazards (e.g. poor weather). We also examine the ways in which air transportation impacts the well-being of the remote and predominantly First Nation communities it serves. The focus of this paper is the interdependencies and vulnerabilities of air infrastructure in remote northern Ontario communities.

Air transportation is the only mode of year-round travel in 31 northern Ontario communities. These communities rely on air transportation infrastructure to connect to essential services and resources. Transportation challenges exacerbate community challenges including food insecurity, poor health outcomes, and inadequate housing. Aging infrastructure and climate change are stressing air transportation's physical infrastructure and this is expected to further reduce air service reliability without significant intervention. In parallel, climate change will reduce the viability of other transportation alternatives (e.g. winter roads), therefore increasing future reliance on air travel. We explore system-level interdependencies by analyzing 20 months of cargo data and 12 months of air operations data. The interdependencies are augmented by qualitative data on the lived experience of service providers (i.e. pilots, airline employees) gathered using semi-structured interviews from Fall 2019. Interviews with service providers focus on logistics and challenges of flying in the North. Limitations of this in-progress research, including lack of interviews with First Nation community members related to their usage of air transportation is also discussed. (maximum 300 words)

Keywords:
Air transportation, infrastructure resilience, infrastructure interdependencies, remote communities 3-5 keywords).

1. Introduction

Air transportation is the only year-round available mode of transportation in 31 First Nation communities in northern Ontario. These remote communities rely on air transportation for many essential goods and services including food, fuel, healthcare, and education. Alternative modes are seasonal and not uniformly accessible to communities, such as summer barges and winter roads. Winter roads, which consist of a combination of packed snow and frozen waterways, are crucial for transporting large freight loads (e.g. diesel fuel) to communities more economically than by air. The operating season of winter roads is highly variable, however, and the disproportionate climatic warming in northern Ontario is expected to reduce the viability of winter roads [1]. Consequently, the importance of air transportation is expected to increase in the future due to climate change.

In parallel, the remoteness of communities illustrated by their reliance on air transportation is a contributing factor in the health and wellbeing disparities between northern communities and the rest of Canada. For example, 52 percent of households in northern Ontario First Nations communities were classified as food insecure in 2012 compared to 8.2 percent for Ontario overall [2]. Reading and Wien note that food insecurity in northern Canada is a consequence of high rates of poverty and high food costs, to which transportation costs contribute [3]. In comparing the healthcare and education infrastructure indicators developed by the Centre for the Study of Living Standards, the ones for remote First Nations communities in Canada are significantly lower than remote non-Indigenous communities (0.34 compared to 0.83 and 0.44 to 0.76, respectively) [4]. This difference is partially due to the lack of healthcare and education services located in communities and is partially addressed by air transportation. Air ambulances, for example, play a key role in emergency healthcare. Air service reliability is therefore connected to a community's access to essential goods and services that determine the community's quality of life and well-being.

The main objective of this research is to understand how remote communities and their infrastructure

systems depend on air transportation. The second objective, assuming some dependence of remote communities on air transportation, is to understand what factors impact air service reliability.

2. Resilience and interdependencies

An infrastructure resilience lens provides a useful perspective through which to assess air transportation in this remote context. From the resilience literature arises the concept of infrastructure interdependencies, where different infrastructure systems rely on one another in order to function (e.g. clean water and distribution is reliant on reliable electricity). For example, in the majority of the remote communities, electricity generation is completely reliant on diesel generators and diesel is predominantly transported by winter road. If a community is not able to put in their winter road or if they run out of diesel fuel before the winter road season, then diesel will need to be transported by air. If water treatment and distribution require electricity, then clean water is also reliant on diesel and its transportation.

The interdependent infrastructure systems and the community they service is then exposed to a set of external shocks and stresses. Shocks and stresses, which can range from large-scale natural disasters to regular isolated thunderstorms, impact the function of one or more infrastructure systems. Due to the interdependencies, however, the consequences of a singular shock impacting one infrastructure system may cascade and impact other infrastructure systems and functions. Figure 1 illustrates how infrastructure systems may be interdependent and how this could affect community well-being.

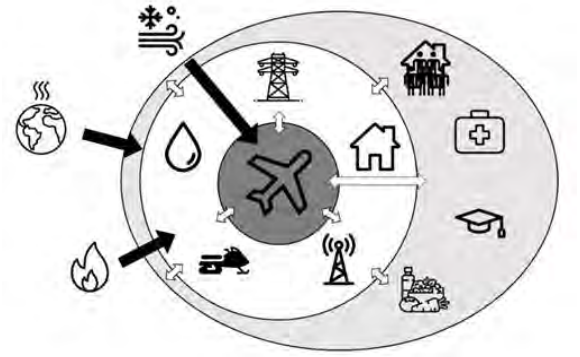

Fig 1: Schematic of interdependencies between air transportation and other infrastructure systems. Community concerns that may be impacted (grey area) and example shocks and stresses (black arrows) are represented.

3. Data collection and analysis

At the outset of this research, the authors identified several data sources as critical for a robust and complete analysis, but have not yet engaged with all of them at the time of writing. Of particular note, is the lack of input from the First Nations communities in the area of research and the Ontario Ministry of Transportation, who is the responsible authority for remote airports in the region. At the time of writing, the authors have had a number of engagement meetings with First Nations members in the region and are in the process of scheduling visits to two First Nations. The authors acknowledge that the lack of direct input and data from the involved communities and residents is an important limitation of this work to date.

The principal source of data for this work is North Star Air (NSA), an airline operating in the region. NSA has been operating in the provincial and territorial North since 1997 [5]. In 2017, NSA was acquired by the North West Company, which is a large retailer in northern Canada that owns many grocery stores in the North. Due to the singular nature of the data, the findings may not be representative of all aviation business in the region. However, some of the interviewees have worked in the region for a long time across many companies and so their insights may be more representative.

The data consists of cargo, flight operations, 13 semi-structured interviews with NSA employees and pilots, and observations from shadowing air operations for one week in Fall 2019.

Cargo

The cargo dataset consists of all the goods shipped by NSA from February 15, 2018 to October 27, 2019. A description of the good, its weight, date it was received into NSA operations, date it was shipped, origin, and destination are the data points of interest. Based on the goods' descriptions, a set of 15 cargo type categories were developed. After counting the total weights associated with each category, five categories (hunting, batteries, baby-related, chemicals, and fire extinguishers) were found to represent less than 0.03% of the total cargo respectively and 0.058% collectively, so they were removed as categories and became part of the "other" category. The remaining ten categories are: food, fuel, appliances, furniture, construction, general merchandise, toilet paper, water, transportation, and other.

Flight operations

The flight operations data is contained in two datasets, one for cancelled flight legs and one for operational flight legs. Flight legs, in comparison to flights, are the components of a flight between two points. For example, Flight 100 may fly from Community A, to Community B, to Community C, and then back to Community A. In this case, Flight 100 consists of three flight legs. The timeframe represented by the datasets is August 30, 2018 to August 30, 2019. The scheduled departure and arrival time, actual departure and arrival time, origin, destination, flight number, and user-entered reason for cancellation or delay where applicable are the data points of interest.

Semi-structured interviews

Semi-structured interviews were conducted by one researcher according to the protocols approved by the University of Toronto's ethics board in Fall 2019. The questions for airline employees and pilots revolved around the factors that impact air service reliability, such as infrastructure quality, facility quality (e.g. maintenance, fueling), and poor weather. The semi-structured nature of the interviews allowed the interviewees to share their experiences and encouraged discussion of factors that may not have otherwise been considered. Overall, 13 interviews were conducted, 12 in person, and one over the phone. Recordings and subsequent transcriptions of nine interviews were made with the consent of the interviewees. For the remaining four interviews, detailed notes were made.

Operations observation

During the same visit to conduct interviews, the researcher shadowed NSA operations at three bases and flew on five passenger flights and one non-passenger flight. The observations and field notes that were made during this time, while not necessarily representative of aviation in northern Ontario overall, contextualized the quantitative and qualitative data collected.

4. Results and discussion

Cargo

The cargo totals were compared across categories and analyzed temporally. Overall, there is an upward trend of total cargo weight transported, increasing by 1.4 tonnes over the 19 months. Comparing the eight months for which there is 2018 and 2019 data to the previous year (i.e. March 2018 and March 2019), seven of these months had an increase in total cargo compared to the year before. The most significant differences are March and April, which both saw a 137% increase in total cargo from 2018 to 2019. There are myriad possible contributing factors to this growth, which remain unknown at the time of writing.

In looking at the breakdown of cargo types, the vast majority of cargo by weight is food (89.0%). For the remaining 11%, only two categories make up more than 1% of total cargo weight individually: general merchandise (5.0%) and fuel (2.6%). The food majority is unsurprising given NSA is owned by a retailer, but the fuel percentage is low because it does not agree with the observations of how much diesel fuel is transported. At the time of writing, the reason for the disagreement had not been found.

Though food is the majority of cargo, other cargo types should not be overlooked. Figure 2 shows the temporal changes in four cargo types linked to other community infrastructure systems: construction, water, transportation, and fuel. Temporal changes in cargo categories do not seem to follow each other strictly, though the low points of the graph occur close to each category's low point at February/March and July/August both years. These low points coincide with potential alternative mode availability, namely winter roads and summer waterways, though there may be other explanatory factors, including variation in NSA capacity.

Flight data

Of the total flight legs (n = 42,114), 13,722 were delayed (32.6%) and 8,926 were cancelled (21.2%). Delayed flights were identified one of two ways: either the actual departure time was 15 minutes greater than the scheduled departure time or by the user-entered delay code. Some proportion of delayed flights did not have an associated reason and so an "unknown" reason code was introduced for 48.9%. A proportion of delayed flights have a delay reason but insufficient delay duration information (10.5%) and are excluded from Figure 3.

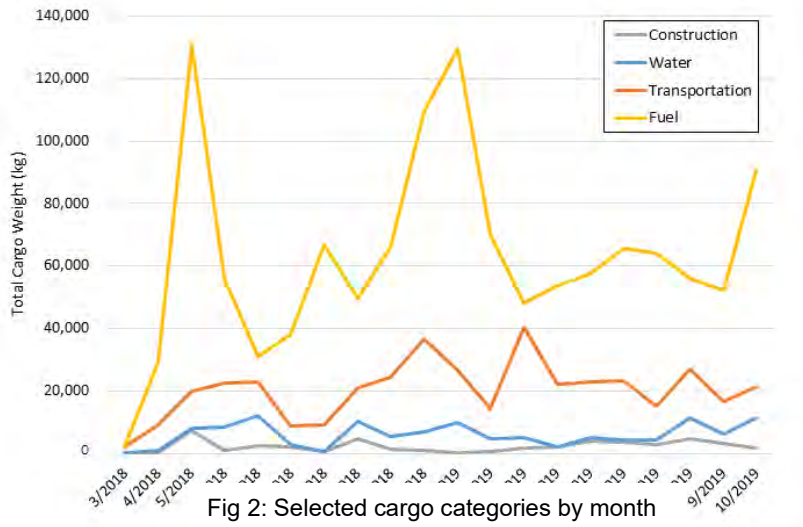

Fig 2: Selected cargo categories by month

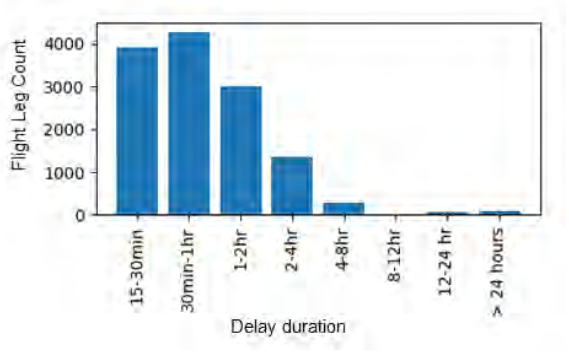

Fig 3: Distribution of delayed flight legs

Preliminary analyses of delay reasons showed that the majority of delays were attributed to "Late Inbound Aircraft", meaning an earlier delay in the system. By looking at the previous flight legs that matched aircraft and logically agreed with the origin and destination, the original reason for the delay could be determined. From that point, the propagating impact of delays could be tracked, specifically whether a delay was the original delay, secondary, tertiary, etc. The longest propagation showed a 16th delay. Table 1 shows the distribution of delay orders. Of the total delays, 40% were found to be delay origins, meaning that 40% of delays are responsible for creating the remainder of delays in the system.

Table 1: Delayed flight leg counts by delay order

Delay Order	Number of delayed flight legs	Percentage of total delays (%)
1st	5,384	39.8
2nd	3,335	24.6
3rd	1,899	14.0
4th	1,204	8.9
5th or more	1,900	14.0

Semi-structured interviews

The interviewees' experience in aviation in the region was quite varied, ranging in time from less than a year to several decades and in positions from pilot to dispatch. While each interviewee spoke from their unique experiences, a number of key takeaways relevant to this work arose across multiple interviews. The majority of the key takeaways fall into one of two categories: 1) reliance on base infrastructure and resources and 2) changes in infrastructure and operating environments.

Base airports are key in delivering air service in the region due to the fact that there is very limited infrastructure and services at the remote airports. For example, only two communities have jet fuel outside of NSA bases. Therefore, aircraft generally need to carry enough fuel for roundtrip flights and do not have much flexibility in their routing. Similarly, only bases have significant de-icing facilities. At remote airports, each airline is wholly responsible for having de-icing fluid and equipment, but it is not necessarily effective or safe for pilots to use. Therefore, if icing conditions arise on route to a remote community, it is likely that the pilot will not land and will continue the route to another community or back to the origin point. The people and goods onboard the plane will also miss that landing and continue the route, often going back to the base where accommodations can be found. Additionally, agents or cargo handlers at remote airports are infrequent unless a larger amount of people and goods is expected. Pilots then are the ones loading and unloading planes, checking in passengers, and weighing bags.

From an infrastructure perspective, there have been some improvements in runway lighting and expansion of limited weather reporting (e.g. weather cameras that transmit what the airport runway looks like). However, there are still remote airports that have no weather reporting and the relatively short runways are a safety concern. Limitations in other community infrastructure, like telecommunications, exert regular stress on airline operations.

A number of interviewees with lengthier careers noted the negative impacts of climate change on the operating environment, specifically an increase in freezing rain, icing conditions, and thunderstorms. With the climatic warming, the period before winter and after it where icing conditions are present is lengthening and significantly impacting air operations. The lack of adequate de-icing facilities at remote airports amplifies the impact. The increase in thunderstorms is also problematic, especially compounded with the lack of weather reporting in the region.

5. Conclusions and outlook

While the current work is a preliminary analysis of the relationship between air transportation and community infrastructure in northern Ontario, it is a step towards that end.

There are clear interdependencies between air transportation and other community infrastructure systems, for example air transportation of other land and water vehicles (e.g. snowmobiles, canoes). Variations in fuel transportation by air similarly suggest that reliance on air transportation grows in response to other modes' availability. Due to the limited resources at remote airports, air transportation relies less on community infrastructure, with the exception of a community's telecommunications.

When examining shocks and stresses on the communities and air transportation, climate change and its associated inclement weather are proving a regular and significant hindrance. Other climate change-related shocks such as wildfires and flooding

have been affecting the region and should similarly be assessed for their impacts on air transportation infrastructure and communities.

Acknowledgements

The authors would like to thank North Star Air for their generosity in sharing data and allowing Pia to shadow their operations and interview employees.

References (suggested style)

[1] Woudsma, C., and Towns, W. (2017). Ontario. In K. Palko and D.S. Lemmen (Eds.), Climate risks and adaptation practices for the Canadian transportation sector 2016 (pp. 139-179). Ottawa, ON: Government of Canada.

[2] L. Chan, O. Receveur, M. Batal, W. David, H. Schwartz, A. Ing, K. Fediuk, A. Black and C. Tikhonov. (2014) First Nations Food, Nutrition and Environment Study (FNFNES): Results from Ontario (2011/2012). Ottawa: University of Ottawa.

[3] C. L. Reading, and F. Wein. (2009). Health Inequalities and Social Determinants of Aboriginal Peoples' Health. National Collaborating Centre for Aboriginal Health, pp. 1-47.

[4] N. Johnston and A. Sharpe. (2019). An Infrastructure Index for Remote Indigenous Communities. Centre for the Study of Living Standards.

[5] North Star Air. (2020) History. Online. Available : http://www.northstarair.ca/article/history-2194.asp

INFLUENCE OF STEAM CURING PARAMETERS ON CONCRETE STRENGTH AND OPTIMIZATION AT 28 DAYS

. Radad Azhari Elsir Elnour ,

Department of Civil Engineering, Faculty of Engineering, University of Khartoum
Khartoum, Sudan
radadazhari@gmail.com

Abstract:
Steam curing provides moisture and increases the temperature, which are important, factors for accelerating the concrete curing process. This paper is the second of the authors' series that identifies the effect of atmospheric-pressure steam curing parameters for producing precast concrete. These parameters include a delay period after casting (DT) of 0, 1, 2, 3, 4 & 6 hours, maximum curing temperatures (T) of 50, 60 & 70°C maintained for a specific curing period (CT) of 2, 3, 4 & 5 Hours. To attain this aim, several laboratory experiments have been carried out to measure and optimize compressive strength after 28 days. Taguchi methodology has been utilized to identify that DT, CT and T have the same effective weight on compressive strength and DT=3Hours, CT= 4Hours & T= 70ºC as the optimum curing regime at 28 days (stored on air) after steam curing .The optimum steam curing cycle will be carried out that to compare with the values of compressive strength specimens subjected to conventional water curing method at different ages. Results showed that the optimum steam cured type has better performance than water curing at early age.

Keywords:
Curing time, curing temperatures, delaying time, steam curing cycle, Taguchi Method.).

1. Introduction

The primary objective of steam curing is to obtain a sufficiently high early strength so that the concrete products may be handled soon after casting; the molds can be removed, or the pre-stressing bed vacated earlier than the case with ordinary moist curing, moreover, less curing storage space is required. This means an economic advantage. For many applications, the long-term strength of concrete is of lesser importance (Neville, 2011). The strength enhancement depends on the steam curing cycle.
The aim of this study is to:
Studying the influence of 3 variable parameters of steam curing (i.e.) delay time (DT) before curing (0 to 6 hours), curing time (CT) in a range between (2 to 5 hours) at three different maximum curing temperatures (T) of (50, 60 & 70ºC). For this purpose, a concrete mixture of C40 grade at 28 days was employed.
Optimize the steam curing cycles for 28 days old conventional concrete, for strength and productivity purpose and then compare it with water cured specimens.
Note : the author had done almost the same study for age of 7 days (Radad .A & Yousif.A, no date).
Many researchers have investigated the three parameters of the steam curing cycle (T, DT & CT) to optimize the steam curing cycle for conventional concrete.
Erkdem [2] studied the effect of delay period before steam curing application on concrete which causes expansion and induce tensile stress in the exterior rigid shell.
Oztekin (E., 1984) showed that for compressive strength development, duration of steam curing is also an important parameter as well as temperature. The curing period (CT) and temperature (T) is adjusted according to the targeted one-day strength level. A rise in (T) speeds up the chemical reactions of hydration and reduces the length of the dormant period and hence the overall structure of the hydrated cement paste gets established very early. However, rapid initial hydration provides less time for diffusion of products which leads to formation of local areas of lower strength. When the curing temperature of concrete changes, the composition of the hydrated cement changes. Accordingly, this change influences the diffusion and penetration of the hydration products related to the medium or long-term strength of the concrete(Yi, Moon and Kim, 2005) .
This research utilizes primary and secondary sources to attain its objective. The primary sources include observations from laboratory experiments carried out on a predesigned concrete mixture used at the plant (Noor Pole Factory). The secondary sources include review of hard and soft copies of books and scientific journal articles for gaining know-how about designing the optimization experiments and statistical methods to analyses their results.
The concrete mixture will be subjected to different combination of the identified three variable parameters, i.e. DT before curing (between 0 and 6 hours), CT (between 2 and 5 hours), at three different

curing temperatures T of 50º, 60º and 70ºC. Then the concrete compressive strength is measured and the results are statistically analyzed to identify an optimum steam curing cycle at 28 days. Furthermore, the product cured at the identified optimum steam cycle is compared with water cured cubes at different compressive strength ages.

2. Materials and Methods:

2.1 Materials and Mix Proportions:

According to the results of tests on raw materials, in this research, River sand has been used from (Nile River State) conforming to BS882-1992 with absorption=3.3%, 39.5% passing 0.6mm sieve, and a specific gravity=2.5 is used as a fine aggregate. A crushed stone from with a maximum size =20mm, conforming to BS882-1992 ,water absorption=2.5% and a specific gravity=2.7 is used as a coarse aggregate (Radad .A & Yousif.A, no date).

Ordinary Portland cement has been used. Its initial and final setting times were 2.5 hours and 4 hours respectively (Radad .A & Yousif.A, no date).

Materials, DoE mix design procedure (Department, 2010) is used to design in the following limiting values:

A. *Production limitation:*

1. Slump should be ≤ 30 mm due to centrifugal compaction used to form hollow cylindrical poles.
2. Two hours stripping strength after steam curing period should be ≥20N/mm^2 to meet the requirement for de-stressing and handling.
3. Total steam curing cycle (CT+DT+Destressing time (2Hours)) not exceeds 9 hours.

B. *Long-term time limitation:*

1. 7 days compressive strength (store in air) should be ≥ 30 N/mm^2 (Radad .A & Yousif.A, no date) .
2. 28 days compressive strength (store in air) should be ≥ 40 N/mm^2.

The mix proportion used to manufacture the poles without any admixtures is 450kg cement, 740kg sand, 1030 kg coarse aggregates and 220kg water (including aggregate absorption water) (Radad .A & Yousif.A, no date).

2.2 Curing Regimes

2.2.1 Steam Curing

The steam curing was applied using an automatically controlled cabinet of steam temperature with timing control of the steam curing period ((**Error! Reference source not found.**). The cabinet has a steam generator capable of generating steam in different types of temperature by feeding pure water at a fixed rate of heat and the cooling temperature of 90ºC/hr. (Radad .A & Yousif.A, no date).

Fig 1: Steam Curing Cabinet

Curing Temperatures (T):

Is defined as a target temperature to which the sample specimen is raised and held constant during the CT. Based on the literature; the experiments in this study have been carried out for temperatures of 50º, 60º, and 70ºC

Delaying time (DT):

An initial delay prior to steaming or a “preset time.” Concrete should sit for a predetermined period of time (minimum of 30 minutes, recommended two to three hours) or until initial set (Neville and Brooks, 2010a). In this study values of DT are set to 0, 1,2,3,4, and 6 hours.

Curing Time (CT):

CT is defined as a period of heating time and holding the maximum temperature constant.

Based on the literature the experiment investigations were carried out for curing time for four curing periods 2,3, 4, and 5 hours.

2.2.2 Water curing:

In this study, samples were left in a fog cabinet with relative humidity ≥ 95% for 24 hours, then immersed in a water tank having temperature of 25ºC to be considered as reference samples tested at ages of 12 Hours,3 days,7 days and 28days. These specimens compared to optimum steam-cured specimens at early 2 Hours and 28 days age compressive strength (Radad .A & Yousif.A, 2018).

2.3 Methods:

After mixing concrete in a laboratory mixer in temperature of 25ºC, slump was measured and found to be 300mm +/-(50mm). Six cubes were cast for each cycle to be tested at 7 days (Radad .A & Yousif.A, no date) and 28 days. In total, 72 (cycles) * 6 = 432 cubes were cast to cover all steam curing cycles (delay time, curing time, curing temperature). The steam cured specimens were stored in air until testing time at 28 days using 3 cubes for each day. The compressive test was carried out using a standard machine and the average of three cubes strength was calculated.

From the above steam curing cycles the Taguchi engineering method (Dotchin and Oakland, 1994) was used to identify the effective strength weight of each parameters of steam curing, and then conduct the optimum steam cycle that produced the optimum

28days compressive strength and lowest production time and cost to compare it with water cured concrete.

3. Results Of Compressive Strength And Optimization For Steam Cycle Parameters

3.1 Results of Compressive Strength:

The influence of the three steam curing parameters on the 28 days average compressive strengths at different steam curing cycles are shown **Error! Reference source not found.** and **Error! Reference source not found.**. It is observed that the peak strength for T=50º and 60ºC are obtained for DT between 3 & 4Hours, while for T= 70ºC, the peak is between DT= 4 and 6 Hours. All strengths for DT below the initial setting time of the cement used, i.e. 2 Hours. is lower than the peak with the minimum at DT=0ºC. This agrees well with the A .M. Neville (Neville, 2000) that before the initial setting time the microstructure is fragile and affected by shrinkage.
For curing time, when CT increases one hour the compressive strength increase too mostly 7% (Ramezanianpour, Khazali and Vosoughi, 2013)(Neville and Brooks, 2010b).
After 28 days steam curing period, when the curing temperature increases to 10ºC the average strength will almost increase by 10%.

3.2 Optimization:

3.2.1 Robust Design Engineering Method:

For optimizing results, Taguchi Robust Design Engineering methodology (Oakland, 2003)(Dotchin and Oakland, 1994) has been used as a tool to identify the parameter that influences the compressive strength significantly relative to the other parameters considered in the study.

3.2.2 Identification Of Parameter Significantly Affecting The Compressive Strength After 28 Days Using Steam Curing:

The average of the 28 days compressive strength of the steam cured for all 72 cycles' samples of different 3 parameters (delay time, curing time and curing temperature) was determined to be 35.3N/mm^2.
By taking the following factors to represent the effect of every variable where Fa represents effect of curing temperature (T), Fb represents effect of delay time (DT) and Fc represents effect of curing time (CT).
Effect of curing temperature (T):
Fa_1 represents the effect of temperature corresponding to 50°C regardless of other two parameters values. It is calculated as the average strength of cubes having steam curing temperature 50°C at 28 days by neglecting the other two parameters (i.e. DT & CT) as follows:
Fa_1(50C) = (22.7 + 24.7 + 28.2 + 31.1 + 31.4 + 31.7 + 24.7 + 29.3 + 34.3 + 33.6 + 35.1 + 33.6 + 29 + 29.4 + 31.8 + 41.3 + 38.3 + 39.6 + 29.9 + 35.8 + 32.6 + 37.4 + 34.1 + 39.3) / 24 = 31.5 N/mm^2, Similarly, for 60°C and 70°C;
Fa_2(60°C) = 34.44 N/mm^2, and Fa_3(70°C) = 38.9 N/mm^2.
Effect of delay time (DT):
Fb_0 represents the factor effect of DT corresponding to zero Hours. It is calculated as the average strength of cubes after 28 days having delay period zero Hours. By varying the other 2 parameters.
Fb_0 = (22.7 + 25.1 + 29.2 + 24.7 + 27.5 + 33 + 29 + 29.9 + 36.4 + 29.9 + 33.7 + 35.9 +) / 12 = 29.75 N/mm^2. Similarly, Fb_1(1Hours.delay) = 32.95 N/mm^2, Fb_2 = 35.3 N/mm^2, Fb_3 = 37.95 N/mm^2, Fb_4 = 37.93 N/mm^2, and Fb_6 = 37.63 N/mm^2.
Effect of curing time (CT):
Fc_2 represent the factor effect of steam curing period corresponding to 2 Hours. and is calculated as the average strength of cubes after 28 days having steam CTs of (2, 3, 4 and 5Hours) by varying the other 2 parameters.
Fc_2 (2 Hours. steam curing period) = 31.2 N/mm^2, Fc_3=32.04 N/mm^2, Fc_4=37.3 N/mm^2, and, Fc_5=37.82 N/mm^2.
Now by considering differences between the influence factors for each parameter value and the average strength of 72 cycles denoted as μ= 35.3N/mm2: as shown in Table 1.

Table 1: Difference between effect of each factor and average strength of all steam curing cycle

Name	*Difference (N/mm^2)*		
a_1	Fa_1-μ	31.5-35.3	-3.8
a_2	Fa_2-μ	34.44-35.3	-0.86
a_3	Fa_3-μ	38.9-35.3	3.6
b_0	Fb_0-μ	29.75-35.3	-5.55
b_1	Fb_1-μ	32.95-35.3	-2.35
b_2	Fb_2-μ	35.3-35.3	0
b_3	Fb_3-μ	37.95-35.3	2.65
b_4	Fb_4-μ	37.93-35.3	2.63
b_6	Fb_6-μ	37.63-35.3	2.33
C_2	Fc_2-μ	31.2-35.3	-4.1
C_3	Fc_3-μ	32.04-35.3	-3.26
C_4	Fc_4-μ	37.3-35.3	2
C_5	Fc_5-μ	37.8-35.3	2.5

By using ANOVA (analysis of variance) method: A_1= a_1^2+ a_2^2+ a_3^2= 28.16%, B_1= b_0^2+ b_1^2+ b_2^2+ b_3^2+ b_4^2+ b_6^2= 55.76% and C_1= c_2^2+ c_3^2 + c_4^2+ c_5^2=37.69 %.
Here A1 is representative of the deviation in compressive strength after 28days obtained by changing the parameter value of temperature by 10°C. Then the FT ratio defined as weighted percentage of the effect of a parameter on the compressive strength, e.g. for temperature parameter (T),
F_T (%) = ((N_T * A_1) / ((N_T * A_1) + (N_{DT}* B_1) + (N_{CT}* C_1)) *100%
the F_T is calculated as follows:
= ((24 * 28.16) / ((24 * 28.16) + (12*55.76) + (18 * 37.69)) *100% = 33.4%
Similarly, for DT = F_{DT}%
F_{DT}(%) = (N_{DT} * B_1) / ((N_T * A_1) + (N_{DT}* B_1) + (N_{CT}* C_1)) *100%

& CT period = F_{CT}%
$F_{CT}\% = (N_{CT} * C_1) / ((N_T * A_1) + (N_{DT} * B_1) + (N_{CT} * C_1)) *100\%$
Where;
N_T: No. of cycles having constant T, e.g. 50,
N_{DT}: No. of cycles having constant DT, e.g. = 2Hours, and,
N_{CT}: No. are cycles having constant CT, e.g. =4Hours.
Similarly, for DT, F_{DT} =33%
And for steam CT, F_{CT} =33.5%.
Based on the results obtained using the Robust Design Engineering Methodology, it is inferred that the effect of parameters of steam curing cycle is almost equal for 3 variables at long term compressive strength .mean while the effect of same parameters of steam curing at 7 days done by same author were DT is (52.7%) more significant compared to T (17.7 %) and CT (29.54%)(Radad .A & Yousif.A, 2018).

3.2.3 OPTIMUM STEAM CURING CYCLE:

From experiments results in this research, besides the limitations for strength there are extra limitations on productivity time imposed by production department as follows:

The steam curing cycle total time should not more than 9 hours as production department caution see (2.1 Materials and Mix Proportions:). It is worth noting that the cycle includes DT+ CT+ de-molding and de-stressing time. The de-molding and stressing time is estimated by the production team for a typical steam chamber containing 18 poles to about 100minutes, i.e. about 5 minutes for each pole.

This means the constraints for DT+CT should be about 7 Hours. Given that from **Error! Reference source not found.** and **Error! Reference source not found.** that the DT should be between 3 & 4Hours, this means the CT should be between 4 & 3Hours see(3.1 Results of Compressive Strength:).
To identify the optimum cycle, Fa, Fb and Fc values obtained from Taguchi method are examined and parameters that fulfill the minimum strength of 40 N/mm2 and water –cured strength of 39N/mm2 are identified. They are Fa3 (70oC)= 33.2 N/mm^2, i.e. = 70oC and (Fb3, Fb4 and Fb6) for DT =3, 4 & 6Hours respectively and (Fc4 & Fc5) for CT= 4 & 5hrs respectively. Therefore, the optimum steam curing cycle should have C= 70oC, DT = 3 or 4hrs and CT= 4 or 5 hrs. To fulfill the condition of DT+CT=7hrs, the CT=5hrs and DT=4hrs should be ruled out, leaving DT=3hrs as the only option for CT is 7-3= 4hrs.
So the Optimum steam curing cycle was:
C= 70oC, CT= 4hrs and DT= 3hrs.
For this identified optimum steam cycle, it is important to verify that the 2hrs stripping strength should be ≥20N/mm^2. Therefore, a set of 12 cubes of optimum steam curing cycle were cast, cured and crushed at ages of 2hrs after CT, 3days, 7 days and 28days The strength values are 20, 30.5, 37.8 and 42N/mm^2, fulfilling all engineering and operational requirements.
.then compare with water cured specimens at same age see (**Error! Reference source not found.**).

4. Results And Discussion Of Comparison Between Optimum Steam And Water Cured:

Error! Reference source not found. Show the compressive strength of the specimens cured in the optimum steam curing and water. The steam cured specimen provided higher strength at all ages early, 3, 7 and 28 days age especially at early strength which was peak. May be this due to steam cured has higher rate of hydration at early age more than water-cured specimen.

5. Conclusions:

The results obtained from experimental studies can be summarized as follows:-
1. By using Robust Design Engineering (Taguchi) methodology it has been found that the effect of delaying time (DT) ,steam curing period (CT),and temperature (T) are have almost the same effect on compressive strength compared after 28 days of steam.
2. The optimum steam curing cycle for strength and productivity and long live requirements in the factory have been found to be T= 70oC, DT= 3hrs and CT = 4hrs at 28 days age.
3. The steam cured specimen provided higher strength at all ages early, 3,7 and 28 days age especially at early strength which was peak.

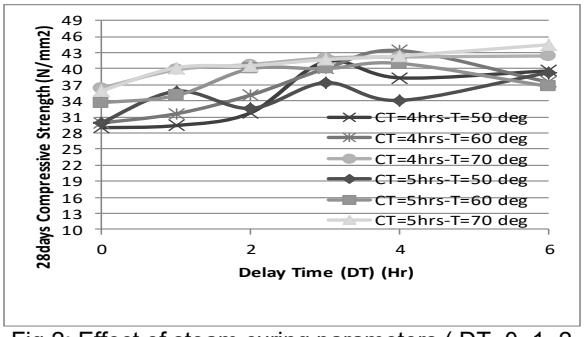

Fig 2: Effect of steam curing parameters (DT=0, 1, 2, 3, 4 and 5hrs, CT=2 and 3hrs , T=50, 60 and 70oC) on 28days compressive strength.

Error! Not a valid link. Fig 3: Effect of steam curing parameters (DT=0, 1, 2, 3, 4 and 5hrs, CT=4 and 5hrs , T=50, 60 and 70oC) on 28days.compressive.strength.

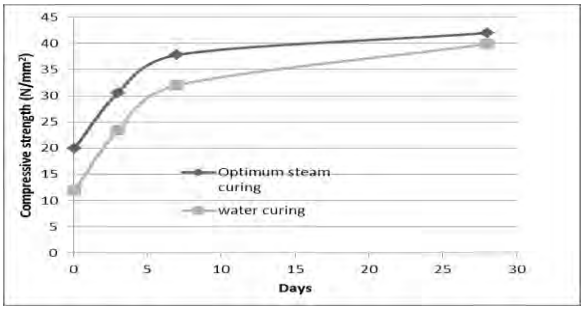

Fig 4: Compare Between Optimum Steam Curing Cycle Compressive Strength at Different Ages and Water Curing

Acknowledgements

The authors would like to thank Dr. yousif humida and protech multi activates company for the technical and financial support .

References

[1] Department of civil engineering in SEDC company. (2010) Specification for Prestressed Concrete Poles sudanese electricity distribution company (SEDC).

[2] Dotchin, J. a. and Oakland, J. S. (1994) 'Total Quality Management in Services: Part 2: Service Quality', International Journal of Quality & Reliability Management, 11(3), pp. 271–281. doi: 10.1108/02656719410056468.

[3] E., O. (1984) "Determination of Heat Treatment Cycle for Cements', Turkish cement manufacturers' association, Cem. Bull., 206 (3), pp. 24-26.

[4] Neville, A. M. (2000) Properties of Concrete, 4th ed., England: Longman.

[5] Neville, A. M. (2011) Properties of concrete. 5th edn. Person.

[6] Neville, A. M. M. and Brooks, J. J. J. (2010a) 'Concrete Technology', Building and Environment, p. 442. doi: 10.1016/0360-1323(76)90009-3.

[7] Neville, A. M. M. and Brooks, J. J. J. (2010b) 'Concrete Technology', Building and Environment. doi: 10.1016/0360-1323(76)90009-3.

[8] Oakland, J. S. (2003) Statistical Process Control, Control.

[9] Radad .A & Yousif.A (2018) 'Objectives', Effect Of Steam Curing Parameters On Concrete Strength And Durability, 10 pages, 2nd Conference of Civil Engineering in Sudan, University of Khartoum, 3-5 Dec 2018, pp 48-54.

[10] Ramezanianpour, A. A., Khazali, M. H. and Vosoughi, P. (2013) 'Effect of steam curing cycles on strength and durability of SCC: A case study in precast concrete', Construction and Building Materials, 49, pp. 807–813. doi: 10.1016/j.conbuildmat.2013.08.040.

[11] Yi, S. T., Moon, Y. H. and Kim, J. K. (2005) 'Long-Term Strength Prediction Of Concrete With Curing Temperature', Cement and Concrete Research, 35(10), pp. 1961–1969. doi: 10.1016/j.cemconres.2005.06.010.

Cost and limiting efficiency of silicon solar panels past and future

T. Tiedje

Electrical and Computer Engineering Department
University of Victoria, Victoria, BC, V8W 2Y2, Canada

Abstract:
This paper describes the evolution over the past 40+ years of the cost of silicon solar modules, the volume produced and their efficiency. The production volume is projected to saturate over the next few years, which will slow down the rate of cost reductions according to usual expectations for learning in manufacturing after about 2025. The efficiency of silicon solar panels is approaching physical limits, however further increases in output per unit area can be expected from bifacial panels and new heterojunction contact technology. The cost of electricity for stand-alone residential systems is about a factor of 5 higher than the cost of electricity from utility-scale projects. Canada has an abundant solar resource with natural advantages, yet is falling behind leading trading partnes in the implementation of solar photovoltaic generation. Wind turbines and solar photovoltaics are now the lowest cost ways to produce bulk electricity.

Keywords:

Solar photovoltaics, efficiency of silicon solar cells, cost of solar modules, learning curves, solar electricity in Canada

1. Introduction

Over the last 45 years the cost of silicon solar panels has dropped by three orders of magnitude, annual production has increased by five orders of magnitude and the efficiency has doubled [1]. Although these things could have been predicted, and in some cases were predicted long ago, on the basis of a standard learning curve approach which applies to industrial production [2], nevertheless few people from the early days would have believed that crystalline silicon panels could be produced at the cost that they are today. Historically the solar photovoltaic (PV) market relied on remote applications, government subsidies and early adopters. The PV industry is now in a new era. As Seb Henbest of Bloomberg New Energy Finance said in 2018 “wind and solar have won the race to produce the lowest cost bulk electricity” [1]. Solar module costs are down by 83% since 2010 due to aggressive price reductions by large volume Chinese manufacturers [1]. In the future the levelized cost of electricity from solar and wind is expected to be lower than the operating cost of existing coal and nuclear plants. In other words plant operators can save money by shutting down the legacy units and replacing them with new solar plants. As a result it is not surprising that in developed countries most of the new electricity generating capacity built today is wind and solar [3]. Of course the wind and solar resource is intermittent so cost is not the only consideration.

2. Growth of silicon PV production

We consider how the solar PV industry is likely to evolve in the future now that it is the lowest cost way to produce bulk electricity. Over many years the solar PV industry experienced average annual growth rates of 30%. This period of rapid growth is coming to an end. Now that most of the new-build electricity generating capacity is wind and solar, there simply isn’t as much room to grow as in the past. The reduction in the annual growth rate will in parallel lead to a slow-down in the rate of cost reductions associated with the learning curve. In a typical learning situation the cost of manufacturing a commodity declines by 20% for each doubling of cumulative production. In the case of solar panels the cost reduction has been faster, an average of 28% for each doubling of cumulative production over more than 40+ years. In Fig. 1 we show how the cost of

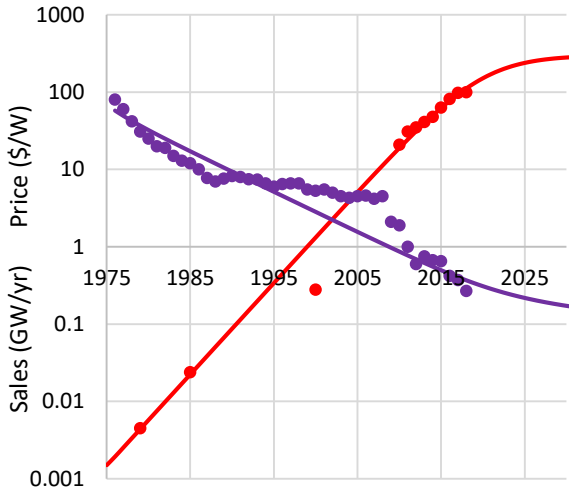

Fig. 1: Module price (purple) and sales volume (red) as a function of time for PV panels. The lines are fits to the data. The PV growth rate slowed from 1990 until 2008 when Chinese manufacturers ramped up their production and reduced selling prices. The fit to the sales volume is a logistic curve (see Eqn.1) with a saturation production volume of 297 GW/yr. The purple line projects the price into the future assuming a constant learning rate consisting of a 28% drop in price for each doubling of cumulative production.

silicon solar modules may play out in the future.

The annual electricity production world-wide was 26,700 TWh in 2018 [3]. If the working lifetime of an electrical power generating asset is 30 yr, then 890 TWh of electricity must be produced by new generating assets each year to maintain electrical power generation constant. We assume that 50% of the new electrical power will be produced by PV and that 1 GW of solar PV peak capacity produces 1500 GWh of power over one year (see Table 1 below). In this case 297 GW of new solar capacity will be needed every year to maintain annual electricity production at current levels. This number is used to extrapolate historical production of solar modules into the future with the following fitting equation:

$$P = \frac{297}{1+e^{(2019.9-t)/3.68}} \qquad [1]$$

where P is the annual production of solar panels in GW and t is the year. This fitting curve and extrapolation is shown in Fig. 1.

The fitting curves show that the production volume is beginning to saturate now, however the associated rate of cost reduction predicted by the learning curve does not change very much until after 2025. It is important to point out that the fits in Fig. 1 reproduce long term trends but do not do a good job of predicting shorter term price levels and production changes.

3. Efficiency of silicon PV panels

The efficiency of a solar panel determines how much output power it produces for a given area and is therefore critical in establishing the cost of solar electricity. The efficiency of solar panels over time has followed a similar trajectory to other technologies for example the efficiency of steam engines. The time evolution of the efficiency follows a logistic curve with an initial exponential rise followed by a saturation close to but below the physical limit set by thermodynamics. The logistic curve for the efficiency of silicon solar panels is,

$$\eta = \frac{29.5}{1+e^{(1979-t)/13}} \qquad [2]$$

where the efficiency η is in % and t is the year. This logistic curve is shown in Fig. 2 along with the experimental data on the record measured silicon solar cell efficiencies over time. The highest reported efficiency for a silicon solar cell in the lab is 26.7±0.5% [4], whereas the most efficient commercial solar panels today are around 21% [5]. The most efficient lab cells have heterojunction contacts rather than the diffused contacts that are more common in commercial panels.

There have been many attempts to further improve the efficiency of solar cells. There are two basic approaches: (1) find a better material than silicon or (2) make a multijunction cell [6]. Thin film GaAs, a III-V semiconductor, has a maximum measured efficiency of 29.1% but this technology has not caught on because of cost challenges associated with the manufacturing process. High efficiency multijunction cells (up to 45%) typically involve several different III-V semiconductors, complex manufacturing processes and expensive substrates. However multijunction solar cells have found applications in space satellites. To date all attempts to find something better than silicon for terrestrial PV have so far failed to displace silicon from its dominant position in the market place.

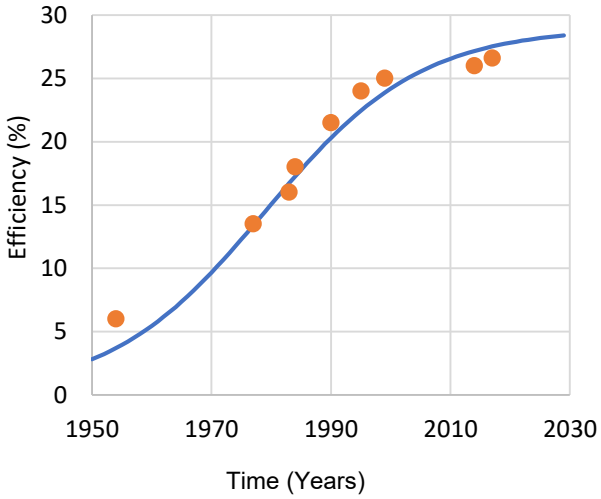

Fig 2: Silicon solar cell efficiency as a function of time fitted with the logistic function Eqn. [2]. The maximum efficiency achieved to date is 26.7±0.5% [4]

An approach in which a wide bandgap perovskite material is deposited on top of the silicon solar cell is being pursued by Oxford PV, which they claim could achieve efficiencies of more than 30% [7]. The long term stability of the perovskite material is a concern for this class of materials. Another approach to achieving higher output power is the bifacial cell which is sensitive to light incident on both sides [8]. Bifacial panels have two layers of glass, one on the front and one on the back and can be manufactured at only modestly higher cost than a monofacial cell. The intensity of the light incident on the back side depends on the albedo of the ground and tilt angle of the panel among other things. Field tests show a 10%-30% increase in output power can be obtained with bifacial panels compared with monofacial panels [8]. It is likely that bifacial panels will dominate utility-scale applications in the future. In architectural applications in which the back side of the panels is visible, bifacial panels may be preferred because they are more appealing visually, from the back. The thermodynamic limit to the efficiency of bifacial silicon PV cells is 28.9%, only slightly lower than limiting efficiency of monofacial cells of 29.5% [9].

4. Solar PV in Canada

The rapid reduction in the cost of solar electricity discussed above applies to utility scale projects. The cost of electricity from residential roof-top PV installations has not fallen as quickly and is 5-6x higher than the cost of electricity from a utility scale

project. For example in 2019, one roof-top residential installation in the Capital Regional District of Vancouver Island cost $30K for a 13 kW system, designed to produce 14,500 kWh annually. With a retail electricity price of 11 cents/kwh and a return of 5% on the capital investment this is about 5x the cost of recent utility scale projects in the US for which the levelized cost of electricity is about 2 cents/kWh.

At the utility scale Canada is a laggard in the generation of solar electricity compared with China, USA and Europe. For example, Germany, which has similar insolation characteristics to many parts of Canada, has 45 GW of solar generating capacity while in 2018 Canada had only 3.0 GW [10,11]. This is probably due in part to the availability of abundant hydroelectric power in Canada and therefore less need to make use of solar electricity. There is also a misconception that because Canada is a northern country with short days in the winter that the solar resource is weak. The available resource is illustrated in Table 1 below, which shows the annual solar energy incident on a flat surface tilted at the angle of the latitude per kW of solar panel capacity in four different cities in western Canada. The insolation for the most favourable desert locations is ~2000 kWh/kW or approximately twice the insolation in Yellowknife. In partial compensation for weaker insolation, northern locations have several competitive advantages compared with southern deserts. The presence of snow for part of the year means that

Table 1: Average annual insolation for a panel facing south tilted at an angle equal to the latitude [10]. 1000 kWh/kW means there are 2.7 hr/day of full sun averaged over the year.

City	Annual Insolation (kWh/kW)
Victoria	1091
Yellowknife, NWT	1094
Calgary, AB	1291
Regina	1360

bifacial panels will have better back illumination since snow has a higher albedo than a desert landscape and will scatter more of the incident light. Also solar cell efficiency goes up as the operating temperature drops, favouring cooler locations [9]. Finally in relatively remote northern locations the cost of competing sources of electricity is generally high.

5. Conclusions and outlook

The levelized cost of electricity produced by solar panels has dropped dramatically over the past 40 or so years to the point where on average it is the lowest cost way to generate bulk electricity. The rapid growth in production experienced in the past will begin to slow down now that a substantial fraction of new electrical generating capacity world-wide is supplied by solar PV. Manufacturing cost reductions will continue. New technologies including heterojunction cells and bifacial panels offer opportunities to continue to grow the power output per square meter of solar panel area, at a modest rate. Increases in efficiency for tandem perovskite-silicon panels are promising for the future but unproven in the commercial marketplace.

Acknowledgements

I would like to thank Akira Engelbrecht for helpful discussions.

References

[1] Bloomberg New Energy Finance, see for example: about.bnef.com/blog/henbest-power-system-will-dance-tune-wind-solar-batteries/

[2] G. D. Cody, T. Tiedje, "A Learning Curve Approach to Projecting Cost and Performance in Thin Film Photovoltaics", Proc. IEEE Photovoltaic Specialists Conf. (1996).

[3] World Energy Outlook 2019, International Energy Agency (available online 2020)

[4] K. Yoshikawa, H. Kawasaki, W. Yoshida, T. Irie, K. Konishi, K. Nakano, T. Uto, D. Adachi, M. Kanematsu, H. Uzu, K. Yamamoto, Silicon heterojunction solar cell with interdigitated back contacts for a photoconversion efficiency over 26%, Nature Energy 2, 17032 (2017).

[5] M. Kasu, J. Abdu, S. Hara, S. Choi, Y. Chiba, A. Masuda, Temperature dependence measurements and performance analyses of high-efficiency interdigitated back-contact, passivated emitter and rear cell, and silicon heterojunction photovoltaic modules, Jpn. J. of Appl. Phys. 57, 08RG18 (2018)

[6] M. A. Green, Y. Hishikawa, E. D. Dunlop, D. H. Levi, J. Hohl-Ebinger, A.W.Y. Ho-Baillie, Solar cell efficiency tables (version 52), Prog. Photovolt. Res. Appl. 26, 427–436 (2018).

[7] www.oxfordpv.com

[8] C. D. Rodríguez-Gallegos, M. Bieri, O. Gandhi, J. P. Singh, T. Reindl, S.K. Panda, Monofacial vs bifacial Si-based PV modules: Which one is more cost effective? Solar Energy 176 412–438 (2018)

[9] A. Engelbrecht, T. Tiedje, Temperature and intensity dependence of the limiting efficiency of monofacial and bifacial solar panels (to be published)

[10] Natural Resources Canada, Photovoltaic and solar resource maps (available online, 2020)

[11]Recent facts about photovoltaics in Germany, Jan. 7, 2020: www.ise.fraunhofer.de/en/publicatioins/studies/recent-facts-about-pv-in-germany.html

In-situ Envelope Performance and Actual vs Modeled Energy Consumption of a Passive House Certified Research and Testing Facility in Northern BC

A. Conroy[a*], G. Wimmers[b]

[a] PhD student, University of Northern British Columbia, Canada, conroy@unbc.ca
[b] Associate Professor, University of Northern British Columbia, Canada, guido.wimmers@unbc.ca

Abstract:
The Wood Innovation Research Lab (WIRL) was completed in July, 2018. Constructed as a research and testing facility by the University of Northern British Columbia (UNBC), it is the first industrial research facility constructed and certified in North America to the International Passive House standard. The building was constructed using a glulam post and beam system and a unique high-performance standing truss wall and flat truss roof assembly. Of particular interest are the hygrothermal behavior of the wall assembly and the annual energy consumption of the building compared to the predicted values included in the Passive House Planning Package (PHPP) computer model. To investigate the hygrothermal behavior, a total of 20 temperature and 16 humidity sensors were installed in the north and south exterior wall assemblies. Initial findings show that the exterior walls did not experience 100% relative humidity during the data collection period but that high readings of relative humidity (>80%) did occur during the heating and cooling seasons for short periods of time. Energy consumption agreed with the predicted consumption values included in the PHPP model, however not all laboratory testing and research equipment had yet been installed when the initial analysis was completed. This paper will report on the initial findings of the hygrothermal performance and energy consumption of the WIRL building with a particular focus on the behavior of high-performance wall assemblies in heating-dominated climates and a comparison of modeled versus actual energy consumption for Passive House Certified buildings.

Keywords:
Passive House, Hygrothermal Behavior, Energy Efficiency, Cold Climate, Predicted vs Actual Energy Consumption

1. Introduction

The purpose of this research is to investigate what differences, if any, exist between the modeled energy consumption and building envelope performance of the Wood Innovation Research Laboratory (WIRL) building following seven months of in-situ data collection. The WIRL building was completed in July of 2018 by the University of Northern British Columbia (UNBC) and is located in Prince George, British Columbia. The building was designed to meet Passive House standards, a building certification system that requires the building to have low energy input requirements due to high levels of thermal insulation and minimal air leakage. To ensure the building achieves the established energy use targets, a computer model of the proposed building must be completed prior to the start of construction using the Passive House Planning Package (PHPP) software. Inputs to the model include envelope design, mechanical energy use, building location and airtightness value. Key outputs included the predicted annual heating demand (kWh/m2a), total primary energy demand (kWh/m2a), and air tightness of the building envelope (ACH@50pa).
Based on the final building design model and test results achieved following completion, the WIRL building was deemed to have met all Passive House requirements and certification was achieved.
To help meet the low thermal energy demand requirements of the Passive House certification system, a unique vertical truss assembly was constructed for the exterior walls of the building. The walls measure 53.3cm deep, and have a calculated thermal resistance value of RSI 12.66 m^2*K/W.
The use of thick-wall assemblies in cold climates has raised concern for long-term durability issues compared to standard or exterior insulated wall assemblies [1, 2]. To examine the hygrothermal behavior of the WIRL walls, temperature and humidity sensors were installed in the north and south assemblies. In addition, gas and electrical energy use meters were installed to monitor the building's heating and energy consumption.

2. Building energy use

The Passive House Planning Package (PHPP), a static simulation software, was used to predict the energy consumption of the equipment installed in the WIRL and the energy performance of the building itself. To calculate the natural gas and electric consumption for auxiliary systems for heating (or cooling) purposes, ISO 13790 is used to balance all thermal losses through opaque and transparent envelope components, ventilation losses and solar heat gains as well as internal heat gains to establish the remaining specific heating (or cooling) demand and the heating (or cooling) load of the mechanical equipment. For the calculation of the internal heat gains the type, power and user intervals of all equipment such as lights, plug loads for computers and miscellaneous equipment is calculated. Of particular interest for the WIRL building PHPP model

and certification is the energy consumption of the workshop and testing equipment. The use of saws, sanders, shapers and various other tools had to be estimated. By far the largest energy consumers are the Hundegger CNC machine, the hydraulic power unit and actuators for the structural testing and the dust extraction system. The user cycles had to be estimated carefully.

To maintain a consistent indoor environment, the WIRL building is separated into two climate-controlled zones. The first is the lab and research space, which is maintained at 15C, and the office and classroom space, which are maintained at 20C. Space heating and hot water are provided through a condensing natural gas boiler, while all electricity is provided through hydro power. Ventilation is provided to the building through two heat recovery ventilators (HRVs), which are designed to exhaust stale air and supply fresh air throughout the building.

3. Exterior wall performance

The exterior walls of the Wood Innovation Research Lab were constructed using 508mm thick vertical truss panels filled with mineral fiber insulation. The panels were sheathed on both the interior and exterior side with oriented strand board (OSB) with a vapour diffusion resistant adaptable membrane installed on the exterior face of the interior OSB sheathing for airtightness and vapour diffusion.
20 temperature and 16 relative humidity sensors were installed in the north and south exterior wall cavities to measure their thermal and moisture performance (Figure 1).

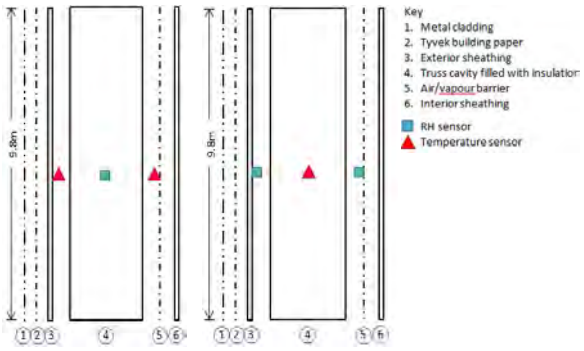

(a) (b)

Figure 1. Sensor placement in the exterior north and south wall assemblies of WIRL building. Sensor groups N01, N02, N05 and N06 and S01, S02, S05 and S06 are configured as shown in (a). Sensor groups N03 and N04 S03 and S04 are configured as shown in (b).

The sensors were installed in 6 groupings of three sensors each separated vertically in a single panel. Four of the six sensor arrangements in each wall were configured with two temperatures and one humidity sensor (N01, N02, N05 and N06, and S01, S02, S05 and S06) (Figure 1a), and two arrangements were configured with two humidity and one temperature sensors (N03 and N04 and S03 and S04) (Figure 1b). For configurations N01, N02, N05 and N06 and S01, S02, S05 and S06, the temperature sensors are located on the exterior face of the interior OSB sheathing layer and the interior face of the exterior OSB sheathing layer, with the humidity sensor located in the center of the insulated assembly. The two additional sensor configurations, N03 and N04 and S03 and S04, were configured with two humidity sensors and one temperature sensor. Here, the two humidity sensors are located on the exterior face of the interior OSB sheathing layer and the interior face of the exterior OSB sheathing layer, with the temperature sensor located in the center of the insulated assembly.

4. Results and discussions

Fuel and electricity consumption meters were installed to measure the energy consumption of the WIRL building. Results provided below reflect the findings from the first seven months of data collection. The heating for the building is provided by a radiant in-floor hydronic loop supplied by a natural gas boiler. A gas consumption meter was installed and data collection began on December 6, 2018. Electrical power to the building is supplied by BC Hydro. An electrical consumption meter was installed and data collection began on July 13, 2018.
The PHPP model completed for the WIRL building predicted a Heating Demand of 12 kWh/(m²a), a Heating Load of 10 W/m² and an overall Primary Energy Demand of 116 kWh/(m²a) based on a climate model that uses the average weather data of the last 10 years. Under specific circumstances when energy intensive equipment is used extensively in the summer months, a potential cooling load of 1 W/m² was predicted as well.
The total specific heating demand calculated by the PHPP software is compared to the actual natural gas consumption for the period of December 6 to 31, January 1 to 31 and February 1 to 28 (Figure 2).
When evaluating the predicted values versus the known natural gas consumption, we can see that a performance gap exist between the two. While the term ‘performance gap’ is more commonly used for discrepancies found between predicted versus actual energy use [3, 4], here we broaden the use of the term to include thermal heating demand as well. It is important to review the assumptions made by PHPP when calculating the specific heating demand for the building so that we may better understand the possible cause(s) of this performance gap. Validation of building energy use models with in-situ collected data can help improve the accuracy of future building models including user inputs and energy use predictions.

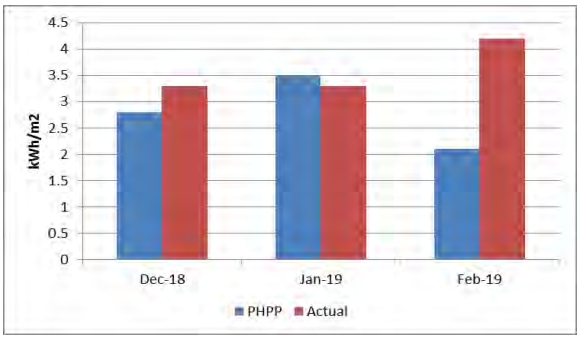

Figure 2. WIRL specific heating demand calculated vs actual energy consumption

The first cause of discrepancy that can be found between the PHPP model and actual performance of the WIRL building is in the climatic data used in the PHPP model versus the actual recorded temperatures for the months during which gas consumption has been recorded. These values can be seen in Figure 3.

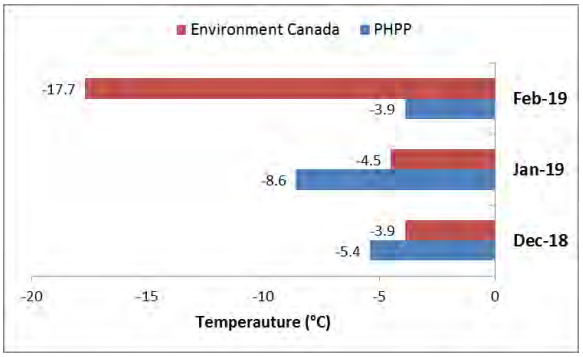

Figure 3. Modeled ambient temperature vs. actual weather data for WIRL building.

From Figure 3 we can see that discrepancies exist between the ambient temperatures used in the PHPP model versus the actual recorded average temperatures for Prince George for the months of December 2018 and January and February of 2019. February 2019 shows a particularly large difference between the two values, which may be accounted for in the fact that it was the coldest February on record in the city's history, with an average temperature of -17.7°C. For the month of January, PHPP used an average ambient temperature of -8.6°C, while the actual measured average temperature was -4.5°C. This is reflected in the heating energy use for the building, which is 0.2kWh/m2 lower than the predicted heating energy demand by PHPP.

For the month of December, we find that the average outdoor temperature was warmer than that used by PHPP as the ambient design temperature; however, the gas consumption for the building is higher than predicted by the PHPP model. In investigating the energy use for the month of December, we found an anomaly in the gas consumption for the first hours in which the gas meter was operational on the building. The total amount of gas used for this period is 1.9527GJ, or 542kWh of gas consumption. We find this to be comparable to the difference in modeled versus actual gas consumption for the month, which is 520kWh of consumption. In reviewing the consumption data for the remaining reporting period, we find that the consumption is consistent thereafter. Therefore, we feel confident that the discrepancy for energy consumption for the period of December can be accounted for in the startup errors in the gas metering device.

In calculating a building's estimate energy demand, the PHPP software multiplies the energy demand for the relevant components by a Primary Energy (PE) factor. The PE factor is used to account for the energy content of the raw material and the losses from distribution, conversion and delivery of the selected energy type for the given component to the end-user. Based on the energy consumption of the WIRL building, the projected annual energy demand for the building was 53.9kWh/m2*a (56,109.90kWh/a). Multiplied by the appropriate PE factors, the total estimated annual Primary Energy consumption for the building was 116.0kWh/m2*a.

The cumulative energy consumption for the WIRL building has been recorded since July 13th, 2018. The total energy consumption of the building on Feb. 28, 2019 was 65,166.36kWh of energy.

At the time energy consumption readings began, an initial 20,127.22kWh of energy had already been consumed. It is unknown when the actual start date for this energy consumption began, and whether it included construction work being done in the building before completion. Therefore, when calculating the average energy consumption per month, this initial energy consumption was removed.

For the period of July 2018 to Feb. 2019, the average monthly energy consumption for the WIRL building was 4.22kWh/m2, (4392.63kWh) per month (Table 1). If we are to use these values to estimate the projected annual energy consumption of the building, we find the building is estimated to use 50.64kWh/m2*a (52,711.59kWh/a). This is 3.26kWh/m2*a (3398kWh/a) less than estimated by the PHPP model which was completed for the building.

Month	Total kWh consumption (for month)
Jul-18	3324.55
Aug-18	5281.64
Sep-18	4576.79
Oct-18	4213
Nov-18	4219
Dec-18	4213
Jan-19	4213
Feb-19	4032

Table 1. WIRL total cumulative energy consumption (kWh) for the period of July 13, 2018 to Feb. 28, 2019.

A review of the data collected from the six sensor groups located in the north and south wall of the

WIRL building show that at no point during the data collection period of July 18, 2018 to Jan. 12, 2019 was 100 percent relative humidity achieved in either the north or south wall assembly (Figure 4-5). The maximum relative humidity values were recorded by sensor N06 on Jan. 8, 2019 at 22:00, with a value of 76.59%, and sensor S03 on Jan. 7, 2019 at 17:00 at 94.24%. The dates of these readings correspond to one of the coldest weather periods recorded during the data collection period. The large fluctuations in relative humidity readings in the south wall are attributed to temperature fluctuations due to solar gain.

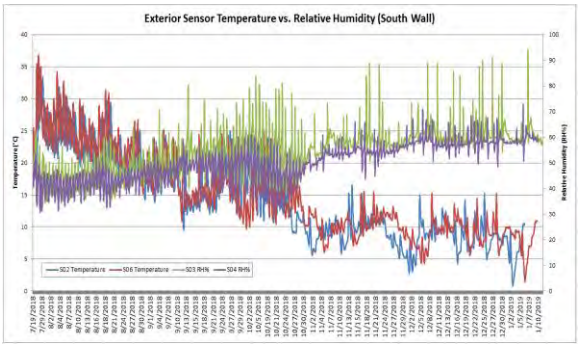

Figure 4. South wall exterior sensors (S02, S06, S03 and S04) relative humidity vs temperature

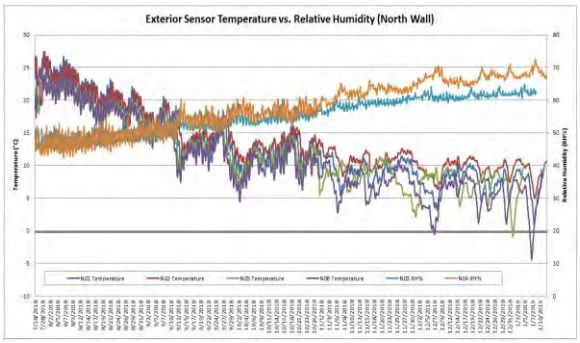

Figure 5. North wall exterior sensors (N01, N02, N03, N04, N05 and N06) relative humidity vs temperature

Critical moisture levels for mould growth in building materials have been reported as low as 75-80% RH, however sustained periods of high relative humidity are required for significant growth (>12weeks) [5]. Although the peak relative humidity values recorded by sensors S03 and N06 are high enough to support mould growth in the exterior sheathing of the wall assemblies, these critical moisture levels were not sustained for periods deemed sufficient to allow growth to occur. Annex 14 of the International Energy Agency (IEA) recommends that the surface relative humidity of an assembly be kept below 80% on a monthly mean basis [6]. Similarly, ASHRAE Standard 160 recommends a 30-day running average surface relative humidity be less than 80% when the average surface temperature for the same period is between 5 and 40°C [7]. For the data collection period, the highest monthly mean relative humidity levels occurred in sensors N04 and S03, with values of 68.19% and 60.89%, respectively. Therefore for the reported data collection period we feel confident that the exterior wall assembly has performed sufficiently and not experienced conditions susceptible to decay organism growth.

5. Conclusions and outlook

The thermal performance and energy consumption of the WIRL building to date has shown good correlation with the values predicted by the PHPP model. The sensors that were installed in the north and south walls demonstrate good hygrothermal behavior, with no record of 100% relative humidity occurring in the assembly. Ongoing data analysis will continue to better understand the long-term hygrothermal performance of the thick-wall assembly under variable climate and conditions.

The monthly fuel consumption of the building supports the thermal performance and thermal energy consumption estimates made by the PHPP model. Discrepancies between the modeled thermal energy (natural gas) consumption of the building and the actual consumption correlate strongly with discrepancies between the design heat loss temperatures used by the software and the actual temperature profiles for each month.

Current energy consumption values show a strong correlation with the PHPP model. However, it is believed that no substantial claim on the final energy consumption of the building can be made at this time due to the inconsistent operation of testing equipment. Further conclusions and discussion may be made following the completion of a full one-year data collection period.

Acknowledgements

This research was funded by Forestry Innovation Investment Ltd. The authors thank UNBC's Facilities Management team and UNBC staff for providing information and support throughout the data collection and analysis that was used in the writing of this case study.

References

[1] H. Ge et al. Building and Environment 160 (2019)
[2] T. M. Trainor et al. ASHRAE Thermal Performance of the Exterior Envelopes of Whole Buildings XIII International Conference, Clearwater Beach, FL, December 2016
[3] A. C. Menezes et al. Applied Energy, 97 (2012) 355-364
[4] S. J. Rees Building Service Engineering Research and Technology 38(2) (2017) 125-132.
[5] P. Johansson et al. International Biodeterioration & Biodegradation 73 (2012) 23-32.
[6] H. Hens International Energy Agency Annex XIV: Condensation and Energy, Vol. 2. (1990) Leuven, Belgium: K.U. Leuven, Laboratory for Building Physics
[7] ANSI/ASHRAE Standard 160 (2009) 14 p.

Hygrothermal Performance and the Effect of an Exterior Air Barrier on High-Performance Building Envelope Assemblies

A. Conroy[a*], G. Wimmers[b]

[a] PhD student, University of Northern British Columbia, Canada, conroy@unbc.ca
[b] Associate Professor, University of Northern British Columbia, Canada, guido.wimmers@unbc.ca
* Corresponding author, Tel: 250-960-6714

Abstract:
Government bodies increasingly recognize the contribution residential housing has on Greenhouse Gas emissions and the need to implement or encourage energy-efficient design and construction. In 2017 the government of British Columbia introduced the BC Energy Step Code, a compliance path option provided to fulfill the requirements of Section 9.36 of the Provincial Building Code. The goal of the Step Code is that all new residential construction will be built "Net-Zero-Energy-Ready" by the year 2032. To meet the energy consumption requirements of the Step Code, building envelopes will have to increase in thermal resistance, requiring thicker assemblies utilizing higher levels of insulation and air tightness. As building durability becomes a greater focus in the construction industry, the hygrothermal behavior of high-performance envelope assemblies must be considered. Thick envelope assemblies combined with air leakage and vapour diffusion may lead to moisture accumulation and long-term fungal growth in the assembly. Convective looping may contribute to increased levels of moisture transport and deposition on building envelope materials. Depending on the position of the air barrier within a given assembly, higher rates of convective looping may occur. The purpose of this research is to investigate the impact the position the air barrier has on the occurrence and rate at which convective looping takes place in an envelope assembly, and the increased risk of long-term durability issues due to moisture accumulation. Preliminary research findings and future testing to be conducted will be discussed.

Keywords:
Hygrothermal Behavior, Energy Efficiency, Convective Looping, Building Durability, BC Energy Step Code

1. Introduction

Current residential building practices in Canada allow builders to choose the location of the air barrier system in the envelope assembly to fit the design of their selected wall assembly and construction methodology. The air barrier system may be comprised of several materials adhered or sealed together through the use of sealants or tapes to form the continuous barrier, and it is not uncommon for more than one air tight layer to be found within the assembly.

Unlike the air barrier, the vapour retarder does not need to be a continuous system. It is understood that while the installation of the vapour retarder is to retard the movement of water vapour across the building envelope by the process of diffusion, the majority of moisture problems resulting from the condensation of water vapour in the building envelope are caused by the exfiltration of moisture-laden air within and through the building envelope materials [1].

Although wood-frame construction practices in Canada still primarily use sealed polyethylene sheeting installed behind the interior drywall to act as both the air barrier and vapour retarder, the use of an exterior air barrier system is becoming more prevalent in the construction of buildings designed to meet high performance energy and air tightness targets [2] and [3]. The use of an exterior air barrier system has been promoted as a viable option to achieving high-performance building envelope systems by industry organizations and educators within the Province of British Columbia [4-6].

It is important that the performance of wood-frame wall assemblies using exterior air barriers be fully understood before they become widespread in practice to reduce the potential for long-term durability issues due to the growth of decay organisms in susceptible building materials, including framing and sheathing material. As demonstrated by [7], convective air movement within an exterior wall assembly can occur as a result of one or more leakage path scenarios when a difference in pressure exists in the assembly, including leakage across the assembly, from the exterior side into the assembly, from the interior side into the assembly, and within a completely closed assembly (Figure 1). Should the air which is transported within, or through the assembly also carry moisture from either side of the envelope, the moisture content of the materials found within the assembly may increase to levels at which decay organism growth can occur. Of concern for the research is the transportation of moisture via convective air movement from the conditioned interior living space into the exterior wall assembly and the redistribution of this moisture on assembly components susceptible to decay when the primary air barrier (or most airtight element) is installed towards the outside of the assembly (Figure 2).

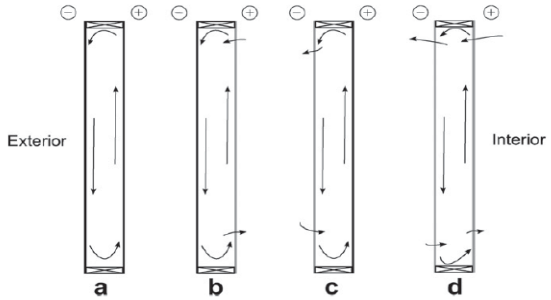

Figure 1. Buoyancy driven air flow in a light weight wall: a) airtight interior and exterior sheathing, b) air open interior sheathing, c) air open exterior sheathing, d) air open interior and exterior sheathing. Of particular interest for this study is the convective looping process that occurs as illustrated in example (b) [7].

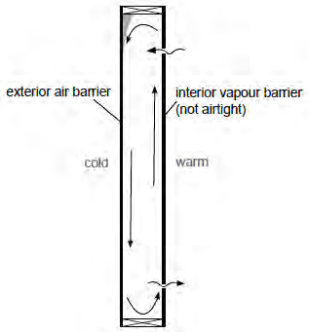

Figure 2. Moisture redistribution in vapour open wall designs (moisture accumulation in grey) with an exterior air barrier [8].

2. Preliminary hygrothermal model setup

Nine wall assembly configurations were chosen based on designs which are representative of those used in the province, including three split-wall assemblies, four deep stud walls with service cavities, and two standing truss assemblies (Table 1). The nine assemblies are designed to meet three effective thermal resistance values: RSI 3.87 (W1, W2, W3), 7.04 (W4, W5, W6) and 8.81 (W7, W8 W9) m2·K/W. In each assembly the air barrier is located to the exterior of the framing insulation layer.

The nine wall assemblies were modeled in the WUFI® Plus software for a one year period starting December 1, 2018 using a weather file created for Prince George, BC, Canada using hourly weather data records from Environment Canada. Material properties used for preliminary hygrothermal modeling were selected from values cited in [8-11]. Initial assembly conditions were set at 80% relative humidity and 21°C. Indoor climate design conditions were set at temperature 21°C (min) and 24°C (max) and 40% RH (min) and 70% (max). An internal loads/occupancy file was selected from the WUFI® Plus database for a family of four. To simulate the presence of convective looping within the assembly up to the location of the airtight layer, a moisture source was added to the critical layer on which moisture accumulation is predicted to occur (exterior sheathing layer). This air infiltration model is adapted from [9] and calculates the amount of condensed moisture transported to a designated surface or assembly layer from interior air. The method is based on the assumption that the heat effect of the penetrating air is neglected. Boundary conditions for the model were set using a depth of 5cm starting at the interior face of the critical layer material, a stack height of 2.4m and a 0.0 Pa overpressure. A user-defined air tightness class was set with an envelope infiltration rate of 0.0 m3/m2h.

Table 1: Selected wall assembly designs

	Framing	Framing insulation	Exterior insulation
Split Wall			
W1	38x140mm	glass fiber batt	38mm XPS
W2	38x140mm	Loose fill cellulose	38mm XPS
W3	38x140mm	Glass fiber batt	32mm semi-rigid mineral wool
Deep Stud w/service Cavity			
W4	38x89mm, 241mm I-joist	Glass fiber batt, loose-fill cellulose insulation	-
W5	38x89mm, 241mm I-joist	Glass fiber batt, glass fiber batt	-
W7	38x140mm , 302mm I-joist	Glass fiber batt, loose-fill cellulose insulation	-
W8	38x140mm , 302mm I-joist	Glass fiber batt, glass fiber batt	-
Standing Truss			
W6	302mm vertical truss	Loose-fill cellulose	-
W9	406mm vertical truss	Loose-fill cellulose	-

In addition to the WUFI® Plus hygrothermal simulation models, WUFI® Bio was also used as a preliminary analysis tool to assess the risk of mould growth in each of the nine assemblies based on the stated boundary conditions. Mould growth risk was calculated for each of the assemblies at the defined critical layer. WUFI® Bio uses the hourly hygrothermal conditions that occur at the designated layer and compares it to the growth conditions needed by mould, calculating the moisture content of mould spores which are compared to the critical water

content that allows a spore to germinate. Results are presented either as mould growth or mould index (Viitanen model).

3. Experimental design and setup

The first stage of the research work is the completion of the hygrothermal analysis on the predicted behavior of the nine wall assemblies using the WUFI Plus software. Modeling of the high-performance wall assemblies must be completed before laboratory testing of the assemblies can be completed so that benchmark reference values are available for comparison of results.

Following the completion of the initial hygrothermal computer models, the assemblies will be constructed and tested in a natural exposure test facility located on campus at the University of Northern British Columbia. The nine assemblies will be grouped and constructed so that a single test panel will be made up of three different test assemblies, each measuring 2.4m x 2.4m in size. Duplicates of the three panels will be constructed so that each can be tested in the north and south exposures available at the testing facilities to factor in the hygrothermal influence of solar radiation. In total, therefore, 6 panels will be constructed.

To record the response of each assembly to the interior heat and moisture loads and exterior climate conditions, temperature, moisture content, relative humidity and heat flux sensors will be installed in each assembly. This information will be collected by data loggers, with one data logger being used for each assembly. The panels will be constructed in such a way that each will have removable specimen which may be removed and measured for moisture evolution on a regular basis.

Once all data collection from the tested panels is complete, analysis of the in-situ performance may be conducted. These results will be compared to the initial predicted hygrothermal response completed using the WUFI® Plus software, which can then be validated and used to predict the long-term performance of each assembly under various interior loads and climatic conditions.

4. Results and Discussion

The results of the preliminary WUFI® Plus and WUFI® Bio analysis are shown in Figures 3-5. In Figure 3, the results of the calculated relative humidity at the interior face of the critical layer are shown. The initial relative humidity for the materials within all nine wall assemblies was set at 80% in accordance with ASHRAE Standard 160 and the IEA Annex 14 when determining mould growth risk [12 and 13].

The results shown in Figure 3 show an initial spike in the critical layer RH in all assemblies followed by a decrease in all wall assemblies except W7 and W9. W8 maintains a high RH that decreases only a small amount over the course of the simulation period. W1, W2 W4, W5 and W6 show similar results while W3 shows similar results but at a consistently lower RH value than the other assemblies. None of the assemblies returns to a RH level lower than 80% over the simulation period.

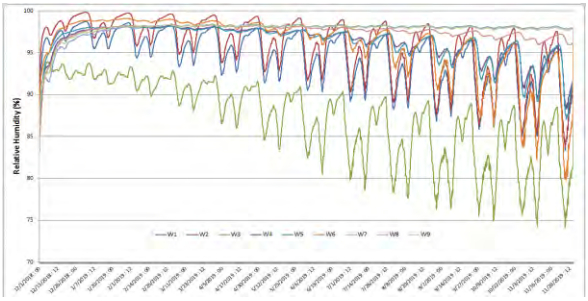

Figure 3. Relative humidity of critical layer in assemblies W1-W9.

The WUFI® Bio assessment tool classifies mould growth risk for indoor surface of positions in contact to indoor air according to the values presented in Table 2. WUFI® Bio uses a signal light indicator when displaying the results of each assessment, with green signaling an assembly deemed to have no, or acceptable risk, yellow for assemblies where caution should be taken and additional investigation is needed for assessing acceptability and red for assemblies deemed not acceptable. All WUFI® Bio simulations were run using an initial RH in spore of 50% and substrate class II, which is defined as adverse recyclable building materials.

Table 2. WUFI® Bio mould growth risk index

	Acceptable	Caution	Not Acceptable
Mould Growth (g_m)	<129mm/year	129 < w_s ≤ 176 mm/year	> 176 mm/year
Mould-index (MI)	≤1	1<MI≤2	>2

Based on the moisture levels found at the critical layer in each of the nine wall assemblies, four of the assemblies were deemed not acceptable (W1, W2, W3 and W9), two noted with caution (W7 and W8) and three as acceptable (W4, W5 and W6) (Figure 4). Figure 5 shows the results for W9 with the water content of spore displayed in blue and the critical water content in red. The calculated water content of the spore exceeds the critical water content of the sheathing long enough over the course of the calculation period that the assembly is deemed not acceptable (red signal light).

The results of the preliminary WUFI® Plus and WUFI® Bio analysis demonstrate the influence of the properties of the materials used in the different assemblies.

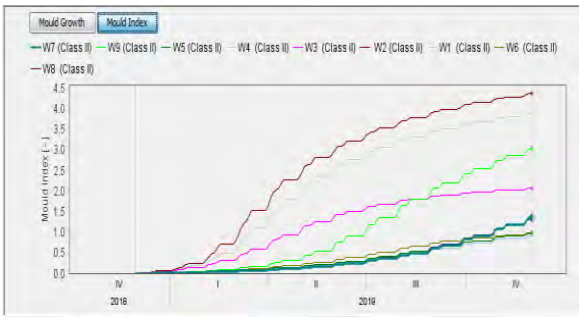

Figure 4. Mould Index values for the nine wall assemblies as calculated by WUFI® Bio

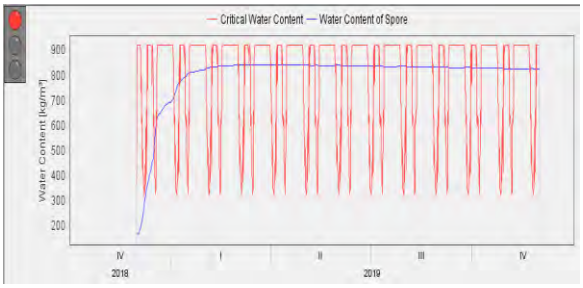

Figure 5. Critical water content (red) and water content of spore (blue) for W9.

While W1, W2 and W3 are all deemed unacceptable by WUFI® Bio, the mould index value calculated for W3 is significantly lower than W1 and W2. This is also reflected in the critical layer RH as shown in Figure 3, and can be attributed to the use of mineral wool as the exterior insulation. In addition to material properties, the total depth of the assembly is shown to have a significant impact on both the assessed mould growth risk and critical layer RH. W7, W8 and W9 all have assembly depths over 400mm. W9 is calculated to have an unacceptable mould growth risk and maintains a sheathing RH over 95% over the one year calculation period. While W7 and W8 maintain similarly high RH levels at the critical layer over the course of the calculation period, their calculated mould assessment risk is to proceed with caution. This is due to lower critical water content fluctuations that result from smaller temperature fluctuations in the critical layer in these two assemblies.

5. Conclusions and outlook

Nine wall assemblies designed to meet three thermal resistance values have been designed as a part of ongoing studies to assess the hygrothermal behavior of high-performance wall assemblies that use an exterior air barrier system. The transportation of moisture laden interior air into the wall assembly up to the point of the air barrier system has been simulated by the use of the air infiltration model in the WUFI® Plus software and mould risk assessment conducted using the WUFI® Bio software. Preliminary results show an unacceptable mould risk for four of the assemblies when an initial assembly material RH of 80% is used. Further analysis must be completed at additional initial material RH levels and for a greater simulation time period. Future work includes the construction and in-situ testing of the nine wall assemblies in a natural-exposure facility to collect in-situ performance data which will then be used for preliminary model validation and further long-term hygrothermal behavior predictions.

Acknowledgements
The authors would like to thank UNBC for their ongoing support of this research project.

References

[1] National Research Council of Canada. National Building Code of Canada. Ottawa: National Research Council of Canada (2015)
[2] J. Langmans, R. Klein, M. De Paepe, S. Roels, Potential of wind barriers to assure airtightness of wood-frame low energy construction. Energy and Buildings, (2010) 2376-2385
[3] J. Lstiburek, Understanding Air Barriers. BSD-104 (2006)
[4] BC Housing. Illustrated Guide - Achieving Airtight Buildings. Burnaby: BC Housing (2017)
[5] City of Vancouver. Illustrated Guide - R22+ Effective Walls in Residential Construction in British Columbia. Burnaby: BC Housing (2017)
[6] FP Innovations. Pathways to High-Performance Housing in British Columbia. Vancouver: FP Innovations (2014)
[7] J. Langmans, R. Klein, S. Roels, Hygrothermal risks of using exterior air barrier systems for highly insulated light weight walls: a laboratory investigation. Building and Environment, (2012) 192-202
[8] J. Langmans, S. Roels. What are the hygrothermal consequences of applying exterior air barriers in teimber frame construction in Europe? Journal of Building Performance Simulation 8:3 (2015) 191-204
[9] L. Wang, H. Ge, Effect of air leakage on the hygrothermal performance of highly insulated wood frame walls: comparison of air leakage modeling methods. Building and Environment, (2017) 363-377
[10] D. Watt, S. Sjoberg, P. Wahlgren, Hygrothermal performance of a light weight timber wall assembly with an exterior air barrier. Energy Procedia, (2015) 1419-1424
[11] K. Riesner, C-E. Hagentoft, G-W. Mainka, Condensation risk within loose fill insulation due to natural convection in vertical cavities. 9th International Conference on Performance of the Exterior Envelopes of Whole Buildings Florida, USA, (2004)
[12] S. Glass, Hygrothermal Analysis of Wood-Frame Wall Assemblies in a Mixed-humid Climate. Forest Products Laboratory, (2013) FPL-RP-675
[13] E. Vereecken, D. Saelens, S. Roels, A comparison of different mould prediction models. 12th Conference of International Building Performance Simulation Association, Sydney (2011)

Pros and Cons of Different Strategies and Levels of Prefabrication and the Influence of the BC Energy Step Code on the Manufacturing of Buildings

G. Wimmers[a], L.Wimmers[b]*

[a] Dr. Guido Wimmers, Chair, Associate Professor, Master of Engineering, Integrated Wood Design, University of Northern British Columbia, 3333 University Way Prince George, BC, V2N 4Z9 guido.wimmers@unbc.ca
[b] Lewin Wimmers, Master Student MNRES, University of British Columbia, 3333 University Way Prince George, BC
* Corresponding author: Lewin Wimmers: lenny.wimmers@alumni.unbc.ca

Abstract:
In 2017 the British Columbian Energy Step Code [1] was introduced with the goal to create a road map to higher energy efficiency of the built environment in 4 or 5 steps until reaching the highest defined level in 2032. The logical consequence of implementing more insulation and subsequently building thicker walls and better airtightness is the adaptation of prefabrication and production of building components in a controlled environment. This can be done with open panels, one side or even both sides closed panels, already including other components such as windows and doors and conduit for electrical installation and plumbing. Several different strategies and levels of automation of prefabrication are compared and advantages and disadvantages discussed.

Keywords:
Prefabrication, Automation, Energy-efficiency, Building Assemblies, BC Energy Step Code

1. Introduction

The British Columbian Energy Step Code [1] defines the energy efficiency for new buildings in 4 or 5 steps. The highest level for large residential and commercial buildings (Part 3) and for smaller residential buildings (Part 9) is occasionally also referred to as “Net-Zero-Energy-Ready”. This step is not as challenging or energy efficient as the internationally well-established Passive House Standard [2], but it will increase the energy efficiency of code compliant buildings drastically over the remaining 12 years. To achieve these energy efficiency goals, the thermal performance of the envelope and the airtightness will have to be increased. Assuming the predominant use of traditional insulation materials, the thickness and consequently the weight of the envelope assembly can increase by 42% to 77% and the volume might increase by 87% to up to 100% compared to step one of the BC Energy Step Code [1]. Increased accuracy is demanded to achieve higher airtightness requirements which trigger potentially more labour steps. The logical consequence of implementing more insulation and subsequently building thicker walls and better airtightness is the adaptation of prefabrication and production of building components in a controlled environment. Prefabrication has the potential to optimize the processes and reduce costs for materials and labour [3].
Prefabrication and off-site construction have been developed over decades on several continents with slightly different approaches and emphasis. Other countries have been more successful than Canada in the adaptation of prefabricated construction: while the market volume in Australia in 2011 was around $1.5 billion, the same year in Canada the volume was only about $250 to 300 million [4].

2. Several Different Strategies and Levels of Automation of Prefabrication

Prefabrication can be categorized in several ways, for example in non-volumetric, volumetric and modular buildings [5], in 1D for precut packages and log construction, 2D for panelized systems and 3D for volumetric and modular systems.
One of the more recent attempts was made in the report “Cost Implications of Accelerated Construction Schedules” by Forestry Products Innovation(FPI) [6], with 4 levels of prefabrication.
Following those 4 levels are taken and further refined and clarified where deemed to be necessary to better reflect the industry:

2.1. Level 1: Components that are Manufactured in a Factory

The production of these components or elements typically involves only one trade, contractor or supplier. Level 1 can be further subdivided in level 1a for light weight components and 1b for heavy timber components.
Level 1a are components such as framed trusses and light frame wall panels, only comprise the structural system. The manufacturing of roof trusses and light framed wall panels do not necessarily involve a higher level of automation, but this is advantageous if mass production applied. Consequently, the level of specialised production expertise and equipment varies.

Level 1b are components such as precut or machined glued laminated timber (glulam), or precut mass timber elements (CLT, NLT, LVL panels, etc.). For heavy timber components such as glulam, CLT and similar products, usually a high level of expertise and automation is necessary to produce cost efficiently and manage quality control. The production of glulam still allows for several manual steps, the production of CLT is usually highly automated. These products are in several countries typically called precut, but not prefabricated.

2.2. Level 2: Panelized Components

The prefabrication of panelized components can be further subdivided in one side closed or both sides closed panels. Both have in common that several trades will be involved, the investment in automation depends often on the volume of the production line. Generally, Level 2 is globally referred to as prefabrication.

2.2.1. Level 2a: One Side Closed Prefabricated Panels

In this category, assembly involves several trades (i.e. carpenters, insulators, window installers, etc.) and additional expertise in the form of building science, transportation and installation is required. The prefabrication company may play a more central role in the design and construction process through the preparation of shop drawings, coordination of sequencing, provision of specialized equipment, etc. Examples include “one side closed” exterior wall panels that include cladding, insulation, vapour/air barrier, and can also include the glazing. The level of applied automation in production varies strongly as this level can be pursued by small and medium size companies as well. Depending on the production volume, automation can be implemented in stages. The same system can be applied for roof and floor panels. The installation of mechanical and electrical systems is normally done on-site, after the wall, roof, and floor panels are installed and structurally connected. Architecturally these buildings are very versatile and flexible in the design and cannot be identified as a prefabricated building. This level can utilize advantages in production efficiency and quality control, combined with efficient shipping. Construction time on-site is significantly faster than Level 1.

2.2.2. Level 2b: Both Sides Closed Prefabricated Panels

This category involves an even wider range of trades (e.g. carpenters, insulators, window installers and electricians, plumbers, installers of mechanical systems, etc.) and in addition to level 2a the design has to be further optimized to allow for easy connections between all panels and their included services on-site. The prefabrication company plays a vital role in the design and construction of the project and in addition to the multiple trades, an interdisciplinary design team is included. Similar to level 2a automation can be introduced in stages but companies pursuing level 2b are usually producing larger volumes and therefore higher level of automation are typical. On-site all components will be fit together, structurally connected, and all services will be connected. Only minor finishing work such as the transition from panel to panel will be done on-site. Similar to level 2a mass customization is possible and an identification as prefabricated building difficult or impossible. Advantages of prefabrication to optimize cost efficiency and quality control are fully utilized. Shipping is very efficient and construction on-site very short. Lifting costs on-site are still relatively low as typically only one component at the time is lifted. Only under specific circumstances such as labor shortage on-site or extremely short construction period demanded Level 4 might be preferred.

2.3. Level 3: Volumetric Pre-Assembled Pods

Three-dimensional, highly specialized elements are fabricated by multiple trades and are shipped fully finished from a factory to a project site for integration into a permanent or semi-permanent building or to a prefabrication plant to be integrated into larger modular elements. The specialized company works with the project team to customize, assemble, transport and install the units. Examples include fully equipped mechanical rooms, most common application are bathroom and/or kitchen “pods”. This type of prefabrication is typically done in larger series, many units with the same design will be produced by applying a high level of automation. On site these pods are then typically connected to either prefabricated panels according to Level 2a or 2b or to modules as described in Level 4. The use of pods can decrease the total construction period on-site significantly.

2.4. Level 4: Volumetric Prefabricated Modules

Three-dimensional elements are fabricated by multiple trades and shipped fully finished from the factory to the project site then integrated into a permanent or semi-permanent building. The prefabrication company works with the project team to customize, assemble, transport, and install the units. Examples include: fully finished residential modules, office spaces, or hotel rooms, and can be combined with fully equipped mechanical rooms, a bathroom and/or kitchen “pods”, hospital rooms, as described in Level 3. These modules are fully finished, including final surface of walls, ceiling and floor and built-in furniture are installed as well. Ideally, to be more architecturally appealing, the level of prefabrication should not be obvious, once the building is finished. The installation on-site becomes crucial to allow for the full benefits of this “plug and play” approach. This level has the potential to fully utilize all advantages of prefabrication as the construction time on-site is the shortest of all levels. Particularly if larger numbers of similar units are needed, i.e. hotel rooms, the application of volumetric modules can be attractive. This level comes with the disadvantage of inefficient shipping and high lifting costs on-site.

3. International Comparisons

The shift from building on-site to off-site construction is indirectly triggered by the energy efficiency requirements for new construction in the building code. The increase of thermal resistance is generally achieved by increasing the envelope thickness, the volume, and consequently the weight of the construction will be increased. Energy efficient buildings with envelope performance of RSI 10.57 resulting in wall thicknesses of about 38cm to 45cm [7]. Those envelopes can be constructed on-site but due to the mass, volume and several labour steps, prefabricated envelope components will be more cost efficient. A comparison with countries whose building codes are requiring similar energy efficiency as the 2032 BC Energy Step Code since many years can help to better understand in which direction the local industry might develop.

Level 1a light frame prefabrication is not a significant player in either of the two regions, leading wood based prefabrication, the alpine region in Europe with Austria, Germany, Italy and Switzerland and northern Europe with Denmark and Sweden. This is likely due to the utilization of only a small portion of the potential benefits, hence making this type of prefabrication simply uncompetitive in these markets. Only in North America this level is currently widely spread but as the demand for more energy efficient envelopes increases, resulting in thicker (>35cm) and consequently heavier envelopes [7], the use of level 1a will probably be reduced due to being uncompetitive compared to Level 2a and 2b.

Level 1b heavy timber prefabrication, including glulam, CLT, DLT, and NLT, is dominated by Austria, Germany, Northern Italy and Sweden.
For example, in 2018, the annual production of Canada's entire glulam industry was smaller than the production of a midsize Austrian glulam manufacturer with 120,000m³ while the largest Austrian manufacturer produced about 400,000 m³ [8]. Canada's largest glulam producer produced 30,000 m³ [9]. Out of the worldwide 5 largest CLT producers 4 are Austrian owned companies, and the largest, a Swedish/Finish company has their largest production plants in Austria [10].

For several decades Level 2 has been the standard for wood construction in Scandinavia as well as central Europe. Companies, based in Germany, Austria, Switzerland, Italy, Slovenia, Slovakia, Hungary, and France typically have semi or fully automated production lines. Generally, smaller companies have a lower level of automation focused on Level 2a, but offering a high level of customization. Large companies have typically a significantly high level of automation focused predominately on 2b. This type of prefabrication is uncommon in North America. For many years in the US only a few has been investing into 2a and 2b [11]. The Asian market with China and Japan is actively involved. China is fairly new in this segment, but after having heavily invested in European technology is ramping up volume quickly [12].

Level 3 prefabrication of pods is relatively new on the European market and has grown rapidly over the last 10 years. This market is in the start-up phase in North America, although for the past few years there have been several companies in the US offering pods.

Level 4 is very heterogeneous, as modular construction is popular in the North American as well as the European, markets but the implemented processes and the resulting product are hardly comparable. European companies do offer Level 4 for very specific types of projects, including high numbers of repetition and design tailored to modular construction or were shortest possible construction period on site is essential. In North America the production of modular homes was historically related to lodging camps and trailer homes and is working relentlessly to overcome the rather poor reputation triggered by their heritage. In Level 4, the Asian market recently became very active, in particular, China is rapidly increasing its productivity. Comparing Level 2b and 4, both systems have their advantages and disadvantages. In the European market, companies typically explore modular prefabrication after gaining decades of experience with panelized prefabrication. This natural progression ensures a high level of quality and efficiency optimization in the process. Modular prefabrication has, potentially, an advantage if large numbers of the same units can be stacked to produce a building and if construction speed on-site is of utmost importance. However, modular construction has also some significant disadvantages compared with panelized prefabrication. In modular construction, almost all surfaces of a module are built for transportation, but eventually, each module gets connected to the next one, leading to doubling walls and double floors. This doubling up increases the production and material costs and the weight when lifting but has the advantage of better sound insulation. Fire control and compartmentalization are other aspects of concern. Potentially, hidden cavities in modular construction can be problematic, specific attention must be paid to the continuous separation of units. Modular construction typically triggers higher shipping costs as a large volume of air is shipped to the site and the load for the crane is significantly higher than for panelized prefabrication. Panelized prefabrication is usually overall more efficient and more flexible, allowing for many different sizes but, need a few days of installation work on-site [13].

4. Discussions

Although we observed crucial differences in the application and the processes of prefabrication technology in different European markets, there are

general differences between the European market and the Canadian. On the European market, each panel of a module is generally finished to the highest level possible (typically Level 2b) to benefit from the full range of prefabrication advantages and then either shipped to site or assembled in a controlled environment to a 3D volumetric structure, if this makes sense. Historically, prefabrication companies had decades of experience with panelized 2D prefabrication before venturing into 3D modular prefabrication. 3D is only applied if there is sufficient repetition of the same modules to justify the disadvantages of higher transportation and lifting costs. This can be, for example, the case if larger hotels, social housing projects, or student homes are built and many similar components can be shipped over relatively short distances and time at the construction site is extremely valuable.

In Canada, we observed that the assembly of the 2D panels into 3D modules happens at the very beginning of the process (typically Level 1). Assembling to a 3D structure as soon as possible automatically eliminates some of the advantages of prefabrication as not all advantages of working ergonomically optimized at a table can be utilized and in many cases, the finishing of an upright structure or even over-head components are more time consuming and rather comparable with on-site construction.

5. Conclusions and Outlook

The BC Building Code (BCBC) [14] influences two key factors in the decision of BC's industry to start transitioning towards prefabrication. The first one is the energy efficiency defined in the BC Energy Step Code, as this code influences the thickness of the building envelope of every building. The second key influence is the allowable height increase of wooden buildings to 12 floors. Prefabrication is essential for taller wood construction as manufacturing on-site is not just significantly slower but triggers a few disadvantages in the fields of worker's safety, accuracy, overall performance and impact on the surrounding area including noise pollution and traffic infringement.

These newly implemented regulations are indirectly influencing the industry and are leading to an adaptation of prefabrication in the BC construction industry. The direct consequences as well as the customized adaptation of prefabrication for the BC and Canadian market must be further explored.

References

[1] BC Energy Step Code Council: BC Energy Step Code. The government of British Columbia, 2017.

[2] Passive House Institute Darmstadt: Criteria for the Passive House, EnerPHit and PHI Low Energy Building Standard, version 9c, revised 29.09.2015.

[3] Lopez D., Froese T. M.: Analysis of Costs and Benefits of Panelized and Modular Prefabricated Homes. Procedia Engineering, 145, 1291–1297, 2016.

[4] Bernstein H.M., Gudgel J.E., Laquidara-Carr D.: Prefabrication and modularization: increasing productivity in the construction industry. US Department of Commerce, 2011.

[5] Goodier C., Gibb A.: Future opportunities for offsite in the UK. Construction Management and Economics, 25(6), 585–595., 2007.

[6] Goodland H., Lam A., Taylor M., Zadeh P.: Cost Implications of Accelerated Construction Schedules. Vancouver: FP Innovations, 2019.

[7] Wimmers G., Conroy A.: Consequences of the BC Energy Step Code on Offsite Construction. Modular and Offsite Construction Conference, Banff, AB, 2019.

[8] Timber Online: Mayr-Melnhof To Take Over Hüttemann. 2020. https://www.timber-online.net/holzprodukte/2018/02/brettschichtholz-top-10.html.

[9] Nordic Engineered Wood: Non-residential design Construction Guide, Quebec, CA, 2015.

[10] Imarc Group: Top 5 Cross-Laminated Timber Manufacturers Worldwide - Imarcgroup.com, 2020. https://www.imarcgroup.com/top-cross-laminated-timber-manufacturers-worldwide.

[11] Haas C.T., O'Connor J.T., Tucker R.L., Eickman J.A., & Fagerland W.R. Prefabrication trends and effects on the construction workforce. Austin, TX: Centre for Construction Industry Studies, 2000.

[12] Hong J., Shen G. Q., Li Z., Zhang B., & Zhang W. Barriers to promoting prefabricated construction in China: A cost–benefit analysis. Journal of Cleaner Production, 172,649–660, 2018.

[13] Blismas N., Pasquire C., & Gibb A. Benefit evaluation for off-site production in construction. Construction Management And Economics, 24(2), 121-130, 2006.

[14] BC Building Code (BCBC): BC Building Code. The government of British Columbia, 2018.

Fiber Holder to Assist in Sputter Deposition of Optical Fibers

C.A. Vail[a,*], G. Burton[a], P.M. Wild[b], H.L. Buckley[a]

[a] Dept. of Civil Engineering, University of Victoria
[b] Dept. of Mechanical Engineering, University of Victoria
* Caitlin Vail, cvail@uvic.ca

Abstract:
Sputter deposition is used to coat 100 nm of aluminum on the tips of single mode optical fibers. A fiber holder was built to secure the fibers in the sputter deposition chamber while being sputter coated. Our findings show that the distance between the target and the tips of the optical fibers has a large effect on the Al thickness of the coating. The goal of the fiber holder is to maximize repeatability of the sputter deposition by ensuring the fibers are held in the same position every time sputter deposition occurs. We expect increased repeatability between tests when using the sputter deposition machine.

Keywords:
Sputter deposition, optical fibers, holder.

1. Introduction

Magnetron sputtering can be traced back to the 19th Century to Grove's observations of pulsed diode sputtering [1]. In the past two decades, sputter deposition has been used to deposit thin-films onto a surface, analyze trace impurities of materials, treat and process surfaces, and numerous other technological applications [2]. This paper does not review the history or latest developments of magnetron sputtering, which is a mature and widely used industrial technology and is reviewed elsewhere [1]. Most commonly, sputter deposition is used in industry for large-area deposition of thin films however, magnetron sputtering is a flexible and scalable technique that can be used for a wide range of thin film deposition [2]. We use magnetron sputtering for an uncommon application: coating the tips of single-mode optical fibers with 100 nm of aluminum. In doing so, our goal is to develop a sensor to detect fluoride concentrations in groundwater. Common materials to be coated would be able to lay flat across the top of the substrate within the sputter deposition chamber. The substrate is where the material goes that is to be coated with a thin film, and the target is the material which coats the substrate. We need the tips of the optical fibers to be perpendicular to the surface of the target, meaning the fibers cannot lay across the top of the substrate. For this reason, we have designed a fiber holder.

Sputter deposition uses a vapor-based physical deposition method [3]. As shown in Figure 1, particles are removed from the surface of a target through ion bombardment [1]. The released particles condense on the surface of the substrate, creating a coating [1].

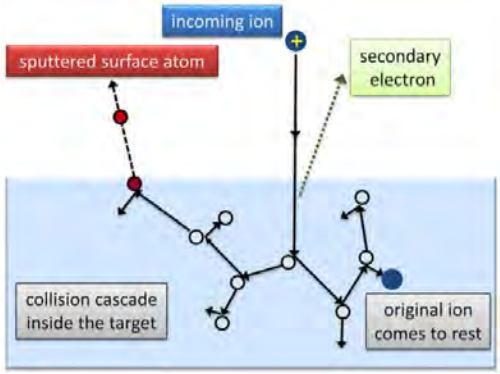

Figure 1: Ion bombardment of Argon ions bombarding the target surface releasing surface atoms and secondary electrons into the plasma [1]

Factors such as the number of particles removed off the surface of the target, penetration depth of ions, and nature of the collisions are influenced by the mass and energy of ions and the characteristics of the target material [1]. Monte Carlo simulation gives the best representation of the particle collision cascades [1]. As the name suggests, a magnetron is used to create a magnetic field [1]. This allows electrons to perform numerous gyrations along magnetic field lines thus forcing electrons to travel a longer path in front of the magnet [1].

Energetic electrons collide with process gas atoms, effectively ionizing them and creating a plasma which consists of both electrons and ions [1]. The plasma and its boundaries determine the local electric field [1]. The positive ions are attracted to the target, which is negatively charged, and continue sputtering the target [1]. Sputtered atoms travel to the substrate to coat it with a thin film [1]. Substrate temperature and energy of the atoms determine the microstructure of the thin film coating [1]. Process parameters for

sputtering are limited and consists primarily of controlling the substrate temperature and the gas pressure [1]. This process is illustrated in Figure 2.

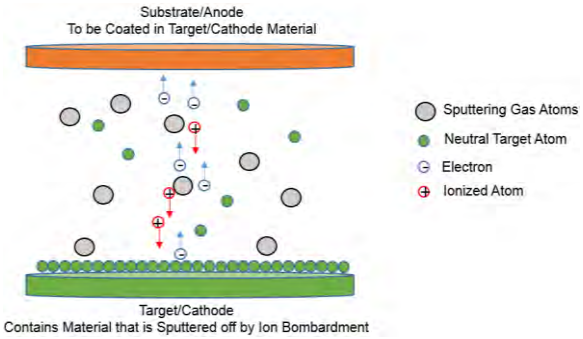

Figure 2: Sputter Deposition Process

An additional process parameter is the distance between the substrate and the target which has a strong effect on the distribution and characteristics of the deposition molecules [4]–[7]. As the distance between the substrate and the target increases, the uniformity of the distribution of the depositing atoms increases however, the kinetic energy of the depositing atoms decreases [4]. Furthermore, the substrate-target distance has an effect on the deposition rate, as well as the microstructure and hardness of the thin-film coating [4].

This paper does not give an extensive review on the underlying physics of magnetron sputtering as entire books have been written on the subject [8]. Rather, the goal is to explain how the fiber holder we have built compliments sputter deposition to make it a more robust, reliable, and repeatable process.

2. Design

The fiber holder is designed to hold up to 17 single-mode optical fibers in a vacuum-sealed chamber under 10^{-3} mbar pressure. As shown in Figure 3, the fiber holder consists of a ring to lay atop the substrate, threaded rods, and a bottom portion containing an O-ring that clamps the fibers in place.

The material was chosen based on what can be exposed to plasma for a long period of time, meaning non-magnetic materials are required so the magnetic and electric fields created by the plasma and magnetron are not affected. Moreover, no material containing pockets of air, such as foam or wood, can be used because it compromises the vacuum state of the chamber. Table 1 summarizes the materials used to build the fiber holder.

Table 1: Materials

Piece	Material
Top Plate	Aluminum 6061-T6
Threaded Rods	Stainless Steel 18-8
Bottom Clamp	Aluminum 6061-T6
Fasteners	Electron-plated Stainless Steel
O-Ring Clamp	Viton

The O-ring clamp made from Viton is inside the bottom clamp, as shown in Figure 4. Its purpose is to prevent the fibers from slipping. The parts and labor to build this fiber holder cost $200 CAD in total for the production of a single fiber holder. The mass production of several fiber holders would decrease the cost of each individual fiber holder.

Figure 4: O-Ring Clamp and Vacuum Tape

The threaded rods are adjustable, a major advantage to this design. The closer the tips of the fibers are to the target, the more direct and concentrated the stream of sputtered atoms will be. The further away the tips of the fibers are from the target, the broader the array of sputtered atoms are, and the higher the likelihood that the fibers will be evenly coated. Additionally, the rods may be bent so the fibers are perpendicular to the target surface effectively allowing the tips to be facing the oncoming stream of sputtered atoms. The limitation to this design is that, while it fixes the vertical distance between the tip of the fibers and the surface of the target, it does not fix in place the holder with regards to rotating it atop the substrate. Figure 5 illustrates the rotation movement of the fiber holder.

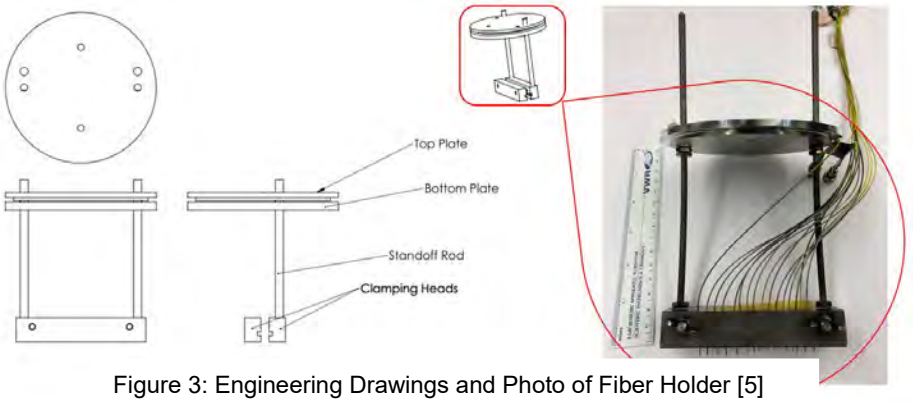

Figure 3: Engineering Drawings and Photo of Fiber Holder [5]

Overall, the fiber holder increases the parameters we can control of the sputter deposition process, mainly fixing the fibers perpendicular to the surface of the target and at a set vertical distance from the surface of the target.

3. Sample and Instrument Operation

Single-mode optical fibers are stripped of their yellow plastic outside coating for about 3 cm from the distal end. The tip that was previously coated and submersed in a fluoride solution, about 1 cm from the distal end, is then cleaved, and the exposed optical fiber core is cleaned with acetone. The optical fibers we use in our experiments are Pigtail FC/APC SM SX Ø0.9 1M. Securing the fibers into the holder is best assisted with vacuum tape to ensure they do not slip out of place. We leave 3 mm between each fiber. Once the fibers are in place, we clamp the second bottom piece with fasteners so the O-ring helps grip the fibers in their desired position. Now the fiber holder may be inserted into the sputter deposition chamber as shown in Figure 5. The top circular substrate of the fiber holder is slid on top of the substrate in the chamber. The fiber holder can be twisted so that the tips of the optical fibers are perpendicular to the surface of the target. The rods are made of 18-8 Stainless Steel and can be bent to better position the tips of the optical fibers to being perpendicular to the surface of the target; however, note that this compromises the ability to adjust the rods height. At this stage, the machine can be sealed for sputter deposition.

Figure 5: Fiber Holder in Chamber

In our tests, we use a Mantis QUBE sputter deposition machine and we coat single-mode optical fibers with 100 nm of aluminum. Argon gas is used as the sputtering gas however, nitrogen gas is used to vent the chamber. The argon gas is vented into the chamber at a flow of 35 standard cubic centimeters per minute, power applied is 60 W, and the pressure in the chamber once under vacuum is 10^{-3} mbar. The temperature at the bottom of the chamber is 28°C, at the bearing is 27°C, and at the motor is 26°C. The Mantis QUBE uses a 13.56 Mhz generator.

4. Research Findings

We coated 17 single-mode optical fibers using the fiber holder with the sputter deposition machine. We fixed a 1 cm^2 piece of glass to the fiber holder such that the glass is held at the same position as the tips of the optical fibers so that the distance between the target the piece of glass is the same as the distance between the target and the tips of the optical fibers. We sputter coated the optical fibers with Al. The sputter deposition machine measured the Al coating thickness at the substrate to be 10 nm. Using a profilometer, we measured the Al thickness on the glass to be 100 nm.

We conclude that the distance between the target and the tips of the optical fibers has a large effect on the thickness of the Al coating. The large variability in data we observed at the beginning of our research

may very well be due to the fact that we were not using a fiber holder and that the fibers were positioned at slightly different distances from the target each time we sputter coated. We expect the use of the fiber holder to be key in ensuring repeatable and reliable data for our research moving forward because it ensure the Al thickness on the tips of the optical fibers is consistent each time we sputter coat.

5. Results and discussions

The concept with the same materials can be applied to other sputter deposition machines using various target materials, sputtering gases, chamber pressures, and temperatures. Furthermore, the fiber holder can be used outside the scope of single-mode optical fibers, and can hold in place any object that fits within the clasp.

The holder increases the process parameters of sputter deposition that can be controlled, namely, placement within the chamber. This decreases the number of variables to consider when analyzing the results of sputter deposition. Through adjusting the distance between the surface of the target and the tips of the optical fibers, further control over the nature of the thin film coating is achieved.

6. Conclusions and outlook

The fiber holder is sturdy and able to hold up to 17 single-mode optical fibers at once. It can be adjusted to hold the fibers closer or further away from the target and thus accommodates the desired outcome of the user. Future work will be to find a way to set the device so it does not rotate on the substrate, but is set in one position so each test is rotated the same angle towards the target. In conclusion, we think the design was successful. It achieves the goals set out at the on-start of building this holder. The fiber holder is capable of increasing repeatability between tests when using the sputter deposition machine.

Acknowledgements

The authors would like to thank Jonathan Rudge, the Nanofabrication Lab manager at the University of Victoria, for support and advice regarding the use of the sputter deposition machine.

For financial support the authors would like to thank NSERC Discovery, CFI JELF, BCKDF, IESVic CESAP, UNAC GreenSpaces, Electricity HR, UVic IRCPG, and the Wighton Engineering Fund.

References

[1] A. Anders, “Tutorial: Reactive high power impulse magnetron sputtering (R-HiPIMS),” *J. Appl. Phys.*, vol. 121, no. 17, 2017.

[2] D. Depla and S. Mahieu, *Reactive Sputter Deposition*. 2008.

[3] D. Lundin and K. Sarakinos, “An introduction to thin film processing using high-power impulse magnetron sputtering,” *J. Mater. Res.*, vol. 27, no. 5, pp. 780–792, 2012.

[4] R. Wuhrer and W. Y. Yeung, “Effect of target-substrate working distance on magnetron sputter deposition of nanostructured titanium aluminium nitride coatings,” *Scr. Mater.*, vol. 49, no. 3, pp. 199–205, 2003.

[5] P. J. Kelly and R. D. Arnell, “Magnetron sputtering: A review of recent developments and applications,” *Vacuum*, vol. 56, no. 3, pp. 159–172, 2000.

[6] M. Yusupov, E. Bultinck, D. Depla, and A. Bogaerts, “Behavior of electrons in a dual-magnetron sputter deposition system: A Monte Carlo model,” *New J. Phys.*, vol. 13, 2011.

[7] M. Ohring, “Materials Science of Thin Films,” in *Materials Science of Thin Films Deposition & Structure, 2nd ed.*, Second Edi., vol. 1, no. 2001, Academic Press, 2002, pp. 106–117.

[8] R. Behrisch and W. Eckstein, *Sputtering by Particle Bombardment: Experiments and Computer Calculations from Theshold to MeV energies*, vol. 110. 2007.

Simulation of wind-driven rain exposure of a heritage façade using future climate weather data

J. Bourcet [a], A. Kubilay [b*], D. Derome [c], J. Carmeliet [a]

[a] ETH Zurich, Rämistrasse 101, 8092 Zurich CH
[b] Empa - Swiss Federal Laboratories for Materials Science and Technology, Überlandstr. 129, 8600 Dübendorf CH
[c] Université de Sherbrooke, 2500, boul. de l'Université, Sherbrooke Qc CA
* Dr. Aytaç Kubilay, Aytac.Kubilay@empa.ch

Abstract:
Wind-driven rain (WDR) is a primary consideration for analyses of overall building durability in regions that receive consistent rain events such as the west coast of Canada. With recent advances in computational resources, it has become feasible to numerically model complex urban geometries and specific building features for their exposure to wind-driven rain. However, these models typically utilize current weather data and do not consider the potential changes in rain intensity that could occur due to climate change. In this study, representative weather events are selected to assess if climate change predictions will influence WDR exposure of a historical building façade. Based on climate change models (assuming an RCP8.5 Scenario), the current weather data is modified using a simplified weather morphing method to reflect the potential changes in expected WDR events. Numerical simulations of WDR are performed using the current weather data and the modified future climate data for comparison. The results show that the rainfall intensity predicted by future climate models will have an impact on the WDR exposure at various locations on the façade. This impact, along with potential changes in temperature and relative humidity, needs to be considered when analyzing building durability over the expected lifespan of the building.

Keywords:
Urban Physics, Wind-Driven Rain, Computational Fluid Dynamics, Building Durability, Climate Change

1. Introduction

With increased computational power, it is feasible to perform computational fluid dynamics (CFD) simulations not only for wind flow around a complex arrangement of buildings, but also their wind-driven rain (WDR) exposure while taking into account the effect of façade detailing. Numerical simulations of WDR patterns on building facades create significant potential for the analyses of durability of new buildings and the preservation of existing buildings, particularly those with significant historical and cultural significance. However, the results of these complex simulations are only as relevant as the data that is utilized as input into the model. Further, as these buildings are expected to continue to function for the foreseeable future, the effects of climate change has to be taken into account in their preservation and maintenance.

This paper applies a methodological framework utilizing publicly available climatic data and climate prediction models, along with open-source CFD and WDR modeling tools using an Eulerian Multiphase (EM) approach, to provide insights into the long-term WDR performance of a historically important building located in Victoria, BC.

2. Climate analysis

2.1. Real climate data synthesis

Measured climatic data is used for the current weather analysis, instead of standardized typical meteorological data. The measured data is modified using climate change model predictions to represent future weather data. Both datasets are then used to numerically simulate WDR exposure in order to predict potential effect of the climate change. It has been shown by [1] that the measured data has to be collected at 10-minute intervals (15-minute maximum) to ensure that errors related with the averaging are minimized [1]. Larger sampling rates can introduce errors unless the data is not weight-averaged [1], since large-period data could provide erroneous results for the WDR simulation as a highly intense but short duration even could be flattened to a moderate event over a full hour. Taking this criterion into account, data is collected from various weather stations in the British Columbia Capital Regional District. Unfortunately, the collection of weather data in Canada is typically done at one-hour intervals which makes data synthesis at the required frequency difficult. The University of Victoria collects weather data, specifically rain data, at 15-minute intervals.

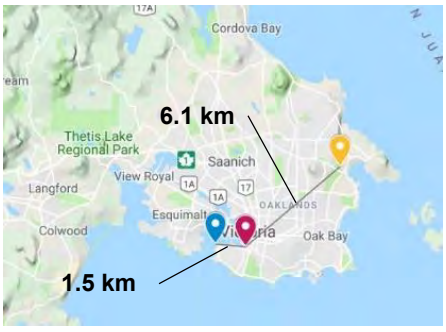

Fig 1: Weather station locations (yellow = rain, blue = wind), red is the location of the studied building) © Google Maps

Finding a compromise between the sampling rates of weather stations and their distances from the building of interest, the stations shown in Fig. 1 are chosen for the analysis. Taking the rainfall intensity data from the University of Victoria and combining it with the one-hour wind data collected at a weather station within 1 km of the building, an appropriate weather data set is synthesized, where the one-hour wind data is applied to each 15-minute interval of rain data.

2.2. Current wind-driven rain trends

An analysis of the existing weather data is performed to determine typical WDR event frequencies in the Capital Regional District over the course of three years (2016-2018). The results of this analysis are shown in Fig. 2.

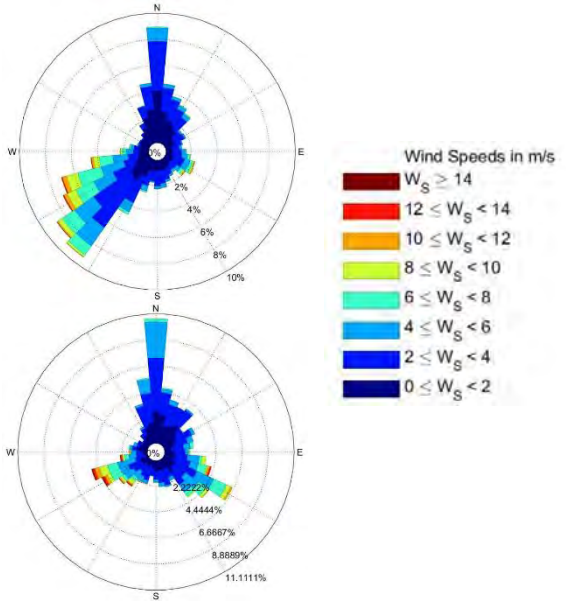

Fig 2: Wind roses from measured data considering all wind (top), and wind co-occurrent with rainfall (bottom).

Fig. 2 shows that wind from north appears to have a relatively consistent presence. Interestingly, although the majority of wind events come from the south-west and due north when including both WDR and non-WDR events, the wind events which come from the south east, while infrequent, typically come with rain whereas the wind events coming from the south west typically do not have rain events. However, when the wind is stronger from the south west, there is a higher likelihood of there being rain.

Over the three-year period 2016 to f 2018, the average annual precipitation is 680 mm, while the average rain intensity is 1.70 mm/hr, representing light rain. This analysis provides information for the next steps involving CFD simulations as only specific climate conditions need to be simulated, lowering the total calculation time.

2.3. Future climate prediction and modification

A literature review is conducted to determine if wind, rain or both are anticipated to shift due to climate change. Based on [2], [3] , it is anticipated that the effects of climate change on wind patterns and intensities will be modest. [3] notes that there is the potential for an increased number of high-intensity gust events.

Per the IPCC report on Climate Change 2013 [4], it is assumed that there will be an overall increase in global precipitation with the increase in global temperatures. Further, these changes will be subject to spatial variation with some regions receiving more rain, some receiving less, and others remaining relatively unchanged [4]. These changes in rainfall amount are included in the Canadian Earth System Model CanESM2 [5] . For this analysis, the Pacific Climate Impacts Consortium Climate Explorer tool [6] is utilized to gather climate change predictions. The CanESM2 model assuming an RCP8.5 scenario is utilized for predicting potential changes in precipitation. The RCP8.5 model is selected as it is the assumed worst-case scenario in terms of carbon production [7]. It should be noted that climate change prediction scenarios and their effects on quantities of rain vary greatly depending on the region, prediction period, and the yearly season.

Fig 3: Comparison of rainfall predictions for Victoria, BC, for RCP2.6, RCP4.5, and RCP8.5

When considering building durability, it is prudent to select worse-case scenarios as over-design reduces risks of building failure. The Capital Regional District (CRD) which includes Victoria is selected within Climate Explorer as the analysis region. As shown in Fig. 3, the RCP8.5 scenario is predicted to cause the greatest increase in the total rainfall in the CRD.

The average daily precipitation values r_h for each month are selected for current baseline model predictions, along with predictions for 2070-2099. These values are compared to provide a percentage change from baseline ($\boldsymbol{\Delta r_{h\%}}$). With this value, a modification factor ($\boldsymbol{r_{h_{mod}}}$) is calculated for each month in each timeframe (Eq.1).

$$r_{h_{mod}} = r_h \frac{\Delta r_{h\%}}{100} + 1 \qquad (1)$$

The modification factors applied to the existing weather data to create a modified dataset are summarized in Table 1.

Table 1: Predicted average daily precipitation (2070-2099) and percent change from baseline (1980-2010)

Month	Average Daily Precipitation (1980-2010) (mm/day)	$\Delta r_{h\%}$ (%)
JAN	6.05	17.31
FEB	3.92	24.71
MAR	3.33	11.34
APR	2.15	-1.29
MAY	0.98	25.52
JUN	1.12	3.85
JUL	0.61	-55.08
AUG	0.71	-62.68
SEP	1.23	-40.4
OCT	3.40	6.44
NOV	6.39	20.72
DEC	5.50	-0.03

3. Wind-driven rain analysis

3.1. Modeling of wind flow

The wind-flow simulations are performed using steady Reynolds-Averaged Navier Stokes (RANS) with the realizable k-ε turbulence model. For each wind direction, a single reference wind speed (U_{ref} = 10 m/s at 10 m height) is used for wind-flow calculations. The resulting wind-flow field is then linearly scaled for the remaining reference wind speeds (Uref = 1, 4, 8 and 18 m/s), which is allowed for high-Reynolds number flows around sharp-edged bluff bodies according to the Reynold number independence for high Re numbers. The computational model of the building along with the surrounding buildings is shown in Fig. 4. The domain size is chosen based on the guidelines given in [8] and the blockage ratio is ensured to be less than 3%.

To ensure that the approach wind flow profiles are as accurate as possible, nearby buildings are explicitly modeled. The effects of the buildings further away are taken into account through surface roughness. For the ground surface, wall functions with appropriate surface roughness modifications have been used to limit unwanted flow acceleration. The atmospheric boundary layer profiles at the inlet are based on the log-law relation which reflects the aerodynamic roughness length of a fetch of 5km upstream of the inlet.

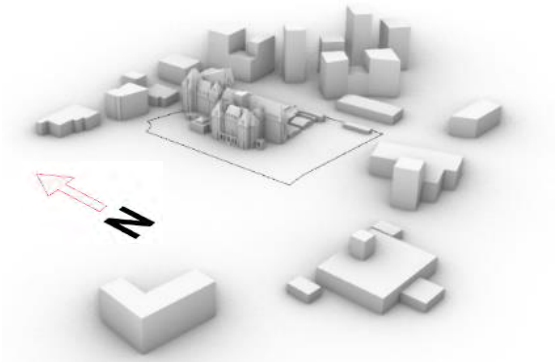

Fig 4: Building model utilized in simulation

3.2. Modeling of wind-driven rain

The WDR simulations are performed using an Eulerian Multiphase (EM) model [9]. In the EM model, rain is regarded as a continuum and the governing equations for 16 different rain phases are solved (Eq.2 and Eq.3). Each rain phase corresponds to a different class of raindrop sizes. OpenFOAM-based solver windDrivenRainFoam [9][10] is used, which solves the governing equations given in Eqs. 2 and 3, where α_k and $u_{k,j}$ denote the phase fraction and velocity of rain phase k, respectively, u_i the velocity component of wind, ρ_w the density of the raindrops, μ_a is the dynamic air viscosity, g_i the gravitational acceleration and C_d the drag coefficient.

$$\frac{\partial \alpha_k}{\partial t} + \frac{\alpha_k \overline{u_{k,j}}}{\partial x_j} = 0 \qquad (2)$$

$$\frac{\alpha_k \overline{u_{k,i}}}{\partial t} + \frac{\alpha_k \overline{u_{k,i}}\ \overline{u_{k,j}}}{\partial x_j} = \alpha_k g_i + a_k \frac{3\mu_a C_d Re_R}{4\rho_w d^2}\left(\overline{u_i} - \overline{u_{k,i}}\right) \qquad (3)$$

In Eq. 3, the terms on the right-hand side represent the gravity and the drag forces. Re_R denotes the relative Reynolds number calculated using the relative velocity between the air and rain phases. It is assumed that rain is one-way coupled with the wind [11], this follows guidelines as the volume of rain within a unit volume of air is below $1x10^{-3}$ for rain intensities up to 20 mm/hr and $1x10^{-2}$ for even higher rain intensities noted in [12]. This implies that, while the wind can influence the raindrops, the raindrops do not have a significant impact on the wind flow.

The primary concept which is utilized in the analysis of WDR simulations is the catch ratio, which provides the ratio of the amount of rain hitting a façade element over a unit area to the horizontal rain falling through a unit area. A specific catch ratio for each rain drop size can be defined as given in Eq. 4, where $R_{wdr}(k)$ and $R_h(k)$ denote the wind-driven rain intensity and the horizontal rain intensity of the k^{th} rain phase, respectively. $V_n(k)$ is the velocity magnitude of the k^{th} rain phase in the direction normal to the element and $f_h(k)$ is the probability density function of the raindrop size falling through a horizontal plane.

$$\eta_d(k) = \frac{R_{wdr}(k)}{R_h(k)} = \frac{\alpha_k |V_n(k)|}{R_h f_h(k)} \quad (4)$$

Once the specific catch ratios are calculated for a discrete number of rain drop sizes, it is possible to utilize the rain drop size probability distribution function as function of rainfall intensity by [13] to create a (global) catch ratio distribution for each unit area on the surface of the model as function of rainfall intensity, wind speed and wind direction:

$$\eta = \int_d f_h(R_h, d)\eta_d dd \quad (5)$$

4. Results and discussion

The results of the simulations are visualized to illustrate the potential difference in surface wetting between the measured data representing current weather in 2018 and the modified future weather data representing 2099. The impact of future climate on the WDR exposure of the façade is dependent on the meteorological characteristics such as average wind speed and average rainfall intensity. Therefore, instead of using a complete annual period, periods which can be more critical in terms of WDR are chosen. Table 1 shows that February will experience a large increase in rainfall intensity. Here, as an example, the results are presented for February considering rain events with a wind direction from west as the western façade is relatively more exposed.

Fig. 5 shows the catch ratio distribution determined using data from 2018, η_{2018}, which is defined as the total wind-driven rain reaching the surface, $S_{wdr,2018}$ [mm] and the total horizontal rain, $S_{rain,2018}$ [mm]. The results show that, in addition to the roof, particularly the southern edge of the façade and all chimneys receive a considerable amount of rain. Fig. 4 also indicates that there is a significant portion of the façade reaching a catch ratio around 0.3.

In order to estimate the impact of future climate on WDR exposure of the façade, Eq. (6) is defined, where $S_{wdr,2099}$ and $S_{wdr,2018}$ represent the total wind-driven rain [mm] for future and current weather, respectively.

$$\theta_S = \frac{S_{wdr,2099} - S_{wdr,2018}}{S_{rain,2018}} \quad (6)$$

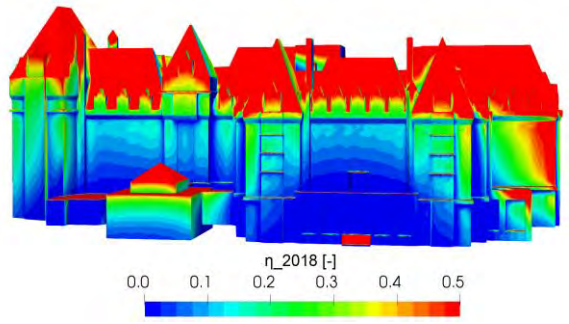

Fig 5: Catch ratio for February using current data for rain events from west.

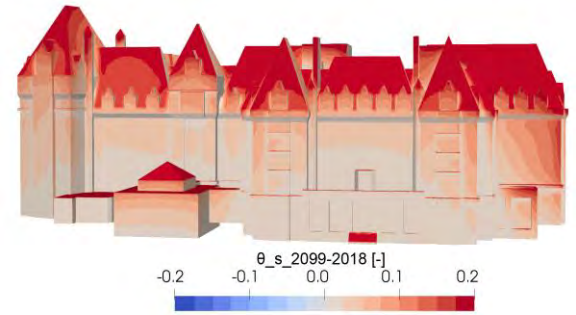

Fig 6: Relative difference in WDR exposure between future and current data for month of February.

As illustrated in Fig. 6, WDR exposure increases for almost all locations on the façade, while some façade elements show an increase in surface wetting of up to 20%. Note that the locations with the highest increase happen to be similar to the ones that already receive more rain in Fig. 5, which provides important insights into potential areas for worst-case durability problems such as rain infiltration, degradation of built in wooden elements, degradation of the mortar pointing.

5. Conclusions and outlook

As illustrated in Figs. 5 and 6, there is a non-trivial amount of difference in surface wetting of the façade between the 2018 and the modified 2099 data, particularly in specific locations and specific months. As buildings are intended to remain in service for multiple decades, consideration for future climate change will be essential for the design of their long-term durability.

In terms of hygrothermal modeling, the ability to understand both the surface wind pressure on the façade from the wind flow calculations, as well as the quantity of surface wetting from the WDR modeling, could open a new avenue for modeling wall assemblies. By modifying the model input for incidental water ingress through the façade based on the horizontal rain intensity, wind speed, and wind direction, the hygrothermal model could incorporate a more accurate “worst case” methodology which would be more reflective or real-world conditions, where water infiltration values through the façade would be specific to the location of the building. Further, by applying the modification factor methodology for changes in climate noted in section 2.3 the same model could be analyzed for current conditions as well as future weather predictions, leading to and understanding of the long-term behavior of the building façade with respect to wind-driven rain.

References

[1] B. Blocken and J. Carmeliet, “Guidelines for the required time resolution of meteorological input data for wind-driven rain calculations on buildings,” *J. Wind Eng. Ind. Aerodyn.*, vol. 96, no. 5, pp. 621–639, 2008.

[2] B. N. & A. W. SCOTT EICHELBERGER, JAMES MCCAA, “Climate Change Effects On Wind Speed,” *North Am. Wind Power* , no. June 2017, 2008.

[3] C. S. Cheng, E. Lopes, C. Fu, and Z. Huang, “Possible impacts of climate change on wind gusts under downscaled future climate conditions: Updated for Canada,” *J. Clim.*, vol. 27, no. 3, pp. 1255–1270, 2014.

[4] IPCC *et al.*, “AR5 Climate Change 2013: The Physical Science Basis — IPCC,” 2013.

[5] Environment Canada, “Environment Canada - Climate Change - CCCma: CanESM2 / CGCM4 model output,” 2019. [Online]. Available: http://climate-modelling.canada.ca/climatemodeldata/cgcm4/CanESM2/index.shtml. [Accessed: 23-Nov-2019].

[6] Pacific Climate Impact Consortium, “PCIC Climate Explorer.” [Online]. Available: https://services.pacificclimate.org/pcex/app/#/data/climo/ce_files. [Accessed: 23-Nov-2019].

[7] K. Riahi *et al.*, “RCP 8.5-A scenario of comparatively high greenhouse gas emissions,” *Clim. Change*, vol. 109, no. 1, pp. 33–57, Nov. 2011.

[8] B. Blocken, “Computational Fluid Dynamics for urban physics: Importance, scales, possibilities, limitations and ten tips and tricks towards accurate and reliable simulations,” *Build. Environ.*, vol. 91, pp. 219–245, 2015.

[9] A. Kubilay, D. Derome, B. Blocken, and J. Carmeliet, “CFD simulation and validation of wind-driven rain on a building facade with an Eulerian multiphase model,” *Build. Environ.*, vol. 61, pp. 69–81, 2013.

[10] J. Carmeliet and A. Kubilay, “Wind-driven rain solver for OpenFOAM – Chair of Building Physics | ETH Zurich,” *ETH Zurich*. [Online]. Available: https://carmeliet.ethz.ch/research/downloads/winddrivenrainfoam.html. [Accessed: 19-Dec-2019].

[11] A. Kubilay, D. Derome, B. Blocken, and J. Carmeliet, “Numerical simulations of wind-driven rain on an array of low-rise cubic buildings and validation by field measurements,” *Build. Environ.*, vol. 81, pp. 283–295, 2014.

[12] D. A. De Wolf, “On the Laws-Parsons distribution of raindrop sizes,” *Radio Sci.*, vol. 36, no. 4, pp. 639–642, Jul. 2001.

[13] A. C. Best, “The size distribution of raindrops,” *Q. J. R. Meteorol. Soc.*, vol. 76, no. 327, pp. 16–36, Jan. 1950.

Why Wood – Building the case for more wood education

1. Reed Kelterborn, P.Eng.[a]

[a] National Education Manager, Canadian Wood Council
* 613.747.5544 ext. 235, rkelterborn@cwc.ca

Abstract:
Canada's forests are an effective carbon sequestration tool that can play an integral role in mitigating climate change. Wood products, and the sustainably managed forests they come from, naturally create an endless cycle of carbon absorption and storage. Meanwhile, productivity in the construction sector is stagnant. As the industry looks to improve efficiencies, it is challenged with skilled labour shortages and increasing costs. Prefabrication and other industrialized building processes are creating promising opportunities for wood construction. These opportunities are further magnified through advanced engineered wood materials and sophisticated fabrication technologies that are re-shaping the ways buildings are planned, designed, and constructed. These advances in wood construction technology are also facilitating increasingly larger, and taller, wood structures in denser urban areas.

A challenge is that the design and construction industry are dominated by concrete and steel, with greater focus traditionally devoted to those materials in Canada's post-secondary education curriculum. More wood focused education is needed so that when new design and construction professionals enter the workforce, they have the required skillsets to plan, design, fabricate, and assembled advanced wood structures. Increasing market demand for Canadian wood products, which in turn helps to mitigate climate change through sequestration and substitution. Wood design and construction curriculum is expanding across Canada driven in part by the existing shift to more efficient industrialized construction.

Keywords:
Wood, education, sustainability, industrialized construction, curriculum development

1. Introduction

The Canadian Wood Council's Advanced Wood Education Roadmap program aims to address knowledge and skills gaps with a focus on supporting post-secondary educators, and students, by developing curriculum and additional learning resources. The goal is to help students, our future engineers, architects, and builders, obtain the knowledge and skillsets required to design and construct the modern wood structures needed to help mitigate climate change. This effort also advances the existing paradigm shift to more efficient industrialized construction.

2. Why we need more wood education

2.1 Sustainability in Construction

Wood products, and the sustainably managed forests they come from, play an essential mitigating role in climate change. Forests are one of the Canada's greatest carbon sequestration tools, and sustainable forestry naturally creates an endless cycle of carbon absorption and storage. As trees grow, they absorb carbon dioxide from the atmosphere, storing the carbon in their wood fiber, roots, leaves, needles, and surrounding soil. In exchange trees release oxygen back into the atmosphere for humans to breathe. Young, vigorously growing trees absorb the most carbon dioxide, with the absorption rate slowing as they reach maturity.

When trees die and begin to decay, or when forests are lost to wildfire, insect attack or disease, the stored carbon is released back into the atmosphere. In sustainably managed forests the trees are harvested before the end of this lifecycle and the carbon remains captured in the wood products made from the felled trees. For each tree that is felled approximately 4 are planted in its place, and less than 0.2% of Canada's 347 million hectares of forest are harvested annually [1]. Wood products and building systems can store large amounts of carbon, for example 1m^3 of SPF lumber stores approximately 1 tonne of CO_2 equivalent.

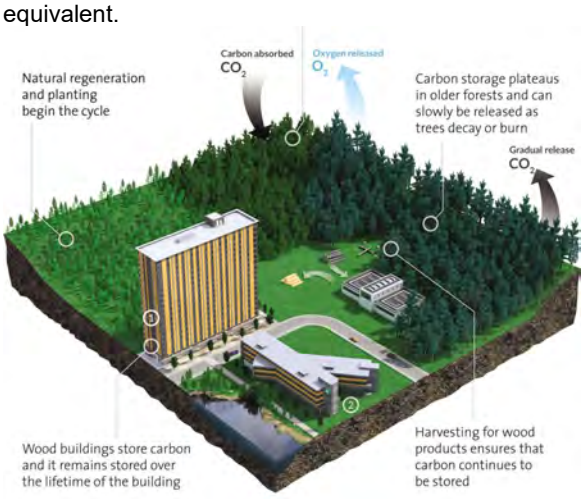

Fig 1: Growing forests absorb carbon dioxide and release oxygen. *Image courtesy of naturallywood.com*

2.2 Productivity in Construction

In addition to the environmental benefits of building with wood, there is also promising economic incentive as wood's respectable strength to weight ratio and ease of processing lends itself well to more efficient

industrialized construction processes, including prefabricated elements and modular construction. This is significant as productivity in the construction industry is historically weak. In the United States, labour productivity in construction has declined since 1968 [2], in contrast to rising productivity in other sectors.

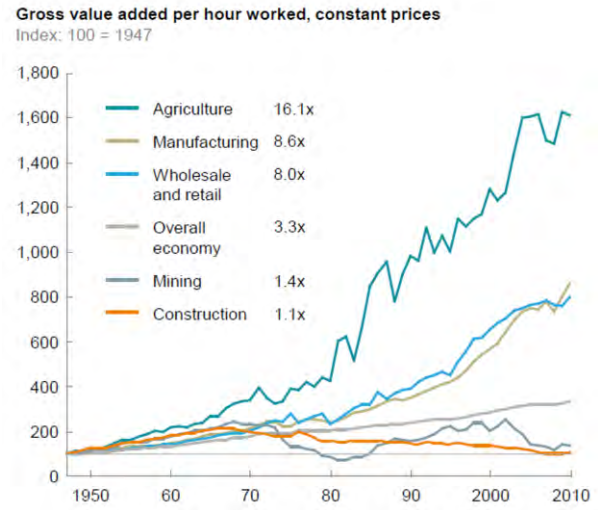

Fig 2: Many sectors have transformed and achieved huge advances in productivity; construction is a laggard and has changed very little since 1947, limiting productivity gains [2].

Mass timber products like CLT that can be made in a factory to high tolerances with CNC'd connections and M.E.P. routing represents a new opportunity for industrialized construction processes. Incorporating the concept of Design for Manufacture and Assembly (DfMA) a design approach that focuses on ease of manufacture and efficiency of assembly, which has long been used in automotive and consumer products manufacturing, can create a boost in construction productivity in the order of 5x to 10x [3]. Wood construction, specifically mass timber, embodies this systems approach where the structure is design from the beginning with the intention of being prefabricated off-site and then assembled on-site as a kit of parts.

Fig. 3: A CLT floor panel is craned in to place during construction of the 18-storey Brock Commons student residence at UBC. *Image courtesy of ThinkWood.com and KKLaw.*

It is important that future architects, engineers, and builders have knowledge in wood design and construction as a significant amount of new infrastructure is required to meet the needs of a growing population. Globally, the World Bank, predicts that 300 million new housing units will need to be constructed in the next 10 years [4]. To meet this demand it is estimated that 15-20% of all construction in the US and Europe will need shift to more productive modular or off-site processes by 2030 [5]. This represents a huge potential opportunity for wood construction given its desirable characteristics in those applications.

3. How to expand wood education in Canada

The focus of the Advanced Wood Education Roadmap is to support and expand the existing efforts of Canadian post-secondary institutions and avoid duplicating them. Through the planned initiatives the aim is to help fill the gaps that exist in traditional curriculum and encourage students to study wood design and construction. The program consists of three focus areas, namely outreach and engagement, curriculum development, and thirdly tools, support, and technology transfer.

3.1 Outreach and Engagement

Expanding wood education at the post-secondary level requires connecting with, and supporting, an engaged network of enthusiastic educators. This is the supply side of the network, with qualified educators who can equip future architects, engineers, and construction professionals with the right wood design and construction skillsets. A new website at woodSMART.ca will serve as a mechanism to connect educators and disseminate newly developed teaching resources. The website will host the Resource Hub containing up-to-date course content and teaching resources, that are freely available to any educator in Canada. In addition, a peer-to-peer networking app called Wood Expert Exchange, or woodEX, is scheduled to launch in March, 2020. This tool will help connect educators to design professionals through an online database that will facilitate learning through interaction.

Fig. 4: The National Workshop on Wood Education was held in Ottawa, ON in February 2020 where the leading wood educators and practitioners participated

in strategic and tactical discussions to expand wood education in Canada.

The opposite side of the equation, the demand side, requires connecting with students to build excitement around taking wood design and construction courses. This is done by increasing the awareness of the benefits of building with wood and promoting the potential career path advantages. To facilitate this engagement with students, the Advanced Wood Education Roadmap supports in-class guest lecturers where leading practitioners can challenge the student's perception of what is possible with wood construction. Sponsorship of events like NHICE-02, where advanced wood buildings can be showcased as the future of construction and not the past, help increase student awareness.

3.2 Curriculum Development

Currently, most post-secondary design and construction curricula focuses on concrete and steel. More wood education content is needed so new graduates are familiar with the knowledge of wood design and construction. New and up-to-date course content for architecture, engineering, and construction management programs are being developed with the help of expert practitioners and leading educators. All the material including lectures, presentations, and design examples, will be freely available through the Resource Hub on woodSMART.ca.

Fig. 5: 3-storey Mass Timber Office Building design example, freely available to educators through woodSMART.ca shortly, with full engineering calculations, construction documents, and a detailed Revit model.

A 2-step approach has been taken to implement this initiative. Firstly, a discovery exercise consisting of a needs assessment study for architecture and engineering curriculum was conducted to better understand what knowledge new graduates need when entering the workforce and what resources educators require to be able to teach those skills. The second step is developing tailor made course content, informed by the needs assessment studies combined with regular engagement with educators and practitioners. This material will then be readily available to educators. With a goal of making easier for educators and institutions to deliver wood design and construction courses. Either starting from the beginning with a new course or enhancing an existing offering.

3.3 Tools, Support, and Tech Transfer

Wood design and construction technology is progressing so quickly that knowledge transfer is often a bottleneck for growth. New tools and resources can help educators equip students with the current in-demand skillsets. To assist with this knowledge transfer 3 new teaching manuals are being developed for architecture, engineering, and construction management programs respectively.

Introduction to Wood Design for Architects will focus on the historical relevance of wood construction in North America. Discussing early indigenous typologies through to modern light wood frame and mass timber building systems. The Advanced Wood Engineering Manual will include content that goes beyond current Canadian and North American wood standards provisions and will constitute a state-of-the-art resource for structural wood design. The new textbook will address the growing knowledge gaps to help equip graduate level engineering students and practising engineers with the expertise to design increasingly larger, taller, and more complex wood structures. A third manual, the Builder's handbook, will focus on planning, procurement, fabrication, and assembly considerations for non-residential wood buildings, specifically low-rise commercial, mid-rise multi-family and tall wood typologies.

To further support in class instruction new case studies with BIM resources for low-rise commercial, mid-rise multi-family, and tall wood structures are in development. Detailed Revit models will permit interactive and dynamic learning, allowing students to visualize how the different systems work and better understand the construction processes.

Fig. 6: Defi Cecobois Student Design and Build competition facilitates interdisciplinary collaboration and applying design principles learned in class.

Student competitions are recognized by educators, practitioners, and students as a very effective way to explore interdisciplinary collaboration, apply design principles learned in class, understand constructability issues, engage future employers, and learn about career path options. A national scale student design and build competition is currently under development. Existing competitions including TimberFever

presented by Moses Structural Engineers and Defi Cecobois will be continuing to be supported.

4. Conclusions and outlook

The construction of the built environment is changing. The shift to more sustainable, and industrialized, construction processes require that new architecture, engineering, and construction management graduates know more than just concrete and steel as building materials. The Canadian Wood Council's Advanced Wood Education Roadmap aims to expand wood education resulting in an increased market demand for Canadian wood products, support for job growth, promotion of innovation in research and technology, and mitigation of climate change through carbon sequestration and substitution.

Acknowledgements

The author would like to thank Natural Resources Canada, ThinkWood.com, NaturallyWood.com, and the Canadian Wood Council.

References

[1] Beaudoin, A., et al. Species composition, forest properties and land cover types across Canada's forests at 250m resolution for 2001 and 2011. Natural Resources Canada–Canadian Forest Service, Laurentian Forestry Centre, Quebec, Canada. (2017).

[2] Filipe Barbosa et al. McKinsey Global Institute Reinventing Construction: A Route to Higher Productivity (2017) 23.

[3] Filipe Barbosa et al. McKinsey Global Institute Reinventing Construction: A Route to Higher Productivity (2017) Contents In Brief.

[4] Gloria M. Grandolini et al. World Bank "Housing for All" (2016).

[5] Michael Chui et al. McKinsey Global Infrastructure Initiative, The Impact and opportunities of automation in construction (2019) 5.

Morphing Weather Data for Climate Resilient Building Design: A Study on Lifetime Thermal Comfort, Energy Demand and Energy Consumption

M. Fakoor[a]

[a] RJC Engineers Ltd., Vancouver, Canada
* Corresponding author, +1 (778) 865 5040, mfakoor@rjc.ca

Abstract:
Projected and "morphed" weather data have been used in this research to investigate the lifetime thermal comfort, building thermal energy demand, and building energy consumption of a representative building. Currently, there is a lack of understanding regarding building performance/occupant thermal comfort in British Columbia under future extreme conditions. Such extreme events will become more common in the future as a result of climate change. As such, a low-rise multi-unit residential building (MURB) has been considered for energy simulation. The studied building is a naturally cooled building with electric baseboard heaters for heating and central gas-fired condensing boilers for the domestic hot water system. The project is located in Victoria, British Columbia (ASHRAE climate region 4C). The CWEC weather file referenced in the City of Vancouver (COV) Energy Modeling guideline (EMG) has been used as the baseline case. Subsequently, the most recent climate projections from Intergovernmental Panel on Climate Change (IPCC) referred to as Representative Concentration Pathways or RCPs have been used. As such, RCP 8.5 and RCP 4.5 are used to simulate the building at different periods namely 2020-2040, 2050-2070, and 2080-2100 represented by 2030, 2060 and 2090 for each time slice, respectively. Mid-point, and upper tail warmings of 50th and 90th percentiles of RCPs for each period are used to analyze long-term occupant thermal comfort and to determine life-time thermal and energy demand intensity of the building. The results of this study demonstrate a significant occupant thermal discomfort in naturally cooled buildings under future weather data, and a dramatic decrease in the thermal energy demand intensity of the buildings.

Keywords:
Climate Change, Morphed Weather Data, Building Simulation, Thermal Comfort, Energy Modeling.

1. Introduction

The scientific consensus is that our global climate is rapidly changing mainly due to anthropogenic greenhouse gas emissions which have increased significantly since the pre-industrial era, and more recently break historical records [1]. These changes directly impact the application of building science to the development of our built environment [2]. Buildings designed or retrofitted today will see dramatically different climates in future. Considering the rapidly changing environment, three main design/retrofit strategies must be considered for buildings: i) climate resilient building enclosures; ii) adaptability to future extreme weather conditions; and iii) mitigation of the detrimental impacts of climate change on building enclosures.

Whole building energy simulation is an important tool to analyze the performance of building enclosures and passive and active systems for heating and cooling. The foundation of the energy model is climate data which significantly impacts the relationship between building enclosure, mechanical systems, passive systems and surrounding environment. Historical weather data, based on a typical meteorological year (TMY), are currently used for building simulation and code compliance modeling. In addition, most building rating systems rely on energy simulations with historical weather data to develop new energy codes and validate baseline conditions for comparison. However, such weather data does not represent projected trends, nor account for variability in future climate conditions [3], i.e., designing buildings for typical/historical conditions leads to future vulnerability. The weather files that are currently used for energy simulation in British Columbia are CWEC files which are outdated and are almost 10 years old.

The concept of TMY was first introduced by Hall *et al*. [4] which is based on concatenating typical meteorological months (TMM) over a given period to create the weather file for a year. Belcher *et al*. [5] developed "morphing" methodology that generates future weather data by downscaling coarse resolution global circulation models to the fine spatial and temporal resolutions (hourly) required for building performance simulations. There are also other techniques to develop future weather data such as dynamical downscaling, synthesizing weather data, and interpolation which are computationally expensive or deal with large data sets, which seem unlikely to be practical for building energy simulation [5, 6].

Robert and Kummert [7] studied a net-zero energy building, and demonstrated that the net-zero target of the project might not be achievable under future weather data. They remarked on the importance of considering future weather data to assure the building is on track with its energy target over its lifetime.

Moazami *et al*. [8] studied an energy retrofit of a day care center for current and future weather scenarios. Several strategies were developed to assure occupant thermal comfort under future warmer weather data. Ek *et al*. [9] used a morphing technique to generate future weather data to simulate the thermal performance of a 22-storey multi-unit residential building in Vancouver, Canada. The morphing technique in [9] is based on daily rather than monthly projections. In addition, thermal comfort and risk analysis of heating/cooling systems were not in the scope of [9]. Moreover, United States Green Building Council (USGBC) recently conducted a study [10] to determine the impacts of climate change on building energy performance in different regions in the USA. It was pointed out in [10] that multiple climate files must be used in the process of designing a building to account for future extreme conditions.

Our literature review indicates that for residential buildings in British Columbia, there is no study on:

- Future energy consumption of naturally cooled buildings,
- Thermal comfort under future weather data,
- Risk analysis for heating systems under projected extreme conditions,
- Thermal energy demand intensity under future weather data.

The main objective of this study is to demonstrate that we are currently designing building enclosures for the past, not for the future, leading to future vulnerability.

2. Methodology

The future weather files in this study have been obtained from the WeatherShift™. Each set of future weather files contain three files for the specified location (Victoria), time period and emission scenario (RCP), one each at the 10th, 50th, and 90th percentiles of warming for that period. These weather files have been derived from a larger ensemble of climate projections. The 50th percentile file represents the warming midpoint for that ensemble, i.e., half of the projections are warmer and half are cooler. It is necessary to consider different warming percentiles due to inherent uncertainty of future climate. It is not clear which file closely matches the actual future climate so this represents a risk management approach for thermal comfort and energy simulation of buildings. Since the building under study is naturally cooled, we only considered 50th and 90th percentiles of warming as median and worst case scenarios, respectively.

Another source of uncertainty is the amount of future emissions of Greenhouse Gases (GHG). For the Fifth Assessment projections, the IPCC defined several scenarios as Representative Concentration Pathways (RCPs). The two mandatory RCPs were RCP 4.5 and RCP 8.5. It should be noted that RCP 4.5 can be considered as moderately aggressive mitigation scenario with GHG concentrations stabilizing shortly after 2100. The current pledges under Paris agreement (RCP 2.5) for reduced emissions are less than those required by RCP 4.5. In addition, RCP 8.5 represents a “business as usual” case with GHG emissions continue to increase throughout the 21st century [12].

Building simulations are performed in this study using IES VE 2019 software package. The thermal bridging calculations are performed per the requirements of Building Envelope Thermal Bridging Guide Version 1.2. The building under study is a mixed-use 6-storey wood-framed building with 4460 [m^2] of Gross Floor Area. To assess the performance and thermal comfort of the building under CWEC and future weather data, 50th and 90th percentiles of warming of RCP 8.5 and RCP 4.5 are used. The energy simulations are done for CWEC (baseline), 2020-2040, 2050-2070, and 2080-2100 time slices. Figure 1 demonstrates a schematic of the building in the energy simulation and a floor plate of the top floor showing the critical zone for thermal comfort (South-West facing). The building envelope assemblies and details are designed to meet the requirements of Step 4 of the BC Energy Step Code for the residential portion and Step 3 for the Commercial portion, i.e., net-zero energy ready. Table 1 represents the main building enclosure and mechanical systems of the building.

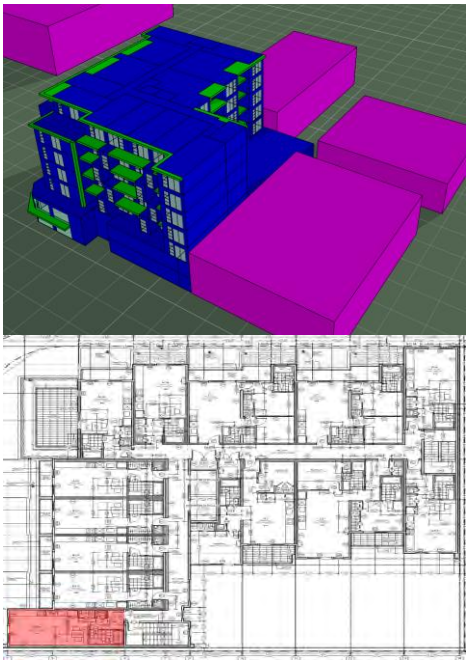

Fig 1: A schematic of the building simulation in IES VE and top floor plate with highlighted critical zone for thermal comfort

It should be noted that for each suite two top hung windows with 30° opening above the guardrail and sliding doors are modeled in the Macro Flow module of IES VE to perform the thermal comfort analysis.

Table 1: Description of the building enclosure and mechanical systems to meet net-zero energy ready per the BC Energy Step Code

Exterior walls	3'' exterior mineral wool, R-22 batt (R-27+ Effective)
Roof	8'' XPS (R-40+ Effective)
Slab-on-grade	5'' XPS under Slab (R-25+ Effective)
Windows	Triple-glazed fiberglass, U-0.18; SHGC 0.25
Heat Recovery Ventilator	80% SRE with bypass damper
DHW	Gas-fired condensing boiler with 96% efficiency
Heating system	Electric baseboard heaters

3. Results and Discussions

Figure 2 illustrates the monthly outdoor air average dry bulb temperature for baseline (CWEC) and future weather data for RCP 8.5 90th percentile for the time slices represented by 2030, 2060, and 2090. As seen in Fig. 2, the monthly average temperature increases significantly based on the RCP 8.5 or "business as usual" case. In particular, for the month of August the average temperature increases from 15.46 to 23.6 °C, i.e., over 8 °C temperature increase in Victoria by the end of this century if no GHG mitigation scenario is taken into account.

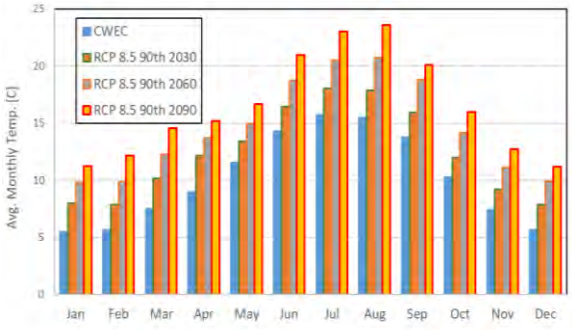

Fig 2: Average monthly outdoor dry bulb temperature for the baseline (CWEC) and RCP 8.5 90th percentile for different studies periods.

Figure 3 represents the yearly average temperature for the baseline (CWEC), RCP 8.5, and RCP 4.5 50th and 90th percentiles for different studied periods. Based on Fig 3, it can be concluded that i) The yearly average temperature estimated by different climate scenarios is much higher than the baseline CWEC value (10.16 °C); ii) the rate of increase in the average temperature associated with RCP 4.5 is significantly lower than RCP 8.5 and start to stabilize by the end of this century; iii) the yearly average temperature at the time slice represented by 2060 for RCP 4.5 90th percentile is higher than that for RCP 8.5 50th percentile.

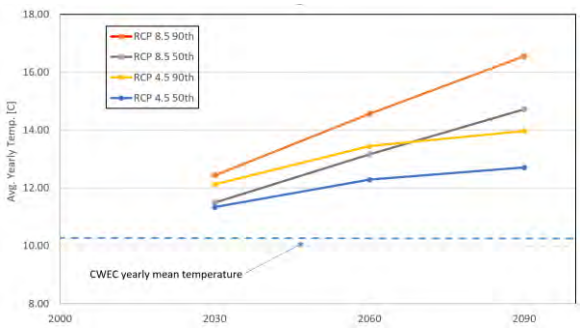

Fig 3: Yearly average temperature for baseline (CWEC), RCP 8.5 and RCP 4.5 50th and 90th percentile for different studied periods.

A comprehensive thermal comfort analysis is done in this study to reduce the unmet cooling hours in the critical zone, see Fig 4. As such, the initial window design is altered to have large openings via sliding doors and top-hung windows. The unmet cooling hours for the CWEC file is determined to be 40 hours. This complies with the requirements of the COV EMG version 2 Section 4, i.e., less than 200 unmet cooling hours. However, the thermal comfort study under future weather data demonstrates significantly higher unmet cooling hours (or occupant thermal discomfort) under projected warmer weather data. As such, the unmet cooling hours for RCP 8.5 90th percentile for 2080-2100 is calculated to be 280 hours showing a 7-fold increase in the unmet cooling hours as a result of future warmer climate data for Victoria. Therefore, it is recommended to reduce the 200-hour threshold of the COV EMG to about 20 hours to mitigate the future impacts of climate change on the occupant thermal comfort.

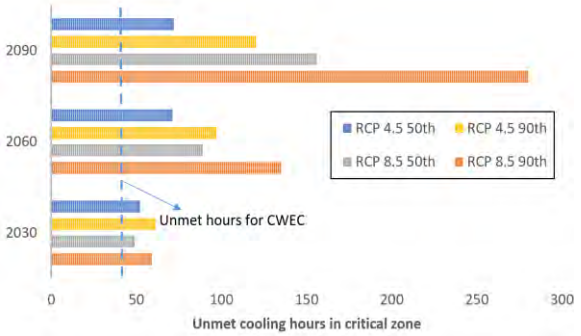

Fig 4: Unmet cooling hours under baseline (CWEC), RCP 4.5 and RCP 8.5 50th and 90th percentiles in the critical zone with highest thermal comfort issue.

Figure 5 illustrates the thermal comfort study that is done per ASHRAE 55-2017. As shown in Fig 5, the indoor operative temperatures in the critical zone fall out of the upper ASHRAE 55 acceptability limit for around 280 hours under RCP 8.5 90th percentile for 2080-2100 period as mentioned before for Fig 4.

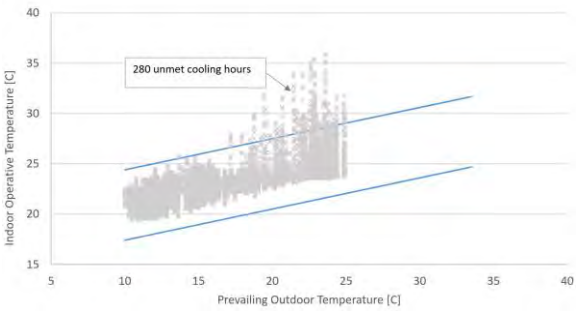

Fig 5: Unmet cooling hours for the critical zone per ASHRAE 55-2017 under RCP 8.5 90th percentile for 2080-2100 period.

Figure 6 depicts the thermal energy use intensity of the building under different climate scenarios. As seen in Fig 6, the TEUI of the building under CWEC (baseline) weather data is calculated 93.13 [kWh/m^2/year] while TEUI for this building under RCP 8.5 90th percentile over 2080-2100 is calculated 75 [kWh/m^2/year]. This represents almost 20% reduction in the building energy use due to warmer future weather data.

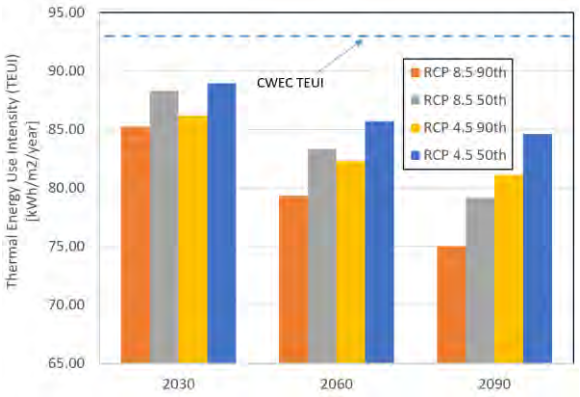

Fig 6: Building Thermal Energy Use Intensity (TEUI) under different climate scenarios.

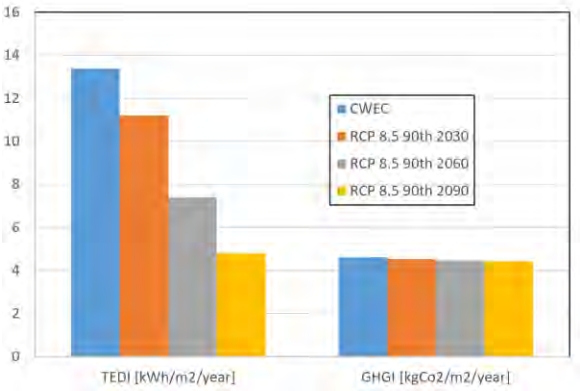

Fig 7: Thermal Energy Demand Intensity (TEDI) and Greenhouse Gas Intensity (GHGI) under baseline (CWEC) and RCP 8.5 90th percentile over different studied periods.

Figure 7 shows the Thermal Energy Demand Intensity (TEDI) and Greenhouse Gas Intensity (GHGI) for the baseline (CWEC) and RCP 8.5 50th and 90th percentile over studied periods. It is clear that TEDI decreases significantly over time under future projected weather data, i.e., from 13.39 to 4.42 [kWh/m2/year]. This translates to approximately 66% decrease in TEDI under RCP 8.5 90th percentile over 2080-2100. In addition, GHGI remain almost constant since electricity in BC has very low emission factor and its reduction does not affect GHGI considerably. We assumed the DHW demand is similar under different periods and studied scenarios.

4. Conclusions and outlook

A life-time thermal comfort and energy study is performed for a naturally cooled 6-storey wood-framed building under future weather data. The building enclosure and mechanical systems are designed to have a net-zero energy ready building per the requirements of the BC Energy Step Code. The results of this study demonstrate that the unmet cooling hours increase approximately by 7 fold under projected weather data. In addition, it is observed that the Thermal Energy Demand Intensity (TEDI) of the building decreases approximately 66% under projected weather data by the end of this century.

References

[1] IPCC, Climate change 2014 : Synthesis report. Summary for policy makers, (2014) 1-31.
[2] L. Troup, D. Fannon, Morphing climate data to simulate building energy consumption, ASHRAE and IBPSA-USA Simbuild (2016).
[3] N. Kegel, Climate change in Canada : impacts on building energy use intensity, IES Ltd.
[4] I.J. Hall, R.R. Prairie, H.E. Anderson, E.C. Boes, Generation of a typical meteorological year, Sandia Lbas (1978).
[5] S.E. Belcher, J.N. Hacker, D.S. Powell, Constructing design weather data for future climates, Building Services Engineering Reasearch and Technology 0 (2017) 1-26.
[6] V.M. Nik, J. Arfvidsson, Using typical and extreme weather files for impact assessment of climate change on buildings, Energy Procedia 132 (2017) 616-621.
[7] A. Robert, M. Kummert, Designing net-zero energy buildings for future climate, not for the past, Building and Environment 55 (2012) 150-158.
[8] A. Moazami, S. Carlucci, F. Causone, L. Pagliano, Energy retrofit of a day care center for current and future weather scenarios, Procedia Engineering 145 (2016) 1330-1337.
[9] M. Ek, T. Murdock, S. Sobie, B. Cavka, B. Coughlin, R. Wells, Future weather flies to support climate resilient building design in Vancouver, NHICE-01 (2018).
[10] L. Larsen et al., Green building and climate resilience : understanding impacts and preparing for changing conditions, US Green Building Council (2015).
[11] City of Vancouver Energy Modeling Guideline, Version 2 (2018).
[12] Agros Analytics, Guidelines for specifying WeatherShiftTM future weather files.

Future Context for Retrofitting Existing Buildings: Impacts of A Changing Climate on Energy Conservation Measures

M. Fakoor[a]

[a] RJC Engineers Ltd., Vancouver, Canada
* Corresponding author, +1 (778) 865 5040, mfakoor@rjc.ca

Abstract:
Climate change will significantly impact the energy conservation measures that we implement in today's building energy retrofit projects. As a result, it is crucial to consider the forthcoming changes and extreme conditions in retrofitting building envelopes for the sake of a resiliently built environment. The main objective of this paper is to determine the effects of energy conservation measures on the energy use of a building for current and future climate. As such, an energy study was performed for Building D of the University of Fraser Valley (UFV) in Abbotsford. As part of the energy study, a whole building airtightness test with multiple blower fans was performed to evaluate the airtightness of the building. An energy model was then calibrated based on monthly energy use over a 4-year period. After validating the numerical model and based on the discussions with UFV, several strategies were considered as Energy Conservation Measures (ECMs) for the project. The most recent climate projections from IPCC referred to as Representative Concentration Pathways or RCPs have been used. As such, RCP 8.5 with mid-point tail warmings of 50th percentile was used to determine the energy use of the building for the time slice of 2080-2099. It has been shown that the cooling load of the building will increase significantly by the end of this century due to improved building envelope and warmer Climate. It is demonstrated that the current retrofit strategies lead to 10% energy saving under current climate, but this will drop to around 5.5% saving under future warmer climate due to the increase in the cooling load of the building.

Keywords:
Building Energy Retrofit, Climate Change; Morphed Climate; Building Simulation; Energy Conservation Measures; Energy Modeling

1. Introduction

Climate change is occurring and buildings designed or retrofitted today will see dramatically different climates in future. The rapid change in climate is mainly due to anthropogenic greenhouse gas emissions which have increased significantly since the pre-industrial era [1]. Canada is committed to reducing its GHG emissions by 30% below the 2005 level of 732 Mt CO2 eq by 2030 [2]. As such, stringent contemporary energy standards have been adopted by different provinces across Canada, e.g., BC Energy Step Code, Toronto Green Standard V3, NECB 2017 in Alberta. For existing buildings, federal, provincial, and territorial governments will work to develop a model code for existing buildings by 2022; this code will help guide energy efficiency improvements that can be made when renovating buildings [2].

Considering the rapidly changing environment, three main retrofit strategies must be considered for buildings: i) climate resilient building enclosures; ii) adaptability to future extreme weather conditions; and iii) mitigation of the detrimental impacts of climate change on building enclosures.

Whole building energy simulation is an important tool to analyze the performance of building enclosures and passive and active systems for heating and cooling. The foundation of the energy model is climate data which significantly impacts the relationship between building enclosure, mechanical systems, passive systems and surrounding environment. Historical weather data, based on a typical meteorological year (TMY), are currently used for building simulation and code compliance modeling. In addition, most building rating systems rely on energy simulations with historical weather data to develop new energy codes and validate baseline conditions for comparison. However, such weather data does not represent projected trends, nor account for variability in future climate conditions [3], i.e., retrofitting buildings for typical/historical conditions leads to future vulnerability. The weather files that are currently used for energy simulation in British Columbia are Canadian Weather Year for Energy Calculation (CWEC) files which are outdated and are almost 10 years old.

Robert and Kummert [4] studied a net-zero energy building, and demonstrated that the net-zero target of the project might not be achievable under future climate. They remarked on the importance of considering future climate to assure the building is on track with its energy target over its lifetime. Moazami *et al*. [5] studied an energy retrofit of a day care center for current and future weather scenarios. Several strategies were developed to assure occupant thermal comfort under future warmer climate. Chen *et al*. [6] performed an investigation on the feasibility and

importance of considering climate change impacts in building retrofit analysis. They concluded that the optimal retrofit strategy of selecting the best Energy Conservation Measures (ECM) combinations under current climate condition will be subject to change in the future climate condition.

Ek *et al*. [7] used a morphing technique to generate future metrological data to simulate the thermal performance of a 22-storey multi-unit residential building in Vancouver, Canada. The morphing technique in [7] is based on daily rather than monthly projections. Shanks [8] performed a study on Retrofit Options to Reduce Climate Change Impacts on United Arab Emirates (UAE) Building Cooling Demand. It is pointed out that retrofit technologies that address conductive heat gain, through glazing and external walls, are the most resilient to projected climate changes whilst those that address solar gain provide the greatest overall reduction in cooling demand.

Our literature review indicates that for existing buildings in British Columbia, there is a lack of understanding on:

- Effects of future metrological data on energy retrofit strategies,
- Cooling energy use intensity under future climate.
- Resilient energy conservation measures (ECMs) for current and future warmer climate.

The main objective of this study is to demonstrate that the changing climate must be considered in our retrofit strategies. We are currently retrofitting building enclosures for the past, not for the future, leading to future vulnerability.

2. Methodology

The future metrological data for this study has been obtained from the WeatherShift^{TM}. The metrological data have been derived from a larger ensemble of climate projections. The 50th percentile file used in this study represents the warming midpoint for that ensemble, i.e., half of the projections are warmer and half are cooler. One of the sources of uncertainty is the amount of future emissions of Greenhouse Gases (GHG). For the Fifth Assessment projections, the IPCC defined several scenarios as Representative Concentration Pathways (RCPs). The two mandatory RCPs were RCP 4.5 and RCP 8.5. It should be noted that RCP 4.5 can be considered as moderately aggressive mitigation scenario with GHG concentrations stabilizing shortly after 2100. The current pledges under Paris agreement (RCP 2.5) for reduced emissions are less than those required by RCP 4.5. In addition, RCP 8.5 represents a "business as usual" case with GHG emissions continue to increase throughout the 21st century [9].
This study is performed to investigate the energy performance of the existing building, and to identify system modifications and/or synergies that can aid in reducing overall building energy consumption, and/or improving occupant comfort when undertaking system renewals. As such, the energy study was done as follows:

- A "whole building air-tightness" testing was performed to determine the air leakage rate of the existing building and to input into the energy model.
- A "whole building energy modeling" was performed using IES VE 2019 software program and calibrated based on the utility data of the past 4 years.

The building under study is a 3-storey building with 5,740 [m^2] of gross floor area; 2 floors of lecture rooms and 1 floor of offices. Figure 1 depicts a schematic of the building modelled in the energy modelling software. Table 1 represents the main building enclosure and mechanical systems of the existing and proposed buildings.

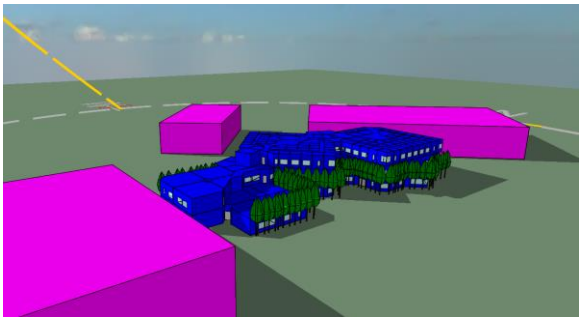

Fig 1: A schematic of the building simulation in IES VE 2019

Table 1: Description of the building enclosure and mechanical systems for the existing and proposed buildings

	Existing BLDG	**Proposed BLDG**
Exterior walls	4'' semi-rigid insulation with thermally broken clips, 6'' steel-framed walls with R-20 batt inside cavities	6'' steel-framed walls with R-20 batt inside cavities
Roof	4'' XPS	
Slab-on-grade	24'' vertical rigid insulation (R-8)	
Windows	Non-thermally broken aluminum windows: U0.65 SHGC 0.4	Thermally broken curtain wall system: U0.38 SHGC 0.4
Heating System	Central AHU with VAV terminal units	
Central Plant (heating)	Non-condensing gas-fired boilers 80% E_t	Condensing gas fired boilers, 94% E_t
Central Plant (cooling)	Air cooled chiller (EER 12.9)	

DHW	Gas-fired water tank with 80% efficiency	Tied into space heating boilers
Air Leakage Rate [L/s/m^2]	0.27 [L/s/m^2] @ operating pressure per actual test	30% reduction

The airtightness test was performed following the requirements of ASTM E779-2019 using 4 fans distributed across two test stations. All the outside air intake/exhaust vents were sealed from outside. Figure 2 shows the two test stations, and sealed mechanical vents.

Fig 2: Views of the two test stations (total of 4 fans), and sealed mechanical systems

3. Results and Discussions

Monthly utility bills were used to calibrate the energy model and to weather normalize the energy consumption of the building. The following figures show the energy consumption by reading period graphically. Heating and cooling degree days have also been represented on the graphs. Figure 3 represents monthly natural gas use intensity from January 2014 to December 2018. The heating degree days have also been shown in this graph. As seen in Figure 3, the natural gas consumption increases in winter time due to the increase in the heating load. Figure 4 demonstrates monthly electricity use intensity based on the utility data from January 2014 to December 2018. The cooling degree days have also been shown in this graph. As seen in this figure, the electricity consumption increases in summer time due to cooling demand of the building.

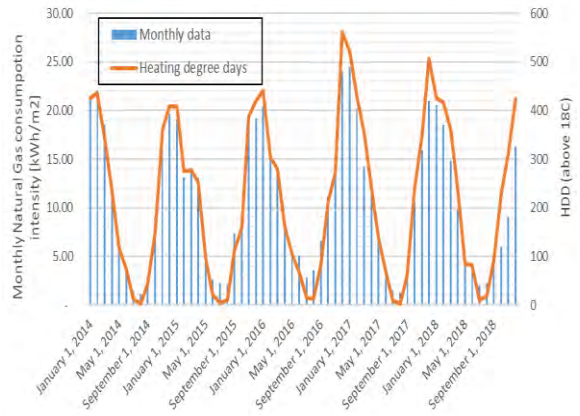

Fig 3: Monthly natural gas use intensity and HDDs (base 18˚C)

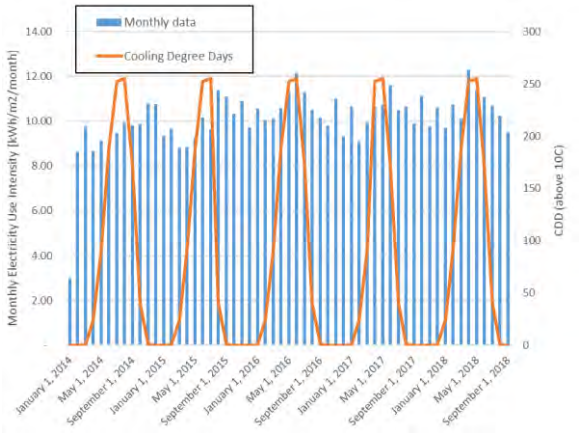

Figure 4: Monthly electrical energy consumption and CDDs (base 10˚C)

Figure 5 shows the metered energy consumption compared with the final calibrated model results for the energy consumption. The maximum percentage difference between the metered and modeled consumption is 11.3% monthly and ±3% annually. To assess the quantity of the model calibration, ASHRAE Guideline 14 describes statistical methods to quantify modeling uncertainty for calibration to monthly utility bills. This involves calculating the coefficient of Variation of the Root Mean Square Error (CVRMSE) and the Normalized Mean Bias Error (NMBE).

The CVRMSE must be less than 15%, and the NMBE less than 5%. The current energy model has a CVRMSE and a NMBE below 4% which is within the recommended limits.

The energy breakdown for the proposed building and the existing building along with the associated energy savings are outlined in Figure 6. The data are presented for the existing and proposed buildings under current climate and future climate (RCP 8.5).

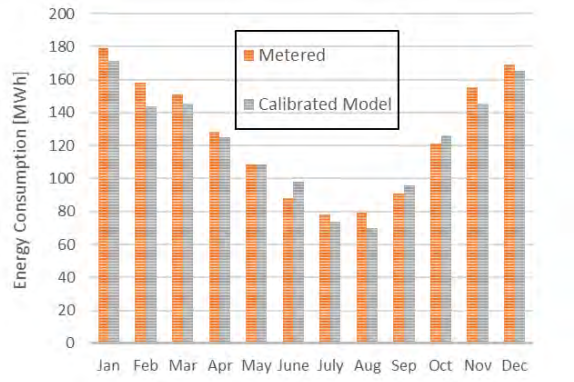

Figure 5: Calibration of the modeled energy consumption against the weather normalized utility data

As seen in Figure 6, the retrofit strategies implemented in this building, i.e., using high performance walls/windows and high efficiency boilers, lead to 25% energy saving associated with space heating. Same strategy by the end of century will lead to only 15% energy saving for space heating due to warmer climate data. In addition, under current climate, the increase in the cooling/heat rejection energy consumption is attributed to the higher wall and window R-value in the proposed building which result in less natural cooling of the building through envelope heat transfer during cool hours of a day.

Figure 6: Annual energy consumption for different end uses-existing and proposed building under current and future climate

It is also evident in Figure 6 that the cooling load of the building will increase significantly under future warmer climate data, i.e., almost 47% increase in cooling energy. The increase in fan energy is also attributed to the increase in cooling load (chiller) and the economizer for free cooling (20% increase). The current building retrofit strategies will lead to a total of 10% energy saving under current climate, and around 5.5% saving under future climate.

4. Conclusions and outlook

An energy study and whole building airtightness test were performed to investigate the effects of current building enclosure strategies on energy saving for current and future metrological data. It was observed that the current retrofit strategies that lead to saving in space heating are not as effective under future warmer climate. For the current case study retrofitting exterior walls, windows, and installing high efficiency boilers lead to 10% energy saving under current climate and around 5.5% under warmer climate data due to increase in the cooling load.

References

[1] IPCC, Climate change 2014 : Synthesis report. Summary for policy makers, (2014) 1-31.
[2] Pan Canadian Framework on Clean Growth and climate change, Dec 2016.
[3] N. Kegel, Climate change in Canada : impacts on building energy use intensity, IES Ltd.
[4] A. Robert, M. Kummert, Designing net-zero energy buildings for future climate, not for the past, Building and Environment 55 (2012) 150-158.
[5] A. Moazami, S. Carlucci, F. Causone, L. Pagliano, Energy retrofit of a day care center for current and future weather scenarios, Procedia Engineering 145 (2016) 1330-1337.
[6] S. Pengyuan, B. William, Y. Yunkyu, The feasibility and impoertance of considering climate change impacts in building retrofit analysis, Applied Energy, Elsevier, vol. 233, pages 254-270.
[7] M. Ek, T. Murdock, S. Sobie, B. Cavka, B. Coughlin, R. Wells, Future weather flies to support climate resilient building design in Vancouver, NHICE-01 (2018).
[8] K. Shanks, Retrofit Options to Reduce Climate Change Impacts on UAE Building Cooling Demand Int. J. of Sustainable Water & Environmental Systems Volume 8, No. 2 (2016) 71-76.
[9] Agros Analytics, Guidelines for specifying WeatherShiftTM future weather files.

Towards Net-Zero Energy Ready: Where Passive House Lies on the High Performance Staircase of the BC Energy Step Code

M. Kennedy-Parrott[a], M. Fakoor[a*]

[a] RJC Engineers Ltd., Vancouver, Canada
* Corresponding author, +1 (778) 865 5040, mfakoor@rjc.ca

Abstract:
The main objective of this research is to study how the Passive House Standard compares with the BC Energy Step Code (ESC). British Columbia is committed to taking incremental steps to increase energy-efficiency requirements in the BC Building Code to make buildings net-zero energy ready by 2032. However, there is a lack of understanding whether Step 4 of the Part 3-BC Energy Step Code (net-zero energy ready) is more or less efficient than the Passive House Standard. In this study, a 4-storey wood-framed multi-unit residential building has been modeled with the Passive House Planning Package (PHPP) to show compliancy with the Passive House standard. Using Passive House principles, the performances of assemblies, building envelope details, and mechanical systems' efficiencies have been determined that will comply with the requirements of the Passive House. The building was then modeled in IES VE software package per the City of Vancouver Energy Modeling Guideline (COV EMG) aligned with the requirements of the BC Energy Step Code. Consequently, the Thermal Energy Demand Intensity (TEDI) and the Thermal Energy Use Intensity (TEUI) have been calculated for the model as per the COV EMG. It is determined that the PH compliant building is significantly more energy efficient than the Step 4 ESC requirements – 40% better in TEDI and 45% better in TEUI. In addition, a comprehensive thermal comfort analysis aligned with the requirements of COV EMG and ASHRAE 55-2017 has been done to investigate the thermal comfort characteristics of a building built to the Passive House Standard. It is shown that the compliant Passive House does not meet the requirements of ASHRAE 55-2017, but it complies with the thermal comfort criteria of the COV EMG.

Keywords:
Passive House; Energy Step Code; Building Simulation; Thermal Comfort; Energy Modeling.

1. Introduction

Energy use of residential, commercial, and institutional buildings accounts for approximately 27% of all energy used in Canada, which corresponds to approximately 23% of total GHG emissions [1]. These numbers exclude any building-specific energy used within the industrial, transportation, and agriculture sectors. In urban settings like Metro Vancouver, the GHG emissions associated with buildings is somewhat higher, at 26% [2]. This means buildings are a large opportunity for reduction in energy use and associated greenhouse gas emissions, and in an effort to take advantage of this, there has been a recent shift in building codes and municipal strategies to address building energy efficiency.

The recent implementation of the BC Energy Step Code (ESC) is one such example, which is a performance-based approach to building energy use in new construction. It offers increasingly stringent 'steps,' each with a set of defined metrics for building envelope, total energy use, and airtightness requirements for new construction. There are 5 steps for Part 9 buildings, 4 steps for Part 3 residential buildings, and 3 steps for Part 3 commercial buildings. The highest step for each building type represents a "net-zero energy ready" building, in an attempt make all new construction net-zero ready by 2032 – a goal laid out in the Pan-Canadian Framework on Clean Growth and Climate Change [3]. The Step Code is an incremental approach to achieving this goal which allows municipalities to choose their own path to the 2032 goal. As of late 2019, 27 municipalities in BC had implemented or incentivized the ESC, with a further 27 formally indicating their intent to do so in the near future [4].

Some municipalities, such as the City of Vancouver, have turned towards the German "Passive House" (PH) standard to achieve high performance envelopes and building systems that reduce energy requirements significantly in an effort to move towards Net-Zero Ready. In addition to this, Step 4/5 of the BC ESC is often cited as equivalent to the PH standard in terms of building performance for "net zero ready" buildings [3]. As PH becomes more popular for all building types, it is clear that this standard is a large part of the conversation relating to achieving net-zero ready buildings by 2032. However, the modelling and individual requirements for PH certification differ from those required for ESC Compliance. This paper aims to quantify those differences, and determine where exactly the Passive House Standard lies on the BC Energy Step Code Staircase.

While there has been significant research into PH and the ESC separately, none verify the equivalency of the higher steps to the PH standard.

Baba and Ge [5] studied the effect of future climates on a single family dwelling modeled to both NECB-

baseline and PH modelling standards. They determined that a single family PH consumes approximately 50% less energy than one modelled to National Energy Code of Canada for Buildings (NECB) baseline modelling, and that due to this lower energy use and improved envelopes, the PH is more resilient to climate change. While useful in terms of TEUI numbers for PH versus NECB baseline modelling, this research does not contextualize the results of PHPP modelling under the BC ESC.

Bagheri *et al.* [6] modeled a small PH daycare in both PHPP and in IES-VE and compare the results of the two models. In IES-VE, the building is modelled using both ASHRAE 90.1 baseline inputs and with the PH inputs, and the results of the three models are presented. The model shows that IES-VE and PHPP modelling result in very similar final values for TEDI and TEUI of the building, with individual differences across end-uses. The research provides useful insight into the similarities and differences between IES-VE modelling and PHPP modelling, but again does not contextualize the results in terms of the ESC. The building is also a commercial daycare, and not a MURB, so does not provide information into the latter building archetype, only into small-scale commercial.

The Zero Emissions Building Plan for the City of Vancouver [7] is one of the main driving forces behind the adoption of PH as a useful tool for achieving net-zero energy buildings in BC. In this plan, there is an acknowledgement that the energy modelling for single family homes, Passive House, and MURBs/offices are all different, which can result in confusion when comparing the results of each. The plan recognizes the need for more understanding of how to employ relative comparisons of building model results in order to drive change in setting targets for future buildings, and how to achieve compliance with these targets.

This paper will help to address this gap by providing one such relative comparison across two energy modelling strategies, to provide some insight into how the results of two different standards can be compared. It will use the results of the two standards to quantify the performance of a PH-certified building in the context of the ESC target requirements.

2. Methodology

A building previously modelled to meet Step 1 of the ESC was chosen to complete the analysis. This building was not originally designed to PH principles, but has simple geometry that lends itself to the PH standard, and had the space necessary to improve envelope systems to PH levels with minimal changes to the existing design. The envelope assemblies were upgraded to achieve PH thermal performances, and systems were changed to reflect PH heating, cooling, and ventilation methods. The entire building was modelled using the Passive House Planning Package (PHPP), using PH-certified components to ensure a PH compliant building. A breakdown of the envelope assemblies and a description of the building systems required to achieve Passive House compliance are given in the table below.

Table 1 - Description of PH Building Design

Exterior walls	8'' exterior mineral wool, R-22 batt in 2x6 wood-framed walls (R-42.4 Effective)
Roof/Roof Decks	3'' mineral wool exterior, R-35 batts in 10" I-beams (R-48.5 Effective)
Floors above Parkade	R-35 batts in 10" floor joists on 8" Concrete slab (R-32.6 Effective)
Slab-on-grade	4'' XPS under 4" Concrete Slab (R-21.4 Effective)
Thermal Bridges	Thermal-bridge free wherever possible (less than 0.01W/mK) All existing thermal bridges designed to 0.03 W/mK or less
Windows	Triple-glazed fiberglass, U-0.80W/m^{2}K; SHGC 0.54
Heat Recovery Ventilator	Two Centralized Zehnder ComfoAir XL1500 80% effective heat recovery efficiency
DHW	40m^2 flat plate solar collector, serving two 119-gallon storage water tanks used to supplement tankless instantaneous electric water heaters in each suite
Heating system	Electric baseboard heaters
On-site renewables	PV generation on West roof, 44 modules of 2m^2 each

Once the PHPP model had been finalized, the building with upgraded PH envelope and systems was modelled in IES-VE, using City of Vancouver Energy Modelling Guidelines (COV EMG) [8] as per the ESC requirements. The purpose of this research was not to duplicate the inputs exactly in both energy models, but to model the same building to two different standards to compare results. A render of the IES-VE model is seen in Figure 1 below.

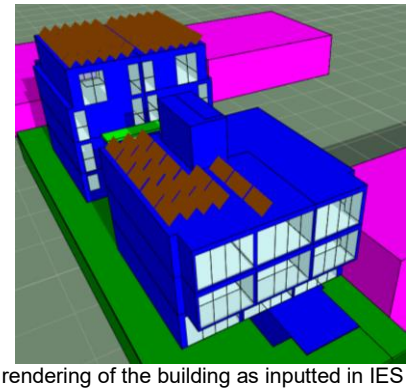

Fig 1: A rendering of the building as inputted in IES VE

Once both the models were finalized, the results of the two models were compared to confirm the key differences in results between the two modelling standards, and to see how a Passive House certified building performs on the staircase of the BC Energy Step Code.

3. Results and Discussions

The relevant ESC metrics from both building models is shown in the table below. Airtightness results inputted into both models to achieve the stated thermal energy demand intensity (TEDI) and total energy use intensity (TEUI) are shown to demonstrate how the inputs of both models compare, though there is no Step 4 airtightness requirement other than complying with the inputted value during final testing. The 0.6 ACH @ 50pa target for Passive House is converted to an operating pressure input for IES-VE, which is determined to be 0.07 [L/s/m^2].

Table 2 – Step Code Results of IES-VE and PHPP modelling

	PHPP	IES-VE	Step 4
TEDI	13 kWh/m^{2}a	8.86 kWh/m^{2}a	15 kWh/m^{2}a
TEUI	45.0 kWh/m^{2}a	55.4 kWh/m^{2}a	100 kWh/m^{2}a
Airtightness	0.6 ACH @ 50pa	0.07 L/s/m^2 @ operating pressure	0.47 L/s/m^2 or lower at 75 Pa

The TEDI calculated by the PHPP is higher than the results given by IES-VE, which is likely due to average monthly temperatures used in the PHPP, rather than hourly temperatures used in IES-VE. The total energy use determined by the PHPP is lower than that determined by IES-VE, with both models assuming an energy generation of 25.8 MWh/year.

Figures 2 and 3 illustrate the end use breakdown of the total energy for both models, and Figure 4 shows a comparison between the two models per end uses.

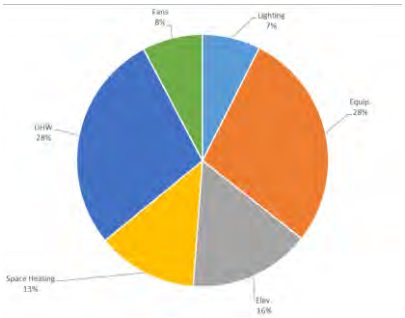

Fig 2: Building final energy use per end-use category, according to IES-VE and COV EMG.

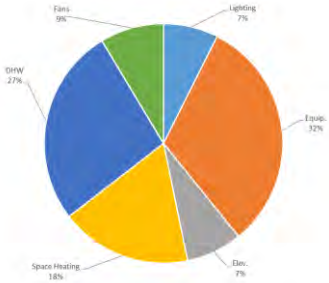

Fig 3: Building final energy use per end-use category, according to Passive House Planning Package.

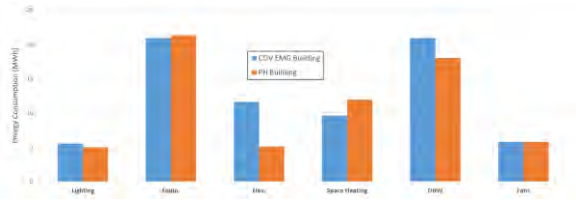

Fig 4: Building final energy use per end-use category.

The results for lighting, equipment, and fans are comparable across the two models. Space heating values vary slightly, as is shown by the TEDI results discussed earlier. The two largest differences between the two models are elevator energy use and energy use required for DHW. The elevator energy use can be explained due to the differences between inputs of the two models – COV EMG require an input of 11 MWh/year (3kW load, NECB G Equipment Schedule), regardless of the specific elevator used. PH requires the actual energy use of the chosen elevator to be inputted, which for this building was estimated using a calculator provided by an elevator manufacturer to be 5.1MWh/year. The differences in DHW energy use can be attributed to the difference between cold water inlet temperatures assigned to the two models. COV EMG dictate a cold water temperature of 5°C, while PH defaults to 11°C.The results of the PHPP model for the building are shown in the table below, along with the criteria for meeting Passive House requirements.

Table 3- PHPP results for PH certification

Building Characteristic	Criteria	Model Results
Heating demand	Less than/equal to 15 kWh/m^{2}a	13 kWh/m^{2}a
Frequency of overheating	Less than/equal to 10% of hours in year	5% (438 hours)
Airtightness	Less than/equal to 0.6 ACH	0.6 ACH
Primary Energy Renewable (PER)	PER demand less than/equal to 74 kWh/m^{2}a	74 kWh/m^{2}a
	Generation of renewable energy* of at least 26 kWh/m^{2}a	40 kWh/m^{2}a

It is important to note that the PH would not meet certification requirements without the energy generation provided by PV and solar DHW systems, since the PER values are too high for standard PER certification (which requires a PER of less than 60 kWh/m^{2}a). In the context of the ESC, the energy generation reduces TEUI of the building from 74.4 to 48.6 kwh/m^{2}a for the IES-VE model, and from 67.2 to 41.2 kwh/m^{2}a for the PHPP model. The TEUI of both models would still meet Step 4 requirements without the requirement for energy generation – it is only needed for PH certification.

Figure 5 illustrates the heat losses and gains of the PH envelope according to the PHPP. These heat losses/gains ultimately result in the 13kWh/m^{2}a heating demand, which is the PH equivalent of the ESC TEDI. The higher than typical solar heat gain coefficient of the window glazing is used in Passive House to allow for useful gains in the winter time to offset heating requirements.

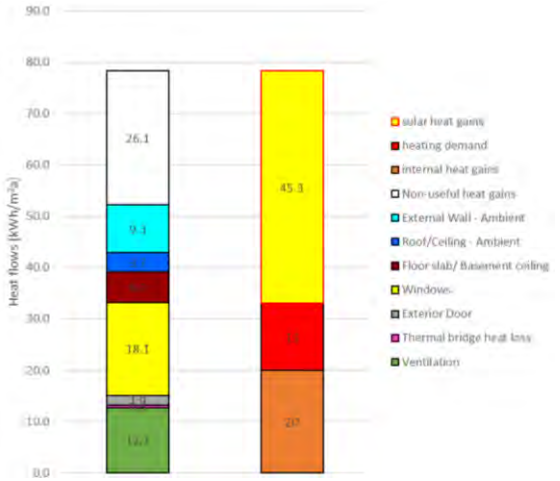

Fig 5: Passive House breakdown of heat losses and gains throughout the building envelope, according to the monthly method

The high solar heat gains achieved by this building need to be offset by shading in the summertime, which is achieved in this building primarily through self-shading of courtyard windows and the use of interior roller blinds. The use of these shading methods result in 438 hours of overheating throughout the entire building over the year. PHPP does not identify which part of the building is experiencing this overheating, which is why completing a further thermal comfort study for the building is useful and often necessary for PH buildings.

Figure 6 illustrates the thermal comfort study that is done per ASHRAE 55-2017 using the IES-VE model. As shown in Fig 6, the indoor operative temperatures in the critical zone fall out of the upper ASHRAE 55 acceptability limit for around 81 hours for the critical zone, i.e., Suite 403 in the building, one of the upper penthouse suites (West facing).

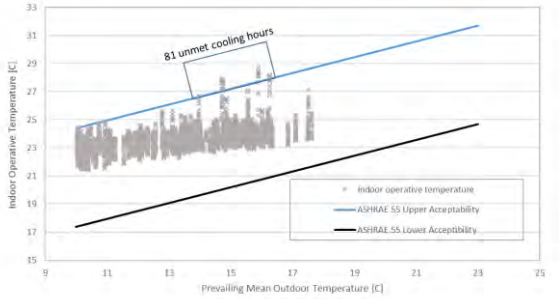

Fig 6: Unmet cooling hours for the critical zone.

The 81 unmet cooling hours is lower than the 438 hours indicated by the PHPP, but only takes into account the critical zone, whereas the PHPP looks at the entire building. The 81 unmet hours does not comply with ASHRAE 55, but complies with COV EMG requirements of fewer than 200 unmet cooling hours for any one zone.

4. Conclusions and outlook

An existing building design is upgraded according to PH principles: improving envelope performances, using PH-certified components, and including energy generation to become fully PH certified according to PHPP modelling. The building with upgraded envelope and systems is then modelled in IES-VE according to COV EMG to assess performance according to BC ESC target requirements. It is determined that the PH compliant building is significantly more energy efficient than the Step 4 ESC requirements – 40% better in TEDI and 45% better in TEUI.

References

[1] Natural Resources Canada, Energy Efficiency Trends in Canada (2016).
[2] Metro Vancouver – Services and Solutions for a Livable Region, Caring for the Air (2018).
[3] Energy Step Code Council and the Building and Safety Standards Branch, BC Energy Step Code: A Best Practices Guide for Local Governments v1.2 (2017)
[4] Energy Step Code Council, Building and Safety Standards Branch, Implementation Updates (2019)
[5] F. Baba and H. Ge, Effect of climate change on the annual energy consumption of a single family house in British Columbia, MATEC Web of Conferences 251, IPICSE-2018 (2018)
[6] F. Bagheri, M. Fakoor, B. Young, C. Cranswick, Comparison of Energy Use Indicators of a Non-Residential Passive House with ASHRAE 90.1 Budget Building, ICCE2018 Proceedings (2018)
[7] City of Vancouver Policy Report, Development and Planning, Zero Emissions Building Plan (2016)
[8] City of Vancouver Energy Modeling Guideline, Version 2 (2018).

Towards Net-Zero Carbon Buildings: A Comparative Study Between Operational and Embodied Carbon Emissions

L. Polovina[a], M. Fakoor[a]

[a] RJC Engineers Ltd., Vancouver, Canada
* Corresponding author, +1 (778) 865 5040, mfakoor@rjc.ca

Abstract:
The construction industry is one of the largest contributors of carbon emissions: one of the key causes of climate change. Embodied carbon (EC) emissions of buildings are often overlooked, but they play a significant role in the total carbon footprint of a building. As British Columbia is taking incremental steps to reduce operational carbon emissions of new buildings, the effects of embodied emissions become increasingly more significant. Currently, calculating and reporting the embodied emissions is not mandatory under most Green Building Standards. As a result, there is a lack of understanding on how embodied emissions compare with the operational carbon emissions. In this study, a 6-storey low-rise building in Victoria, BC is considered. Three different structural systems are considered for the building structure: i) Concrete Frame, ii) Steel Frame, and iii) Wood Frame. In addition, three different configurations are taken into account for the building's mechanical systems, which significantly affect the operational GHG emissions of the building: all-electric, all natural-gas, and hybrid gas-electric systems for HVAC and Domestic Hot Water systems. IES VE 2019 software package is used to simulate the energy performance of the building. The building envelope and mechanical systems of the building are designed for compliance with Step 1, 3 and 4 of the BC Energy Step Code. Athena Impact Estimator is used to perform Life Cycle Assessment (LCA) analysis for the case studies. The impacts of project location and assembly groups were also explored. It is shown that only in the case of an all-gas system, the building's GHG emissions are governed by building envelope systems rather than the mechanical systems.

Keywords:
Embodied Carbon; Energy Step Code; Building Simulation; Life Cycle Assessment; Energy Modelling

1. Introduction

The construction industry is a significant contributor to greenhouse gasses in the atmosphere. As climate change becomes a growing concern, reducing carbon emissions in the building sector has become an important opportunity to impact the fight against climate change. Cities are central in mitigating climate change, as they occupy 2% of the earth's surface, but use 75% of human resources and generate 75% of all waste [1].

The carbon footprint of a building can be divided into two categories: embodied and operational carbon. Embodied carbon includes energy consumed during manufacturing, maintenance and decommissioning of a structure [2]. Operational carbon includes heating, cooling, lighting, ventilation and equipment use [1]. Currently, operational carbon (OC) makes the largest contribution to life cycle impacts. Building energy use depends on interactions between building shape and orientation, construction materials, weather, building equipment and occupational requirements [3]. As buildings become increasingly energy efficient, embodied carbon plays a significant role in reducing upfront carbon emissions.

Currently, green building rating systems such as LEED and BREAM do not focus on addressing embodied carbon and focus more on operational performance. Under LEED v4, LEED Platinum can be achieved without embodied carbon considerations [1]. However, some jurisdictions, such as the City of Vancouver, has a Zero Emissions Building Plan that aims for 90% reduction in emissions by 2025 and uses LCA to inform future policies. The BC Energy Step Code does not consider EC but has progressive performance targets [2]. Many countries in the EU have policies and programs to address embodied carbon, such as national Environmental Product Declaration (EPD) databases, requiring whole building LCAs and EC reporting.

LCA captures the overall environmental footprint of a building, by looking at different phases, or assembly groups, of the project lifecycle: product, construction, use and end-of-life (assembly groups A-D respectively). The foundation, floors and walls have the greatest impact, followed by roof and insulation [4]. The manufacturing phase has the highest impact for both steel and concrete [6]. Steel has the largest embodied carbon by volume whereas concrete has high impact because of sheer volume used in construction [7]. Increasing the transportation distance and number of distribution centers for steel and reinforcing steel also increases EC [6]. Integrating LCA with tools such as Building Information Modelling (BIM) can conceptualize the environmental impact of structural systems and increase the accuracy of an LCA; however, it is limited by the level of detail that can be entered into the program. Regional variations in energy grids, building codes, manufacturing processes and construction practices make LCA benchmarking difficult to achieve [4]. There are also

inconsistencies between study boundaries and methods [5].

Using supplementary cementitious materials (SCM's), thinner walls and more sustainable materials can also reduce EC [1]. Increasing air-tightness and reducing window to wall ratios has a modest effect on EC and a greater benefit in OC savings [3], [8]. Innovations that have been demonstrated to result in low EC include: alternative fuels like biomass, electric arc furnaces for steel production, synthetic limestone aggregate that uses carbon capture and mineralization, bio-based insulation alternatives [1] and insulated concrete forms [3].

Our literature review indicates that for residential buildings in British Columbia, there is a knowledge gap on:

- The comparison between different structural framing systems and mechanical heating systems for optimum energy performance
- The embodied carbon impacts of energy efficiency measures
- The comparison between operational carbon and embodied carbon – what is the optimum balance between materials used and energy performance?
- The comparison between operational and embodied carbon for Steps 1, 3 and Step 4 of the BC Energy Step Code

The main objective of this paper is to compare the interaction of different envelope, mechanical and structural systems and illustrate their effects on operational and embodied carbon under Step 1, 3 and 4 of the BC Energy Step Code.

The paper also explores the EC of different assembly groups and the effect of changing the project location to illustrate the magnitude of geographic influences.

2. Methodology

In this study, a 6-storey low-rise building in Victoria, BC was considered. Three different structural systems were considered for the building structure: i) Concrete Frame, ii) Steel Frame, and iii) Wood Frame. Reflecting local construction practices, the first two floors were modelled as concrete for all three structural scenarios and the remaining floors were modelled as concrete, steel or wood. The building was designed under the respective frame system and foundations were sized for each building type. Athena Impact Estimator was used to perform the LCA for the case studies. In addition, three different configurations were considered for the building's mechanical system: all-electric, all natural-gas, and hybrid gas-electric systems for HVAC and Domestic Hot Water systems. IES VE 2019 energy modelling software was used to simulate the energy performance of the building. The building envelope was modelled for Step 1, Step 3, and Step 4 compliance of the BC Energy Step Code.

Figure 1 shows the modelling parameters that this paper explores and Table 1 describes the structural, building envelope and mechanical systems:

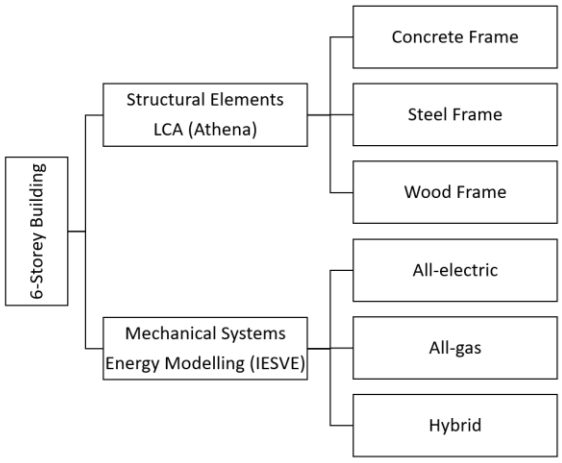

Fig 1 : Modelling parameters in this study

Table 1: Description of the structural, building envelope and mechanical systems

	Step 1	Step 3	Step 4
Columns & Beams	Concrete: 35 MPa Concrete Benchmark		
	Steel: Hollow Structural Steel/ Open Web Joists		
	Wood: 2x10 Laminated Veneer Lumber Beams		
Foundation	30 MPa Concrete Benchmark, 5" rigid Under Slab (all structures)		
Exterior Walls	Concrete and Steel: Steel-Stud @ 16"o/c		
	R-22 batt	3'' Semi-rigid, R-22 batt	5'' Semi-rigid, R-22 batt
	Wood: Wood Stud @ 16" o/c		
	R-22 batt	2" semi-rigid, R-22 batt	3" semi-rigid, R-22 batt
Interior walls	Elevator Core: 30 MPa Concrete Benchmark (all structures)		
	Wood: (Shear Walls) 2x8, 1/2" Plywood, Wood Stud @ 12" o/c		
Floors	Concrete: 35 MPa Suspended Concrete Slab Benchmark		
	Steel: Composite Steel Deck		
	Wood: 2x10 Joists, Plywood Deck		
Roof	Concrete:35 MPa Concrete Benchmark		
	Steel: Composite Steel Deck		
	Wood: 2x10 Joists, Plywood Deck		
	all: 4" rigid	6" rigid	8" rigid
Glazing	Double-glazed PVC	Double-glazed fiberglass	Triple-glazed fiberglass
	U-0.32; SHGC 0.4	U-0.25; SHGC 0.25	U-0.18; SHGC 0.25
Heat Recovery Ventilators (HRV)	Per Suite		
	65% SRE	81% SRE	81% SRE

Table 2 below represents the building description used to create the LCA model.

Table 2: Building description

Building Area	4,461 m^2
Building Footprint	880 m^2
Building Height	21m
Number of Floors	6
Project Location	Vancouver, BC
Building Type	Multi-Unit Owner-Occupied Residential
Building Life Expectancy	60 years

Note that the main differences between Steps 1, 3 and 4 are the glazing type and insulation levels. The structural system remains the same throughout. It was assumed that the concrete reinforcement density was 2% for structural components. Vancouver is used in the model's Project Location due to Athena's limited geographic options.

The mechanical systems for the scenarios described in Figure 1 are listed in Table 3:

Table 3: Description of the mechanical systems

	All-Electric	**Hybrid**	**All-Gas**
Heating	Electric Baseboards		Hydronic Base-boards
DHW	Electric Tanks 95% EF	Condensing Gas-Fired Boilers 96% E_t	
Ventilation	Heat Recovery Ventilator (HRV)		

3. Results and discussions

Figure 2 illustrates the embodied and operational Greenhouse Gas Intensity (GHGI) for the different mechanical and structural systems under Steps 1, 3 and 4 of the BC Energy Step Code. Under Step 4 for wood frame, the all-electric system has 63% and 47% lower total Greenhouse Gas Emission Intensity (GHGI) compared to the all-gas and hybrid system, respectively. This demonstrates that mechanical systems play a key role in the carbon footprint of the building. When it comes to structural systems, a wood frame building has approximately 50% lower embodied carbon compared to equivalent concrete and steel structures. The concrete system has 10% higher embodied carbon than steel. For a wood frame building, EC is 21–29% of total carbon for a gas system under Step 1–4 respectively. The range is 72–77% for electric and 39–41% for hybrid. For concrete frame, the range for EC is 38–48% for a gas system, 85 – 89% for electric and 60–61% for hybrid. The conclusion of Figure 2 is that the Energy Step Code can significantly reduce the total GHGI of the building only for the all-gas case study. When electricity is used for space heating, improving the building envelope (higher steps of the energy step code) does not reduce GHGI noticeably. This is highly dependent on the carbon footprint of the electrical generation since most of Victoria's electrical energy is provided by hydro dams as opposed to fossil fuel generation.

Figure 3 compares the EC of different assembly groups (A-D) under Step 4. For a concrete frame system, floors make up 40% of EC, followed by foundation at 29% and walls at 23%. For a steel frame building, floors lead at 40%, foundation at 30% and walls at 22%. For wood frame, floors contribute to 34%, followed by foundation at 31% and walls at 29%.

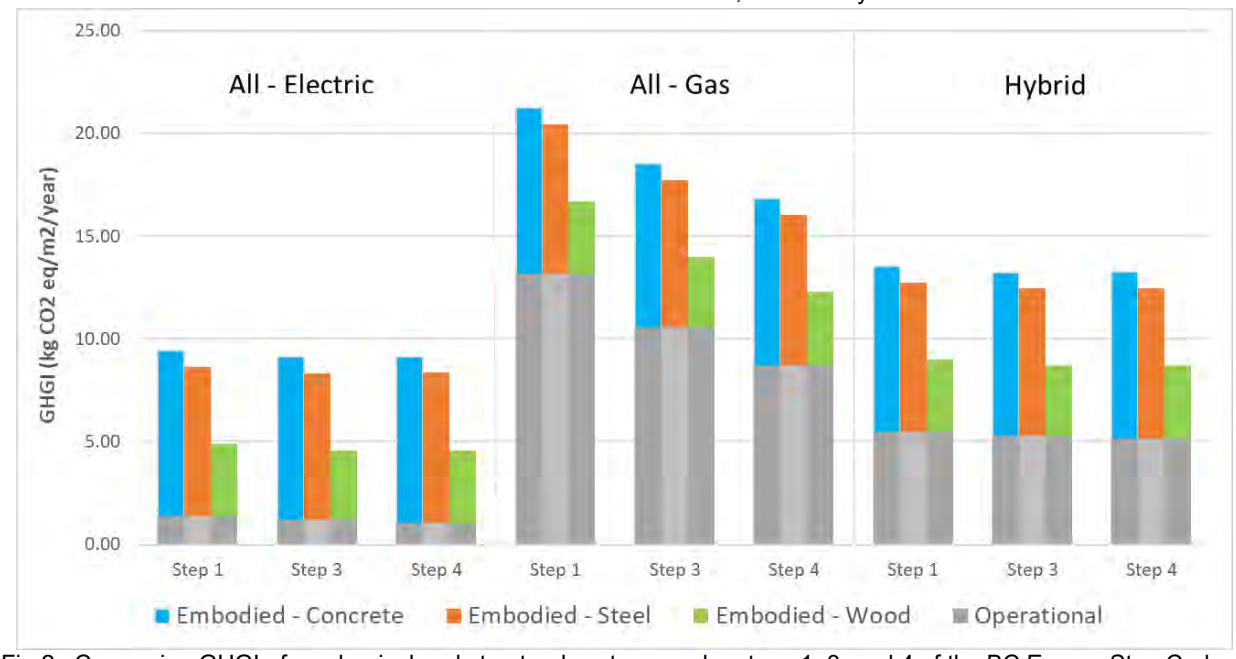

Fig 2 : Comparing GHGI of mechanical and structural systems under steps 1, 3 and 4 of the BC Energy Step Code

It is also shown in Figure 4 that for a Step 4 building, changing the site location from Vancouver to Los Angeles increased EC by 12% for concrete, 11% for steel and 16% for wood due to higher material transportation distances.

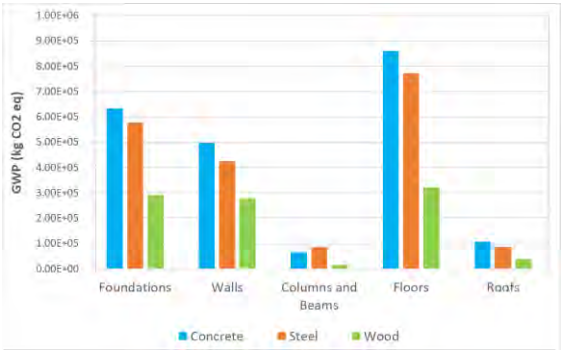

Fig 3 : Comparing global warming potential (GWP) by assembly group (A-D) for Step 4

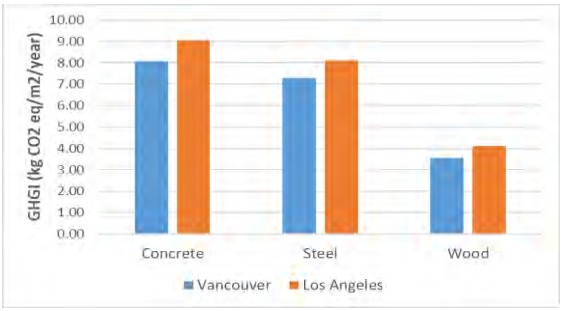

Fig 4 : Comparing effects of project location on GHGI for a Step 4 building

Figure 5 below illustrates the total GHGI of the wood frame building under different scenarios for mechanical systems and steps of the BC Energy Step Code. As seen in Figure 5, the building envelope has the greatest effect for a gas system; going from Step 1 to 4 led to a 27% reduction in total GHGI using an all-gas system. The reduction was 6% for an all-electric system and 3% for the hybrid system.

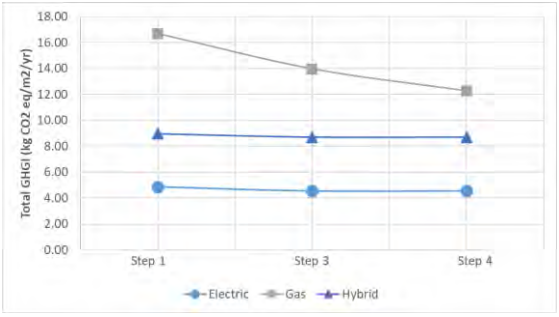

Fig 5 : Comparing GHGI for wood frame system

Considering Figures 2 and 5, it is evident that improving building envelope does not have a significant effect on the embodied energy and carbon intensity for all-electric hybrid buildings, provided the electrical energy is generated with low GHGI (hydro, solar, wind, etc.). For buildings with all-gas systems, a better building envelope decreases the OC/EC ratio due to less heat loss from the building envelope, which in turn reduces the natural gas consumption.

4. Conclusions and outlook

The main conclusions of this study are as follows:

I. The building's mechanical system governs GHG emissions rather than the building envelope systems for higher steps of the BC Energy Step Code.
II. Switching from gas to electric system, under Step 1 reduces GHG emissions by approximately 60% for concrete/steel, and almost 70% for wood frame due to the low carbon footprint of electricity generation.
III. The building envelope has a significant effect for a gas system, reducing operational GHGI by 34% when moving from Step 1 to Step 4 for a wood frame building
IV. For concrete/steel structures, embodied carbon accounts for more than 80% of the total GHG emissions for an all-electric system, and around 50% for the hybrid system, respectively.
V. A wood frame system has approximately 50% lower embodied carbon than concrete or steel.
VI. Among all structural elements, columns, beams, and roofs have the least impact on EC (less than 10%). Foundation, floors, and walls are the major contributors to EC.

References

[1] N. Wheating, Embodied carbon: A framework for prioritizing and reducing emissions in the building industry, University of San Francisco, (2017)
[2] R. Zizzo, J. Kyriazis, H. Goodland, Embodied carbon of buildings and infrastructure – international policy review, Forestry Innovation Investment (2017)
[3] J. Ochsendorf, L. Keith Norford, D. Brown, H. Durschlag, S. Lisbeth Hsu, A. Love, N. Santero, O. Swei, A. Webb, M. Wildnauer, Methods, impacts, and opportunities in the concrete building life cycle, MIT (2011)
[4] R. Ghattas, J. Gregory, E. Olivetti, S. Greene, Life cycle assessment for residential buildings: A literature review and gap analysis, MIT (2013)
[5] N. Yokoo, K. Yokoyama, Evaluation of embodied energy and CO2 for building construction – Energy in Assessment of Building Structural Systems Using Building Information Modeling, ISARC (2018)
[7] H. Zhou, Embodied Energy Assessment of Building Structural Systems using Building Information Modeling, Lakehead University (2017)
[8] S. Dulmage, M. Mousa, Embodied carbon white paper, Sustainable Buildings Canada (2018)
[9] A. Pak, Concrete High Rise LCA Study City of Vancouver, Priopta, (2019)

Designing Buildings for a Warming Climate

L. Westerhoff[a,*], S. MacDougall[b], C. Dedels[c], S. Shepherd[d]

[a] Integral Group, lwesterhoff@integralgroup.com
[b] Focal Engineering, susan@focaleng.com
[c] Integral Group, cdedels@integralgroup.com
[d] Focal Engineering, sarah@focaleng.com
* Corresponding author, 604-687-1800 x 2084, lwesterhoff@integralgroup.com

Abstract:
The Province of British Columbia will experience significant changes in climate over the next several decades. Temperature increases of between 1.3 and 2.7°C are projected out to 2050, and the province is already experiencing more extreme weather, including frequent and severe heat waves and wildfire events as a result. The impacts of these events pose serious risks to British Columbia's buildings, along with the safety, well-being, and financial investments of their owners and occupants. As building design can play a key role in enhancing our resilience to these current and projected impacts, designers must increasingly consider how buildings can be adapted for a warmer world.

This paper provides an overview of how designers can begin to improve building resilience, focusing on two significant climate-related issues: overheating and indoor air quality. It will present a set of principles, strategies and practices that can enhance building resilience to climate change, improve overall building quality, and increase occupant comfort and health. The paper will include an introductory approach to assessing a building's performance with respect to overheating, including a method of analyzing necessary weather files as well as key overheating metrics. It concludes with a presentation of a set of high-level strategies that designers can use to ensure the longevity and sustainability of their designs.

Keywords:
Resilience; Overheating; Air Quality; Energy Code; Energy Policy; Future Climate; Building Adaptation

1 Introduction

In the era of the climate emergency, building professionals must now approach building design using the dual lens of both mitigating and adapting to climate change. *Mitigation* action is already underway in many areas in the form of efforts to reduce energy use and greenhouse gas (GHG) emissions in new buildings. In British Columbia (BC), both the Province and the City of Vancouver have developed new codes and standards in order to encourage energy efficient and/or low-carbon building design via the *BC Energy Step Code* (Step Code) and Vancouver's *Zero Emissions Building Plan* (ZEBP), respectively.

Despite these efforts to reduce emissions in new construction, however, past and current emissions have already guaranteed some degree of climate warming. Climate data for BC projects temperature increases of between 1.3 and 2.7°C by 2050 [1], accompanied by longer dry spells, more heat waves, and more severe wildfire events. Given this new climate reality, professionals must also incorporate *adaptation* measures into building design to reduce the negative impacts associated with changes in climate, maintain the safety, comfort and well-being of occupants, and protect financial investments.

Among the impacts expected for BC's building sector are the interrelated issues of overheating and indoor air quality. As temperatures rise and summer precipitation rates fall, buildings are increasingly at risk of extreme heat and wildfire-related air quality events that can pose serious consequences for occupants – particularly those most vulnerable (e.g. children, pregnant women, elderly people, and those who are ill or immunocompromised)[2]. Designers now face a new challenge of ensuring that new building projects are able to both maintain safe and comfortable spaces for their occupants while continuing to reduce emissions. This dual approach falls under the umbrella of *low-carbon resilience*, or the need to anticipate, prepare for, and respond to the negative impacts of climate change while simultaneously reducing emissions[3].

To help support this goal, this paper provides an overview of a new and more resilient approach to building design. It identifies a set of key strategies for the achievement of low-carbon and resilient buildings focusing on the risk of overheating, and air quality issues associated with wildfire events. The paper concludes with a summary of key takeaways and potential areas of future exploration.

2 Limitations of Current Design Practice

To understand the need for a new approach to building design, it is important to first identify the limitations of current methodologies. In general, high-performance building design includes energy modelling, used to estimate a building's expected energy use, as well as its heating and cooling needs. Energy models use a set of core assumptions around the performance and operation of a building, expected occupancy, and importantly: the expected weather conditions under which the building will operate. In BC, energy models are often created using Canadian Weather for Energy (CWEC) files, which are based on 30 years of weather observations (i.e. the most typical results for each month). Mechanical heating and cooling equipment is sized using *BC Building Code* (BCBC) data that are also based on historical design conditions.

However, current conditions are already warmer than those represented in CWEC 2016 files, with further warming anticipated still. As a result, the use of past weather puts buildings at risk of overheating as warmer temperatures go unaccounted for. Without adequate passive and/or mechanical cooling measures, spaces may become too warm for occupants, leading to discomfort and disruption. Prolonged or dangerously high temperatures can also lead to a range of health risks, including heat stress, heatstroke, increased morbidity or even mortality.

Alongside overheating, the building sector is also facing increasing concerns over indoor air quality. Stipulations for indoor air quality are now included in the BCBC and ASHRAE *Standard 62.1*, which generally require either Class 1 or Class 2 air filter units for occupied spaces. However, the changing climate presents additional risks to consider. Extreme wildfires are projected to increase, which emit heavy smoke that contains a mixture of fine particulate matter, carbon monoxide, nitrous oxides, and volatile organic compounds, all which have been linked to numerous short- and long-term negative health impacts (e.g. fatigue, respiratory diseases, cancer), especially in vulnerable populations. This smoke can travel great distances, and so the air quality concerns can extend well beyond those buildings at the wildfire interface.

3 A New Approach to Building Performance

In order to appropriately design new buildings to adapt to changes in climate, design professionals must consider the performance of their buildings under future conditions. This requires a consideration of projected future conditions in energy modelling to evaluate building performance for both emissions reductions and improved resilience. The key steps of such an approach are noted below.

Projected Future Conditions

3.1.1 Climate Scenarios

To properly assess a building's future performance, it is first necessary to identify the likely future climate under which the building will operate. Three future climate scenarios have been developed by the Intergovernmental Panel on Climate Change (IPCC) to indicate the potential severity of climate change, or *Representative Concentration Pathways* (RCPs) These represent possible trajectories for global temperature changes that differ according to varying global efforts to mitigate atmospheric GHG emissions:

- The **best-case scenario** (RCP-2.6) assumes that GHG emissions will be drastically reduced, and existing GHGs will start to be removed from the atmosphere.
- The **stabilization scenario** (RCP-4.5) assumes that all countries will undertake measures to mitigate emissions simultaneously and effectively.
- The **worst-case scenario** (RCP-8.5) assumes that the planet will experience high population growth and relatively slow income growth with modest rates of technological change and energy intensity improvements.

While global efforts to reduce emissions are underway, the current political and economic landscape indicates that emissions will continue to rise[4]. As such, current best practice is to use the RCP-8.5 scenario as an estimate of future climate[5].

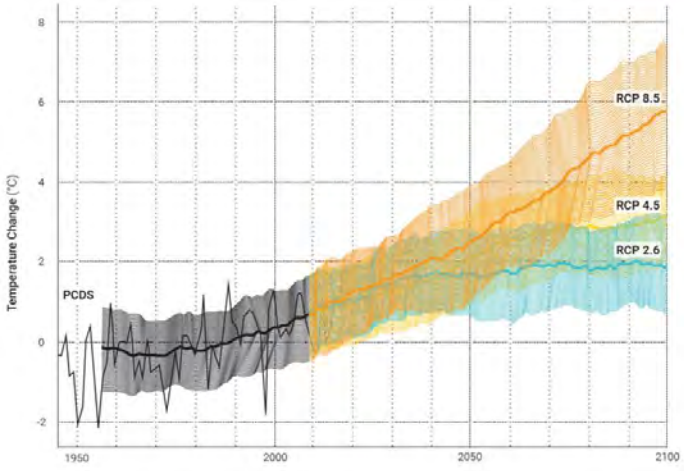

Figure 1: The range of potential temperature increases projected under different emissions reduction scenarios. Adapted from the IPCC's 2013 Summary for Policy Makers[6].

3.1.2 Future Weather Files

To explore how a warmer climate will impact building performance, future weather files exist based on the RCP scenarios listed above for three different time periods: the 2020, 2050 and 2080 decades. Where budgets allow, all three years can and should be

modelled, with several sources of reliable future weather files currently available for BC[7,8, 9]

When using a future weather file to model building performance, designers should explore and present an overview of the weather file selected for use in modelling. Characteristics such as heating degree days (HDD), cooling degree days (CDD), and any peaks that are present in the weather file should all be noted and compared against the CWEC 2016 file to highlight the predicted changes.

During this process, designers should note that climatic conditions are also expected to increase in variability as well as overall temperature. While weather files developed for future conditions are often based on existing weather files and trends, future peak conditions will be different and extreme weather events will become more frequent. As such, currently available weather files may not capture this variability. This presents a significant challenge for designers to fully capture climate-related hazards such as peak heat wave temperatures or extended periods of extreme cold. Further development of methodologies will be needed to capture these aspects; in the interim, however, the use of available future weather files is nevertheless current good practice.

Future Energy Models

3.1.3 Metrics

Once climate and weather files have been selected, designers must identify the key metrics to model. In BC, the provincial Step Code currently evaluates overheating for buildings without mechanical cooling using an upper temperature limit, which varies depending on the building's location. The temperature inside new buildings may not exceed these "80% acceptability limits" for more than 200 hours during the summer months, or a more stringent 20 hours for buildings that house vulnerable populations. This limit is calculated using a methodology defined in ASHRAE *Standard 55*[10], modified by the City of Vancouver *Energy Modelling Guidelines* (Version 2)[11].

However, the Step Code's metric is not intended as a guarantee of thermal comfort for occupants, but rather intended to encourage designers to be mindful that designing for a better envelope does not lead to an increase in overheating. As such, additional metrics should be considered to understand both the magnitude and the distribution of overheating in buildings. These could include:

- The peak interior temperature per space;
- The number of hours in which each occupied space exceeds 26°C (as per maximum indoor temperature standards adopted by the Toronto Board of Health[12]); and
- Metrics described in CIBSE *TM52: Comfort Analysis*[13], such as summer air speed and building category.

The Step Code also provides guidelines for simulating infiltration and requires as-built airtightness testing for compliance. Achieving or exceeding the recommended airtightness is an important way of managing indoor air quality by preventing uncontrolled migration of outdoor air into the building.

3.1.4 Design Simulations

With climate scenarios, future weather files, and energy model metrics in place, designers can use energy simulations to evaluate various design options under future climate conditions.

Future weather conditions can be used to estimate how mechanical cooling equipment sizes may need to increase as the climate warms. When making estimates for future cooling equipment sizes, appropriate future design data must be used. Peak temperatures experienced in energy simulation weather files are usually less extreme than design conditions from the BCBC used for mechanical equipment sizing, since weather files are intended to represent a standard year. While there is no published source of future *design data*, energy modellers can compare peak temperatures in the CWEC 2016 and future weather files, and increase the current design temperatures by the same increment. This should be discussed and agreed upon with the entire design team using an integrated design process.

However, it is important to note that oversizing equipment can lead to decreased efficiency and maintenance issues in the near term, so installing oversized equipment is generally not recommended. Instead, design teams can consider how the design can be adjusted to allow for larger cooling equipment to replace current equipment once it reaches end of life. Examples include:

- Oversizing equipment pads;
- Upsizing mechanical chases; and
- Increasing terminal unit sizes (even if central plant equipment is sized for current loads).

4 Strategies for Low-Carbon Resilient Design

Beyond a new approach for estimating future building performance under a warmer climate, building professionals should also integrate strategies to enhance resilience to the interrelated risks of overheating and wildfire-related indoor air quality events. Many of these strategies have the added benefit of reducing energy use and, when coupled with a low-carbon energy source, can reduce GHG emissions as well. Note that these strategies will need to be considered for each specific project and that there is no "one size fits all" solution. Designers will need to navigate trade-offs to ensure that the building achieves climate mitigation goals, while also ensuring resilience.

Three main groups of strategies should be considered. First, *passive cooling* strategies typically rely on either blocking solar gains from entering a building or enhancing airflow movement through a

building. As exterior temperatures warm, passive strategies may have less of an impact on mitigating overall building temperature, prompting designers to need to consider *mechanical cooling* (e.g. heat pumps) or *mixed-mode* (i.e. hybrid) strategies that incorporate both passive and mechanical measures. Passive cooling strategies that rely on airflow can also compromise indoor air quality based on outdoor conditions. As such air filtration methods should also b considered.

4.1.1 Passive Cooling Strategies

Passive cooling can play a major role in either preventing heat from entering the building or removing heat from a space. In this way, it can drastically reduce the building's overall cooling needs, reducing energy use and associated emissions, and helping to meet climate mitigation goals. Designers can employ a range of building-level passive cooling measures at different stages of the project. Strategies that should be maximized and considered early in the design process for greatest impact include:

- Exploring complex building geometries that increase passive cooling opportunities, such as operable windows and self-shading;
- Maximizing north and south facades, where solar gains are easier to control;
- Utilizing thermal mass, where building materials absorb and store heat during the day and release it at night;
- Incorporating lower window-to-wall ratios to reduce solar gains in the summer; and
- Designing cool roofs that use reflective materials and light colours to reflect solar gains, or green roofs with planted materials to absorb solar radiation.

Additional passive cooling strategies that are easier to implement in later design stages include:

- Adding exterior shading, both fixed and operable;
- Planting deciduous trees and other drought-resistant local foliage to provide shading, focusing on the south- and west-facing facades; and
- Installing high-performance windows to reduce solar heat gain, such as those that incorporate low solar heat gain coefficients (SHGC), low-emissivity coatings, and electrochromatic glazing.

Once the above passive cooling strategies have been thoroughly explored, designers can further reduce overheating risk using natural ventilation methods, such as vents in the building's envelope or the introduction of operable windows. Natural ventilation has the benefit of reducing energy use and reliance on mechanical systems, and many occupants enjoy being able to quickly adjust temperatures by opening a window. Important to note, however, is that operable windows pose the risk of allowing wildfire smoke and other airborne contaminants inside when left open. In addition, the viability of natural ventilation as a cooling method will steadily decrease as the climate warms, and so it should only be counted on as a supplement to other cooling strategies.

4.1.2 Partial Cooling Strategies

Designers can supplement passive strategies with mechanical systems that help increase overall airflow through the building. These partial cooling approaches can be a cost-effective way to reduce overheating risk and the need to add mechanical cooling. Possible partial cooling strategies include:

- Driving air movement with supply/exhaust fans or ceiling fans;
- Tempering supply air from central ventilation units and increasing air supply rates when required; and
- Using a bypass in heat or energy recovery ventilation (H/ERV) systems to prevent cooler outside air from absorbing heat from warm air being exhausted.

4.1.3 Mechanical Cooling Strategies

Under a warming climate, even the most effective passive cooling strategies will likely be insufficient to ensure thermal comfort during the warmest months of the year. Recognizing this, designers will need to consider mechanical cooling systems. Recommended options that achieve cooling using low-carbon sources of energy include high-efficiency electric heat pumps and variable refrigerant flow (VRF) systems.

Where a project does not yet require mechanical cooling, design teams can prepare for future climate conditions by incorporating "rough-ins" that allow for easier retrofits later in the building's life. This might include:

- Mapping routes for future refrigeration or chilled water lines;
- Sizing airflow rates to meet future cooling loads; and
- Ensuring adequate electrical capacity to power future mechanical cooling.

In general, designers should consider mixed-mode cooling systems that offer the ability to cool a mechanically-ventilated space using both passive and mechanical strategies. For example, a space might use operable windows as an adequate source of cooling during the shoulder seasons and then convert to mechanical cooling when outdoor summer temperatures become too hot. Such an approach can help to ensure thermal comfort under current and projected peak climate conditions, while optimizing energy efficiency and reducing energy demand. When taking this approach, designers should separate ventilation and cooling air wherever possible to increase the flexibility of the system.

4.1.4 Air Filtration

Mechanical systems that provide cooling can also be designed for higher levels of filtration to reduce the impact of air quality advisories from wildfire smoke and other pollutants. Designers can enhance building resilience by including filtration that exceeds industry standards (e.g. MERV 13 or HEPA) and may also consider secondary filters (e.g. activated carbon) that are only installed during poor outdoor air quality events. Because adding enhanced filtration can increase the building's total energy use intensity (TEUI), these measures need to be accounted for to help ensure that the building still achieves the performance targets of either the Step Code or Vancouver ZEBP.

5 Conclusions and Outlook

The potential negative impacts of climate-related overheating and air quality on occupants highlight the complexity of interactions between climate and building systems. Without an integrated approach that considers these interactions, conflicting design strategies and missed opportunities for improving building resilience can arise. For example, the higher performance envelopes of energy efficient buildings can increase overheating risk during summer months if adequate cooling measures are not included. Similarly, wildfire smoke events reduce the viability of passive ventilation measures that some high-performance buildings rely upon for low-carbon cooling. While integrated design is becoming more common, there remains a need to bring together different disciplines and areas of expertise under a methodology to ensure buildings are designed for the future climate.

Building designers can help to limit overheating risk and mitigate air quality concerns using both passive and mechanical strategies. These strategies are particularly effective when coupled with GHG mitigation efforts, helping to promote low-carbon resilience. Key takeaways for teams aiming to design more resilient buildings include:

- Use future climate scenarios, weather files, and energy simulation tools to understand the building's projected performance;
- Plan for the addition of mechanical cooling equipment if not initially included, or future increased sizing beyond the original design;
- Utilize integrated design processes to identify synergies and limit conflicting strategies.

Beyond individual building projects, there are three areas of future work that could help to encourage a more resilient building sector:

- Explore the possibility of the Step Code requiring that buildings in BC are modelled to future climate conditions;
- Conduct research on how modelling for future conditions can better simulate variability and extreme weather conditions.
- Determine additional metrics and limits to assess overheating and air quality risks.

6 Acknowledgements

The authors would like to thank BC Housing and the Pacific Climate Impacts Consortium (PCIC) for their support on this project. They would also like to thank the reviewers of the *Guideline on Energy Modelling for Future Climate & Overheating Analysis*, including Remi Charron, Christian Cianfrone, Ralph Evins, Ted Kesik, Colin Mingus, Liam O'Brien, and Ralph Wells.

References

[1] Government of British Columbia. (2019). *Impacts of Climate Change.*
[2] National Collaborating Centre for Determinants of Health (NCCDH). (2019). *Glossary – Vulnerable Populations.* A
[3] Adaptation to Climate Change Team (ACT). (2019). *Low Carbon Resilience.*
[4] United Nations Environment Programme. (2019). *Emissions Gap Report 2019.*
[5] BC Housing & Focal Engineering. (2019). *Guideline on Energy Modelling for Future Climate & Overheating Analysis.*
[6] Intergovernmental Panel on Climate Change (IPCC). (2013). *Summary for Policy Makers.*
[7] Pacific Climate Impacts Consortium (PCIC). (2019). *Weather Files.*
[8] ClimateData.ca. (2019). *Climate Data for a Resilient Canada.*
[9] WeatherShift. (2019). *WeatherShift v2.0.*
[10] ASHRAE. (2017). *Standard 55 - Thermal Environmental Conditions for Human Occupancy.*
[11] City of Vancouver. (2018). *Energy Modelling Guidelines.*
[12] City of Toronto. (2015). *Update on Extreme Heat and Maximum Indoor Temperature Standard for Multi-unit Residential Buildings.*
[13] Integrated Environmental Solutions Limited. (2014). *CIBSE TM52: Comfort Analysis.*

Experimental Study on the Thermal Performance of Green Roof Substrates as a Function of Temperature and Moisture Content

B. Shao[a], C. Valeo[a], P. Mukhopadhyaya[a] and J. He[b]

[a] University of Victoria, Victoria, British Columbia, Canada
[b] University of Calgary, Calgary, Alberta, Canada
* Corresponding Author: valeo@uvic.ca

Abstract:
Green roofs have seen an increase in popularity in recent years due to the numerous environmental benefits as well as the reduction in building energy consumption. Many studies use numerical models to analyze the energy performance of green roofs; but these approaches are plagued by a lack of accuracy in thermal properties that are input to the model. The objective of this research is to provide better estimates of parameters used to model energy and moisture budgets in green roof systems. In this study, an experimental study into the thermal conductivity at different temperature and moisture content was performed using four different commercially available substrates for green roofs. The results show that at the same temperature and moisture content, Eagle has the highest thermal conductivity while Sopraflor I has the lowest thermal conductivity. In the unfrozen state (T>5℃), there is no significant relationship between thermal conductivity and temperature; but in the phase transition zone (between +5℃ and -10℃), as temperature decreases, thermal conductivity increases sharply during the transition from water to ice. When ice is present, the higher the substrate moisture content prior to freezing, the larger the thermal conductivity.

Keywords:
Green Roof, Thermal Conductivity, Moisture Content, Heat Flow Meter, Energy Balance.

1. Introduction

Green roofs are becoming more popular in recent years due to the numerous environmental, social and economical benefits. Researches have shown that green roofs can reduce stormwater runoff and unban heat island, provide habitats for wildlife, enhance quality of air and water, reduce energy consumption of buildings and noise pollution[1-3] which protect residentials' living quality.

Many studies have investigated the energy performance of vegetated green roofs, which includes two important layers: the vegetation layer and the substrate layer, but few of them focus on substrates which is to insulate the influence between vegetation and substrate. And for those who use numerical models to analyze thermal performance of green roof substrate, they are plagued by a lack of accuracy of model input. Heat transfer through green roof substrate is affected by its moisture content and temperature. [4]

In this study, to achieve a better understanding of green roof substrate thermal properties and to provide better estimates of parameters used to model energy and moisture budgets in green roof systems, an experimental study of thermal conductivity at different temperature and moisture content for four different commercially available substrates for green roofs (Sopraflor I, Sopraflor X, ZinCo Blend and Eagle Lake) were performed. An experimental study of two green roof test cells with Sopraflor X substrate were constructed outdoor to further study the thermal performance of green roof substrate.

2. Materials and Methods

2.1 Experimental study of thermal conductivity
Four different commercially available substrates for green roofs (Sopraflor I, Sopraflor X, ZinCo Blend and Eagle Lake) were used in this study, as shown in Figure 1.

Fig 1: Sopraflor I, Eagle Lake, ZinCoBlend and Sopraflor X (From left to right)

Fig 2: Holding Frame

Figure 3. Substrate with frame and sheet.

To determine the thermal conductivity of substrates using heat flow meter, a holding frame is needed to contain substrates. According to Heat Flow Meter Manuel, dimension of sample should be 300×300mm and height of frame should be ideally around 55mm. ASTM C687 standard specifies thermal conductivity of frame four edges should be lower than 0.12W/m·K to decrease the effect of edge heat flow and the bottom which support the loose fill materials should be a thin, thermally insignificant membrane[5]. Pine wood with thermal conductivity of 0.106W/m·K was chosen as frame edges to satisfy low thermal conductivity demand. A paper based phenolic board with thickness of 1.6mm and thermal conductivity of 0.12W/m·K was used as the base frame. The base board was attached by screws and whole frame was coated with two layers of epoxy to waterproofed, joint edges between frame edge and base board was coated with silicone derivative to prevent water from leaking. Final holding frame are shown in Figure 2.

According to Clarke[6], for samples with thermal resistance lower than 1.0 m^2K/m, the most significant error may come from interface resistance. Standard ASTM C518 also suggests for sample which is hard to obtain a good surface contact with testing plate, a thin sheet of suitable homogeneous material could be used between the sample and the plate surfaces. Since surface of substrates used in this test is uneven which may result a high interface resistance, a buffer sheet was used to minimize the influence of interface resistance. Clarke used four different buffer sheet materials to perform the test and found silicone sponge provides the most uniform results. In this experiment, two silicone sponges with thickness of 9mm were used as buffer sheet, sits on the top surface of substrate and bottom of frame individually. The buffer sheets were slightly compressed during the test to perform a good contact with substrate surface as well as the bottom frame, as shown on Fig 3.

Substrate together with holding frame and buffer sheet were put into heat flow meter together to measure the thermal conductivity at -10, 5, 15, and 30℃. Thermal conductivity for substrate only was calculated by subtracting reference thermal properties.

3. Results and discussions

Table 1 Eagle Lake Thermal Conductivity ($W/m \cdot K$)

Eagle Lake		Mean Temperature (℃)			
		-10	5	20	35
Moisture content by mass	0%	0.197	0.202	0.197	0.208
	10%	0.549	0.313	0.367	0.389
	20%	2.183	0.622	0.693	0.618
	30%	13.540	0.874	1.102	1.020

Table 2 ZinCo Blend Thermal Conductivity ($W/m \cdot K$)

ZinCo Blend SI		Mean Temperature (℃)			
		-10	5	20	35
Moisture content by mass	0%	0.140	0.149	0.154	0.134
	10%	0.423	0.224	0.251	0.312
	20%	0.835	0.344	0.419	0.487
	30%	2.306	0.481	0.537	0.513
	40%	10.138	0.658	0.659	0.732

Table 3 Sopraflor I Thermal Conductivity ($W/m \cdot K$)

Sopraflor I		Mean Temperature (℃)			
		-10	5	20	35
Moisture content by mass	0%	0.127	0.138	0.149	0.148
	10%	0.286	0.204	0.233	0.250
	20%	0.578	0.258	0.297	0.345
	30%	1.010	0.346	0.414	0.4
	40%	2.412	0.465	0.522	0.492
	50%	8.760	0.724	0.761	0.790

Table 4 Sopraflor X Thermal Conductivity ($W/m \cdot K$)

Eagle Lake		Mean Temperature (℃)			
		-10	5	20	35
Moisture content by mass	0%	0.197	0.202	0.197	0.208
	10%	0.549	0.313	0.367	0.389
	20%	2.183	0.622	0.693	0.618
	30%	13.540	0.874	1.102	1.020

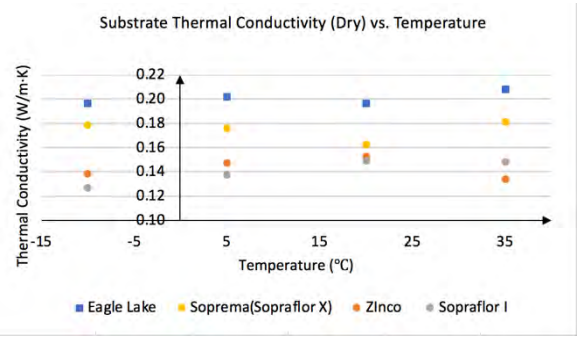

Fig 4 Dry Substrate Thermal Conductivity vs T

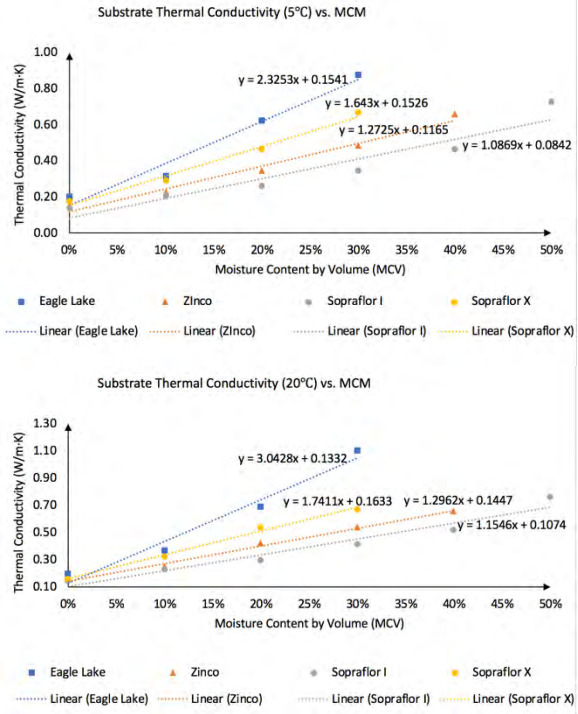

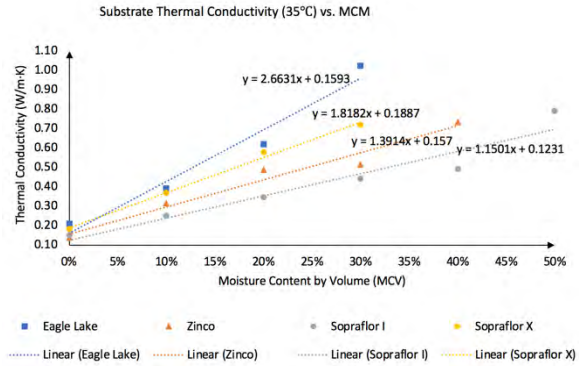

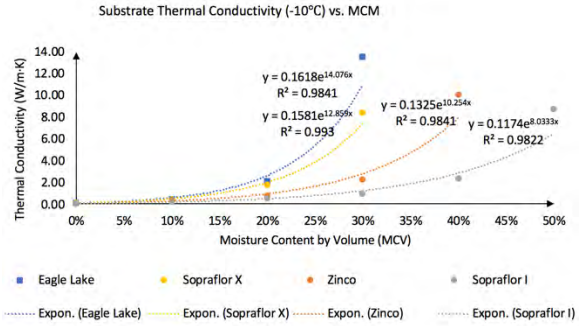

Fig 5 Substrate Thermal Conductivity vs. MCM

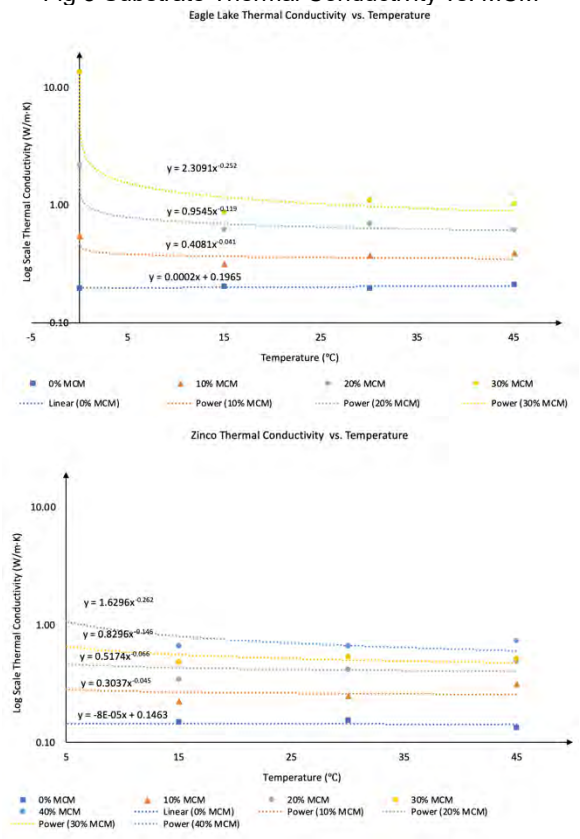

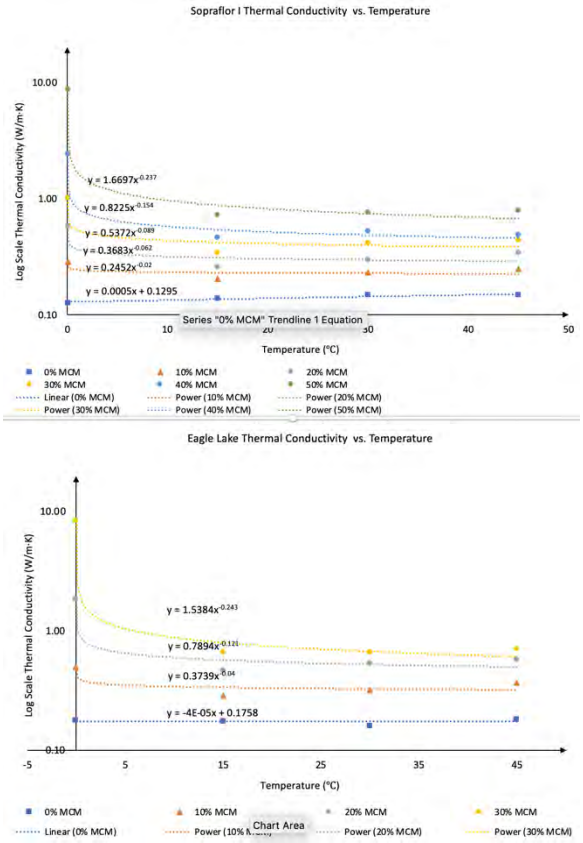

Fig 6 Thermal Conductivity vs. Temperature

(1) ,Maximum moisture content by mass or Eagle Lake, Sopraflor X, ZInCoBlend and Sopraflor I are 30%, 30%, 40%, and 50% individually.
(2) According to figure 4, the higher the dry substrate density, the higher the substrate thermal conductivity.
(3) According to figure 5, as substrate moisture content goes higher, thermal conductivity goes higher linearly.
(4) According to figure 6, in the unfrozen state (T>5℃), there is no significant relationship between thermal conductivity and temperature; but in the phase transition zone (between +5℃ and -10℃), as temperature decreases, thermal conductivity increases sharply during the transition from water to ice.
(5) When ice is present, the higher the substrate moisture content prior to freezing, the larger the thermal conductivity.

References

[1] Muhammad Shafique, Reeho Kin, Muhammad Rafiq. Green roof benefits, opportunities and challenges-A review. Renewable and Sustainable Energy Reviews(2018).
[2] Fioretti R, Palla A, Lanza LG, Principi P. Green roof energy and water related performance in the Mediterranean climate. Build Environ 2010;45:1890–904.
[3] Andrea Pianella, Robin E. Clarke. Steady-State and transient measurements of green roof substrates. Energy and Buildings(2016).
[4] Salah-Eddine Ouldboukhitine, Rafik Belarbi. Experimental characterization of green roof components. Energy Procedia(2015).
[5] G. Apparatus, H. Flow, and M. Apparatus, "Standard Practice for Determination of Thermal Resistance of Loose-Fill Building," Significance, vol. 04, pp. 1–11, 2003.
[6] R. E. Clarke, "Flexible Buffer Materials to Reduce Contact Resistance in Thermal Insulation Measurements," 2014.

Identification of model pioneer bacteria used to test biofouling on reverse osmosis water treatment membranes and related protocol

A. Curtin[a,*], M. Thibodeau[a], A. Piper-Arroliga[a], H.L. Buckley[a]

[a] University of Victoria, Civil Engineering Department, Green Safe Water Lab, 3800 Finnerty Road, Victoria, BC V8P 5C2
* Corresponding author, (250) 472-5879, annacurtin@uvic.ca

Abstract:
Due to increasing water scarcity across the globe, scientists are pursing cost-effective drinking water treatment processes that make use of alternative water sources. One promising method is reverse osmosis. The application of reverse osmosis, however, is limited by fouling, especially biofouling. Biofouling occurs when a biofilm forms at the water-membrane surface. A biofilm is a complex of microorganisms, including bacteria, fungus, and algae, and extracellular polymeric substances, which microorganisms excrete on the membrane to condition it for attachment. Biofouling progressively clogs the membrane, which increases the energy demand to maintain flux across the membrane, causing reverse osmosis to be a more energy intensive and expensive process. Unfortunately, treating biofouling is a complex problem because the components of biofilms vary depending on the type of microorganisms in the water and on the environmental and operational conditions. Investigating treatment methods for removing these organisms, therefore, tends to focus on single-species biofilms. Here we establish a consensus from the literature via a semi-systematic review of model biofilm-forming pioneer bacteria involved in biofilm formation on reverse osmosis membranes, including *Acinetobacter, Bacillus, Escherichia, Methylobacterium, Pseudomonas, Staphylococcus, Stenotrophomonas, and Sphingomonas*. It was found that the most important constituents of biofilms from a treatment perspective are those that initiate biofilm formation. We also recommend a modified protocol to test antifoulant chemicals on single species suspension cultures of the identified model pioneer organisms grown in 96-well plates. Although not an established predictive method, treatment methods that are able to either kill or prevent functioning of these organisms in suspension cultures could potentially prevent biofilm formation and the difficulties associated with treating mature biofilms.

Keywords:
Reverse osmosis; biofouling; preservative; antimicrobial; safer alternative.

1. Introduction

Water scarcity is characterized by a lack of access to clean and affordable drinking water, as well as water for hygienic and economic needs [1]. Approximately half of the global population currently lives in an area that faces extreme water scarcity for at least one month per year [2]. This situation is a result of an imbalance between the water availability in a region and the amount of water consumed in the region; however, it is exacerbated by climate change, population growth, improperly managed water sources, and over consumption of water for food production, industry, and to sustain urban and rural populations [3]. In 2015, according to the World Economic Forum, the water crisis posed the largest risk in terms of impact to economies, environments, and people [4]. To help address water scarcity, alternative water sources can be processed to provide drinking-water quality permeate. Desalination of water via reverse osmosis (RO) is one promising method of treating alternative sources of drinking water.

RO water treatment can lead to the utilization of typically non-potable water sources, ranging from brackish water (5-30 grams salt/liter) to seawater (30 grams salt/liter) [5]. Desalination via RO, however, is limited significantly by fouling of the filtration membrane [6]. Fouling can clog membrane pores causing decreased membrane flux, which then requires increased pressure and energy input to return to the original flux. It can lead to the biodegradation or corrosion of the membrane. Additionally, anti-fouling treatment methods can wear down membranes, which shortens their lifespan. Ultimately, fouling decreases the efficiency of RO membranes, consequently increasing operational and maintenance costs for water treatment plants. These drawbacks cause RO to be disadvantageous for promoting cost-effective, sustainable communities and cities.

The most significant form of fouling is biofouling, which is responsible for approximately 30-45% of fouling cases [6], [7]. Biofouling occurs when a biofilm forms on membrane material at the water-membrane interface. A biofilm is a complex of microorganisms, including bacteria, fungus, and algae, and extracellular polymeric substances (EPS) [8]. The process of biofilm formation proceeds as follows: 1. conditioning of the membrane by EPS secreted by microorganisms, 2. attachment of pioneer microorganisms, which are the first organisms to attach to the membrane, 3. diversification, growth, and metabolism of attached microorganisms, and 4. development into a mature biofilm [9]. Many treatment

methods attempt to treat biofouling after mature biofilms have formed [6]. Treating mature biofilms is difficult for many reasons. First off, physical cleaning methods are ineffectual or near impossible on spiral-wound membranes [10], which are the most common type of membrane used in RO systems [6]. The structure of biofilms also protects microorganisms from chemical and physical treatment methods. Additionally, microorganisms in biofilms experience enhanced gene transfer, which allows microorganisms to share beneficial traits, such as antimicrobial resistance, which increases the resistance of mature biofilms to treatment [9]. The protective mechanisms facilitated by the microenvironment of a biofilm, especially increased antibiotic resistance, make biofouling one of the most difficult forms of fouling to treat [9]. Moreover, treating biofilms is a complex problem because the components of biofilms vary depending on the type of microorganisms in the water and on the environmental and operational conditions [11].

One treatment approach for biofouling of RO membranes is the addition of antimicrobials to the feed water, which will either kill bacteria (bactericidal) or prevent reproduction of bacteria (bacteriostatic) and either prevent or remove biofouling depending on the time of application. Chlorine is one antimicrobial agent that is commonly used to treat biofilm-forming organisms in almost all industries, including in RO plants [12]. Although a relatively effective bactericidal oxidant, it tends to damage the membrane, decreasing the effectiveness and the lifespan of the membrane [13]. Additionally, [14] points out that antimicrobial resistance can form against chlorine due to repeated treatments. Chlorine also has the potential to react with natural organic matter in the water and form disinfection by-products, which can be carcinogenic [15].

Due to the drawbacks of chlorine treatment of RO membranes, scientists are searching for antimicrobials that are safer for humans, the environment, and the membrane, while remaining effective. One sector that aims to use safer and effective antimicrobials is the home and personal care product industry. [16] investigated chemical antimicrobials used in home and personal care products to identify the safest, most effective chemical preservatives. The chemicals identified in [16] may be able to be applied to RO systems to remove or prevent biofouling of the membranes (antifoulant), while causing less damage to the membrane and posing lower risk to humans and the environment, including mitigating the development of antimicrobial resistance. The research team investigates bacteriostatic chemicals that prevent the reproduction of microorganisms rather than bactericidal chemicals because there is a lower chance of bacteriostatic-treated bacteria developing resistance [16], [17].

Antimicrobial treatment methods that attempt to remove mature biofilms are only temporarily successful at best, and often become ineffective when organisms in biofilms become resistant. Ultimately, any treatment that is not 100% successful will leave behind organisms that can regrow a mature biofilm [6], [18]. A proactive treatment method, which targets pioneer organism that condition the membrane, would be ideal because it could avoid the obstacles associated with treating mature biofilms. It is therefore integral to test antimicrobial efficacy against biofouling on common pioneer microorganisms in biofilms on RO membranes to determine best practice treatment methods. To do so, we reviewed the scientific literature to determine whether there is a consensus of microorganisms used to study antimicrobial efficacy against biofouling on RO membranes. We then investigated whether or not these organisms were considered to be pioneer organisms. Additionally, we developed a protocol to test antifoulant efficacy of safer chemicals identified in [16] against the organisms identified as commonly tested pioneer organisms. The current protocol focuses on treating suspension cultures, rather than formed biofilms. Although results from suspension culture tests may not be directly applicable to removal of mature biofilms, results from these tests should be generally indicative of biofouling prevention efficacy.

2.1 Literature review methods and materials

We performed a semi-systematic review to gain a consensus of the common microorganisms used to test antimicrobial efficacy against biofilms on RO water treatment membrane. The Web of Science © database was used to identify articles that study antimicrobial efficacy against biofilms on RO membranes. The final search terms resulted in 197 articles. After reading through the abstracts, 182 articles appeared to meet the semi-systematic review criteria. Upon a more detailed review of the articles, 37 articles were not included in the final analysis including, review articles (13), articles that used real water samples that were not analyzed to identify bacterial organisms (12), and articles that did not include necessary content (12). The final analysis, therefore, included 145 of the articles identified via the semi-systematic review.

The articles included studies that tested antimicrobial chemicals and membrane modifications in experiments ranging from biofilms in 96-well plates to bench-scale reverse osmosis systems. Some articles included antimicrobial tests against suspension cultures (planktonic phase cells) prior to biofilm tests. We included all organisms used in those studies, even if some organisms were only used for the suspension culture aspect of the paper. We chose to include these because even though the organisms were not grown as biofilms, the data was still used to

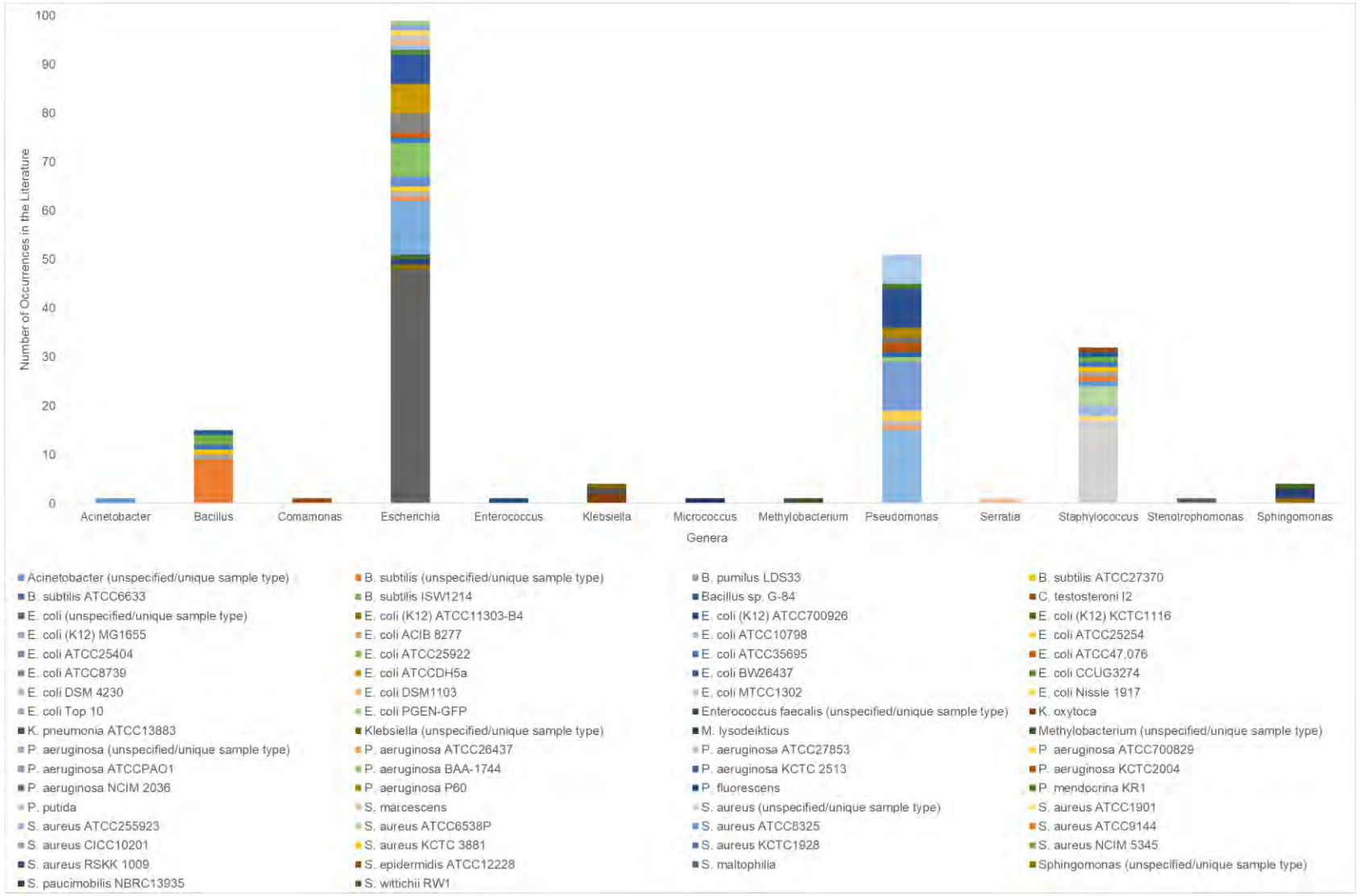

Figure 1: Frequency of occurrence of common microorganisms in biofilms on reverse osmosis membranes cited in the literature. Data was acquired from an analysis of 155 articles related to biofouling in water treatment systems.

inform following tests against biofilms. The 145 articles were analyzed to extract pertinent information including antimicrobial type, organism(s) tested, the organism phase (suspension culture, agar plate, or biofilm), type of research, and whether or not the paper mentioned that the test bacteria was chosen because it is a model organism.

2.2 Literature consensus results

One-hundred-and-forty-five articles contributed to a consensus from the literature of common microorganisms used to test antimicrobial efficacy against biofilms on RO membranes. Upon analyzing these articles, thirteen genera were identified in at least one article including *Acinetobacter* (1), *Bacillus* (15), *Comamonas* (1), *Escherichia* (99), *Enterococcus* (1), *Klebsiella* (4), *Micrococcus* (1), *Methylobacterium* (1), *Pseudomonas* (51), *Serratia* (1), *Staphylococcus* (32), *Stenotrophomonas* (1), and *Sphingomonas* (4) (Figure 1). Of the analyzed literature, approximately 93% of the identified species came from four different genera including: *Escherichia*, which occurred in about 47% of the articles, *Pseudomonas*, which occurred in about 24% of the articles, *Staphylococcus*, which occurred in 15% of the articles, and *Bacillus*, which occurred in 7% of the articles. The remainder of the genera occurred in less than 2% of the articles. The most commonly used strain was *Escherichia coli* (*E. coli*) K12 MG1655, which was tested in 11 articles, followed by *Pseudomonas aeruginosa* (*P. aeruginosa*) ATCC PAO1, which was tested in 10 articles. We also found that 73% of the articles included in the final analysis stated that the organism they used was a model or typical organism or simulate biofouling. Five genera were not described in any of the articles as model organisms, including *Acinetobacter*, *Methylobacterium*, *Stenotrophomonas*, *Serratia*, and *Sphingomonas*.

2.3 Literature consensus discussion

Selecting an appropriate model biofilm-forming organism to use for a benchtop study about antimicrobial efficacy against biofouling in an RO system is key for gaining relevant results. Ideally the model organism is a pioneer organism, which is one of the first organisms to attach to the membrane. If tests are performed against model pioneer organisms the results can be representative of preventing biofilms, which can be easier to do than removing biofilms. Removal of biofilms is difficult because it employs reactive treatment methods that are often not completely successful for many reasons. Organisms in mature biofilms have increased protection due to the microcolony structures that form [19]. Treatments therefore, do not always successfully penetrate deeply enough to completely eradicate a mature biofilm. Organisms also experience enhanced gene transfer in a biofilm, allowing organisms to pass on beneficial traits, such as antibiotic resistance. For example, bacteria integrated into biofilms have been shown to have about 1,000 times more resistance to antibiotics compared to the same organisms in the planktonic phase [20]. Additionally, mature biofilms consist of multiple organisms and different types of EPS, which often require different treatment methods [9]. It is therefore advantageous to treat biofouling in the early stages or prevent conditioning of the membrane in the first place. To choose successful proactive antifoulants, studies should perform tests against model biofilm-forming organisms that are also pioneer organisms in biofilms on RO membranes. A consensus from the literature of which model biofilm-forming organisms are commonly tested and an analysis of which of the tested organisms are pioneer organisms will be useful for optimizing future studies on antimicrobial treatment of biofouling on RO membranes.

In this analysis, we found that many of the organisms used in the studies were used because they are considered model organisms. For example, *P. fluorescens* was used in [21] because it was considered convenient and a relevant model organism for biofilm formation. Similarly, [22] describes that *Pseudomonas* spp. are useful model organisms for studying biofouling based on secretion of EPS. Only five of the genera were not specifically described as model organisms in any of the analyzed literature, however, this does not mean that they are not model organisms. For example, *Shingomonas* spp. are recommended as a model organism for biofouling, especially for studying initial attachment and growth of biofilms [23].

Of the thirteen genera identified in the semi-systematic review, eight of the genera including, *Acinetobacter, Bacillus*, *Escherichia*, *Methylobacterium*, *Pseudomonas, Staphylococcus, Stenotrophomonas*, and *Sphingomonas,* all contain species that are considered to be pioneer organisms of biofilms [9], [23]–[28]. The first step of biofilm formation on a membrane is conditioning by EPS, which is excreted directly onto the membrane by pioneer organisms. One type of EPS released by microorganisms such as the ones in this study are biosurfactants. Biosurfactants are released by cells and can facilitate the attachment and detachment of organisms to the membrane by increasing the surface area of organisms; creating a layer of separation between the organisms and the hydrophobic, water-soluble membrane; and by increasing the solubility of organisms [10], [29]. Specific examples for the organisms in this study include, *B. subtilis*, which releases the biosurfactant surfactin, and *P. aeruginosa*, which releases the biosurfactant rhamnolipids [9]. Additionally, A*. braumannii* releases a slime and has been shown to bridge organisms in biofilms [9]. Aside from conditioning the membrane for attachment, biosurfactants determine the constituents of a biofilm by making it more favorable for certain organisms to attach to the biofilm and deterring others

based on toxicity [29]. EPS is therefore integral for biofilm formation, especially for determining the specific organisms that integrate into the biofilm. If treatment methods were focused on preventing the excretion of EPS and attachment of pioneer organisms, mature biofilms would not form, negating the need for the complex treatment methods that are required for mature biofilms.

Although this analysis identifies genera that contain species that are commonly used to test antimicrobial efficacy against biofilms on reverse osmosis membranes, are model biofilm organisms, and are pioneer organisms, which would provide relevant organisms for antimicrobial efficacy studies, there are some limitations to its application. First off, our analysis included organisms that were only tested in the suspension culture phase in a biofilm study. This could have caused some organisms to appear more popular in studies, even though they were not used to grow biofilms (i.e. [32]). For example, [31] noted that they did not use their E. coli strain for some of the biofilm tests they performed because it formed a mature biofilm very slowly and did not allow for clear comparisons between adhered cells and non-adhered cells. In addition, [30] states that many studies related to biofouling in water treatment-related systems, focus on opportunistic pathogens, including *Pseudomonas, Staphylococcus, and Escherichia.* An opportunistic pathogen is an organism that normally has a commensal relationship with a host, but is able to infect hosts under certain circumstances, such as individuals that have compromised immune systems. The organisms, therefore, are a public health concern, which warrants increased attention in the literature. This could account for some of the use of *E. coli* in 47% of the articles and P*. aeruginosa* in 24% of the articles. Although opportunistic pathogens are important from a public health perspective, these organisms may not be the most relevant for treating biofilms.

3. Protocol Development

We recommend a modified protocol based on [16] and [17] to test the biofilm prevention efficacy of safer antifoulants identified in [16] on the identified model biofilm-forming pioneer microorganisms (Appendix). The protocol outlines microdilution antifoulant efficacy tests on single species suspension cultures grown in 96-well plates. Preliminary tests focus on treating *P. aeruginosa,* a commonly used model biofilm-forming microorganism with greener antifoulants identified in [16]. Antifoulant efficacy data will be collected in the form of minimum inhibitory concentrations and log-reductions. This data will provide a general understanding of biofouling prevention. The results from these preliminary studies will guide tests on the species in biofilms.

The modified protocol for testing antifoulant efficacy against representative microorganisms in suspension cultures has a potential limitation for its application to biofilm research. In the protocol, tests are performed against single species suspension cultures. Single species suspension cultures contain one organism in planktonic phase. This type of culture is relatively easy to create in a laboratory using sterile techniques and it simplifies the complexity of studying multi-species biofilms [9]. However, in the natural world, bacterial organisms are typically found in multi-species biofilms on surfaces, not in the planktonic phase. Organisms generally exist in planktonic phase based on environmental conditions that would drive organisms to detach from biofilms [19]. Planktonic phase organisms exhibit different morphological, chemical, and metabolic characteristics than species complexed in biofilms [19]. Ultimately, conclusions drawn from studies that focus on single species suspension cultures have limited applicability to real world biofilm situations which have bacterial community interactions. For example, [33] compared the behavior of organisms in single species biofilms to dual species biofilms and found disparities between the two, suggesting using a model biofilm-former is not sufficient to gain accurate results. Results from these tests can, however, be useful for determining foundational knowledge related to organisms in biofilms and may provide representative results for preventing the formation of biofilms.

4. Conclusions and outlook

In this study, we identified nine common biofilm-forming pioneer genera on membranes in RO systems. We also designed a protocol to test the efficacy of safer antifoulants on single species suspension cultures. This protocol will be used to investigate prevention efficacy of safer antifoulants, rather than biofilm treatment efficacy. The results from these studies will be used to develop protocols to study treatment efficacy against biofilms, in order to obtain results relevant to treating biofouling and to allow for the comparison of treatment efficacy against suspension cultures to efficacy against biofilms.

Acknowledgements

The authors would like to thank Ellen Busby (University of Victoria, Department of Microbiology) for providing organisms for this study; and Rebecca Hof (University of Victoria, CAMTEC).

References

[1] V. Komnenic, R. Ahlers, and P. van der Zaag, “Assessing the usefulness of the water poverty index by applying it to a special case: Can one be water poor with high levels of access?,” *Phys. Chem. Earth*, vol. 34, no. 4–5, pp. 219–224, 2009.

[2] UNESCO World Water Assessment Programme and A. -write. of foreword Azoulay, *The United Nations world water*

development report 2019 : Leaving no one behind. 2019.

[3] A. Y. Hoekstra, M. M. Mekonnen, A. K. Chapagain, R. E. Mathews, and B. D. Richter, "Global monthly water scarcity: Blue water footprints versus blue water availability," *PLoS One*, vol. 7, no. 2, 2012.

[4] M. M. Mekonnen and A. Y. Hoekstra, "Sustainability: Four billion people facing severe water scarcity," *Sci. Adv.*, vol. 2, no. 2, p. e1500323, 2016.

[5] Y. C. Kim and M. Elimelech, "Potential of osmotic power generation by pressure retarded osmosis using seawater as feed solution: Analysis and experiments," *J. Memb. Sci.*, vol. 429, pp. 330–337, 2013.

[6] T. Nguyen, F. A. Roddick, and L. Fan, "Biofouling of water treatment membranes: A review of the underlying causes, monitoring techniques and control measures," *Membranes (Basel).*, vol. 2, no. 4, pp. 804–840, 2012.

[7] S. Jakka Ravindran, R. Kumar, A. Srimany, L. Philip, and T. Pradeep, "Early detection of biofouling on water purification membranes by ambient ionization mass spectrometry imaging," *Anal. Chem.*, vol. 90, no. 1, pp. 988–997, 2018.

[8] S. Jiang, Y. Li, and B. P. Ladewig, "A review of reverse osmosis membrane fouling and control strategies," *Sci. Total Environ.*, vol. 595, pp. 567–583, 2017.

[9] K. Zhang, H. Choi, D. D. Dionysiou, G. A. Sorial, and D. B. Oerther, "Identifying pioneer bacterial species responsible for biofouling membrane bioreactors," *Environ. Microbiol.*, vol. 8, no. 3, pp. 433–440, 2006.

[10] C. Whittaker, H. Ridgway, and B. H. Olson, "Evaluation of cleaning strategies for removal of biofilms from reverse-osmosis membranes," *Appl. Environ. Microbiol.*, vol. 48, no. 2, pp. 395–403, 1984.

[11] A. S. Ziegler *et al.*, "Dynamics of the fouling layer microbial community in a membrane bioreactor," *PLoS One*, vol. 11, no. 7, pp. 1–14, 2016.

[12] N. P. Gule, N. M. Begum, and B. Klumperman, "Advances in biofouling mitigation: A review," *Crit. Rev. Environ. Sci. Technol.*, vol. 46, no. 6, pp. 535–555, 2016.

[13] A. Antony, R. Fudianto, S. Cox, and G. Leslie, "Assessing the oxidative degradation of polyamide reverse osmosis membrane-Accelerated ageing with hypochlorite exposure," *J. Memb. Sci.*, vol. 347, no. 1–2, pp. 159–164, 2010.

[14] M. L. Ludensky, "An automated system for biocide testing on biofilms," *J. Ind. Microbiol. Biotechnol.*, vol. 20, no. 2, pp. 109–115, 1998.

[15] G. A. Boorman *et al.*, "Drinking Water Disinfection Byproducts : Review and Approach to Toxicity Evaluation," *Environ. Health Perspect.*, vol. 107, pp. 207–217, 1999.

[16] H. L. Buckley *et al.*, "Design and Testing of Safer, More Effective Preservatives for Consumer Products," *ACS Sustain. Chem. Eng.*, vol. 5, no. 5, pp. 4320–4331, 2017.

[17] W. M. Hart-Cooper, K. Johnson, and D. M. Lanueva, "Self-Assembled Active Agents," 2018.

[18] J. Mansouri, S. Harrisson, and V. Chen, "Strategies for controlling biofouling in membrane filtration systems: Challenges and opportunities," *J. Mater. Chem.*, vol. 20, no. 22, pp. 4567–4586, Jun. 2010.

[19] M. E. Davey and G. A. O'toole, "Microbial biofilms: from ecology to molecular genetics," *Microbiol. Mol. Biol. Rev.*, vol. 64, no. 4, pp. 847–867, 2000.

[20] P. Gilbert, J. Das, and I. Foley, "Biofilm susceptibility to antimicrobials," *Adv. Dent. Res.*, vol. 11, no. 1, pp. 160–167, 1997.

[21] J. Lei, C. Mayer, V. Freger, and M. Ulbricht, "Synthesis and characterization of poly(ethylene glycol) methacrylate based hydrogel networks for anti-biofouling applications," *Macromol. Mater. Eng.*, vol. 298, no. 9, pp. 967–980, 2013.

[22] S. Yamanouchi *et al.*, "Enhancement effects of cationic contaminants from bacteria on cake layer formation and biofouling on an RO membrane," *Biotechnol. Bioprocess Eng.*, vol. 22, no. 3, pp. 281–286, 2017.

[23] L. A. Bereschenko, A. J. M. Stams, G. J. W. Euverink, and M. C. M. Van Loosdrecht, "Biofilm formation on reverse osmosis membranes is initiated and dominated by Sphingomonas spp," *Appl. Environ. Microbiol.*, vol. 76, no. 8, pp. 2623–2632, 2010.

[24] L. Vanysacker, C. Denis, P. Declerck, A. Piasecka, and I. F. J. Vankelecom, "Microbial adhesion and biofilm formation on microfiltration membranes: A detailed characterization using model organisms with increasing complexity," *Biomed Res. Int.*, vol. 2013, 2013.

[25] J. Luo, P. Lv, J. Zhang, A. G. Fane, D. McDougald, and S. A. Rice, "Succession of biofilm communities responsible for biofouling of membrane bioreactors (MBRs)," *PLoS*

One, vol. 12, no. 7, pp. 1–23, 2017.

[26] L. Sala-Comorera, A. R. Blanch, C. Vilaró, B. Galofré, and C. García-Aljaro, “Pseudomonas-related populations associated with reverse osmosis in drinking water treatment,” *J. Environ. Manage.*, vol. 182, pp. 335–341, 2016.

[27] L. Hou, Q. Zhou, Q. Wu, Q. Gu, M. Sun, and J. Zhang, “Spatiotemporal changes in bacterial community and microbial activity in a full-scale drinking water treatment plant,” *Sci. Total Environ.*, vol. 625, pp. 449–459, Jun. 2018.

[28] I. Douterelo, R. Sharpe, and J. Boxall, “Bacterial community dynamics during the early stages of biofilm formation in a chlorinated experimental drinking water distribution system: Implications for drinking water discolouration,” *J. Appl. Microbiol.*, vol. 117, no. 1, pp. 286–301, 2014.

[29] E. Z. Ron and E. Rosenberg, “Natural roles of biosurfactants,” *Environ. Microbiol.*, vol. 3, no. 4, pp. 229–236, 2001.

[30] D. Davies, “Understanding biofilm resistance to antibacterial agents,” *Nat. Rev. Drug Discov.*, vol. 2, no. 2, pp. 114–122, 2003.

[31] H. L. Buckley *et al.*, “Design and Testing of Safer, More Effective Preservatives for Consumer Products,” *ACS Sustain. Chem. Eng.*, 2017.

[32] A. P. Byrne, W. M. Hart-Cooper, K. Johnson, and L. H. Stanker, “Testing for sustainable preservative,” vol. 42, 2016.

[33] L. C. Simões, M. Simões, and M. J. Vieira, “Biofilm interactions between distinct bacterial genera isolated from drinking water,” *Appl. Environ. Microbiol.*, vol. 73, no. 19, pp. 6192–6200, 2007.

Appendix :

Minimum Inhibitory Concentration (MIC) LB Broth Microdilution Tests on Bacterial Suspension Cultures

1 PURPOSE

This document outlines the Standard Operating Procedure (SOP) for performing Minimum Inhibitory Concentration (MIC) broth microdilution tests on bacteria cultures with various antifoulants in microtiter plates.

2 PROCEDURE

1. Resuspend bacteria in new LB Broth (remove waste/add nutrients)

1) Transfer 5 mL of overnight culture to a sterile falcon tube and pellet out cells by centrifuging at 3000 rpm for 5-10 minutes (until a visible pellet has formed/the solution is no longer cloudy).
2) Decant the supernatant and add 5 mL of LB Broth.
3) Thoroughly vortex tube to resuspend the bacteria in the new LB Broth.

2. Prep Overnight Culture for Inoculation

1) Dilute overnight culture to about 5 x 10^6 CFU/mL [1, 2].

3. Broth and Antibiotic Dilutions

1) Dispense 80 uL of LB broth into all wells in column 2-12.
2) Add 160 uL of LB broth (the diluent used to make the antifoulant) into Column 1 in Row A and C (negative controls).
3) Using new tips, dispense 160 uL of 2X antifoulant into Column 1 (left side of plate), except for Row A and C.
4) Use the multichannel pipettor set at 80 uL to mix contents in wells in Column 1 of all Rows thoroughly (draw liquid up and down about 6-8 times (don't push pipette button all the way down); be gentle as to not contaminate, splash, etc.).
5) Draw up 80 uL from Column 1 and dispense in Column 2 wells. Carefully mix using multichannel pipettor. Repeat step up to Column 12 and discard remaining 100 uL from Column 12.
6) Dispense an additional 20 uL of LB into all wells in Row A and B. Fill Row B from right to left in order to not carry AF to wells with lower concentrations).

4. Inoculation and Incubation

1) Pour bacterial dilution (made in Part 1) into a sterile petri dish.
2) Set multichannel pipettor to 160 uL to dispense bacteria. **This applies to Rows C-H only**. Starting in Column 12 and working to Column 1 (IN THAT ORDER). Do not inoculate Row A or Row B.
3) Cover with air permeable film. Label the air permeable film side (white sheet still attached) with your initials, lab group initials (Buckley), organism (including strain), media, and antifoulant. Consider recording time incubation started. Ensure you have recorded what is contained in each well (probably best done in excel before starting the experiment).
4) Put plate in shaker incubator and tape down so it doesn't fall off shaker. Incubate plates at appropriate temperature (usually 37°C) until satisfactory growth (approximately 18 hours). Be sure to put plates in shaker incubator.

5. Read Plates

1) The next day, rinse the wells with 125 uL of saline.
2) Add in 60 uL of trypsin to each well. Incubate the plate on the shaker for four minutes.
3) Add 40 uL of Live/Dead Baclight Stain mixture.

a. The final concentration of PI should be 20 M and final concentration of Syto 9 should be 3.34 M. The stain should be made in sterile saline.

4) Read each well with full well scan at an excitation of 485 nm for both stains and an emission at 528 nm for Syto 9 and 645 nm for PI.

3 REFERENCES

[1] H.L. Buckley, W.M. Hart-Cooper, J.H. Kim, D.M. Faulkner, L.W. Cheng, K. L. Chan, C. D. Vulpe, W.J. Orts, S.E. Amrose, and M.J. Mulvihill, Design and testing of safer, more effective preservatives for consumer products, ACS Sustainable Chemistry & Engineering 5 (2017) 4320-4331.

[2] A.P. Byrne, W.M. Hart-Cooper, K. Johnson, L.H. Stanker, D.W.S. Wong, and W.J. Orts, Testing for sustainable preservative, Household & Personal Products Industry, 53.1 (2016) 42.

In-Situ Temperature and Moisture Monitoring of a High-Performance Tiny House with Vacuum Insulation Panels

C. Campbell[a,*], S. Bucking[b], C.A. Cruickshank[c]

[a] MASc Candidate, Department of Mechanical and Aerospace Engineering, Carleton University, Ottawa, Canada
[b] Associate Professor, Department of Civil and Environmental Engineering and the Azrieli School of Architecture and Urbanism, Carleton University, Ottawa, Canada
[c] Associate Professor, Department of Mechanical and Aerospace Engineering, Carleton University, Ottawa, Canada
*Corresponding author, chriscampbell@cmail.carleton.ca

Abstract:

In Canada, many new high-performance residential buildings exhibit relatively thick walls to improve thermal insulation, at the cost of reduced living space that could be worth tens of thousands of dollars in some cities. Vacuum insulation panels (VIPs) offer a potential solution to reduce wall thickness, as they provide insulation values much higher than typical insulation materials. Recent work has proven the thermal performance of VIPs in new and retrofit construction, yet the ageing characteristics of VIPs in buildings and of the building enclosures themselves are have yet to be fully understood. VIPs lose thermal performance over time due to gas and moisture permeation through the foil casing. They may also impact the moisture transport through the envelope, potentially causing inadequate drying after moisture infiltration and consequently increasing the risk of degradation of the construction materials. This paper describes the ongoing building envelope research conducted using a net-zero energy tiny house at Carleton University that incorporates VIPs in different configurations throughout the roof, walls and floor to achieve high levels of insulation while maximizing useable floorspace. Temperature, moisture content and relative humidity sensors were installed in the building envelope to monitor the conditions of areas proximity to the VIPs. The objective was to collect in-situ temperature and moisture data from a building envelope containing vacuum insulation panels and use the findings to advise future VIP ageing studies and envelope designs. Several months of data are presented and preliminary results are discussed.

Keywords:

Vacuum insulation panels, Moisture in Buildings, In-situ testing, Tiny House

Introduction:

The housing industry in Canada provides a significant opportunity to reduce greenhouse gas emissions by researching and implementing highly efficient and durable building envelope technologies. In 2011, residential buildings accounted for approximately 19% of the total energy consumption in Canada [1]. As the population of Canada steadily grows, the need for such technology grows as well. In 2019, Statistics Canada reported a record population growth of 1.4% (531,000) from 2018 [2]. During the same period, nearly 200,000 new homes were built; 66,000 of which were single-detached houses [3]. If each of these houses could be built using highly insulated and durable enclosures, millions of future residents could enjoy comfortable and long-lasting living spaces at minimal cost to the environment.

Highly insulated houses usually feature very thick wall assemblies. Double stud walls commonly contain around 240 mm (9.5 inches) of fiberglass-batt or blown cellulose insulation to achieve an RSI value of 5.8 (R-33) in an overall thickness of over 330mm (13 inches) [4]. Extreme examples can have as much as 410 mm (16 inches) of insulation to achieve an RSI value of 9.9 (R-56). Other walls reduce thermal bridging effects by using exterior rigid polystyrene insulation, commonly achieving an RSI value of 6.7 (R-38) at around 290 mm (11.5 inches) thick [5]. These walls types may be appropriate in the rural settings in which they are typically found but closely packed suburban and urban dwellings demand thinner walls due to smaller lot sizes and higher property costs. Tiny homes also benefit from thinner walls that can maximize floor space. In these applications, vacuum insulation panels (VIPs) may be a suitable solution.

VIPs outperform fiberglass batt insulation by up to 10 times per unit thickness [6]. The lifespan of VIPs in buildings is worth investigation due to the potential energy savings that could be realized. Previous work has revealed the ageing effects that VIPs exhibit due to vapour permeation through seams of the foil casing, increasing the thermal conductivity of the core. A recent study estimated that VIPs could lose half of their thermal performance in approximately 23 years when installed in a new building in Ottawa [7]. This ageing rate is largely determined by the vapour pressure surrounding a VIP which varies depending on climate, construction type, initial conditions and other factors. The collection of real-world data in this area is useful to verify estimates about VIP ageing.

The objective of this work was to collect in-situ temperature and moisture data in order to accurately estimate the lifespan of VIPs in buildings in Canada.

Methodology:

In-situ testing was done using the Northern Nomad tiny house: a net-zero house designed and built by students at Carleton University in Ottawa, Canada in 2018. Figure 1 shows a photograph of the house viewed from the south-west. Built upon a 7.3 m (24') long trailer frame, the house features a 3.6 kW roof integrated photovoltaic array with battery storage, 900 litres of potable water tanks and vacuum insulation panels incorporated into the roof, floor and south facing wall. The south wall achieves a measured RSI value of 6.1 (R-35) in just 170 mm (6.75") of overall thickness. Figure 2 shows details of the roof, walls and floor construction. The walls were built with 38 mm x 89 mm (2x4) studs and 16 mm (5/8") OSB sheathing with closed-cell polyurethane spray foam insulation on the interior. The north, east and west facing walls are covered with 25 mm (1") XPS with 13 mm pressure treated strapping and cedar siding. The south facing wall is layered with 13 mm VIPs and 13 mm XPS with 13 mm pressure treated strapping and cedar siding. The VIPs are spaced from each other with strips of XPS to allow fastening of the siding to the sheathing, shown in Figure 3. The roof was built with photovoltaic (PV) panels, a 51 mm (2") air gap for convective cooling, ice barriers and 16 mm (5/8") plywood on 38 mm x 140 mm (2x6) rafters. Roof insulation is 13 mm VIPs and close cell spray foam on the interior. Figure 4 shows a VIP installed in the roof with instrumentation. Roof pitch is 43 degrees on the north and south sides with a 3-degree dormer on the north side. The 2x4 floor is insulated with 13 mm VIPs and closed cell spray

Figure 1: The Northern Nomad net-zero tiny house designed and built by students at Carleton University

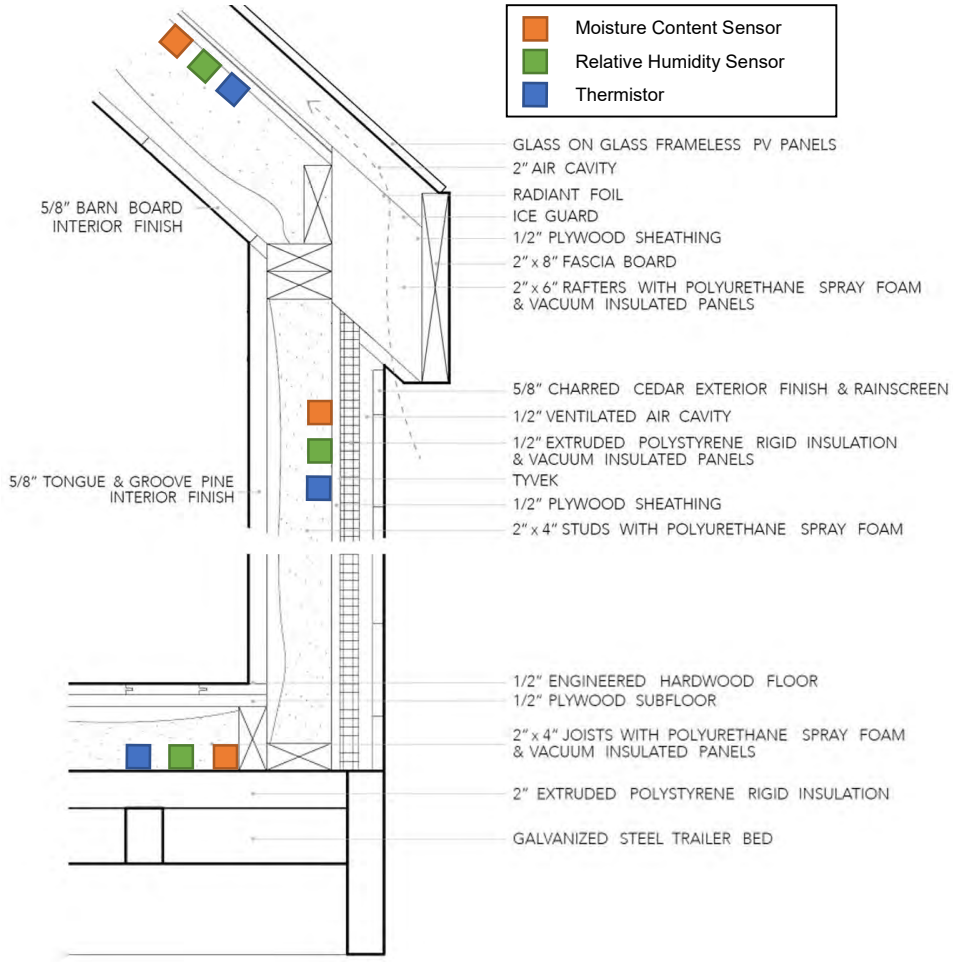

Figure 2: Wall, floor and roof detail of the Northern Nomad house with approximate locations of sensors

foam on top of the steel trailer frame which is insulated with 51 mm thick XPS.

The Northern Nomad house contains several unique features that can provide data related to VIP ageing and enclosure durability. During construction, sensors were installed at 12 specific locations. To contrast the differences between the north and south facing walls, temperature, moisture content and relative humidity sensors were installed on the inside faces of the sheathing in each of the two walls. This data provides conditions in proximity to VIPs on the south facing wall for ageing. In the floor, temperature and moisture content sensors were installed in the 2x4 joists to monitor the durability of this unique building feature. To monitor conditions in proximity to the floor VIPs, temperature, moisture content and relative humidity sensors were installed in the floor sheathing. To monitor the roof sheathing conditions near the VIPs,

Figure 3: VIPs installed on the exterior of the south facing wall

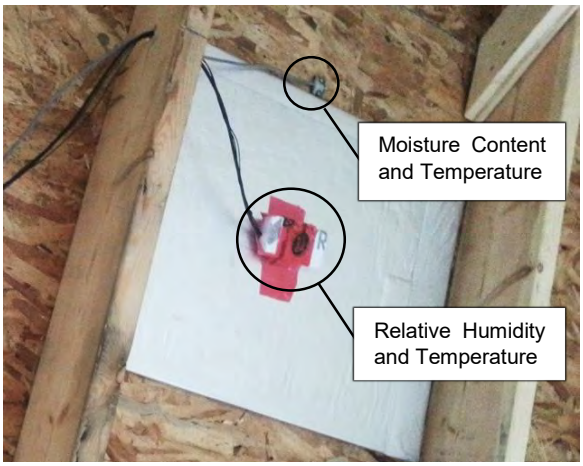

Figure 4: VIP installed between rafter in the roof with instrumentation

temperature, moisture content and relative humidity sensors were installed in the north and south facing roof sheathings adjacent to the VIPs. Additionally, temperature and relative humidity sensors were added to the inside face of the VIPs in the north and south facing roofs.

The house was located at Carleton university during testing. The sensors were connected to SMT data acquisition units and data logging began in February 2019, measuring at 10-minute intervals. SMT BiG software and cloud-based Analytics were used to save and convert resistance and voltage measurements to engineering units. The house was conditioned with a ductless air source heat pump and smart thermostat. Indoor conditions were generally maintained between 19°C and 24°C with some variation over the measurement period due to different electrical work and media activities that took place. An energy recovery ventilator ran continuously for most of the measurement period at a balanced flow rate of 14 litres per second (30 CFM) with 75% sensible effectiveness and 45% latent effectiveness. No consistent moisture loads occurred in the house. Hourly weather data from the Ottawa Airport was used for this study [8].

Results and Discussion

Six months of sensor data was collected from February through July along with accompanying weather data which is shown in Figure 5 [8]. Daily average data samples from five moisture content sensors and five temperature sensors are shown in Figures 6 and 7 respectively. Some sensors were suspected to have been damaged during construction as they gave readings that were consistent with open circuit values, so they are excluded from the study.

Most sensor locations experience reasonably dry conditions, from 13% in February to 10% in July. The south roof consistently experiences the highest temperatures and lowest moisture content in the

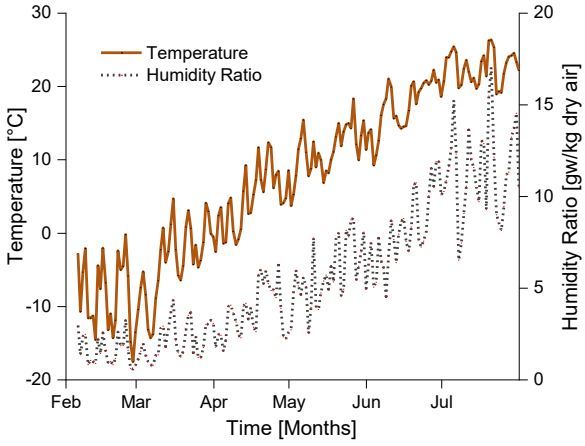

Figure 3: Daily average temperature and humidity ratio of ambient air measured at the Ottawa Airport from February 1 to July 31 [8]

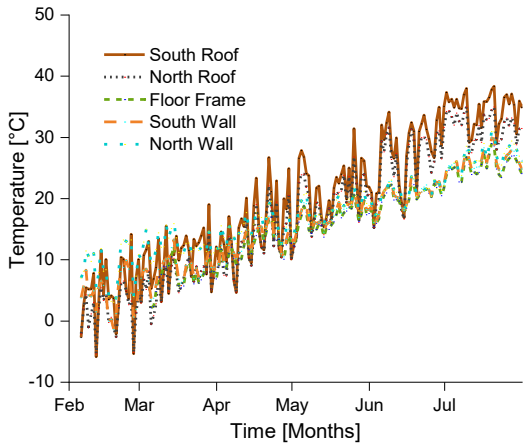

Figure 6: Daily average temperature measured at several locations in the enclosure of the house from February 1 to July 31

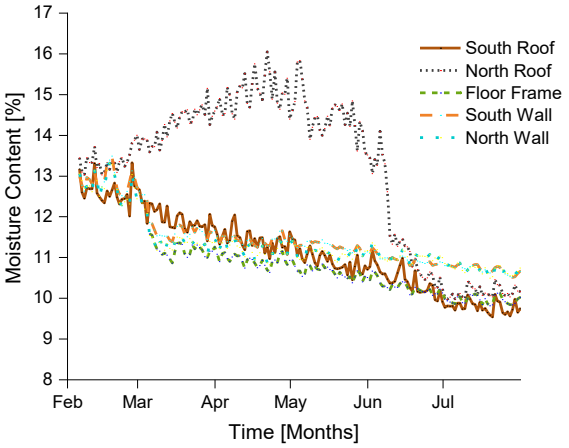

Figure 7: Daily average moisture content measured at several locations in the enclosure of the house from February 1 to July 31

house, making it a suitable location for VIP longevity. The north roof sheathing is the only location that appears to have increased in moisture content through the spring, from 13% in February to 16% in April, before it dropped to 10% in July. This may be a result of the lack of sun exposure on the north roof causing snow, ice or liquid water to sit on or behind the PV panels. This would remain until May when sun exposure increased, and the roof dried adequately. Moisture content in the north and south facing wall sheathings were similar, even though the south façade received more solar irradiance which helps drying. This indicates that the VIPs in the south facing wall kept the sheathing cooler, reducing the rate of drying to be like that of the north facing wall.

Conclusions and Outlook

Moisture content and temperature data was collected in the envelope of a highly insulated tiny house in Ottawa, Canada incorporating vacuum insulation panels in the floor, roof and south facing wall. Results indicate that VIPs may experience the most longevity when used inside of sun-exposed roof sheathing where it is hot and dry, and the least longevity in shaded roofs where it is cool and moist. South facing walls may have reduced drying rates when VIPs are installed exterior of the sheathing.

Data collection in the Northern Nomad is ongoing, with plans to introduce consistent internal moisture loads through 2020 to achieve conditions that more accurately represent an occupied dwelling. To further examine the hygrothermal behaviour of the house, additional instrumentation has been installed in the energy recovery ventilator and in the roof air gap behind the PV panels. Future work should involve applying data from this ongoing study to VIP ageing simulations to verify service life estimates.

References

[1] Natural Resources Canada, "Survey of Household Energy Use," Natural Resources Canada, Ottawa, 2011.

[2] Statistics Canada, "Annual Demographic Estimates: Canada, Provinces and Territories, 2019," Statistics Canada, Ottawa, 2019.

[3] Statistics Canada, " Table 34-10-0135-01 Canada Mortgage and Housing Corporation, housing starts, under construction and completions, all areas, quarterly," Statistics Canada, Ottawa, 2019.

[4] Building Science Corporation, "Double Stud Wall Construction," Building Science Corporation, Westford, MA, 2014.

[5] Building Science Corporation, "2x6 Advanced Frame Wall Construction," Building Science Corporation, Westford, MA, 2014.

[6] P. Mukhopadhyaya et al., "Building application and thermal performance of vacuum insulation panels (VIPs) in Canadian subarctic climate," *Energy and Buildings,* vol. 85, pp. 672-680, 2014.

[7] T. K. Ulmer, "Predicting the Lifespan of Vacuum Insulation Panels in Buildings Using Hygrothermal Simulation," Carleton University, Ottawa, 2019.

[8] Ottawa International Airport, "Historical Data," Government of Canada, Ottawa, 2019.

Feasibility study of integrating carbon capturing and utilization in building level natural gas heating systems

Don Rukmal Liyanage[a], Kasun Hewage[b*], Hirushie Karunathilake[c,d] Rehan Sadiq[e],

[a,b,c,e] School of Engineering, University of British Columbia (Okanagan Campus), 1137 Alumni Avenue, Kelowna, BC V1V 1V7, Canada
[d] Department of Mechanical Engineering, University of Moratuwa, Katubedda, Moratuwa 10400, Sri Lanka
* Corresponding author, Phone: 1.250.807.8176, Fax: 1.250.807.9850, Email: kasun.hewage@ubc.ca

Abstract:
Building sector is the third largest energy consumer in Canada, and over 81% of the Canadian GHG emissions are due to energy. The bulk of the energy consumed in Canadian buildings is for space and water heating, due to the extreme winter conditions. Even though it is commonly believed that heating via electricity produces less GHG emissions in some regions such as BC, most buildings are still equipped with natural gas (NG) heating systems due to financial considerations. Furthermore, regions such as Alberta produces higher emissions when using electricity for building heating rather than natural gas, due to the dominance of fossil fuels in the electric grid. Implementing carbon capturing and utilization (CCU) is a potential solution for these problems, as it can mitigate up to 80% of the CO_2 emissions in power generation plants. However, integrating these systems at building level is a topic that has received limited attention, despite the significance of the potential benefits in terms of emissions reduction. In this study, a scenario based analysis will be conducted to determine the potential of retrofitting existing NG building heating systems with CCU. Furthermore, CCU equipped NG heating systems are compared with electric baseboard systems, ground source heat pumps, and air source heat pumps to analyze the economic and environmental performance of carbon capturing systems. Residential and commercial buildings with natural gas heating systems are considered under different climatic regions to identify the feasibility of building-level carbon-capturing systems in various Canadian provinces. The results will demonstrate the feasibility of integrating building level carbon capturing systems in natural gas heating systems in the Canadian building sector. The study outcomes will benefit building owners, community developers, and policymakers with an interest in emissions mitigation to consider the possibility of carbon capturing implementation in the future.

Keywords:
Carbon capturing; Building heating systems; Emissions reduction; Carbon utilization; Natural gas

1 Introduction

Greenhouse Gases (GHG) especially Carbon Dioxide (CO_2) released due to various human activities such as fossil fuel combustion for energy generation accelerate the climate change [1]. In 2016, buildings consume 67% [2] of the energy and emit 12% of the GHG emissions [3] in Canada. Furthermore, residential buildings contribute 57% of the GHG emissions assigned for buildings [3]. Therefore, buildings are equipped with high insulation building envelops [4] and high efficient building heating systems [5] to reduce the energy demand. Even though reducing the energy demand can reduce the building GHG emissions, still the buildings require energy for building heating. Therefore, it is important to consider the building heating systems and their energy sources when reducing the building GHG emissions.

Provinces such as BC and Ontario produce less emission when generating electricity [6]. Therefore, using electricity as the energy source for building heating can be more environmentally friendly in these provinces. However, the cost of electricity is significantly high compared to natural gas. Furthermore, more than 50% of the buildings are equipped with natural gas heating systems [2]. Therefore, replacing these systems by only considering environmental impacts would not be practical due to economic concerns. In contrast, provinces such as Alberta produce higher GHG emissions when producing electricity. In these provinces, using electricity as the heating energy source has less possibility to reduce the GHG emissions.

Integrating carbon capturing with NG heating systems have a possibility to reduce GHG emissions without compromising the operational cost. Post-combustion carbon capture technology is considered as the most matured carbon capturing technology [7]. In post-combustion technology, the CO_2 is captured after the combustion is completed [8]. Chemical absorption is the commonly used method with the post-combustion technology to separate the CO_2 from the flue gas. The separated CO_2 can be stored in geological storages [9] or utilized as chemical feedstock [10]. Furthermore, there are carbon-capturing technologies that produce by-products during the CO_2 separation [11].

This paper presents lessons learnt from a feasibility assessment study on integrating carbon-capturing technology on natural gas (NG) heating systems. The study considers residential single-family house located in three different provinces to evaluate the operational cost and the CO_2 emission reduction. Furthermore, the results are compared with the performance of electric baseboards, air-source heat pumps, and ground-source heat pumps. HOT2000 energy simulation software is used to evaluate the space heating loads in the houses.

2 Methodology

In this study, Single-family 2000 ft^2 house is modeled in HOT 2000 based on National Building code 2015 [12]. Six scenarios are considered to evaluate and compare the performance of building level carbon capturing technologies. The base scenario, which is named as Scenario 0 considers that the building is equipped with natural gas space heating system. In Scenario 1, Methyl Ethanol Amine based chemical absorption method is used to separate CO_2. The separated CO_2 will be transported to a utilization facility. In Scenario 2, the CO_2 is captured using Potassium Hydroxide (KOH). The chemical will be converted in to Potassium Carbonate (K_2CO_3) during the reaction with CO_2. The by-product created during the reaction will be transported to a facility. The rest of the scenarios are based on replacing the current heating system with electrical baseboard system, air-source heat pump, and ground-source heat pump. The scenarios are further explained in section 2.1.

2.1 Scenario development

The study consider seven different scenarios including base scenario to analyze the feasibility of building level carbon capturing. Using natural gas as the heating energy source is considered as the base scenario. Furthermore, there are three carbon capturing and utilization scenarios. Apart from that, there are three scenarios that uses electric energy. The scenarios are described in detail below.

Scenario 0 - The study consider the base scenario as the building equipped with natural gas heating system. The annual fuel utilization efficiency (AFUE) is assumed as 92 based on the national building energy code. Furthermore it is assumed that the furnace has induced draft technology and the sizing factor is 1.1 when estimating the furnace size.

Scenario 1 - In this scenario, CO_2 from the flue gas is separated using MEA based chemical absorption method. The separated gas is compressed in to 50 bar pressure and temporary stored in a gas storage tank that has 0.5 m^3 storage volume. In each month, the stored gas will be transported to a utilization facility.

It is assumed that the carbon capturing system consume electricity for auxiliary components and thermal energy from natural gas. Furthermore, the MEA solvent has to be added to the system frequently and it is assumed that the MEA consumption is 0.0015 kg/ kg CO_2) [13]. The auxiliary energy is considered as 0.0432 $MJ_e/kgCO_2$ (Electrical energy) and regeneration energy is 3.53 MJ_{th}/ $kgCO_2$ (Thermal energy) [13].

Scenario 2 - In this scenario, CO_2 is captured using Potassium Hydroxide pellets. The reaction is shown in Equation 1. The by-products will be transported in to a facility that use Potassium Carbonate as a chemical feedstock. The transportation distance, emission factor, and the cost are same as in Scenario 1. Furthermore, the auxiliary energy input also assumed as 0.0432 $MJ_e/kgCO_2$.

$$2KOH + CO_2 \rightarrow K_2CO_3 + H_2O \quad \text{---- Equation 1}$$

Scenario 3 - In this scenario, it is considered as the building is equipped with electric baseboard system. The system efficiency is considered as 100%.

Scenario 4 - In this scenario, the building is equipped with electric air source heat pump as the main heating system with natural gas furnace as the secondary heating system.

Scenario 5 - In this scenario, the building is equipped with electric ground source heat pump as the main heating system with natural gas furnace as the secondary heating system.

2.2 Building energy simulation using HOT2000

The study compares environmental and economic performance in of building CC systems with electric baseboards, air source heat pumps, and ground source heat pumps. The environmental performance of above-mentioned building heating energy sources are significantly changes with the energy sources used to generate electricity. Therefore, building locations are chosen based on the emission factor of the grid electricity. Apart from that the building energy requirement considerably change with the climate region. Therefore, the provinces are chosen so that they are fallen in to the same climatic zone.

The study consider House 1 located at Ottawa, Ontario (20 gCO_2 eq/ kWh), House 2 located at Saint John in New Brunswick (330 gCO_2 eq/ kWh), and House 3 located at Truro in Nova Scotia (720 gCO_2 eq/ kWh) as the provinces and the cities where the buildings are located [6]. The provinces are selected so that the emission factor varies from 20 CO_2 eq/ kWh to 720 CO_2 eq/ kWh. Furthermore, all the cities are in climate 6, where the annual heating degree days varies from 4000 to 4999 [12]. The study considers 2000 ft^2 two story single-family house for the building simulation. The details of the developed building model based on the National energy code 2015 are,

- Above grade heated flow area – 1430 m^2
- Below grade heated floe area – 620 m^2
- Number of doors in the main floor – 2
- Number of windows in the main floor – 7
- Number of doors in the main floor – 0
- Number of windows in the main floor – 4
- Number of occupants – 2 adults and 2 children

The overall thermal transmittance values of each building component based on national energy code 2015 [12] are given in the Table 1.

Table 1: Overall thermal transmittance values used in the building simulation

Building component	Overall thermal transmittance W/ (m^2.K)	RSI value m^2.K/ W
Above-ground opaque building assembly		
Walls	0.247	4.05
Roofs	0.183	5.46
Floors	0.183	5.46
Assembly in contact with the ground		
Walls	0.284	3.52
Roofs	0.284	3.52
Floors	0.757	1.32
Other components		
Doors	2.2	0.45
All fenestration	2.2	0.45

The building heating systems used in the building simulations are natural gas furnaces, electric baseboard heaters, air source heat pumps, and ground source heat pumps. The capacities of the heating systems mentioned in all the scenarios are estimated using HOT2000 building simulation software.

2.3 Emission reduction and operational cost estimation

In Scenario 1, the monthly natural gas consumption is increased due to the thermal energy consumption of the carbon capturing system. The monthly natural gas consumption is estimated using the Equation 2. However, this equation is only valid when the captured CO_2 is less than the maximum amount of CO_2 that can be stored in the temporary storage tank.

$$E_1 = \frac{E_0}{1 - EF_{NG} \times \eta_{CO2} \times E_3} \quad \text{---- Equation 2}$$

Where,

- E_1 = Monthly natural gas consumption with carbon capture (MJ)
- E_0 = Monthly natural gas consumption without carbon capture (MJ)
- η_{CO2} = Carbon capturing efficiency (90%)
- EF_{NG} = Emission factor of NG ($kgCO_2$ /MJ)
- E_3 = Regeneration energy consumption (MJ/ $kgCO_2$)

The maximum CO_2 storage capacity for the Scenario 1 is calculated by applying ideal gas equation. The maximum CO_2 storage capacity for the Scenario 1 is calculated by applying mass balance on the reaction mentioned in Equation 1. The CO_2 captured per month is equal to the multiplication of total CO_2 emissions per month and Carbon capturing efficiency when it is less than maximum CO_2 storage capacity. If the CO_2 captured per month is greater than the maximum storage capacity, maximum storage capacity is considered as the CO_2 captured per month.

The total operational cost of Scenario 1 and Scenario 2 is calculated using the Equation 3.

$$C_{total} = C_{NG} + C_E + C_T + C_{Raw} - C_B \quad \text{---- Equation 3}$$

Where,

- C_{total} = Total cost
- C_{NG} = Cost of NG
- C_E = Cost of electricity
- C_T = Cost of Transportation ($0.15 per km) (Based on the average fuel cost in Canada in October 2019 – 1.20$/l) [14]
- C_{Raw} = Cost of Raw material
  - Scenario 1 – MEA ($1.2/ kg) [15]
  - Scenario 2 – KOH ($1400/ kg)
- C_B = Selling price of by-products
  - Scenario 1 – CO_2 ($0.02/kg) [16]
  - Scenario 2 – K_2CO_3 ($1700/kg)

In Scenario 3, 4, and 5, the electricity and NG fuel cost are considered as the operational cost.

The Table 2 shows the electricity cost schemes used in Ontario, New Brunswick, and Nova Scotia.

Table 2: Electricity cost schemes used in provinces

Province	Electricity variable cost		
	Supplier	Cost of electricity	Rebates
Ontario	Hydro one [17]	**Summer (May1 – Oct 31)** Up to 600 kWh – 7.7 ¢/ kWh Over 600 kWh – 8.9 ¢/ kWh **Winter (Nov1 – April 30)** Up to 1000 kWh – 11.9 ¢/ kWh Over 1000 kWh – 13.9 ¢/ kWh **delivery charges** – 2.37 ¢/ kWh **regulatory charges** – 0.412 ¢/ kWh	31.8% of base invoice [18]
New Brunswick	Energie NB Power [19]	**All units** – 11.18 ¢/ kWh	-
Nova Scotia	Nova Scotia Power [20]	**All units** – 15.603 ¢/ kWh	-

The natural gas cost is considered as coming from the same source. The cost is calculate based on FortisBC rates. It is assumed that the basic charge per month is $12.66 and all other variable costs are $7.36 per GJ [17].

3 Results and discussion

The Figure 1 shows the monthly CO_2 emissions from the heating system. The figures indicate that the house located in Ottawa emits maximum monthly CO_2 emissions of 1.28 tons. The yearly CO_2 emissions of all three houses vary from 5.2 tons to 5.7 tons. The house 2 and house 3 do not require heating in July and August months whereas, House 1 does not require heating in June, July, and August months.

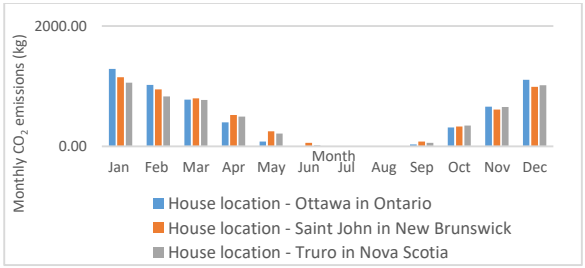

Figure 1: Monthly CO_2 emissions from all houses in Scenario 0

3.1 CO_2 capturing performance

The Figure 2 and Figure 3 show the monthly CO_2 reduction percentage in scenario 1 and scenario 2 for the house 1 accordingly. The results show there is a less carbon capture percentage in months that has higher energy load due to the restrictions of the CO_2 storage capacity and the material handling capacity in a residential house.

In scenario 1 and 2, the monthly carbon capture percentage is less than 20% except May and September. Furthermore, the total GHG emission is considerably low in May and September. This result shows that, it is not necessary to use very high efficient carbon capturing technologies in building scale with the identified carbon utilization scenarios.

The carbon capturing systems consume energy for their operation. It is assume that, the carbon capturing system indicated in scenario 1 consume thermal energy from

natural gas and electricity energy from the grid electricity supply. Furthermore, carbon capturing system in scenario 2 consume electrical energy. Therefore, the figures further indicate that the directly captured CO_2 percentage in each month is higher than the CO_2 reduction percentage compared to the baseline scenario as the CO_2 emitted due to the excess natural gas combustion and during the generation of the extra electricity consumed by the carbon capturing systems.

More interestingly, it is observed that the difference between the captured CO_2 percentage and the reduced CO_2 percentage is increasing from house 1 to house 3 accordingly. The reason is that the emission factor for the electricity generation is increased in house 1 to house 3. In provinces such as Ontario has less emission factor for electricity production than natural gas combustion. In these provinces, using electricity for the thermal energy required by the carbon capturing systems is more environmentally friendly. In contrast to that, the thermal energy for carbon capture can be supplied using natural gas combustion in provinces such as Nova Scotia, which has higher emission factor for the electricity generation.

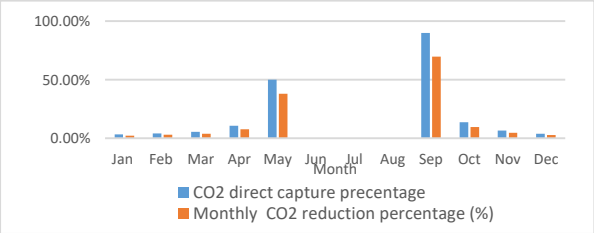

Figure 2: Monthly CO_2 capture rate and reduction rate of Scenario1 in House 1

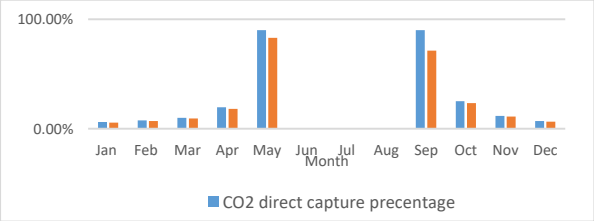

Figure 3: Monthly CO_2 capture rate and reduction rate of Scenario 2 in House 1

3.2 Annual CO_2 emissions and operational cost

The Figure 4, Figure 5, and Figure 6 show the percentage change of the annual CO_2 emissions and operational cost of scenario 1 -5 compared to the base scenarios in each house. The carbon capturing scenarios shows CO_2 emission reduction in all three houses as expected. However, the annual CO_2 emission reduction is limited to 5% in scenario 1 and 12% in scenario 2. More importantly, the scenario 2 has negative operational cost in all the houses due to the profit obtained from selling the by-products. Furthermore, scenario 3, 4, and 5 has significant operational cost increase in all houses, as the cost of electric is higher than the cost of natural gas in all the provinces considered in the study.

In Ontario, the electricity emission factor is considerably lower than the emission factor of natural gas combustion. Therefore, using a ground source heat pump can be considered as the highest environmentally friendly action as it can reduce the CO_2 emissions by 98% according to the figure. Since the heat pumps are combined with natural gas furnaces, adding an air source heat pump has higher CO_2 emissions than when entirely depend on electric baseboard. However, the operational cost reduced considerably when using any type of a heat pump compared to the electrical baseboard.

In New Brunswick, using electric baseboards and air source heat pumps increases the CO_2 emissions in contrast the house located at Ontario according to the figure. However, using ground source heat pumps still reduces CO_2 emissions by 47%. Furthermore, scenario 3, scenario 4, and scenario 5 show high cost increment compared to the house 1 as the electricity charges in Ontario is considerably low due the rebates given by the government. The same variation of annual CO_2 emissions and operational cost can be observed in house 3 according to the figure 3. However, all the heating systems that uses electricity as the main energy source increases the annual CO_2 emissions by more than 32% due to the higher emission factor for generate electricity in Nova Scotia. Furthermore, the operational cost of electricity also increased considerably compared to house 1 and house 3 due to the high electricity cost in Nova Scotia.

The carbon capturing scenario considered in scenario 1 reduces the CO_2 emissions by 4.3% in house 1 and approximately 5% in house 2 and house 3. In scenario 2, the CO_2 emissions in house is reduced by 10% where other houses have 12% CO_2 reduction. The maximum CO_2 mass handled in a month is constrained to 43.6 kg in scenario 1and 78.5 in scenario 2. Therefore, the difference of the CO_2 emissions reduction percentage in scenario 1 and scenario 2 can be expected.

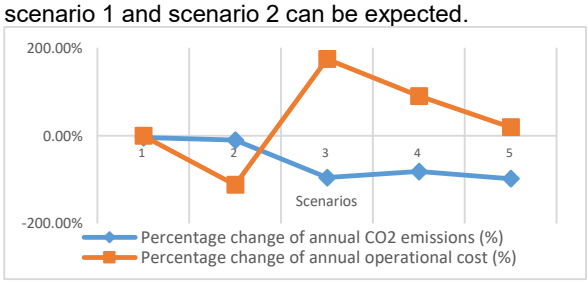

Figure 4: Percentage change of annual CO_2 emissions and operational cost in House 1

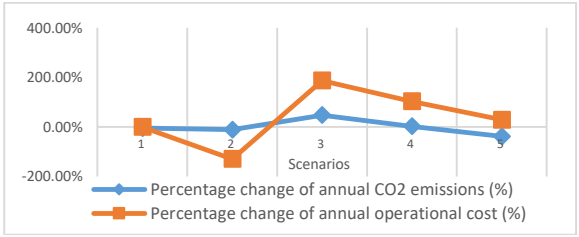

Figure 5: Percentage change of annual CO_2 emissions and operational cost in House 2

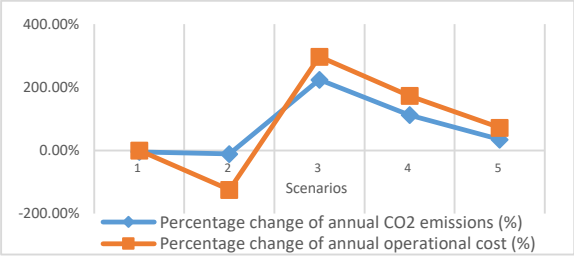

Figure 6: Percentage change of annual CO_2 emissions and operational cost in House 3

4 Conclusion

The above results demonstrate the performance of using carbon capturing technologies on building level natural gas heating systems. This study clearly shows that the scenario 2 performs better than other scenarios in terms of economic aspects. It shows that there is a potential to reduce the emissions by converting CO_2 in to a useful product that can reduce the operational cost significantly. The emissions reduction is low due to the constraints of the material handling, storage, and transporting. Furthermore, CO_2 capture level is not exceeded to its maximum levels in most of the times. Therefore, increasing the material handling capacity increases the emission reduction capacity.

The carbon capturing method describe in Scenario 1 reduce less CO_2 emissions while increasing the operational cost slightly. However, this method does not need higher amount of raw material compared to the scenario 2. The scenario 1 require approximately 70 grams of solvent, while scenario 2 require 200 kg of chemicals per month. Therefore, scenario 1 needs less effort on maintenance and transportation compared to scenario 2. On the other hand, scenario 1 needs to compress CO_2 gas from 1 atm to 50 bar which may need more energy and equipment cost.

Since scenario 2 require considerable effort on material handling, this method may not have the interest in residential building owners despite the fact it reduces the operational cost of heating significantly. However, if this technology can be used in industry that use the by-products for their own production, it may gain more interest. Other than the higher effort required to handle material in scenario 2, there are other drawbacks that are not considered in this study. The operational cost of scenario 2 can be vary with the market price of raw material and by-products. If the revenue generated by the by-product is less than the raw materials, the operational cost can be significantly increased.

Even though scenario 2 reduces the operational CO_2 emissions of heating system, it is necessary to focus on the emissions during the production of raw material and by-products as there is considerable amount of material is consumed and generated during the carbon capturing process. Apart from that, the study did not consider the capital cost when considering the performance of the heating systems. Furthermore, the feasibility of the building level carbon capturing is entirely depend on the interest of building owners. Therefore, further studies need to evaluate the feasibility of building level carbon capturing by considering capital cost, life cycle environmental impacts and costs, with the social interest.

5 References

[1] N. Oreskes, “The Scientific Consensus on Climate Change,” *Science (80-.).*, vol. 306, no. 5702, pp. 1686–1686, Dec. 2004.

[2] NRCan, “Energy Use Data Handbook,” 2019.

[3] Environment and Climate Change Canada, “National Inventory Report 1990–2017: Greenhouse Gas Sources and Sinks in Canada Canada’s Submission To the United Nations Framework Convention on Climate Change,” 2019.

[4] H. Jang, L. Jones, and J. Kang, “Prioritisation of old apartment buildings for energy-efficient refurbishment based on the effects of building features on energy consumption in South Korea,” *Energy Build.*, vol. 96, pp. 319–328, Jun. 2015.

[5] R. Saidur, “Energy savings and emission reductions in industrial boilers,” *Therm. Sci.*, vol. 15, no. 3, pp. 705–719, 2011.

[6] Environment and Climate Change Canada, “National Inventory Report 1990-2017: Greenhouse Gas Sources and Sinks in Canada,” 2019.

[7] IEA, *20 Years of Carbon Capture and Storage*. 2016.

[8] L. Petrescu, D. Bonalumi, G. Valenti, A. M. Cormos, and C. C. Cormos, “Life Cycle Assessment for supercritical pulverized coal power plants with post-combustion carbon capture and storage,” *J. Clean. Prod.*, vol. 157, pp. 10–21, 2017.

[9] Rosa M. and A. Azapagic, “Carbon capture, storage and utilisation technologies: A critical analysis and comparison of their life cycle environmental impacts,” *J. CO2 Util.*, vol. 9, pp. 82–102, 2015.

[10] I. González-Aparicio, Z. Kapetaki, and E. Tzimas, “Wind energy and carbon dioxide utilisation as an alternative business model for energy producers: A case study in Spain,” *Appl. Energy*, vol. 222, pp. 216–227, Jul. 2018.

[11] D. Bonaventura, R. Chacartegui, J. M. Valverde, J. A. Becerra, and V. Verda, “Carbon capture and utilization for sodium bicarbonate production assisted by solar thermal power,” *Energy Convers. Manag.*, vol. 149, pp. 860–874, 2017.

[12] Canadian Commission on Building and Fire codes, “National Energy Code of Canada for Buildings.” National Research Council of Canada, Ottawa, 2015.

[13] T. Grant, C. Anderson, and B. Hooper, “Comparative life cycle assessment of potassium carbonate and monoethanolamine solvents for CO2capture from post combustion flue gases,” *Int. J. Greenh. Gas Control*, vol. 28, pp. 35–44, 2014.

[14] “Monthly average retail prices for gasoline and fuel oil, by geography,” *Statistics Canada*, 2018. [Online]. Available: https://www150.statcan.gc.ca/t1/tbl1/en/tv.action?pid=18100 00101. [Accessed: 03-Dec-2019].

[15] E. S. Rubin, M. B. Berkenpas, and A. B. Rao, “An Integrated Modeling Framework For Carbon Management Technologies,” Pittsburgh, Pennsylvania, 2004.

[16] E. S. Rubin, J. E. Davison, and H. J. Herzog, “The cost of CO 2 capture and storage,” *Int. J. Greenh. Gas Control*, vol. 40, pp. 378–400, 2015.

[17] “Natural gas rates - residential,” 2019. [Online]. Available: https://www.fortisbc.com/accounts-billing/billing-rates/natural-gas-rates/residential-rates. [Accessed: 03-Dec-2019].

[18] “Ontario Electricity Rebate to take effect on November 1.” [Online]. Available: http://www.ieso.ca/en/Sector-Participants/IESO-News/2019/10/Ontario-Electricity-Rebate-to-take-effect-on-November-1. [Accessed: 28-Nov-2019].

[19] “Residential Rates (effective July 18, 2019),” 2019. [Online]. Available: https://www.nbpower.com/en/products-services/residential/rates. [Accessed: 28-Nov-2019].

[20] “Rates & Tariffs | Nova Scotia Power.” [Online]. Available: https://www.nspower.ca/about-us/electricity/rates-tariffs. [Accessed: 28-Nov-2019].

The physics of the outdoor urban climate

J.Carmeliet[a,*], A. Kubilay[b], A. Ferrari[a], D. Derome[c]

[a] Chair of Building Physics, Department of Mechanical and Process Engineering, ETH Zurich, Switzerland
[b] Laboratory of multiscale studies in building physics, Empa, Switzerland
[c] Department of Civil and Building Engineering, Université de Sherbrooke, Canada
* Corresponding author, cajan@ethz.ch

Abstract:
An urban microclimate model is proposed to study the local urban heat island in street canyons of cities and to propose mitigation measures for thermal discomfort. The microclimate model is composed of a computational fluid dynamics model for solving the turbulent air, heat and moisture flow in the air domain of a street canyon, a model for heat and moisture transport in porous urban materials, a radiative exchange model, determining the net solar and longwave radiation on each urban surface and a wind driven rain model. The model is used to evaluate the evaporative cooling potential for different pavement systems wetted by rain. A two-layer pavement system combining principles of capillary pumping and capillary break is designed for optimal evaporative cooling. A smart wetting protocol is proposed answering the questions 'when', 'how much' and 'how long' street pavements have to be artificially wetted for having a maximum cooling effect during the next day-night cycle.

Keywords:
Urban physics, heat wave, urban heat island, urban microclimate, mitigation by evaporative cooling

1. Introduction

The increase in occurrence of heat waves, together with global and local urban heat islands (UHI), seriously threatens the future urban comfort and health of inhabitants worldwide. Hence, the accurate assessment of urban heat islands and strategies to implement mitigation of UHI's are becoming increasingly important for many affected countries and cities. UHI refers to the higher air temperatures in urban environment compared to rural areas. The higher temperature in cities can be attributed to more sensible heat storage of solar radiation in urban materials with low albedo, high heat capacity and thermal diffusivity, radiation entrapment in between buildings by multiple reflections, reduced cooling by evapotranspiration due to less vegetation and water bodies, lower heat removal by urban ventilation due wind shielding by buildings and less longwave radiation to the colder sky at night (reduced sky view factor). The UHI effect has an unfavorable impact on thermal comfort, building energy use for cooling and public health [1]. Different mitigation measures for UHI have been proposed combining the use of cool materials with high albedo and/or evaporative cooling, promotion of vegetation, water bodies, urban ventilation and shading.

In this paper, we study the effect of evaporative cooling by pavements. Such pavements can be used in pedestrian urban zones with high local heat island as one of the mitigation measures. A smart wetting protocol for artificial wetting is designed for mitigating UHI during heat waves. Finally, conclusions are drawn.

2. Microclimate model and case study

The microclimate model aims at simulating the heat and mass transport in the city composed of air and porous material domains, the latter consisting of porous walls, roofs, streets and underneath ground. The heat and mass transport in these domains is solved by four coupled models. A Computational Fluid Dynamics (CFD) model is used to solve the turbulent, convective air, heat and moisture flow in the air domain. The heat and moisture flows in the porous domain are solved by a coupled heat and moisture (HAM) transport model. In the radiation model, all urban surfaces are assumed to be opaque, grey and diffusive. Multiple reflections of both solar and thermal radiation are considered in order to account for the possible radiation entrapment within buildings. The net longwave and shortwave radiative heat fluxes for each surface (urban surfaces and sky) are determined using a radiosity approach. Finally, an Eulerian multiphase model [2] determines the wind driven rain (WDR) fluxes. The four sub-models (CFD, HAM, radiation and WDR) are implemented in OpenFOAM 6.0 [3]. At each time-step, information between the models is exchanged at the urban surfaces imposing continuity of heat and moisture fluxes. When capillary saturation is attained at a material surface, extra water reaching the surface is removed, while runoff is not explicitly modelled. The reader is referred for more information on these models and their validation [4, 5, 6].

In Fig.1a, we present the case study of a single street canyon with two long buildings (10 x 10 x 50 m^3) oriented south-north and exposed to west wind. The total computational domain measures 60 x 230 x 250 m^3. The finite volume meshes for air domain and

material domain are shown in Figs. 1b and 1c. Figure 1d describes the porous domain, consisting of 9 cm brick walls and a street composed of 15 cm pavement and 1.85 m soil underneath. The interior part of the building envelope is modelled with a thermal resistance of 2.5 m^2K/W and a constant indoor temperature of 20°C. A constant temperature of 10°C is imposed at 2 m depth in the soil. All exterior surfaces have an albedo value of 0.4.

A fully developed atmospheric boundary layer wind velocity profile is imposed at the inlet assuming neutral stratification. Ambient inflow temperature and humidity ratio are assumed to be uniform over height. We consider as a first case hourly varying meteorological conditions for an average sunny summer day (21st of June, Zurich) with moderate air temperature between 11-19°C, RH between 62-85%, wind from west and clear sky conditions.

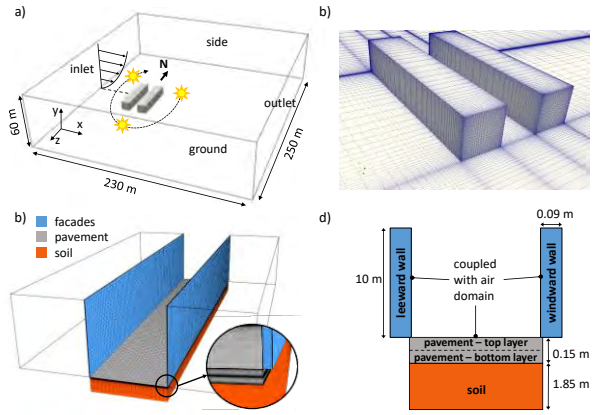

Fig 1: a) Computational domain of street canyon. b) Mesh used in the air subdomain. c) Geometry of street canyon and mesh. d) Cross section of the porous building subdomain with coupling to air domain (figures based on [6] with permission).

3. Requirements for evaporative cooling

In this section, we focus on the pavement and answer first the question which pore structure of the material maximizes the evaporative cooling effect. We aim at maximizing the evaporative cooling effect during the first drying period, where evaporation takes place at the material surface at high moisture content maintained by liquid transport from inside the wet material to the surface. During the first drying period, the drying rate is high and a high reduction in surface temperature by latent heat is obtained. Once the liquid transport within the porous medium is too low to maintain the outer layer of the material at high moisture content, the second drying period starts and the evaporative cooling effect diminishes. In order that the first drying period lasts as long as possible, the permeability of the material has to be sufficiently high to conduct water to the material surface. We refer to this as the capillary pumping effect. The pores cannot be too coarse otherwise gravity may overrule the capillary forces inversely proportional to pore size. A second requirement for maximizing the evaporative cooling effect of pavements is that the loss of water to the underneath soil is limited and water is kept close to the surface. This requirement can be guaranteed by installing a capillary break under the top pavement layer. The capillary break can be made of a material showing coarse pores, preventing capillary transport from top layer to the soil. Multilayer solutions can combine these requirements where the surface pavement layer acts as a capillary pump, while the second acts as a capillary break. For this purpose, we designed different pavement materials PA1, PA2 and PA3 with different pore volume distributions (Fig. 2). As reference, the pore volume distribution of concrete is given showing very fine pores and limited porosity leading to a material with low liquid permeability. PA1 with a porosity of 10% shows much coarser pores than concrete leading to a higher liquid permeability. PA3 shows even more coarse pores with a porosity of 30%. PA1 is used as top pavement layer guaranteeing a long first drying period with high evaporative cooling effect, while PA3 acts as capillary break preventing water loss to the soil. The properties of PA2 lie in between those of PA1 and PA3.

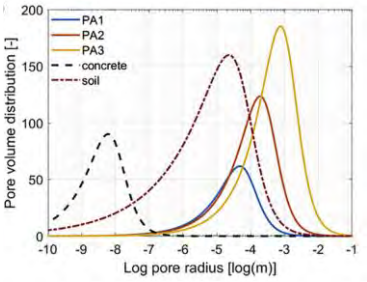

Fig. 2. Pore volume distributions of different materials (with permission based on [6]).

4. Evaporative cooling of multilayer pavements

We evaluate the evaporative cooling effect by the reduction in surface temperature and improvement in pedestrian thermal comfort. We use the Universal Thermal Climate Index (UTCI) for assessing the thermal comfort. The UTCI can be determined knowing the mean radiant temperature including solar radiation and longwave radiation from surrounding surfaces on a person and local variables such as air temperature, relative humidity (RH) and wind speed. We consider three consecutive (similar) meteorological days. During the night of the second day, the pavement is wetted by a rain event of 1 mm/h for 10 hours. Fig. 3a gives the average surface temperature for different pavement solutions. The second day is marked by a clear reduction in surface temperature due to evaporative cooling. Fig. 3c shows that the pavement combination PA1-PA3 leads to the highest cooling effect, followed by PA1-PA2. These pavement arrangements combine capillary pumping by PA1 and capillary break by PA3 or PA2. PA3

shows the most effective capillary break effect due to its coarser pores and higher porosity. When omitting a capillary break and using only PA1, water is lost to the soil and not sufficient water remains for guaranteeing an evaporative cooling effect. Figure 3b shows that for PA1-PA3 the first drying period, characterised with a RH close to 100%, lasts the longest. Figure 3d shows that by optimal evaporative cooling by pavements, we can achieve reductions in UTCI up to 2.5 degrees.

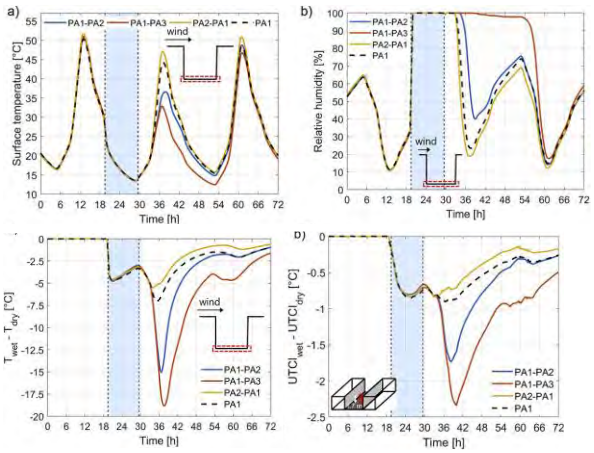

Fig. 5. Results for different pavement solutions averaged over the total street surface: (a) surface temperature; (b) relative humidity at surface; (c) drop in surface temperature comparing wet and dry days; (d) reduction in UTCI comparing wet and dry days (with permission based on [6]).

5. Smart wetting

Having designed a two-layer pavement system combining capillary pumping in the top layer and a capillary break in bottom layer for evaporative cooling, we can now optimize the wetting process by artificial wetting (spraying). We answer the questions 'when', 'how much' and 'how long', which are related to the total amount and intensity of the wetting process. Preferentially, the wetting should guarantee a long-lasting evaporative cooling effect over at least one day-night cycle, while the spraying process has limited disturbance of urban life and traffic.

Figs. 4a-b show the surface temperature and RH at the surface for three days during the three hottest days of the heat wave of 2017 (21st, 22nd and 23rd June) in the city of Zurich. Air temperatures are in the range of 22 - 35°C and the RH between 30 - 80%, with rather low wind speeds. Artificial wetting occurs between 8 and 10 for 2 hours at different intensities (1, 2.5 and 3 mm/h) amounting to quantity of 2, 5 and 6 mm. The ambient temperature and the results for dry concrete are given for comparison. The results show that a wetting intensity of around 2.5 ~ 3 mm/h guarantees maximal evaporative cooling effect during the next day and night cycle. The reductions in surface temperature amount to 10 – 15°C compared to these of dry concrete.

Further analysis showed that the duration of wetting could be reduced from 2 hours to 10 minutes with a total amount of 5 mm/day. We also found that wetting daily in the morning guarantees the same evaporative cooling effect during each day and night cycle.

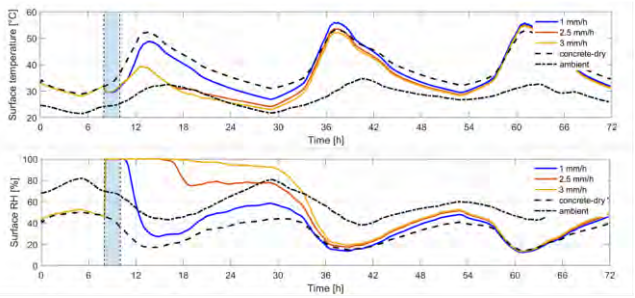

Fig. 4. Results for pavement PA1-PA3 for different spraying intensities. Comparison with dry concrete. (a) Average surface temperature. (b) Average relative humidity.

6. Conclusions and outlook

An urban microclimate model was used to design layered pavements maximizing the evaporative cooling effect during heat waves. The optimal pavement system consists of two layers where the first layer acts as a capillary pump bringing the liquid water from inside its pore structure to the material surface. Second layer acts as a capillary break preventing water loss to the underneath soil. Smart wetting of these pavements includes artificial spraying with an amount of 5 mm/day during 10 minutes in the morning hours. Future research will cover the further design of such pavement systems including the analysis of their durability, their impact in case studies and a demonstration project analyzing their behavior during real environmental exposure.

Acknowledgements

This research project is supported by the Swiss Competence Center for Energy Research SCCER FEEB&D of the Swiss Innovation Agency Innosuisse and the Swiss National Science Foundation (SNF) - Project no. 169323, CTI.1155002539.

References

[1] P. Moonen, T. Defraeye, V. Dorer, B. Blocken, & J. Carmeliet, Urban physics: effect of the micro-climate on comfort, health and energy demand. Front. Arch. Res. 10 (3), 197–228 (2012)
[2] A. Kubilay, D. Derome, B. Blocken, J. Carmeliet, CFD simulation and validation of wind-driven rain on a building facade with an eulerian multiphase model. Build. Environ. 61, 69–81 (2013)
[3] OpenFOAM v6.0 User Guide. The OpenFOAM Foundation (2018).

[4] A. Kubilay, D. Derome, and J. Carmeliet. Coupling of physical phenomena in urban microclimate: A model integrating air flow, wind-driven rain, radiation and transport in building materials. Urban Climate, 24, 398-418 (2018).
[5] A. Kubilay, D. Derome, and J. Carmeliet. Impact of evaporative cooling due to wetting of urban materials on local thermal comfort in a street canyon. Sustainable Cities and Society, 49, 101574, (2019).
[6] A. Ferrari, A. Kubilay, and J. Carmeliet. The use of permeable and reflective pavements as a potential strategy for urban heat island mitigation. Urban Climate, 31, 100534 (2020)

Modeling wood performance? The challenge of using natural materials.

D. Derome[a], M. Chen[b], C. Zhang[c], A. Shomali[b], B. Coasne[d], J. Carmeliet[b]

[a] Department of Civil and Building Engineering, Université de Sherbrooke, Canada
[b] Chair of Building Physics, Department of Mechanical and Process Engineering, ETH Zurich, Switzerland
[c] Laboratory of multiscale studies in building physics, Empa, Switzerland
[d] Liphy, Université de Grenoble, France
* Corresponding author, dominique.derome@usherbrooke.ca

Abstract:
Wood is a natural material with manifold applications in buildings. Its durability depends on intrinsic properties and on environmental loading, which proper modeling all comes with challenges. Wood has a hierarchical configuration, which plays different roles in its hygromechanical behavior: adsorption/desorption, swelling/shrinkage and mechanical softening upon moistening. Different modeling approaches are required at different scales and upscaling between models is required to achieve a proper understanding of wood behavior through computational means. The approach presented here allows to study holistically the hygromechanical behavior of this material using a multiscale approach. The benefit of this approach for durability or long-term performance assessment of wood, or of other natural materials, is demonstrated.

Keywords:
Wood, multiscale modeling, durability, hygro-thermo-mechanical behavior.

1. Introduction

Wood is considered as one of the 'greenest' building materials, not only for structural applications, but also as building components and envelope finishes. The question still persists on how to assess the long-term performance of wood under different loadings (mechanical, hygrothermal, biodegradation, etc).

Wood is a hierarchical material, where the configuration at different scales (lumber, growth ring, cellular and cell wall material) plays different roles in its behavior: adsorption/desorption, swelling/shrinkage and mechanical softening upon. Different modeling approaches are required at different scales and upscaling between models is required. Our approach allows to study holistically the hygromechanical behavior of this material using a multiscale approach.

The atomistic simulation efforts paid off in allowing to reveal the underlying physics of water-porous material interactions. We showed that the origin of sorption hysteresis lies in the coupling of sorption and swelling of the material as elucidated from studying hydrogen bonding networks. This cell wall material behavior is upscaled using a poromechanical approach.

In this presentation, we outline the main elements of this multiscale modeling framework and endeavor in applying this knowledge towards understanding the behavior of wood in partly deteriorated state.

2. Cell wall scale

The origin of sorption and swelling lies at the nanoporous material scale, where water molecules are adsorbed into the hydrophilic matrix of the cell walls, inducing fluid-solid interaction forces, which result in swelling of these cell walls. Therefore, we study in-depth the coupled effects of water sorption and swelling on the hygric and mechanical properties of different polymeric components with atomistic modeling. We aim at understanding all the ramifications of this intricate nanocomposite, with the specific goal of upscaling the results to cellular and macroscopic scales. In order to study the behavior of S2 layer, we analyze the different configurations of cellulose microfibril aggregates and S2 matrix using molecular simulations, as laid out in Figure 1 and Table 1.

For such nanoscale systems, in the last years, a knowledge base and specific methodologies to investigate polymers at this atomistic scale by molecular simulations were developed. This methodological framework is presented in detail in a recent overview paper [7] paving the way for this promising research approach. The realm of hygromechanical behavior is captured for several components of the wood cell wall material and simplified composite systems, obtaining good agreement with experimental data [15-21,39,40]. This work led to the unraveling of the origin of fluid/solid interactions at nanoscale and the ensuing sorption hysteresis. The origin of sorption and swelling hysteresis in a nanopolymer, used as a model system for wood, is studied by considering the configuration of hygroden bonds in the polymer undergoing adsorption and desorption. In adsorption from dry state, as water molecules increase their presence, the polymer to polymer hydrogen bonds are broken, making sorption sites available for water sorption. As water finds its way in, the system swells. Upon desorption, water molecules sit on these sorption sites and prevent the reassembly of the original polymer bonding configuration, delaying the shrinkage and the

attainment of a lower moisture content for a same relative humidity exposure [8].

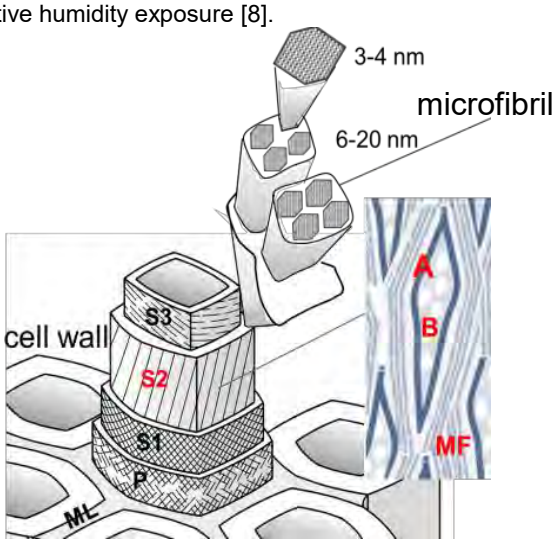

Fig 1: Schematic representation of the cell structure with middle lamellar (ML), primary cell wall (P), the first, second and third secondary wall layers (S1, S2, S3) and the microfibrils (MF), A and B refer to mix as described in Table 1 (illustration partly based on [9]).

Table 1. Chemical components of wood S2 cell wall layer

components of S2 layer	S2 polymers
cellulose microfibril	cellulose
microfibril aggregates	crystalline cellulose water accessible surface or amorphous cellulose hemicellulose possibly
polymeric matrix	
adjacent to microfibrils (matrix A)	hemicellulose galactoglucomannan lignin G (guaiacyl)
in lenticular spaces (matrix B)	hemicellulose glucoronoarabinoxylan (xylan) lignin G

This approach can be used to study the hygromechanical behavior of moisture sensitive cellulose-based materials such as wood, but also synthetized different wood polymer systems, in order to quantify the physical impact of microclimatic conditions. Many contributions demonstrated the validity and efficiency of this innovative approach. The resulting scientific insights lead to possibilities of developing new biomaterials with tailored properties [42,43].

3. Cellular structure scale

At cellular scale, both experimental and modeling investigations can be performed. Experimental advances in imaging acquisition were instrumental. In effect, in order to track water configuration or its effects on porous media, an expertise is developed using advanced imaging technologies ranging from optical light (fast imaging) to neutron projection and X-ray tomography, among others. Original experimental setups and innovative analysis methods are developed to extract complex information [24,26]. Such acquisition of state-of-the-art images is possible with proposal-based access to different imaging modalities, including the imaging beamlines of Paul Scherrer Institute, Villigen, Swirzerland, using neutron [14,37,38] and synchrotron X-ray radiation [10].

Upscaling cell wall behavior to cellular scale is informed through accurate geometrical description of the cellular structure using in particular X-ray CT at different relative humidity, at different scales, namely sub-cellular, cellular and growth ring scales [11,22,26,28]. From actual cellular configuration changes from spring- to summer wood, the swelling behavior of a growth ring can be predicted [29,30,32,33]. Further, parametric analyses have shown the sensitivity of wood behavior to different geometrical metrics.

4. Timber scale

In this multiscale framework, we upscale the hygromechanical observations using a poromechanical constitutive model [3,6,27].

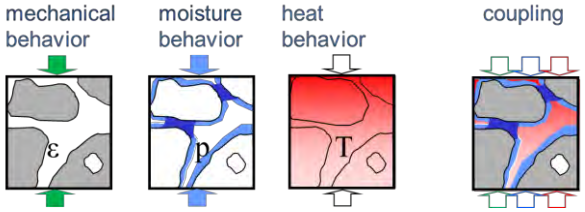

Fig 2: Schematic illustration of the poromechanical approach, where the effects of different fields, here mechanical, hygric and thermal, are modelled by an extensive coupling between the fields, as done in [1,2]

We have upscaled from the cellular scale to the growth ring to timber scales and compared with experimental results to find good capacity in delineating in particular the tangential and radial swelling behavior [31].

5. Wood used as a component of the building envelope: retrofit, climate change, durability, sustainability.

The application of knowledge of wood in building and urban physics problems can be used e.g. to address evaluating and proposing applied solutions. Energy efficiency and retrofitting of the building envelope is a longstanding theme. Assessing and developing building envelope retrofit measures with the aim to reduce building energy consumption has relied on properly modeling and assessing hygrothermal performance and risks of deterioration due to biological degradation (mold and rot), corrosion [36-38], freeze-thaw occurrence. Combining experiments with long term environmental loading in large chambers [4,5,12,14] with smaller scale moisture transport experiments, and with different modeling

methods, [4,5] has proven to be a fruitful approach. A sustainable future requires low-energy and durable buildings, but this assessment has also to consider the changing boundary conditions of the future, thus requiring the selection of moisture reference years taking into account climate change prediction, using our methodology [41]. The multiscale approach can provide the required consistent material properties to be used in durability analysis.

6. Towards predicting the behavior of damaged or deteriorated wood: application for the study of archeological wood treated with PEG

The Mary Rose ship, belonging to King Henry XIII's fleet, sunk in the 16th c. and was raised in the 1970's, to be later housed in a museum. Archaeological wood of shipwrecks buried for centuries under sea sediments is highly degraded due to the chemical changes and material loss. Some polymeric constituents have vanished while others have lower degree of polymerization or other damage. A consolidation technique used consists of spraying polyethylene glycol (PEG) for decades at the surface of shipwrecks to both penetrate the wood and reinforce the wood structure. The microscopic-level mechanisms governing the hygromechanical behavior of PEG-treated archeological wood are still not fully elucidated. Atomistic simulation is used to provide molecular-level insights into the PEG and wood cell wall polymers interactions. Sorption curves are obtained. By applying mechanical tests in silico, the adsorption-induced mechanical softening in the wood cell wall structure is also studied. The mechanism by which the PEG consolidant affects the mechanical stability of wood will be elucidated through studying porosity change and hydrogen bonding formation/breaking at different moisture content.

This first use of our approach to consider damaged systems is expected to yield a better understanding of the physics of polymeric mixtures in general, but also will help for considering novel consolidant materials in the future.

7. Conclusions and outlook

The ensemble of results documents the co-occurrence of sorption and swelling and its hysteresis. This methodology provides new insights into understanding wood behavior and its material properties. Such insights cannot be directly determined solely from experiments. This multiscale methodology is used to explore new pathways for material development and durability of wooden components. Next steps are towards a completely integrated modeling of the hygro-thermo-mechanical behavior of wood, including hysteresis.

Acknowledgements

Support of Swiss National Science Foundation SNF in projects CRSI22-125184, 200021-143601, 200021-162957 and 200020L-182512.

References

[1] Abbasion S, Carmeliet J, Sedighi Gilani M, Vontobel P, Derome D. (2015) A hygrothermo-mechanical model for wood: part A. Poroelastic formulation and validation with neutron imaging – COST Action FP0904 2010-2014: thermo-hygro-mechanical wood behavior and processing. Holzforschung, 69: 825-838.

[2] Abbasion S, Moonen P, Carmeliet J, Derome D. (2015) A hygrothermo-mechanical model for wood: part B. Parametric studies and application to wood welding – COST Action FP0904 2010-2014: thermo-hygro-mechanical wood behavior and processing. Holzforschung, 69: 839-850.

[3] Carmeliet J, Derome D, Dressler M, Guyer R. (2013). Nonlinear poro-elastic model for unsaturated porous solids, Journal of Applied Mechanics, 80:020909.

[4] Carmeliet, J, Derome D. (2012a) "Temperature driven inward vapor diffusion under constant and cyclic loading in small-scale wall assemblies: Part 1 experimental investigation". Build. Envir. 48: 48-56.

[5] Carmeliet, J. Derome D (2012b) "Temperature driven inward vapor diffusion under constant and cyclic loading in small-scale wall assemblies: Part 2 Heat-moisture transport simulations". Building and Environment 47: 161-169.

[6] Chen M, Coasne B, Derome D, Carmeliet J. (2020) Coupling of sorption and deformation in soft nanoporous polymers: molecular simulation and poromechanics, J. Mech. Phys. Solids, 137:103830.

[7] Chen M, Coasne B, Guyer R, Derome D, Carmeliet J. (2019). Molecular simulation of sorption-induced deformation in atomistic nanoporous materials, Langmuir, 35:7751-7758.

[8] Chen M, Coasne B, Guyer R, Derome D, Carmeliet J. (2018). Role of hydrogen bonding in hysteresis observed in sorption-induced swelling of soft nanoporous polymers, Nature Comm., 9:3507.

[9] Derome D, Rafsanjani A, Patera A, Guyer R, Carmeliet J. (2012). Hygromorphic behaviour of cellular material: hysteretic swelling and shrinkage of wood probed by phase contrast X-ray tomography, Philosophical Magazine, 92: 3680-3698.

[10] Derome, Zillig, Carmeliet (2012) "Variation of measured cross-sectional cell dimensions and calculated water vapor permeability across a single growth ring of spruce wood", Wood Science and Technology, 46:827-840.

[11] Derome, D., Griffa, M., Koebel, M., Carmeliet, J. (2011) "Hysteretic swelling of wood at cellular scale probed by phase contrast X-ray tomography", J. Structural Biology, 173:180-190.

[12] Derome, D., Sananeijad, S. (2010) "Inward vapor diffusion due to high temperature gradients in experimentally tested large-scale wall assemblies", Building and Environment, 45: 2790-2797

[13] Desmarais G, Sedighi Gilani M, Vontobel P, Carmeliet J, Derome D. (2016) Transport of polar and nonpolar liquids in softwood imaged by neutron radiography, Trans. in Porous Media, 113:383-404

[14] Guizzardi M, Carmeliet J, Derome D. (2015) Risk analysis of biodeterioration of wooden beams embedded in internally insulated masonry walls, Construction & Building Materials, 99, 159-168.
[15] Kulasinski K, Salmen L, Derome D, Carmeliet J. (2016) Moisture adsorption in glucomannan and xylan hemicelluloses, Cellulose, 23:1629-1637
[16] Kulasinski K, Guyer R, Derome D, Carmeliet J. (2015). Water adsorption in wood microfibril-hemicellulose system: role of the crystalline-amorphous interface, Journal Biomacromolecules, 16, 2972-2978.
[17] Kulasinski K, Keten S, Guyer R, Derome D, Carmeliet J. (2015). Impact of moisture adsorption on structure and physical properties of amorphous biopolymers. Macromolecules, 48, 2793-2800.
[18] Kulasinski K, Guyer R, Derome D, Carmeliet J. (2015). Poroelastic model for adsorption-induced deformation of biopolymers obtained from molecular simulations, Phys. Rev. E, 92, 022605.
[19] Kulasinski K, Guyer R, Derome D, Carmeliet J. (2015) Water diffusion in amorphous hydrophilic systems: a stop and go process, Langmuir, 31:10843–10849.
[20] Kulasinski K, Keten S, Churakov S, Derome D, CarmelietJ.(2014)Acomparative Molecular Dynamics study of crystalline, paracrystalline and amorphous states of cellulose, Cellulose, 21:1103-1116.
[21] Kulasinski K, Keten S, Churakov SV, Guyer R, Carmeliet J, DeromeD.(2014). Molecular mechanism of moisture-induced transition in amorphous cellulose, ACS MacroLetters 3:1037-1040.
[22] Patera A, Van den Bulcke J, Boone MN, Derome D, Carmeliet J. (2018). Swelling interactions of earlywood and latewood across a growth ring: global and local deformations, Wood Sci Techn. 52:91-114.
[23] Patera A, Carl S, Stampanoni M, Derome D, Carmeliet J. (2018). A non-rigid registration method for the analysis of local deformations in the wood cell wall, Advanced Struct. and Chemical Imaging, 4:1.
[24] Patera A, Derluyn H, Derome D, Carmeliet. (2016) Influence of sorption hysteresis on moisture transport in wood,Wood Sc. and Techn., 50:259-283.
[25] Patera A, Jefimovs C, Rafsanjani A, Voisard F, Derome D, Carmeliet J. (2014) Micro-scale restraint methodology for humidity induced swelling investigated by phase contrast X-ray tomography, Experimental Mechanics, 54:1215-1226.
[26] Patera A, Derome D, Griffa M, Carmeliet J (2013). Hysteresis in swelling and in sorption of wood tissue. J. of Structural Biology, 182:226-234
[27] Rafsanjani A, Derome D, Carmeliet J. (2015). Poromechanical modeling of moisture induced swelling anisotropy in cellular tissues of softwoods. RSC Advances 5 (5): 3560-3566.
[28] Rafsanjani A, Stiefel M, Jefimovs K, Mokso R, Derome D, Carmeliet J. (2014) Hygroscopic swelling and shrinkage of latewood cell wall micropillars reveal ultrastructural anisotropy, J. Royal Society Interface, 11:20140126.
[29] Rafsanjani A, Derome D, Guyer R, Carmeliet J. (2013) Swelling of cellular solids: From conventional to re-entrant honeycombs, Applied Physics Letters, 102:211907.
[30] Rafsanjani A, Derome D, Carmeliet J. (2013). Micromechanics investigation of hygro-elastic behavior of cellular materials with multi-layered cell walls. Composite Structures 95, 607-611.
[31] Rafsanjani A, Lanvermann C, Derome D, Niemz P, Carmeliet J. (2013) Multiscale analysis of free swelling of Norway spruce, J. Composites Part A., 54:70-78
[32] Rafsanjani A, Derome D, Carmeliet J. (2012). The role of geometrical disorder on swelling anisotropy of cellular solids. Mechanics of Materials 55: 49-59, 2012
[33] Rafsanjani A, Derome D, Wittel F K, Carmeliet J. (2012). Computational up-scaling of anisotropic swelling and mechanical behavior of hierarchical cellular materials. Composites Science and Technology 72:544-551.
[34] Sedighi Gilani M, Abbasion S, Lehmann E, Carmeliet J, Derome D. (2014). Neutron imaging of moisture displacement due to steep temperature gradients in hardwood,Int. J.Thermal Sci., 81: 1-12.
[35] Sedighi Gilani M, Vontobel P, Lehmann E, Carmeliet J, Derome D. (2014). Liquid uptake in Scots pine sapwood and heartwood visualized and quantified by neutron radiography, Materials and Structure, 47: 1083-1096.
[36] Zelinka S, Glass S, Boardman C, Derome D. (2016). Comparison of the corrosion of fasteners embedded in wood measured in outdoor exposure with the predictions from a combined hygrothermal-corrosion model, Corrosion Science, 102:178-185.
[37] Zelinka S, Glass S, Derome D. (2014) The effect of moisture content on the corrosion of fasterners embedded in wood subjected to alkaline copper quartenary treatment, Corrosion Science, 83:67-74
[38] Zelinka S, Derome D, Glass S (2011) “Combining hygrothermal and corrosion models to predict corrosion of metal fasteners embedded in wood”, Building and Environment 46:2060-2068.
[39] Zhang C, Coasne B, Guyer R, Derome D, Carmeliet J. (2020). Moisture-Induced crossover in the thermodynamic and mechanical response of hydrophilic biopolymer, Cellulose, 27:89-99.
[40] Zhang, C, Shomali, A, Guyer, R, Keten, S, Coasne, B, Derome, D, Carmeliet, J. (2020). Disentangling Heat and Moisture Effects on Biopolymer Mechanics, Macromolecules.
[41] Zhou X, Derome D, Carmeliet J. (2016) Robust moisture reference year methodology for hygrothermal simulations, Build. Envir., 110:23-35.
[42] Song J, Chen S, Zhu C et al. (2018) Processing bulk natural wood into a high-performance structural material, Nature, 554:224–228.
[43] Zhu H, Luo W, Ciesielski et al. (2016) Wood-Derived Materials for Green Electronics, Biological Devices, and Energy Applications, Chem. Rev. 116:9305-9374.

Impact of Climate Change on Energy Demand of a Mid-Rise Office Building

Chinmay Jha[a], Shweta Lall[a], E. Rajasekar[a]

chinmayjha91@gmail.com, slall@ar.iitr.ac.in, raj.fap@iitr.ac.in
Department of Architecture and Planning, Indian Institute of Technology Roorkee, Roorkee, Uttrakhand, India
*Shweta Lall, +919646677911,slall@ar.iitr.ac.in

Abstract:
Globally climate change driven thermal severity has resulted in increased demand for comfort conditioning. Buildings which are designed to the present day scenarios are subject to performance variations in such contexts. It is essential to establish the impact of climate change severity on building energy demand not only in terms of its amplitude but also the periodicity. This study investigates the impact of climate severity on a mid-size office building located in a composite climate of India (New Delhi). The study has the following objectives (a) to map the impact of climate change based on the magnitude and temporal variations of climate variables (b) to establish the effect of climate change on the energy use of a mid-size office building and (c) to delineate design strategies for climate change resilient building envelope. The weather data used in the simulations is made available by ISHRAE for the year 1990 and is morphed for the years 2020 and 2050 using the climate change world weather file generator. This tool uses IPCC TAR model summary data of the HadCM3 A2 experiment ensemble. A statistical analysis of climate variables is carried out to map the magnitude and temporal variation between the years 1990, 2020 and 2050. An energy model of the building was developed for simulations and the results are validated with the actual energy data of the building. The building was found to experience reduction in heating load and increased cooling load in a climate change scenario. Further analysis of periodicity reveals that there is significant increase in cooling demand in the pre-summer and post-summer durations. The study concludes with a set of interventions so as to maintain the current-day energy demand in the future scenario.

Keywords: Climate change, energy demand, Thermal severity, Energy efficiency

1. Introduction

There is a growing concern worldwide about energy use and its implications towards the environment. The fifth assessment report of the Intergovernmental Panel on Climate Change (IPCC) clearly states that since the mid-19th century, the average increase in the temperature of the Earth's surface is 0.85 degrees centigrade (°C). It has also stated that the world temperatures could rise by 1.1 to 6.4 °C during 21st century[1]. Thus, providing a lot of scope for uncertainty in the indoor thermal environment. As the energy consumption and thermal comfort in the building is majorly dependent on outside weather conditions [2]. It is fair to state that climate change plays a vital role in the change of space cooling and heating energy demands globally. Various studies conducted for existing buildings has shown that there is a nearly linear correlation between the increase of average air temperature and the increase of building cooling load. To study the implication of climate change on the building energy consumption three methods are used namely, observation based regression/prediction, global/regional energy modelling and individual building energy simulation [3][4]. The objectives of this paper are (a) to map the impact of climate change based on the magnitude and temporal variations of climate variables (b) to establish the effect of climate change on the energy use of a mid-size office building and (c) to delineate design strategies for climate change resilient building envelope.
The scope of this project is limited to a typical mid-size office building, which comes under the commercial building type as per Indian energy conservation building code (ECBC) [5].

2. Research methodology

The research methodology is divided into three main stages 1) To study the impact of thermal severity of climate change on current and future scenario, 2) to evaluate the actual and simulated building model energy demands, 3) to identify the mitigation and design strategies for built envelope.
Stage 1: Impacts of thermal severity of climate change for current and future scenario are quantified using present-day climate data and A2b emission scenario for future weather files. The selection of A2b scenario for future weather file generation is done based on IPCC third assessment report model summary data of the HadCM3A2 experiment ensemble. Climate change world weather file generator tool based on 'morphing' methodology for climate change transformation of weather data is used in the production of weather data files for 2020, 2050 and 2080 [6]. Analysis of all these years including the current weather data is performed on parameters namely, Dry Bulb Temperature (T), Relative Humidity (RH), Diffuse Horizontal Irradiation (DHI) and Direct Normal Irradiation (DNI).
Stage 2: Changes are established in thermal performance and overall energy demand of a medium-sized office building in New Delhi, for current and future climates. Building simulation model on the basis of various parameters including building materials, architectural details through Plan/Elevation/sections/HVAC system is modelled. These simulations are performed to assess the thermal performance and energy demand of the building model for the current and future climate scenarios.

Following a comparative analysis between simulated and actual energy consumption data.
Stage 3: Identifying the mitigation and design strategies for the built envelope to improve the thermal comfort conditions and building energy demands. Thermal properties of the building envelope includes the U- value and solar heat gain coefficient (SHGC).

3. Case study

Development Alternatives World Headquarters (DA HQ) building is considered for the study. It is recognized for its energy conservation measures which reduce the overall energy consumption by 25-30% when compared with similar typology. It is located in New Delhi, India which represents a humid sub-tropical as per Köppen-Geiger climate classification. Delhi experiences hot summers starting from April to May with an average temperature of approximately 32°C with occasional heat waves, followed by monsoon from June to September and then short winters starting from late November with an average temperature 6-7°C till January.The building is modeled as per the actual specifications. Its total built-up area is 4500 sqm. with a six storey construction. It is modeled with density of 0.11 people/sqm, with scheduled occupancy as per actuals.

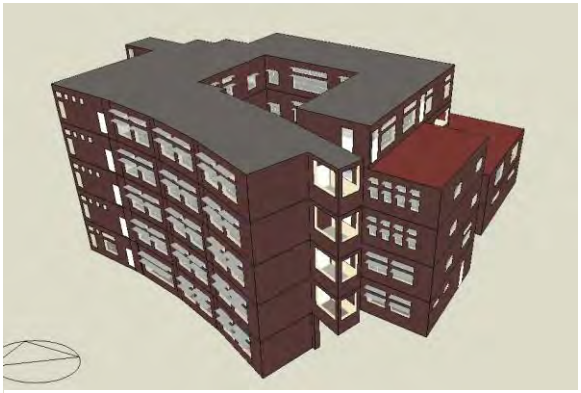

Figure 1: DA headquarters building simulation model.

The building simulation model for DA HQ building shows 91.37% similarity between simulated vs actual energy consumption data. Further analysis on monthly energy data comparison shows that the simulated model performed similar with the summer and monsoon months (May to Oct) with 102.31% similarity, while winter months (Nov to Apr) works with 74.06% efficiency.
Simulations are performed to quantify the impact of energy consumption for 1990, 2020 and 2050. The comparison between heating energy demand, cooling energy demand and total HVAC energy is shown in Figure 2,3 and 4. To validate the energy performance of the simulated model of DA Building (New Delhi), a collective mean monthly energy consumption for 2016 to 2018 is calculated. This monthly mean and annual average data is further used to validate the energy consumption of 2020 for DA building.

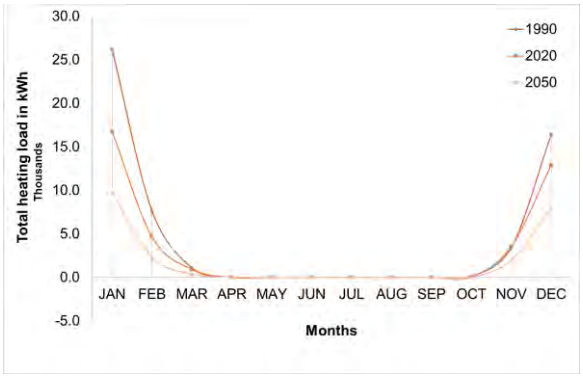

Figure 2: Heating load in kWh for DA HQ building

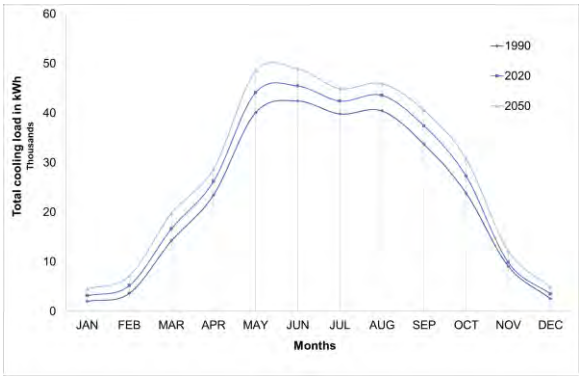

Figure 3: Cooling load in kWh for DA HQ building

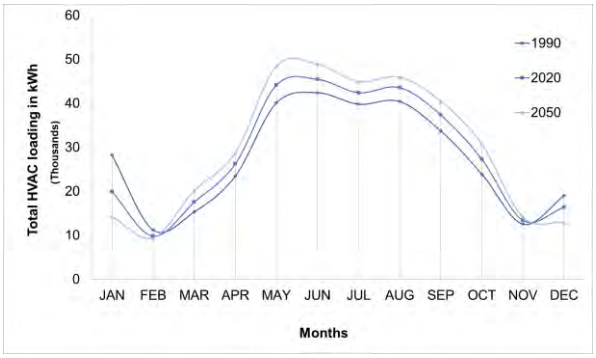

Figure 4: Total HVAC in kWh for DA building

The heating energy load decreased by 16032.6 kWh (-29.93%) from year 1990 to 2020 and 16256.3 kWh (-41.97%) from year 2020 to 2050 (Fig 2). Whereas, cooling energy load increased by 29271 kWh (11%) from year 1990 to 2020 and 31873 kWh (10%) from year 2020 to 2050 (Fig 3). The total HVAC energy demand increased by 13162 kWh (4%) from year 1990 to 2020 and by 15574 kWh (5%) from year 2020 to 2050.

4. Result and discussions

In order to quantify the impact of climate change on building energy consumption. Climate clustering for base year (1990) and 2050 (A2b) future scenario is done.

4.1 Impact of climate change based on the magnitude and temporal variations of climate variables

In the context of present study, a two-step cluster analysis yielded nine climate clusters based on their homogeneity. Data in a specific cluster has attributes namely, daily maximum temperature (T_max), daily minimum temperature (T_min), daily average relative humidity (RH_avg) and daily average global horizontal irradiation (GHI_avg). Table 1 presents the summary of the clustering for summer, winter and monsoon seasons.

	SEVERE		MODERATE		LOW	
	1990	*2050*	*1990*	*2050*	*1990*	*2050*
Summer	**3(25)**	**1(16)**	**2(37)**	**2(41)**	**4(24)**	**4(32)**
Tmax	40.4	43.5	38.6	40.2	33.3	36.9
Tmin	25.9	31.2	27.2	29.7	20.0	23.3
GHIavg	610	608	520	503	560	553
RHavg	38	38	52	53	40	39
Winter	**7(76)**	**9(56)**	**5(19)**	**8(41)**	**8(70)**	**5(63)**
Tmax	22.6	25.3	18.2	23	29.3	30.9
Tmin	9.9	11.7	10.9	13.9	14.8	17.3
GHIavg	373	384	261	296	443	436
RHavg	69	65	84	80	58	61
Monsoon	**6(45)**	**7(31)**	**9(1)**	**6(1)**	**1(68)**	**3(84)**
Tmax	31.8	32.6	31.6	33.7	34.8	35.3
Tmin	24.6	27.6	18	20.9	26	28
GHIavg	368	333	280	310	455	411
RHavg	77	85	51	55	65	71

Table 1 Cluster days Comparison
() denotes number of days

These clusters are further identified into three seasons- summer, monsoon and winter. Clusters with highest daily T_max and T_min are classified into summer and winter clusters while high RH_avg and low GHI_avg are classified into monsoon clusters. Every season is assigned three clusters severe, moderate and low. From the climate clustering analysis, it is clear that the number of days shifting from winter clusters (5) are compensated into summer (3) and monsoon (2).

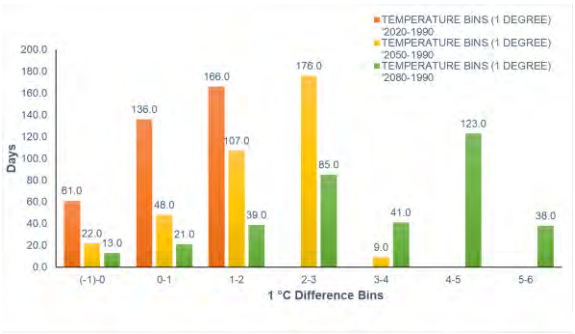

Figure5 : Frequency difference between 2020, 2050 and 2080 to 1990 (T_max)

Compared to the base year (1990) a significant increase in the number of days with higher temperature difference is observed, 4-6°C for 2080, 2-4°C for 2050 and 1-2°C for 2020 as shown in Figure 5 and 6. Comparison of GHI_avg shows a similar trend to temperature.

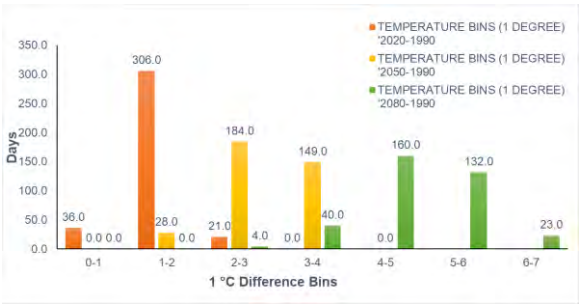

Figure6 : Frequency difference between 2020, 2050 and 2080 to 1990 (T_min)

Comparison of RH_avg for the three years 2020, 2050 and 2080 with base year shows a significant increase in extreme category of 10%-20% and 90%-100% .Refer Table 2 to infer the frequency differences in RH_avg.

	DIFFRENCE AS TO 2020	DIFFRENCE AS TO 2050	DIFFRENCE AS TO 2080
RH (10-0)	0	0	1
RH (20-10)	-3	-4	61
RH (30-20)	-115	-102	-147
RH (40-30)	-131	-128	-207
RH (50-40)	-198	-179	-184
RH (60-50)	-268	-249	-346
RH (70-60)	-167	-141	-170
RH (80-70)	-205	-159	-263
RH (90-80)	-1	1	10
RH (100-90)	229	102	386

Table2 :Frequency difference between 2020, 2050 and 2080 to 1990 (RH_avg)

4.2 Effect of climate change on the energy use

To understand the energy consumption of DA HQ building an ECBC prescribed base case of the same is modelled and simulated to compare the seasonal clusters energy consumption of year 1990 and 2050.

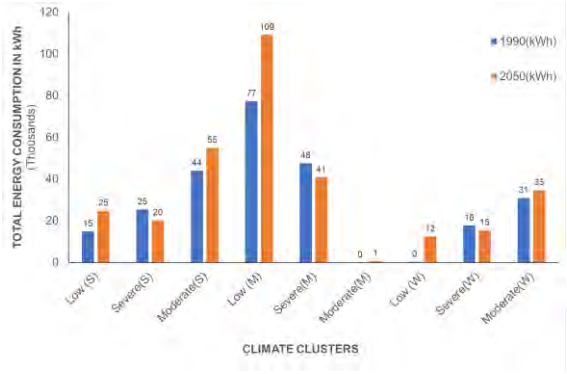

Figure7 : Total energy consumption of DA HQ building (ECBC compliant) 1990 and 2050

From Figure 7, it is determined that the total energy consumption for severe summer, monsoon and winter months decreases when the year 1990 is compared to 2050 and increases for all the three seasons for low and moderate clusters.This simultaneous comparison between change in the number of days and change in energy consumption

shows a similar pattern. Energy consumption changes as the number of days shift among the clusters.

4.3 Design strategies for climate change resilient building envelope

In this study we focus on the U-Value (External Wall, Window) and Solar Heat Gain Coefficient (SHGC) of the building envelope for energy performance improvement.
Optimization of each property is done to estimate the suitable U-Value, which can bring down the energy consumption of the year 2050 to the same level as that of the base year (1990) for DA HQ building. Through various iterative runs of the building model, the U-value for external wall of 0.14 W/m^{2}K yielded a comparable HVAC energy consumption between the year 2050 and the base year. This meant a 66.82% decrease in heating load and 12.50% increase in cooling energy load. Further for an SHGC of 0.1, the decrease in the heating load is 44.28% and the increase in cooling energy load is 9.02%. Similarly, when the U-value of window is considered as 0.1 W/m^{2}K it yields a comparable HVAC energy consumption between the year 2050 and the base year. This meant a decreased by 70.7% in heating load and 20.51% increase in cooling energy load.

5. Conclusion and outlook

This paper maps the impact of climate change based on the magnitude and temporal variations as well as establishes the effect of climate change on the energy use and delineates the resiliency measures to future proof the building.
A comparative cluster analysis of climate variables T_max, T_min, RH_avg and GHI_avg for base year 1990 and 2050 indicates that the decrease of 5 days from winter cluster are compensated in summer cluster by increase of 3 days and in monsoon cluster by increase of 2 days.
Energy simulations for DA Building indicates a decrease in heating energy demand by 35.6% on average, increase in cooling energy demand by 10.5% and overall increase in HVAC energy demand by 4.5%.
A single mitigative factor is able to limit the energy consumption of future scenario (2050) to the base year scenario (1990). The paper presented a change in envelope U-value for external wall of 0.14 W/m^{2}K, U-value for window of 0.1 W/m^{2}K and glazing SHGC which leads to changing building energy demand as per base case scenario as 0.1.

Acknowledgements

This work is carried as a part of Zero Peak Energy Building Design for India (ZEDi), grant no. DST/TMD/UKBEE/2017/17.

References

[1] N. Adger and A. Coauthors including Fischlin, "Summary for policymakers," *Clim. Chang. 2007 Impacts, Adapt. vulnerability. Contrib. Work. Gr. II to Fourth Assess. Rep. Intergov. Panel Clim. Chang.*, no. vii, 973, pp. 7–22, 2007.

[2] H. Wang and Q. Chen, "Impact of climate change heating and cooling energy use in buildings in the United States," *Energy and Buildings*, vol. 82. pp. 428–436, 2014.

[3] J.Huang, "The variation of climate change impact on building energy consumption to building type and spatiotemporal scale." .

[4] K.K.W Wan, "Impact of climate change on building energy use in different climate zones and mitigation and adaptation implications." .

[5] Energy Conservation building code, 2017,vol. 1, no. 4, p. 53, 1389.

[6] M. F. Jentsch, P. A. B. James, L. Bourikas, and A. B. S. Bahaj, "Transforming existing weather data for worldwide locations to enable energy and building performance simulation under future climates," *Renewable Energy*, vol. 55. pp. 514–524, 2013.

[7] Beepindia.org. (2018). BEEP Case Study - Aranya Bhawan

[8] Trupti J. Dabe, Vinayak S. Adane, The impact of building profiles on the performance of daylight and indoor temperatures in low-rise residential building for the hot climatic zones 2018.

Parametric Design of Balconies in Multi-Unit Residential Buildings

T. Peters[a*], T. Kesik[b]

[a] Department of Architectural Science, Ryerson University, Toronto, Canada
[b] John H Daniels, Faculty of Architecture, Landscape and Design, University of Toronto, Canada
* Corresponding author, Terri Peters terri.peters@ryerson.ca

Abstract:
Condominiums have become the predominant housing form in Canada, and connection to the outdoors, adequate fresh air, and appropriate levels of daylight are essential to people's quality of life. The majority of new condos have balconies, but there are no climate-specific balcony guidelines for comparing design options for multi-unit residential buildings (MURBs) with balconies. To date, studies of MURBs have focused on other important parameters including energy efficiency, indoor comfort, daylight, and resilience, but there is a significant research gap relating to balcony design. Balcony spaces are often underutilized, and shade both the living spaces inside and the units below. This research presents a research framework and preliminary results of a simulation-based study to quantify the impacts of three typical balcony designs on daylight in MURB dwellings. The framework and findings presented form part of a larger and more comprehensive simulation-based study that will provide the basis of design guidelines for balconies.

Keywords:
Daylight, Multi-unit residential building (MURB), simulation, balcony, parametric design,

1. Introduction

Daylight and connection to the outdoors are important in all housing types, but multi-unit residential buildings (MURB) housing has specific performance challenges [1, 2]. MURB units tend to have inadequate daylighting, and poor connection to the outdoors [3,4] Most new MURB units have balconies, and these are one of the defining architectural and programmatic elements that distinguish tall urban buildings from offices. In cities such as Vancouver, there are a range of balcony types and sizes being constructed, but no climate-specific guidelines for comparing design options for suites with balconies. This paper presents preliminary findings of a simulation-based study focused on the impacts of balcony design on daylight.

Fig 1: Examples of balcony types in MURB housing.

2. Methodology

This study seeks to understand significant balcony design parameters that impact daylight. This study evaluated daylight in the condo units using climate--based daylight simulation (CBDM) [5]. Daylight autonomy (DA) is used as the metric in order to understand, quantify, and compare the impacts of balconies on the interior floor area [6]. DA is an annual metric that describes the percentage of floor area that receives a specified target illuminance for at least half of the space's annual occupied hours. This DA metric was chosen, rather than Spatial Daylight Autonomy (SDA), another metric often used to understand annual daylight in spaces, as this study does include the use of a blind control model that predicts the status of moving shading devices at all time steps of the year [6].

The results presented here are part of a larger study to understand and quantify the impacts of balcony design on daylight in MURB. It is imagined that this study will help inform early stage design of new condos. In this paper, a single geographic location is presented, Vancouver BC, but the larger study examines a number of Canadian climates and regions. Overheating and glare are considered to be less of a concern in MURB than in offices, due to the typical 1:2 or 1:3 aspect ratio in condo floorplates, and also because it is not assumed that people are sitting along the facades in fixed positions. For these reasons the study focuses on how much natural light can enter the unit with the different balcony options, due to the energy saving, quality of life, and health and wellbeing benefits of daylight. An upper illuminance threshold to study visual discomfort, glare, and overheating are not specified.

The study examines MURB floorplans that are single aspect, size lit, one bedroom units with a floor to ceiling height of 8' (2.4m). While our earlier research found that window to wall ratios above 70% did not positively impact daylight [1] in this study we did not vary the WWR, we used 100% WWR to simplify our massing model and maximize the amount of light that could possibly enter floorplans. This study assumed the units are occupied 8am-6pm with Daylight Savings Time (DSTI) invoked, analyzed in 60 minute increments. For the analysis grid, the node height and spacing assumptions are 0.5 m high, the node spacing is 0.5 m apart. Furniture and partitions are highly variable and

so the maximum potential illumination was examined. The façade glazing simulated represents commonly used MURB façade materials (Table 1).

Table 1: Surface reflectance and glass transmittance used in DIVA simulations.

Materials	Reflectance/transmittance *
Ceiling	70%
floor	20%
glazing	65%*
Glazed balcony panels	88%*
Solid balcony panels	70%
Outside ground	20%

As expected, the results of this study show that any balcony at all negatively impacts the daylight in the unit. The amount of impact varies depending on the qualities of the balcony. The impacts are studied in relation to the best performing option. The DA of the south facing unit without a balcony is DA 300 lux [50%]=62.84% which is the highest relative to other orientations. For comparision, the East facing is DA 300 lux [50%]=54.81%; the North facing is DA 300 lux [50%]=44.05%; and the West facing is DA 300 lux [50%]=54.39%.

Balcony Impacts Relative to Baseline Study

To be able to interpret the relative impact of balconies on the daylight in condo units in this study against an ideal, no balcony option, this study evaluates the impact of balconies on DA as a percentage of the baseline DA of the best performing South facing, no balcony unit (Table 2).

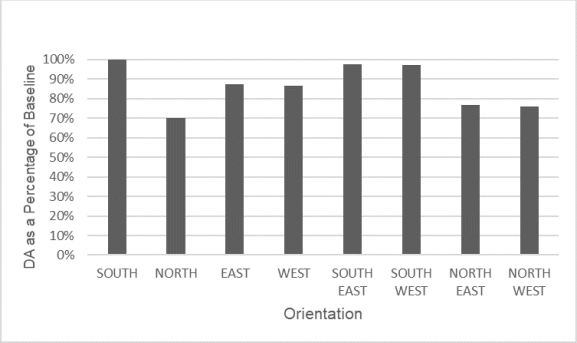

Fig 2: The results showed that the South orientation had the best daylight in the typical MURB unit and so the three balcony options were evaluated using this orientation.

3. Results and Discussions

Size, Geometry, Materials, Positions of Balconies

The results confirmed the assumption that balcony size and geometry are the most important parameters as the added depth creates deeper floorplates therefore limiting daylight access to the indoor living space. Other important considerations in this study were found to be the materials of the outer balcony wall, studied here as solid and glazed. Another important parameter is the position of the balcony on the facade. Balconies are normally stacked one above the other along a facade, and so the balcony above shades units below. Both a stacked and staggered design were tested. Both glazed and solid balcony handrail options were studied with a height of 1.2m.

Table 2: Results of the impact of balcony design on south facing unit floorplates showing both glazed and solid balcony walls

Balcony Type	Relative Daylight Autonomy of unit floorplan (assuming no balcony is 100%)
No balcony	100%
Option 1: 1m Continuous	78% glazed (67% solid)
Option 2a: 2m x 2m Staggered	95% glazed (88% solid)
Option 2b: 2m x 2m Stacked	87% (glazed) (81% solid)
Option 3: 3m x 2.5m inset loggia	80% glazed (76% solid)

Several balcony sizes and geometries were modelled and simulated and this paper reports on the best performing options for typically used balcony geometries (Table 2). Typically in offices, the target illuminance is 300 lux and the height of the task plane (desk height) 0.8m is used. The daylight was measured at typical task height, the convention for daylight simulation in buildings, although further studies will test other heights.

The study used typical balcony types based on size and geometry. Simulations were carried out for:

Option 1. This balcony type is long and shallow, located along the whole facade of the unit. The balcony measures 1.0m wide along length of façade (Figure 3). In this case, the balcony functions not as an usable room, and is more of a facade element than outdoor space. Option 1 is a shading device on the building façade, and is the worst performing of the three options. Simulations were carried out for two material options: a glazed balcony wall and a solid balcony wall (Table 1). The results showed that this option had the most significant performance difference in the two material studies. A solid balcony achieved 67% DA relative to the option with no balcony, whereas the glazed handrail allowed more daylight into the unit, and achieved 78% DA relative to the option with no balcony.

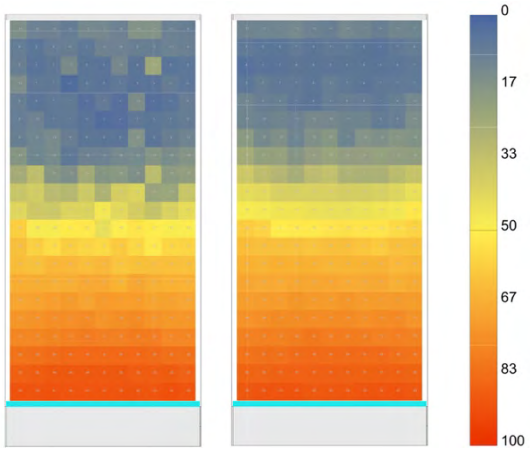

Fig 3: Option 1a on the left assumes a solid balcony wall and achieves DA 300lux [50%]= 42.23% DA, and Option 2b on the right assumes a glazed balcony wall and achieves DA 300lux [50%]= 44.65%

Option 2. This balcony type is an extruded square balcony, that juts out from the building the length of the façade (Figure 4). This was modeled at 2.0m wide and 2.0 meters long over half of the façade (typically the living room). In this case, the balcony is more of a useable outdoor room where the inhabitant could put a small table and chairs, and step outside and possibly see the sky. Two options were tested in terms of facade position. Option 2a is a staggered arrangement where the units are not directly above one another on the façade. Option 2b is a stacked arrangement where the units are directly above one another one the façade, shading the balcony below and unit interior. Option 2a is the best performing balcony option followed by 2b. Simulations were carried out for two material options for each Option 2a and 2b: a glazed balcony wall and a solid balcony wall.

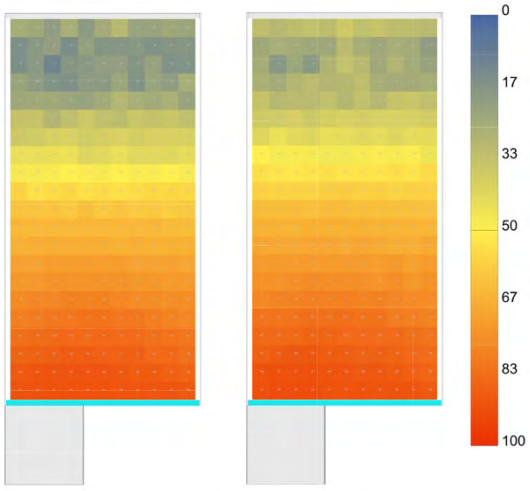

Fig 4: Option 2a on the left assumes a solid balcony wall and achieves DA 300lux [50%]= 55.32% DA, and Option 2b on the right assumes a glazed balcony wall and achieves DA 300lux [50%] = 58.83%

Option 3. This balcony type is inset into the façade, as a loggia, modeled at 3.0 meters deep and 2.5 meters wide (Figure 5). In this option, the balcony does not protrude along the façade of the building and so does not shade the unit below it. This design is shown to significantly reduce the amount of DA in the unit because it has the effect of creating a deeper living space. Simulations were carried out for two material options: a glazed balcony wall and a solid balcony wall. The simulation showed no significant difference when comparing solid or glazed railings, in this option, uniquely the impact is in how the design of the loggia balcony create a deeper floorplate.

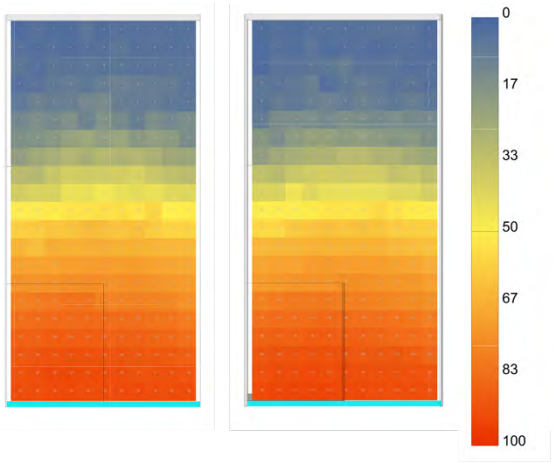

Fig 5: Option 3a on the left assumes a solid balcony wall and achieves DA 300lux [50%] =48.07% and Option 3b on the right assumes a glazed balcony wall and achieves DA 300lux [50%] =47.78%

4. Conclusions and Outlook

This study examined several balcony design options and compared the relative impact of different balcony designs on daylight in the unit. Based on the design of typical MURB units, and typical balcony units a number of parameters were considered: geometry and size of balcony, location of the balcony in relation to the unit, material of the balcony railings.

The balconies in Option 1 created a shading screen across the building, so a significantly lower amount of daylight entered into the living space. Option 1 showed that the limited benefit of a 1m wide balcony, which would be difficult to practically use as a living space, unacceptably shaded the living space inside, which would only get 67% of the DA in the solid option and 78% in the glazed handrail option compared to the baseline no balcony option. This would greatly impact people sitting in the living room on a sofa, as the light would be shaded at this level. A follow up study will work to understand the impact at multiple

illuminance planes as this study focused on desk height.

The balconies in Option 2 are also a common balcony type and can be considered more of a usable outdoor room. Unfortunately, there are also significant trade-offs with daylight, depending on materials used and position on the façade. This study showed that the position of the balcony on the façade greatly impacts daylight in a unit. By staggering the balconies on the façade (Option 2b), the negative impacts of the balcony are lessened, due to minimized shading. The most significant result in this study is that a good-sized balcony, 2m x 2m can be designed for a small unit, as long as there is a glazed handrail and the balconies are staggered along the façade. Results of Option 2B shows that there is a very small difference between the daylight in this unit, and a no-balcony unit. It achieves 95% of the baseline DA.

The balconies in Option 3 are inset into the façade, as indoor/outdoor rooms within the living space, partly enclosed with a 1.2m high handrail. This option has no impact on shading units below. Unsurprisingly, this balcony design has the lowest performing daylight of the studies presented, because the balconies serve to create a deeper floorplate, limiting daylight penetration into the room behind. They do also have a benefit in creating some articulation in the façade, allowing light to come in from two panes of glazing. In both the option with a glazed handrail (80% of baseline) and the option with a solid handrail (76% of baseline), the DA is much lower than the no-balcony option. The geometry and orientation are still the most significant parameters in balcony design, rather than materials or small differences in balcony depth. Option 3 could have some non-daylight benefits because the balcony is a room that is covered and yet open to view and air from the front. This may prove desirable in a rainy climate like Vancouver but more research needs to be done to understand people's satisfaction with balcony design. Some studies have asked residents about their environmental satisfaction in MURB, but not directly about balconies [7].

Based on this initial study the following general conclusions about balcony design and MURB can be drawn:

1. Balconies are desirable in MURB and their design including size, orientation, and materials are important. However, this study shows that any balcony limits daylight penetration into the unit, and in some cases also shades the unit below, thereby limiting what little daylight does come in to a MURB unit.

2. There is a need to examine the simulation parameters and assumptions relating to daylight and MURB design. For example, MURB-specific criteria must be developed relating to occupancy and uses of rooms, the most relevant target illuminance levels to achieve visual comfort given that there is no 'task' associated with some spaces, and more consideration must be placed on appropriate metrics for MURB units in relation to daylight. For example, DA is normally evaluated at 300 lux but in MURB there are a range of activities and program types making this a problematic assumption.

3. In MURB, there are numerous important parameters aside from daylight that must be considered when designing balconies, including impact on energy efficiency and indoor thermal. For example, balconies can create thermal break between interior and exterior resulting in poor thermal comfort and performance. This trade-off will be analyzed in future studies. Other important trade-offs include quality of life parameters including the relative size of the unit to the balcony space, views, and privacy.

Acknowledgements

The authors would like to thank BC Housing for their support of this research.

References

[1] T. Peters, T. Kesik. Daylight simulation for multi-unit residential buildings: occupant-centered approaches to assessment, in eSIM 2018 Conference Proceedings, Available:http://www.ibpsa.org/esim-2018-conference--proceedings/

[2] M.S. Andargie, M. Touchie, W. O'Brien. A review of Factors affecting occupant comfort in multi-unit residential buildings. Building and Environment, 160 (2019) 106-182.

[3] J. Veitch, A. Galasiu. 2012. The physiological and psychological Effects of Windows, Daylight, and View at Home: Review and Research Agenda. National Research Council of Canada Institute for Research in Construction NRC-IRC Research Report RR-325.

[4] T. Kesik, L. O'Brien, T. Peters. MURB design guide: enhancing the liveability and resilience of mulit-unit residential buildings (MURBs) v2. February 2019. Available:https://www.daniels.utoronto.ca/faculty/kesik_t/MURB-Design-Guide/MURB-Design-Guide-v2--Feb2019.pdf

[5] Mardaljevic, J. (2006). Examples of climate-based daylight modelling. CIBSE National Conference 2006: Engineering the Future, 21-22 March, Oval Cricket Ground, London, UK.

[6] C. Reinhart, J. Mardaljevic, Z. Rogers. Dynamic daylight performance metrics for sustainable design. Leukos Vol 3, No 1, July 2006, p.7-31

[7] P. Xue, C.M Mak, Z.T Ai. A structured approach to overall environmental satisfaction in high rise

residential buildings. Energy and Buildings, 116(Complete) 181-189.

Optimizing mass timber-concrete composite floor systems with respect to embodied carbon

T. Joyce[a,*], H. Daneshvar[b], Y.H. Chui[c], L. Zhang[d]

[a] PhD Student, Dept. of Civil and Environmental Engineering, University of Alberta, Edmonton, AB, Canada
[b] Post-doctoral Fellow, Dept. of Civil and Environmental Engineering, University of Alberta, Edmonton, AB, Canada
[c] Professor, Dept. of Civil and Environmental Engineering, University of Alberta, Edmonton, AB, Canada
[d] PhD Candidate, Dept. of Civil and Environmental Engineering, University of Alberta, Edmonton, AB, Canada
* Corresponding author, +1 778 991 1248, tpjoyce@ualberta.ca

Abstract:
Efforts to reduce the environmental impacts of the construction industry have resulted in growing interest in the use of low carbon materials such as timber. For long span floors found in common office buildings, serviceability issues (mainly vibration and deflection) restrict the application of timber floors and have fueled the development of timber-concrete composite (TCC) systems. A comparison of cross-laminated timber (CLT) floors with and without structural concrete topping was performed using common TCC floor design methods, with and without satisfying vibration criteria. In both cases, lower embodied carbon values were found by using a thicker CLT panels rather than adding concrete topping. Increasing timber thickness also resulted in a lower floor weight, which would contribute toward reducing the size of supporting framing members and foundations, resulting in further reductions in the embodied carbon of the whole building. Severe span limits and large discrepancies with methods in CSA O86 were observed for the vibration criteria obtained from the literature, and suggest the need for further research on appropriate vibration criteria for TCC systems.

Keywords:
Embodied carbon, Timber-concrete composite (TCC), Cross-laminated timber (CLT), Timber, Sustainability.

1. Introduction

In recent years the use of timber for tall non-residential and multi-unit residential buildings has increased worldwide, including in North America, motivated primarily by perceptions surrounding the sustainability of timber as the main structural material [1]. In particular, timber structures are generally associated with lower levels of embodied carbon due primarily to lower emissions during manufacturing of the materials. In addition, some life cycle accounting practices permit the inclusion of carbon sequestered from the atmosphere during tree growth that is captured within timber products for the duration of their life [2].

One of the main applications of engineered timber products such as glue-laminated timber or Cross Laminated Timber (CLT) is the usage in floor or roof systems, as a part of both vertical and lateral load resisting systems of the building. At typical floor spans found in office buildings, however, the lighter weight and lower stiffness of timber floors can make them more susceptible to serviceability limit states such as vibrations and excessive deflections, while satisfying the strength requirements. Increasingly timber-concrete composite (TCC) floor systems, wherein a structural concrete topping layer is provided over the timber, are being used to address these issues [3]. Since concrete products are more carbon intensive than timber, there is a trade-off between additional concrete for improved vibration performance and increased embodied carbon. This study seeks to explore this trade-off, particularly around the application of structural concrete topping on CLT floor panels.

2. Background

Despite the on-going research in the field of the mass timber products, at present there is no standardized method for designing TCC floor systems in Canada. Various methods have been proposed, of which the γ-method, based on Annex B of Eurocode 5 [4] is commonly used to account for the imperfect composite action [5]. In this method, the degree of composite action depends on the connector stiffness, which is a function of the connector type and spacing. The thickness of the concrete layer is chosen based on several requirements, including: anchorage of the fastener; limits for concrete crushing; minimum cover to reinforcement; sound transmission; and, a minimum thickness required for diaphragm action. Generally, concrete thicknesses of 75 mm to 100 mm (approximately 3 in to 4 in) are used in practice, though past studies have considered thicknesses as low as 57mm with inclined self-tapping screws [6] and 48mm with notches and dowels (approximately 2 in), using steel fibre reinforcement to remove the cover requirements [7]. Ultra-thin toppings of only 12.5mm (1/2 in) were tested by [8], and showed significant reductions in both stiffness and strength relative to comparable connections with inclined self-tapping screws in thicker concrete layers. Despite this, the topping was found to be effective in reducing the perception of human-induced vibrations by increasing the natural frequency [8].

CSA O86 [9] provides a vibration-based limitation on the allowable span for CLT floors, however the calculation does not adequately account for potential composite behavior. Other simplifying assumptions

such as the added weight of concrete topping are neglected, and the limiting span may be increased by 20% if the floor covers extends over more than one span and has a non-structural element that enhances the vibration performance. Hamm et al. [10] proposed a method for checking the vibration performance of TCC floors. For floors with higher vibration demands (including office spaces), the natural frequency should be above 8Hz and the deflection under a static, centrally-located 2kN point load should be less than 0.5mm. For floors having a natural frequency less than 8Hz but greater than 4.5Hz, an additional check on the floor peak acceleration under a defined impulse is required that shall be less than 0.05m/s^2.

3. Methodology

An analysis comparing the embodied carbon of floor systems using CLT completed with structural concrete topping was made to investigate the effect of floor span and connector stiffness. The properties of the CLT panels were determined for a unit width of 1.0 meter using CSA O86 [9] for the V1 stress grade. The specified compressive strength and modulus of elasticity of concrete topping were assumed to be 35MPa and 26600MPa, respectively. Dead loads were obtained from the self-weight of the timber and concrete materials with an additional uniformly distributed superimposed load of 0.5kPa and a live load of 2.4kPa, corresponding to an office occupancy.

The composite floors were designed using the γ-method in Annex B of Eurocode 5 [4] for short term loading only, despite the time dependent behaviour of TCC systems. This choice was supported by the results, which showed that the designs tended to be governed by short-term effects, such as vibrations and deflections under live loads alone.

To reflect a variety of connector setups γ-values of 0.25, 0.5, 0.75, and 1.0 were selected. The analysis was repeated for spans from 2.0 to 12.0m, for 3-ply (105mm thick), 5-ply (175mm), and 7-ply (245mm) CLT panels. In each case, a minimum concrete thickness was selected for each CLT panel thickness that satisfied the strength requirement in bending, deflection, and vibration requirements. From preliminary calculations it was found that the vibration criteria in [10] resulted in thick concrete layers that did not align with the results from floor vibration tests. This is partially due to conservative assumptions for boundary conditions (i.e. simply-supported members). A simplified set of vibration criteria was chosen based on [10] but omitting the additional check for floors where 4.5Hz ≤ f_n < 8Hz. Bare CLT (using the vibration criteria in [9]) and simply supported concrete systems (taken as 1/20 times the span, with a 100mm lower cutoff for cover to reinforcement) were included for comparison.

The embodied carbon content of the floors was determined using carbon intensities (kgCO_2eq/m^3) obtained from Athena Impact Estimator for Buildings [11]. Since the analysis does not explicitly consider any particular connection between the concrete and timber elements, only the cradle-to-gate carbon associated with the concrete and timber elements were considered. For the purposes of this study, the building was assumed to be owner-occupied and located in Vancouver, Canada. In order to focus exclusively on near-term embodied emissions, carbon storage in the timber material was excluded. The carbon intensity of the CLT from Athena was compared with available environmental product declaration values from major CLT producers in Canada and was found to over-estimate the intensity by 15-30%. This implies that the results are shifted up slightly, however the effect on the general conclusions was observed to be minimal.

4. Results and discussions

The design of the timber-concrete floors was governed at all spans by the vibration criteria, which generally agrees with common practice. Relative to the vibration-controlled span limit in CSA O86 [9], the set of selected vibration criteria was found to be more severe, with 65% to 80% reductions in the maximum spans achieved with bare CLT. This was partially a product of the strict static deflection criterion; supports the need for further research on the vibration performance of both bare CLT and TCC floors.

Additionally, the results of the analysis show that the lowest embodied carbon values are generally found for floors with bare CLT or thin skim coats (Fig 1). If a minimum concrete thickness of 12.5mm (1/2 in) is assumed for composite action (based on the minimum thickness tested by [8]), then the range of spans for which the lowest embodied carbon is achieved with TCC is quite limited (Fig 2). As such, it is preferable, from the perspective of minimizing embodied carbon, to use a thicker CLT panel than to use a TCC system. While the analysis was only performed for up to 7-ply CLT, it is likely to apply for longer spans with 9-ply or thicker panels.

Given the discrepancies between the selected vibration criteria and the bare CLT check in CSA O86 [9], the analysis was repeated considering deflection (less than L/360 and L/480 for total dead and live load and solely live load, respectively, in which L is the span length) and strength only. As in the previous case, the deflection criteria governed for all spans. CLT alone was found to be acceptable at much larger spans (approximately 175% longer), after which the required concrete thickness increased rapidly. As a result, the range of spans for which the TCC floors had less embodied carbon was more restricted, further supporting the recommendation to increase the size of the timber panel rather than introduce thicker concrete toppings.

The effect of the γ-value, representing the degree of composite action, diminished as γ increased (Fig 4), with relatively little variation for γ ≥ 0.5. The trend was most pronounced for the vibration criteria, which reflects the strong relationship between vibration performance and floor stiffness. Since γ is a function of connector stiffness, the results indicate that there is little benefit to increasing the stiffness of connectors beyond a moderate threshold. Considering typical connector stiffness values (see [4]), this suggests that there is little difference in the embodied carbon-related performance of TCC floors assembled using adhesives, notches, or nail plates; for dowel-type and inclined self-tapping screw connectors the behaviour will depend on the fastener dimensions and spacing. Further, as the designs were limited by vibration, the ultimate strength of the connectors was similarly not influential in the design outcome. Together these results indicate that the choice of connection between the timber and concrete elements has only a minor impact on the design beyond a threshold level (γ = 0.5), and the thickness of concrete required for acceptable vibration performance for a given span and timber element is more strongly determined by the anchorage requirements of the connectors.

In addition to changing the properties of the floor, the addition of timber or concrete material to the floor increases the weight, which can create a demand for larger framing members and foundations due to increase in dead and seismic loads. The floor weight expressed as unit area load is given in Fig 5, and mirrors the embodied carbon plots since the ratio of assumed weights (2400kg/m^3 for concrete; 500kg/m^3 for CLT) is similar to the ratio of carbon intensities for the two materials. Lower demands on the rest of the structure, and therefore potentially smaller member sizes, occur when thicker timber panels are used instead of adding concrete topping.

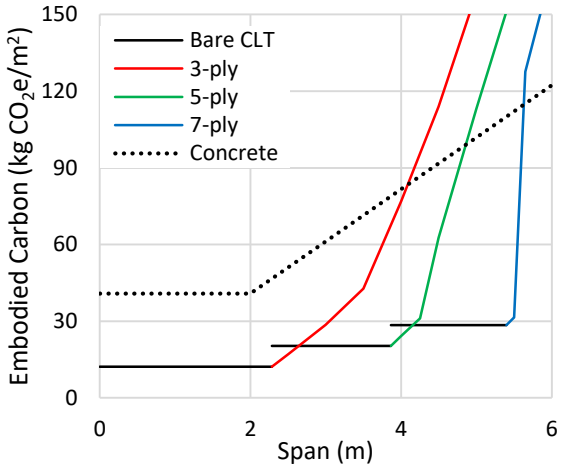

Fig 1: Minimum embodied carbon content of TCC floor systems with 3-, 5-, and 7-ply CLT (γ = 0.25). Reinforced concrete option shown for comparison.

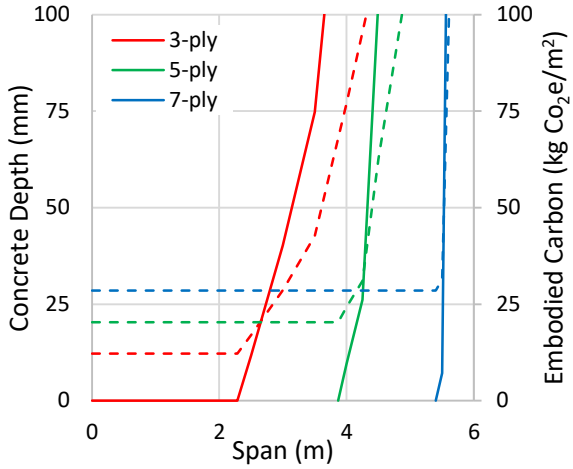

Fig 2: Interaction between concrete topping thickness and embodied carbon for TCC floor systems (γ = 0.25). Dashed lines: minimum required concrete thickness; solid lines: embodied carbon.

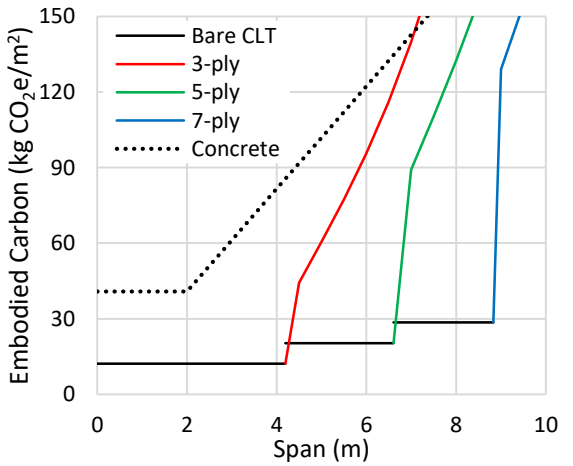

Fig 3: Minimum embodied carbon content of TCC floor systems based on deflection criteria (γ = 0.25). Reinforced concrete option shown for comparison.

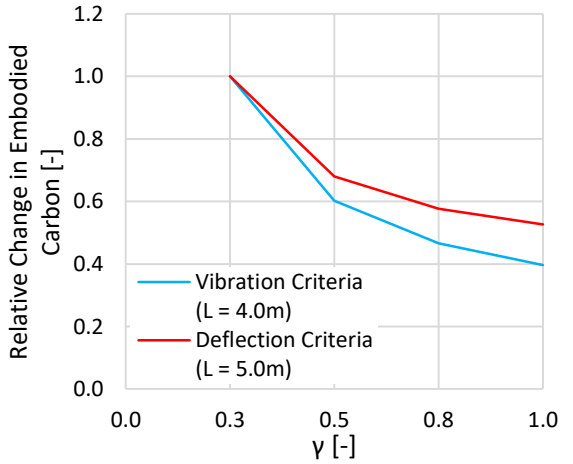

Fig 4: Effect of γ-value on embodied carbon content of TCC floors (3-ply CLT). Relative to γ = 0.25.

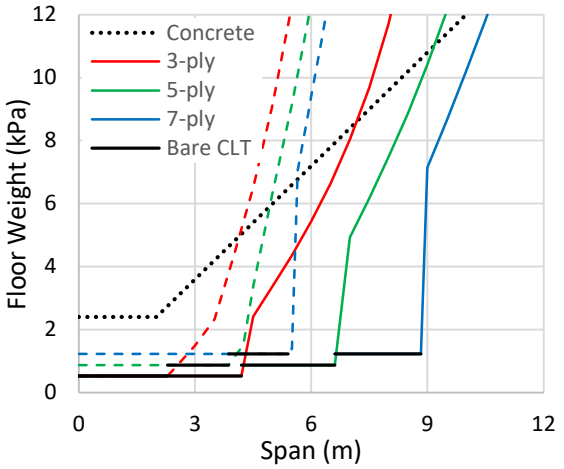

Fig 5: Floor unit weight by span based on criteria (vibration: dashed lines; deflection: solid lines) (γ = 0.25).

5. Conclusions and outlook

The literature review revealed that only a limited number of studies have considered the effect of and opportunities for reducing the thickness of structural concrete topping layers in TCC floors. Accordingly, minimum requirements for composite action for different connection systems could not be identified.

By using current design practices for TCC systems, it was shown that using structural concrete toppings increases the embodied carbon in a structure significantly. A lower carbon building can be achieved by increasing the thickness of timber elements instead. Also, it is observed that the results were not significantly affected by changes in the γ-value above $\gamma \geq 0.5$, which indicates that the choice of connector has a minor influence on the required concrete depth provided they produce a moderate degree of composite action.

Given that the carbon intensity of the TCC floor system increased rapidly with topping thickness, more research on the minimum limits is needed. Additionally, this research focused on embodied carbon as a single metric and did not account for cost or other environmental impacts from the material selection e.g. eutrophication or acidification potential and on-site construction. Further analysis including these effects and accounting for the relationship between embodied carbon and cost is recommended.

Acknowledgements

The authors would like to thank the Natural Sciences and Engineering Research Council of Canada for providing financial support through the Industrial Research Chair in Engineered Wood and Building Systems.

References

[1] A. Gosselin, P. Blanchet, N. Lehoux, Y. Cimon, Main motivations and barriers for using wood in multi-story and non-residential construction projects, BioResources 12(1) (2017), 546-570.

[2] L.F. Cabeza, C. Barreneche, L. Miró, J.M. Morera, E. Bartolí, A.I. Fernández, Low carbon and low embodied energy materials in buildings: A review, Renewable and Sustainable Energy Reviews 23 (2013), 536-542.

[3] D. Yeoh, M. Fragiacomo, M. De Franceschi, K.H. Boon, State of the art on timber-concrete composite structures: Literature review, Journal of Structural Engineering 137(10) (2011), 1085-1095.

[4] European Committee for Standardization (CEN), Eurocode 5 – Design of timber structures – Part 1 – General – Common rules and rules for buildings, EN 1995-1-1 (2014).

[5] A. Dias, J. Schänzlin, P. Dietsch, Design of timber-concrete composite structures, COST Action FP1402/WG4 (2018).

[6] C. Higgins, A.R. Barbosa, C. Blank, Structural tests of concrete composite-cross-laminated timber floors, Oregon State University, Report 17-01 (2017).

[7] K. Holschemacher, S. Klotz, D. Weisse, Application of steel fibre reinforced concrete for timber-concrete composite constructions, Lacer, No. 7 (2002), 161-170.

[8] J. Skinner, J. Bregulla, R. Harris, K. Paine, P. Walker, Development of ultra-thin timber-concrete composite upgrades, World Conference on Timber Engineering (2014).

[9] CSA Group, Engineering design for wood, CSA O86 (2019).

[10] P. Hamm, A. Richter, S. Winter, Floor vibrations – new results, World Conference on Timber Engineering 2010.

[11] Athena Impact Estimator for Buildings v5.4 Software and Database, Athena Sustainable Materials Institute, Ontario, Canada (2019).

Recent developments in engineered wood products for green building constructions

Marc Oudjene[1,2]
[1] Civil and Water engineering Department, Laval University, 1065 avenue de la Médecine G1V 0A6 Québec (Qc), Canada
[2] Université de Lorraine, LERMAB, 27 rue Philippe Séguin 88026 Épinal, France

Corresponding author, email: marc.oudjene@gci.ulaval.ca, Tel.: +1 418-656-2131

Abstract:
This paper presents comprehensive experimental investigations to design novel adhesive free engineered wood products (AFEWPs), namely adhesive free laminated beams (AFLB) and adhesive free cross-laminated timber panels (AFCLT). Compressed wood (CW) dowels were used as a joint element as an alternative to the traditional glue and metallic fasteners. The following structural elements were studied: (i) compressed solid timber beams, (ii) middle-scale and large-scale three-layer AFLB and (iii) AFCLT panels. Both structural and vibrational serviceability performances of the developed EWPs are addressed.

Keywords:
Experiments, Engineered wood products, eco-construction, FE modeling.

1. Introduction

In the current global sustainable development policies addressing the climate changes, the European commission has invested for moving towards a competitive low carbon economy by 2050, in different industrial sectors. In the construction sector, this consists on reducing greenhouse emissions (GHE), energy consumption, waste and volatile organic compounds (VOCs) in the new generation of buildings and products. In the last decade, timber engineered wood products (EWPs), such as glulam and cross-laminated timber (CLT) has becoming an effective alternative approach that has been adopted across the world given that timber is a natural, renewable and sustainable material.
In timber construction, gluing and/or mechanical metallic fastening are valid and still extensively used techniques to produce and assemble conventional EWPs. However, in a more environmentally friendly approach the use of petrochemical products can be regarded as drawbacks that affect the sustainability, the recyclability and the broader environmental impact of those EWPs. In fact, gluing leads to problems of real potential or perceived pollution, as well as problems of deposits on the glue-applicators and of cleaning which is in general costly. Furthermore, structural wood working such as cutting, planning, etc. is incompatible with the presence of metallic fasteners in the wood.
In this context, a consortium with six partners from six different European countries was formed through a joint research project funded by the North-West-European Interreg program called: "Towards Free Adhesive Buildings - AFTB" [1]. Its objective is to develop and validate new free adhesive EWPs (Fig. 1), as an alternative to the conventional ones involving a high degree of petrochemicals. The idea was to use compressed wood dowels to develop structural joints and to connect laminations to form adhesive free laminated beams (AFLB) and CLT panels (AFCLT).

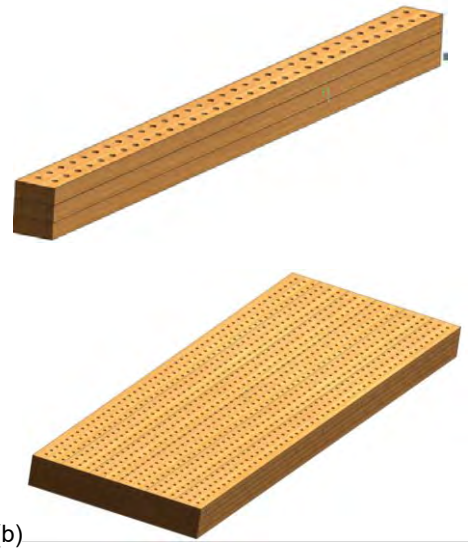

(a)

(b)

Fig. 1: Illustration of the developed engineered wood products: (a) adhesive free layered timber beams (AFLTB), (b) adhesive free CLT panels (AFCLT)

A large experimental program has been undertaken by the different project partners [1-2]. The tests include material properties characterization of compressed wood, destructive bending tests on AFLB and AFCLT panels. The vibrational serviceability was also included in the testing program [3]. In addition to the experimental program a predictive 3D-FE model that enable accurately predict both the local and global behaviors of such structural elements has been developed to support the present research and developments.

2. Manufacturing process

Softwood and hardwood, namely spruce timber and oak timber, have been used in this study to manufacture AFEWPs. The mean density values of spruce and oak were, respectively, 437 kg/m^3 and 620 kg/m^3. Compressed wood (CW) dowels were obtained from compressed (densified) spruce timber blocks, with initial density of 437 kg/m^3, in the radial direction up to compression ratio of 68% (initial and final thickness ratio).
Defects free spruce timber blocks were conditioned at 8% Moisture Content (MC) and an ambient temperature of 20°C prior to the compression process. The compression of the spruce timber blocks was done using a hot-pressing machine with a maximum pressure force of 2000 kN (Fig. 2).

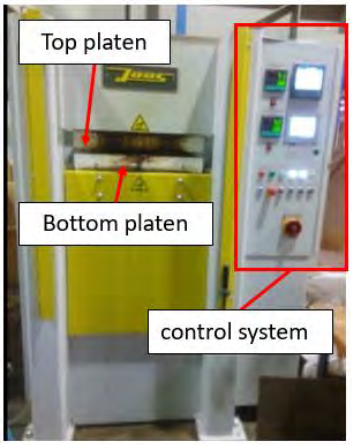

Fig 2: The hot press machine

The hot-pressing machine as shown in Fig. 2 consists of two main parts: two hot metallic pressing apparatus and pressure/temperature control system.
The typical shape of spruce timber before and after densification process in the radial direction can be seen in Fig. 3. Once the spruce timber blocks were compressed in the radial direction at a CR of 68%, they were cut and planned to obtain plates with a desired thickness of 16 mm.

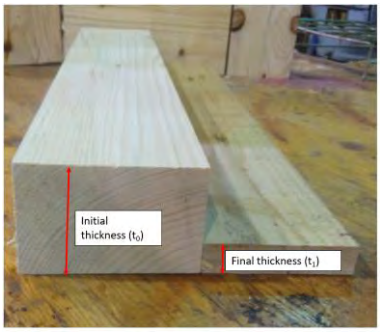

Fig. 3: Typical thicknesses of timber block before and after compression (CR= 68%)

From the densified plates, rounded CW dowels with 16 mm diameter were produced (Fig. 4). All dowels were weighed, and MC measured prior to assembly and testing.
It is worth noting that all spruce blocks were weighed before and after the densification process to obtain information on the increase of the density and the results are summarized in Table 1.

Table 1: Density mean values before and after compression.

Mean Density (kg/mm^3)	Before	After
	437	1133

Fig. 4: Typical produced CW dowels

Two types of EWPs were manufactured, namely adhesive free laminated beams (AFLB) and adhesive free cross-laminated timber panels (AFCLT). The AFLB were manufactured by stacking three layers made of oak timber and having the following dimensions: 70 mm x 22.5 mm x 1450 mm. The layers were drilled to obtain one row of holes with 16 mm diameter. The dowels were made of 68% compressed spruce with 16 mm diameter (d=16 mm). In addition, similar conventional three-layer glued (glulam) beams were manufactured and tested for comparison purpose. The dowels were regularly spaced and inserted by hammer insertion (Fig. 5). Two spacing distances were tested: 50 and 112 mm.

Fig. 5: Assembly of AFLB by hammer insertion of the dowels

The dimensions of AFCLT panels were: 75 mm x 105 mm x 2100 mm (Fig. 6). They are built using oak

timber layer having 25 mm thick and 150 mm width. A total of 196 CW dowels were used for each panel.

Fig. 6: Typical manufactured AFCLT panels assembled using CW dowels

3. Experimental program

The experimental program includes: (i) bending tests on solid timber and three-layer AFLB, (ii) bending tests on AFCLT panels and (iii) vibrational serviceability performance.
The schematic illustration of the conducted bending tests is shown in Fig. 7. In order to evaluate the relative mechanical performance of compressed wood ten small beam specimens, with dimensions: 400 mm x 20 mm x 20 mm, made either of compressed or non-compressed spruce timber were manufactured and tested under three-point bending tests. The global flexural modulus of elasticity (MoE) as well as the modulus of rupture (MoR) were obtained and compared.

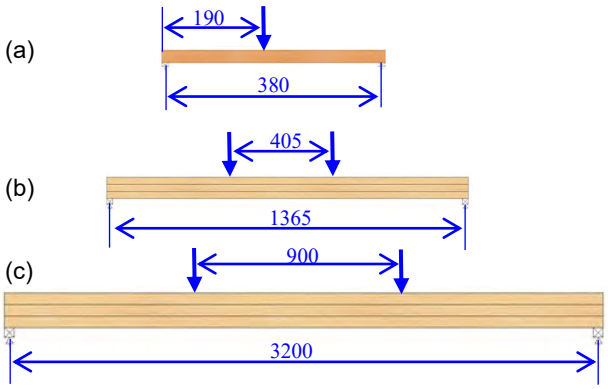

Fig. 7: Illustration of the bending test set-ups

The structural performance of AFLB was verified based on the tests shown in Figs 7b and 7c.
The destructive bending tests were performed in accordance with the both EN 408 [3] and EN 16351 [4] standard requirements. Similarly to the bending tests of beams, the mid-span deflection for the major axis of each panel was recorded using an LVDT displacement transducer (Fig. 8) and the load-vs-deflection curves were recorded during the tests for all the specimens for subsequent analysis and comparison against the numerically-predicted ones.
Furthermore, experimental modal analysis has been performed for the AFLB and AFCLT panels to study their vibrational serviceability performance. In the case of AFLB, the results were compared to similar glued beams (glulam) in order to evaluate the relative vibrational performance.

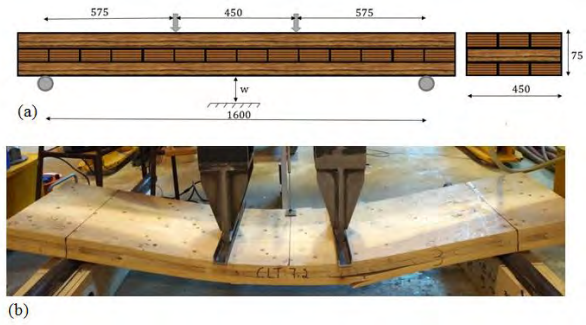

Fig. 8: Schematic and experimental set-ups

The experimental data were recorded and analyzed using the LMS Test Lab system. All beams and CLT panels were tested under free–free conditions. The free–free conditions were achieved thanks to the mineral wool system placed at the two end supports of the beam and suspension hook as shown in Fig. 9 and Fig. 10, respectively. The stiffness of the mineral wool is very low, which ensures free–free conditions. The beams and AFCLT panels were excited by hammer, respectively, impact at 11 points regularly spaced and 15 impact points. One 3D sensor was used to record measurements. Responses at these points were obtained using the reciprocity theorem.

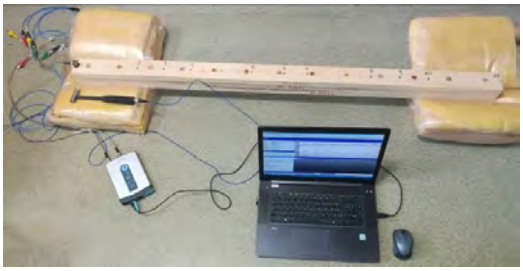

Fig. 9: Experimental set-up for the AFLB under free – free conditions

4. Results and discussions

First of all, the performance of the compressed wood was characterized and evaluated against non-compressed wood (Fig. 11). It can be seen a clear improvement of the density as well as the stiffness and strength characteristics, thanks to the compression process.
Fig. 12 depicts the load-mid-span deflection curves for both glued and AFLB large scale specimens (Fig. 7c).

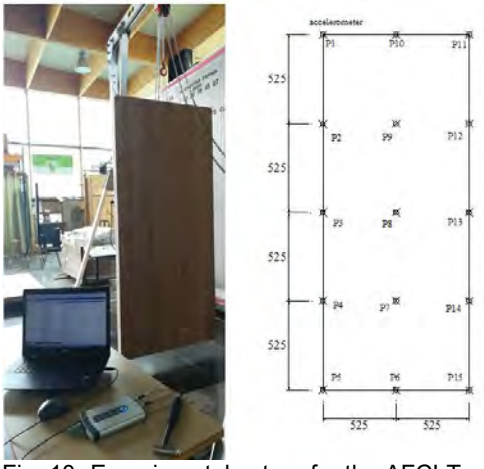

Fig. 10: Experimental set-up for the AFCLT panels under free – free conditions

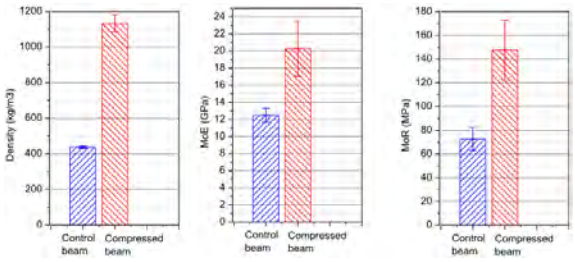

Fig. 11: Comparison between compressed and non-compressed wood (three-point bending tests)

The AFLB specimens exhibit load-carrying capacity nearly the glued ones, however they suffer from relatively lower stiffness (Fig. 12).

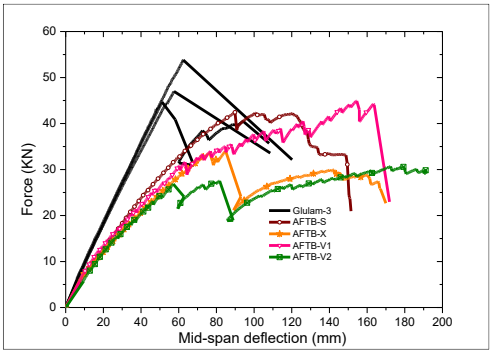

Fig. 12: Load-deflection curves for the glued and AFLB beam specimens

Fig. 13 compares the first three vibrational frequencies for the glued beams and the AFLB, and it can be seen that the AFLB exhibits a good vibrational characteristic. The results for the AFCLT panels were used to calibrate the developed FE model which in turn was used to simulate large scale AFCLT panel showing good vibrational serviceability comfort with regard to the Eurocode 5 design requirements.

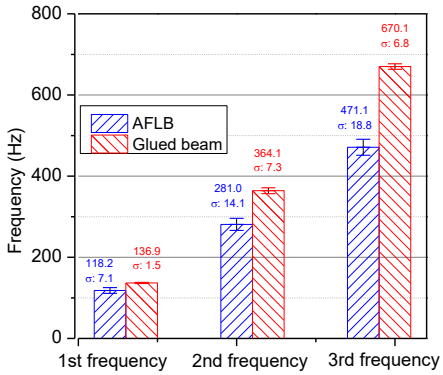

Fig. 13: Comparison between average vibrational performance of glued and AFLB specimens

5. Conclusions and outlook

AFEWPs have been manufactured and tested experimentally. The preliminary results show that those AFEWPs present acceptable performance and are suitable for structural uses. However, several issues need to be studied in more depth before they can enter the construction market. For example, the improvement of their stiffness and their behavior under long-term loading are necessary perspectives.

Acknowledgements

The project was funded by the European Regional Development Fund (ERDF) via Interreg NWE grant 348 “Towards Adhesive Free Timber Buildings”, AFTB. Special thanks to PhD and post-doc students, Pr. Yann Rogaume, Pr. Pascal Lardeur, Pr. Mourad Khelifa, Pr. Zhongwei Guan and Pr. Daniel Bradely.

References

[1] A. I. El-Houjeyri, V-D. Thi, M. Oudjene, M. Khelifa, A. Sotato, Z. Guan, Experimental investigations on adhesive free laminated oak timber beams and timber-to-timber joints assembled using thermo-mechanically compressed wood dowels. Construction and Building Materials, Vol. 222 (2019), pp. 288-299

[2] T. A. Bui, P. Lardeur, M. Oudjene, Experimental study of vibration uncertainty of multilayered timber beams assembled through compressed wood dowels. ISMA-USD 2018 - International Conference on Noise and Vibration Engineering, 17-19 September, Leuven, Belgium.

[3] EN 408, Timber structures – Structural timber and Glued-Laminated timber – Determination of some physical and mechanical properties. Bruxelles, November 2010.

[4] EN 16351, Timber structures — Cross laminated timber — Requirements. Afnor 2015

Coastal resiliency of Canadian low-rise light wood frame buildings against climate change

H. Daneshvar[a,*], T. Joyce[b,*], Y.H. Chui[c]

[a] Post-doctoral Fellow, Dept. of Civil and Environmental Engineering, University of Alberta, Edmonton, AB, Canada
[b] PhD Student, Dept. of Civil and Environmental Engineering, University of Alberta, Edmonton, AB, Canada
[c] Professor, Dept. of Civil and Environmental Engineering, University of Alberta, Edmonton, AB, Canada
* Corresponding author, +1 780 604 8093, Hossein.daneshvar@ualberta.ca

Abstract:

In Canada, the majority of low-rise residential buildings, including coastal buildings, are made using wood as the main structural material. These buildings — some of which have stood for several decades — were designed to meet the building codes or the best common practice at the time of construction. However, with the new challenges due to changes in the environment, such as more frequent and intense storms and sea level rise, it is necessary to revisit the resiliency of current design and construction methods. In addition, an aggressive coastal environment accelerates the rate of changes in material properties. Having said that, the vulnerability of wood as a biomaterial and metal connections should be investigated thoroughly in order to avoid catastrophic failures. The current study seeks to initiate a comprehensive research on the resiliency of current coastal communities in terms of structural integrity due to different natural hazards, mainly long-term climate-induced ones. The research work lies primarily in the field of resilient-based assessment of timber coastal structures, including members and connections. This research provides a comprehensive approach for designing, constructing and maintaining residential wood frame buildings in coastal environments using the best common engineering practices based on the information collected from state-of-the-art literature in US and applied to Canadian coastline construction. The main outcome of the research is to provide recommendations for increasing the resiliency of light wood frame residential coastal buildings against hazards induced by changes in the climate and environment.

Keywords:
Coastal resiliency, Low-rise light wood frame buildings, Climate change, Resilient communities, Hazard identification.

1. Introduction

Coastal residential buildings have increased significantly at some sites that have higher risks of vulnerability to natural hazards due to climate changes than in the past in recent years. Also, nowadays residential buildings constructed on the coastlines tend to be larger and more expensive, which creates a heightened risk of large economic losses in the event of a natural disaster. These buildings were designed based on building codes or the best common practice at the time of their construction. However, with all the new challenges due to changing environment and extreme natural hazards, such as more frequent intensified storms, seasonal flooding and sea level rise, it is necessary to revisit the resiliency — the ability to withstand and recover from an extreme event — of current design and construction methods. Also, aggressive coastal environments accelerate the rate of change in the characteristic properties of materials, which affect the structural response. The vulnerability of wood as a biomaterial and the metal connections typically used in timber construction should be investigated thoroughly in order to avoid catastrophic failures. The current study seeks to initiate a comprehensive research study on the resiliency of coastal light wood frame buildings subjected to natural hazards, including those due to climate changes. As a result, it is crucial to identity the common and potential future hazards that should be considered in the design of buildings in coastal areas.

For instance, flooding is a case of natural hazard as a result of changing environment. Fig 1 shows how the average annual maximum flow of a 1000 square kilometer river basin varies across different regions of Canada [1]. The water peaks at some level, which may cause flooding of surrounding lands mainly probable in the Canadian coastlines. This observation highlights the required attention towards the coastal areas considering the changing environment. It is noted that while the focus of this document is on the particular conditions experienced in coastal areas of the country such as British Columbia and Atlantic Provinces, some of the guidelines are applicable to areas farther inland including Prairies, Ontario and Quebec, where some of the hazards, notably higher risk of flooding, are increasingly likely. More information regarding the historical cases of major weather events that made headlines from coast to coast, during recent years can be found on the Environment and Climate Change Canada website [2].

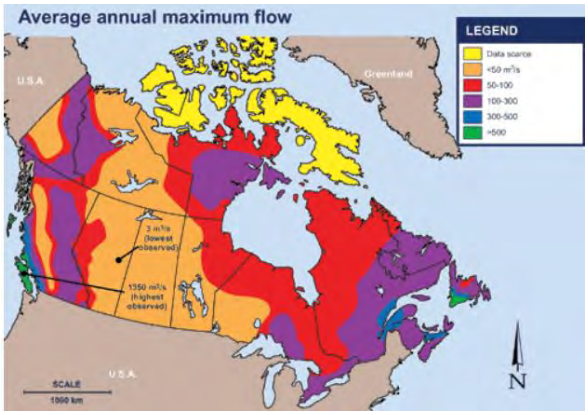

Fig 1: Canada's average annual maximum flow [1]

In the current study, a comprehensive discussion of hazards affecting coastal structures is given, followed by recommendations for the design, construction and maintenance of residential wood frame buildings are provided using the best common engineering practice identified from the existing literature. The primary targeted users for the proposed research are design professionals, building officials, and those involved in decision-making processes around the resiliency and required retrofitting criteria for coastal structures. Recommendations regarding site selection, foundation systems, building envelope considerations, material comparisons and risk assessments are outside of the scope of this study.

2. Background

One of the leading references in this field is the *Coastal Construction Manual (FEMA P-55)* [3, 4]. This two-volume publication presents valuable information on the design and construction of houses in the coastal areas of U.S. and its territories. These two documents are the main references for this study. To the best of knowledge of the authors, there is no such publication with similar content within the Canadian context. Insight on hazards in Canada, including Canadian coastlines, is given in [5]; however the publication is directed to the general audience, not design professionals. As a result, the lack of such a document for the Canadian coastal environment is obvious, necessitating the need for current research. The FEMA publication *Local Officials Guide for Coastal Construction (FEMA P-762)* [6] is suggested for readers with less familiarity with design and construction practice.

In terms of best practices in coastal design and construction, other codes provide specific dedicated sections or clauses. The International Residential Code (IRC) [7] asks for 1 foot of freeboard — additional height that the building is elevated above the base flood elevation — in special flood hazard areas. Also, the International Building Code (IBC) [8] requires conformance with American Society of Civil Engineers (ASCE) Standard 24-05 [9], for design and constructions requires special flood hazard criteria, and ASCE 7 provides guidelines for calculating flood-related loads [10]. To-date no similar best practice or design documents focusing on the Canadian context are available.

3. Hazard Identification

It is crucial to understand and identify the hazards that affect the performance of coastal developments, particularly residential buildings, to evaluate their resiliency. FEMA P-55 [3] identified four major categories of natural hazards affecting coastal buildings: earthquakes, high winds, flooding (including wave action), and erosion. Many studies have been conducted to address the former two hazard groups, and building codes are generally well-developed and engineers are familiar with how to address them through design and construction. However, the latter two categories, flooding and erosion, are least discussed in the current literature, guidelines and building codes [3, 11].

In general, low-rise wood frame buildings designed based on the prescriptive methods in the National Building Code of Canada (NBCC) [11] perform satisfactorily during major seismic events in non-coastal environments [12]. In Canada, high seismic risk areas lie along the Pacific Coast and sections of the St. Lawrence River through Quebec [11]. Parts of both regions are susceptible to flooding due to both sea level rise and trends toward more severe storms causing increased rainfall. Typical design measures for flood-resistance for buildings in low-lying areas and along shorelines may conflict with conventional seismic design guidelines. For example, elevating a structure to allow flood waters to pass under with minimal obstruction could conflict with the need to provide adequate lateral bracing to resist seismic loads. In such cases, proper design for coastal hazard must consider a balance between the need to elevate the building above flood hazards with minimal obstructions to let the water flow and the requirement to sufficiently brace or stabilize the building against lateral seismic motions. Geotechnical hazards particularly liquefaction of supporting soil — such as situations of granular solid with high water tables which is very common in coastal areas — should be considered as well [3].

High winds are a major hazard for coastal buildings and are the main source of failure in both structural components and cladding. Changing ocean conditions are predicted to result in more frequent and severe hurricanes and tropical storms in Atlantic Canada, bringing higher wind speeds than are historically typical for the region [13]. Following the wind load calculations in NBCC [11] and ASCE 7 [10] as well as paying careful attention to connection details are necessities to mitigate failure, satisfying minimum requirements. Design for high wind hazards such as tornadoes are beyond the scope of most building codes including Part 4 of NBCC. The risk of tornados to Canadian coastal

communities is limited to the Maritime provinces, particularly New Brunswick and Prince Edward Island [14]. Higher wind speeds create a range of additional hazards, including wind-borne debris damages and consequent rainfall penetration, higher lateral forces, and heightened risk of uplift on roofs.

Coastal flooding originates from difference sources and should be considered in building analysis in the form of hydrostatic, hydrodynamic, wave, and flood-borne debris forces. Hydrostatic loads include buoyancy effects and lateral loads from standing water, slowly moving water and non-breaking waves. These effects can cause structural failure, deteriorate wooden members through rot, and result in health issues due to the potential for mold growth. Hydrodynamic loads include lateral loads due to rapidly moving water and breaking waves. Some areas along the Atlantic and Arctic coasts of Canada are also vulnerable to hazards caused by floating ice [4].

Erosion — defined as the washing away of coastal lands — is one the most important hazards facing structures near shorelines. Erosion can threaten the structure in different ways by weakening the foundation or increasing the flood and wave effects. Large seasonal fluctuations of the shorelines might not be an indication of long term erosion, however localized scour, overwash and sediment burial, landslides and ground failures are categorized in the erosion hazard group [3].

Sea and lake level rise, both short term (occurring over a period of hours or days) and long term (over years and decades as a global climate change effect) should be considered in the design. Also coastal land masses can move up or down, — called uplift and subsidence, respectively — independent of water level. The most significant consequence of coastal subsidence, even when it is small, is an increase in coastal flood hazards due to an increase in flood depth that should be considered in flood load calculations. Salt spray and moisture effects are two other commonly overlooked hazards that might lead to corrosion and decay of light wood frame materials in coastlines. Salt spray accumulated on metal connectors, straps and clips cause corrosion in the humid conditions. Changes in temperature, sunlight, aging, and chemicals can also cause decay in wood. With temperatures in northern areas increasing, the range in which termites are active is likely to increase. Termites are of particular concern in coastal areas subject to high humidity and frequent and heavy rainfall [3 & 4].

4. Design and Construction

The design development process in the coastal areas mainly considers the natural hazards discussed earlier in Section 3 that are feasible to occur in the building site and afterwards, and involves designing structural components and systems so they can withstand the potential damaging effects adequately. The following is a brief set of recommendations for the effective design of light wood frame buildings in coastal areas to increase their resilience and structural integrity against short-term and long-term hazards arising due to climate change [3 & 4]:

Provide continuous load path: In resilient building construction the capability of structural components, from rooftop to foundation, to resist and transfer the anticipated loads is essential. This is of particular importance coastal structures subject to high wind and seismic loads. Each element in the load path should be designed to transfer the applied load without failure or excessive deformation since localized failure might lead to disproportionate failure of total load path and consequently the whole building. Added brackets and hurricane straps are commonly required to resist uplift at the perimeter of roofs and at overhangs; these connectors may not be present in older structures, which should be retrofit to reduce the risk of uplift failure.

Adequate connection design is key: Most failures along a load path happen at the connections, not at individual structural elements. All connections, e.g. those shown in Fig. 2 and including roof sheathing to framing connection (Link #1), roof framing to exterior wall (Link #2), wall top plate to wall studs (Link #3), wall sheathing to window header (Link #4), window header to exterior wall (Link #5), wall to floor framing (Link #6), floor framing to support beam (Link #7) and floor support beam to foundation (Link #8) should be controlled carefully to assure adequacy.

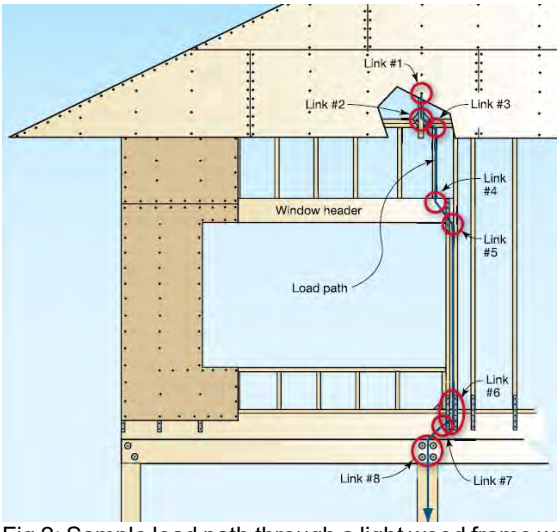

Fig 2: Sample load path through a light wood frame wall section [4].

Design for extreme wind and seismic events: Designers should consider the effects of long-term erosion causing topographic effects which may speed up the winds a building may experience during its life time as well. For conventional light wood frame buildings, it is uneconomical to design the entire

building to resist tornadoes. It is suggested to have a portion of the building in the coastal high hazard coastal areas using good practices for wind-resistant buildings to mitigate damage. Although generally rare in Canada, parts of the Pacific coast (the west and south shores of Vancouver Island, Haida Gwaii, and the central coast) have a high risk of experiencing tsunamis following a major earthquake along the Cascadia Subduction zone. Designer shall consider tsunami run-up, flooding, erosion and debris loadings in these high hazards zones.

Use corrosion protected mechanical connectors: Metal connectors and fasteners should be hot-dip galvanized or stainless steel to increase durability. Typically, mechanical connectors are available with various levels of corrosion resistance, e.g. levels of hot-dip galvanizing and plating for corrosion-resistance. In very aggressive corrosive environments stainless steel connectors are recommended, since exposed galvanized metal fasteners can corrode in a few years. Stainless steel connectors should be used with stainless steel fasteners only to avoid galvanic corrosion between dissimilar metals.

Avoid moisture penetration: Protection against moisture is a key to protect wood against decay and hence increase resiliency. Since pressure treated wood is not recommended for interior wood construction, this shall be achieved by appropriate detailing of building envelope joints in exterior walls to shed rain water, and proper installation of water-resistive barriers.

Protect the wood against termites: This can be accomplished by use of borate-treated wood products including field treatment of notches, holes, and cuts, use of naturally termite-resistant wood species, and installation of barriers to termites in susceptible coastal areas.

Exercise precaution when combining materials: It is essential to consider material compatibility since dissimilar metal fasteners in contact with each other may corrode in the presence of salt and moisture. There are also some issues when galvanized fasteners are in contact with certain types of treated wood as well. Using wood adjacent to other material such as masonry should be exercised with precaution due to potential differential settlements caused by moisture changes in the two materials.

5. Conclusions and Outlook

The current study has initiated the process of hazard evaluation and proposing recommendations to increase the resiliency of light frame wood buildings in coastal environments. Considering the variety of hazards in this context, a multi-hazard approach is the most practical way to address all potential hazards and their consequences. Considering the use of mass timber products is recommended in order to overcome the weak points that inherently exist in conventional light wood frame buildings which has been neglected in the current literature related to coastal construction. As the use of mass timber in residential construction increases, the need for resilient design and detailing recommendations will also increase.

Acknowledgements

The authors would like to thank the Natural Sciences and Engineering Research Council of Canada for providing financial support through the Industrial Research Chair in Engineered Wood and Building Systems.

References

[1] Government of Canada, Environment and Climate Change Canada, Flooding events in Canada: https://www.canada.ca/en/environment-climate-change/services/water-overview/quantity/floods/events-canada.html (2013)
[2] Government of Canada, Environment and Climate Change Canada, Canada's top ten weather stories archive:https://www.ec.gc.ca/meteo-weather/default.asp?lang=En&n=3318B51C-1 (2017).
[3] Federal Emergency Management Agency (FEMA). Coastal Construction Manual: Principles and practices of Planning, Siting, Designing, Constructing, and Maintaining Residential Buildings in Coastal Areas, FEMA 55, Fourth Edition, Volume I (2011).
[4] Federal Emergency Management Agency (FEMA). Coastal Construction Manual: Principles and practices of Planning, Siting, Designing, Constructing, and Maintaining Residential Buildings in Coastal Areas, FEMA 55, Fourth Edition, Volume II (2011).
[5] Institute for Catastrophic Loss Reduction, Building Resilient Communities. Canadians at risk: Our exposure to natural hazards. Canadian Assessment of Natural Hazards Project (2010).
[6] Federal Emergency Management Agency (FEMA). Local officials guide for coastal construction: Design Considerations, Regulatory Guidance, and Best Practices for Coastal Communities, FEMA P-762 (2009).
[7] International Code Council (ICC). International Residential Code (IRC) (2015).
[8] International Code Council (ICC). 2018 International Building Code (IBC) (2015).
[9] American Society of Civil Engineers (ASCE). Flood Resistant Design and Construction. ASCE Standard ASCE 24-05 (2005).
[10] American Society of Civil Engineers (ASCE). ASCE. Minimum Design Loads for Buildings and Other Structures. ASCE Standard ASCE 7-10 (2016).
[11] National Research Council of Canada (NRC). National Building Code, NRC, Ottawa, ON, Canada (2015).
[12] Canadian Wood Council. Wood-frame Construction: Meeting the Challenges of Earthquakes (2003).
[13] Natural Resources Canada. From Impact to Adaptation: Canada in a Changing Climate: https://www.nrcan.gc.ca/environment/resources/publications/impacts-adaptation/reports/assessments/2008/10253
[14] Institute for Catastrophic Loss Reduction, Building Resilient Communities. Increasing High Wind Safety for Canadian Homes: A Foundational Document for Low-Rise Residential and Small Buildings. (2019).

Mapping of the Renewable Energy Generation Potential in India

Mr. Nimai Sundar Manna[a] , Prof. (Dr.) Binoy Krishna Choudhury[b]

[a] Ph. D. Research Scholar, Dept. of Business Management, University of Calcutta
[b] Professor- Energy Management Dept., IISWBM, University of Calcutta

* Corresponding author: Mr. Nimai Sundar Manna Tel: 07890038030, email: drnsmanna@gmail.com

Abstract:
With the ever increasing demand for clean and green energy in coping up with Sustainable Development Goals (SDGs) of United Nations Organization (UNO) India needs to produce more renewable energy as the fossil fuel based conventional energy may not met the per capita energy consumption to achieve desired Human Development Index (HDI) with 130 million heterogeneous population of diverse energy usage pattern as there are plenty resources for renewable energy such as Solar, Wind and Biomass which are mostly untapped till date. Due to geographical position India's climatic condition is tropical in nature and as such ample opportunities of solar radiation in daytime in most part of the country and in the wide length of western (Arabian Sea) and eastern (Bay of Bengal) sea coastal region there is huge potential of wind energy generation too. The present wind power installed capacity in the country is around 28.28 GW with which in terms of wind power installed capacity India is globally placed at 4th position after China, USA and Germany. India has an estimated renewable energy potential of about 900 GW from commercially exploitable sources viz. Wind – 102 GW (at 80 m mast height); Small Hydro – 20 GW; Bio-energy – 25 GW; and 750 GW solar power, assuming 3% wasteland. Economic growth, increasing prosperity, a growing rate of urbanisation and rising per capita energy consumption has increases the energy demand of the country.
In the proposed research the renewable energy sources for solar, wind and biomass etc. are identified and potential generation capacity to be estimated using statistical package. For this purpose last 10 years monthly data of all 36 states & UTs in India are analyzed on the basis of state wise and segment wise generation of renewable energy with respect to the potential capacity of energy. Being a colour coded map over the geographical map of India it would instantly help in identifying the supply- demand scenario in any place, etc.

Keywords:
Solar energy, Wind energy, Renewable Energy potential, color coded map.

1. Introduction

India is implementing reforms towards a secure, affordable and sustainable energy system to power a robust economic growth. The country has made huge strides to ensure full access to electricity, bringing power to more than 700 million people since 2000. It is pursuing a very ambitious deployment of renewable energy, notably solar, and has boosted energy efficiency through innovative programmes such as replacing incandescent light bulbs with LEDs (under the Ujala scheme).

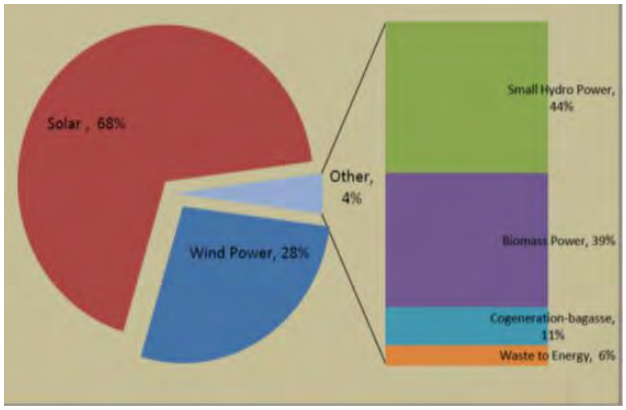

Fig. 1:Sourcewise Renewable energy generation as 31.3.18

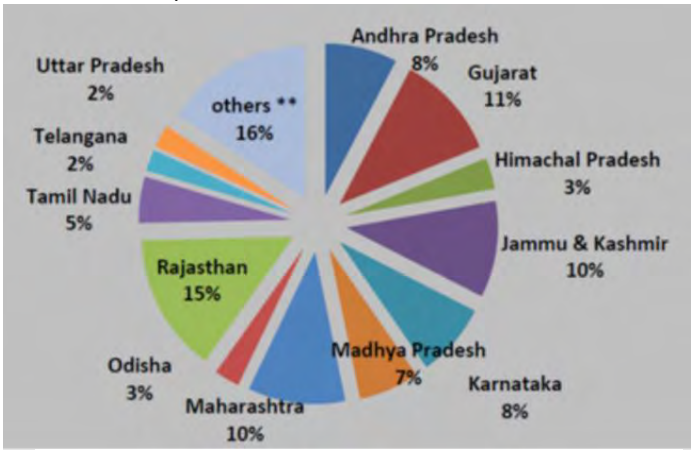

Fig. 2:Sourcewise Renewable energy generation as 31.3.18

There is high potential for generation of renewable energy from various sources like - solar, wind, biomass, small hydro and cogeneration bagasse and waste to energy. Within last 4 years India has done tremendous progress in electrifying the nation with 99.9% household electrification and 80 million LPG connection for cleaner cooking.

The total potential for renewable power generation in India (as on 31.03.18) is estimated at 1096081MW. This includes solar power potential of 748990 MW (68.33%), wind power potential of 302251 MW (27.58%) at 100m hub height, SHP (small-hydro

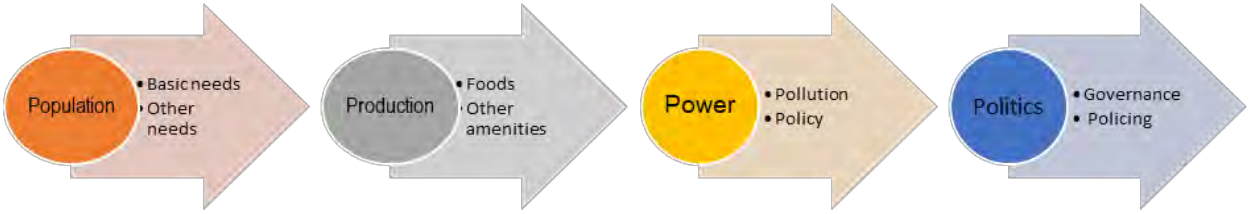

Fig.3: Integrated Need chain with 4 Ps'

power) potential of 19749 MW (1.80%), biomass power of 17,536 MW (1.60%), 5000 MW (0.46%) from bagasse-based cogeneration in sugar mills and 2554 MW (0.23%) from waste to energy.

The geographic distribution of the estimated potential of renewable power (as on31.03.2018) reveals that Rajasthan has the highest share of about 15% (162238MW), followed by Gujarat with 11% share 122086 MW) and Maharashtra with 10% share (113933MW), mainly on account of solar power potential and also Jammu & Kashmir (10%).

2. Perspective:

As per 2019 data the renewable share of the total energy mix in India's total install capacity is 35.4% whereas Coal is 53.9% while in 2016 it was 16.1% and coal accounted for 59.8%. This indicates the reality of paradigm shift of the scenario that India is harvesting more and more renewable energy coping up with the sustainable development goal (Goal-7) too. The strong initiative of the Government towards National Solar Mission and clean and sustainable energy for all is the driving force for this paradigm shift. With the growing population there is need of growth of production to produce more there is need of more energy. Though fossil fuel (majorly coal) based primary energy source is dominating but the trends in the recent years is showing a gradual declining whereas the renewable source is rocketing high. Among the renewables Solar (68%) and wind power (28%) are contributing 96% in the renewable energy(RE) mix.

The emergence of electric vehicles is also a very good sign of future energy consumption in the transportation sector as petroleum reserve is very limited in India and the transportation consumption is a major concern. The charging stations are installing solar PV in grid connecting configuration therefore grid integrated RE will be a next business in this line. The per unit cost of generating RE is gradually decreasing whereas the same cost for conventional is increasing fast. This cost benefit leverage also pushes RE towards a bright future along with the newer technological breakthrough increases the efficiency of the RE generation. The Govt. intervention and policy directives towards fulfilling ambitious target is the driving force towards RE generation and increasing the potential with newer technology and new avenues for generating RE.

3. Materials & Methods:

In our study we have used all authenticated data from Govt. of India and its different related Department like, MNRE, BEE, NIWE, Ministry of Power (MoP) etc. Time series data for the last 10 years have been used for wind power, solar energy, biomass & cogeneration bagasse, small hydro, waste to energy of all 36 states & UTs have been analyzed. We use quadratic trend analysis model for future potential for each of the RE options like solar, wind, biomass etc.

A methodology developed [1] for identification of potential areas for solar power generation in India is presented in the (Fig. 4) and more details process

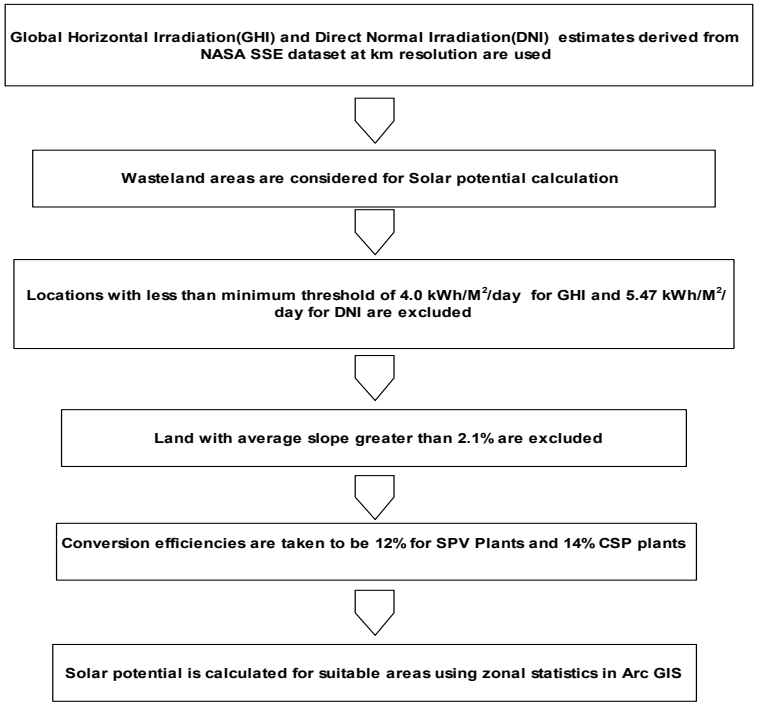

Fig.4: Methodology used for Solar potential calculation

with wasteland use [4] for solar radiation and wind speed data is also available. To begin with identification of wasteland we use 23 types of wasteland as marked in the wasteland atlas from

Dept. of land resource, ministry of rural development, Govt. of India. For potential sites acceptable value of annual average solar radiation DNI and GHI is considered as per Fig -1. Then land slope is also taken into account upto 2.1% slope is accepted for calculation of potential solar energy generation. As the technological efficiency varies in CSP than to SPV, we take 12% for efficiency for SPV and 14% for CSP.

4. Results and discussions

We have analyzed the monthly data of last 10 years for all the 36 states & UT of India in MW unit (source: CEA, MoP, Govt. of India).

time stamp	Wind	Solar	Biomass	Bagasse	Small Hydro
Apr-18	3322.74	3178.88	255.43	1263.94	384.14
May-18	4441.09	3322.72	253.59	728.01	472.04
Jun-18	8336.94	3012.37	285.86	393.48	761.27
Jul-18	11365.27	2553.02	225.10	319.56	1193.60
Aug-18	11771.66	2635.79	185.61	218.28	1530.91
Sep-18	6093.34	3209.96	177.17	231.36	1001.29
Oct-18	2822.78	3452.61	206.31	426.26	872.37
Nov-18	2181.03	3140.99	199.72	1558.80	678.16
Dec-18	2789.24	3078.47	247.01	2311.49	516.72
Jan-19	2851.89	3392.66	230.98	2351.84	428.57
Feb-19	2983.75	3589.39	242.53	1964.41	397.9

Table 1: A sample consolidated table (all India value)

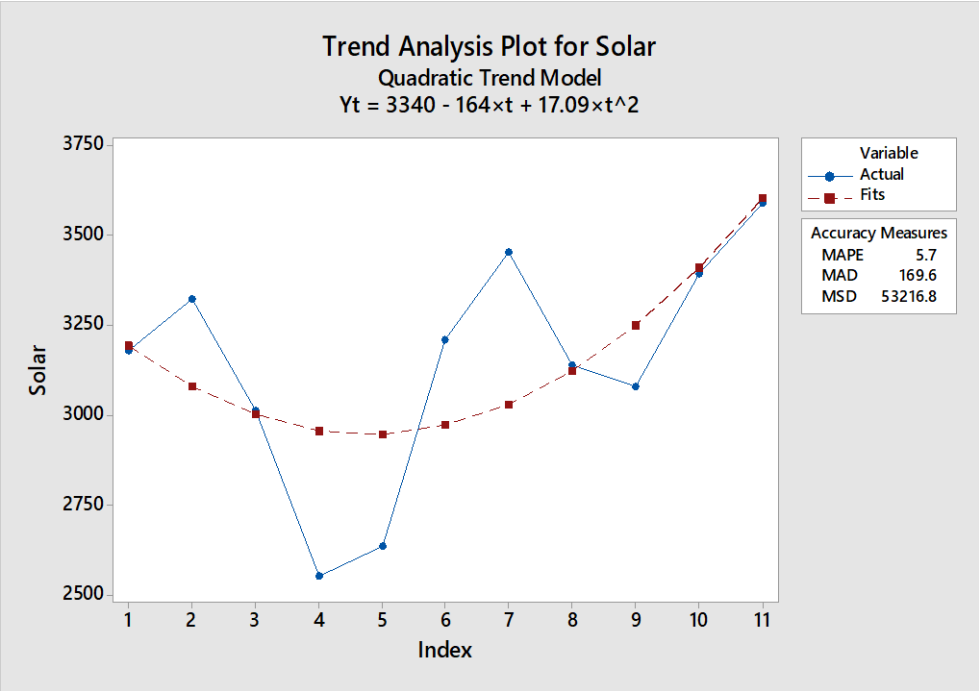

Fig.5:Trend Analysis plot for Solar Energy in India

The analysis shows that in the long run the potential electricity generation potential from Solar energy is exponentially increasing trend which is also revealed in the past year on year estimated potential electricity generation from Solar energy.

In case of wind energy, it is found a gradual decreasing trend over the period of future time which may indicate the climate change impact on wind speed and seasonal change in weather condition.
The trend of potential energy generation from the Biomass source is also showing a gradual increasing in nature which may indicate growth of population and as such related inter-alia.
Again the potential electricity generation from the small hydro project is having a downward trend over the period of time which indicate the scarcity of water resources and water recharge issues caused due to global warming and climate change effect.

5. Conclusions and outlook

The analysis of the potential renewable energy generation from all sources in all the 36 states and UTs on the basis of last 10 years' monthly data shows the naturally available solar energy will dominate the renewable energy sector as it has already having more than 68% of the RE mix and in the total energy mix the share of Coal based energy is decreasing whereas the RE share is increasing at very faster rate which is due to the Govt. intervention to boost up the national solar mission towards producing 175 GW renewable energy by 2022. With 99.9% household electrification as the challenge is to provide non-stop availability of electricity to achieve desired development on the context of limited fossil fuel reserve harvesting solar energy is the way forward to implement SDG (goal -7). However, this approach may not predict the disruptive technology which may suddenly change the potential like SPV to CSP in tapping solar energy.

6. References

[1] Richa Mahatta, P.K. Joshi, A.K. Jindal. Solar power potential mapping in India using remote sensing inputs and environmental parameters, Renewable Energy 71 (2014) 255-262
[2] Ramchandra T.V. Spatial mapping of renewable energy potential Renewable and Sustainable Energy Reviews 11 (2007) 1460–1480
[3] Katrina Adam, et al. Methodologies for city-scale assessment of renewable energy generation

potential to inform strategic energy infrastructure investment, Cities 54 (2016) 45–56
[4] Sharma Chandan, et al. Assessment of solar thermal power generation potential in India. Renewable and Sustainable Energy Reviews 42(2015)902–912
[5] Vikas Khare et al. Status of solar wind renewable energy in India, Renewable and Sustainable Energy Reviews 27(2013)1–10
[6] Ramchandra T.V et al, Hotspots of solar potential in India, Renewable and Sustainable Energy Reviews 15 (2011) 3178– 3186
[7] Ashwani Kumar et al, Renewable energy in India: Current status and future potentials. Renewable and Sustainable Energy reviews 14(2010) 2434-2442

7. Source of data:

1. Tentative State-wise break-up of Renewable Power target to be achieved by the year 2022 So that cumulative achievement is 1,75,000 MW

https://mnre.gov.in/file-manager/UserFiles/Tentative-State-wise-break-up-of-Renewable-Power-by-2022.pdf

2. State-wise Potential of Various Renewable Energy Technologies
https://data.gov.in/catalog/state-wise-potential-various-renewable-energy-technologies?filters%5Bfield_catalog_reference%5D=91931&format=json&offset=0&limit=6&sort%5Bcreated%5D=desc and
https://data.gov.in/sites/default/files/datafile/State-wise_Potential_of_Various_Renewable_Energy_Technologies_1.xls

3. Recent State Wise Statistical Review of Renewable Energy in India
https://www.researchgate.net/publication/333210879_Recent_State_Wise_Statistical_Review_of_Renewable_Energy_in_India

4. Energy Statistics 2019 - Ministry of Statistics
http://www.mospi.gov.in/sites/default/files/publication_reports/Energy%20Statistics%202019-finall.pdf

5. Report of the Expert Group on 175 GW RE by 2022 - NITI Aayog
https://niti.gov.in/writereaddata/files/175-GW-Renewable-Energy.pdf

6. CEA GoI State Wise Renewable Energy Generation Data
http://cea.nic.in/reports/monthly/renewable/2019/renewable-05.pdf

7. NITI AAYOG State Renewable Energy Capacity Addition Roadmap
https://niti.gov.in/sites/default/files/energy/Executive-Summary.pdf

8. State-wise Renewable Energy Potential in India
https://www.jagranjosh.com/general-knowledge/what-is-the-state-wise-renewable-energy-potential-in-india-1520941871-1

9. https://www.iea.org/reports/india-2020

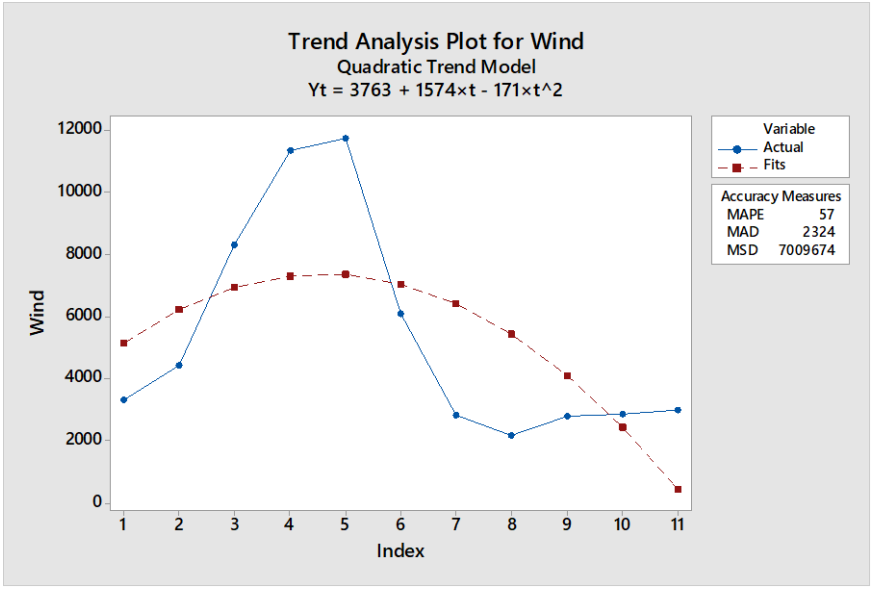

Fig. 6 : Trend analysis plot for Wind energy

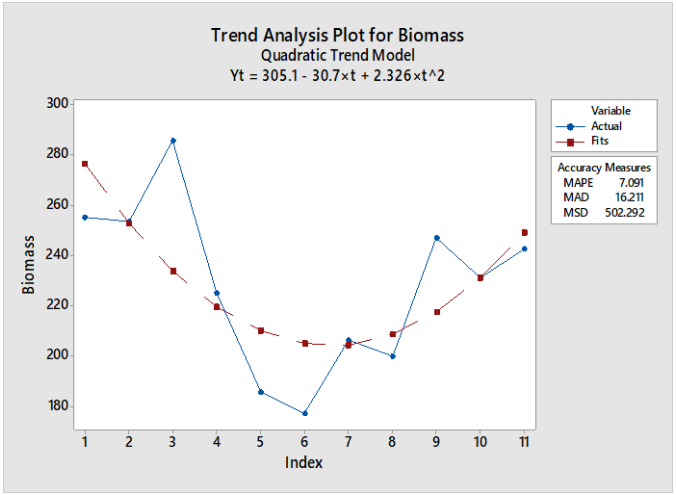

Fig.7 : Trend analysis plot for Biomass

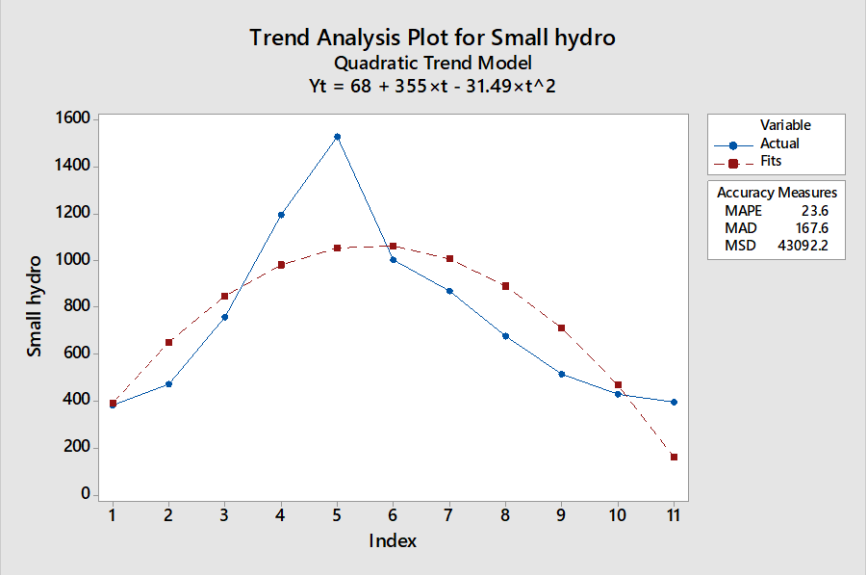

Fig.8 : Trend analysis plot for Small Hydro power

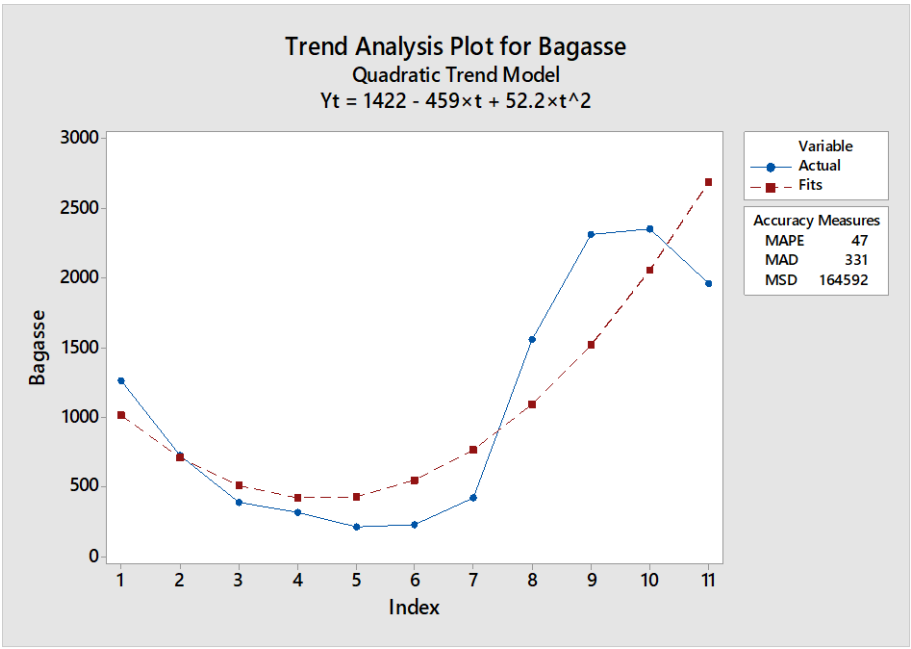

Fig. 9 : Trend analysis plot for Bagasse

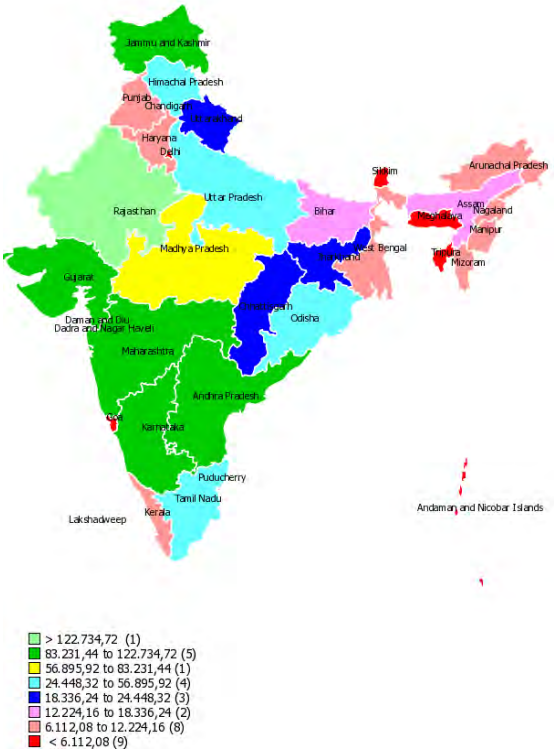

Fig.10 :Total estimated Renewable Energy Potential

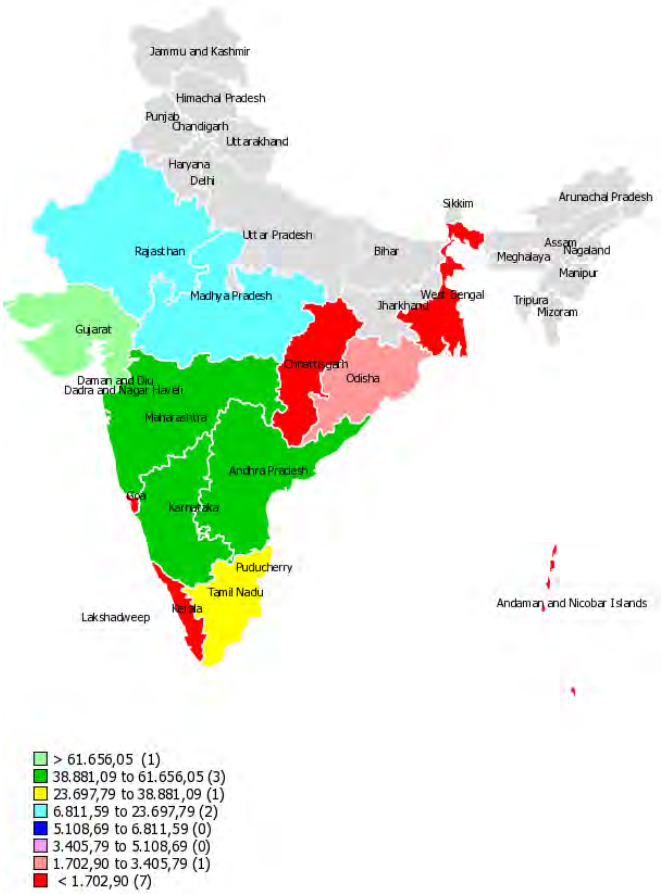

Fig.12 : Wind power generation potential

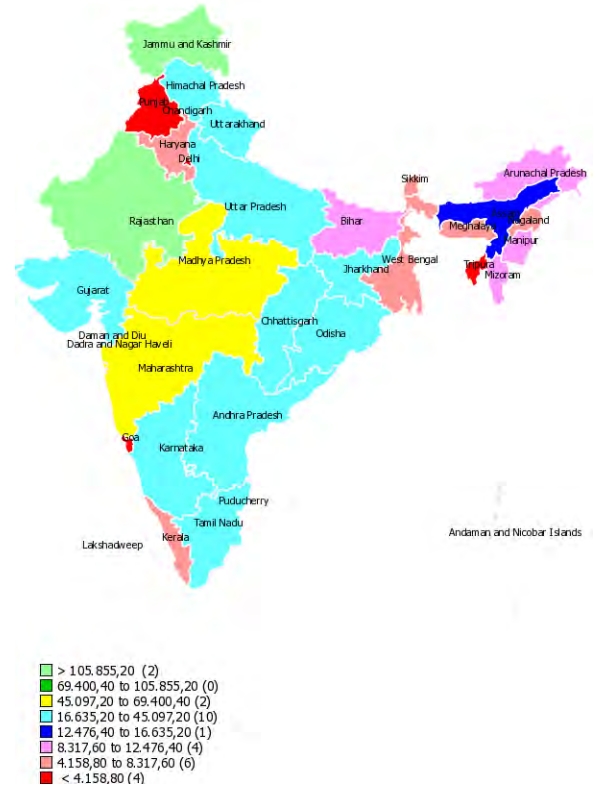

Fig.11: Potential Solar Energy Generation Map

Microscale Characteristics of New Bitumen-Based Carbon Fibers (BBCF)

Maryam Monazami, Rishi Gupta*
Civil Engineering Department, University of Victoria, Victoria, BC, Canada
* Corresponding author, e-mail address: guptar@uvic.ca

Abstract
Used as secondary reinforcement, fibers can modify concrete properties in various ways. Self-monitoring concrete is a type of concrete with small portion of carbon fibers that work as sensors to detect flaws in concrete. Carbon fiber reinforced concrete is highly suitable to maintain longevity of infrastructure where corrosion of steel can shorten the useful service life of the structure. This paper provides a concise review of recent advancements in carbon fiber reinforced concrete as well as introducing a new sustainable and low cost type of Bitumen-Based Carbon Fibers. A systematic study on microstructure and elemental composition of Bitumen-based, Pitch-based and PAN-based carbon fibers were carried out to compare the newly introduced fiber with the previous widely used carbon fibers. Scanning Electron Microscopy (SEM) was carried out to investigate the physical morphology including surface texture of the three groups of fibers and energy-dispersive X-ray (EDX) was employed to obtain the elemental spectrum of the specimens.

Key words:

Bitumen-based carbon fibers; Pitch-based and PAN-based carbon fibers; Morphology; Texture; Elemental spectrum

1. Introduction

The development of high-performance engineering products such as a new type of smart concrete is increasing worldwide. Among the many different types of fibers which are being used in concrete, carbon fibers have been extensively exploited over the past few years due to their ability of self-sensing. Therefore, this paper presents an overview of the developments made in the area of carbon fiber reinforced composites, in terms of their types and properties, morphology and application in concrete, and a new type of bitumen-based carbon fiber for future application is introduced, which underscore the roles of material scientists and manufacturing engineers, for the future of this new carbon fiber through value addition to enhance its use.

The interest for application of sustainable and renewable materials in new composite as well as enhancing several desired properties of the composites makes industries imply a wide variety of shapes and materials ranging from synthetic to natural in their new products. The incorporation of reinforcements, such as fibers into composites, affords a means of extending and improving the properties of composites that meets the requirements of most engineering applications. These improvements may happen economical and functional aspects. According to ACI 544 committee [1], there are four categories for FRC: SFRC (Steel Fiber Reinforced Concrete) GFRC (Glass Fiber Reinforced Concrete), SNFRC (Synthetic Fiber Reinforced Concrete) and NFRC (Natural Fiber Reinforced Concrete). Carbon fibers can be classified as synthetic fibers. Recently, the use of carbon fibers in various industries has been rapidly expanding. Aerospace, automobile, construction, sports and transportation are examples of some industries that adopt carbon fibers for different reasons. The idea of carbon-fiber-reinforced concrete was developed by using low-cost pitch-based carbon fibers in the 1980s [2]. One of the first studies on incorporation of carbon fibers in cement mortar was done by Ohama et al [3], who reported that increasing the content of pitch carbon fibers will improve the hardened properties of mortar. However, 3mm carbon fibers showed superior results in comparison with 10 mm fibers. In early 1990s, Banthia et al [4] investigated the impact resistance of carbon fiber reinforced mortar. A significant increase in fracture energy was observed in carbon fiber reinforced samples. A comprehensive study was done by Dr. Chung research group about carbon fibers [5-11]. They studied the capability of concrete for detecting flaws [5] and introduced the new type of concrete as a new strain-stress sensor [6]. Traffic monitoring, fatigue damage self-monitoring and drying shrinkage of carbon fiber reinforced concrete was also investigated [7-9]. The results approved the positive effects of reinforcing concrete with carbon fibers. However, in recent years, many of the researchers have focused on special effects of carbon fibers in concrete such as ice prevention [12], deicing [13,14], reinforcing pervious concrete [15], being used in repair material [16] and other special properties [17-19] that makes it a special type of fiber with multi beneficial aspects.

In this scientific article, different types of carbon fibers, their overall characteristics, as well as their mechanical properties will be reviewed. Furthermore, the optical and microscopic characteristics of three types of carbon fibers, Pitch, PAN and bitumen-based will be studied to obtain some information about the diameter and surface treatment of the fibers. EDX is performed to find the elements inside the fibers. This paper is a preliminary investigation of an ongoing project to assess the feasibility of using the new type of carbon fiber in concrete composites.

2. Carbon fibers

2.1. Properties

Carbon fibers also have useful properties that could improve concrete behavior such as durability and strength. Commercially available carbon fibers when compared to other fibers are generally more expensive. They usually have high tensile strength and elastic modulus depending on the type of fiber. Also, a very useful property of carbon fibers is that they are inert to most chemicals. Carbon fibers can be broken down into two major subcategories called Pan and Pitch, which are created by different precursors and thus yield different mechanical and physical properties [20]. However, some other precursors of carbon fibers can be classified as cellulosic, silk, chitosan and rayon. Carbon fibers can also be classified on the basis of the fiber structure and degree of crystallite orientation: ultrahigh-modulus (UHM), high-modulus (HM), intermediate-modulus (IM), high-tensile-strength (HT), and isotropic carbon fibers [21]. Table 2 shows the classification of carbon fibers.

Table 1: Classification of carbon fibers [21]

Carbon fiber type	Heat treatment temperature (°C)	Crystallite orientation	Long-distance order	
Type 1 high modulus	> 2000	Mainly parallel to fiber axis	High	UHM
				HM
Type 2 high strength	≈ 1500	Mainly parallel to fiber axis	Low	IM HT
Type 3 isotropic	< 1500	Random	Very low	Isotropic

2.1.1. PAN fibers

Over the years, acrylic precursors have been used for carbon fiber preparation by many manufacturers. Polyacrylonitrile (PAN) is the most used acrylic precursor to create carbon fibers. Approximately 70-80% of commercially produced carbon fibers are created from PAN polymer [22]. Pan carbon fibers are produced by carbonizing polyacrylonitrile at high temperatures and then aligning the crystallites by stretching to create the fibers [20].

2.1.2. Pitch fibers

Precursors for Pitch carbon fibers have a high modulus of elasticity in comparison to PAN carbon fibers. Although the elasticity is high, Pitch carbon fibers have poor compressive properties when compared to Pan fibers. Pitch precursors are usually a mix of polyaromatic molecules and heterocyclic compounds. Normal Pitch fibers are produced by refining petroleum or the distillation of coal which tends to be a less expensive process than producing Pan fibers [23].

2.1.3. Morphology

Chae et al [24] have reported that most PAN-based carbon fibers exhibit a particulate morphology, whereas pitch-based carbon fibers exhibit a sheet-like morphology. PAN-based carbon fibers show higher tensile and compressive strengths than pitch-based carbon fibers because PAN-based fibers consist of particle-like structures and smaller crystals in comparison with the sheet-like structure and larger crystals in pitch-based fibers. However, the reports on morphology of carbon fibers are pretty diverse in different papers and based on the classification of fibers. Kim et al [25] The SEM photos of PAN film shows that they are relatively flat and exhibited a dense sponge-like structure. Naito et al [26] suggested that there is a big difference in the morphology of high and ultrahigh strength PAN-based carbon fiber with high modulus PAN-based carbon fibers. From the SEM photos, the fractured surfaces of the high and ultrahigh strength PAN-based carbon fibers exhibit a rough, rather poorly defined granular texture, with no indication of a sheet-like structures but, high modulus PAN-based carbon fibers have slightly sheet-like structures in their cross sections.

2.2. Carbon fibers in concrete

Carbon fibers are usually added to concrete to give it a property of self-sensing. Electrically conducting concrete, as provided by the addition of carbon fibers to concrete, can function as smart structure material that allows non-destructive electrical probing for the monitoring of flaws [27]. There have been lots of studies which investigated the effects of incorporation of different types of carbon fibers in concrete. Table 2 shows properties of some types of carbon fibers used in concrete.

Table 2: Carbon fiber properties in previous studies

Type	length (mm)	Equivalent diameter (μm)	Specific gravity	Tensile strength (MPa)	Elastic Modulus (GPa)	Reference
PAN	3	18		650	35	[28]
PAN	5	7	>1.75	1950	>175	[29]
PAN	spool	-	1.6	3600	230	[30]
PAN		6.5	1.79	4000	240	[31]
PAN	spool	-	1.6	5600	276	[30]
Pitch	5.1	10	1.6	690	48	[32]
Pitch	5	10				[8]
Pitch	5	15	1.6	690		[33]
Pitch	5	15± 3	1.6	690	48	[7]
Pitch	5	7	1.78	>3000	220-240	[34]
Pitch	-	11.49	-	3200	940	[35]
Pitch	Plain weave	7	-	3530	920	[36]
Pitch	5	11.55	-	4000	935	[37]
×	5	7	1.6	2500	240	[38]
×	5	7	>1.75	1950	>175	[39]

Chen et al [40] investigated the conductive behavior of carbon fiber cement-based composites. They studied influence of carbon fiber volume, size, cement-based matrix, relative humidity and curing age on the characteristic of the new composites. They reported that the relationship between conductivity and volume fraction of carbon fiber obeys the statistical percolation theory and the theory is applicable for the change rule of conductivity of system with the volume of carbon fiber.

Shi et al [7] were one of the first researchers who investigated the effects of carbon fibers to be used for traffic monitoring. They added 5 mm pitch carbon into their concrete mixtures (0.5% or 1.0% by weight of cement), and reported that self-monitoring concrete containing short carbon fibers is effective for traffic monitoring and weighing in motion. They concluded that the resistance decreases reversibly with increasing stress up to 1 MPa and is independent of speed up to 55 mph. Other researchers also approved the effects of other carbon-cement composites such carbon black filler and carbon nanotubes to be used in traffic monitoring [41-42].

Capability of carbon fibers to be used as thermal sensors has been reviewed in several studies [43-46]. In 1999, Mingqing et al [43] examined the relationship between the temperature differential and thermoelectric force, the sensitivity and repeatability in carbon fiber reinforced concrete. The results showed that thermoelectric force is proportional to temperature change over a wide range of temperature, and the thermal self-monitoring carbon fiber reinforced concrete possesses high sensitivity and good repeatability. The final result revealed that carbon fibers can be used as a thermal sensor embedded in massive concrete structures.

Piezoelectric and piezoresistive properties of carbon fibers in mortar and concrete was also studied by a few researchers. Sun et al [47] studied the piezoelectric properties of concrete with short carbon fibers under dynamic loading. The results revealed that the new composite can be used as good sensors for monitoring dynamic loading. Azhari et al [48] worked on developing a new composite with 5 mm pitch-based carbon fibers and carbon nanotubes that enhance the electrical conductivity of concrete. They resulted that under cyclic loading, the changes in resistivity mimic the changes in applied load and also the material strain with high fidelity. Bontea et al [49] classified damage in concrete in two groups of minor and major damage and studied the effects of adding short pitch carbon fibers on resistance of concrete. Fibers in the amount of 0.5%, 1%, and 2% by weight of cement were used in concrete samples and the damage in concrete reinforced with short carbon fibers was monitored by measurement of the DC electrical resistance in the stress direction during repeated compressive loading at increasing and decreasing stress amplitudes. They resulted that minor damage that didn't change the compressive modulus was revealed by a partially reversible increase in resistance, which occurred mainly during loading, particularly at a stress above that in prior loading cycles. They also reported that major damage that was accompanied by a decrease in modulus was revealed by the damage-induced resistance increase occurring in every loading cycle irrespective of the prior loading and by an irreversible increase in the baseline resistance.

During the past few years, self-heating concrete has become a new attractive topic among researchers. The aim is to produce a type of concrete which can thaw the snow and ice above it. Gomiz et al [50] studied the self-heating property of carbonaceous cement paste produced by the application of an electric current to conductive cement pastes. One of the carbonaceous materials was 3 mm carbon fiber used in the cement paste. The results indicated that Addition of carbonaceous compounds to cementitious materials will reduce the electrical resistance of the resulting material, so that application of a potential difference produces an electric current by Joule effect, which quickly melts the ice accumulated or to prevent its formation. Galao et al [51] also had another research on the feasibility of conductive carbon fiber reinforced concrete as a self-heating material for ice formation prevention and curing in pavements. Tests were carried out in lab ambient conditions at different voltages and then specimens were put in a freezer at 15 °C. The specimens inside the freezer were exposed to different fixed voltages when reaching +5 °C for prevention of icing and when reaching the temperature inside the freezer, i.e., -15 °C, for curing of icing. They resulted that the new type of concrete with 2 % oxidized PAN carbon fiber (by weight of cement) could act as a heating element in pavements with risk of ice formation. It also consumes a reasonable amount of energy for both anti-icing and deicing. Wu et al [52] used three kinds of electrically conductive material in concrete, namely, steel fiber, carbon fiber, and graphite to deice concrete pavements. The results revealed that 1% volume fraction of steel fiber, 0.4% volume fraction of carbon fiber, and 4% volume fraction graphite are the optimum percentage for deicing pavements.

2.3. Bitumen

Bitumen is a semi-solid material that can be produced either from certain crude oils or in nature as "natural asphalt". Bitumen consists of a mixture of hydrocarbons of different molecular sizes containing hetero atoms like Sulphur and nitrogen as well as traces of metals like vanadium and nickel, However, the true nature of bitumen is not completely known. Many books and papers on bitumen chemistry describe that bitumen is a colloidal dispersion of asphaltenes in maltenes [53]. According to SARA separation, bitemen can be classified in 4 groups: saturants, aromatics, resins and asphaltenes [54]. High-quality carbon fibers can be produced from bitumen due to its composition and molecular constituent [55]. bitumen can be used to produce PAN

(from cracked gas propane) and potentially a pitch product, utilizing the high-asphaltene content that makes oil sands bitumen unique [56].

3. Fiber characterization

Three types of Pitch, bitumen and PAN-based fibers according to Fig. 1 were investigated in this study. Pitch fibers were acquired from Mitsubishi Chemical Carbon Fiber And Composites and PAN fibers were acquired from Teijin company. The properties of fibers as provided by the manufacturers are summarized in table 3.

Table 3: Properties of fibers

Type	Equivalent diameter (μm)	Specific gravity	Tensile strength (MPa)	Elastic Modulus (GPa)
Pitch	11	2	2345	186
PAN	7	1.8	4890	227

(a) (b) (c)

Fig 1: (a) Pitch-based carbon fibers, (b) Bitumen-based carbon fibers, (c) PAN-based carbon fibers

3.1. Scanning Electron microscopy

Fig 2 shows the morphology of the microstructure of the three types of fibers. It is observed that the pitch and PAN based fibers has small cavities and hollows on its outer surface, and the surface of the BBCF is smoother than that of the two other fibers. The presence of rough cavities can improve the mechanical anchoring (i.e. improve the quality of the fiber/matrix interface) when using the fiber in composite materials [57], however these pores seems to be too small to affect the fiber/matrix bonding. Fig 3 shows SEM photos of the newly developed BBCF in different scales and locations. The cross-section of this fiber is circular and the fibers are arranged in parallel to each other in a bunch. Furthermore, the thickness of fiber ranges from 10 to 15 μm. The SEM photo of the cut of the surface of the fiber approves its smooth texture on the diameter.

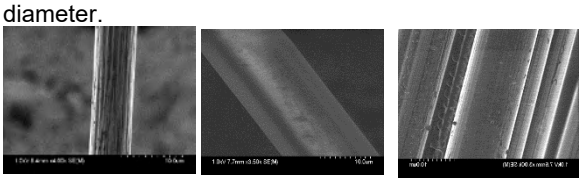

Fig 2: SEM photos of (a) Pitch-based carbon fibers (b) Bitumen-based carbon fibers (c) PAN-based carbon fibers

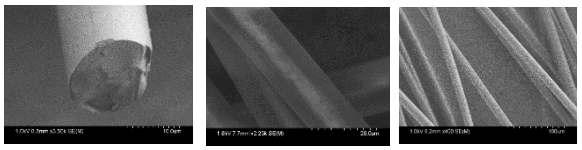

Fig 3: SEM photos of (a) cross-section (b) longitudinal view and (c) bunch of bitumen-base carbon fibers

3.2. Energy dispersive X-ray (EDX)

Energy dispersive X-ray was tested at least on three different points and surface on fibers to confirm the validity of the results. EDX results can be found in Fig 4. **EDX** provides information on carbon(C), Oxygen(O), Nickel(Ni), Vanadium(V), Titanium(Ti) and Sulphur(S) content of three groups of carbon fibers. As it was predicted carbon is the major component of all types of fiber, but the amount of carbon is different in different fibers, 81% carbon in bitumen-based carbon fiber is a low amount in comparison with other available fibers, Moreover, bitumen fibers contain approximately 6% of Sulphur which necessitates further investigation and analysis of additional samples. Other types of Pitch and PAN fibers didn't show any traces of Sulphur in their combination.

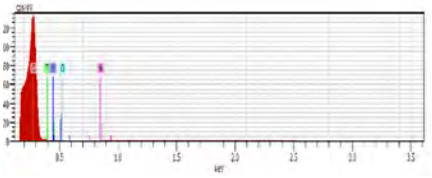

EL	AN	unn.	C norm.	C Atom	C Error
		(wt.%)	(wt.%)	(wt.%)	(%)
C	6	93.81	93.81	95.29	28.2
O	8	6.16	6.16	4.7	1.9
S	16	0	0	0	0
V	23	0	0	0	0
Ti	22	0	0	0	0
Ni	28	0.02	0.02	0	0

(a)

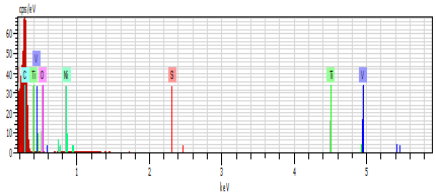

EL	AN	unn.	C norm.	C Atom	C Error
		(wt.%)	(wt.%)	(wt.%)	(%)
C	6	81.1	81.1	87.48	24.6
O	8	12.1	12.1	9.8	3.9
S	16	6.61	6.61	2.67	0.3
V	23	0.08	0.08	0.02	0
Ti	22	0.05	0.05	0.01	0
Ni	28	0.06	0.06	0.01	0

(b)

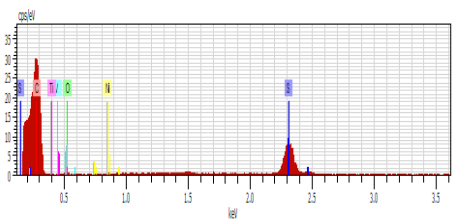

EL	AN	unn.	C norm.	C Atom	C Error
		(wt.%)	(wt.%)	(wt.%)	(%)
C	6	97.97	97.97	98.55	29.4
O	8	1.88	1.88	1.42	0.6
S	16	0	0	0	0
V	23	0	0	0	0
Ti	22	0.01	0.01	0	0
Ni	28	0.14	0.14	0.03	0.1

(c)

Figure 4. EDX results of a) Pitch-based, b) Bitumen-based, and C) PAN-based carbon fiber

4. Conclusion

This paper presents a review of various carbon fibers available today that can be used for producing cementitious composites. In this article, the properties of a new carbon fiber extracted from bitumen were studied in order to evaluate the possibility of using it as reinforcement in cementitious materials. The following conclusions were drawn from the results of the microstructural tests of this new natural fiber.

The study of the surface morphology by SEM revealed that the cross-section of bitumen-based carbon fiber has a circular shape similar to other fibers and the surface of it is smooth. No cavities were found on the surface and in the cross section of the new fiber. Bitumen fibers are located in parallel to each other in bundles.

Energy dispersive X-ray results showed around 6% of Sulphur in bitumen fibers which necessitate the need for further confirmatory investigation.

Acknowledgment

The authors would like to acknowledge financial support received from Alberta Innovates. The technical advice offered by Dr. Axel Meissen is greatly acknowledged. The authors would like to thank the staff members in the Advanced Microscopy Facility at UVic for their support. The support received from the tech team in Department of Civil Engineering is also acknowledged.

References

[1] ACI 544.IR-96, State-of-the-art report on fibre reinforced concrete, Manual of concrete practice, Farmington Hills, 1998 (CD-ROM).
[2] Ohama, Y. (1989). Carbon-cement composites. Carbon, 27(5), 729-737.
[3] Ohama, Y. et al. (1985). Concrete International, 7(3), 58-62.
[4] Banthia, N. et al. (1989). Fiber Reinforced Cements and Concretes: New Developments, 251-60.
[5] Chen, P. W. et al. Smart Materials and Structures, 2(1), 22.
[6] Chen, P. W. et al. Composites Part B: Engineering, 27(1), 11-23.
[7] Shi, Z. Q. et al. Cement and Concrete Research, 29(3), 435-439.
[8] Fu, X. et al. Cement and concrete research, 26(1), 15-20.
[9] Chen, P. W. et al. Composites Part B: Engineering, 27(3-4), 269-274.
[10] Chung, D. D. L. (2000). Composites Part B: Engineering, 31(6-7), 511-526.
[11] Chen, P. W. et al. (1993). Composites, 24(1), 33-52.
[12] Galao, O. et al. (2016). Materials, 9(4), 281.
[13] Sassani, A. et al. (2018). Journal of cleaner production, 203, 799-809.
[14] Wu, J. et al. (2015). Construction and Building Materials, 75, 129-135.
[15] Rangelov, M. et al. (2016). Construction and Building Materials, 126, 875-885.
[16] Karzad, A. S. et al. (2017). In MATEC Web of Conferences (Vol. 120, p. 01008). EDP Sciences.
[17] Tanyildizi, H. (2018). Advances in Civil Engineering, 2018.
[18] Song, W. et al. (2016). Materials, 9(8), 704.
[19] Jeon, E. B. et al. (2015). Composite structures, 134, 27-35.
[20] ACI Report pdf (Report on Fiber Reinforced Concrete
[21] Park, S. J. (2015). Carbon fibers (p. 74). Dordrecht, Heidelberg, New York, London: Springer.
[22] Donnet, Jean-Baptiste, and Roop Chand Bansal. Carbon fibers. Crc Press, 1998.
[23] Park, Soo-Jin, et al. Carbon Fibers. Springer, Dordrecht, 2015. 31-66.
[24] Chae, H. G. et al. (2006). Polymer, 47(10), 3494-3504.
[25] Kim, S. S. et al. (2014). Carbohydrate polymers, 102, 231-237.
[26] Naito, K. et al. (2008). Carbon, 46(2), 189-195.
[27] Chen, P. W. et al. (1993). Smart Materials and Structures, 2(1), 22.
[28] Ivorra, S. et al. (2010). Materials & Design, 31(3), 1553-1558.
[29] Sun, M. Q. et al. (1998). Cement and concrete research, 28(12), 1707-1712.
[30] Chae, Han Gi, et al. Carbon 93 (2015): 81-87.
[31] Wang, W. et al. (2006). Materials Science and Engineering: A, 434(1-2), 347-351.
[32] Chen, P. W. et al. (1993). Smart Materials and Structures, 2(3), 181.
[33] Aydin, A. C. (2007). Construction and Building Materials, 21(6), 1149-1154.
[34] Chen, B. et al. (2008). Construction and Building Materials, 22(11), 2196-2201.
[35] Naito, K. et al. (2009). Journal of the American Ceramic Society, 92.1 186-192
[36] Reimer, T. et al. Ceramics and Composites VII 252 (2015): 277.
[37] Naito, K. Carbon 126 (2018): 346-359.
[38] Yao, W. ET AL. (2003). Cement and concrete research, 33(1), 27-30.
[39] Sun, M. et al. (2000). Cement and Concrete Research, 30(10), 1593-1595
[40] Chen, B. et al.(2004). Cement and Concrete Composites, 26(4), 291-297.

[41] Han, B. et al. (2009). Nanotechnology, 20(44), 445501.
[42] Monteiro, A. O. et al. (2017). Construction and Building Materials, 154, 1079-1086.
[43] Mingqing, S. et al. (1999). Cement and Concrete Research, 29(5), 769-771.
[44] Sun, M. et al. (2000). Cement and Concrete Research, 30(8), 1251-1253.
[45] Sun, M. Q. (1998). Cement and concrete research, 28(12), 1707-1712.
[46] Bahar, D. et al. (2008). New Carbon Materials, 23(1), 21-24.
[47] Sun, M. et al. (2000). Cement and Concrete Research, 30(10), 1593-1595.
[48] Azhari, F. et al. (2012). Cement and Concrete Composites, 34(7), 866-873.
[49] Bontea, D. M. et al. (2000). Cement and Concrete Research, 30(4), 651-659.
[50] Gomis, J. et al. (2015). Construction and Building Materials, 75, 442-449.
[51] Galao, O. et al. (2016). Materials, 9(4), 281.
[52] Wu, J. et al. (2015). Construction and Building Materials, 75, 129-135.
[53] Redelius, P. G. (2000). Solubility parameters and bitumen. Fuel, 79(1), 27-35.
[54] K.H. Altgelt, D.M. et al. Marcel Dekker, New York (1979), pp. 194-196
[55]https://albertainnovates.ca/wpcontent/uploads/2018/04/BBC-Report-1.pdf
[56]https://albertainnovates.ca/wpcontent/uploads/2018/04/BBC%20-%20Report%202.pdf
[57] Maache, M. et al. (2017). Carbohydrate polymers, 171, 163-1

Smart Buildings – A Road Map: Where we are, where we are going, and how we get there

N. Hodge[a], A. Crosson[a]

[a] Integral Group, Victoria BC; Tel: 250-418-1288; Email: acrosson@integralgroup.com, nhodge@integralgroup.com

Abstract:
Over the past century, the design and construction of buildings has changed dramatically – buildings are getting smarter. Smart buildings utilize connected systems and automated processes to collect data that can be used for a multitude of purposes. Smart buildings are integral to green building and reaching net zero targets in the future. Traditional buildings have typically been designed with independent control systems for components including HVAC, lighting, access control, and IT networks. Smart buildings break the silos that have long existed between systems by collecting and sharing information to optimize building performance. Modern building design today often includes building controls for systems that, while largely independent of each other, have gateways of communication so that there is limited control between silos. Data that is collected can be analysed and used in dashboards to show energy consumption, usage, and can be used as a tool for facility management. As technology evolves and advances in passive optical networks (PON) and wireless networks (5G) continue, higher bandwidth and higher speeds are being realised which enables more devices to be connected and more data to be collected with low latency. The Internet of Things (IoT) and network convergence will enable robust, scalable software defined networks where OT and IT integration can be used for the management of both physical processes and information in real time. Big data and machine learning can be utilized to optimize design leading to reduce maintenance costs and energy consumption while increasing efficiency, sustainability, and the quality of the living or working environment for the occupants. Smart buildings will continue to evolve and are an important part of our future.

Keywords:
Smart buildings, sustainability, machine learning

1. Introduction

Smart buildings use automated processes and connected systems to control building performance. Sensors within the building are used to collect raw data which can be analysed and used to make decisions for building operation. Smart buildings enhance occupant experience and create healthy environments while increasing productivity, energy efficiency, and reducing greenhouse gas emissions [1].

The building and building construction sector account for over 30% of the world's energy consumption. The sectors also account for roughly 40% of global CO2 emissions both directly and indirectly [2]. The opportunities to increase building energy efficiency are integral to the success of green building and net zero targets. According to the International Energy Agency (IEA), primary sources of wasted energy in a building include space heating, space cooling, water heating, and lighting [2]. These sources of wasted energy can be reduced by realizing synergies between the systems and optimizing overall performance. Meeting 2030 targets of net zero, in which new construction would be either net zero energy or net zero emission, requires smart buildings to play a key role [3]. Smart buildings are an important step toward reducing emissions in both new construction, and existing buildings.

This paper will explore where current smart building technology is at today, current challenges, where smart buildings are going, and how advances in technology will enable performance to be optimized further.

2. Modern Building Systems – Where we are

Buildings have come a long way in the last century. From simple wooden structures to skyscrapers, technology has had a profound impact on the way buildings are designed and constructed today. As technology has advanced, building control systems have become more advanced as well. Examples of building systems includes, but is not limited to, HVAC, plumbing, life safety, security, access control, communications, lighting, audio visual, and power systems. Modern buildings usually incorporate basic building system integration and control. This allows for information to be shared between systems and building equipment in order to enable effective operation.

Modern buildings use sensors within building systems to collect raw data to be analysed by the building management system to control the equipment within the building. This can be used to monitor and measure system performance. The ability to collect data and high-level information on energy usage is important for assessing building performance and implementing corrective measures to reduce energy consumption.

Dashboards can be used to display high level information to inform occupants about building performance in real time. Providing a visual representation of building performance data helps to communicate information quickly and easily. This can

empower occupants to make informed decisions on energy usage. When people see the effects of their actions, they are more likely to make informed decisions on energy consumption [4]. Having access to performance data also allows for facilities management to schedule preventive maintenance so that all systems function properly and as designed, to increase overall efficiency.

As building systems become increasingly integrated, more information becomes available. Sensors can be used to collect information about occupancy and the building usage. Occupancy sensors for lighting control allow for greater efficiency by reducing energy consumption for lighting when it is not needed. Sensors can measure daylight and communicate with lighting control systems to maintain a desired light level, thus lights that are not required to maintain specified light levels in an area can be dimmed or turned off. Occupancy sensors and room booking systems can be used to collect data on space utilization, which can be used to determine building needs. Energy can be reduced by appropriate heating and cooling specific areas based on occupancy, rather than continually heating and cooling an entire floor.

Figure 1: Modern Building Control System

Figure 1 depicts a modern building control system, where most systems within the building can communicate with one another to improve overall performance.

3. Challenges with modern building control

In modern buildings, a variety of different teams work on different parts of the building. To develop a unified building control system, having a clear vision at the start of the project of how the building will need to function will allow for successful and integrated buildings.

A challenge with modern building control systems today is that systems can be isolated from other systems within the building. When systems operate independently of each other however, silos of information can be created [5]. This causes systems to work independently of one another which negatively affect system performance. This leads to higher maintenance costs and decreased equipment life spans. As buildings are renovated or building systems are upgraded, the risk of silos increases. Another issue arises with proprietary systems as they follow communication protocols which may not be compatible with other systems.

Disparity exists between operational technology (OT) and information technology (IT). Generally, OT and IT use different communication protocols which lead to challenging integration and analysis of data. OT monitors the physical state of systems and uses industrial communication protocols, while IT usually uses IP communication. The communication gap between OT and IT must be bridged to optimize building performance successfully.

Sensors can provide a wealth of information, but there is not always the ability to analyse and use the data effectively. This can be due to an oversaturation of information, or an inability to process it properly into useful information. Bandwidth and latency are restrictions on the amount of data that can be transferred, and it can be challenging to process the data accurately and efficiently. Today, proactive problem solving is limited in its applications and corrective actions are mostly reactive. Currently there are massive amounts of data being collected by individual systems, but the data needs to be used more efficiently to optimize building performance. [6]

In addition to the physical and technological challenges smart buildings face, the evolving workforce must also be taken into consideration as well. Remote and mobile workers can add a challenge with space utilization and planning as the number of people within the space can vary greatly. Buildings will need to adapt to this by using data to determine what is available and to predict what will be required.

4. Digital Buildings – Where we are going

The next step in building control is seamless integration of monitoring and control for all systems within the building. Using real time analytics as well as historical data would allow the system to predict what will need to happen before an event occurs. This enables increased efficiencies within the building due to proactive action.

Advances in technology allow for higher bandwidth and higher data speeds, allowing more devices to be connected to a network with quicker response times. With instantaneous access to data, and seamless communication, buildings would be much more efficient.

Figure 2: Full System Integration

Figure 2 depicts a smart building with full system integration, where all systems communicate on a single unified network.

5. Future Trends – How will we get there

The increasing trend of connected devices has led to more data available than ever before. Gartner Inc forecasts the number of connected devices with the Internet of Things (IoT) to reach 5.8 billion in 2020 [7]. The number of connected devices will soon outnumber people in the world, and this number is increasing rapidly, the world is becoming constantly more connected. Smart buildings have many different streams of data, including system data, facility data, and occupant data. With growing number of connected devices and the IoT, the amount of data that can be used to provide information for building management is increasing significantly. The term Big Data is used to describe large and varied data sets, with high volume, high velocity, or high variety [8]. The analysis of big data allows for machine learning and predictive analysis.

Network convergence enables connected devices to communicate effectively. The integration of OT and IT will allow for increased data analysis and control. Network convergence enables robust, scalable software defined networks (SDN). With the ability to send information over a single streamlined network less infrastructure is required. Software defined networks improve network control and do not require as much physical hardware or powered equipment. With SDN, greater flexibility and control of the network can be achieved. Encouraging open protocol as well for sensor and device communication will reduce data silos and help to bridge the gap for OT and IT integration.

The fifth generation mobile network – 5G will also play an important role in smart buildings, IoT, and network convergence. 5G uses millimeter waves to transmit information with high bandwidth and low latency which enables more devices to access the mobile network. 5G will facilitate seamless communication between devices.

Passive optical networks (PON) use fibre optic technology to transmit information with higher bandwidth and speed capacity than a traditional copper network. PON networks require significantly less space and require up to 45% less power than copper networks [10]. Fiber cables are lighter, and require less structural support within the building, and have a much longer lifespan than copper cables. Also, fiber cables are not as susceptible to EMI (electromagnetic interference) as copper networks. PON networks enable more information to be transferred within the building.

Operational efficiency can be increased through mobile workstations to accommodate more employees as workforce trends evolve. In an IoT enabled smart building created by Intel in 2016, employee capacity was increased 30% by using sensors and data collection to use space more efficiently [9].

As technology evolves and the world becomes more connected, buildings will become smarter. Taking advantage of these trends will allow buildings to take the next step towards achieving greater levels of energy efficiency and sustainability.

6. Conclusions and outlook

Smart buildings are critical to realizing green building initiatives and net zero targets. They are a way to increase energy efficiency within the building and to optimize the way that the building is used. They will create healthier environments where productivity is increased, and space is used more efficiently. The benefits of smart buildings and the evolution of smart building technology include reduced maintenance costs, fewer unplanned equipment outages, increased energy efficiency and reduced greenhouse gas emissions.

Overcoming current challenges and interoperability issues with modern smart buildings will allow the smart buildings of the future to achieve greater energy efficiency. More connected devices will allow greater amounts of data to be analysed and processed. As advancements in artificial intelligence and machine learning continue, the ability to use the data to provide information for building management will increase. Network convergence will enable connected devices to communicate effectively. As technology advances, the opportunities to apply intelligence to building systems grow as well. Taking advantage of emerging technology, network optimization, and data analysis enables connected systems to make smart decisions on how to optimize building functionality.

References

[1] Government of Canada - Public Services and Procurement (November 6, 2019), Smart Buildings Initiative, accessed November 2019 from, https://www.tpsgc-pwgsc.gc.ca/biens-property/intelligents-smart/index-eng.html

[2] IEA.org (n.d), Energy Efficiency: Buildings, accessed November2019 https://www.iea.org/topics/energyefficiency/buildings/

[3] Frappé-Sénéclauze, T.P, Kniewasser, M (2015), "*The Path to "Net-Zero Energy" Buildings in BC The case for action and the role of public policy*", retrieved November 2019 from https://www.toolkit.bc.ca/Resource/Path-%E2%80%9CNet-Zero-Energy%E2%80%9D-Buildings-BC

[4] Wilson, A. (November 24, 2008), Energy Dashboards: Use Real-Time Feedback to Influence Behaviour, accessed November 2019 from https://www.buildinggreen.com/feature/energy-dashboards-using-real-time-feedback-influence-behavior

[5] Cole, C. (July 2, 2018), From Silos to Shared: Smart technology makes its mark, accessed November 2019 from https://crej.com/news/from-silos-to-shared-smart-technology-makes-its-mark/

[6] Linder L., Vionnet D., Bacher, J.P., Hennebert J. (2017), Big Building Data - a Big Data Platform for Smart Buildings, Energy Procedia 122 (2017), 589-594, retrieved from www.sciencedirect.com

[7] Gartner Press Release (August 29, 2019), accessed November 2019 retrieved from https://www.gartner.com/en/newsroom/press-releases/2019-08-29-gartner-says-5-8-billion-enterprise-and-automotive-io

[8] IBM.com (n.d), Big Data Analytics, accessed November 2019 https://www.ibm.com/analytics/hadoop/big-data-analytics

[9] Khandalilli, S. (2017) *Intel Creates Smart Building Using IoT* [White Paper], retrieved November 2019 from www.intel.com

[10] Optical Fiber (n.d), Comparison between copper networks vs. fiber optic networks, accessed November 2019 from https://www.opticalfiberco.com/en/pon/698-copper-vs-fiber

A Comparison of carbon capturing technologies for community energy systems: A techno-economic assessment

Ravihari Kotagoda Hetti[1], Hirushie Karunathilake [2, 3], Kasun Hewage[4], Rehan Sadiq[5]

[1,2,4,5] School of Engineering, University of British Columbia (Okanagan Campus), 1137 Alumni Avenue, Kelowna, BC V1V 1V7, Canada

[3] Department of Mechanical Engineering, University of Moratuwa, Katubedda, Moratuwa 10400, Sri Lanka

* Corresponding author: Dr. Kasun Hewage, Phone: 1.250.807.8176, Email: kasun.hewage@ubc.ca

Abstract:

Global climate is being affected by the increasing greenhouse gas (GHG) emissions, of which the most significant is carbon dioxide (CO_2). According to the Pan-Canadian framework on clean growth and climate change, Canada has set ambitious targets to realise a low carbon future for the nation. Amongst strategies that are available for emission reduction, on-site carbon capturing, storage, and utilization (CCSU) have proven its' potential to reduce CO_2 emissions from large-scale industrial facilities. However, the integration of CCSU units with on-site energy generation applications such as district energy systems has not been explored adequately in literature. This study evaluates the techno-economic feasibility of retrofitting different carbon capturing technologies in community energy systems. A scenario-based approach was employed in assessing the performance of the energy systems with and without CCSU units. Potential carbon capturing technologies were identified through a thorough literature review. The chosen energy system scenarios are conventional coal power plant with post combustion carbon capture, and oxy fuel carbon capture, integrated gasification combined cycle plant with pre combustion carbon capture, and natural gas combined cycle (NGCC) power plant with post combustion carbon capture. The main parameters considered to compare the technical performance are technology readiness level, abatement efficiency, capture potential, and the efficiency penalty. The economic evaluation focuses on the levelized cost of electricity, cost of CO_2 avoided, and the cost of CO_2 capture. Based on the results from the techno-economic evaluations the technologies were ranked using multi-criteria decision-making approaches. The Technique for Order of Preference by Similarity to Ideal Solution (TOPSIS) was used to rank the technology scenarios. Neutral weights were given for all performance criteria. The data envelopment assessment (DEA) methodology was further adopted to evaluate the performance efficiency of technology options. NGCC plant with post combustion capture ranked the first amongst the chosen scenarios while all scenarios were proven to perform well. The findings from this study will be useful for the municipalities and policy makers in making investment decisions to reach net-zero emissions communities.

Keywords: Carbon capturing and utilization, community energy systems, techno-economic analysis, greenhouse gas, zero emission communities

1. Introduction

Climate change has garnered much attention in the present day due to negative impacts caused on the society and the eco-system. Some of them are extreme weather conditions, rising sea levels, and change in weather patterns that are linked with global warming [1]. Anthropogenic sources contribute significantly to atmospheric greenhouse gas (GHG) levels [2]. Energy generation from fossil fuel combustion is the largest contributor for GHG release to the atmosphere from Canada. It records 45% of the overall Canadian emissions [3]. This highlights the importance of rapid implementation of emission mitigation and reduction strategies for the energy sector.

There are three strategies that are commonly used to reduce the carbon emissions from energy generation namely, (a) enhance system and process efficiencies; (b) develop and implement alternative low-emission fuel technologies and use renewable energy; (c) on-site carbon capturing, storage, and utilization (CCSU) [4]. However, energy efficiency enhancement and energy conversation has a limited applicability in large-scale energy generation facilities such as energy intensive industries and power plants. Moreover, although Canada is the 4th largest renewable energy producer in the world [5], 9% of electricity is generated from coal and 10% of the generated electricity is consumed by the oil and gas sector [6] [7]. This is due to the differences in the regional applicability of renewable technology that varies with several geographical, technical, and socio-economical aspects [8]. Other aspects are issues associated with intermittent power supply, high costs, and federal and provincial policies that are either settling or contradicting [9][10]. Moreover, on-site energy generation applications associated with industries have comparatively limited access to alternative clean power technologies than future low carbon plants [11].

Canada has invested significant resources into developing renewable energy technologies. However, fossil fuel still plays and will continue to play a major role in energy systems of some regions. Under the present stage of emission abating strategies, CCSU is the only technology available to avoid carbon emissions from fossil fuel and gas power plants, and other on-site energy generation applications [12]. Carbon capturing technology allows two options for the captured carbon. Carbon storage is one of them. Canadian regions in Western Canadian Sedimentary Basin (WCSB) that includes Alberta, Northeastern British Columbia, South

Western Manitoba and southern and central parts of Saskatchewan are known as regions with a huge potential for carbon storage [13]. On the other hand, carbon utilization is deemed to be much beneficial due to its' potential for additional revenue generation. However, the applicability of carbon capture technologies for on-site energy generation applications such as community energy systems is yet to be explored. Hence, this study aims to conduct a preliminary investigation on technically viable carbon capture strategies for community scale energy systems.

The objective of this study is to present a framework to assess the techno-economic viability of selected carbon capture scenarios in planning zero emissions communities in Canada. Different carbon capture integration scenarios are compared in the study. The data needed for the assessment was gathered from literature and the Integrated Environmental Control Model (IECM) software developed by the Carnegie Mellon University [13], [14]. The evaluation is based on multiple criteria decision-making approaches to rank the optimum scenarios and determine the performance efficiency. The findings will be useful to the urban planners in making their investment decisions for zero emissions community development.

2. Methodology

The technology readiness level (TRL) is an important indicator when establishing the viability of a CCSU project.

A higher maturity ensures the reliability, feasibility, and the safety of technology [15]. Therefore, carbon capture technologies with a technology maturity with 7 – 9 (7-functional prototype demonstration, 8 - full scale technology demonstration at commercial scale, 9 – first of a kind commercial deployment) [16][17], were chosen for further analysis. They are post combustion capture with monoethanolamine (MEA), pre combustion capture with selexol, and oxy fuel combustion capture. Carbon capture integration scenarios were defined based on different combination of fossil fuel combustion systems. They are,

(a) Conventional coal power plant with post combustion capture (PC - MEA)
(b) Conventional coal power plant with oxy fuel combustion capture (PC – Oxy fuel)
(c) Integrated gasification combined cycle (IGCC) coal power plant with pre combustion capture (IGCC - Selexol)
(d) Natural gas combined cycle (NGCC) power plant with post combustion capture (NGCC - MEA)

A coal power plant without any carbon abatement strategy was selected as the reference plant. For the case of an IGCC power plant, IGCC without carbon capture was not selected as the reference plant. This is due to the lack of reliable cost data since the IGCC technology is still considered a novel technology compared to the conventional coal power plant [18]. Table 1 presents parameter details of the carbon capture integration scenarios. For the purpose of the study some literature based assumptions were made on the plant capacity factor, fixed charge factor, electricity charges, and fuel prices, and miscellaneous site specific costs [13], [19]–[23]. Moreover, certain performance and cost estimations were obtained from the IECM software tool.

Table 1: Carbon capture integration scenarios

	PC	PC - MEA	PC – Oxy fuel	IGCC	IGCC - Selexol	NGCC	NGCC - MEA
Power plant performance							
Gross power output (MW)	500	500	500	706.9	688.9	605.8	550
Net power output (MW)	461	371.5	359.7	604.1	544.5	590	505
Net plant efficiency (%)	28.84	22.03	28.29	36.20	30.56	50.4	42.89
CO_2 emission rate before capture (tCO2/ MWh)	1.14	1.44	1.116	0.85	0.99	0.36	0.42
Capacity factor (%)	70	70	70	70	70	70	70
Capture plant performance							
Capture technology	-	MEA	Oxy fuel combustion	-	Selexol	-	MEA
Capture system efficiency (%)	-	90	80	-	90	-	90
CO_2 emission rate after capture (tCO_2/ MWh)	-	0.1448	0.062	-	0.09	-	0.04
Cost performance							
Fixed charge factor	0.109	0.109	0.109	0.109	0.109	0.109	0.109
Total capital cost ($/kW)	1377	4748	4000	2443	3695	779.8	1421
Capture plant capital cost ($/kW)	-	1952	1745	-	799	-	528.8

IECM is a software tool available for the public, which is developed by the Carnegie Mellon University to estimate performance of fossil fuel based energy systems [24], [25].

Figure 1 presents the methodology followed in this study. Technical and economic performances were evaluated for defined criteria indicators. Under the technical evaluation carbon capture efficiency, and the technology readiness level were obtained from the literature [16], [17], [22]–[24], [26]. CO_2 emissions from the plant, and total CO_2 captured under the defined scenarios were obtained from the IECM software tool.

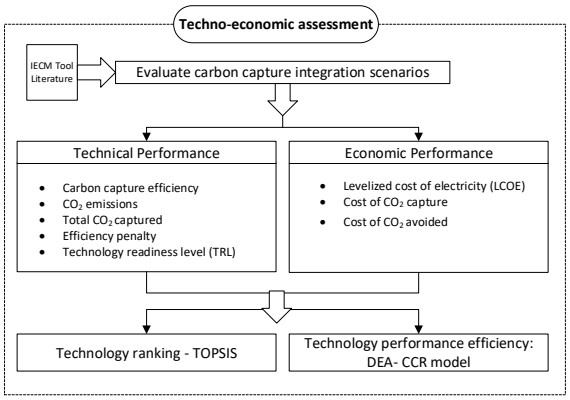

Figure 1: Methodology followed

2.1 Technical and cost performance assessment

Efficiency penalty is one criterion indicator that was calculated for the technical performance of carbon capture integration scenarios. It is an indicator of the reduction in rated power output due to additional fuel consumed in the carbon capture plant [27]. The efficiency penalty was calculated using the equation 1.

$$(1)\ \text{Efficiency penalty} = \frac{\eta\text{ref} - \eta\text{cc}}{\eta\text{ref}}$$

Where, ηref = plant efficiency without carbon capture and ηcc = plant efficiency with carbon capture.

The levelized cost of electricity (LCOE) characterises the average revenue per unit of electricity required to cover the operations and other fixed costs for a defined financial life [28]. This measure was used to compare the cost performance of selected scenarios. LCOE ($/MWh) is defined in equation 2 [29]:

$$(2)\ \text{LCOE} = \frac{(\text{TCC})(\text{FCF})+(\text{FOM})}{(\text{CF})(8766)(\text{MW})} + \text{VOM} + (\text{HR})(\text{FC})$$

Where, TCC = total capital cost ($), FCF = Fixed charge factor (fraction/year), FOM = Fixed O&M costs ($/year), VOM = Variable non fuel O&M cost ($/MWh), HR = net heat rate (MJ/MWh), FC = fuel cost ($/MJ), CF = capacity factor (fraction), and MW = net plant capacity (MW) [26].

Cost of avoidance and capture gives the average cost to avoid and capture one unit of CO_2 while generating the same amount of power as the reference plant without CCSU respectively [28]. The cost terms are defined as (equation 3, 4) [26];

$$(3)\ \text{Cost of } CO_2 \text{ avoided} = \frac{(\text{LCOE})_{\text{ccs}} - (\text{LCOE})_{\text{ref}}}{(\text{tCO}_2/\text{MWh})_{\text{ref}} - (\text{tCO}_2/\text{MWh})_{\text{ccs}}}$$

$$(4)\ \text{Cost of } CO_2 \text{ captured} = \frac{(\text{LCOE})_{\text{ccs}} - (\text{LCOE})_{\text{ref}}}{(\text{tCO}_2/\text{MWh})_{\text{captured}}}$$

2.2 Multi-criteria approach for technology ranking and performance efficiency evaluation

This study adopted a multi-criteria decision making approach to rank the carbon capture integration scenarios and to evaluate their performance efficiencies. The DEA methodology with standard Charnes-Cooper-Rhodes (CCR) model was used to evaluate the performance efficiencies of the selected technologies based on the values of the cost (input) and benefit (output) attributes [30]. The main benefits offered by DEA method over other MCDM techniques are that it is simple and no subjective inputs are required [31]. Microsoft Excel Solver was used for the DEA analysis. The mathematical approach to DEA is provided below [32]. Consider n DMUs (DMU_1, DMU_2, …, DMU_j, .., DMU_n), with m inputs (x) and s outputs (y).

$\text{Min}\ \theta = \theta_p$

Such that,

$\sum_{j=1}^{n} x_{ij}\gamma_j \leq \theta_p\, x_{ip}$ j= 1……n, i = 1…..m

$\sum_{j=1}^{n} y_{rj}\gamma_j > y_{rp}$ r = 1…..s

$\gamma_j \geq 0$

γ_j : Weight or the intensity of the DMU

After assessing the technical and performance efficiencies of the defined carbon capture scenarios to establish the feasibility, the feasible scenarios were further ranked to determine the most suitable integration scenario amongst them. TOPSIS (Technique for Order of Preference by Similarity to Ideal Solution) method was selected for this purpose due to its simplicity and straightforwardness [15]. Neutral weights were given for the technical and economic performance criteria. However, weights can be adjusted based on expert judgements. This method follows a step wise approach given below [33].

1. Calculate the weighted normalized decision matrix

$a_{ij} = W_{ij}\, r_{ij}$

Where,

a_{ij}: Weighted normalized matrix element

W_{ij}: Weight of criteria j

r_{ij}: Normalized matrix element

1. Determine the ideal and negative ideal solution

$A^+ = \{A_1^+, \ldots\ldots, A_n^+\} = \{(j_{max} a_{ij} | i \epsilon I'), (j_{min} a_{ij} | i \epsilon I'')\}$

$A^- = \{A_1^-, \ldots\ldots, A_n^-\} = \{(j_{min} a_{ij} | i \epsilon I'), (j_{max} a_{ij} | i \epsilon I'')\}$

I' and I'' are increasing and decreasing criteria

2. Measure distance to ideal and negative ideal solution

$S_i^+ = \sqrt{\sum_{j=1}^{n} (a_{ij} - A_j^+)^2}$

$S_i^- = \sqrt{\sum_{j=1}^{n} (a_{ij} - A_j^-)^2}$

3. Calculate similarity index

$C_i^* = \frac{S_i^-}{S_i^+ + S_i^-}$

Alternatives with higher similarity indices are ranked higher.

3. Results and Discussion

Figure 2 depicts the overall techno-economic performance of chosen carbon capture integration scenarios. It can be seen from the figure that the highest LCOE is associated with the conventional coal power plant integrated with MEA post combustion capture, where as the least is for the conventional coal power plant without any capture technology. Thus, high LCOE is associated with the capital and operational costs for the capture unit. The largest efficiency penalty of 28.1% is recorded for the coal power plant with oxy fuel combustion capture. The PC – MEA integration scenario follows this. High-energy requirement by the carbon capture facility is the main reason behind this. NGCC plant without a capture technology holds the lowest efficiency penalty. This is because NGCC power plants usually hold higher overall thermal efficiencies [27].

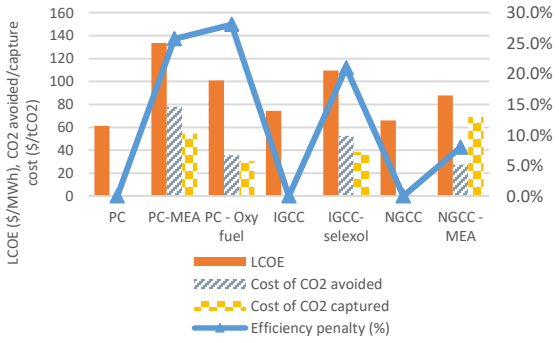

Figure 2: Techno-economic performance of carbon capture scenarios

The cost of CO_2 avoided is highest for again coal power plant with MEA post combustion capture and it is least for the NGCC plant integrated with MEA carbon capture technology. The IGCC plant with carbon capture depict less costs than conventional coal power plant with carbon capture. However, the above cost calculation does not include carbon transportation and storage or utilization costs, since they highly depend on site specific characteristics [26]. Therefore, the evaluated costs may increase when transport, storage, and utilization costs are included to the calculation. Literature suggests that the expected costs of early full commercial scale (TRL 8-9) CCSU projects are expected to drop to \$30-45 /tCO_2 avoided once operating experience and economies of scale are gained [26][19]. Thus, above cost estimates may drop in the coming years with further developments to the carbon capture technologies.

Table 2 gives the performance efficiencies and technology ranks for the defined scenarios. As per the DEA, results all the integration scenarios provided the value of 1. This indicates that all carbon capture scenarios are technically and economically efficient. Hence, it is safe to deduce that the all four integration scenarios are technically and economically sound. Technology ranks obtained from TOPSIS provide that NGCC with MEA carbon capture as the best integration option based on the technical and economical performance criteria. This is due to the low LCOE, carbon mitigation costs, and efficiency penalty associated with the NGCC-MEA scenario. Moreover, the MEA carbon capture holds the highest technical maturity level of 9. However, PC- MEA option ranks the last. This could be due to high costs associated.

Table 2: Technology ranks and performance efficiency

	DEA	Efficient?	TOPSIS
PC-MEA	1	YES	4
PC - Oxy fuel combustion	1	YES	2
IGCC- Selexol	1	YES	3
NGCC - MEA	1	YES	1

4. Conclusion

The key findings from this study are, (a) compared with the chosen scenarios conventional coal power plant holds the highest cost elements, (b) NGCC power plant shows the potential to be a competitive emission reduction strategy with and without any carbon capture technology, (c) oxy fuel combustion is a competitive option for coal power plants, (d) under coal based power plants IGCC holds comparatively higher capture costs.

Coal power generation hold highest cost elements. This high costs can be attributed to the low thermal efficiencies, and high additional energy requirement. Moreover, IGCC plant has high cost that could mainly due to relatively high contingency charges associated with limited operational experience. Oxy fuel combustion holds the TRL of 7. However, it is a competitive option due to high carbon capture rates and low costs involved. Amongst the considered scenarios NGCC is the most favorable to be integrated with carbon capture technologies due to positive economic and technical performance. Moreover, NGCC plants emits the lowest CO_2 content in the flue gas. Thus, it can be considered as the most environmentally favorable energy generation option as well.

The obtained results indicate that more research is required in the area of reducing the energy demand of carbon capture facilities and improving the power plant thermal efficiency [34]. There is continuous research and development on more efficient and novel technologies for carbon capture, storage, and utilization to speed up the commercialization of this technology. This provides the prospects for the reduction in capture costs in future along with the economies of scale [19].

Furthermore, the study ranked the technologies based on technical and economic performance criteria. However, a carbon capture project should not be prioritized solely based on the mentioned criteria. Environmental, political, legal, and societal aspects should also be integrated into the ranking framework, in order to obtain further valid results. In addition to that, the study only considered capital and operational costs in the economic evaluation. However, more meaningful results

could be obtained if complete life cycle costs are in cooperated considering all parts of its value chain. Other than that, the results could be improved if uncertainty is integrated in to the decision making process. The data used in this study can be used to develop a carbon capture selection tool for Canadian energy systems. Hence, the approach used in this can be extended with triple bottom-line life cycle thinking to determine the suitability of carbon capture to Canadian provinces to develop zero emissions communities.

5. Acknowledgements

The support provided by FortisBC for this research work is gratefully acknowledged.

6. References

[1] IPCC, *Climate Change 2013 - The Physical Science Basis*. Gian-Kasper Plattner, 2014.

[2] N. Oreskes, "The Scientific Consensus on Climate Change," *Science (80-.).*, vol. 306, no. 5702, pp. 1686–1686, Dec. 2004.

[3] "Where Do Canada's Greenhouse Gas Emissions Come From?" [Online]. Available: http://prairieclimatecentre.ca/2018/03/where-do-canadas-greenhouse-gas-emissions-come-from/. [Accessed: 30-Apr-2019].

[4] P. Nogia, G. K. Sidhu, R. Mehrotra, and S. Mehrotra, "Capturing atmospheric carbon: Biological and nonbiological methods," *Int. J. Low-Carbon Technol.*, vol. 11, no. 2, pp. 266–274, 2016.

[5] Generation Energy Council, "Canada's Energy Transition," 2018.

[6] Natural Resources Canada, *Energy Fact Book, 2018-2019*. 2018.

[7] The Conference Board of Canada, "Power Shift: Electricity for Canada's Remote Communities," 2016.

[8] D. Y. C. Leung, G. Caramanna, and M. M. Maroto-Valer, "An overview of current status of carbon dioxide capture and storage technologies," *Renew. Sustain. Energy Rev.*, vol. 39, pp. 426–443, 2014.

[9] J. P. Gee, "Summary for Policymakers," *Clim. Chang. 2013 - Phys. Sci. Basis*, pp. 1–30, 2013.

[10] M. I. al Irsyad, A. Halog, and R. Nepal, "Renewable energy projections for climate change mitigation: An analysis of uncertainty and errors," *Renew. Energy*, vol. 130, pp. 536–546, 2019.

[11] D. Leeson, N. Mac Dowell, N. Shah, C. Petit, and P. S. Fennell, "A Techno-economic analysis and systematic review of carbon capture and storage (CCS) applied to the iron and steel, cement, oil refining and pulp and paper industries, as well as other high purity sources," *Int. J. Greenh. Gas Control*, vol. 61, pp. 71–84, 2017.

[12] International Energy Agency, "20 Years of Carbon Capture and Storage - Accelerating Future Deployment," 2016.

[13] Canadian Energy Research Institute, "a Comprehensive Guide To Electricity Generation Options in Canada," 2018.

[14] Carnegie Mellon University, "Integrated Environmental Control Model." [Online]. Available: https://www.cmu.edu/epp/iecm/index.html. [Accessed: 29-Nov-2019].

[15] H. Karunathilake, K. Hewage, W. Mérida, and R. Sadiq, "Renewable energy selection for net-zero energy communities: Life cycle based decision making under uncertainty," *Renew. Energy*, vol. 130, pp. 558–573, Jan. 2019.

[16] "Technology readiness levels - Innovation Canada." [Online]. Available: https://www.ic.gc.ca/eic/site/080.nsf/eng/00002.html. [Accessed: 04-Nov-2019].

[17] IEAGHG, "Assessment of emerging CO2 capture technologies and their potential to reduce costs," 2014.

[18] ZEP (Zero Emissions Platform), "The Costs of CO2 Capture - Post-demonstration CCS in the EU," Brussels, 2011.

[19] E. S. Rubin, J. E. Davison, and H. J. Herzog, "The cost of CO2 capture and storage," *Int. J. Greenh. Gas Control*, vol. 40, pp. 378–400, 2015.

[20] G. of Canada, "Reduction of Carbon Dioxide Emissions from Coal-fired Generation of Electricity." [Online]. Available: http://www.gazette.gc.ca/rp-pr/p2/2012/2012-09-12/html/sor-dors167-eng.html. [Accessed: 24-Nov-2019].

[21] "Coal facts | Natural Resources Canada." [Online]. Available: https://www.nrcan.gc.ca/science-data/data-analysis/energy-data-analysis/energy-facts/coal-facts/20071#L6. [Accessed: 24-Nov-2019].

[22] "Electricity Rates - Canadian Electricity Association." [Online]. Available: https://electricity.ca/learn/future-of-electricity/electricity-rates/. [Accessed: 25-Nov-2019].

[23] Hydro-Québec, "Comparison of electricity prices in major North American cities," *Hydro-Québec*, pp. 27–28, 2015.

[24] E. S. Rubin, C. Chen, and A. B. Rao, "Cost and performance of fossil fuel power plants with CO 2 capture and storage," *Energy Policy*, vol. 35, no. 9, pp. 4444–4454, 2007.

[25] A. B. Rao and P. Kumar, "Cost implications of carbon capture and storage for the coal power plants in India," in *Energy Procedia*, 2014, vol. 54, pp. 431–438.

[26] E. S. Rubin, J. E. Davison, and H. J. Herzog, "The cost of CO 2 capture and storage," *Int. J. Greenh. Gas Control*, vol. 40, pp. 378–400, 2015.

[27] S. D. Supekar and S. J. Skerlos, "Reassessing the Efficiency Penalty from Carbon Capture in Coal-Fired Power Plants," *Environ. Sci. Technol.*, vol. 49, no. 20, pp. 12576–12584, 2015.

[28] IPCC, *IPCC Special Report on Carbon dioxide Capture and Storage*. 2005.

[29] E. S. Rubin, J. E. Davison, and H. J. Herzog, "The cost of CO 2 capture and storage," *Int. J. Greenh. Gas Control*, vol. 40, pp. 378–400, 2015.

[30] M. Dvo and J. Klicnarová, "On the differences between DEA and selected MCDM methods," in *The International Scientific Conference INPROFORUM 2017*, 2017, pp. 338–343.

[31] A. Ishizaka and P. Nemery, *Multi-Criteria Decision Analysis Multi-Criteria Decision Analysis*. Wiley, 2013.

[32] M. Tavana, M. Keramatpour, F. J. Santos-Arteaga, and E. Ghorbaniane, "A fuzzy hybrid project portfolio selection method using Data Envelopment Analysis, TOPSIS and Integer Programming," *Expert Syst. Appl.*, vol. 42, no. 22, pp. 8432–8444, 2015.

[33] B. K. P. Yoon and C. Hwang, "Topsis," in *Multiple Attribute Decision Making*, 2019, pp. 39–45.

[34] H. H. Khoo, J. Bu, R. L. Wong, S. Y. Kuan, and P. N. Sharratt, "Carbon capture and utilization: Preliminary life cycle CO2, energy, and cost results of potential mineral carbonation," *Energy Procedia*, vol. 4, pp. 2494–2501, 2011.

Critical road network recovery in the District of North Vancouver

A. Deelstra[a,*], D. Bristow[b]

[a] PhD student – Department of Civil Engineering – University of Victoria, British Columbia, Canada
[b] Assistant Professor – Department of Civil Engineering – University of Victoria, British Columbia, Canada
* Corresponding author, adeelstra@uvic.ca

Abstract:
Transportation of goods and services is critical to support the recovery of communities in the days and weeks following a disaster. In the District of North Vancouver, British Columbia, road and highway systems are a primary transportation option and are considered essential for post-disaster recovery. The southern-central portion of the District is especially critical in providing connections to the west, east, and to the greater Vancouver region, where resource availability may be higher following a disaster. The work presented here specifically focuses on the road network and a number of points of interest within this central area that connect the various parts of the District with one another and the City of Vancouver. Data from a previous study for an earthquake scenario in the region provides estimates of damage to the road network in the District. Using the Graph Model for Operational Resilience (GMOR), this damage data is combined with repair time estimates from the literature to assess the recovery time of the roads that connect the points of interest along specific paths. Repair resource allocation is specified in some trials and randomized in others to evaluate how the allocation affects the recovery of the paths of interest. Results indicate that the time required to connect the points across the district can be reduced by up to 37% by prioritizing the recovery of certain roads over others. This work can be further expanded for larger road networks to better understand how their recovery influences the restoration of communities and neighbourhoods as a whole.

Keywords:
Disaster recovery; road restoration; critical infrastructure lifelines.

1. Introduction

The District of North Vancouver (DNV) is located in southwestern British Columbia, just north of the City of Vancouver. This area is at risk of a large seismic event in the future and as a result has been subject to an extensive study detailing the effects that a magnitude 7.3 earthquake would have on the District's residents, buildings, and critical infrastructure lifelines. The work presented here provides additional assessment of the road network in a critical area of the District and offers a comparison of two resource prioritization techniques. Based on results from the previous study, a map of road damage within the neighbourhoods in the District was established and can be seen in the inset of Figure 1.
The darkest sections of the map indicate the areas that are most likely to experience road failure in a disaster. This area happens to be in a critical location given its importance in connecting the west and east parts of the District, as well as connecting the east part to the City of Vancouver to the south.
The District is separated into three main sections by the Lynn Creek and Seymour River canyons. These canyons run roughly north-south, so the District is separated into west, central, and east sections. A number of bridges cross the canyons to provide road access throughout the District.
The west and central sections of the District are well-connected via road networks and bridges to West Vancouver, the City of Vancouver, and other communities along the west coast of British Columbia. The east part of the District, however, is bounded to the north by forested terrain and to the east by the Indian Arm inlet. No other roads to external locations are available within the eastern part of the District. As such, the east part of the District is heavily dependent on the road network in the central section for access to goods and services.

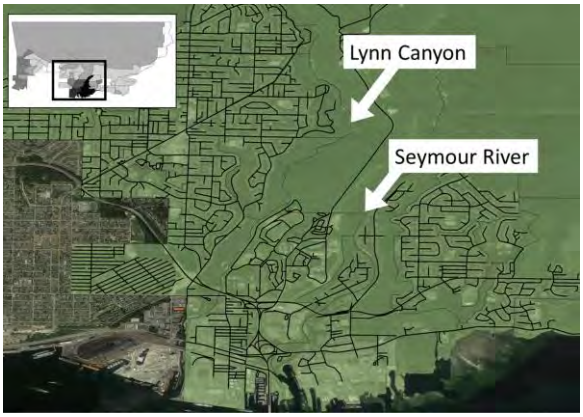

Fig 1: Map of the District of North Vancouver, showing areas of likely road damage due to earthquake (inset), and the road network in the highlighted section of the District. The City of Vancouver is located directly south of the area shown.

This work focuses specifically on the recovery time of roadway transportation routes within the central part of the District based on the level of damage indicated in the previous study and estimated repair time data gathered from previous disasters. The recovery is based on the functionality of three origin points in the west and south of the study area, and two destination

points in the east. These points represent critical locations that, once functional, are assumed to provide reliable road connection across the District. A key goal of this work is to identify changes in connection time observed by altering the priority of repairs for the road segments in the study area.

Just over seven thousand people live within this study area. Additionally, more than twenty thousand residents live in the eastern part of the District and are also dependent on the studied road network. This area is shown in Figure 1 and includes three bridges that span Lynn Canyon, one bridge that crosses the Burrard Inlet to the City of Vancouver, and two bridges that cross the Seymour River. The roads are in the area that is subject to the most extensive levels of damage identified in the previous study (see the inset of Figure 1) and are considered crucial for connecting the different parts of the District.

2. Background

Most studies related to damage and restoration of roads can be grouped into a few main categories: planning repairs for standard road maintenance activities; measuring the level of damage and planning access and repairs of road networks due to natural or other disasters; performance characteristics of novel road repair techniques and materials; and optimizing road repair activities.

Studies done by [1], [2], and [3] address resource constraints, optimization of maintenance schedules, prioritizing repairs, and work zone planning for pavement repairs. These studies focus primarily on standard road repair activities and do not address emergency repairs or extensive levels of damage to road networks. Other studies consider full-depth reclamation of roads [4] and are chiefly interested in the performance characteristics of the rehabilitated roads. With respect to road damage after disaster, [5], [6], and [7] have studied methodologies for categorizing damage as well as the impacts of failed roads on communities, while others provide an assessment of material performance after emergency repairs are conducted [8], [9].

Very few of these studies explicitly mention the repair times of roads. One exception is [10], which indicates a standardized value of 0.5 kilometres of repairs per hour, but does not differentiate based on the level of damage that the road experiences.

One reference that does include information related to road repair time is the Hazus technical manual, which is produced by the United States Federal Emergency Management Agency [11] and indicates mean repair time and standard deviation per kilometre of road based on the level of damage experienced. While Hazus results are useful in providing overall repair times for road networks, the work presented here seeks to detail more fully how prioritizing the repairs of specific road segments affects the overall recovery time of the network.

To process the information gathered from Hazus related to the road repairs, Bristow and Hay's Graph Model for Operational Resilience (GMOR) is utilized [12], [13]. The capabilities provided by GMOR allow for the generation of paths to connect points of interest in the road network, prioritization of repairs, and variation of repair times based on level of damage for each entity within the model. Repair times indicated in ATC-13 and subsequently included in Hazus documentation clarify that restoration "follow[s] normal nonemergency construction schedules" [14]. Since the size and capabilities of repair crews in the original survey data is aggregated from a variety of sources, the repair times indicated in Hazus documentation are assumed to be accurate for use in the GMOR model as well.

3. Methodology

Road data from a GIS model of the District (with multiple extraneous and redundant road segments removed) is shown in Figure 2 along with the selected origin and destination points mentioned in Section 1. Each origin point, destination point, and road segment is used to create a node in a graph model. These nodes are joined by edges that represent the connections between the roads in the study area.

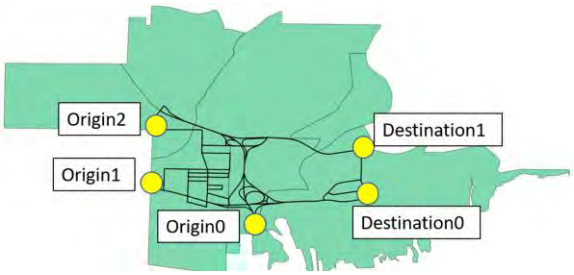

Fig 2: Selected origin and destination points for the road network within the study area

A set of shortest paths between each origin and destination point is produced, determined by the number of nodes (road segments) between the origin and destination, rather than by the length of the road representing each node. These paths may not be the shortest by distance, but this difference is assumed to be negligible.

Each road segment has four failure entities associated with it, one for each possible damage state the road can experience – none, slight, moderate, and extensive/complete. Repair time parameters are then added for each damage state for each road. Repair times are generated for each damage state using road lengths and per-kilometre repair time estimates from Hazus [11]. A single resource entity is assigned for the repair of all road segments in this model.

Dependencies between origin and destination points are added in the GMOR model. The dependencies provide an indication that a destination point is only accessible after a path of fully repaired road segments connects it to an origin point. The repair resource in the model limits the number of road segments that can be repaired at a time.

4. Assumptions

One key assumption made in the modeling process is that the results represent the path repair times only after origin points are functional in the aftermath of a disaster. Since it is unknown which point (if any) would be accessible at a given time, this assumption provides an understanding of how repairs propagate from each origin to each destination. Since each path is associated with a specific origin and destination point, results for the individual paths in the model can be assessed as needed.

Various additional assumptions are made in the generation of this model which may have an effect on the results that are produced as well. These assumptions are primarily related to repair time and resource issues that are difficult to model and could vary widely in actual disaster scenarios. It is assumed that the uncertainty in repair times included in the model (via normally distributed times indicated in Table 1) account for and accommodate this variability. Specifically related to assumptions surrounding repair time are access issues that could impede repair crews and prevent them from quickly reaching damaged sections of roadway. Travel and access times are not included in the GMOR model, but it is assumed that they are generally smaller than the times necessary to perform repairs on damaged road segments.

Additionally, ATC-13 documentation indicates that repair times are reported under the assumption that "[u]nlimited resources are available for reconstruction", which may not realistically be the case [14] but falls beyond the scope of this work.

Table 1: Mean and standard deviation of normally distributed road repair times per kilometre of road based on level of damage

	Repair time (days per km)	
Damage	**Mean**	**Standard Deviation**
None	0	0
Slight	0.9	0.05
Moderate	2.2	1.8
Extensive/complete	21	16

5. Trials

A beneficial feature in the GMOR model used here is the capability to prioritize resource allocation for performing repairs. This feature allows for the specification of entities (in this case, road segments) that are to be repaired before others. Prioritization may also be randomized, providing insight into how a network recovers beyond the influence of modelers. In the initial trials of the model presented here, the prioritization of resource allocation is randomized, so all roads are considered equally in performing repairs. Further trials explicitly prioritize certain groups of road segments over others to determine how the order of repair affects overall network repair time.

In trials where repair order is specified, three levels of priority are assigned to the various road segments. The list of road segments is split into groups based whether they are included in one of the shortest paths or not. The highest priority roads are those that are associated with an origin or destination point. Next are the segments that are identified as being part of one of the shortest paths. Finally, the road segments that are not included in any shortest path are repaired. Within each of the differing levels of priority, the repair order of road segments is randomized. That is to say, a road segment included in a path will be repaired before one not included in a path in every trial, but will be randomly assigned a priority among all roads included in a path. This prioritization is not highly complex for the purposes of these trials, but further detail can be included as desired in future models.

6. Results

Results are presented here for the two sets of trials identified in Section 5. Five hundred trials were generated for each trial type, all based on the initial earthquake scenario identified previously.

Table 2: Mean (μ) and standard deviation (σ) of recovery time for origin and destination points. All values given in days.

	Random				**Ordered**			
	Dest. 0		Dest. 1		Dest. 0		Dest. 1	
	Mean	σ	Mean	σ	Mean	σ	Mean	σ
Orig. 0	42	18	44	18	27	15	28	15
Orig. 1	46	19	45	18	30	16	30	16
Orig. 2	47	19	47	19	30	16	30	15

For trials in which no repair order was specified, the average time required to provide a functional path from any origin point to either destination is 42.0 days, with a standard deviation of 17.9 days. The minimum and maximum times required for repairs to reach a destination are 6.6 and 105.7 days, respectively. Histograms for each destination are shown in Figure 3. The average repair times and standard deviations for each origin-destination pair are shown in Table 2.

For trials in which three levels of priority were modeled, average repair time to reach either destination drops to 26.6 days with a standard deviation of 15.2 days. A minimum of 0.7 days and maximum of 97.3 days is required to reach a destination point. Histograms for these results are shown in Figure 3. For each origin-destination pair, results are shown in Table 2.

7. Results and discussions

As can be clearly seen in the results, prioritizing repairs to road segments that are included in paths

connecting origin and destination points drastically improves the repair times needed to reach those points. It is interesting to note, however, that even though the required repair time drops substantially, the standard deviation is reduced by a comparatively small amount. This indicates that individual repair times for specific road segments are subject to roughly the same amount of variability in each set of trials, but the prioritization of repairs shifts the mean to a much lower overall repair time.

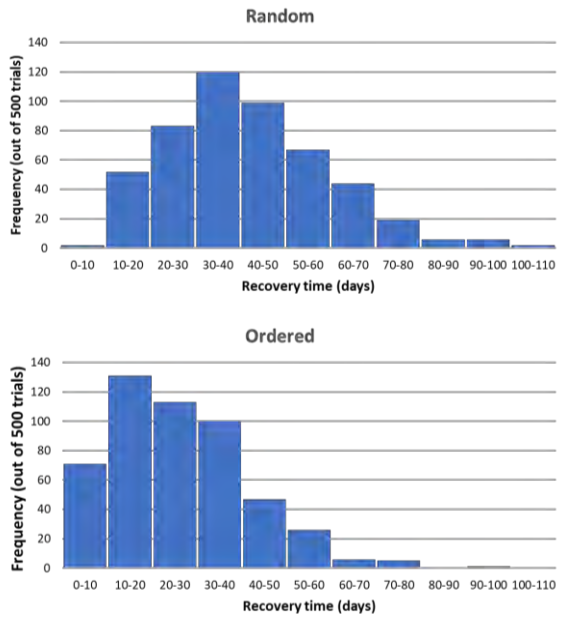

Fig 3: Recovery time distributions for random (top) and ordered (bottom) road recovery trials.

A number of important details must be mentioned when discussing these results. The first is that the repair time shown here is for the complete repair of the included road segments, not simply for access or the ability to traverse a specific road segment. For example, “Slight Damage” and “Moderate Damage” (damage states 2 and 3) in Hazus documentation is characterized by anywhere from a few inches to several inches of settlement in a roadway [11]. While this level of damage would certainly require repairs, it would not necessarily prevent access for repair crews, emergency responders, or even residents. As such, the repair times indicated here are not meant to indicate that no supplies or emergency services are able to travel through the District in case of a disaster, but that returning to normal roadway function in those areas will take time.

8. Conclusions and outlook

Several options exist to expand and improve on this work in the future. Further optimizing the priority of repairs for roads and paths is one area that can be developed. For example, considering the length, probability of failure, and resulting estimated repair time for specific road segments could provide an opportunity to prioritize repairs of those that are likely to provide the quickest access to the desired origins and destinations. In addition, identifying other key areas within the district could be considered in future modeling scenarios as well. Prioritizing routes to hospitals, shopping centres, or other supply routes, for example, may increase overall repair time in the certain neighbourhoods but improve outcomes for citizens by providing earlier access to critical facilities.

In addition, these trials only cover a small area of a single part of the District, but the same methodology could be extended to larger municipal-scale regions. Key paths within a region may be identified and can then be used to perform larger trials and inform stakeholders for the purposes of coordinating and planning at a regional scale.

As mentioned previously, the trials run for the purposes of this study do not consider travel time or access issues related to the process of performing road repairs. It is assumed that extra time required is mitigated by the inclusion of standard deviations for repair times, and that travel time is limited in comparison to actual repair time. In the future, it may be possible to improve accuracy by accounting for impassable roads, crew set up time and resource acquisition. Each of these additions introduces its own variability, so understanding the effect of each on overall recovery time and uncertainty is crucial.

Further benefit could be provided by performing rapid assessment of in the immediate aftermath of a disaster to produce quick plans for post-disaster reconstruction. Incorporating observed damage states in the models presented here rather than estimates from simulations would improve the accuracy of results and provide an opportunity to plan for realistic recovery. While the computing resources and time required to run models are significant, improvement in recovery outcomes based on results from those models would likely far outweigh those challenges. That being said, reducing the complexity of models to improve computational efficiency without negatively impacting results should certainly be pursued.

The work presented here provides an overview of the repair time necessary to connect points of interest within a set of neighbourhoods in the District of North Vancouver after a disaster. Results indicate that prioritizing specific sections of road results in a reduction in the time required to connect these points. The effects of prioritization are highlighted and offer a clear picture of the impact that simple changes may have on recovery at a municipal scale.

This work may be used to support decision-makers and stakeholders as they plan for post-disaster reconstruction or provide insight into where resources should be located or how they should be distributed to prepare before a disaster strikes. Communication with residents in neighbourhoods, recognizing their needs, and understanding the resources and processes that support their well-being should be a critical consideration in developing resilient strategies throughout their communities.

Acknowledgements

The authors would like to thank those involved in the previous study of the District of North Vancouver for their excellent research that made this project possible.

References

[1] L. Janani, R. K. Dixit, V. Sunitha, S. Mathew, and S. Mathew, “Prioritisation of pavement maintenance sections deploying functional characteristics of pavements,” *Int. J. Pavement Eng.*, vol. 0, no. 0, pp. 1–8, 2019.

[2] V. Donev and M. Hoffmann, “Optimisation of pavement maintenance and rehabilitation activities , timing and work zones for short survey sections and multiple distress types zones for short survey sections and multiple distress types,” *Int. J. Pavement Eng.*, vol. 0, no. 0, pp. 1–25, 2018.

[3] A. A. Lempert, D. N. Sidorov, A. V Zhukov, and G. L. Nguyen, “A Combined Work Optimization Technology under Resource Constraints with an Application to Road Repair,” vol. 77, no. 11, pp. 1883–1893, 2016.

[4] M. Bocci *et al.*, “Full-depth reclamation for the rehabilitation of local roads : a case study,” vol. 8436, 2014.

[5] P. Anbazhagan, S. Srinivas, and D. Chandran, “Classification of road damage due to earthquakes,” pp. 425–460, 2012.

[6] T. R. Robinson and T. R. Robinson, “Road impacts from the 2016 Kaikōura earthquake : an analogue for a future Alpine Fault earthquake ? Road impacts from the 2016 Kaik ō ura earthquake : an analogue for a future Alpine Fault earthquake ?,” *New Zeal. J. Geol. Geophys.*, vol. 61, no. 3, pp. 403–411, 2018.

[7] X. Gao and D. Sun, “Assessment of Road Damage and Schedule Study of Road Repair after Earthquake,” in *World Automation Congress, 2012*, 2012.

[8] A. Hawa, D. Tonnayopas, W. Prachasaree, and P. Taneerananon, “Development and Performance Evaluation of Very High Early Strength Geopolymer for Rapid Road Repair,” 2013.

[9] I. L. Howard *et al.*, “Emergency paving using hot-mixed asphalt incorporating warm mix technology,” vol. 8436, 2014.

[10] S. Li and K. L. Teo, “Post-disaster multi-period road network repair : work scheduling and relief logistics optimization,” *Ann. Oper. Res.*, 2018.

[11] FEMA, “Hazus – MH 2.1 Earthquake Model Technical Manual,” Washington, D.C., 2011.

[12] D. N. Bristow and A. H. Hay, “Graph Model for Probabilistic Resilience and Recovery Planning of Multi-Infrastructure Systems,” *J. Infrastruct. Syst.*, vol. 23, no. 3, p. 04016039, 2017.

[13] D. N. Bristow, “How Spatial and Functional Dependencies between Operations and Infrastructure Leads to Resilient Recovery,” *J. Infrastruct. Syst.*, vol. 25, no. 2, pp. 1–8, 2019.

[14] Applied Technology Council, “ATC-13: Earthquake Damage Evaluation Data for California,” Redwood City, CA, 1985.

What are the extent and opportunities of Sustainable Development in the Construction Industry?

Suzana C N L. Espindola [a,*], Thomas M. Froese [b]

[a] Ph.D. Candidate at The University of British Columbia - CAPES Scholarship holder (Brazil), Vancouver-BC-Canada
[b] Supervisor and Professor at The University of Victoria, Victoria-BC-Canada
* Corresponding author, Tel +1 (604) 779-9484, email suzanacarlaespindola@gmail.com

Abstract:
Since the United Nations Conference on the Human Environment held in Stockholm in 1972, sustainability has been a significant focus across a broad range of human activities. In 1983, the World Commission on Environment and Development (WCED) introduced the popular definition of sustainable development: to meet the needs of the present generation without compromising the ability of future generations to meet their needs [1]. Our understanding of sustainable development has expanded to engage further complex issues such as economic development models, world food supply, poverty reduction, justice, and nature conservation [2]. Furthermore, sustainability issues and the ways that organizations address them impact not just the environment, but also employees, nearby communities, and material sources. Sustainable development is defined as the combination of the three pillars of sustainability: social, environmental, and economical. Approaches that address just one or two of the sustainability pillars does not fit the definition as a sustainable development [3]. The 2030 Agenda for Sustainable Development, adopted in 2015 by the United Nations and committed by more than 193 countries, contains 17 Sustainable Development Goals (SDG) approaching the three pillars of sustainability [4]. For the purposes of this research, the definition of sustainable development consists of sustainable practices involved in achieving sustainability objectives approaching the three pillars defined as sustainably developed and detailed by the 17 United Nations SDGs. This research is reviewing several relevant sustainable development codes, certification systems, and frameworks to understand the extent and opportunities of Sustainable Development in the construction industry. This research presents a consolidated list of 100 Sustainable Development Indices (100 SDI), including the sustainability targets, indicators and assessment methodologies, giving a better understanding of where and how the construction industry can contribute to the sustainable development goals.

Keywords:
Sustainable construction impact analysis, sustainable development goals of the construction industry, sustainability construction indicators, SDGs in the construction industry

1. Introduction

Since the United Nations Conference on the Human Environment, held in Stockholm in 1972, sustainability has been a major focus of discussion. The term has become a political and ethical argument for addressing the ecological and social crises of the world. The World Commission on Environment and Development (WCED) presented in 1983 the most popular sustainable development interpretation: to meet the needs of the present generation without compromising the ability of future generations to meet their needs [1].

Although the initiative to implement sustainability in daily operations starts with a desire to impact the world positively, organizations are detecting the benefits of sustainable practices such as to reduce costs and to improve corporate image [5].

However, there is an excessive number of articles and standards that describe different interpretations of sustainability across diverse fields. The diversity of studies makes it hard to consolidate an approach, justifying the lack of understanding and the difficulty of implementing sustainability management into the daily operations of the organization.

Likewise, a sustainability approach will be different according to the diverse interpretations across fields and depends on the priorities, demands of the stakeholders and the impacts of the sector. The sustainability approach in the construction industry has several standards, rating systems, and other materials for helping to capture and codify sustainable practices. Each of these materials helps to approach some of the sustainability targets, complementing or overlapping each other. A more well-defined understanding of sustainable development in the construction industry would provide a foundation for sustainable development management in the sector.

2. Sustainable Development

Our understanding of sustainability has been changing for the last three decades and has expanded to engage further complex issues. The focus of sustainability from 1960 to 1970, 1990 to 2000, and 2010 to the present day have expanded from air & water pollution to safety & consumer protection to climate change, respectively [7].

Nowadays, sustainable development engages further complex issues such as economic development

models, the world food supply, poverty reduction, justice, and also nature conservation [2]. Sustainable development became a significant term to describe the balance between the use and preservation of current resources (Grober, 2007), and the relationship between human beings and nature.

Sustainability is commonly conceptualized as involving the three pillars: social, environmental, and economic—and Sustainable Development is understood to require to address all three of these domains [3]

Upon a decade of major United Nations conferences and summits, world leaders came together at United Nations Headquarters in New York, In September 2000 to adopt the United Nations Millennium Declaration. The nations committed to a new global partnership to reduce extreme poverty and to set out a series of time-bound targets - with a deadline of 2015 - that is known as the Millennium Development Goals [8].

The Sustainable Development Goals (SDGs) are the continuation of the United Nations Millennium Development Goals (MDGs). On September 25th of 2015, the United Nations General Assembly formally adopted the universal, integrated and transformative 2030 Agenda for Sustainable Development, along with a set of 17 Sustainable Development Goals and 169 associated targets and committed by more than 193 countries [4]:

- *SDG 1* No Poverty;
- *SDG 2* Zero Hunger;
- *SDG 3* Good Health and Well-Being;
- *SDG 4* Quality Education;
- *SDG 5* Gender Equality;
- *SDG 6* Clean Water and Sanitation;
- *SDG 7* Affordable and Clean Energy;
- *SDG 8* Decent Work and Economic Growth;
- *SDG 9* Industry, Innovation and Infrastructure;
- *SDG 10* Reduced Inequalities;
- *SDG 11* Sustainable Cities and Communities;
- *SDG 12* Responsible Consumption and Production;
- *SDG 13* Climate Action;
- *SDG 14* Life Below Water;
- *SDG 15* Life and Land;
- *SDG 16* Peace, Justice, and Strong Institutions;
- *SDG 17* Partnerships for the Goals

The United Nations acknowledges the construction industry as having an essential role in delivering the SDGs and their associated targets [9]. The contribution includes significant economic, environmental and social impacts and benefits associated with construction products, buildings and infrastructure throughout their lifecycles.

For this research project, the definition of Sustainable Development consists of sustainable practices that are involved in achieving sustainability objectives as understood by the three pillars of sustainability and detailed by the United Nations with the 17 SDGs.

Hence, the scope of sustainability in the construction industry, introducing the sustainability targets of the three pillars of sustainability, is an essential reference for sustainable development management in this sector.

3. Scope of Sustainable Development in the Construction Industry

This study focused on the following international and American standards and rating systems used in the construction industry and business focusing on the three pillars of sustainability (social, economic, environment) to identify the scope of sustainable development in the construction industry:

UN-SDGs – The 17 goals and 169 targets focus on five main critical areas for humanity and the planet: people; planet; prosperity; peace; partnership [4].

OECD – Organization for Economic Co-Operation and Development is an international organization that works on establishing international norms with the participation of governments, parliaments, policymakers, businesses and citizens to elaborate policies focus on prosperity, equality, opportunity and well-being for all [10].

ICC – International Chamber of Commerce is the world's largest business organization with a global network to assist businesses of all sizes to operate both internationally and responsibly and represent business interests at the highest levels of intergovernmental decision-making such as World Trade Organization and United Nation [11].

WBCSD – World Business Council for Sustainable Development is a global network with more than 200 leading businesses and almost 70 national business councils that work together to bring best practices to accelerate the implementation of sustainable development into the business activities [12].

GRI – Global Reporting Initiative is an independent international organization that helps businesses, governments, and other organizations to identify and report their impacts on issues such as climate change, human rights and corruption [13].

BREEAM – Building Research Establishment's Environmental Assessment Method is a rating system and the world's first established method of sustainability assessment for buildings that reflect the performance achieved by a project and its stakeholders measuring [14].

LEED – Leadership in Energy and Environmental Design is an internationally recognized third-party certification program and the most common green building rating system developed by the non-profit U.S. Green Building Council (USGBC) [15].

ENVISION – Envision Rating System for Sustainable Infrastructure is a framework that provides a

consistent, consensus-based assessment of sustainability and resilience in all types and sizes of infrastructure projects [16].

LBC – Living Building Challenge is a philosophy, certification, and advocacy tool for projects to be not only less harmful but truly regenerative, coming from negative environmental impacts to positive environmental impacts. The standard is a performance-based on the indicator's outcome [17].

SPeAR – Sustainable Project Appraisal Routine is a sustainability appraisal tool developed to monitor and evaluate project performance and informed decision making throughout the project life cycle [18].

Green Globe – Green Globes is an on-line assessment and user-friendly assessment protocol with chiefly three main phases: a self-assessment through a questionnaire-based, the submittal requirements, and the formal certification request utilized primarily in Canada and the USA [19].

ISO – International Organization for Standardization is the world's largest developer of voluntary international standards, an independent, non-governmental international organization with standards for business, government and society as a whole [20].

FSDS – Federal Sustainable Development Strategy is the Canadian Government plan and reports for sustainable development, setting sustainable priorities and establishing goals and targets [21].

Table 1: Sustainability targets analyzed for each standard and certification.

Standard/ Certification	Sustainability Targets Analyzed
UN-SDGs	17
OECD	64
ICC	10
WBCSD	17
GRI	93
BREEAM	54
LEED	55
ENVISION	60
LBC	20
SPeAR	24
Green Globe	47
FSDS	13

It was analyzed 474 targets to elaborate a consolidated list with sustainability targets for the construction industry.

4. Results and Discussions

Through a meta-analysis, this research identified a set of 99 sustainability targets for the construction industry calling the *100 Sustainable Development Indices* (*100 SDI)*.

This research performed a meta-analysis of the sustainability indicators from different codes and standards for the construction industry to identify the consolidated list of sustainable targets for the building construction industry. It was analyzed more than 800 indicators from the 474 sustainability targets of the 12 codes and standards mentioned in the previous section, cross-listing them to identify the lack and overlapping between the references.

Table 2: 100 SDI categorized and the number of sustainability targets for each one

Category	Subcategory	Targets	%
Environmental	Soil	4	45%
	Air Emission	11	
	Biodiversity	4	
	Energy	6	
	Local Impact	7	
	Resource Consumption	6	
	Waste	1	
	Water	6	
Social	Social Development	17	27%
	Human Rights	10	
Economic	Economy Growth	5	9%
	Business Growth	4	
Governances	Innovation	2	18%
	Social Development	7	
	Environment	2	
	Management	7	
100 SDI		99	100%

5. Conclusions and Outlook

Sustainable Development spans an extensive range of issues. To identify which topic areas need to be managed within the domain of Sustainable Development for construction, this research reviewed several relevant Sustainable Development codes, certification systems, and frameworks, identifying the common and overlapping indicators. The result was a consolidated list of 100 Sustainable Development Indices (100 SDI).

The ongoing research is validating the 100 SDI and the connection with the UN-SDGs. The 100 SDI give the construction industry a set of targets to contribute to the UN-SDGs. You can contact the author for more information.

Fig 1: 100 SDI Relationship with UN-SDGs

Acknowledgements

The authors acknowledge the financial support from the Brazilian Government – CAPES, The University of British Columbia and The University of Victoria. We also thank Mr. Bert Paul for the contribution to this work, and to God, whom I give all honour.

References

[1] United Nations, "Earth Summit," 23 May 1997. [Online]. Available: http://www.un.org/geninfo/bp/enviro.html. [Accessed 19 01 2017].

[2] maribus gGmbH, "World Ocean Review," 24 February 2017. [Online]. Available: http://worldoceanreview.com/en/wor-4-overview/concepts-for-a-better-world/what-is-sustainability/. [Accessed 2017 February 2017].

[3] Circular Ecology Ltd, "Circular Ecology," 09 April 2019. [Online]. Available: http://www.circularecology.com/sustainability-and-sustainable-development.html. [Accessed 09 April 2019].

[4] United Nations, "United Nations - Sustainable Development," 2015. [Online]. Available: https://sustainabledevelopment.un.org/?menu=1300. [Accessed 06 October 2017].

[5] G. Weybrecht, The Sustainable MBA: A Business Guide to Sustainability, John Wiley & Sons, 2014.

[6] R. Fowke and D. K. Prasad, "Sustainable Development, Cities And Local Government: Dilemmas and definitions," *Journal Australian Planner,* pp. 61-66, Issue 2 Volume 33 1996.

[7] M. Rosenberg, Strategy and Sustainability: A Hardnosed and Clear-Eyed Approach to Environmental Sustainability For Business, IESE Busines Collection, 2015.

[8] MDG - Millenium Project, "Millenium Project," 2006. [Online]. Available: http://www.un.org/millenniumgoals. [Accessed 23 February 2017].

[9] Building Research Establishment Ltd, "BREEAM," 01 August 2018. [Online]. Available: https://www.breeam.com/. [Accessed August 2018].

[10] OECD, "OECD - Better policies for better lives," May 2019. [Online]. Available: oecd.org/about. [Accessed 22 August 2019].

[11] International Chamber of Commerce, "ICC - International Chamber of Commerce," 22 March 2017. [Online]. Available: https://iccwbo.org. [Accessed 22 March 2017].

[12] WBCSD - World Business Council for Sustainable Development, "WBCSD Business Solutions for a Sustainable World," n/a n/a 2019. [Online]. Available: http://www.wbcsd.org. [Accessed 02 September 2019].

[13] GRI, "GRI - Empowering Sustainable Decision," 2017. [Online]. Available: https://www.globalreporting.org. [Accessed 09 03 2017].

[14] Building Research Establishment Ltd, "BREEAM," 01 March 2018. [Online]. Available: https://www.breeam.com/. [Accessed 2018 March 2018].

[15] U.S. Green Building Council (USGBC), "USGBC - LEED," USGBC, 10 January 2019. [Online]. Available: https://new.usgbc.org/. [Accessed 10 January 2019].

[16] Institute for Sustainable Infrastructure, "Institute for Sustainable Infrastructure," 2015. [Online]. Available: sustainableinfrastructure.org. [Accessed November 2016].

[17] International Living Future Institute, "International Living Future Institute," International Living Future Institute, 25 February 2019. [Online]. Available: https://living-future.org/. [Accessed 25 February 2019].

[18] Arup Group Ltd., "Arup - SPeAR Manual," n/a n/a 2017. [Online]. Available: https://sustainabilitytoolkit.arup.com/assets/support/SPeAR_manual.pdf. [Accessed 18 September 2019].

[19] Green Building Initiative - GBI, "Green Globes," n/a n/a 2019. [Online]. Available: http://www.greenglobes.com. [Accessed 17 September 2019].

[20] ISO - International Organization for Standardization, "ISO - International Organization for Standardization," n/a n/a n/a. [Online]. Available: https://www.iso.org. [Accessed 16 November 2019].

[21] Government of Canada, "Government of Canada - Federal Sustainable Development Strategy (FSDS)," Government of Canada - Federal Sustainable Development Strategy (FSDS), 19 November 2019. [Online]. Available: https://www.fsds-sfdd.ca/index.html#/en/goals/. [Accessed 19 November 2019].

A neural network metamodel for predicting hygrothermal performance of wood framed envelopes under future climatic loads

Lin Wang[a*], Hua Ge[a]

[a] Centre for Zero Energy Building Studies, Department of Building, Civil and Environmental Engineering, Concordia University, Canada.

* Corresponding author, email: forestwang2013@gmail.com

Abstract:
Climate change has become a new challenge for designers to develop sustainable, resilient and energy efficient building envelopes. Understanding the hygrothermal response of building envelopes to climatic loads is important to investigate the potential moisture problem risks under future climate. Traditionally, the hygrothermal behaviors of the building envelopes can be investigated through hygrothermal simulations under the current and projected future climatic data to study the effect of climate changes on the hygrothermal performance of building envelopes. However, there are uncertainties in the projected future climatic loads, such as different greenhouse gas emission scenarios and the frequency of extreme weathers. Stochastic modelling approach can be applied to investigate these uncertainties and their influences on the hygrothermal behavior of building envelopes. However, the high computational cost inhibits the wide application of stochastic modelling. This paper proposes a neural network metamodel as a substitute of traditional hygrothermal model, to predict the hygrothermal response of building envelopes to future climatic loads. A Long short-term memory (LSTM) neural network model is used to predict the time series of moisture content, relative humidity and temperature of the wood sheathing in a typical 2x6 wood framed wall. Stochastic simulations are firstly performed under current climatic conditions to obtain the input and output samples. Then, the input and output samples are used to train the neural network model. Finally, the developed metamodel is used to predict the hygrothermal responses of the wall to current and future climatic loads. The performance of the metamodel is evaluated by root mean square error (RMSE) between the results of original hygrothermal model and metamodel. It is found that the metamodel is able to reasonably predict the hygrothermal behaviors of the wall under future climatic loads.

Keywords:
Neural network meta-model, Hygrothermal performance, Wood framed envelopes, Future climate

1. Introduction

Climate change has become a new challenge for designers to develop sustainable, resilient and energy efficient building envelopes. Understanding the hygrothermal response of building envelopes to climatic loads is important to investigate the potential moisture problem risks under future climate. The hygrothermal behavior of the building envelopes can be investigated through hygrothermal simulations under the current and projected future climatic data to study the effect of climate changes on the hygrothermal performance of building envelopes. However, there are uncertainties in the projected future climatic loads, such as different greenhouse gas emission scenarios and the frequency of extreme weathers. In some studies, stochastic modelling approach is applied to investigate the uncertainties of hygrothermal behavior of building envelopes [1][2][3]. However, the high computational cost inhibits the wide application of stochastic modelling. To improve the computational efficiency, the statistical metamodels can be developed as a substitute for the hygrothermal model to predict the hygrothermal performance of the building envelopes. Annex 55 has summarized different metamodelling methods, such as polynomial regression, multivariate adaptive regression splines (MARS), and neural network [4]. And these methods have been applied in some studies to predict the cumulative hygrothermal performance indicators such as heat loss or moisture gain in a certain period [5]. While, the time series of the performance indicators such as the variation of moisture content, relative humidity and temperature with time are also important to reveal the trend of hygrothermal behaviors throughout years, particularly when future climate conditions are taken into account. Recently, Tijskens et al. reviewed different neural network methods to develop the metamodels for predicting the time series of hygrothermal behaviors [6]. Their study showed that Long short-term memory (LSTM) neural network and Convolutional neural network (CNN) are powerful in learning and predicting the time series of hygrothermal responses to climatic loads.

This paper uses LSTM neural network to develop the metamodel as a substitute of hygrothermal model, to predict the hygrothermal responses of a typical 2x6 wood framed wall to future climatic loads. The LSTM neural network model is trained by stochastic input and output time series under current climatic conditions. Then the trained metamodel is used to predict the hygrothermal responses of the wall to the future climatic loads. The root mean square error (RMSE) is used as a performance indicator to evaluate the performance of the developed metamodel under current and future climatic conditions.

2. Method

2.1 Hygrothermal model

The metamodel is developed based on the hygrothermal model of a conventional 2×6 wood framed wall, which is created by DELPHIN 5.8. Figure 1 shows the configuration of the investigated wall.

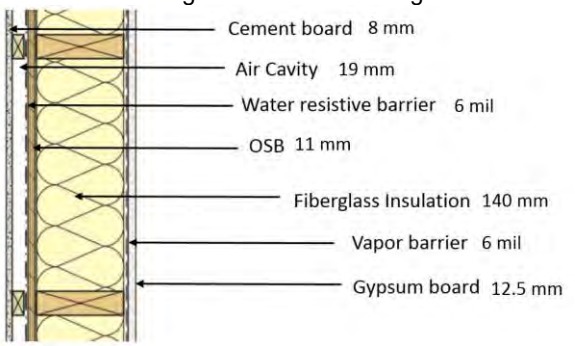

Fig. 1 Configuration of 2x6 wood framed wall

The material properties are determined based on literatures [7] [8]. The boundary conditions of wind-driven rain and solar radiation are considered as imposed fluxes, which are directly deposited on the exterior surface of the wall. The wind-driven rain is calculated based on ASHRAE 160 empirical formula [9]. The incident solar radiation is calculated based on the solar calculation procedure presented in ASHRAE Fundamental [10]. Table 1 lists some critical boundary condition coefficients for wind-driven rain and incident solar radiation.

Table 1 Boundary condition coefficients

Wind-driven rain		Incident solar radiation
F_D	F_E	α_s
0.5	1	0.6

F_D – rain deposition factor; F_E – rain exposure factor; α_s – short-wave absorptivity.

The Ottawa weather data, which is provided by National Research Council of Canada (NRC), is used in this study. The moisture reference year (MRY) for current climatic data is picked up from historical data in between1986 and 2016, and that for future climatic data is from the projected data in between 2062 and 2092 [11][12]. The selection of the MRY is based on Severity Index [9]. The climatic data of the year 2009 and 2066 are selected to represent the current and future climatic conditions separately.

2.2 Data preparation

Stochastic simulations are performed for current climatic conditions (reference year 2009) to generate the data for training the metamodel. Orientation is considered as a stochastic variable and uniformly distributed from 0° to 360°. The stochastic time series of wind-driven rain and incident solar radiation on the exterior wall surface are calculated based on the stochastic orientations and local climatic conditions, as well as boundary condition coefficients (wind speed, wind direction, horizontal rain and rain factors for wind-driven rain; direct and diffuse solar radiation, short wave absorptivity for incident solar radiation). In total, 100 samples are generated with different orientation, wind-driven rain flux and incident solar radiation flux. The time series of outdoor temperature and relative humidity are the same for the 100 samples. The material properties, surface transfer coefficients, as well as the rain factors and short-wave absorptivity are considered as deterministic parameters. Simulations are performed for 2 years to get the stochastic results, including the moisture content, relative humidity and temperature on the interior surface of the OSB sheathing. In summary, four input time series (outdoor temperature, relative humidity, wind-driven rain flux and incident solar radiation flux) and three output time series (moisture content, relative humidity and temperature of OSB sheathing) are involved in developing a neural network metamodel. For each time series, there are 100 samples.

2.3 LSTM metamodel

Long and short-term memory (LSTM) is a typical recurrent neural network (RNN) that has memory mechanism, and is able to learn and simulate time series. LSTM has been commonly used for time series prediction and sequence to sequence regression. A detailed review of LSTM network can be found in [6]. The LSTM network used in this paper has 1 hidden layer with 200 hidden units. The data obtained from stochastic simulation are used for training the neural network, 80 samples are used for training and 20 samples are used for testing. The root mean square error (RMSE) between the results of original model and metamodel is used to evaluate the metamodel. The developed motamodel is also applied to predict the hygrothermal behaviors of the wall under future climatic loads of 2066. Stochastic simulations are performed for the 20 test samples (same orientations with those of 2009) under future climatic loads (2066) using hygrothermal model to get the time series of moisture content, relative humidity and temperature. And these time series are also predicted by the metamodel developed based on 2009 climatic data. And then the results from the original hygrothermal model are compared with the those from the metamodel.

3. Results and discussions

Fig. 2 shows an example of the comparison between original model and metamodel. It is the sample with the orientation of 58° , which receives relatively higher amount of wind-driven rain but less solar radiation. From Fig. 2a to c, it can be seen that the results from metamodel have the same trend with the those from the original model. The moisture content of metamodel is higher than original model at the beginning stage in the fall 2009, while they get closer in the winter time and the spring time of 2010. During the winter time at the end of 2010 and the beginning of 2011, the metamodel has lower moisture content than original

model, while they get closer in the spring and summer time 2011.

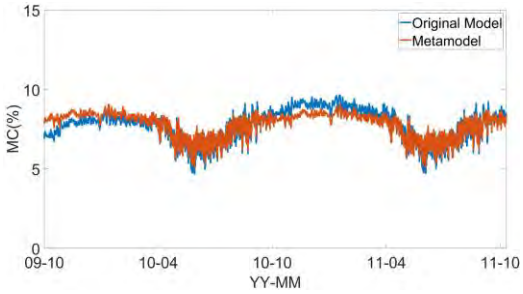

a) Moisture content_ 2009

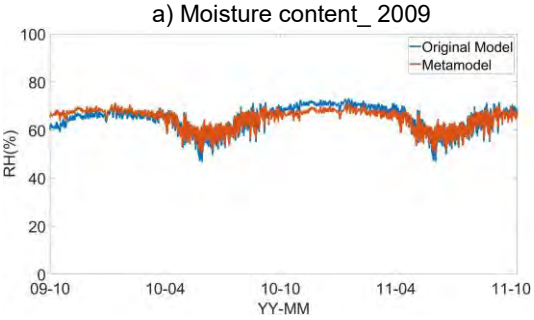

b) Relative humidity_ 2009

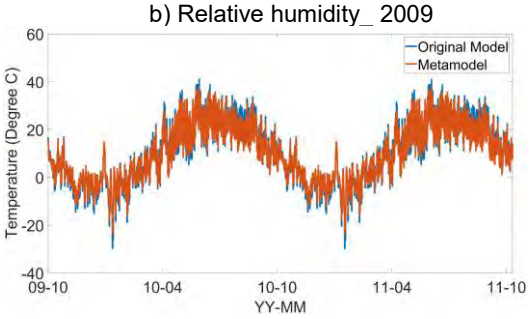

c) Temperature_ 2009

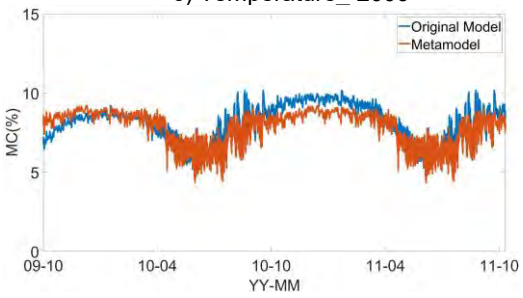

d) Moisture content_ 2066

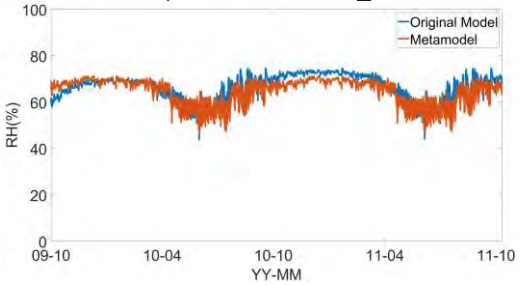

e) Relative humidity_ 2066

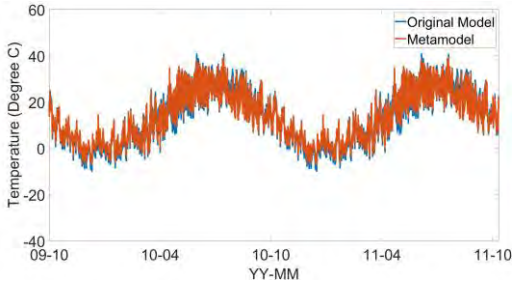

f) Temperature_ 2066

Fig. 2 Comparison between original model and metamodel

The relative humidity has similar trend with the moisture content, but less difference between the original model and metamodel. The difference in temperature between original model and metamodel is less than that in moisture content and relative humidity. Similar trend can be observed from Fig. 2d to f, the comparison between original model and metamodel under future climatic loads. The differences in moisture content and relative humidity are higher than those under current climatic loads, especially in the period with some peaks of MC and RH during the late summer and the beginning of fall, during which period when the rainfall amount is higher in the future year than the current year as shown in Fig. 3a. The temperature is overall higher than that under current climatic loads because of the increase of outdoor temperature as shown in Fig. 3b, while the difference between original model and metamodel is still much less than that in moisture content and relative humidity.

Table 2 shows the RMSE between the original model and metamodel for all the 20 test samples. It can be seen that the RMSE of MC and RH is higher than T, which means the metamodel performs worse in predicting MC and RH than temperature. And the RMSEs in 2066 are higher than those in 2009, which indicates the metamodel performs worse in future climatic conditions than in current climatic conditions. This is because the metamodel is developed with current climate data, which has less extreme weather than future climate data. Therefore, the hygrothermal responses of the building envelope to the extreme weather are not well trained with current climatic data.

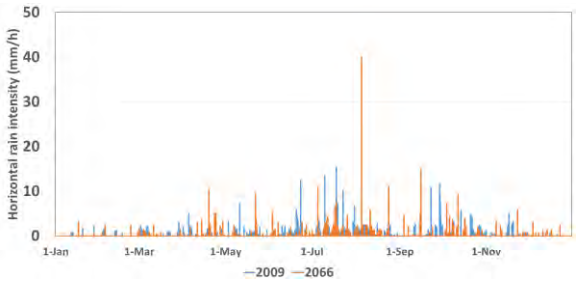

a) Horizontal rain

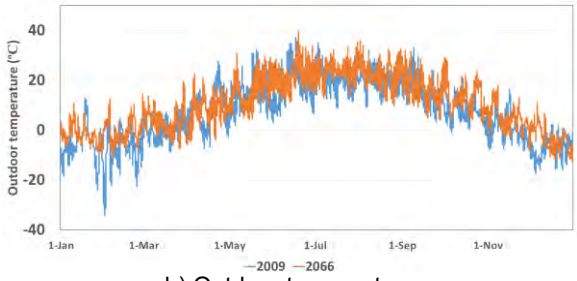

b) Outdoor temperature

Fig. 3 Comparison of climatic parameters between current and future years (2009 v.s. 2066)

Table 2 RMSEs under current and future climatic conditions

	MC (kg/m^3)	RH (%)	T (℃)
RMSE(2009)	2.69	2.05	1.61
RMSE(2066)	5.05	3.72	2.52

Although there is a bit loss of accuracy by using the metamodel, the simulation time is significantly reduced compared to the original hygrothermal model. For 2 years simulation of 20 test samples, the original DELPHIN hygrothermal model takes about 40 minutes to complete the simulation, while the metamodel only takes about 30 seconds to get all the results.

4. Conclusions and outlook

This paper developed a metamodel as a substitute for hygrothermal model to predict the hygrothermal behaviors of a conventional 2x6 wood framed wall under current and future climatic loads. The metamodel is developed based on Long short-term memory (LSTM) neural network, and trained by the stochastic time series of inputs and outputs under current climatic conditions. The developed metamodel showed a good performance in predicting the moisture content, relative humidity and temperature under both current and future climatic loads, although the performance in future climatic conditions is slightly worse than that in current climatic conditions. The simulation time is significantly reduced by using the metamodel with a minor sacrifice of accuracy. Therefore, metamodeling approach can be applied to study the hygrothermal responses of building envelopes to future climatic loads, and it will significantly improve the simulation efficiency especially when considering different scenarios of future climatic loads.

Since this paper is a preliminary exploratory study, only four input time series (outdoor temperature, relative humidity, wind-driven rain flux and incident solar radiation flux) and three output time series (moisture content, relative humidity and temperature) are used to develop the metamodel. In the future study, more time series such as long-wave radiation flux, rain penetration rates and air leakage rates will be included to make the metamodel to be more robust.

Acknowledgement

The authors would like to thank National Research Council of Canada (NRC) for providing the historical and projected future climatic data.

References

[1] L. Wang, H. Ge. Stochastic modelling of hygrothermal performance of highly insulated wood framed walls. Building and Environment, 146 (2018), 12–28.

[2] J. Zhao, R. Plagge, A. Nicolai, J. Grunewald, J.S. Zhang. 2011. Stochastic study of hygrothermal performance of a wall assembly-the influence of material properties and boundary coefficients. HVAC&R Research, 17(4) (2011), 591-601.

[3] T. Defraeye, B. Blocken, J. Carmeliet. Influence of uncertainty in heat–moisture transport properties on convective drying of porous materials by numerical modelling. Chem. Eng. Res. Des., 91 (1) (2013), pp. 36-42

[4] H. Janssen, S. Roels, L.V.Gelder, P.Das. Final report of IEA Annex 55- Subtask 2: Probabilistic tools. Gothenburg, Sweden: International Energy Agency (2015).

[5] L. Van Gelder, P. Das, H. Janssen, S. Roels. Comparative study of metamodelling techniques in building energy simulation: guidelines for practitioners. Simulation Modelling Practice and Theory, 49 (2014), 245-257.

[6] A. Tijskens, S. Roels, H. Janssen. Neural networks for metamodelling the hygrothermal behavior of building components. Building and Environment. 162 (2019), 106282.

[7] M.K. Kumaran, J. C. Lackey, N. Normandin, F. Tariku, D. van Reenen. Variation in the hygrothermal properties of several wood-based building products. In Proceedings of Second International Building Physics Conference, Leuven, Belgium. 2003.

[8] P. Mukhopadhyaya, M. K. Kumaran, J.C. Lackey, D. van Reenen, F. Tariku. Hygrothermal properties of exterior claddings, sheathing boards, membranes and insulation materials for building envelope design, NRCC-50287. National Research Council of Canada, Ottawa, Canada. 2007

[9] ASHRAE. ANSI/ASHRAE Standard 160-2016 Criteria for moisture-control design analysis in buildings. Atlanta, GA: American Society of Heating Refrigerating and Air Conditioning Engineers Inc. 2016.

[10] ASHRAE ASHRAE Handbook: Fundamentals (SI. Ed) ASHRAE. 2013.

[11] A. Gaur, M. Lacasse, M. Armstrong. Climate Data to Undertake Hygrothermal and Whole Building Simulations Under Projected Climate Change Influences for 11 Canadian Cities. Data, 4(2) (2019), 72.

[12] Environment and Climate Change Canada. Memorandum of Understanding between National Research Council and Environment and Climate Change Canada. Government of Canada: Ottawa, ON, Canada. 2018.

A New Sensing System to Detect Liquid Water Penetration through Water Resistant Barriers

W. Qi[a], C. Valeo[b,*], P. Mukhopadhyaya[c]

[a] Wenqin (Sarah) Qi, Department of Mechanical Engineering, University of Victoria, Victoria, BC, Canada, qsarah@uvic.ca
[b, *] Caterina Valeo, Department of Mechanical Engineering, University of Victoria, Victoria, BC, Canada, valeo@uvic.ca
[c] Phalguni Mukhopadhyaya, Department of Civil Engineering, University of Victoria, Victoria, BC, Canada, phalguni@uvic.ca
* Corresponding author, Tel: (+1) 250-721-8623, Email: valeo@uvic.ca,

Abstract:
This research investigates a Hydrostatic Pressure Test Apparatus (HPTA) provided by SMT Research Ltd, which was designed to test the liquid water penetration factor. The HPTA was designed according to AATCC 127: *Water Resistance: Hydrostatic Pressure Test*, with a greater focus on liquid water penetration as opposed to pressure. The HPTA sensing system was composed of a housing unit that holds the water column to provide pressure, an electrical resistance sensor with 42 channels - each reading an individual electrical resistance and a data logger. Lower electrical resistance indicates that more liquid water has penetrated the sensor. Initial test results using Typar and HAL-TEX barrier samples showed significant leakage, which rendered results unusable. Thus, a new system was designed with a completely redesigned housing system. The new system was tested for accuracy and repeatability.

The revised HPTA 2.0 contained two transparent round acrylic plates and eight bolts to clamp the barriers being tested. HPTA 2.0 showed no water leakage through any joint and proved to be highly functional. Nine types of WRBs, SIGA-Majvest, MENTO PLUS, INTELLO X, Blueskin VP100, Blueskin VP160, Tyvek Commercial, TYPAR, Stormtite and HAL-TEX 30 MINUTE, were tested by HPTA 2.0. Among all results, Typar and Stormtite were determined to be the best water-resistive material, which did not leak over 5 hours. Mento had the least water resistance since the average time to penetrate three spots was only 7 minutes. Results of all the barriers showed reasonable repeatability, but further verification is recommended. A new version of the device is under development to fix the sensor pin sealing problem as well as to improve the ease of handling and operation of the device.

Keywords:
Water resistive barrier, liquid water penetration factor, hydrostatic pressure test apparatus, accuracy, repeatability.

1. Introduction

Building science is a broad subject that contains knowledge and technologies from different areas. Buildings need to be built using strong engineering fundamentals to ensure the safety and wellbeing of the occupants. Many factors influence the performance of a building such as the energy efficiency, HVAC system, air leakage, and hygrothermal response of building materials while moisture management has the most critical role. In this work, liquid water penetration of a water resistive barrier is going to be the main focus.

In building envelopes, moisture enters the building in three forms: liquid water, water vapor, and solid like snow. This work mainly focuses on liquid water, and the other two forms will not be discussed. In order to prevent liquid water entering the building envelope and possible water accumulation, the International Building Code [1] suggests that the design and construction of an exterior wall should allow a water-resistive barrier to be applied behind the exterior veneer. As defined in the literature [2], “A water resistive barrier is a material behind an exterior wall covering that is intended to resist liquid water that has penetrated behind the exterior covering from further intruding into the exterior wall assembly”. The terms “building paper” and “building wrap” are also used.

In this work, a factor that describes the ability of each WRB to resist liquid water penetration is going to be discussed. This liquid water penetration factor is investigated by the Hydrostatic Pressure Test Apparatus (HPTA) provided by SMT Research Ltd, a company that provides structural monitoring solutions and analysis for clients engaged in building design, construction, management, and restoration [3]. The HPTA apparatus was designed to create a consistent, empirical method for membrane testing [4]. It was developed based on AATCC 127 [5]. Modifications of the device were applied for better performance.

2. Literature Review

In ASTM E2556 [6], *Standard Specification for Vapor Permeable Flexible Sheet Water-Resistive Barriers Intended for Mechanical Attachment*, several types of

WRBs were given based on material difference: felt-based barrier composed of asphalt-saturated organic felts, paper-based barrier mainly composed of sulfate pulp fibers, and polymer-based barrier made of plastic sheet materials. This standard categorized WRBs into two groups: Type I WRB with base-level water resistance and Type II WRB with enhanced water resistance as shown in the modified table below. One thing to note here is this specification only apply to vapor permeable flexible sheet materials.

Table 1: Requirement for Water Resistive Barriers, modified from [6]

Test Requirement	Test Method	Minimum Performance Requirements	
		Type I	Type II
Water resistance test	Test Method D779 [7]	10 min minimum	60 min minimum
	Ponding Test (A1.1)	Ponding Test (A1.1)	not applicable
	AATCC Test Method 127	not applicable	No leakage is permitted to the underside of any specimen in 5 h

The ASTM D779 introduced the “boat test” that folding a piece of sheathing membrane into a boat with a moisture indicator on it and placing the boat on water while AATCC Test Method 127 introduced the “hydrostatic head test” and “hydrostatic pressure test” that measured the water penetration resistance of a fabric with respect to hydrostatic pressure.

The UU-B-790a, *federal specification of building paper, vegetable fiber: (Kraft, waterproofed, water repellent and fire resistant)* [8] gave a more complex classification. The building papers were classified into four types, from grade A to G in 11 styles. Only Type I, Barrier paper is going to be discussed here. See table 2 concluded from the specification below.

Table 2: Grade requirements, modified from [8]

Water Resistance	Grade			
	A	B	C	D
Hours min	24	16	8	1/6

The Grade A and Grade B paper were high water-vapor resistant and moderate water-vapor resistant respectively. The Grade C paper was water resistant and the Grade D paper was water-vapor permeable.
The third classification was from JC/T 2291-2014, *Water resistive & vapor permeance barriers* [9] shown in Table 3. Type I barrier and Type II barrier had different requirements on other physical properties such as tensile strength and water vapor transmission rate which were not included here. The water column height was the height of a testing method given in EN 1928, *Flexible sheets for waterproofing - Bitumen, plastic and rubber sheets for roof waterproofing - Determination of Watertightness* [10].

The results of these standards and their relevant apparatuses were relatively subjective and none of them can rigorously quantify the amount of liquid water that passes through. Thus a more precise and quantifiable method should be developed.

Table 3: Water resistive & vapor permeance barriers physical properties, modified from [9]

	Type I (wall)	Type II (metal roofing)	Type III (tile roofing)
Water-tightness	1000mm water column 2h	1000mm water column 2h	1500mm water column 2h

3. The Hydrostatic Pressure Test Apparatus

The main difference between the Hydrostatic Pressure Test Apparatus (HPTA) and the testing methods discussed above is that HPTA has a sensor platter that reads electrical resistance directly in contact with the testing specimen. In Figure 1, (a), it can be seen that the sensor has 42 channels of measurement (38 inside a circle and four edge sensors outside the circle). The gold plated feature gives the sensor excellent corrosion resistance and conductivity. Each of the 42 pads reads value separately. The pads are numbered alphabetically row by row as shown in Figure 1, (b).

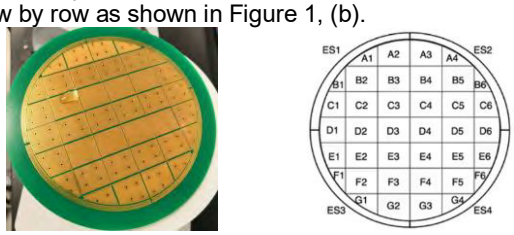

Figure 1: (a) Sensor Platter (b) Pad Number

The data are collected by a data logger, and read by BiG, a software developed by SMT Research. Data exportation and cloud sync functions are available. The reading is completed in a time sequence from one pad to another with a coded order. The values of electrical resistance indicate if each pad was dry or wet. The original value of a dry pad is 1,000,000,000 Ohms. When the pad is getting wetter, in other words, when liquid water is penetrating the WRB specimen, the electrical resistance decreases. An alarm can be set in the software; for example, the threshold value of a WRB specimen gets penetrated is 2,000,000 ohms, and any reading below this value will trigger the Alarm. It allows relating the amount of water passing through the membrane with the electrical resistance then the water penetration rate can be determined. A full assembly of HPTA is shown below in Figure 2.

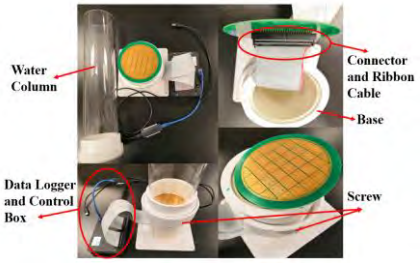

Figure 2: SMT HPTA Apparatus

3.1 Materials to be tested

Nine WRB materials are available: Stormtite, HAL-TEX 30 MINUTE, SIGA-Majvest, MENTO PLUS, INTELLO X, Blueskin VP100, Blueskin VP160, Tyvek Commercial, and TYPAR. Most of them are polymer-based. Some of them are vapor permeable while others are not. The Blueskin WRBs from Henry Company have a self - adhesive feature and can adhere to the exterior wall without mechanical attachment.

3.2 HPTA Performance Test

Several performance tests were conducted using HPTA. The sensitivity of the sensor platter was confirmed by adding the same or different amount of water right on the sensor surface via a pipette. The readings of each inner pad are generally consistent as they gave similar curves in the test with same amount applied. The sensors response rapidly to the test with increased water amount. Figure 3 shows a plot of column C Pads. In the beginning, 5 µl distilled water was added to each pad. After 5 minutes and 20 seconds, another 5 µl distilled water was added to each pad. The sensor caught this change in the following reading cycle. It can be seen that every curve had a noticeable drop at around 6 minutes, which verified the inverse relationship between electrical resistance and the amount of liquid water.

Tests with the application of WRBs were then conducted using Typar and HAL-TEX 30. Three tests were done for both materials, and every test started with a new sample. Water leakage happened to five of the six tests, thus lead to inaccurate and unrepeatable results. Figure 4, (a) shows how water leaked through the screw connecting location. Another problem, material edge wicking, was also found (see Figure 4, (b). The sodden edge indicated that the clamping method is not appropriate since the water did not penetrate the material but went to the sensor surface from the edge. the HPTA apparatus was updated to a new version, HPTA 2.0 to address the problems.

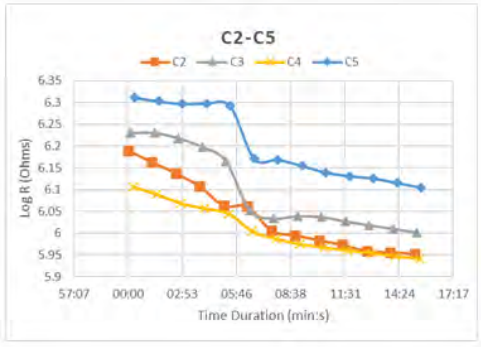

Figure 3: Sensor Response to Water Amount Change

Figure 4: (a) Water Leakage (b) Edge Wicking

3.3 Development of HPTA 2.0

The objective of this design was to upgrade the current HPTA apparatus so that it can have better accuracy and repeatability which directly influence the experiment results to evaluate the water penetration rate of WRB materials. The 3D model built in SolidWorks, prototype machined in UVic machine shop, and the assembled device are shown in Figure 5. The original screw mechanism was changed to bolts clamping. The two transparent acrylic plates allowed easy observation of the specimen.

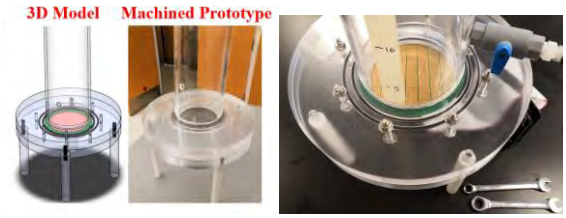

Figure 5: HPTA 2.0 CAD, Prototype and Assembly.

4. Results and discussions

Performance tests were done for HPTA 2.0 and the leaking problem was solved for all kinds of materials.
The device gave adequate results at this stage but there are still some disadvantages regarding the sealing method of the sensor pin (possible circuit shortage caused by water), the portability of the apparatus, and the complexity of assembling hence a new version of the device is under development.
The test results of HPTA 2.0 were imported to a data analyzer scrip that specially wrote for this project by a CS student. The analyzer enabled visualization of collected data so the user can tell the real-time condition of each pad, as shown in Figure 6. The green color from light to dark indicated the decrease in electrical resistance. The color turned to red when the threshold value was reached.

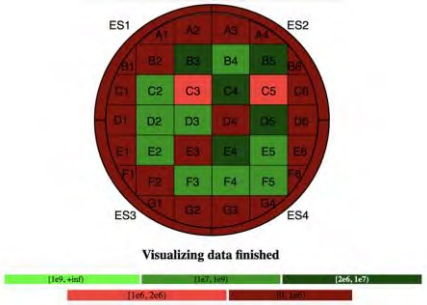

Figure 6 Data visualization

The data analyzer also processing the data in a more readable way compares to the data exported from BiG. An example is given in Table 4. The first column showed the order that each pad got penetrated, date, time, electrical resistance reading, and log reading. Other features such as duration and day/wet phase change can be added by changing the code in the script.

Table 4: Data output from the Analyser

#	name	date	time	reading	log_reading
1	D4	2019/8/15	17:56:43	1209824	6.083
2	C5	2019/8/15	18:04:23	1744194	6.242
3	B1	2019/8/15	18:07:51	1151744	6.061
4	B2	2019/8/15	18:07:52	855554	5.932
5	Edge Sensor 1	2019/8/15	18:08:00	721211	5.858
6	Edge Sensor 2	2019/8/15	18:08:01	489456	5.69
7	A3	2019/8/15	18:08:03	682109	5.834
8	A4	2019/8/15	18:08:08	500174	5.699
9	B6	2019/8/15	18:08:14	603316	5.781
10	E1	2019/8/15	18:08:18	965855	5.985
11	F1	2019/8/15	18:08:19	464261	5.667
12	F2	2019/8/15	18:08:22	1301801	6.115
13	Edge Sensor 3	2019/8/15	18:08:28	683143	5.835
14	Edge Sensor 4	2019/8/15	18:08:30	740952	5.87
15	G3	2019/8/15	18:08:34	1306145	6.116
16	F6	2019/8/15	18:08:41	1587647	6.201
17	D1	2019/8/15	18:09:03	784273	5.894
18	A2	2019/8/15	18:09:11	721516	5.858
19	G2	2019/8/15	18:09:43	767885	5.885
20	A1	2019/8/15	18:10:25	471740	5.674

Tests were conducted for every material. The results were relatively consistent and a table summarized the average time that three spots got penetrated by water for each material is given below. The high and low extreme values were deducted from the average time calculation since they always occurred when there was an edge wicking. Improper installation of the assembly could cause the fault value and material edge wicking. Results showed Mento got penetrated in the shortest time, whereas Typar and Stormtite can resist liquid water penetration for more than 5 hours.

Table 5: Average Time of First Leak

Material	Time(min)
SIGA	13.83
Tyvek	18.16
Mento	7.3
Hal-Tex 30	26
INTELLO X	13
Blueskin VP100	15
Blueskin VP160	29
Stormtite	>360
Typar	>360

The difference between tests using a same piece of specimen for several times and tests using a new piece of specimen is not obvious. No rule was found for material fatigue in this stage. Further investigation and tests need to be done in order to find more convictive results for all materials.

5. Conclusions and outlook

In this work, the original Hydrostatic Pressure Test Apparatus (HPTA) was tested for sensitivity and repeatability. The device was very prone to water leakage through the joints. A new design to prevent water leakage was proposed and the modified version, HPTA 2.0, was constructed at UVic. The HPTA 2.0 showed excellent water leakage resistance. Using HPTA 2.0, nine WRB materials were tested without any sign of water leakage through the joints. Most results were reasonably repeated while occasional wicking through the edge of the WRB was found with the presence of extreme values. Therefore, further verification tests of different WRBs are necessary. The sensor pin sealing method, ease of handling and operation of the device is going to be addressed in an updated device.

Acknowledgments

Authors would like to acknowledge the financial support provided by the Natural Sciences and Engineering Research Council of Canada (NSERC) and research support extended by the SMT Research Ltd, more specifically, Mr. Gamal Mustapha, Mr. Khaleed Khondoker, Mr. Jason Teetaert and Ms. Paige Merko. Authors would also like to thank Dr. Armando Tura, Mr. Mitch Anderson, Mr. Art Makosinski, and Mr. Rodney Katz for their technical input and operational support. Computing support provided by Mr. Tianyi Liang is highly appreciated.

References

[1] I. C. Council, *2003 International Building Code ®, December 2002 ISBN # 1-892395-56-8 (soft)*. 2004.

[2] A. Dunlap and S. Flock, “Research of air/water leakage at fasteners through the air barrier,” 2019.

[3] “SMT Research.” [Online]. Available: https://www.smtresearch.ca/.

[4] “NSERC Engage 2 Page Proposal,” 2018.

[5] AATCC Technical Manual, “Water Resistance: Hydrostatic Pressure Test,” *AATCC Tech.*

[6] ASTM, “E2556 - Standard Specification for Vapor Permeable Flexible Sheet Water-Resistive Barriers Intended for Mechanical Attachment 1,” *Astm*, vol. 10.

[7] ASTM, “D779 Standard Test Method for Determining the Water Vapor Resistance of Sheet Materials in Contact with Liquid Water by the Dry Indicator Method 1,” pp. 1–4, 2019.

[8] “Federal Specification Building Paper, Vegegetable Fiber: (Kraft, Waterproofed, Water Repellent and Fire Resistant),” 1964.

[9] Z. Zhiyuan et al. “JC/T 2291 Water resistive & vapour permeance barriers”.

[10] “EN 1928 Flexible sheets for waterproofing - Bitumen, plastic and rubber sheets for roof waterproofing - Determination of watertightness,” 2000.

Impact of Insulating the Rough Opening Gap on the Total Heat Flow at the Window to Wall Interface

Edward Lau and Fitsum Tariku

Building Science Centre of Excellence
British Columbia Institute of Technology, Burnaby, BC

Abstract:
This paper investigated the impact on the total heat flow at the window to wall interface by insulating the rough opening gap. A total of 32 THERM models were created to investigate four different wall assemblies combined with two different window frames along with four different thicknesses of insulation in the rough opening gap. In general, the results indicate that there is a reduction in heat flow even with a minimal amount of insulation in the rough opening gap. The heat flow reduction is more significant when the thermal barrier is not thermally aligned with the window frame. When the window frame and wall assembly is thermally aligned, the maximum heat flow reduction was calculated to be only 1.7%. Results also indicate that for a split insulated wall assembly, insulating the rough opening gap has more heat flow reduction effects when the window frame is positioned near the back of the wall where the cavity insulation and studs are more conductive than the exterior insulation. For non-thermally aligned conditions, adding insulation in the rough opening gap can potentially reduce the heat flow by up to 15%. Lastly, adding insulation in the rough opening gap appears to have a more significant effect for highly conductive windows.

Keywords:
Window to wall interface, thermal bridge, insulation, rough opening gap

1. Introduction

Buildings are becoming more stringent in terms of energy performance due to evolving building codes around the world. As higher R-values of the building envelope become more common, closer attention needs to be given to thermal bridges as they can create significant heat loss. The window-to-wall interface is an example of a thermal bridge and is the focus of this paper.

Totten et al (2008) modelled an aluminum storefront frame on 3 different wall assemblies and concluded that the window to wall interface thermal bridge caused up to 20% additional heat flow. Cappelletti et al. (2011) modelled a wood frame window to wall detail with varying amounts of insulation interior and exterior of the frame to analyze its effects on the ψ-values. They concluded that the greatest ψ-value reduction can be realized when the window jamb frame is located in the middle position with insulation on the exterior and by shifting the window from an internal to an external position. Barnes et al (2013) investigated the impact on the ψ-values of a window to wall interface for a bridged flashing and unbridged flashing condition and concluded that the ψ-values on average dropped by 86% for the unbridged condition. Misiopecki et al (2013, 2017) modelled a wood frame window on 8 different wall assemblies with varying window positions to investigate the optimal window position with the lowest ψ-value and concluded that the optimal window position is located in the middle exterior of the thermal insulation. Sierra et al (2014) studied the difference between two UK standards of modelling the condensation risk of a window header and concluded that including the window frame in the model is important as it has a significant impact on ψ-values. Ilomets et al (2014) conducted computer modelling and field measurements of the window to wall interface in rehabilitation projects in older Eastern European buildings to study the impacts of increasing the insulation in the wall assembly and relocating the window position. They concluded that with the window at the original position and 200mm more of interior insulation, 34% of the heat loss was due to thermal bridges, whereas repositioning the window to be more thermally-aligned, only 10% of the heat loss was due to thermal bridges. Chapter 7 in the CSA A440.4-2019 standard requires the rough opening gap to be insulated for locations where the January 2.5% design temperature is below -15°C. This paper focuses on quantifying the impact of insulating the rough opening gap with varying thicknesses on the total heat flow of four different window to wall interface designs.

2. Thermal Modelling Methodology

Thermal simulation models were conducted using LBNL's THERM 7.4 program. A total of 32 THERM models were simulated for this paper accounting for four different wall types, two different fenestration systems, and four rough opening sizes. For the first set of THERM models, a vinyl window frame was modelled with a 2x6 wood frame wall assembly with R18 batt insulation inside the cavity along with a top plate, wood siding, and gypsum board construction. The model indicated that the wall achieves an effective R-value of R17. **Figure 1** illustrates the typical model and **Table 1** summarizes the materials data used in this set of models.

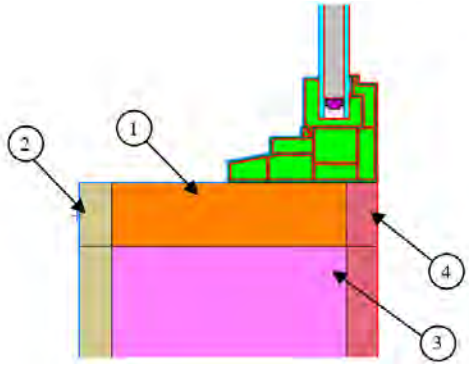

Figure 1: Vinyl Window Frame to Wood Frame Wall

Table 1: Material Data for Models #1-8

#	Material	Conductivity (W/mK)
1	Wood, Coniferous (Softwoods)	0.1400
2	Plywood (Douglas Fir)	0.106
3	Wood Studs @ 400mm o.c. with R18 batt in cavity	0.049
4	Gypsum Board	0.1586

For the second set of THERM models, an aluminum curtainwall mullion was modelled with an 203mm thick concrete wall assembly, interior insulated with 76mm XPS along with a steel stud and gypsum board construction. The model indicated that the wall achieves an effective R-value of R15. **Figure 2** illustrates the typical model and **Table 2** summarizes the materials data used in this set of models.

Table 2: Material Conductivity for Models #10-17

#	Material	Conductivity (W/mK)
1	Concrete, Heavy Weight	1.9464
2	XPS Insulation	0.0290
3	Steel Stud @ 400mm o.c with air in cavity	0.2175
4	Gypsum Board	0.1586

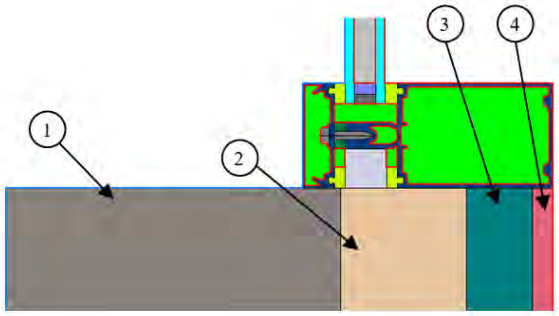

Figure 2: Curtainwall Mullion to Concrete Wall

For the third set of THERM models, a curtainwall mullion was modelled with a 152mm deep steel stud wall assembly with a 101mm exterior mineral wool insulation and an R18 batt insulation inside the cavity along with plywood and gypsum board construction. The model indicated that the wall achieves an effective R-value of R32. **Figure 3** illustrates a typical model and **Table 3** summarizes the materials data used in this set of models.

Table 3: Material Data for Models #20-27

#	Material	Conductivity (W/mK)
1	Mineral Wool Insulation	0.0288
2	Plywood (Douglas Fir)	0.106
3	Steel Studs @ 400mm o.c. with R18 batt in cavity	0.0742
4	Gypsum Board	0.1586
5	Steel – Stainless (Oxidized)	17.00

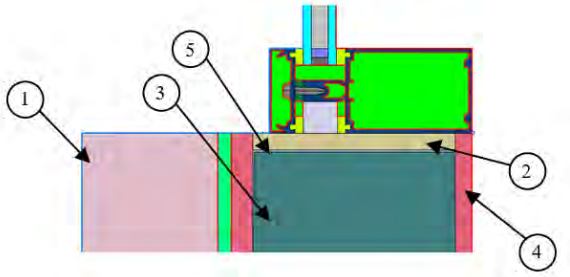

Figure 3: Curtainwall Mullion to Steel Stud Wall

For the fourth set of THERM models, a vinyl window frame was modelled with a 2x6 wood frame wall assembly with a 152mm exterior EPS insulation and an R24 batt insulation inside the cavity along with a top plate, plywood sheathing and gypsum board construction. The model indicated that the wall achieves an effective R-value of R42. **Figure 4** illustrates a typical model and **Table 4** summarizes the materials data used in this set of models.

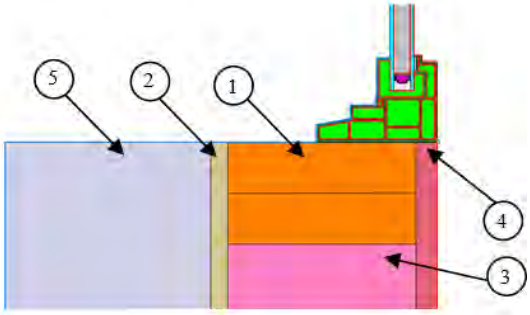

Figure 4: Vinyl Window to Split Insulated Wood Frame Wall

Table 4: Material Data for Models # 30-37

#	Material	Conductivity (W/mK)
1	Wood, Coniferous (Softwoods)	0.1400
2	Plywood (Douglas Fir)	0.106
3	Wood Studs @ 400mm with R24 batt in cavity	0.0411
4	Gypsum Board	0.1586
5	EPS Insulation	0.038

The vinyl window frame achieves a U-value of 1.87 W/m^2K and utilizes a warm edge spacer. The curtainwall frame achieves a U-value of 7.93 W/m^2K and utilizes a “Super Spacer”.

The insulated glass units (IGU) were created in WINDOW 7.4 using conventional NFRC simulation guidelines and boundary conditions. **Table 5** summarizes the IGU's U-value used for both the vinyl window frame and curtainwall mullion.

Table 5: Insulated Glass Unit U-value

Frame Used	Exterior Pane	Interior Pane	U-value (W/m2K)
Vinyl Frame	3mm Cardinal LoE 366	3mm Clear Glass	1.361
Aluminum Curtainwall	6mm Cardinal LoE 272	6mm Clear Glass	1.405

The THERM models used conventional boundary conditions common to the building envelope field for both IGU, frame, and wall. The boundary conditions according to NFRC conventions, where the IGU has its own boundary condition, were not used in these simulations. The boundary conditions are summarized in **Table 6**.

Table 6: Boundary Conditions

Boundary Condition	Temperature (°C)	Film Coefficient (W/m2K)
Interior Vertical Surface	21.1	8.29
Exterior Winter	-17.8	34.00

All 32 THERM models were modelled as the sill along with a 1220mm tall IGU and a 1000mm tall wall assembly. When XPS insulation is added in the rough opening gap, the wall assembly including the thickness of the insulation stays constant at 1000mm tall. This creates a comparable heat flow number based on the same surface area. Total heat flow results are then recorded from the THERM models.

Each window to wall assembly combination was simulated with a front and back window position along with a 0mm, 10mm, 25mm, and 50mm thick XPS insulation (conductivity = 0.0290 W/mK) in the rough opening gap for a total of 8 models per combination. The steel stud and the wood studs were assumed to be spaced @ 400mm o.c. Horizontal cross-sections were first modelled to obtain the effective R-values of studs and insulation inside the cavity. These values were then inputted into the vertical cross-section models as a new material. **Figure 5** illustrates an example of a model that has insulation in the rough opening gap.

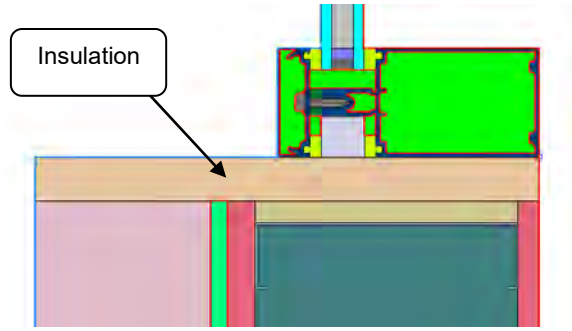

Figure 5: Example of Rough Opening Insulation

3. Results and discussions

Heat flow results and their percentage changes from the uninsulated base case are summarized in **Table 7.** In general, the results indicate that adding insulation in the rough opening gap does reduce the overall heat flow of the interface. Moreover, insulating the rough opening gap only has a more significant effect when the window position is not properly aligned with the thermal barrier in the first place.

When the window is already aligned with the thermal barrier, adding insulation in the rough opening gap does not significantly reduce the heat flow. The minimal reduction in the overall heat flow is likely due to the insulation having a lower conductivity than the wall assembly itself rather than reducing the thermal bridge effect. For the thermally aligned window models, the smallest heat flow reduction was 0.079% from Model # 35, while the largest heat flow reduction was 1.765% from Model #13.

However more importantly, the results indicate that aligning the thermal barrier with the thermal break of the window frame and the IGU does help in reducing the overall heat flow. For a split insulated wall assembly, the thermal barrier is considered aligned when the window is aligned with the lowest conductive material. As evident in the steel stud wall assembly and the split-insulated wood frame wall assembly for both curtainwall mullions and vinyl frames, the cavity insulation is more conductive than the exterior insulation. Therefore, adding insulation in the rough opening gap does help reduce the overall heat flow when the window frame is positioned above the cavity insulation. As shown in the results of Models #20-23 and Models #30-33, the effect could be as much as 3.399%, depending on the thickness of the insulation. From a structural perspective, it is more feasible that the window sill be installed on top of a wood or steel stud structure rather than on top of the exterior insulation where there's limited structural capacity.

The most extreme heat flow reduction is when the curtainwall mullion was modelled in the front position of the concrete wall from Models #14-17. This detail is

quite common for industrial warehouses without a thermal break in the precast concrete wall. As shown in Table 7, the heat flow could potentially be reduced by 15.76%. Because the wall's insulation is located at the back of the wall assembly, there is a huge misalignment of the thermal barrier. The results appear to indicate that adding even 10mm of insulation can reduce the total heat flow by 11.508%.

Lastly, the reduction in heat flow appears to be more significant for poorly performing window frames and wall assemblies. However, this difference is minimal. For example, in the thermally aligned position of the steel stud wall and split insulated wood frame wall, the heat flow reduction is 0.614% for the curtainwall from Model #27, while the heat flow reduction is 0.199% for the vinyl window frame from Model #37. Adding insulation to the rough opening gap in poorly performing wall assemblies also have a more significant effect. For example, in the thermally aligned position of the concrete wall the heat flow reduction reached a maximum of 1.7% from Model #13, while the split insulated wood frame wall assembly only reduced up to 0.199% from Model #37.

Table 7: Modelling Results

Position	Model #	Substrate	Heat Flow (W)	% Change
Back of Wood Wall	1	Vinyl Frame with no insulation	86.2	
	2	Vinyl Frame with 10mm insulation	85.7	-0.550%
	3	Vinyl Frame with 25mm insulation	85.3	-0.957%
	4	Vinyl Frame with 50mm insulation	85.0	-1.303%
Front of Wood Wall	5	Vinyl Frame with no insulation	85.5	
	6	Vinyl Frame with 10mm insulation	85.1	-0.434%
	7	Vinyl Frame with 25mm insulation	84.9	-0.668%
	8	Vinyl Frame with 50mm insulation	84.7	-0.907%
Back of Concrete Wall	10	Curtainwall with no Insulation	104.3	
	11	Curtainwall with 10mm Insulation	103.3	-1.025%
	12	Curtainwall with 25mm Insulation	103.0	-1.265%
	13	Curtainwall with 50mm Insulation	102.5	-1.765%
Front of Concrete Wall	14	Curtainwall with no Insulation	124.3	
	15	Curtainwall with 10mm Insulation	110.0	-11.508%
	16	Curtainwall with 25mm Insulation	106.5	-14.325%
	17	Curtainwall with 50mm Insulation	104.7	-15.760%
Back of Steel Stud	20	Curtainwall with no Insulation	101.7	
	21	Curtainwall with 10mm Insulation	99.5	-2.130%
	22	Curtainwall with 25mm Insulation	98.8	-2.859%
	23	Curtainwall with 50mm Insulation	98.2	-3.399%
Front of Steel Stud Wall	24	Curtainwall with no Insulation	98.2	
	25	Curtainwall with 10mm Insulation	97.8	-0.401%
	26	Curtainwall with 25mm Insulation	97.6	-0.557%
	27	Curtainwall with 50mm Insulation	97.6	-0.614%
Back of Split Insulated Wall	30	Vinyl Frame with no insulation	80.9	
	31	Vinyl Frame with 10mm insulation	80.1	-0.987%
	32	Vinyl Frame with 25mm insulation	79.5	-1.731%
	33	Vinyl Frame with 50mm insulation	79.0	-2.348%
Back of Split Insulated Wall	34	Vinyl Frame with no insulation	78.1	
	35	Vinyl Frame with 10mm insulation	78.0	-0.079%
	36	Vinyl Frame with 25mm insulation	78.0	-0.140%
	37	Vinyl Frame with 50mm insulation	78.0	-0.199%
Components		Curtainwall 6mm LowE/6mm, 1220mm IGU	90.0	
		Vinyl 3mm Low E/3mm, 1220mm IGU	72.3	
		Concrete Wall, 1000mm	14.1	
		Wood Frame Wall, 1000mm	12.4	
		Steel Stud Wall, 1000mm	6.9	
		Split Insulated Wood Frame Wall, 1000mm	5.2	
		Vinyl Window U-Factor	1.9	W/m2K
		Curtainwall Mullion U-factor	7.9	W/m2K

As much as building envelope engineers want to align the thermal barrier with the window, it may not always be feasible due to architectural and structural considerations. Coordination between professionals to achieve thermal barrier continuity might also be a challenge especially for lower budget projects. Therefore, adding insulation in rough opening gap is a potential design option that can help reduce the overall thermal bridging effects in most situations.

4. Conclusions and Outlook

This paper investigated the impact on the total heat flow at the window to wall interface by insulating the rough opening gap. A total of 32 THERM models were created to investigate four different wall assemblies combined with two different window frames along with four different thicknesses of insulation in the rough opening gap. In general, the results indicate that there is a reduction in heat flow even with a minimal amount of insulation in the rough opening gap. The heat flow reduction is more significant when the thermal barrier is not thermally aligned with the window frame. When the window frame and wall assembly is thermally aligned, the maximum heat flow reduction was calculated to be only 1.7%. Results also indicate that for a split insulated wall assembly, insulating the rough opening gap has more heat flow reduction effects when the window frame is positioned near the back of the wall where the cavity insulation and studs are more conductive than the exterior insulation. For non-thermally aligned conditions, adding insulation in the rough opening gap can potentially reduce the heat flow by up to 15%. Lastly, adding insulation in the rough opening gap appears to have a more significant effect for highly conductive windows.

Future work should focus on the practicality of an insulated rough opening gap design where structural, architectural, building envelope, and installation issues are also considered.

Acknowledgements

The authors of this paper wish to thank BCIT, NSERC, and CRC for their continual support of fostering young professionals in research and development.

References

1) Totten P.E., S.M. O'Brien, M. Pazera, 2008. The Effects of Thermal Bridges at Interface Conditions. Retrieved from: https://www.semanticscholar.org/paper/The-Effects-of-Thermal-Bridging-at-Interface-Totten-Pe/082a0380c8febd2a8bd9af01b4871b828105664b on Feburary 25, 2019.

2) Cappelletii F., A. Gasparella, P. Romagnoni, P. Baggio, 2011. Analysis of the influence of installation thermal bridges on windows performance: the case of clay block walls. Energy and Buildings 43: 1435-1442.

3) Barnes B, A. Pagan-Vazquez, R. Liesen, J. Yu, N. Alexander, 2013. Window Related Thermal Bridges. Thermal Performance of the Exterior Envelopes of Whole Buildings XII International Conference.

4) Misiopecki C., L.M. Decheva, B.P. Jelle, A. Gustavsen, 2013. Practical Methods for Ensuring Energy Efficient Window-to-Wall Connections. Thermal Performance of the Exterior Envelopes of Whole Buildings XII International Conference.

5) Misiopecki C., M. Bouquin, B.P. Jelle, A. Gustavsen, 2017. Thermal Modelling and Investigation of the Most Energy-Efficient Window Position. Energy and Buildings, 158: 1079-1086.

6) F. Sierra, J. Bai, T. Maksoud, 2014. Impact of the simplification of the methodology used to assess the thermal bridge of the head of an opening. Energy and Buildings (87): 342-347

7) Ilomets S., K. Kuusk, L. Papp, E. Arumagi, T. Kalamees, 2014. Impact of Thermal Brdiges on Thermal Transmittance of Renovated Apartment Buildings. Journal of Civil Engineering and Management, 23(1): 96-104.

8) CSA A440.4 – 2019. Windows, Doors, and Skylights Installation.

Quantifying overheating in highly glazed buildings and evaluating glazing films as a mitigation strategy

Shengbo Zhang[a,*], Jamie Fine[a], Marianne F. Touchie[a,b], William O'Brien[c]
[a]University of Toronto, Department of Mechanical and Industrial Engineering, 5 King's College Road, Toronto, ON, M5S 3G8, Canada
[b]University of Toronto, Department of Civil and Mineral Engineering, 35 St. George St., Toronto, ON, M5S 1A4, Canada
[c]Carleton University, Department of Civil and Environmental Engineering, 3432 Mackenzie Building, Ottawa, ON, K1S 5B6, Canada
∗Corresponding author; Email addresses: Shengbo.Zhang@mail.utoronto.ca (Shengbo Zhang), Jamie.Fine@utoronto.ca (Jamie Fine), Marianne.Touchie@utoronto.ca (Marianne F. Touchie), liam.obrien@carleton.ca (William O'Brien)

Abstract
Glass façades have become increasingly common in contemporary high-rise residential and commercial buildings throughout urban centers globally. Despite the aesthetic and daylighting benefits that glass façades may provide, overheating has also increased due to the additional solar heat gain. The objectives of this study are to i) demonstrate a simulation approach for quantifying this overheating, and ii) examine the tradeoff between energy and overheating for different aftermarket glazing films. First, a simulation approach using EnergyPlus for energy modeling and a Fanger-based approach for quantifying overheating is presented. Next, simulations are performed on a hypothetical zone with a fully glazed facade in four different orientations. Six film products and three blind control strategies are also simulated for each orientation, and the resulting overheating and energy consumption are reported. Finally, the trade-off between overheating and energy use are compared and discussed.

Keywords
Overheating; thermal comfort; glass façade; solar radiation

1 Introduction

Glass façades with WWR greater than 90% have gained popularity in recent years. Thus, for occupants residing in these buildings, the risk of overheating is a concern largely due to excessive solar heat gain through the windows.

Given the above scenario, the objectives of this paper are to i) demonstrate a simulation approach for quantifying overheating, and ii) examine trade-offs between energy and overheating for different mitigation strategies using glazing films. The assessment of window films is based on two perspectives: overheating; and heating and cooling energy performance. Three interior shading strategies are included in this study: always closed; always open; and closed during the presence of direct beam solar radiation.

To begin, a review of overheating and its quantification methods is presented in Section 2. Next, the simulation process and the simulation set-up are presented in Section 3, followed by results and discussions in Section 4. The results from this analysis demonstrate the spatiotemporal variations of overheating and the trade-off between overheating and energy performance among the selected window film products and blind control strategies.

2 Literature Review

Overheating is a phenomenon where an occupant becomes uncomfortably hot due to the indoor environment. Indoor overheating is not only the subject of research for tropical and subtropical climates such as Australia [1], [2], but also for heating-dominated climates like Canada [3], [4]. Numerous approaches for quantifying overheating have been proposed by thermal comfort standards and studies. The quantification approach varies by ventilation strategies. Specifically, for naturally ventilated buildings, the primary approach for defining thermal comfort uses the operative temperature, which has been used in international standards such as the Chartered Institution of Building Services Engineers (CIBSE) [5], ASHRAE Standard 55 [6], and ISO 7730 [7]. For mechanically ventilated buildings, Fanger's Predicted Mean Vote (PMV) and Predicted Percentage Dissatisfaction (PPD, which is a function of PMV) [8] is often used to evaluate thermal comfort. When using PMV, the range of -0.5 < PMV < 0.5 has been recommended to represent the comfort range by both ASHRAE Standard 55 and ISO 7730.

When determining PMV, many energy modeling software, such as EnergyPlus, evaluate PMV based upon the conditions at the center of a zone [9]. However, this assumption might not be sufficient if a particular region in a room is exposed to direct solar radiation or is in close proximity to a cold or warm surface. First, solar loading on the human body can have a significant impact on thermal comfort, and thus it can result in overheating [10], [11]. Second, the mean radiant temperature (MRT) and the corresponding thermal comfort of an occupant in close proximity to a surface depends on the temperature of that surface [12].

To account for these limitations, the methodology proposed in this study evaluates the PMV of occupants at multiple points within the room, and at different times, to produce a spatiotemporal thermal comfort metric.

3 Methodology

This section details the computer simulation setup and the methodologies used for quantifying overheating.

3.1 Thermal Discomfort from Overheating

The spatiotemporal distribution of thermal comfort is based on Fanger's PMV model. The model requires the definition of occupant variables including clothing and metabolic rate, as well as thermal environment parameters including dry-bulb air temperature, relative humidity, MRT, and airspeed. Though all the above parameters are typically output from energy modeling

software, additional steps are required to incorporate both the effect of infrared heat exchange and the additional heating effect of direct solar radiation, which results in a modified MRT. First, the zone is discretized into a structured grid and view factors to each of the surrounding surfaces are determined along with the intensity of direct solar radiation at each grid point. Then, the MRT from infrared-only sources is determined from interior surface temperatures in combination with surface view factors. Next, the Effective Radiant Field (ERF [w/m^2]) of the human body [13] is utilized to determine the additional MRT from direct solar radiation by first equating the solar radiation intensity received by the body (E_{solar} [w/m^2]) to the ERF of the human body [6], [14], as shown in Equation 1 [6]:

$$\text{ERF}_{\text{solar}} = \frac{\alpha_{\text{SW}}}{\alpha_{\text{LW}}} E_{\text{solar}} \quad (1)$$

where α_{SW} and α_{LW} represent the shortwave and longwave absorptivity of the human body.

Next, the additional MRT (ΔMRT), which is added to the original MRT, can be determined using Equation 2 [6]:

$$\Delta\text{MRT} = \frac{\text{ERF}_{\text{solar}}}{f_{\text{eff}} h_r} \quad (2)$$

where f_{eff} is the fraction of the body exposed to solar radiation, h_r is the heat transfer coefficient.

Finally, Fanger's model is employed to determine the PMV at each grid point, at each time in the simulation period, using the previously determined modified MRT value and the other input parameters mentioned above. In this study, these calculations were performed using the Rhinoceros platform and Ladybug plugins [15].

With the PMV values determined at each grid point, a single scoring metric is then determined for each window configuration, such that they can be compared for overheating. We first define the discomfort percentage (DP), which evaluates the area-based percentage of the zone exceeding the warm comfort threshold (i.e. PMV > 0.5), averaged over the simulated year. Similarly, we also define the discomfort severity (DS), which is determined by finding the average of the PPD over only the portion of the zone where the warm comfort threshold is exceeded, which is then also averaged over the simulated year. Finally, the single-value metric is then the product of DP and DS and is referred to as the *overheating index*.

It is important to note that the methodology used in this study does not consider adaptive occupant behavior to restore comfort (e.g. moving away from the window or adjusting clothing level). Despite this limitation, the method is useful to understand the impact of design on the passive performance of the building regarding thermal comfort.

3.2 Simulation set-up

The simulated zone measures 8 m in width, 6 m in depth, and 2.7 m in height, which is based on the ASHRAE Standard 140 [16]. This zone represents a typical suite in a multi-unit residential building such that only one wall is exposed to the ambient environment. In this simulation, a WWR of 100% (on the 8 m by 2.7 m exterior wall) is selected. It should be noted that many energy standards (e.g. ASHRAE Standard 90.1 [17]) prescribe a WWR not exceeding 40%. However, fully glazed building envelopes are still a common feature for many condominiums constructed before the introduction of these new standards.

Three interior films and three exterior films are selected for this study, and the properties of each are determined from the International Glazing Database. The solar transmittance (T_{sol}) and the front reflectance of the films ($R_{\text{f,sol}}$) are shown in Table 1, which are derived from when the film is applied to an 8 mm clear substrate, which is defined as the baseline provided in the database. Using these parameters, the overall SHGCs of the double-glazed window system, which are then in the energy simulations, are also reported. For comparison, the double-glazed system with no film applied yields SHGC of 0.67. In addition, it is assumed that window films do not change the U-factor of the window system, such that U = 2.78 W/m^{2}K for all cases. The algorithm used to determine the SHGC is available online [18].

Table 1 Optical properties of the chosen window films

IGDB Ref	Exterior Films		$SHGC_o$	IGDB Ref	Interior Films		$SHGC_o$
	T_{sol}	$R_{\text{f, sol}}$			T_{sol}	$R_{\text{f, sol}}$	
2705	0.229	0.240	0.28	**2747**	0.218	0.146	0.49
2706	0.362	0.244	0.37	**2748**	0.272	0.154	0.50
2707	0.603	0.260	0.53	**2750**	0.363	0.153	0.53

Lastly, in the following simulations three interior shading control scenarios are implemented: always open; always closed; and closed when direct solar radiation is present. The blinds used in the simulations are assumed to be fabric roller shades with 0% solar transmittance, 0.65 solar reflectance, and 0.9 emittance. We acknowledge that it is a limitation to assume the blind remains always closed or always open. However, these two cases represent the lower and upper limits of energy performance and overheating risk which is useful information to be considered by building designers. More advanced blind operations and strategies are recommended for future studies.

4 Results and Discussions

This section first presents detailed spatial and temporal results in Section 4.1, and then the annual comparisons between selected films and blind controls in Section 4.2.

4.1 Spatial and Temporal Variations

Overheating can vary significantly both temporally and spatially. This section describes the dominant variation patterns, to provide context for the averaged results in Section 4.2. The results shown in this section are based on the case where no window films and no window blinds are implemented.

For the spatial distribution of overheating, there is significantly more overheating near the window as shown in Fig 1.

This increased overheating was found to be a result of increased direct radiation, which could be reduced through the use of blinds. However, even with window blinds closed, this phenomenon that the region in close proximity to the window has a high overheating index may still remain. This is due to infrared heat exchange from the elevated blind surface temperatures as the result of the absorbed solar radiation [12].

Next, histograms of PMV values for the south- and east-facing orientations are shown as a function of the season in Fig 2a and Fig 2b, and as a function of solar

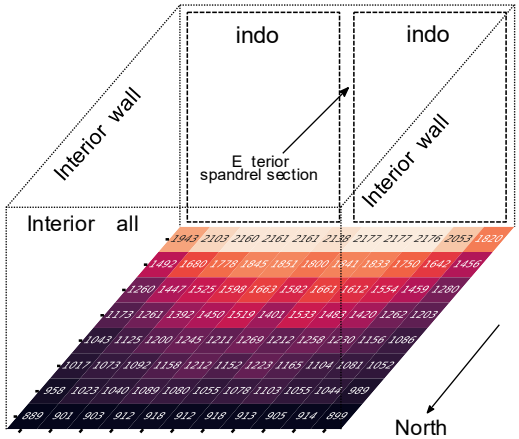

Fig 1: Number of overhating hours in a year exceeding thermal comfort threshold for a south-facing zone with no blind and no window film implemented.

radiation condition in Fig 2c and Fig 2d. The frequency shown in the y-axis represents the total number of grid points in the zone fall in each PMV range over entire zone and over the year. Note that since this study concerns overheating, only grid points with PMV > 0 are accounted for in the histogram shown in Fig 2. Additionally, it should be noted that the span of shoulder season span is as twice as long as other seasons, so a higher frequency in shoulder seasons should not be interpreted as a worse situation.

based HVAC system, the total supply air energy is used to quantify the overall energy performance.

In terms of the overheating index, the south-oriented zone has the highest value for the no-film no-blind case, while the north-oriented zone remains relatively constant regardless of the window film and blind control strategy. Among all orientations, overheating for the no-blind cases are the highest, suggesting that the direct beam and diffuse solar radiation can have a significant impact on thermal comfort.

It is also important to note that the east-oriented zone has a slightly higher overheating index in all cases than the west-facing zone. As explained in the preceding section, this observation is attributed to a thermal storage effect such that, for the east-facing zone, solar heat gain in the morning results in a higher air temperature throughout the day. However, many might believe that west-facing zone performs worse than the east based on the fact that high solar load coincides with high ambient temperature to result in a high zone air temperature in the afternoon period. Therefore, we reiterate that the overheating index used in this study is a temporally averaged value not just based on peak temperature, thus explaining this observation.

As far as the total supply air energy is concerned, the no blind case results in the lowest total energy consumption. As expected, the heating energy requirement is much greater than the cooling energy as the simulation was carried out in a heating-dominant

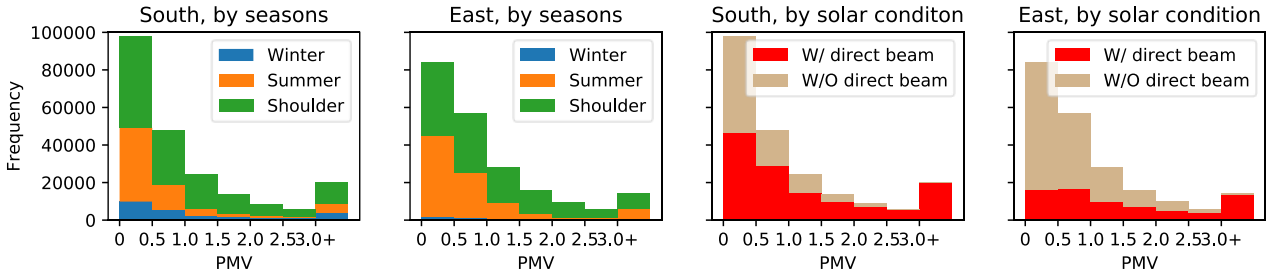

Fig 2: *Stacked* histograms of PMV for south- and east-facing zone categorized by seasons and solar conditions

As shown in Fig 2a and Fig 2b, the frequency of experiencing overheating is the lowest during the wintertime for both orientations, which is expected for a heating-dominated climate. The south-facing zone (Fig 2a), as compared to the east-facing zone (Fig 2b), has a higher overheating frequency during the wintertime due to the lower solar altitude in the winter.

Next, as shown in Fig 2c, overheating is more likely to occur in the south-facing zone during the solar irradiated hours, as is evident from the fact that a greater fraction of points with PMV > 0.5 is within solar-irradiated hours. In contrast, the east-facing zone (Fig 2d) only receives direct beam radiation during the morning hours. However, thermal mass from concrete floors and walls coupled with intense morning irradiation results in overheating that lasts throughout the day, increasing the degree of overheating during unirradiated hours.

4.2 Overheating Index and Energy Intensity

For each of the selected film products, the trade-off between overheating and energy intensity is illustrated in this section, and the results are summarized in Fig 3. In addition, given that the model used an idealized air-

climate. Therefore, solar heat gains offset the conductive heat loss through the window, which results in a decrease in the overall energy consumption. A slight increase in overall supply air energy is also observed for the east-facing zone, as compared to the west-facing zone suggesting that for a higher SHGC the increase in cooling energy offsets the reduction in heating energy.

When examining the tradeoff between energy consumption and overheating, a distinct trade-off is exhibited for all blind control cases for the south-facing zone. For the east- and west-facing zones, there is no substantial tradeoff between energy saving and thermal comfort as energy consumption remains relatively constant as thermal comfort varies. Finally, for the north-facing zone, since overheating is not significant a high SHGC (no film) may be the optimal choice with respect to energy consumption for a heating-dominated climate.

5 Conclusions and outlook

This paper applied an advanced thermal comfort assessment methodology to quantify the impact of windows in buildings. While solar control window films can minimize overheating by reducing solar heat gains,

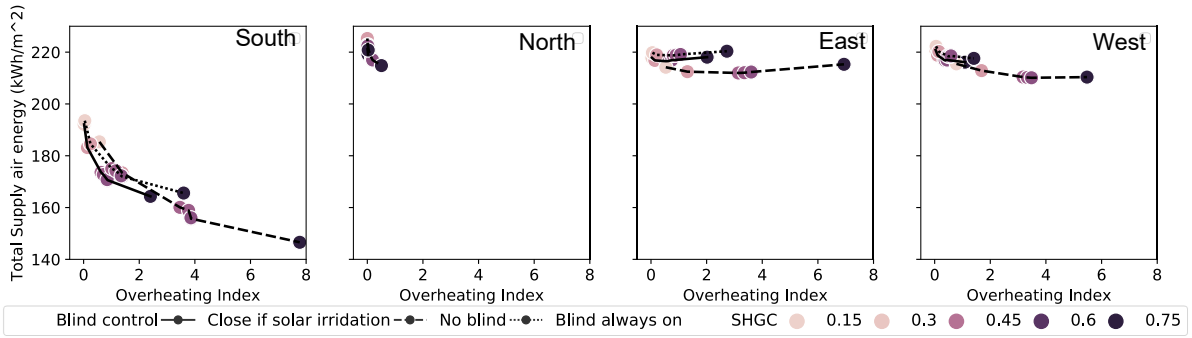

Fig 3: Trade-off between the overheating index and energy performance among selected window films

energy consumption can concurrently be increased as a result of increased heating energy requirements. In this study, the south-orientated zone demonstrated a clear trade-off between energy performance and overheating. For the east- and west-oriented zone, using a solar-control window film does not have a strong potential for energy saving, but does affect overheating. For the north-face zone, window films had little effect on energy consumption or overheating. These results may help homeowners select the correct film as a retrofitting option to optimally balance energy performance and thermal comfort. The methodology presented in this study can also be extended to identify the optimal window products for new building designs. More design choices will be explored in future studies, including electrochromic windows that can automatically adapt to changing conditions.

Acknowledgment

This research was supported by the Natural Sciences and Engineering Research Council of Canada (NSERC), [RGPIN-2016-06325], Ontario Early Researcher Award, and RDH Building Science Inc.

References

[1] G. Hatvani-Kovacs, J. Pockett, and J. W. Boland, “Does the Australian Nation id e House Energy Rating Scheme ensure heat resistance?,” 2016.

[2] N. Willand, I. Ridley, and A. Pears, “Relationship of thermal performance rating, summer indoor temperatures and cooling energy use in 107 homes in Melbourne, Australia,” *Energy Build.*, vol. 113, pp. 159–168, Feb. 2016.

[3] W. O’brien and I. Bennet, “Simulation-Based Evaluation of High-Rise Residential Building Thermal Resilience,” 2016.

[4] M. Touchie, E. Tzekova, J. Siegel, B. Purcell, J. M.-P. of the 13th, and undefined 2016, “Evaluating summertime overheating in multi-unit residential buildings using surveys and in-suite monitoring.”

[5] F. Nicol, “The Limits of Thermal Comfort: Avoiding Overheating in European Buildings: CIBSE TM52, 2013,” 2013.

[6] ASHRAE, *ANSI/ASHRAE Standard 55-2017*. Atlanta, GA: ASHRAE Special Publications, 2017.

[7] The International Organization for Standardization, “ISO 7730: Ergonomics of the thermal environment — Analytical determination and interpretation of thermal comfort using calculation of the PMV and PPD indices and local thermal comfort criteria,” 2005.

[8] P. O. FANGER, *Thermal comfort. Analysis and applications in environmental engineering.* Copenhagen: Danish Technical Press., 1970.

[9] US Department of Energy, “Input/Output Reference: The Encyclopedic Reference to EnergyPlus Input and Output,” 2015.

[10] S. Chaiyapinunt, B. Phueakphongsuriya, K. Mongkornsaksit, and N. Khomporn, “Performance rating of glass windows and glass windows with films in aspect of thermal comfort and heat transmission,” *Energy Build.*, vol. 37, no. 7, pp. 725–738, Jul. 2005.

[11] A. Tzempelikos, M. Bessoudo, A. K. Athienitis, and R. Zmeureanu, “Indoor thermal environmental conditions near glazed facades with shading devices – Part II: Thermal comfort simulation and impact of glazing and shading properties,” *Build. Environ.*, vol. 45, no. 11, pp. 2517–2525, Nov. 2010.

[12] M. Bessoudo, A. Tzempelikos, A. K. Athienitis, and R. Zmeureanu, “Indoor thermal environmental conditions near glazed facades with shading devices - Part I: Experiments and building thermal model,” *Build. Environ.*, vol. 45, no. 11, pp. 2506–2516, 2010.

[13] D. M. Kerslake, *The stress of hot environments*. University Press, 1972.

[14] E. Arens, T. Hoyt, X. Zhou, L. Huang, H. Zhang, and S. Schiavon, “Modeling the comfort effects of short-av e solar radiation indoors,” *Build. Environ.*, vol. 88, pp. 3–9, Jun. 2015.

[15] M. Sadeghipour and M. Pak, “Ladybug: a Parametric Environmental Plugin for Grasshopper To Help Designers Create an Environmentally-Conscious Design,” in *13th Conference of International building Performance Simulation Association*, 2013, pp. 3129–3135.

[16] The American Society of Heating Refrigerating and Air-Conditioning Engineers, “ASHRAE 140—Standard Method of Test for the Evaluation of Building Energy Analysis Computer Programs.” 2017.

[17] The American Society of Heating Refrigerating and Air-Conditioning Engineers, “Energy Standard for Buildings Except Low-Rise Residential Buildings.” Atlanta, GA, 2016.

[18] S. Zhang, “A simple algorithm for calculating overall SHGC and U-factor.” [Online]. Available: https://github.com/zha/window-overall-prop.

Insulation and energy performance of metal exterior curtain wall including thermal bridges

Jin-Hee Song[a,*], Dong-Yun Lee[a], Bo-Hye Choi[b], and Seung-Yeong Song[b]

[a] Research & Development Center, LOTTE Engineering & Construction, 3, Naruteo-ro 10-gil, Seocho-gu Seoul 06527, Republic of Korea
[b] Department of Architectural & Urban Systems Engineering, Ewha Womans University, 52, Ewhayeodae-gil, Seodaemun-gu, Seoul 03760, Republic of Korea
* Corresponding author, Tel +82-2-3483-7892, email cco79@naver.com

Abstract:
The improvement of the energy performance of building envelopes is of considerable importance to save energy in buildings. As a building envelope is the main path through which heat is lost or gained in buildings, its insulation performance is critical to the energy consumption of both heating and cooling. However, building envelopes incorporate various thermal bridges depending on the construction methods and components used, through which heat is transferred in either two or three dimensions. These thermal bridges lead to undesirable heat transfer, thereby resulting in a reduction of the overall insulation performance. Especially, this is considerable for metal exterior curtain walls where metal fastening components, such as steel trusses, brackets, and bolts, penetrate the insulation to be fixed to structural elements. This study aims to evaluate the effective U-value and energy performance of metal exterior curtain walls including thermal bridges. Three-dimensional heat transfer analysis was conducted to obtain effective U-values and annual heat loss and gain including two or three dimensional heat transfer through thermal bridges. Consequently, the existing and alternative effective U-values were 0.524 and 0.168 W/㎡K, respectively. The annual energy consumption of the alternative was reduced by 67.7% compared with that of the existing metal exterior curtain wall. It is shown that the heat loss and gain through thermal bridges are considerable, and such thermal bridges should be minimized to improve the thermal performance of metal exterior envelopes. Furthermore, simplified evaluating graphs of the effective U-values for metal exterior curtain walls were introduced briefly to evaluate the insulation performance easier at the early design stage.

Keywords:
Metal Exterior Curtain Wall, Thermal Bridge, Effective U-value, Annual Energy Performance

1. Introduction

Curtain walls, which are being increasingly constructed in line with the trend toward high-rise and lighter buildings, have various thermal bridges. A metal with low heat resistance is used as the main member, and the various metal members are assembled at the factory or the field. Especially, in opaque exterior wall areas where insulation is installed in the form of metal panels or back panels, various types of steel trusses, brackets, and anchor bolts are used to fix the curtain wall to the structure. Metal fasteners or fastening systems, such as anchor bolts and screws, are installed in multiple positions [1].

However, the Korean current regulations [2] for exterior wall insulation performance use the one-dimensional U-value calculated as the reciprocal of the total heat transfer resistance considering the thermal conductivity and the design thickness of each component. In the case of the one-dimensional U-values, additional heat loss in two or three dimensions from the thermal bridge cannot be considered, which makes it difficult to evaluate insulation performance accurately.

This study aims to evaluate the effective U-value and energy performance of metal exterior curtain walls including thermal bridges. For obtaining the effective U-values and annual energy consumptions of each curtain wall, the overall heat losses and gains through the evaluated areas were calculated. Three-dimensional heat transfer simulation, Physibel VOLTRA [3], was used to calculate heat loss and gain. Furthermore, simplified evaluating graphs of the effective U-values for metal exterior curtain walls were introduced briefly to evaluate the insulation performance easier at the early design stage.

2. Descriptions of metal exterior curtain walls

The metal exterior curtain wall is a non-bearing wall constituting the opaque exterior wall or the spandrel area. As shown in Fig. 1, the method of installing a separate structural member on a building structure and installing an exterior member on the structural member is called the steel truss supporting method. The term steel truss comes from the grid shape of it; a steel rectangular pipe or C-shaped frame is mainly used as the structural member, and using this, the base in grid shape is formed (truss) in the curtain wall. It can be largely divided into the exterior member and the insulation material (1), the interior material (2), the

structural member that supports the self-weight of the metal exterior curtain wall (3), the primary fastening that connects the structural member to the building structure (4), and the secondary fastening that connects the structural member and the exterior member (5).

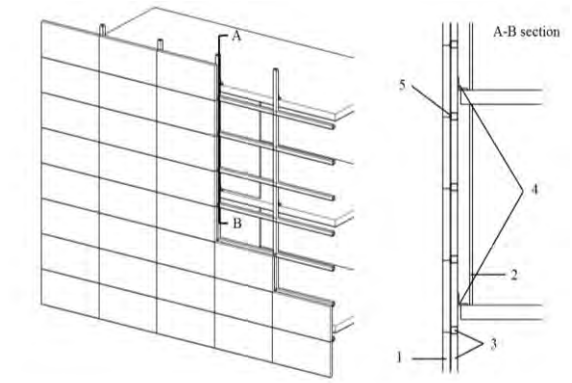

Fig 1: Steel truss supporting method

The steel truss supporting method is widely used for the dry construction of metal and stone exterior curtain walls. C. Keith Boswell [4] classifies the metal framing wall into stick, unitized, unitized on a stick, column cover, and spanned panels depending on the construction method. Among these, the unitized on a stick wall is similar to the metal exterior curtain wall in terms of the construction method and composition.

Metal exterior curtain wall using the steel truss supporting method is simple to design and construct. Moreover, it is possible to reduce the weight of the exterior wall system and shorten the construction period. In addition, it has the advantage of being cheaper than an aluminum curtain wall, and it is being increasingly used in large-scale residential complexes, accommodations, research facilities, and public buildings as well as small and medium commercial or office buildings.

3. Evaluation of insulation and energy performance

The insulation performance of metal exterior curtain walls was evaluated on the metal exterior curtain wall. Two cases were selected depending on the secondary fastening type of the metal exterior curtain wall. Case 1 and Case 2 are described as follows.

Case 1 is a commercially available product with easier installation and higher applicability in the future. It can be installed on the steel truss without penetrating the insulation layer during the secondary fastening as it uses fixing brackets as the secondary fastening. In this case, galvanized steel sheets cover the front and rear sides of the insulation with aluminum molding at the vertical and horizontal edges of the insulation (metal panel). The molding has grooves for bracket fixing, and Azon thermal breaker is inserted in the middle to reduce the heat loss along to the aluminum molding. To achieve the airtightness of the joints between the metal panels, we used the existing product with a 20-mm-long PVC foam pad attached.

Case 2 reduced the length of the aluminum molding of Case 1 to approximately one-third (26 mm) of the panel width, which is the minimum length required to insert the bracket, to reduce the linear thermal bridge owing to the aluminum molding in the joint between panels. In this case, for the remaining two-third of the metal panel width, a PVC foam pad longer than that in Case 1 was attached to prevent exposure of the metal panel internal insulation and to achieve the airtightness of the joint between the metal panels. In addition, a thermally broken bracket with an Azon thermal breaker inserted into the aluminum bracket is applied for the additional improvement of the point thermal bridges.

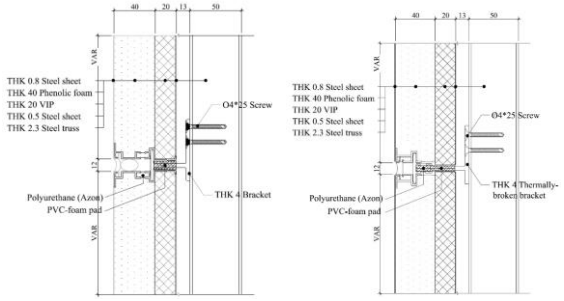

Fig 2: Section drawings of case 1 and 2

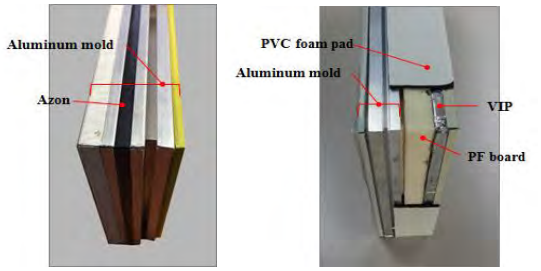

Fig 3: Product images of case 1 and 2

The insulation performance was evaluated on the representative area of the exterior wall including all the thermal bridges, as shown in Fig. 4. The material properties are as shown in Table 1.

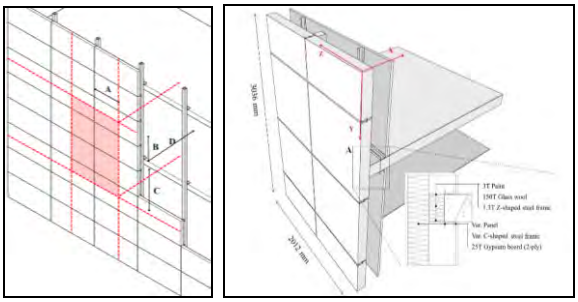

Fig 4: Representative model for the evaluation [1]

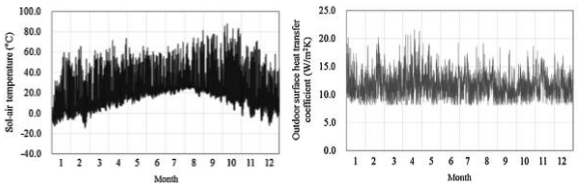

Fig 5: Outdoor boundary conditions [5]

Table 1: Material properties

Materials	Thermal conductivity (W/mK)	Density (kg/m^3)	Specific heat (J/kgK)
Concrete	1.600	2240	879
Phenolic board	0.019	65	1500
VIP	0.0042	192	850
Steel	45.00	7830	500
Aluminum mold	221.0	2740	896
Azon	0.120	1191	1347
PVC foam pad	0.0389	96.1	1434

Table 2: Annual heat loss and gain

Month	Case 1 (MJ/m^2)		Case 2 (MJ/m^2)	
	Heat loss	Heat gain	Heat loss	Heat gain
1	24.3	0.5	7.9	0.1
2	18.7	0.7	6.1	0.2
3	13.2	3.1	4.3	0.9
4	7.0	4.8	2.3	1.5
5	3.5	6.6	1.1	2.1
6	3.0	6.2	1.0	2.0
7	1.7	6.7	0.5	2.2
8	1.2	8.6	0.4	2.8
9	1.4	10.2	0.4	3.4
10	5.0	8.2	1.6	2.6
11	12.8	3.2	4.2	0.9
12	19.1	0.3	6.2	0.1
Total	110.9 (-)	59.0 (-)	36.0 (-67.5%)	18.7 (-68.2%)

The annual heat loss and heat gain per unit area are as shown in Table 2 and Fig. 6. For evaluating annual heat loss and gain, the indoor set point temperature is 20°C in winter, 26°C in summer, and 23°C in autumn and spring. As well, the sol-air temperature in Seoul is used for the outdoor boundary condition as shown in Fig. 5. The annual heat loss was 110.9 MJ/m^2 for Case 1 and 36.0 MJ/m^2 for Case 2, showing a decrease by 67.5%. The annual heat gain is half the heat loss, i.e., 59.0 MJ/m^2 for Case 1 and 18.7 MJ/m2 for Case 2, showing a decrease by 68.2%.

Fig. 6 graphically shows the hourly heat loss and gain for a typical week in winter and summer. The winter week was from January 15 to 21, and the summer week was from August 1 to 7. In the case of winter, the heat loss occurs in general; especially at nighttime, the heat loss increases significantly. In the daytime, the heat loss decreased owing to the effects of solar irradiance, and some heat gain occurred on the day with high solar irradiance. The difference in heat loss between Case 1 and Case 2 increases at night when the heat loss increases, and the difference in heat loss decreases during daytime.

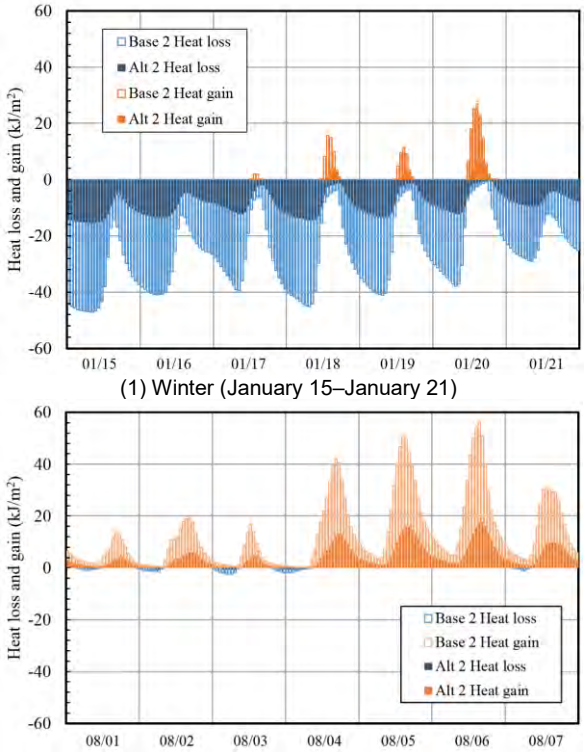

(1) Winter (January 15–January 21)

(2) Summer (August 1–August 7)

Fig 6: Heat loss and gain in winter and summer

Case 2 greatly improves the insulation performance and can significantly reduce the heat loss and heat gain through the exterior wall, leading to saving of annual energy cost. In addition, construction costs are slightly reduced compared with Case 1 [5], and the building life cycle costs are expected to be greatly reduced. Therefore, if the thermal bridge reduction method is applied to actual buildings, there will be sufficient benefits in terms of energy saving and overall life cycle cost.

4. Results and discussions

The thermal bridge of metal exterior curtain walls degrades the insulation performance considerably. Hence, the development and application of the thermal bridge reduction method are necessary in saving energy in actual buildings. The actual impact of reduction of life cycle costs is also observed to be

significant. However, there is a lack of awareness of thermal bridges and its effect of the actual insulation performance of the metal exterior curtain wall at the design and construction stage. Even in the U-value evaluation of metal exterior curtain walls according to the domestic regulations for insulation performance, the effects of thermal bridges are not included. There are very few design guidelines and evaluation tools of insulation performance for reducing thermal bridges.

For the example of simple evaluation tools, the existing study [5] suggested a tool for insulation performance evaluation including thermal bridges by drawing effective U-value evaluation graphs. In order to draw the graphs, design factors that determine the insulation performance of metal exterior curtain walls are derived.

As shown in Fig. 7, the design factors can be defined as length(T1~3), thermal conductivity(λ2~3), and heat resistance(R1) of insulation materials and air cavities. Additional design factor to determine the thermal bridge effect can be defined as sealant width(L4), sealant effective thermal conductivity(λ4), joint width(L5), joint thickness(T5), and additional truss insulation(λ6). The experiment to analyze the effect of the design factors on the insulation performance was designed by DOE (design of experiment) and the experimental cases according to the level of each design factor were obtained. The results for each case were statistically analyzed.

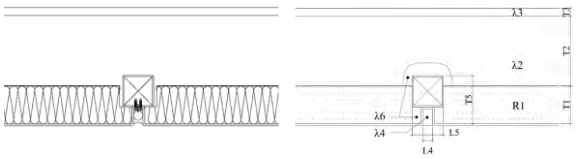

Fig 7: Design factors of metal sheet-type curtain walls

Based on the results of above experiments, the main variables for drawing effective U-value evaluation graphs were determined. The y-axis of the graph was set to the effective U-value, and the x-axis was set to the insulation thickness. The insulation heat resistance level is set to 3.7, 5.0, 6.7 m^2K/W, respectively. If the effective U-value was not significantly affected or the contribution was less than 5%, it was not included as a variable in the graph.

The effective U-value of sheet-type metal exterior curtain walls with size of a rectangular steel truss and with an insulation layer of specific thickness and heat resistance can be evaluated using the graph. In addition, for the additional insulation rear to the steel truss, the improvement in the effective U-value can be easily observed. In addition, it can be used as a design guideline to attain desired insulation performance when designing sheet-type metal exterior curtain walls. In the graph, the narrower the width and height of steel truss, and the thicker the insulation layer, the better is the insulation performance for the same heat resistance.

5. Conclusions and outlook

Based on the above findings, the reduction of thermal bridges of metal exterior curtain walls can contribute to the reduction of building energy by improving the insulation performance of exterior walls. It is beneficial in terms of energy and life cycle costs. Further research and development are required to reduce the thermal bridge of metal exterior curtain walls.

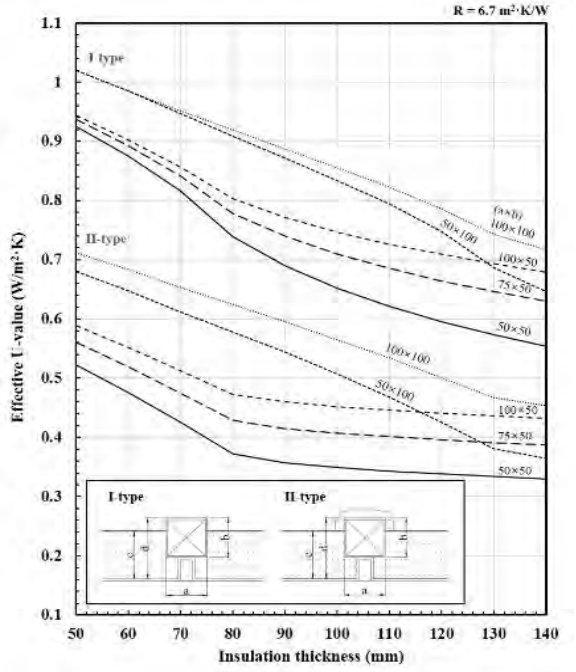

Fig 6: Effective U-value evaluation graph (R=6.7)

In addition, the effective U-value evaluation graph of the metal exterior curtain walls can be used for the simplified evaluation of the effective U-value in the design stage and for the determination on the design factor level of the optimal thermal bridge area to satisfy the required insulation performance standard for insulation design.

Acknowledgements

This research was supported by a grant(19RERP-B082204-07) from Residential Environment Research Program funded by Ministry of Land, Infrastructure and Transport of Korean government.

References

[1] J. Song et al., Influence of thermal bridges on the insulation performance of curtain wall panel systems, J. Asian Archit. Build. Eng. 14 (3) (2015) 741–748.

[2] The Code for Energy-efficient Building Design, Ministry of Land, Infrastructure and Transport (MOLIT), Republic of Korea (2013)

[3] Physibel VOLTRA Manual, Physibel

[4] C. Keith Boswell, Exterior Building Enclosures – Design Process and Composition for Innovative Facades, WILEY (2013)

[5] J. Song, Development of Alternatives for Reducing Thermal Bridges and Simplified Evaluation Method for Effective U-values of Metal Panel Curtain Walls, The Graduate School of Ewha Womans University, Ph.D. thesis (2016)

Development of assessment criteria for overheating risk analysis in buildings

A. Laouadi*, M. Bartko, M.A. Lacasse

Construction Research Centre, National Research Council Canada
1200 Montréal Road, Ottawa, ON K1A 0R6

* Corresponding author: Tel (613) 990 6868, email: aziz.laouadi@nrc-cnrc.gc.ca

Abstract:
Overheating in buildings arising from global warming and extreme heat events (EHEs) is a growing health concern in urban areas of many countries. Overheating is the condition of the indoor environment that results in thermal discomfort or heat-related health stress to building occupants. Overheating is found in naturally ventilated buildings, buildings with limited cooling capacity or intermittent use of air conditioning, and buildings that experience extended periods of power outages or HVAC failure. Despite the extensive studies on this topic, there is a lack of a standard approach to analyse the overheating risk. This paper develops a framework to analyse the risk of overheating in buildings from the perspective of comfort and health of occupants through the use of building simulation. The framework includes four steps: (1) Generation of reference climate data for the historical period and future projections to extract various types of EHEs; (2) Development of heat stress metric to quantity the effect of heat on the comfort and health of occupants; (3) Generation of reference summer weather years for building simulation; and (4) Development of assessment criteria for overheating risk.

Keywords:
Extreme Heat Events, Overheating, assessment criterion, buildings, climate change.

1. Introduction

Overheating in buildings arising from climate change and extreme heat events (EHEs) is a growing health concern in many countries [1-4]. Overheating is the condition of the indoor environment that results in thermal discomfort or heat-related health stress to building occupants. Overheating is found in naturally ventilated buildings, buildings with limited cooling capacity or intermittent use of air conditioning, and buildings that experience extended periods of power outages or HVAC failure. In those buildings, the indoor conditions are consequences of the outdoor conditions, but they may be altered by building constructions and occupant behavior (e.g. opening windows). Continuous exposure to high temperatures over several days strains the human physiological system and may lead to health issues (such as heat cramps, exhaustion, and stroke) or death, particularly for vulnerable people such as the elderly, the sick and children. Indeed, epidemiological studies have found that the excess mortality data during EHEs are higher than any other natural hazard such as floods and storms [3,5,6]. To reduce the risk of overheating, buildings should be designed and operated to be resilient under such extreme climatic conditions. Current design and retrofit of buildings use reference (average or typical) weather years to conduct whole building energy simulations. These reference years may not, however, be suitable to assess the risk of overheating and therefore new reference summer weather years (RSWY), selected from multi-year climate data with various types of EHEs, need to be developed. Development of such reference years requires the use of proper metrics to rank and select representative years having periods of EHEs. Furthermore, the metrics should take into account not only the climate variables, but also the human subjects that are exposed to such EHEs to permit the evaluation of their thermal comfort and heat-related health stress. The Chartered Institution for Building Services Engineers (CIBSE) developed the Design Summer Year (DSY) as the third hottest summer within a 21 year climate data set based on the daily average dry bulb temperature from April to September [7]. Due to the limitations of DSY in predicting known local EHEs, CIBSE [8] has later adopted three types of probabilistic design summer years (moderately warm: pDSY-1, intense: pDSY-2, long and intense: pDSY-3) developed by Eames [4] based on the Weighted Cooling Degree Hours method and the adaptive thermal comfort threshold temperature. Liu et al. [9] used the heat stress metric of the physiological equivalent temperature (PET) to develop probabilistic hot summer years (pHSY) as alternatives to pDSY. As for overheating definition and assessment, there is no universal or agreed-upon methodology [10]. The current definitions are mostly based on the threshold temperatures of the static or adaptive thermal comfort for healthy people [11, 12]. Vulnerable people who would suffer the most from excessive heat are therefore not explicitly addressed.

The goal of this paper is to develop a framework to analyze overheating risk in buildings through the use of building simulation. The specific objectives include the development of: (1) reference summer weather data years; (2) a physiological metric to quantify the effect of heat on thermal comfort and health of human subjects, and to discern outdoor and indoor heat events; and (3) criteria to assess overheating risk.

2. Approach

The proposed framework consists of the following four steps:

1. Generation of reference climate data for the historical period and future projections to extract various types of EHEs;
2. Development of a heat stress metric to evaluate the effect of heat on thermal comfort and health of human subjects;
3. Generation of reference summer weather years (RSWY) to be used for building simulation in selected Canadian cities; and
4. Development of assessment criteria for overheating risk.

3. Reference climate data

Climate data are needed to conduct building simulation. The reference climate data for the historical period and future climate projections (seven scenarios) were collected from the climatic databases of Environment and Climate Change Canada [13]. A methodology was developed to bias-correct the weather variables and produce hourly weather files for selected 11 Canadian cities. More details may be found in Gaur et al. [14]. For the historical period, the most recent data were collected for the period 1986-2016. For each city domain, the weather data were obtained from the associated weather stations and then averaged to produce a single weather file for the selected city. Any missing observational data were filled-in using bias-corrected data from the Climate Forecast System Reanalysis (CFSR) database [15]. For the future climate projections, the simulated climatic database using the CanRCM4 Large Ensemble model with regional corrections were used to extract climatic projections for each city spanning the period 1950 – 2100. The simulated climate data for the historical period 1950-2016 was used to derive bias correction factors for the future years. A set of 15 (parametrizing various cloud physics) simulations comprising of bias-corrected hourly weather data were produced for each city and each future climate change scenario.

4. Metric for heat events

Heat events are time and location dependent. People exposed to such events will undergo heat stresses resulting in thermal discomfort (e.g., sweating) and potential health issues (i.e., dehydration, heat cramps, etc.). Such heat events may also be fatal, particularly for vulnerable people such as the elderly, the sick and children. There exist many heat stress indices for healthy young adults with various degrees of complexity and limitations [16]. A list of suitable indices was compiled from literature and compared against some screening criteria. More details may be found in Laouadi et al. [17]. The standard effective temperature (SET) was selected for this purpose. SET is defined as the temperature of an imaginary indoor environment at 50% relative humidity and mean radiant temperature (MRT) equal to the air temperature, in which an imaginary subject wearing clothing standardized for the activity level has the same heat stress and strain as in the actual environment [18]. SET is calculated using the transient two-node bioheat model of Gagge et al. [19]. The SET bioheat model was modified to suite the transient nature of heat events and subject activities during day and night times. These modifications included fine tuning of some input parameters, accounting for the solar radiation in the MRT definition, incorporation of thermoregulatory controls of a sleeping person, and incorporation of the time limit of exposure algorithms of ISO [19].

The SET index was used to define instantaneous heat events. A heat event is declared when the instantaneous SET value exceeds a threshold value (SET_c). Threshold values are established for outdoor and indoor exposures during daytime when subjects are active and nighttime when subjects are sleeping. Similarly, thresholds for vulnerable subjects may be defined. In this paper, a threshold value corresponding to the initiation of sweating (or slightly warm sensation) of SET_c = 30°C is chosen for r indoor exposure during daytime and SET_c =26°C for sleeping subjects during nighttime. For vulnerable subjects, the threshold SET_c was fixed to 26°C for both day and night time exposures. For outdoor exposure, the thresholds of SET are provided in [22]. For acclimatized subjects, 1.2°C is added to the threshold value. Outdoor heat waves are declared when the cumulative SETH quantity is non zero over at least one or more consecutive days. SETH (°C*hour) is expressed as:

$$SETH = \sum_{days} \sum_{1}^{24} (SET - SET_c) \cdot t \qquad (1)$$

Where t (hours) is the exposure time. The time is counted from the sleeping time to the sleeping time of the following day to account for the effect of sleep disturbance on the physiological response of subjects during daytime exposure. Heat waves are characterized by three features: Duration (number of consecutive days with SETH > $SETH_{min}$ = 4), severity (SETH) and intensity (severity/duration/24; in °C).

5. Generation of RSWY

RSWYs are extracted from a 31 year period of climate data (historic or future) to capture all types of heat waves [22]. The summer period was fixed from May to September for Canadian locations (it may be different for other international locations). The methodology to develop such weather data includes the following steps:

1. Heat waves for each year of the 31 period are identified and sorted by maximum duration, intensity, and severity. The maximum values are assigned to each year.
2. The return period of heat waves is fixed to 15.5 years, which corresponds to the second extreme year out 31 years.
3. The cumulative frequency distribution of the maximum values of duration, intensity and severity are plotted and fitted with suitable distribution functions. The extreme years are then chosen, if their calculated return periods are close to the fixed value of 15.5 years. In most cases, the extreme years are those ranked second by their heat wave maximum values for duration, intensity or severity. If the first ranked years have the same frequency values or are very close, the year with

the highest severity value is chosen to represent the second extreme year as the first extreme year is not known in this case. Similarly, if the second ranked extreme years have the same frequency values, the one with the highest severity value is chosen.

Three types of RSWY (with long, intense and severe heat waves) are thus established to assess the overheating risk in indoor spaces using building simulation. Table 1 lists the extreme years for selected Canadian cities as obtained by the proposed method.

Table 1. Extreme years for selected Canadian cities

City	Long	Intense	Severe
St John's, NF	1990	1990	1990
Charlottetown, PEI	2002	2002	2002
Halifax, NS	1988	1988	1988
Moncton, NB	1997	2013	2002
Montréal, PQ	2010	2010	1987
Ottawa, ON	2010	2006	2010
Toronto, ON	1987	2006	2011
Winnipeg, MB	2005	2007	1995
Saskatoon, SK	2002	1988	1988
Calgary, AB	2007	2007	2007
Vancouver, BC	1989	1989	1989

Figures 1 and 2 compare the hourly SET values during the heat wave periods as obtained by the proposed NRC and CIBSE methods for outdoor and indoor exposures in Ottawa (Ontario), respectively. The CIBSE method [8] uses temperature and the Weighted Cooling Degree Hours (WCDH) method, which is a quadratic sum of the operative temperature deviation from the upper temperature of the adaptive thermal comfort. The proposed method yields the extreme year with long heat waves of 2010 (July 5 to 11), and CIBSE method yields the year of 2012 (Jul. 11 to 17). The indoor SET were calculated for an archetype single detached house without air conditioning. Typical old (1980) constructions and air leakage data were assigned to the house model. Windows are double glazed, distributed over the four facades of the house and equipped with internal Venetian blinds which remain open (slats are horizontal) during the summer period. The house is made of four thermal zones: basement, first floor, second floor (bedrooms) and attic space. The SET values in equation (1) were assigned those calculated for the first floor during daytime (7:00 AM to 22:00 PM) and the second floor for nighttime. In terms of SET, the proposed method yields extreme years that are more extreme than the CIBSE method. In terms of temperature (not shown here), the CIBSE method may yield comparable or higher maximum daytime temperatures, but lower nighttime temperatures than the proposed method. The CIBSE method may therefore lead to the under-estimation of the heat-related health effects, particularly in warm/hot and humid areas.

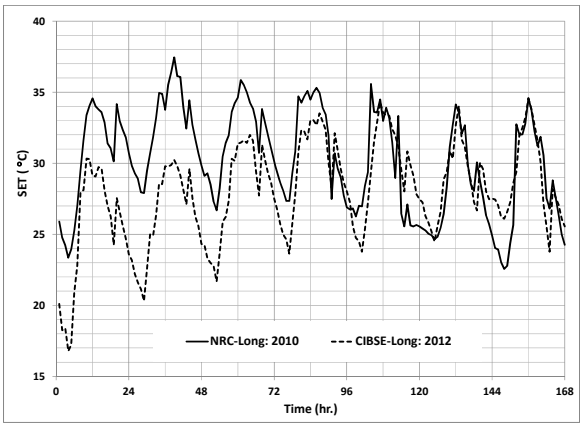

Figure 1. Comparing the outdoor SET of extreme years with long heat waves as obtained by NRC and CIBSE methods for Ottawa

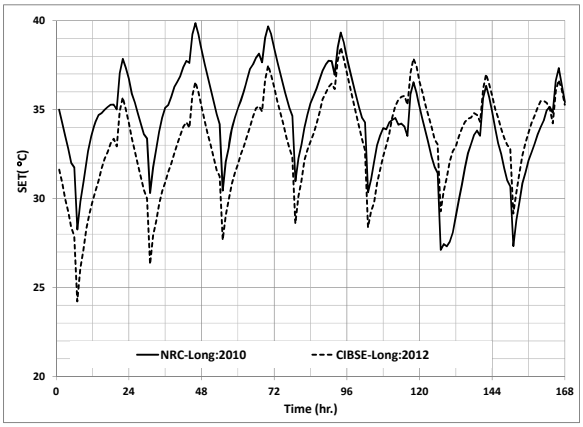

Figure 2. Comparing the indoor SET of extreme years with long heat waves as obtained by NRC and CIBSE methods for Ottawa

6. Assessment criterion for overheating

An indoor overheating event is similar to outdoor heat events, and is thus defined as it relates to the subject under its exposure but not to the fixed space domain which may be unoccupied over certain time periods (e.g., bedrooms are occupied at nighttime versus living rooms occupied during daytime; office or school spaces are occupied only during working hours; patient rooms are occupied 24 hours; etc.). Equation (1) is therefore used as a metric to assess the severity of overheating. The instantaneous value of SET in equation (1) takes on the values calculated for the occupied spaces only during daytime or nighttime with respective SET thresholds. In a typical warm or hot year, there may be more than one heat wave occurring in the summer period, and as a result more overheating events with different severities may occur indoors. To declare that a space is overheated, the severity metric SETH (equation 1) for any overheating event during the summer period should exceed a threshold value ($SETH_c$). This threshold value is calculated based on the total water loss by sweating (dehydration) of subjects exposed to the overheating events.

Dehydration was the leading cause of mortality followed by heatstroke during the 2003 heat wave in France [21]. ISO [20] recommends the maximum allowable dehydration rate of 3% of body weight for healthy people, and indicates that higher dehydration rates are associated with increased heart rates and reduced sensitivity to sweating due to reduced plasma volume of blood. However, for the vulnerable subjects, the maximum dehydration rate should be lower due to age-related changes in their physiology (kidney function, thirst perception, lower body water content. The dehydration rate may be relaxed if subjects rehydrate themselves. The proposed method assumes the rehydration rate of 60% of ISO [20]. The overheating is calculated for the three types of extreme summer years.

Figure 3 shows the severity of overheating (SETH) versus the body water loss for healthy adult subjects under indoor exposure in residential buildings. Based on the body water loss criteria as mentioned before, overheating is declared when the SETH is greater than 127 (°C*h).

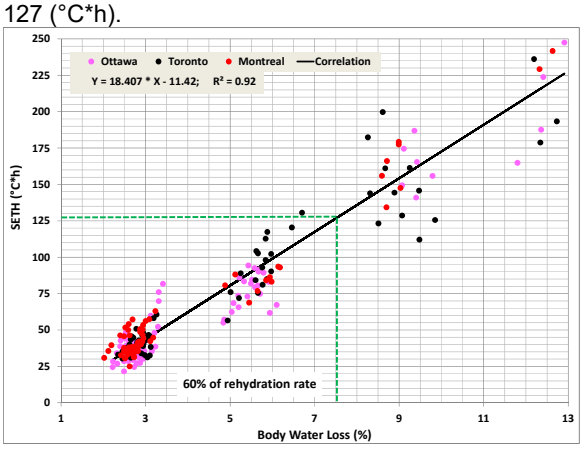

Figure 3. Severity of overheating versus body water loss for healthy subjects

7. Conclusions and outlook

A framework was developed to analyse the risk of overheating in buildings from the perspective of comfort and health of occupants. The framework included four steps: (1) generation of reference climate data to extract various types of extreme heat events at given locations; (2) development of a heat stress metric to evaluate the effect of heat on the comfort and health of human subjects; (3) generation RSWY for 11 Canadian cities; and (4) development of assessment criteria for overheating risk.

The reference historical climate data and future projections were taken from the most recent climate databases from ECCC [13]. The climate data were bias-corrected to produce hourly weather files for 11 Canadian cities.

The SET bioheat model was selected and modified to account for the transient nature of heat events and daily activity levels of subjects, and the physiological response of sleeping person. The transient SET index was used to assess outdoor or indoor heat events based on a set of threshold values for active and sleeping subjects. The severity index (SETH) which is the product of the SET deviation from the threshold value and the exposure time of heat events was used to generate RSWY in 11 Canadian cities. The overheating risk is declared when the SETH exceeds a threshold value of 127 (°C*h), which limits the critical dehydration of subjects during the heat wave periods.

Acknowledgements

This work was carried out by the National Research Council of Canada with funding from Infrastructure Canada in support of the Pan Canadian Framework on Clean Growth and Climate Change. The authors are very thankful for the support.

References

[1] CIBSE. 2005. TM36-2005. London, UK.
[2] HC. 2011. Extreme Heat Events Guidelines. Health Canada, Ottawa.
[3] Saman et al. 2013. National Climate Change Adaptation Research Facility, Gold Coast. PP. 242.
[4] Eames, M.E. 2016. Building Services Engineering Research and Technology. 37: 503-522.
[5] Kenny et al. 2018. Temperature. 1‑26.
[6] Berko et al. 2014. Natl Health Stat Report. (76):1-15.
[7] Levermore, G.J., Parkinson, J.B., 2006. Building Services Engineering Research and Technology, 27(4), pp.311–325
[8] CIBSE. 2014. TM49-2014: Design Summer Years for London. London, UK.
[9] Liu et al. 2016. Build. and Env. 105: 56-68.
[10] Anderson et al. 2013. Perspectives in Public Health; 133(3):158‑164.
[11] CIBSE. 2015. Guide A. London, UK.
[12] Mohamed H. M.H., Hensen J.L.M. Proc. Build. Sim. 7-9 Dec. 2015, Hyderabad, India (pp. 1-8).
[13] ECCC. 2018. Environment and Climate Change Canada. http://climate.weather.gc.ca/.
[14] Gaur et al. 2019. Data, 4, 72.
[15] Saha et al. 2010. Research Data Archive at the National Center for Atmospheric Research, Computational and Information Systems Laboratory.
[16] Walls et al. 2015. Proc. of the 49th Int. Conf. of Arch. Sc. Ass. The Univ. of Melbourne, Australia.
[17] Laouadi et al. 2019. Development of Framework for Overheating Risk Analysis. Report: CRBCPI-Y3-R8. NRC. Ottawa.
[18] ASHRAE. 2017. ANSI/ASHRAE standard 55-2017. Atlanta, GA.
[19] Gagge et al. 1986. AHSRAE Transactions 92: 709-731.
[20] ISO. 2004. ISO 7933:2004. Geneva, Switzerland.
[21] Fouillet et al. 2006. Int. Arch. Occup. Environ. Health. 80(1):16-24.
[22] A. Laouadi, A. Gaur, M. A. Lacasse, M. Bartko & M. Armstrong (2020) Development of reference summer weather years for analysis of overheating risk in buildings, JBPS, 13:3, 301-319.

On the implementation of thermal bridge calculations in the Belgian building code

N. Van Den Bossche[a,*], L. Landuyt[a], A. Janssens[a]

[a] Ghent University, Faculty of Engineering and Architecture, Department of Architecture and Urban Planning, Sint Pietersnieuwstraat 41 B4, 9000 Ghent, Belgium
* Corresponding author, +32 476 97 85 91, nathan.vandenbossche@ugent.be

Abstract:
Numerical tools for two-dimensional or three-dimensional heat transfer are readily available to the building professional to calculate the thermal transmittance of thermal bridges. However, designers need appropriate limits to compare the predicted performance and decide whether it is necessary to improve the detailing. This paper presents a methodology and suggestion for such limiting values. For 5 building typologies all building envelope interfaces were evaluated. For each interface the design was modified to reflect 'business-as-usual', 'standard', or 'thermal bridge avoidance' approach, and the overall impact was evaluated for different insulation levels. The resulting limiting values differ as a function of thermal bridge geometry and take into account the technical feasibility of the requirements. However, when such limits are introduced in a building code, this would imply that every single building envelope interface in every project needs to be simulated. Hence, there is a clear need for a straightforward methodology for the building practice to handle thermal bridge evaluation. In this paper the Belgian approach is presented, which uses easy to apply rules of thumb to check whether a specific building envelope interface is code-compliant. These rules of thumb are based on extensive simulations, and can be applied using only the geometrical information and thermal conductivities of building nodes. Finally, an approach is presented to implement this methodology in an overall heat loss calculation that can cope with different types of input (code-compliant, non-code-compliant, and numerically simulated).

Keywords:
Thermal Bridge, Heat Loss Calculation, Building Code, Numerical Simulations

1. Introduction

The Energy Performance of Buildings Directive (EPBD) in Europe has entailed a standardised energy calculation method and mandatory software in Belgium that was implemented in 2006. As the EPBD did not explicitly require to account for energy loss due to thermal bridge effects, a comprehensive methodology was only developed in 2010 on a national level and implemented in 2011. The main goal was to provide a pragmatic approach that allows an easy implementation by building practitioners. Based on a selection of case-studies it was found that even rather simple residential buildings easily comprise over 30 different building envelope interfaces. The number of point thermal bridges, or situations where important 3D effects come into play is more sensitive to the specific definition. Consequently, a correct calculation would require dozens of building nodes to be simulated in numerical software, an accurate measurement of building envelope length and number of point thermal bridges, and as well, a system to check the accuracy of the simulations and calculations. Such a methodology would entail a large burden on the building industry. In the Belgian context a simplified approach was developed that allows to take the additional energy loss into account, with a reasonable trade-off between accuracy and feasibility. For more literature on thermal bridges and an overview of thermal bridge software, please refer to the Final Report of the European ASIEPI-project (Erhorn et al, 2010). EN ISO 10211 provides guidelines to calculate complex thermal bridges by a linear (W/m.K) or point (W/K) heat transmission coefficient, which is subsequently multiplied with the respective length and number for a specific building. For the majority of European countreis, the detailed calculation of thermal bridges according to this standard is an accepted option to to account for thermal bridge associated energy losses. Other European countries have developed more simplified approaches. The most simplified method is by adding a correction factor ΔU to the U-value of the different envelope areas to take thermal bridging into account (e.g. The Netherlands, Germany, Poland, Spain). More precise, but often still simplified, is the use of tabulated values for specific details or the application of a thermal bridge atlas (e.g. Denmark, France, Germany, Spain) (Roels et al., 2011).
In Belgium, a different approach was developed. Firstly, the typical impact of thermal bridges on energy loss was evaluated for a range of building geometries and building envelope interface design principles. Subsequently, specific limits for linear thermal transmittance were set that take into account geometric and technical boundary conditions. Thirdly, simplified rules of thumb were developed for the building industry, for which detailed simulations were done to ensure that these in fact entail limited additional heat losses in accordance to the linear thermal transmittance values. Finally, an overall approach was developed to incorporate additional energy losses due to thermal bridges in the building code, while maintaining the flexibility to choose a

detailed numerical approach, simplified rules of thumb, default values for poorly designed thermal bridges, or a combination thereof.

2. Impact of thermal bridges on transmission heat loss

To create a better understanding of the relative importance of thermal bridges, the two-dimensional transmission heat loss resulting from all junctions encountered in five typical masonry cavity wall dwelling designs was quantified. The reference dwelling designs have been developed in the framework of a research project on the optimization of building envelopes and services for low-energy residential buildings. The five dwellings are all single-family houses with the same program (four-person families) and the same useful floor area, corresponding to national statistical figures. The dwellings only differ in typology and building compactness, ranging from a detached bungalow to a flat in a six-floor apartment building.

The transmission heat loss related to linear thermal bridges was analyzed for each of the dwellings. The building envelope consisted of traditional constructions that are most commonly found in the Belgian housing stock: insulated cavity walls, warm flat roofs with concrete floors, insulated cathedral ceilings with wood-frame structures, concrete ground floors and floors above grade, etc. To determine a representative linear transmittance for each junction, the two-dimensional heat loss was calculated assuming a thermal insulation thickness of 20 cm (≈ 0.2 W/m2·K). Note that for larger insulation thickness the linear thermal transmittance becomes rather stable, which allows a safe implementation when using standard values.

The analysis is based on three different scenarios with respect to the thermal quality of building details. The difference between the three scenarios is illustrated in Figure 1.

1. **Business as usual**. In this scenario, typical structural intrusions in the thermal insulation are present at window reveals, roof eaves, etc., but not at junctions between the façade and the inner walls and floors. This corresponds to poor building practice in Belgium.
2. **Standard**. In this scenario, the insulation layer is no longer interrupted around window junctions, but structural breaks at other locations (eaves, bearing walls, etc.) remain unsolved.
3. **Thermal bridge avoidance**. In this case, different techniques were applied to achieve continuous insulation over the building envelope. At all structural connections, specific thermal-break materials or components are present to minimize supplementary heat loss.

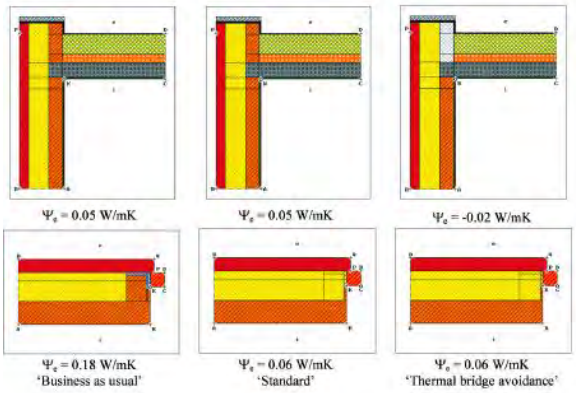

Fig 1: Typological examples (above: roof eaves; below: window reveal) of building junctions for three scenarios with respect to the thermal quality of building details.

The linear thermal transmittances of all building details have been calculated by means of Physibel software. The highest transmittance values are found at junctions where the insulation layer is intruded by a structural concrete floor, such as at balconies. The lowest (negative) values are found at exterior corners where the insulation layer is uninterrupted, such as at building corners and at roof eaves. However, for all detailing scenarios, the two-dimensional heat loss at window junctions is the largest compared to other junctions. Even when the window details are optimized (standard scenario), their influence is still about 40% of the total specific heat loss for all junctions.
Subsequently, the contribution of thermal bridges to the overall thermal transmittance of the buildings was calculated. The increase of the average thermal transmittance as a result of two-dimensional heat transfer at building junctions is given in Figure 2 for the five different reference dwellings.

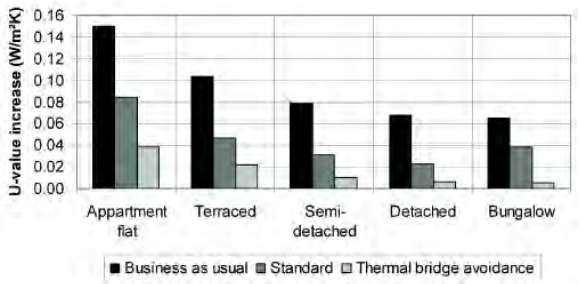

Fig 2: Contribution of building junctions to the average thermal transmittance of the building envelope as a function of the quality of constructional detailing.

The relative importance of building junctions on transmission heat loss increases when the building geometry becomes more compact. When insufficient attention is paid to the avoidance of thermal bridges, the contribution of building junctions to the overall thermal transmittance amounts to 0.06 to 0.15 W/m2·K. Compared to the current requirements in

Flemish building regulation, the construction details thus represent 13% to 17% of acceptable transmission heat loss. These results are obtained with the external building dimensions as a reference for the heat loss surface area. Of course, when internal dimensions are the reference, the heat transfer at building junctions becomes even more important. When attention is paid to thermal bridge avoidance in construction detailing, the contribution of building junctions to the thermal transmittance may be minimized to 0.01 to 0.04 W/m2·K. This represents only 1% to 4% of current transmission heat loss requirements. In low-energy building design. This quality of detailing is certainly necessary to obtain a sufficiently low average thermal transmittance of the building envelope.

3. Limits for linear thermal transmittance

Based on the analysis of thermal bridges for 5 different buildings in the previous section, a new set of limits for linear thermal transmittance was proposed, with limiting values adjusted to the geometrical typology of different junctions (table 1). When a building design meets this set of requirements, the effect of building junctions on transmission heat loss is limited to 0.02 W/m2·K for less compact buildings and to 0.05 W/m2·K for more compact buildings. As a result, the effect of thermal bridges on the thermal transmittance of the building envelope is less than 5%, except for the more compact building types. These figures are found when the limiting values for linear thermal transmittance proposed below are introduced in the analysis of the five reference dwellings.

External wall corners	**ψ < -0.10 W/mK**
Junctions at exterior corners	**ψ < 0.00 W/mK**
Junctions at interior corners	**ψ < 0.15 W/mK**
Balconies	**ψ < 0.10 W/mK**
Window junctions	**ψ < 0.10 W/mK**
Foundations	**ψ < 0.05 W/mK**
Other	**ψ < 0.00 W/mK**

Table 1. Limit values for linear thermal transmittance

These values can thus be used by the building industry to check whether a certain building node is well-designed. The results of numerical simulations are compared to these limiting values. The analysis showed that these performance limits are easily obtained at minimal cost.
Furthermore, these values can also be used as reference value to account for the impact of thermal bridges on the overall energy use of buildings. When the building code was adjusted to take the building nodes into account, an additional heat loss was automatically assigned for each building. As of that point, there was an increase in transmission heat loss in accordance with the values above. Because this supplementary heat loss is automatically calculated, the basis, reference energy calculation thus already assumes that building nodes entail additional heat loss, but as well, that all nodes meet the limits for linear thermal transmittance. By consequence, for the implementation of the thermal bridge effect in the energy calculation, all building nodes that meet the requirements are already accounted for.

4. Practical implementation

By integrating a default energy loss for building nodes, the additional work for the building industry can be significantly reduced. When a node meets the requirements, it is not even necessary to check the length, or the number of building nodes. Hence, the practical implementation has following goals:

- Check whether building nodes meet the requirements
- If not: calculate the linear thermal transmittance, and subtract the limit values (this part is already accounted for)
- If no calculation is done: apply a default conservative, high linear thermal transmittance.

However, the first aspect is not self-evident. To ensure that not every building node in every project needs to be calculated, simple rules of thumb were developed for the building industry. The system works as follows: first one needs to choose between 3 options.

- Option A: detailed method. Every node is numerically calculated, and there is a variable increase in transmission heat loss.
- Option B: pragmatic approach with 'EPB-accepted nodes'. The building nodes are classified into two categories: EPB-accepted, and the other. The first ones can be neglected, the second type entails a variable increase in total thermal transmittance, evidently smaller than the one for option A.
- Option C: there is a fixed penalty, i.e. a large value of 10W/K is applied to the overall thermal transmittance, which can add up to more than 30% for standard buildings.

5. EPB accepter nodes

Option B with the EPB-accepted nodes is a pragmatic approach, which at the same time increases the awareness of good thermal detailing towards the building practitioners involved in the project. The basic rules are defined in such a way that designers, contractors and inspectors can - mainly in a visual way - check whether a detail fulfils the requirements to be an 'EPB-accepted' node. Essentially, the basic rules guarantee a continuous insulation layer within the building envelope.

<u>Basic rule 1: minimal contact length</u>
This rule requires that two connecting insulation layers need a sufficient contact length, which is at least half the thickness of the thinnest insulation layer. The contact length criterion followed from detailed

calculations for all kind of different junctions, which showed that when the contact length is at least half the thickness of the thinnest insulation layer, the extra losses at the junction were minimal.

Basic rule 2: insertion of insulating element
When at a junction of two building envelope parts, it is not possible to bring the insulation layers within each element in contact with one another, an intermediate insulating element has to be foreseen that fulfils certain requirements:

- λ-value should be below 0.2 W/mK
- the thermal resistance R of the intermediate element has to be at least half the smallest thermal resistance of the adjacent insulation layers
- the contact length between insulating elements and adjacent layers has to fulfil basic rule 1

In practice, the majority of the connections and nodes appearing in the building envelope could be covered with an acceptable thermal performance level with basic rules 1 and 2. However, for some specific junctions where the continuity of the insulation layer cannot be guaranteed due to structural requirements (e.g. foundations bearing a heavy load, certain wall-floor connections and balconies), basic rule 1 and 2 are often not applicable. To avoid also for those details complex and time-consuming calculations, while still promoting a good thermal performance, a third rule has been added.

Basic rule 3: path of minimal thermal resistance
In those specific cases where basic rules 1 and 2 cannot be applied, the energy loss can be limited by ensuring a sufficiently long pathway from inside to outside. To determine the necessary length, different typical details have been numerically calculated to determine the linear heat transmission coefficient as a function of the length of the heat flow path. It was found that for different building nodes, a pathway of 1m was sufficient to ensure a reduced linear thermal transmittance that meets the limit values in table 1. Though certainly not the best option, at least basic rule 3 makes it possible to account for those situations where the only solution exists in wrapping insulation around the thermal bridge.

This set of three basic rules is defined in such a way that they can be easily communicated to the building industry and that details can be checked during design and construction phase without any additional calculations.

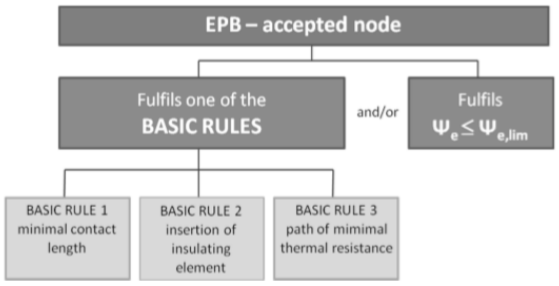

Fig 3: Different options to ensure that a certain building node is EPB-accepted

When for a specific project the majority of the building nodes meet the requirements, it is always possible that one or more nodes have a design which not allows to apply the simple rules. In that case, numerical simulations can be used to prove that in fact the limit values are obtained.

6. Conclusions

In this paper a methodology is presented to develop limiting values for the linear thermal transmittance of building junctions in order to minimize the influence of thermal bridges on transmission heat loss. First, the transmission heat loss resulting from all joints encountered in five reference dwellings with traditional masonry construction was quantified. From that, limit values were derived that account for geometry and technical feasibility. Based on those limiting values, simplified rules of thumb have been derived for the building industry, with a straightforward approach to implement it in practice. The practical experience in the building industry shows that the vast majority of buildings is checked for EPB-accepted nodes, and thus with little to no additional work for architects and contractors.

References

Erhorn H. et al., 2010. An effective handling of thermal bridges in the EPBD context. Final report of the IEE ASIEPI work on thermal bridges.

Janssens A., Van Londersele E., Vandermarcke B., Roels S., Standaert P. & Wouters P. 2007. Development of limits for the linear thermal transmittance of thermal bridges in buildings. Thermal performance of the exterior envelopes of whole buildings X: international conference proceedings, Clearwater, Florida.

Roels S., Deurinck M., Delghust M., Janssens A., Van Orshoven D., A pragmatic approach to incorporate the effect of thermal bridging within the EPBD-regulation. 9th Nordic Symposium on Building Physics - NSB 2011.

A Review of Definition and Classification of Heritage Buildings and Framework for their Evaluation

A. Al-Sakkaf[a,b,*], T. Zayed[c], and A. Bagchi[b]

[a] Department of Building, Civil, and Environmental Engineering, Concordia University, Montreal, QC, Canada.
[b] Department of Architecture & Environmental Planning, College of Engineering & Petroleum, Ḥadhramout University, Yemen.
[c] Department of Building and Real Estate, The Hong Kong Polytechnic University, Hong Kong, Hong Kong.
* Corresponding author, Tel: 001514311929, E-mail: (abobakr.al-sakkaf@mail.concordia.ca)

Abstract:

The unique nature and the significant value of the heritage buildings have created the need for standard unified methods to be used in local heritage building rehabilitation projects. This will allow such important buildings to fit in their own geographical region or policy. This research identified and reviewed three main aspects concerning heritage buildings: definitions, types and conservation treatments, different ways to develop the standard unified assessment. The review followed a comparative analysis of the different methods used by diverse authors and organizations, e.g. the United Nations Educational, Scientific and Cultural Organization (UNESCO), International Council on Monuments and Sites (ICOMOS) and other governmental authorities. Results showed that there is no single way to define the heritage building, classify it into different categories and choose the appropriate treatment for rehabilitation. Each country has its own norms in each of the three aspects. In conclusion, this review has explored the variability of heritage building definitions and types and treatments that are utilized by different organizations. Collaboration between academic institutions and other organization, e.g. UNESCO and ICOMOS, has come up with a standard way to define heritage buildings, classifying them, and selecting the most appropriate strategy for conservation treatment.

Keywords:
Sustainability, heritage buildings, rating systems, architectural rehabilitation, energy.

1. Introduction

Heritage Buildings (HB) inherited from the past are a crucial component in our modern society. Heritage includes those buildings, structures, artifacts, and areas that are historically, aesthetically and architecturally significant. The three factors that determine if a property is worthy to be listed as heritage are historic significance, integrity, and context [2]. Historic significance is related to the importance of a property to history, archaeology, engineering or culture of the community. That includes any heritage building that is associated with past events or important persons or has distinctive physical characteristics of design representing the work of a master. Historic integrity is relevant to the authenticity of a building's identity with evidence of the existence of its physical characteristics during the building's historic period [10]. According to the UNESCO world heritage conservation statistics, the total number of world heritage sites was 1092 by August 2018. These sites were classified as cultural (n=845), natural (n=209) and sites of mixed properties (n=38). They are in 167 states/counties scattered across the world with the following geographic distribution: Europe (47.07%), Asia as well as the Pacific (23.63%), Latin America (12.91%), Africa (8.7%) and the rest resides in the Arab states. Since heritage is constantly under threat by different worldwide ecological and political issues, improvement of *heritage sustainability* has gained a tremendous priority. Heritage sustainability can be defined as designing and managing heritage assets that follow social, economic and ecological sustainability standards [17].

The term 'monument' shall include all real property, whether they contain buildings or not, having archaeological, architectural, historic or ethnographical interest and may include besides the furnishing preserved within them. The term 'site' shall be defined as a group of elements, either natural or man-made, or combinations of the two, which it is in the public interest to conserve [14].
'Cultural property' was regrouped and defined in 1968 as 'movable' and 'immovable.' 'Movable cultural property' was referred to as 'museum collections,' while 'immovable cultural property' was referred to as 'architectural heritage' and was defined to include not only historic sites and features, but also, more importantly, groups of traditional structures and historic quarters in urban and rural areas [18].

The scope of heritage generally remained the same as that introduced by the Council of Europe in 1975, but the Burra Charter introduced three new terms: 1) *Place*: referring to site, area, building or other work, group of buildings or other works together with pertinent contents and surroundings; 2) *Cultural significance*: referring to aesthetic, historic, scientific or social value; and 3) *Fabric*: meaning all the physical material of the place [11], [22].
Unlike the Australia and New Zealand Charters that define their heritage as 'place,' the Chinese define theirs simply as

'heritage sites,' which are accepted as, "the immovable physical remains that were created during the history of humankind and that have significance;" these include archaeological sites and ruins, tombs, traditional architecture, cave temples and historic villages and towns [2]. In the countries of Southeast Asia, cultural heritage is defined as "structures and artifacts, sites and human habitats, oral or folk heritage, written heritage, and popular cultural heritage" [18], [22]. . In Vietnam, for example, heritage is defined as tangible and intangible cultural heritages, and in the Philippines, heritage is now defined as cultural properties, both movable and immovable [2], [3].

For the past 40 years since the adoption of the Venice Charter in 1964, there have been various conservation guidelines as contracts, suggestions, and rules that have completely characterized the extent of the term 'heritage' in the most comprehensive means conceivable. The degree has expanded from a simple concern for individual buildings and sites to incorporate groups of buildings, historical areas, towns, environments, social factors and, recently, immaterial heritage. Regardless of this expanding in scope, the better phrasing of 'heritage' has not been streamlined or institutionalized, and consequently, no consistency exists between nations. While both UNESCO and the International Council on Monuments and Sites (ICOMOS) agreed upon a principle which is that heritage should cover both cultural and natural heritage, the term 'cultural heritage', which includes monuments, groups of buildings and sites, has not been adopted at national levels. Australia refers to its heritage as 'place, cultural significance, and fabric,' Canada refers to it as 'material culture, geographic, environments and human environments', New Zealand as 'place', and China as 'immovable physical remains', to give a few examples. Even though it is the right of each country to set its own terminology and interpretation of heritage, some common terms and terminology should be considered globally. It is recommended that UNESCO and ICOMOS lead the intellectual discussions on common terms, scope, and terminology and that international countries adopt them at the national level [16].

Literature for this review was mainly obtained from heritage-related organizations e.g. UNESCO, ICOMOS, and other governmental organizations that focus on the conversation, restoration and rehabilitation of their heritage buildings. The main objectives of this review were as follows: a) compare different ways of defining heritage buildings; b) review different ways of classifying heritage buildings; and c) investigate different conservation, restoration, and rehabilitation methods that can be used to maintain the sustainability of heritage buildings.

From the review of literature on heritage building, the following five key points have been identified: i) criteria and factors related to the identification and technology of the building; ii) multi-criteria decision-making (MCDM) techniques; iii) sustainability models; iv) rating systems, and v) rehabilitation and renovation methods, as shown in Fig. 1.

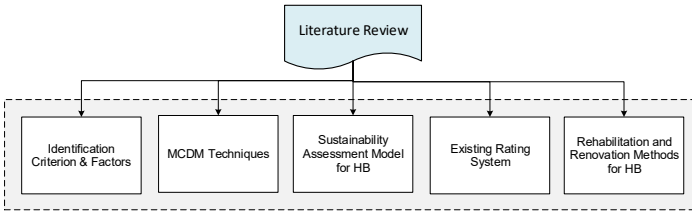

Fig 1: Literature review flowchart

2. Proposed Method

The review was based on searching and screening of relevant journal articles and manuals of renovation procedures published by different organizations. A set of key terms, such as, heritage building definition, types, renovation, rehabilitation have been used in the search criteria. Moreover, unpublished relevant literature was also part of the review, as they have been accessed through Concordia library and the allied system. Published and unpublished literature was assessed for relevance to make sure that they covered the topic of interest Then they were subjected to a subjective comparison to identify the main differences from which the most prominent trends are distinguished as shown in Fig. 2.

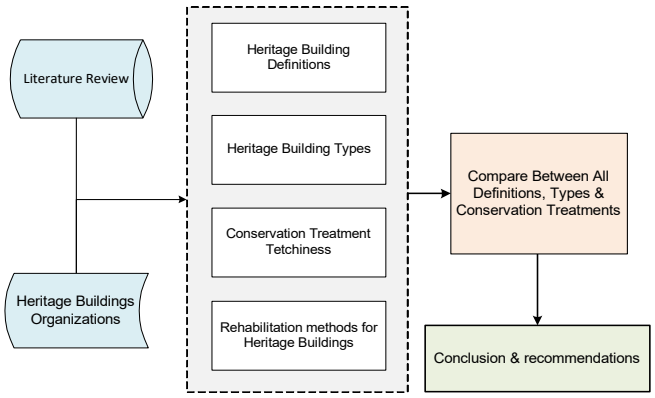

Fig 2: Proposed method flowchart

3. Comparative analysis

Heritage buildings have been defined in different ways in the literature. The definition of heritage buildings showed a lot of discrepancies among organizations as each organization defined them based on their own perspective in addition to other several factors e.g. age, environment, and architectural elements. However, there were four main distinguished definitions described below.

1) Tangible and intangible buildings

There are different definitions of the heritage buildings, among those was the one of cultural heritage. Cultural heritage was defined by UNESCO in 1972 using different wordings such as monuments, architectural works, works of monumental sculpture and painting, elements or structures of an archaeological nature, inscriptions, cave dwellings. However, the common feature of these buildings or sites is that they have a universal outstanding value from the point of view of history, art or science. Furthermore, heritage buildings can exist as a stand-alone building i.e. single or a group of connected buildings which share the same architectural elements or located in the same place in the landscape. Concerning heritage sites, some of them were man-made; however, others were just happened because of climate and environmental changes. In addition, some heritage areas can include more than one archaeological site [23]. The concept of "heritage" in version 7 limited to what is being transmitted across generations, while in that of patrimonies, which has a more social meaning. The vision is only horizontal. To account for vertical vision, it should be of larger dimension, and be able

to encompass more than just the simple inheritance [9], [13], [15].

2) The heritage of directives, charters, and international resolutions

The first definition of the heritage concept was reported in the international charter of Venice (1964). In the heritage, concept was first reported in the international charter of Venice (1964). In the introduction section, it was phrased as "Imbued with a message from the past, the historic monuments of generations of people remain to the present day as living witnesses of their age-old traditions" [13].

3) The scope and definitions of heritage

Although there was an international agreement on including terms of 'tangible', 'intangible' as well as 'environments', in the scope of heritage, it is now the finer terminology of 'heritage' has not been streamlined or standardized, and thus there is no consistency exists among countries [12].

4) Heritage was then defined as monuments and sites

The term monument includes all real properties, whether they contain buildings or not, having archaeological, architectural, historic or ethnographical interests and may also include their preserved furnishing. The term site can be defined as a group of elements, either natural or man-made, or combinations of the two, which are of public interest to conserve [24].

The cultural property was redefined in 1968 in terms of being either movable e.g. museum collections or immovable e.g. architectural heritage. The immovable cultural property was defined to include not only historic sites and features but also and more importantly, groups of traditional structures and historic quarters in both urban and rural areas [22].

The scope of heritage generally remained the same as introduced by the Council of Europe in 1975, but the Burra Charter introduced three new terms by 1979:

- Place referring to site, area, building or other work, group of buildings or other works together with pertinent contents and surroundings.
- Cultural significance, referring to an aesthetic, historic, scientific or social value
- Fabric means all the physical material of a place.

Unlike Australia and New Zealand charters that define their heritage in terms of place, the Chinese defined theirs simply as heritage sites, which was accepted as: 'the immovable physical remains where they have been created during the history of humankind and this has significance'; amongst others, immovable heritage included: archaeological sites, ruins, tombs, traditional architecture, cave temples, and historic villages as well as towns [22].

Different countries defined heritage in a different context. Southeast Asian countries defined the cultural heritage as 'structures and artifacts, sites and human habitats, oral or folk heritage, written heritage, and popular cultural heritage' [1]. While, in Vietnam, heritage was defined as tangible and intangible cultural heritage; and in the Philippines, heritage was defined as cultural properties, both movable and immovable [22].

Since the adoption of the Venice charter in 1964, there have been various conservation guidelines in the forms of contracts, suggestions, or rules that have described the term 'heritage' in a broad scope which extends from a simple concern for individual buildings and sites to incorporate groups of buildings, historical areas, towns, environments, social factors and recently, immaterial heritage. Therefore, there is no exact or explicit way of phrasing the word "heritage" and consequently there is no consistent definition among nations [18].

While both UNESCO and International Council on Monuments and Sites (ICOMOS) agreed that heritage should cover both cultural and natural heritage where the former includes monuments, groups of buildings, and sites. However, this has not been nationally adapted. As for example, it is defined in Australia as 'place, cultural significance, and fabric'; in Canada, 'material culture, geographic environments and human environments'; in New Zealand to 'place'; and in China as 'immovable physical remains [17], [22]. Even though each country has its right to set its own terminology and interpretation of heritage, some of the terminologies need to be standardized or unified globally. Hence, it was recommended that UNESCO and ICOMOS lead the intellectual discussions on common terms, scope, and terminology and that each country adopts them on a country-wide level [15], [16].

4. Heritage Buildings Classification

Based on the existing definitions, heritage buildings are mainly categorized in terms of value and type. Each organization follows its own way of sorting heritage into different types based on their physical, environmental, social and economic value. However, there have been five main distinguished types of heritage buildings as shown in Fig. 3.

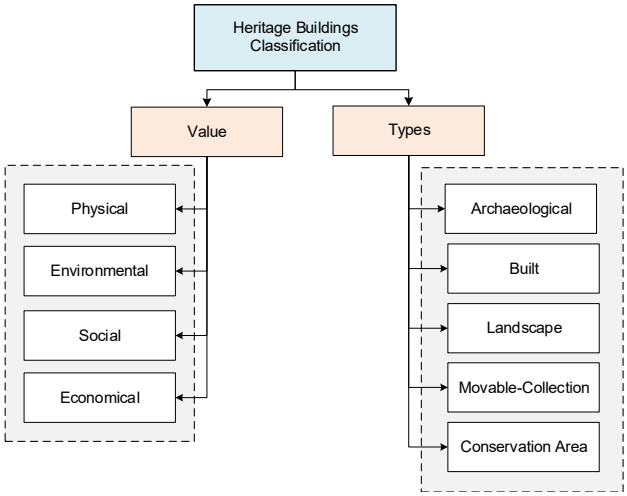

Fig 3: Heritage buildings classification

5. Conservation Treatments

Reviewing the literature revealed that there has been a great variability concerning the strategies used to apply conservation treatments. Table 1 presents a list of the different conservation strategies that can be used for conservation treatments along with their detailed definitions. Preservation includes comprehensively protecting and consistently maintaining the existing form of a historic place. Restoration is about recovering the original condition of a historic place. In addition, Recreating involves replacing exterior features might have missed during restoration. Finally, building rehabilitation is

broader than previous treatment. Rehabilitation is performed in order to reuse, repair or maintain existing features that cannot be restored through renovation.

Table 1: Definitions of different conservation treatments

Action	Definition
Preservation	involves the protection, maintenance and stabilization of the existing form, material and integrity of a historic place.
Restoration	involves the accurate revealing, recovering or representing the state of a historic place as it appeared at a period in its history.
Recreating	missing features of the exterior form that existed during the restoration period, based on physical or documentary evidence; for example, duplicating a dormer or restoring a carport that was later enclosed.
Rehabilitation	involves the sensitive adaptation of a historic place or individual component for a continuing or compatible new use. Rehabilitation is the process that would be used when the repair or replacement of materials and/or features is necessary. It is the only process that allows for additions.

6. Results and discussions

This review has investigated the variability of heritage building definitions and types and treatments that are utilized by different organizations around the globe. By collaboration between academic institutions and other organization, e.g. UNESCO and ICOMOS, has come up with a standard way to define heritage buildings, classifying them, and selecting the most appropriate strategy for conservation treatment. To sum up, the research indicates different conservation treatments that affect the sustainability condition of heritage buildings.

7. Conclusions and outlook

This paper has reviewed three main aspects of heritage buildings: definitions, types, and treatments. Each aspect showed a very diverse picture with some general trends, however, in each aspect, there was no single way standing out as the 'best one' to use especially in terms of sustainability of heritage buildings. Regarding the definition, each country defined the heritage based on their own local geographic or policy context leaving no exact or explicit definition that can be applied worldwide. Regarding value, a heritage building can have the following attributes: physical, social, environmental, and economical. Regarding type, four distinguished categories can be identified: archaeological, built, landscape, movable/collection, and conservation area. Four key conservation strategies have been pointed out: preservation, restoration, recreating and rehabilitation, each can be used deeding on the condition of the building and availability of materials. To conclude, this review has explored the variability of heritage building definitions, types, and treatments among different organizations where collaboration between academic institutions and other organization e.g. UNESCO, ICOMOS to come up with a standard way of defining the heritage building, classifying it into different types and selecting the most appropriate strategy for conservation treatment.

References

[1] Asia Pacific Organization of the International Council of Museums in partnership with the Vietnam Ministry of Culture and Information, (2001). Protection of Cultural Heritage in Southeast Asia Workshop Proceedings, Hanoi, Vietnam, 9-13 April Available from https://www.asef.org/images/docs/Hanoi_Proceedings_Digital_2010.pdf (accessed June 2018).
[2] Akande, O. K., (2015). "Factors influencing operational energy performance and refurbishment of UK listed church buildings: towards a strategic management framework", Ph.D. Thesis, Anglia Ruskin University, UK, May 2015.
[3] Al-Sakkaf, A., Zayed, T., Bagchi, A., & Abdelkader, E. (2019). Sustainability Rating Tool and Rehabilitation Model for Heritage Buildings (pp. 1–11). Annual Conference of the Canadian Society of Civil Engineering (CSCE), Laval, QC, Canada.
[4] Al-Sakkaf, A., Zayed, T. and Bagchi, A. (2020), "A Sustainability Based Framework for Evaluating the Heritage Buildings", *International Journal of Energy Optimization and Engineering*, DOI: 10.4018/IJEOE.2020040105, 9(2), 25 pages.
[5] Al-Sakkaf and Ahmed, R. (2019), "Applicability of BIM in Heritage Buildings", *International Journal of Digital Innovation in the Built Environment (IJDIBE),* DOI: 10.4018/IJDIBE.2019070102 (2), 37 pages.
[6] Arora, J. S., (2012). "Introduction to Optimum Design", Third edition, ed. Waltham, USA: Elsevier Inc.
[7] Asdrubali, Francesco, D'Alessandro, F., & Schiavoni, S Building and Environment 86, 2015. 98e108, *International Initiative for Sustainable Built Environment*. The homepage of iiSBE. [webpage] http://www.iisbe.org/. (accessed May 2019)
[8] Ball, M. (n.d.), 2018. Redshift Retrieved, from Autodesk: http://lineshapespace.com/building-information-modeling-top-10-benefits-of-bim/ (accessed January 2018)
[9] Baker, P., (2011) U-values and Traditional Buildings, In Situ Measurements and Their Comparison to Calculated Values, Historic Scotland Technical paper 10; Glasgow Caledonian: Glasgow, UK (accessed August 2019)
[10] Blake, J. (2002). Developing a New Standard-setting Instrument for the Safeguarding of Intangible Cultural Heritage Elements for consideration. Available from http://unesdoc.unesco.org/images/0012/001237/123744e.pdf (accessed June 2018)
[11] Central public works department, (2013). "Regular establishment and office procedure manual", New Delhi, India, Available from *https://cpwd.gov.in/Publication/RegularManual.pdf* (accessed June 2018)
[12] Dodds, J. D., (2002). "New York Masjid: The Mosques of New York City". New York: Powerhouse.
[13] Economic Commission for Africa (2002). Economic Report on Africa 2002. Tracking Performance and Progress. Available from https://www.uneca.org/sites/default/files/PublicationFiles/era2002.pdf (accessed January 2018).
[14] Gruzinski S., (1993), "Protection of the intangible cultural heritage: Survey and new prospects," Doc. CLT/ACL/IH, 2ndApril, 1993. All the conventions quoted were found on the Unesco website (www.unesco.org).
[15] Feder, E. K. (2007), "Family Bonds: Genealogies of Race and Gender". Oxford UP, 2007. ProQuest library, site.ebrary.com/lib/williams/docDetail.action?docID=10194201.

[16] Francioni, F., and Lenzerini, F. (2003). “The Destruction of the Buddhas of Bamiyan and International Law.” European Journal of International Law 14 (4): 619–651. doi:10.1093/ejil/14.4.619
[17] Francioni, F., (2003). “Beyond state sovereignty: the protection of cultural heritage as a shared interest of humanity”. Mich. J. Int'l L., 25, 1209.
[18] McLennan, Jason F. (2004). The philosophy of sustainable design: the future of architecture. Kansas City, Mo: Ecotone.
[19] Ministers, A. F., (2000). ASEAN Declaration on Cultural Heritage. Bangkok, July.
[20] Nypan, T., (2006). "Cultural Heritage Monuments and Historic buildings as value generators in a post-industrial economy. With the emphasis on exploring the role of the sector as an economic driver. Rev. ed." 17.
[21] The Venice Charter, (1964). International Charter for the conservation and restoration of monuments and sites.
[22] Published at 2nd International Congress of Architects and Technicians of Historic Monuments, Venice, (1964). Available from https://www.icomos.org/charters/venice_e.pdf (accessed January 2017).
[23] Toman, J., (2017). Protection of Cultural Property in the Event of Armed Conflict. Routledge.
[24] UNESCO, 1972. Convention concerning the protection of the world cultural and natural heritage: adopted by the General Conference at its seventeenth session, Paris, 16 November 1972.
[25] Ziffer, K., (1989), Ecotourism: The Uneasy Alliance. Washington, DC: Conservation International, Ernst, and Young.

Operational energy use versus LCA: case study The Mobble for the Solar Decathlon Europe 2019 competition

L. Landuyt[a*], S. De Turck [a] ,S. Lauwerys[a] N. Van Den Bossche[a]

[a] Ghent University, Faculty of Engineering and Architecture, Department of Architecture and Urban Planning, Sint Pietersnieuwstraat 41 B4, 9000 Ghent, Belgium
* Corresponding author, 09 264 32 89, laura.landuyt@ugent.be

Abstract:
Studies have shown that the building sector is the biggest contributor to global warming, generating 40 to 50 % of the global output of greenhouse gas emissions. Furthermore, this industry consumes up to 40 % of the materials entering the global economy and produces one third of the total waste. In Belgium alone, estimations put the building sector's waste output at fifteen million ton of construction waste on a yearly basis. Therefore, a more environmental-friendly thinking is required, that also considers the impact of construction materials on the environment. For highly insulated buildings the environmental impact of additional construction materials might supersede the reduction in energy use that can be obtained throughout its service life. A trade-off should be made between the embedded and operational energy. For the Solar Decathlon competition 2019 in Szentendre an energy efficient house The Mobble was designed and built, for which detailed dynamic energy simulations were performed in Modelica/Dymola, and as well, a life cycle assessment was done using the simulation software Simapro. Even so, the potential of Personal Comfort Systems (PCS) is investigated through the energy simulations. The result of the trade-off for this case-study shows on the one hand a clear potential of advanced demand control HVAC systems and on the other hand clear limits to the increase of insulation thickness. However, for this specific case it was shown that the optimal insulation thickness from environmental point of view is still well above the minimum requirement in the Belgian building code, even for very efficient HVAC systems.

Keywords:
Energy use, LCA, Embedded energy, Case-study, Personal heating

1. Introduction

A student team from Ghent University took part in the Solar Decathlon Europe 2019 competition in Hungary. The Solar Decathlon competition is an international competition for students at an academic level. Universities from all over the world are being challenged to design, build and operate a sustainable and energy efficient pavilion. Studies have shown that the building sector is the biggest contributor to global warming, generating 40 to 50 % of the global output of greenhouse gas emissions. Further, this industry consumes up to 40 % of the materials entering the global economy and produces one third of the total waste. In Belgium alone, estimations put the building sector's waste output at fifteen million ton of construction waste on a yearly basis [1] [2]. Therefore, a more environmental-friendly thinking is required, that also considers the impact of construction materials on the environment. For highly insulated buildings the environmental impact of additional construction materials might supersede the reduction in energy use that can be obtained throughout its service life.

The following question arises: what is the tipping point between the reduction of operational energy of a building and the increased embedded energy. In this paper a trade-off is made between operational energy use and embedded energy for the participating team pavilion 'The Mobble' in the Solar Decathlon Europe 2019 competition.

2. Case study: The Mobble

The dwelling designed and selected for the Solar Decathlon Europe 2019 competition is used as a case-study project to investigate the trade-off between the environmental impact of embedded and operational energy. The building consists of 5 identical modules, dimensions 2.4m x 6m, which are connected and form 1 dwelling with a rather low compactness of 1,2.

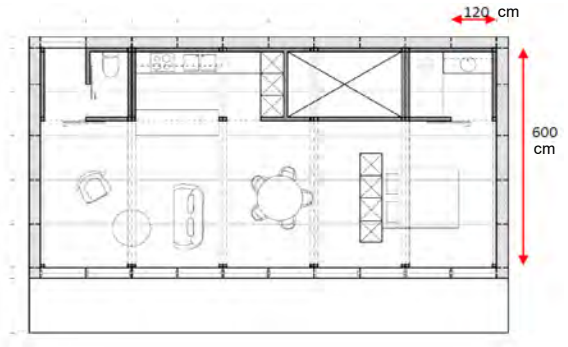

Fig 1: Floor plan of The Mobble [3]

Prefabricated panels are used for the walls, floor and roof. The building parameters are listed in Table 1.

Table 1: Building parameters of the Mobble

Building element	Area [m²]	Thermal transmittance U [W/m²K]
Walls	77,11	0,115
Floor	82,55	0,152
Roof	82,55	0,153
Glazing	27,58	0,7 (triple)
Window frame	3,06	0,7

3. Methodology

First of all, an insight in the operational energy use of the case study is required. Hence, dynamic energy simulations are executed in Modelica/Dymola for both constantly working and demand based HVAC systems. Of course, comfort is a crucial parameter for an indoor environment. Lowering the comfort level in order to save energy in the operational phase is therefore not an option. In literature no consensus is found on the optimal indoor air temperature. As a consequence, the optimal indoor temperature is strongly dependent on which comfort theory – theory of Fanger [4], Zhang [5], … – is adopted. Indoor air temperatures of 20°C and 26°C are chosen for winter and summer respectively, as an acceptable indoor climate and HVAC setpoint. However, during the heating season the indoor temperature of 20°C can be lowered whilst preserving comfort if compensated by Personal Comfort Systems (PCS). Please refer to [6] for more information concerning thermal comfort analysis and PCS for this specific case-study. During the cooling season, the indoor air temperature of 26°C can be increased whilst preserving thermal comfort by adding personal cooling. However, the practical applications of personal cooling are proven to be difficult for a simple reason: comfort issues in summer are related to activities that entail a high metabolism. People typically have a high metabolism while walking around. Therefore, the personal cooling should be mobile and thus integrated in the clothing. However, fans are proven to be the most effective personal cooling devices since the head is the area to tackle and thus the practical applicability of personal cooling is not self-evident. Hence, personal cooling is not included in the energy simulations. To reduce the cooling load, passive measures are taken such as a canopy and sun screens. The remaining cooling load is actively cooled to an indoor temperature of 26°C.

The human comfort simulations have been done in Human Thermal Module, a software of producer Thermo Analytics [7]. This resulted in heat inputs for the local devices as listed in Table 2. The chosen local heating device is a heated chair. As can be seen in Table 2 PCS have their limitations: if the operative temperature is 14 °C, no heated chair can provide enough heat in order to guarantee the comfort of the user, here a single working male. Hence, all simulations with an operative temperature of 14°C and 15°C do not render adequate comfort and are not considered in further analysis.

Table 2: Heat inputs for a heated chair to provide in comfort for various room temperatures

Metabolic rate [met]	Heat input local device per operative temperature [W]						
	20 °C	19	18	17	16	15	14
1.0	0	30	45	60	85	-	-
1.2	0	5	22	50	85	125	-

Subsequently, this operational primary energy use for the combination of PCS and room heating serves as input parameter in the Life Cycle Assessment (LCA), executed in SimaPro using the ReCiPe method [8]. This method considers 18 different environmental performance indices. For the inventory of the data, the Ecoinvent database version 3.5 is used taking a service life of 60 years into account. Although 'The Mobble' is a circular and modular concept, the end-of-life is not taken into account due to the severe uncertainties. A 'Cradle-to-use' approach is chosen, taking into account the production and extraction of materials, transportation to the site and the usage phase by implementing the operational energy from the Dymola/Modelica simulations. Replacements are also accounted for by increasing the amount of material needed, considering a service life of 15 years for finishing layers and 60 years for structural elements. The wall panels have a service life assigned of 30 years due to the modular and circular concept. Note that the LCA of HVAC systems and PCS was not included here.

The combination of LCA and dynamic energy simulations allow a comparison between the environmental impact of the operational energy of the dwelling and the embedded energy of the materials used. Several iterations are done to search for an optimum between the reduction in operational energy use and the increase of embedded energy due to more material-intensive solutions (wall thickness, triple glazing). The configuration in section 2 is referred to as baseline scenario. Next to the baseline, three adaptions are examined. In 'Adaptation 1' the wall panels are insulated with 22 cm of insulation resulting in an increased thermal transmittance of 0,155 W/m²K. In 'Adaptation 2' the window façade has double glazing (U_g = 1,0 W/m²K) instead of triple glazing. In 'Adaptation 3' the wall panels are insulated with 12 cm of mineral wool resulting in a thermal transmittance of 0,27 W/m²K, which is no longer allowed according to the Belgian building code. The three adaptations relative to the baseline were chosen to investigate the balance between operational and embedded energy.

4. Results and discussions

The annual primary energy use for room heating is shown in Fig 2. Evidently the baseline scenario (triple glazing and 30 cm of insulation in the wall panels) has the lowest energy demand for heating. The primary energy use increases for 22 cm of wall insulation (adaptation 1). By replacing the triple glazing by double glazing (adaptation 2) the heating demand and primary energy use will further increase, and finally reducing the insulation package to 12 cm will result in the highest primary energy use. The primary energy use will decrease by lowering the setpoint temperature of the room heating. If the operative temperature of the room heating is lowered from 20°C to 16°C, a reduction in primary energy use for room heating of 40% is obtained (note that the energy use for the PCS to achieve similar comfort is not accounted for).

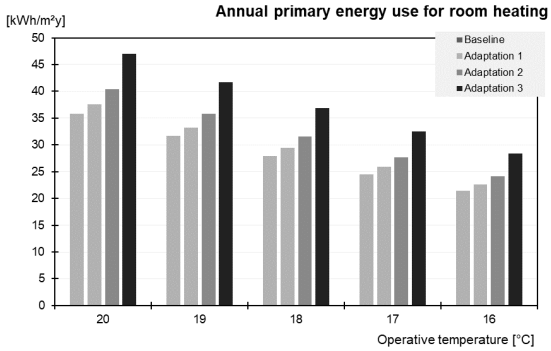

Fig 2: Annual primary energy consumption for room heating (constant temperature)

Considering the total primary energy use of room heating, cooling and personal heating, only a 25% cut in primary energy use can be obtained by lowering the operative temperature from 20°C to 16°C. This is a logical decrease in saving potential because lowering the operative temperature for room heating entails an increased primary energy use for the PCS (Fig 3).

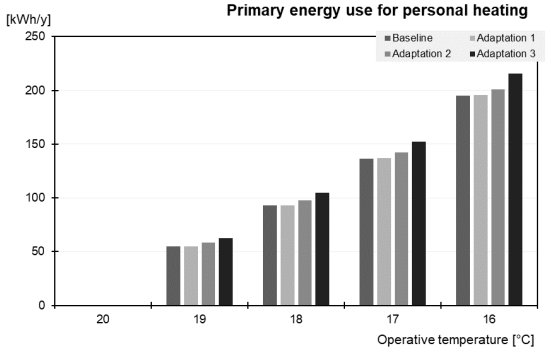

Fig 3: Primary energy use for a heated chair for various operative temperatures (constant HVAC)

If the room temperature does not have to be maintained 24/7 and can be lowered to e.g. 10°C while the dwelling is not occupied, a reduction potential of 17% in primary energy use is found for the simulated user pattern of a working inhabitant.

The trade-off between the total annual primary energy use (heating, cooling, PCS) and embedded energy is shown in Fig 4.

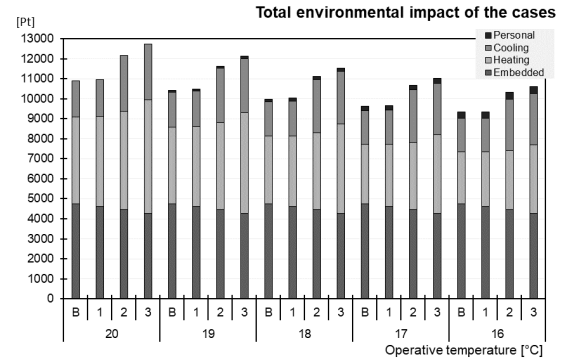

Fig 4: Total environmental impact of the scenarios for varied operative temperatures (constant HVAC)

Again two opposing forces come into play, i.e. the operational phase and embedded energy. On the one hand, lowering the operative temperature results in a decrease in environmental impact due to the saving in total primary energy use of 25%. However, the total environmental impact only decreases by 14%. This can be explained by the low compactness of the case-study. The compactness of a building is defined as the ratio between the volume and the heat loss surface area. A building with a low compactness consequently has a large heat loss surface area and hence a larger material intensity than a highly compact building. On the other hand, Figure 4 shows an increase in environmental impact when the operational energy increases. The increase in operational energy is a result of building components with higher thermal transmittance, resulting in a decreased embedded energy (lower material use). However, the dominance of the operational phase cannot be generalised. Fig. 5 visualizes the contribution of both operational and embedded energy to the total environmental impact of the dwelling.

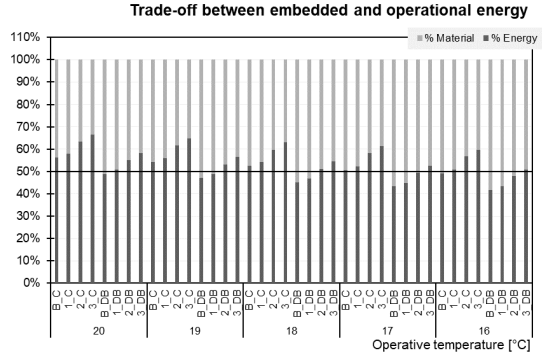

Fig 5: Trade-off between embedded and operational energy (B: baseline, 1-3: adaptation 1-3, C: Constant HVAC, DB: Demand based HVAC)

The question now arises, what is the optimal insulation thickness to minimalize the combination of embedded and operational energy. The result of this optimisation is shown in Fig 6.

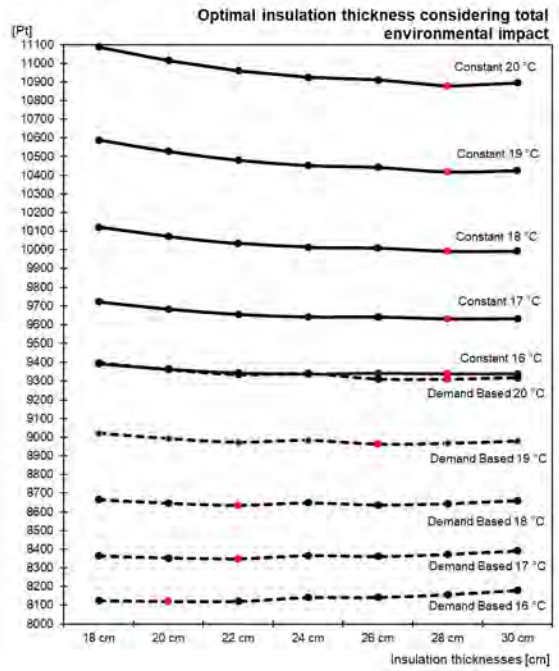

Fig 6: Total environmental impact of insulation thicknesses ranging from 18 cm to 30 cm

For constant heating systems, the optimum insulation thickness from an environmental perspective for operative temperatures ranging from 20°C to 16°C is 28 cm of mineral wool (Fig 6). The energy reduction by using 30 cm instead of 28 cm is only 0,3 %. Thus, the additional 2 cm of insulation material and wood stud size takes more energy to produce. When considering the balance between embedded and operational energy, there is a clear upper limit to the insulation thickness for this case. For demand based systems, the optimum insulation thickness from an environmental perspective for operative temperatures 20°C, 19°C, 18°C, 17°C and 16°C are respectively 28 cm, 26 cm, 22 cm, 22 cm and 20 cm of mineral wool (Fig 6). As there is an upper limit to the insulation thickness, there is also a minimal insulation thickness in this case.

5. Conclusions and outlook

The aim of the research was to investigate whether the environmental impact of additional construction materials might supersede the reduction in energy use that can be obtained throughout its service life. Various influences have been investigated, such as the influence of a constantly working and a demand based HVAC system. Furthermore, the influence of implementing personal heating in order to allow a reduction in operative room temperature to save energy while maintaining comfort was assessed. It can be stated that there are indeed constraints to adding additional construction materials to reduce the operational energy when considering the total environmental impact of the dwelling. When personal heating is not implemented – which is the case for an operative temperature of 20°C – for both the constant and demand based system wall panels with an insulation thickness of 28 cm are most beneficial. The personal heating has the most potential in combination with a demand based system for room conditioning. Here the insulation thickness can be decreased to 20 cm with an operative temperature of 16°C without depriving in comfort. This proves the potential of personal heating systems for reducing the environmental impact of a dwelling. As PCS can be considered as the most efficient demand control HVAC system, for this specific case the increase in system efficiency leads to a reduction around 30% in thermal resistance to achieve the lowest environmental impact. This highlights the susceptibility of LCA assessment towards HVAC efficiency. This research has been focused on one specific user profile, one specific personal heating device, and one specific building. More research on other configurations is required to extrapolate results to building stock level.

References

[1] Khasreen, M., Banfill, P., Menzies, G. (2009). Life-Cycle Assessment and the Environmental Impact of Buildings: A Review. Sustainability 1. 674-701

[2] Romnée, A., & Vrijders, J. (2017). Circulair bouwen "Naar een circulaire economie in de bouwsector".

[3] De Turck, S., Laverge, J., & Van Den Bossche, N. (2018). Personal HVAC: a simulation based feasibility study.

[4] P.O. Fanger, Thermal comfort. Analysis and applications in environmental engineering. Copenhagen, Denmark: Copenhagen Danish Tech. Press; 1970.

[5] Zhang, H., n.d. Human Thermal Sensation and Comfort in Transient and Non-Uniform Thermal Environments 436.

[6] De Turck, S. & Van Den Bossche, Nathan & Laverge, Jelle. (2019). The potential of Personal Conditioning Systems. MATEC Web of Conferences. 282. 02098. 10.1051/matecconf/201928202098.

[7] Huizenga, C., Hui, Z., Arens, E., 2001. A model of human physiology and comfort for assessing complex thermal environments. Building and Environment 36, 691–699.

[8] M.A.J. Huijbregts et al. A harmonized life cycle impact assessment method at midpoint and endpoint level Report I: Characterization. RIVM Report 2016-0104

Effect of render properties on moisture risk in internally insulated masonry walls

X. Zhou[a,b*], J. Carmeliet[b], D. Derome[c]

[a] Laboratory of Multiscale Studies in Building Physics, Empa, Dübendorf, Switzerland
[b] Chair of Building Physics, ETH Zürich, Zürich, Switzerland
[c] Department of Civil and Building Engineering, Université de Sherbrooke, Sherbrooke, Canada
* Corresponding author, Tel +41 58 765 6012, email: xiaohai.zhou@empa.ch

Abstract:
Energy efficiency in buildings with a worth-preserving appearance can be improved with internal thermal insulation. However, internally insulated masonry walls present much higher risk of moisture-related problems in wall components. Render is the most important factor affecting hygrothermal performance and durability of internally insulated masonry walls. This paper studies the influence of water absorption coefficient and vapor diffusion resistance of renders on hygrothermal performance on masonry walls with vapor-closed insulation system and capillary active insulation system. The effect of thermal transmittance and wind-driven rain load on hygrothermal performance of walls are also considered. The hygrothermal performance of the wall envelopes is simulated with a coupled heat and mass transport model and moisture risk is evaluated with mould index. The study indicates that water absorption coefficient of render has much larger influence on moisture risk than vapor diffusion resistance. In most cases, mould index increases significantly with increase of water absorption coefficient. The influence of thermal transmittance and WDR load on moisture risk of retrofitted wall envelope is depend on render properties. When water absorption coefficient of render is considerably large, moisture risk increase dramatically with decrease of thermal transmittance or increase wind-driven rain load.

Keywords:
Interior thermal insulation, vapor-closed insulation, capillary active insulation, mould risk.

1. Introduction

Historical buildings account for about 20 % of the existing building stock in Switzerland. Most of these buildings have been built before 1919. These buildings are mostly not energy efficient and have very high energy consumption. Due to need to preserve the façade of historical buildings, internal thermal insulation is often the only measure for energy retrofitting of these buildings. However, internal thermal insulation is often very risky due to lower temperature and consequently lower drying potential in the existing wall [1,2]. Moisture-related problems such as interstitial condensation and mold growth, freeze-thaw damage of the brickwork or decay in embedded wooden beams could occur after internal thermal insulation. An unthoughtful planned internal thermal insulation will often lead to moisture-related problems in building envelops.

The study from Zhou *et al.* [2] indicates that hygrothermal performance of internally insulated masonry walls depends much more on material properties of exterior render than brick type and masonry structure. Wind-driven rain is the largest moisture sources that influence the hygrothermal performance of building envelopes. Exterior renders provide protections for masonry from moisture-related problems in regions with high wind-driven rain load [3]. Water absorption coefficient (A_{cap}) and vapor diffusion resistance (S_d) are the most important properties of renders. Water absorption coefficient is a parameter that characterize a material's ability for wetting by liquid transport whereas vapor diffusion resistance is a parameter that describes a material's ability to drying by vapor diffusion. In Germany, rain protection coefficient (CRP) of renders, being the product of capillary absorption coefficient and vapor diffusion resistance (A_{cap}*S_d), is required to be smaller than 0.2 kg/(m$h^{0.5}$) to avoid moisture-related problems in wall envelopes. For wall envelopes with interior insulation, the rain protection coefficient is required to be smaller than 0.1 kg/(m$h^{0.5}$) according to the WTA guideline [4]. Such requirement from WTA guideline is often very conservative. Even for building envelopes with the same exterior render, hygrothermal performance can be affected by wind-driven rain load, type of insulation system and U-value of insulation layer. In general, a larger wind-driven rain load and a thicker insulation layer lead to larger moisture risk. However, quantitative relation between increase of wind-driven rain load and insulation thickness and increase of moisture risk is still not clear. It is essential to perform a systematic study to obtain an insight to the quantitative relation between these factors.

The most common internal thermal insulation systems are either vapor tight or capillary active. The vapor tight insulation system restrains vapor diffusion from the indoor environment to cold surface of original wall to avoid interstitial condensation. However, such insulation system limits drying to indoor environment in the summer period, resulting increase of moisture in the existing wall. By contrast, the capillary active insulation system is vapor open but can avoid interstitial condensation by redistributing moisture from the existing wall towards the room by capillary moisture transport.

The objective of the paper is to study the influence of render properties on hygrothermal performance of internally insulated masonry wall under different insulation systems, insulation thicknesses and wind-driven rain loads. A hygrothermal model is used to predict temperature and humidity change in the wall envelopes. Mould index is applied to evaluate the risk of moisture problems.

2. Methodology

Hygrothermal modeling is used to calculate the temperature and moisture distributions in building envelopes.The governing equations for moisture and heat transport are the same as those in HAMFEM [5], and are solved using the finite element solver COMSOL.

The wall envelope is a 250mm thick masonry wall (Fig. 1), which has a U-value of 1.40 W/m2K. The wall envelope used in the 1D simulation is shown between the blue dashdot lines in Fig. 1. The 1D wall envelope consists of a 20 mm thick exterior render, a 120 mm thick brick, a 10 mm thick mortar, a 120 mm thick brick and a 15 mm thick interior plaster. The selected orientation of the wall envelope is 240 degree from the north, where wind driven load is the largest.

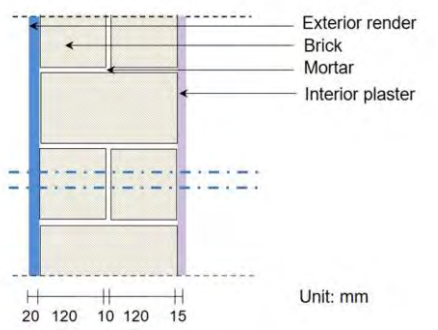

Fig 1: Geometry of wall envelope

To study the influence of different renders, renders with different water absorption coefficient and vapor resistance factor are considered. The material properties of renders are obtained based on a reference render. The reference render is mineral plaster from WUFI database [6], which has a water absorption coefficient 0.1 kg/m^{2}h$^{0.5}$. The material properties of renders are the same as this reference render except liquid permeability and vapor resistance factor. The selected water absorption coefficient for the renders are 0.1, 0.2, 0.4, 0.6, 0.8 and 1.0 kg/m^{2}h$^{0.5}$. The selected water vapor resistance factor for the renders are 5, 10, 20, 30, 40, 50 and 60, which corresponds to vapor diffusion resistance of 0.1, 0.2, 0.4, 0.6, 0.8, 1.0 and 1.2 m. In total, 42 types of render with different combination of water absorption coefficient and vapor diffusion resistance are chosen. Liquid permeability is calculated as the product of moisture capacity and liquid diffusivity. The relation between liquid diffusivity D and water absorption coefficient Acap is [7]:

$$D(w) = 3.8 \cdot \left(\frac{A_{cap}}{w_{cap}} \right)^2 \cdot 1000^{\frac{w}{w_{cap}}-1}$$

where D(w) is the liquid diffusivity (m^2/s), w_{cap} is the capillary moisture content (kg/m^3).

Two insulation systems for internal insulation are selected. The first system is vapor tight system with glass wool and smart vapor barrier. The second one is vapor open, capillary active system with calcium silicate. Glue mortar is needed to attach calcium silicate to the existing wall envelope. For the two insulation systems, new interior plaster of 1.5 cm is added after the insulation material. The wall envelope is internally insulated to the following three thermal transmittances (U-values): 0.25, 0.35 and 0.45 W/m^{2}K.

Twelve years of meteorological data from October 1st 2005 to September 30th 2017 from Meteoswiss station Zurich Kloten are used to drive the numerical model. The meteorological data includes hourly outdoor air temperature, relative humidity, wind speed, wind direction, solar radiation and horizontal rain. The initial condition of building envelope is a uniform temperature of 20 °C and a relative humidity of 60%. The first 2-year meteorological data is used to initialize the numerical model so that simulated hygrothermal condition in the wall envelope is independent from the influence of initial condition. The remaining 10-year data is used for analysis of hygrothermal performance of wall envelopes.

The wind-driven rain load for wall envelope is calculated according to ASHRAE Standard 160 - Criteria for Moisture Control Design Analysis in Buildings, where the WDR intensity is defined by the following equation:

$$R_{WDR} = R_h \times F_E \times F_D \times 0.2 \times V_{10} \times \cos\theta$$

where R_h is the horizontal rainfall amount (kg m^{-2}h^{-1} or mm h^{-1}); F_E is the rain exposure factor; F_D is the rain deposition factor; V_{10} is the wind speed at 10 m above ground (ms^{-1}); θ is the angle between the wind direction and the normal to the façade (rad). Factor F_E depends on the surrounding terrain and the height of the building, while Factor F_D describes the influence of the building itself. In the study, a rain exposure factor of 1.0 is selected. Three deposition factors of 0.5, 1.0 and 2.0 are selected to represent small, medium and large WDR load.

The moisture risk in the wall envelopes is evaluated with VTT Mould Index [8]. Mould index ranges between 0 and 6. A Mould index of 1 is regarded as the maximum tolerable value. The most critical location for internal thermal insulation is the interface between insulation layer and the existing wall. The achieved maximum mould index at this critical location over the 10-year period is used to assess moisture risk in the building envelops.

3. Results and discussions

Figures 2 and 3 show the maximum reached mould index under different conditions in wall envelops with calcium silicate and glass wool. None of the mould index in wall envelopes reaches above 3.5.

In general, wall envelopes with calcium silicate perform better than wall envelopes with glass wool. The contour lines of maximum mould index lie at higher water absorption coefficient and diffusion resistance in wall envelopes with calcium silicate.

For the wall envelopes with calcium silicate, none of the envelopes reach mould index above 1 when the U value of the retrofitted wall is 0.45 W/m^{2}K and rain deposition factor is 0.5 (Fig. 2a). By comparison, the wall envelope with glass wool at the same condition can have mould index above 3 (Fig. 3a). Figure 4 shows mould index and relative humidity over 10 years in envelops with F_D value of 0.5, Acap value of 1.0 kg/m^{2}h$^{0.5}$ and Sd value of 1.2 m but U values of 0.25 and 0.45 W/m^{2}K. When the U value of the retrofitted wall is 0.45 W/m^{2}K, relative humidity in the envelope with glass wool is mostly above 85%. By comparison, relative humidity in the envelope with calcium silicate is above 85% during the winter period and drops below 85% in the summer period. The low relative humidity in the summer period limits the growth of mould. However, when the U value of the retrofitted wall decreases from 0.45 to 0.25 W/m^{2}K, there is significant increase of mould index at the wall envelope with calcium silicate. The maximum mould index increase from 0.72 to 2.54 when the U value decrease from 0.45 to 0.25 W/m^{2}K. It shows that the U value of retrofitted wall envelope has significant influence on moisture risk in this case. Due to the increase of U value, the drying potential of the wall envelope decreases dramatically and thus relative humidity in the summer period becomes mostly above 85%.

However, the influence of U value of retrofitted wall envelope is very small when the render of the water envelope has low water absorption coefficient and diffusion resistance. It could be infered that the decrease of U value of the retrofitted wall will have small influence on wall envelopes with capillary inactive and highly vapor open renders. However, the influence of U value of retrofitted wall has very large influence on moisture risk when renders of wall envelopes is capillary active and not vapor open.

The influence of wind-driven rain load on mould index depends also on properties of render. When the render is capillary inactive and highly vapor open, the influence of wind-driven rain load on relative humidity and thus on moisture risk is small. However, when the render is capillary active and not vapor open, the wind-driven rain load also has very large influence on mould index. When the F_D value increases, the contour lines moves towards lower left (Figures 2 and 3).

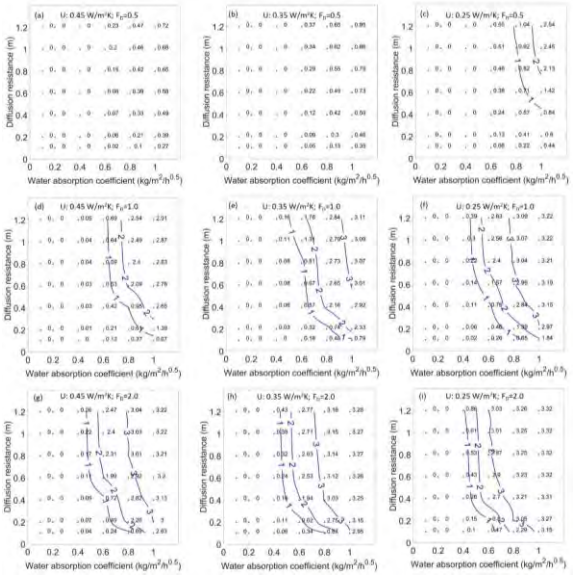

Fig 2: Maximum mould index in wall envelopes with calcium silicate insulation

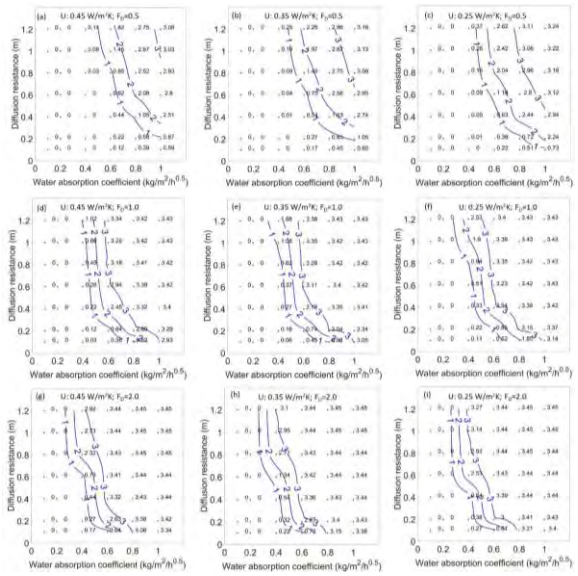

Fig 3: Maximum mould index for wall envelopes with glass wool insulation

When the water absorption coefficient is very low, e.g. 0.1 or 0.2 kg/m^{2}h$^{0.5}$, the diffusion resistance has almost no effect on mould index no matter wall envelopes with calcium silicate or glass wool. Under such conditions, very small amount of rainwater penetrates into the building envelope. A larger diffusion resistance leads slower drying in the summer period. Due to the low wetting potential, a large diffusion resistance does not lead to relative humidity above 85% at the critical location and thus no influence on mould index.

When the water absorption coefficient is considerably large, e.g. 0.6 kg/m^{2}h$^{0.5}$, diffusion resistance has very large effect on mould index. An increase of diffusion resistance leads to increase of mould index. The

larger diffusion resistance lows the drying potential, which results in larger relative humidity in the wall envelope.

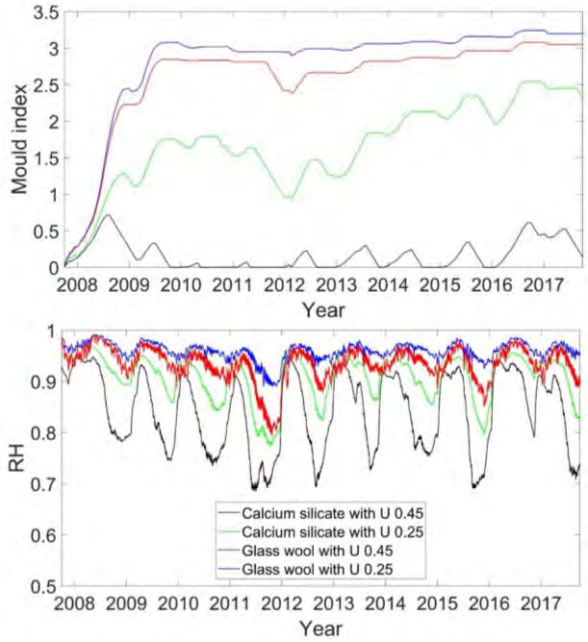

Fig 4: Mould index and relative humidity for wall envelopes with U value of the 0.45 W/m^{2}K and rain deposition factor F_D of 0.5

However, when water absorption coefficient is very large, e.g. 1.0 kg/m^{2}h$^{0.5}$, mould index does not increase significantly with increase of diffusion resistance in some cases, e.g. in envelopes with U value of 0.25 W/m^{2}K and F_D of 2.0. In these cases, mould index is very close to the possible maximum value and an increase of water absorption coefficient does not increase relative humidity greatly and thus mould index.

In general, the influence of diffusion resistance on mould index is smaller than water absorption coefficient. The shape of the contour lines indicate that change of mould index mainly occurs in the X axis. When the diffusion resistance is above 0.6 m, the contour lines become to some extent parallel to the Y axis. This indicates that influence of diffusion resistance on mould index becomes very small when diffusion resistance is above a certain threshold. In most conditions, mould index increases considerably with increase of water absorption coefficient.

4. Conclusions and outlook

The influence of render properties, insulation systems, thermal transmittance and WDR load on moisture risk of internally insulated masonry wall is analyzed. The hygrothermal performance of the wall envelopes is simulated with a coupled heat and mass transport model and moisture risk is evaluated with mould index. In general, wall envelopes with capillary active insulation of calcium silicate perform better than wall envelopes with glass wool. The influence of thermal transmittance and WDR load on moisture risk of retrofitted wall envelope is depend on render properties. When the render of the water envelope has low water absorption coefficient, a decrease of thermal transmittance or an increase of WDR load will have a very small influence on moisture risk of wall envelope. Nevertheless, when the water absorption coefficient is considerably large, a decrease of thermal transmittance or an increase of WDR load will increase moisture risk dramatically. The influence of diffusion resistance on mould index is smaller than water absorption coefficient. In most cases, mould index increases significantly with increase of water absorption coefficient.

Acknowledgements

This research project is part of the Swiss Competence Center for Energy Research SCCER FEEB&D of the Swiss Innovation Agency Innosuisse. The meteorological data have been provided by MeteoSwiss, the Swiss Federal Office of Meteorology and Climatology.

References

[1] X. Zhou, D. Derome, J. Carmeliet, Hygrothermal modeling and evaluation of freeze-thaw damage risk of masonry walls retrofitted with internal insulation, Build. Environ. 125 (2017) 285–298.
[2] X. Zhou, J. Carmeliet, D. Derome, Influence of envelope properties on interior insulation solutions for masonry walls, Build. Environ. 135 (2018) 246–256.
[3] H. Künzel, Criteria defining rain protecting external rendering systems, Energy Procedia. 78 (2015) 2524–2529.
[4] W.T.A. Merkblatt, 6-4-01 (2009): Innendämmung nach WTA I: Planungsleitfaden, Wissenschaftlich-Technische Arbeitsgemeinschaft Für Bauwerkserhaltung Und Denkmalpfl. EV, München.
[5] H. Janssen, B. Blocken, J. Carmeliet, Conservative modelling of the moisture and heat transfer in building components under atmospheric excitation, Int. J. Heat Mass Transf. 50 (2007) 1128–1140.
[6] H.M. Künzel, Simultaneous heat and moisture transport in building components, One-and Two-Dimensional Calc. Using Simple Parameters. IRB-Verlag Stuttgart. (1995).
[7] H.M. Künzel, Effect of interior and exterior insulation on the hygrothermal behaviour of exposed walls, Mater. Struct. 31 (1998) 99–103.
[8] A. Hukka, H.A. Viitanen, A mathematical model of mould growth on wooden material, Wood Sci. Technol. 33 (1999) 475–485.

Hygrothermal performance of mass timber wall assembly with External Insulation Finish System

Villu Kukk[a], Jaan Kers[b,*], Targo Kalamees[a]

[a] Department of Civil Engineering and Architecture, Tallinn University of Technology, Tallinn, Estonia.
[b] Department of Materials and Environmental Technology, Tallinn University of Technology, Tallinn, Estonia
* villu.kukk@taltech.ee

Abstract:
The objective of this research was to evaluate the impact of the rainwater ingress and dry-out capacity on the hygrothermal performance of an MHM external wall with the ETICS. Estonian moisture reference year for mold growth as boundary conditions and wind-driven rain load with 1% of ingress were used in the analysis which were done based on the validated hygrothermal simulation model. Hygrothermal performance of the studied wall was evaluated by the risk of mold growth. The results of this study showed that using a vapor and airtight membrane between ETICS and MHM panels can prevent high humidity on the MHM panel surface in case of 1% of rainwater penetration and thereby avoids the risk of mold growth on a wooden surface. The given solution works only if the thermal insulation composite system provides sufficient dry-out towards the exterior and the use of EPS insulation is not recommended as it poses a high risk of mold growth on the MHM panel surface. In addition, based on the results it was recommended to keep the initial moisture content in mass timber panels below 17% to prevent the possible risk of mold growth.

Keywords:
Mass timber wall assembly, Massiv-Holz-Mauer, External Insulation Finish System, Hygrothermal performance.

1. Introduction

A 'Massiv-Holz-Mauer' (MHM) panel is structurally similar to the CLT (Cross Laminated Timber) product, where the layers of wooden boards are placed crosswise. The layers of wooden boards are nailed together in an MHM panel and the boards are enhanced with grooves on the surface to provide better insulation properties but which may, in turn, result in high air and vapor permeability. In terms of safe hygrothermal performance, the building envelope requires correct rain protection, air tightness, sufficient dry-out capacity (Ott et al., 2015) and the correct location and tightness of the vapor barrier. a ventilated façade, that provides second-stage protection against wind and precipitation, is more moisture safe than a rendered façade such as External Thermal Insulation Composite System (ETICS). Nevertheless, the use of ETICS is strongly desired due to low construction cost. Günther, S., Ringhofer, A., Schickhofer (2016) measured temperature and relative humidity (RH) for a period of two years in a wall with ETICS on CLT and concluded that further investigations are necessary in order to evaluate the differences between measurement and simulations. The objective of this research was to evaluate the impact of the rain-water ingress and dry-out capacity on the hygrothermal performance of an MHM external wall with the ETICS system.

2. Methods

The given study is focusing on the mass timber construction based external wall with ETICS. The external wall studied contained a 205 mm thick 9-layer MHM panel (made from Spruce, Picea abies) covered with 13 mm gypsum board from the inside and with an air and vapor tight membrane from the outside, followed by ETICS consisting of 150 mm high-density mineral wool (Rockwool) insulation with reinforced silicone resin-based plaster with the finish on top (Figure 1). Silicone resin-based plaster is commonly used for ETICS because of its elasticity and high vapor permeability and low water absorption properties. The plaster facade was finished with water-based silicone paint, which also has very high water vapor permeability and the inner surface of the wall was coated with latex paint.

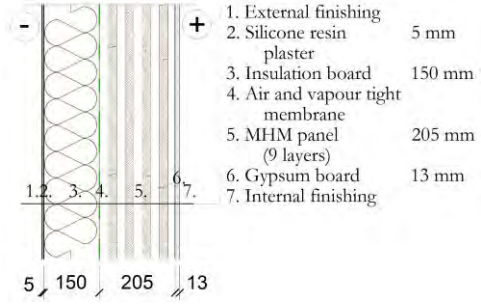

Fig 1: Cross section of the studied external wall with the list of layers of materials.

Hygrothermal simulation software Delphin 5.9.4 was used to create and validate the calculation model for the studied wall. The created hygrothermal simulation model has been validated in the previous study by comparison with results of field measurements, which were done in the same two-floor wooden detached house from where the given wall assembly was taken (Kukk et al., 2019). The studied wall was considered as adiabatic in other directions and therefore a one-dimensional simulation was performed.

The material properties were taken from the software Delphin 5.9.4 database and were adjusted according to the specifications of materials used in building construction. The list of materials together with the main properties used for the hygrothermal simulations are given in Table 1. Vapor resistance (S_d = 2.3 m) and total airtightness (the airtightness of the building (q_{50} = 0.8 $m^3/(m^2 \cdot h)$) was applied on the top surface (between the membrane and the MHM panel) of the MHM panel to represent the air and vapor tight membrane. Extra vapor resistance (S_d = 0.5 m) was also applied on the interior surface of the gypsum board layer to represent the vapor resistance of interior finishing (latex paint). Initial moisture content (MC) of the MHM panel was set at 17%. For all materials, the initial field conditions were set to RH of 80% and to a temperature of 20°C. The hygrothermal simulations began in July and were running repeatedly over a period of five years.

Table 1. Material properties used in the simulation.

Material	**d, mm**	**ρ, kg/m³**	**λ, W/(mK)**	**μ, -**	**γ, kg/(m²·s⁵)**
Gypsum board	13	745	0.18	11 **[**6.0**]**	0.179
MHM panel (*Pine*, 9 layers)	205	390	0.079	30 (RH~ 80%)	0.0024
CLT1/laminated wood (*Pine*)*	205	394	0.12	183	
CLT2/laminated wood (*Pine*)*	205	438	0.12	435	
Air and vapor tight membrane	0.45	-	0.17	5.11 (S_d=2.3 m/ 7.55 ft)	-
Rockwool (mineral wool) insulation board (RW)	150	134	0.039	1 **[**1.5**]**	0
Expanded polystyrene (EPS)*	150	23	0.036	96 **[**60**]**	$1x10^{-5}$
Silicone resin plaster	5	820	0.18	30 **[**10**]**	0.088

*****additional variations for calculations considering uncertainties*

The additional variability values for the water vapor diffusion resistance values as uncertainties of material properties were added in addition to the nominal values (Table 1, values given in brackets [ ]). Variability in properties were used for evaluating the mold growth risk and dry-out capacity (Figure 3 and 4). CLT was considered in simulations as a solid wood panel as an alternative solution in addition to use of the MHM panel and for comparing the dry-out capacity of these different materials in the same wall assembly.

Estonian moisture reference year (MRY) for mold growth that was used for the external climatic conditions is a real year, which was selected by analyzing the Estonian climate data from 1970 to 2000 (Kalamees and Vinha, 2004). For interior climatic conditions, moisture excess class 2 were selected by standard EN ISO 13788, (Ilomets et al., 2017). The moisture excess class 2 stands for ventilated occupational and living spaces with a population density more than 30 m^2 per person where at a temperature below 0°C the moisture excess is 4 g/m^3 in the interior and at a temperature above +20°C it is 1 g/m^3 (Ilomets et al., 2017). The indoor temperature was selected based on the investigations of hygrothermal conditions of Estonian dwellings (Ilomets et al., 2017), which has been considered suitable to be used with the MRY.

Klõšeiko P. (2014) investigated driving rain loads in the Estonian climate on façade orientations (FO) from 0 to 360° degrees (with a ten-degree interval) and the study covered the years 1970 to 2013, including MRY for mold growth analysis. He found the greatest driving load during the MRY and the most exposed façade orientation of 240°, West South West (WSW), with a rain load of 150 kg/m^2a. In addition to the 240°, façade orientations of 180° (115 kg/m^2a), South (S), and 300° (74 kg/m^2a), West North West (WNW), were also considered for the hygrothermal simulations. The simulation considered the possible rainwater penetration (ingress) and therefore 1% of wind-driven rain load was applied on the inner surface of the insulation board, next to the vapor tight membrane (ASHRAE 160).

Besides the considered rainwater penetration, expanded polystyrene (EPS) board was used in the simulation instead of mineral wool (Rockwool) insulation as an alternative solution in the most exposed façade orientation (FO 240 ° EPS).

The hygrothermal performance of the studied wall was evaluated by the risk of mold growth on the material surface. The evaluation was done via a mold growth index (a numerical scale), which is calculated through a function using temperature and relative humidity on the material surface and considers the materials sensitivity to mold growth and exposure time to critical RH (RHcrit.) and temperature (Ojanen et al., 2010). The wall assembly was considered hygrothermally safe when the calculated mold index value remained below one (M < 1 = no growth) during the 5-year period of simulation. An index above one indicates variously: small amounts of mold on surface M=1 (microscopic); several mold growth colonies on the surface (M=2; microscopic); visible mold on the surface, < 10 % coverage, or, < 50 % coverage of mold (M=3; microscopic). In the simulation, the MHM and CLT panels were considered as a pine (Pinus sylvestris.

3. Results and discussions

The location chosen for investigation was the exterior surface of the MHM panel (next to the vapor tight membrane) where the mold growth analyses were done. Figure 2 displays the results from the simulation of the studied wall assembly with wind-driven rain load in each selected façade orientation. The results showed that the façade orientation with 1% of penetrated rainwater did not have any significant effect to conditions between the airtight membrane

and the MHM panel. Neither result of 1% of rain ingress as RH between the membrane and the MHM panel differed less than 4% from the simulation results with (FO 240°) and without (FO 240° WRL – without rain ingress) 1% of rain load applied on the inner surface of insulation board. Membrane kept the MHM surface dry and the penetrated rainwater dried out only towards the exterior direction. After first year, when RH dropped from 70% to 56%, the RH between the MHM panel and membrane varied from 52% to 65% over the rest of the period of simulation. Considering that the favorable humidity conditions for mold growth are above critical RHcrit. (Viitanen and Ojanen, 2007) the simulation results did not show any risk of mold growth in the studied wall.

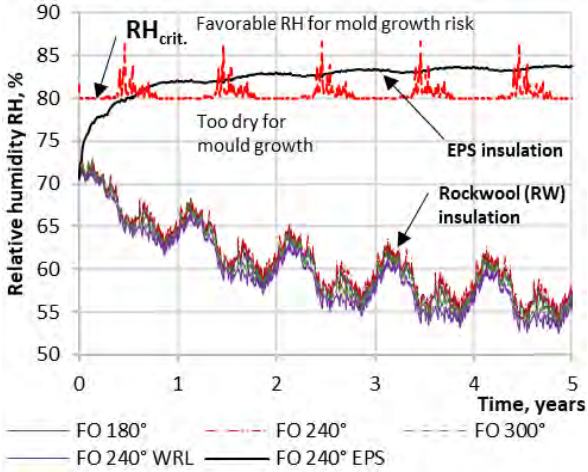

Fig 2: Relative humidity between the air and vapor tight membrane and MHM panel (initial MC of 17%) of the studied wall with 1% of penetrated rainwater in each façade orientation (FO, 0° = North).

When replacing the mineral wool insulation with expanded polystyrene board, the effect of the 1% rainwater ingress is clearly seen. The RH between the MHM panel and membrane increased from 70% to 84% over the period of simulation and the small growth trend continued. The moisture from rain ingress has been accumulating between the EPS and membrane and created favorable conditions for mold growth on the MHM panel surface. The use of mineral wool in an external insulation finished system can be considered essential for mass timber construction and use of EPS as external insulation is not recommended. Künzel M. H. and Zirkelbach D. (2008) found the risk of moisture damage in the lightweight timber structures covered with ETICS caused by the penetration of the driving rain load. They investigated the ETICS with EPS insulation and simulated the scenario where rain ingress occurred on the surface of the OSB sheathing. Moisture risks in timber frame walls with rendered and unventilated facades were found also by Samuelson I., Mjörnell K. and Jansson A. (2008) and they concluded that the ETICS constructions should be avoided for timber frame walls.

The simulation results of the studied wall with an initial MC of 17% in the MHM panel and with 1% of rainwater ingress to the insulation showed safe hygrothermal performance. However, the increase of initial MC in mass timber construction has previously shown an increase in the risk for mold growth (Kukk et al., 2018; McClung et al., 2014) and therefore the simulations of the studied wall assemblies were performed at higher MC in the MHM panel. The simulations were done with initial moisture contents of the MHM panel of 19% and 20% insulated with Rockwool and 13% for the wall assembly insulated with EPS. The results given in Figure 3 are showing that the RH between the MHM panel and the air-tight membrane occurred higher than RHcrit. in the beginning of the simulation period in the wall assemblies insulated with Rockwool due to dry-out of MHM panel at higher MC (MC > 19%). In the wall assemblies insulated with EPS the high RH (> RHcrit.) between the MHM panel and the air tight membrane occurred over a period of time (from 22 to 30 months, depending on the water vapor resistance of EPS) even with very low MC in the MHM panel (13%) due to moisture accumulation between insulation and membrane due to 1% of rainwater ingress. These results are showing that the risk of mold growth occurs with Rockwool insulation due to dry out at a high initial MC, but when using EPS insulation, the mold growth risk occurs even at a very low initial MC due to moisture accumulation caused by rain ingress. This gives another reason to prefer mineral wool insulation over EPS, because the initial MC in a mass timber panel can be kept at a certain value during the production and installation period at the construction site by strictly following a moisture safety plan (the purpose of the moisture safety plan is to protect wooden structures from excessive moisture during construction to prevent any moisture damage), but the moisture accumulation due to rainwater ingress during service life is unpredictable.

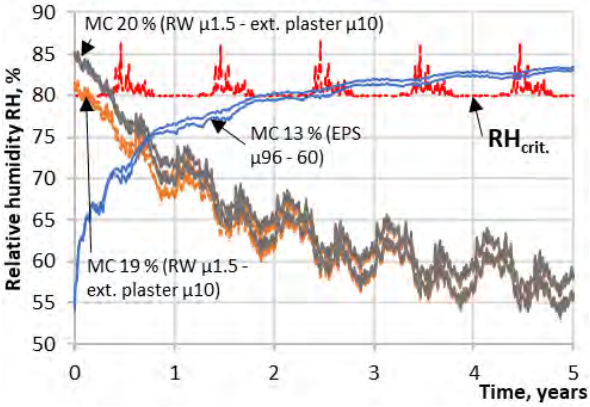

Fig 3: Dry-out capacity of the studied wall assemblies with different initial MC in MHM panels.

As seen from Figure 4, the variability of water vapor diffusion resistance in simulation results is demonstrated as the area between the lowest and highest mold index for each different initial moisture

content in an MHM panel. Most of the results showed a mold growth index exceeding 1 during the calculation period with an initial MC of 20% in the MHM panel in the wall assembly insulated with mineral wool (MHM_MC20%_RW). With an initial MC of 19% in the same wall assembly (MHM_MC19%_RW) the risk of mold growth did not occur. An initial MC of 17% in the CLT (CLT1) panel made from lower density and lower vapor diffusion resistant pine wood and 16% in the CLT (CLT2) panel with higher density and higher vapor diffusion resistance were the upper limits at which the risk of mold growth did not occur. With an initial MC of 13% in the MHM panel in the wall assembly insulated with EPS, the mold index exceeded 1 over a period from 33 to 37 months and exceeded 2 before the 5-year period was completed. Despite the fact that mineral wool insulation ensures sufficient moisture dry-out capacity from rain ingress and an air and vapor tight membrane keeps the timber structure dry from the other side, the high initial MC in mass timber construction may still cause the risk of mold growth. The results of this study confirmed that regulated limits of allowable moisture content for glue laminated timber should be 10-16%. Allowable MC for CLT has been found in several studies to be 15% in wall assemblies with vapor tight interior insulation (Kukk et al., 2018) and 20% with high vapor permeable wall assemblies (McClung et al., 2014).

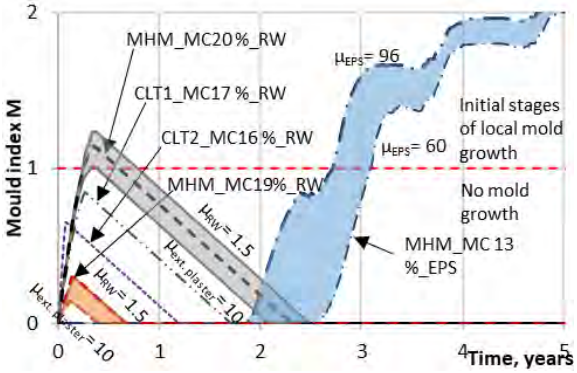

Fig 4: Calculated mold index in five-year simulation of the studied wall assemblies with different initial MC in MHM and CLT panels.

The results of the variations in material properties showed that the vapor diffusion resistance of insulation and the properties of the mass timber panel had the biggest impact on mold growth risk. The increase of diffusion resistance in mineral wool (μRW 1.0 → μRW 1.5) created the upper line (highest mold index/ growth risk) in the area of the variability (MHM_MC19/20%_RW) and the decrease of resistance (μEPS 96 → μEPS 60) in the EPS insulation wall assembly (MHM_MC13%_EPS) created the lower line (lowest mold index). Use of CLT showed the great importance of the properties of the selected timber product for the given wall assembly. Solid wood panels with higher density and higher vapor diffusion resistance have a much lower dry-out capacity and therefore are more sensitive to mold growth risk with a higher initial MC.

The analyze of the results in this study was made only for one location, between the vapor and airtight membrane and the MHM panel, which was considered the most critical from a mold growth risk point of view. Future studies should also cover the analyze of other locations, such as between the plaster and insulation layers and between the insulation and the vapor tight membrane, which may also have an effect on the hygrothermal performance of the studied wall. The MHM panel has been barely studied scientifically and therefore accurate materials properties are unknown. Future studies should include determining the physical material properties of MHM panels for better analysis of the hygrothermal performance of the building envelope. In addition, a two-dimensional simulation is required as an MHM panel cannot be considered as airtight material and the impact of air gaps between the wooden boards in the panel on the material properties needs to be investigated in future studies.

4. Conclusions

Using vapor and airtight membrane between ETICS and the MHM panel can prevent high humidity on the MHM panel surface in the case of 1% rainwater ingress and thereby avoids the risk of mold growth on a wooden surface. The given solution works only if the thermal insulation composite system provides sufficient dry-out towards the exterior and this study showed that the use of mineral wool as external insulation is essential for mass timber wall assemblies. EPS insulation in ETICS for mass timber external walls is not recommended as it poses a high risk of mold growth on the MHM panel surface.

In addition, based on the results it was recommended to keep the initial moisture content of the mass timber panel below 17%, which is the common regulation, to prevent an extended drying-out period and thereby prevent the possible risk of mold growth in the given wall assembly.

Acknowledgements

This research was supported by the Estonian Research Council with Personal research funding PRG483 “Moisture safety of interior insulation, constructional moisture, and thermally efficient building envelope”, Estonian Centre of Excellence in Zero Energy and Resource Efficient Smart Buildings and Districts, ZEBE, grant TK146 funded by the European Regional Development Fund.

The author wishes to thank Estonian manufacturer of prefabricated timber frame houses EstHus OÜ and the owner of the detached house Ermo-Raiki Rebane for cooperation.

References

ASHRAE 160: 2016. Criteria for Moisture-Control Design Analysis in Buildings.

EN ISO 13788: 2017. Hygrothermal performance of building components and building elements - Internal surface temperature to avoid critical surface humidity and interstitial condensation - Calculation methods.

Günther, S., Ringhofer, A., Schickhofer, G., 2016. External thermal insulation composite systems in solid timber construction, in: 2016 World Conference on Timber Engineering, WCTE 2016. Vienna University of technology, Vienna, Austria.

Ilomets, S., Kalamees, T., Vinha, J., 2017. Indoor hygrothermal loads for the deterministic and stochastic design of the building envelope for dwellings in cold climates. J. Build. Phys. 41, 547–577.

Kalamees, T., Vinha, J., 2004. Estonian Climate Analysis for Selecting Moisture Reference Years for Hygrothermal Calculations. J. Therm. Envel. Build. Sci. 27, 199–220.

Klõšeiko, P., 2014. Hygrothermal Performance of a Brick Wall With Interior Thermal Insulation: a Case Study in Kohtla-Järve School Building. Tallinn University of Technology.

Kukk, V., Kers, J., Kalamees, T., 2019. Field measurements and simulation of a massive wood panel envelope with ETICS. Wood Mater. Sci. Eng. (under rev.

Kukk, V., Külaots, A., Kers, J., Kalamees, T., 2018. Influence of interior finishing and insulation on dry-out of CLT walls. Can. J. Civ. Eng. (under Rev.

Künzel, H.M., Zirkelbach, D., 2008. Influence of rain water leakage on the hygrothermal performance of exterior insulation systems, in: 8th Nordic Symposium of Building Physics. pp. 253–260.

McClung, R., Ge, H., Straube, J., Wang, J., 2014. Hygrothermal performance of cross-laminated timber wall assemblies with built-in moisture: field measurements and simulations. Build. Environ. 71, 95–110.

Ojanen, T., Viitanen, H., Peuhkuri, R., Lähdesmäki, K., Vinha, J., Salminen, K., 2010. Mold Growth Modeling of Building Structures Using Sensitivity Classes of Materials, in: Thermal Performance of the Exterior Envelopes of Buildings XI. ASHRAE, Florida.

Ott, S., Tietze, A., Winter, S., 2015. Wind driven rain and moisture safety of tall timber houses – Evaluation of simulation methods. Wood Mater. Sci. Eng. 10, 300–311.

Samuels, I., Mjörnell, K., Jansson, A., 2008. Moisture damage in rendered, undrained, well insulated stud walls, in: Proc. 8th Symposium of Building Physics in the Nordic Countries. Copenhagen, pp. 1253–1260.

Viitanen, H., Ojanen, T., 2007. Improved Model to Predict Mold Growth in Building Materials.

Hygrothermal response of tallwood building enclosures to climate change in different climate zones in Canada

M. Defo[a*], M.A. Lacasse[b]

[a] National Research Council Canada, Ottawa (ON), K1A 0R6
[b] National Research Council Canada, Ottawa (ON) K1A 0R6
* Corresponding author, Phone: (603) 990-0223; Email: Maurice.defo@nrc-cnrc.gc.ca

Abstract:
Within the context of climate change and in order to reduce the carbon footprint of buildings, mass timber products are increasingly used in mid-rise and high-rise buildings. As such, considerable efforts have been invested in developing technical data to support their implementation in North America, with primary emphasis placed on assessing structural, fire, and acoustical performance. Whilst many mass timber buildings have been or are being constructed in many jurisdictions across the country, there are still concerns about the thermal and hygrothermal response and expected moisture performance of mass timber products used in building enclosures. Climate change notwithstanding, tallwood buildings are subjected to increased wind and rain loads given increases in building height. This prolongs the exposure of building enclosures to wind-driven rain and wind loads, and increases the risk of premature deterioration of wood-based wall and roof assemblies. It is also anticipated that future projections of the effects of climate change and extreme weather events will exacerbate the situation. The objective of this study is to assess the potential impacts of climate change on the moisture performance and durability of tallwood building envelopes, using hygrothermal simulations. Deficiencies in the walls that may lead to rain penetration are considered. Potential pathways to adapt design of massive timber to climate change are also explored.

Keywords:
Tallwood buildings, moisture performance, climate change.

1. Introduction

Tallwood buildings have been or are being constructed in many jurisdictions across the country (e.g., Brock Commons tallwood building at UBC, Origine tallwood building in Quebec City). The wall assemblies are designed to ensure moisture durability, energy efficiency, fire safety and noise control. In cold, heating dominated climate zones, the use of exterior insulation is the preferred thermal design approach (Gagnon & Pirvu, 2011; Karacabeyli & Lum, 2014). From exterior to interior, massive timber wall assemblies comprise cladding, drainage cavity, insulation, air barrier/water resistive barrier, and cross-laminated timber (CLT) panel. The CLT panel is encapsulated in drywall for fire safety but where it is permitted, it can be left exposed. The use of vapour permeable insulation is recommended to allow outward drying of the CLT if initially wetted or if there is water penetration due to deficiencies. There is no need for a vapour barrier since the CLT panel provides sufficient outward vapour resistance. The material and thickness of insulation depend on the climate zone in which the building is located. Tall buildings are subjected to increased wind and rain loads given increases in building height. This prolongs the exposure of building enclosures to wind-driven rain and wind loads, and increases the risk of water entry to the wall and thus premature deterioration of wood-based wall and roof assemblies.

There is sufficient evidence that the climate has been warming globally thereby causing more frequent and intense and extreme climate events such as heat waves, droughts, wild fires, snow and ice storms, flooding, as well as wind and hail storms (IPCC 2014). These changes to the climate will have significant effects on building infrastructures and communities, particularly the durability of building materials, as well as the comfort and health of building occupants (Bizikova et al. 2009).

The objective of this preliminary work is to evaluate the effects of climate change on the hygrothermal performance and durability of massive timber products used in tallwood building envelopes in different climate zones across Canada. This will provide a basis for an ongoing and broader study on the impacts of climate change and extreme events on tallwood buildings across Canada to provide a suitable basis for assuring the durable and climate resilient design for these structures.

2. Methods

2.1 Characteristics of cities selected

Five Canadian cities were selected for this preliminary study: Calgary (AB), Ottawa (ON), Vancouver (BC), Winnipeg (MB) and St-Johns NL). Table 1 shows their location and current climate design data as reported in the 2015 edition of the National Building Code of Canada (NBCC 2015). Ottawa and St-Johns are within

the same climate zone but the moisture index (MI) and driving rain wind pressure (DRWP) are higher in St-Johns than in Ottawa. As well, Calgary and Winnipeg are in the same climate zone but the annual rain is higher in Winnipeg that in Calgary while the DRWP is higher in Winnipeg than in Calgary.

Table 1: Location and climate design data of the selected cities

City (province)	Lat (°)	Long (°)	TZO	H (m)	CZ	HDD	MI	Rain (mm)	DRWP (Pa)
Vancouver (BC)[1]	49.3	-123.1	-8	5	4	2825	1.44	1400	160
Ottawa (ON)[2]	45.3	-75.4	-5	125	6	4500	0.84	750	160
St-Johns (NL)	47.6	-52.7	-4	65	6	4800	1.41	1200	400
Calgary (AB)	51.1	-114.1	-7	1045	7A	5000	0.37	325	220
Winnipeg (MB)	49.9	-97.1	-6	235	7A	5670	0.58	415	180

[1]: City Hall; [2]: M-C Int'l Airport; DRWP: Driving Rain Wind Pressure, 1/5; H: Elevation
Lat: Latitude; Long: Longitude; TZO: Time zone; CZ: Climate zone
HDD: Heating Degree-Days below 18 oC; MI: Moisture index

2.2 Building and wall components

A 13-storey (~41 m) building with flat roof was considered for this study. For this type of building, the intensity of rain deposition is higher at the top and edges of the wall in accordance with the studies of Straube and Burnett (2000). In this study, only the top area of the building will be considered.
Fig **1** shows the typical composition of the massive timber wall considered for this study. It is a non-load-bearing wall having a 3-layer CLT. Two claddings were considered: aluminum composite material and fiberboard. The general configuration inboard of the cladding consisted of: (1) drainage cavity of 19 mm; (2) mineral fibre insulation (3) sheathing membrane (30-minute paper, asphalt saturated conforming to CAN/CGSB 51.34-M); (4) 3-layer CLT; (5) air cavity (19 mm); and (6) Interior grade gypsum panel with latex primer and 1 coat of latex paint.

For climate zones 4 (Vancouver, Richmond area), 6 (Ottawa and Saint-Johns), and 7A (Calgary and Winnipeg), the minimum RSI-value as recommended by the National Energy Code for Buildings (NECB 2015) for above grade opaque walls is 3.18, 4.05 and 4.76 m^2K/W, respectively. To meet this requirement, two rows of 64 mm and 89 mm mineral fibre were used as insulation for climate zone 4 and 6, and 7A, respectively.

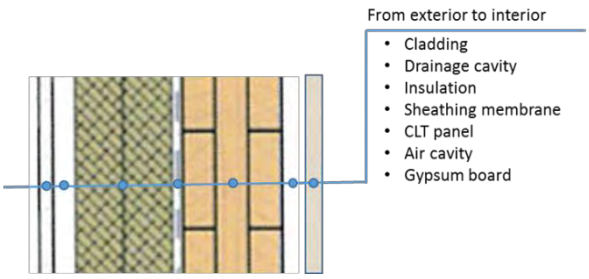

Fig 1: Typical composition of massive timber wall

Material properties were all obtained from the National Research Council hygrothermal material properties database (Kumaran et al. 2002), with the exception of the CLT adhesive layer. The CLT adhesive layer (assumed to extend 2 mm deep in the plank) was modelled with the same material properties as spruce, with the exception that the water vapour permeability and liquid water diffusivity were decreased by 50%. In fact, previous studies on the characterization of the hygrothermal properties of CLT have shown that its vapour permeability and moisture diffusivity are substantially reduced in comparison with solid wood (AlSayegh 2012).

2.3 Climate loads

A detailed description of the procedure used to generate historical and projected future climate data can be found in Gaur et al. (2019). The data is comprised of hourly time-series of climate variables necessary to undertake hygrothermal simulations for a baseline time-period spanning 1986–2016 and 31-year long future time-periods when global warming of 2 ◦C and 3.5 ◦C (with reference to the baseline time-period) are expected to be reached in the future. The climatic datasets were generated to capture the effects of the internal variability of the climate on future climate projections in fifteen hourly realizations that are part of the datasets derived from the large ensemble of climates simulated by the Canadian Regional Climate Model—version 4 (CanRCM4), each initialized under a different set of initial conditions in the CanESM2 global climate model.

For this study, only the 31-year (1986-2016) historical (H) and future (2062-2092) time-period corresponding to global warming of 3.5 ◦C (F) were considered. As mentioned above, each timeline comprises 15 realizations or runs. For this study only the median run based on moisture index (MI) was selected from each timeline. The moisture index (Cornick et al. 2003) of a run was calculated as the average of the 31 yearly MI of that run. The difference in some of the climate variables between the median runs of historical and future data sets for the five cities considered are illustrated in Table 2. It can be observed that: (1) the annual average temperature will increase significantly between the two timelines in all five cities; (2) the relative humidity will not change significantly but due to increase temperature, the partial vapour pressure will increase significantly in all 5 cities; (3) the annual rain will increase Ottawa, St-Johns and Winnipeg but will decrease in Vancouver and Calgary; and (4) the average annual wind speed will remain unchanged but with more fluctuations in St-johns.

2.4 Hygrothermal simulations

For this study, only a one-dimensional horizontal configuration was analyzed as indicated in Figure 1. This configuration excludes the strappings/furring.

Table 2: Comparison of historical (1986-2016) and future (2062-2092) annual average temperature, relative humidity, vapour pressure and wind speed, and annual sum of rain.

		Ottawa		Vancouver		Calgary		Saint-Johns		Winnipeg	
Variable	Statistic	H	F	H	F	H	F	H	F	H	F
Temperature (°C)	Avg	6.7	12.1	10.5	14.7	4.8	9.3	3.7	8.1	3.7	9.0
	SD	1.0	0.8	0.7	0.9	1.2	1.0	0.8	0.8	1.1	1.1
Relative humdidity (%)	Avg	71.4	73.5	62.3	62.5	62.3	62.7	82.7	83.0	71.9	72.4
	SD	1.3	1.4	1.0	0.7	2.5	2.6	0.7	0.7	1.9	2.1
Vapour pressure (Pa)[1]	Avg	703	1037	794	1050	534	736	657	897	572	830
Annual rain (mm)	Avg	762	911	**1250**	**1238**	357	439	1114	1301	408	439
	SD	131	166	181	215	90	104	141	156	115	119
Wind speed (m/s)	Avg	3.5	3.4	2.8	2.6	3.9	3.8	5.6	5.5	4.2	4.0
	SD	0.1	0.1	0.1	0.1	0.2	0.2	0.1	0.2	0.2	0.2

H: historical data (1986-2016); F: future data based on 3.5 °C global warming (2062-2092); Avg: average; SD: Standard deviation

[1]: Vapour pressure was calculated based on averge RH and temperature

Simulations were run using the DELPHIN simulation tool (version 5.9.4).

The moisture reference years (MRYs) were selected based on the Moisture Index (MI) as described by Cornick et al. (2003). The years with the median MI and that with the highest MI of the 31-year series were chosen. MRYs were then formed by concatenating data for the median year followed by the median year again and then the wettest year. This scheme was meant to condition the wall using average conditions and then submit it to the most severe conditions.

The wall orientation was selected as the direction in which the highest wind driving rain quantities occurs for the two MRYs using the wind-driven rain rose. It was for both historical and future timeline SSW for Ottawa, SSE for Vancouver and St-Johns, WNW for Calgary, ENE and ESE for Winnipeg historical and future data, respectively.

The amount of rainwater impinging on building façades was determined using the ASHRAE Standard 160 (ANSI/ASHRAE 2016) assuming an exposure factor of 1.5 (height > 20 m) and a deposition rate of 1.0 (wall subject to runoff). Moisture source was determined assuming water entry beyond the cladding and finding its way through insulation to reach the sheathing membrane. With uncertainties about the quantity of water that penetrates the structure, it was assumed to be 1% of wind-driven rain (WDR) was deposited on the exterior surface of the sheathing membrane based on the ASHRAE Standard 160.

The initial conditions for relative humidity (RH) and temperature (T) for all components were set to 60% and 21 °C, respectively. Indoor T and RH were kept constant at 21 °C and 50%, respectively, assuming that the building is equipped with air conditioning and dehumidification. Referring to ISO 6946 Standard (ISO 2017), the indoor convective heat transfer coefficient was set to 2.5 W/m^{2}K, and the outdoor convective heat transfer coefficient was calculated using Eq. 1:

$$\alpha_{ce} = 4 + 4V \quad (1)$$

Where

α_{ce} = outdoor convective heat transfer coefficient (W/m^{2}K)

V = wind speed (m/s)

The outdoor and indoor convective vapour transfer coefficients were calculated using the Lewis number (Incropera and DeWitt 1996). The indoor radiative heat transfer coefficient was set to 5.5 W/m^{2}K (ISO 2017) whereas the longwave exchange between the cladding surface and the environment was explicitly calculated assuming longwave emissivity of 0.9 for the surface and the surrounding ground, and with ground surface temperature equal to the air temperature. The ground surface albedo was set to 0.2. The shortwave absorption coefficient of the cladding was set 0.6, assuming a red-coloured surface.

The air was assumed still in the air cavity between drywall and CLT but moving in the drainage cavity with an air change per hour (ACH) of 10.

2.5 Performance assessment

The outer layer (~ 0.5 mm) of CLT was used as the critical location from which to compare effects of climate change on the moisture performance of the wall, using the mould growth index (MoI) as the indicator. As recommended by ASHRAE Standard 160, the empirical model used for calculating MoI was the one developed by Hukka and Viitanen (1999) and Ojanen et al. (2010). The maximum and average MoI, as well as the sum of the total hours where MoI remains above 3 (level at which mould is visible) were used for comparison.

3. Results and discussion

The conditions of T and RH of the outer layer of the CLT panel were unfavourable for mould growth in all cities for the fibreboard and aluminum claddings considered and for both historical and future climate data when it was assumed that there were no

deficiencies allowing rainwater to infiltrate the wall beyond the exterior cladding.

Table 3 shows the maximum and the average MoI, and the total number of hours for which the MoI was greater than 3 when water infiltration was considered (1% WDR). In general, risk of mould growth will decrease in the future in Winnipeg and Vancouver, slightly increase in Ottawa and Calgary and significantly increase in St-Johns for both fibreboard and aluminum claddings considered. It should be noted that under the present climate, the design considered with 19-mm drainage cavity and 30-minute asphalt saturated paper, presents a risk of mould development in Vancouver and St-Johns, especially for fibreboard cladding. In fact, the maximum MoI, the average MoI and the total number of hours with MoI greater than 3 are 5.0, 3.7, and 17618, respectively, in Vancouver, and 3.6, 2.3, and 12035, respectively, in St-Johns. While the risk will be significantly reduced in Vancouver due to a reduction in rainfall (Table 2), the increase in rainfall in St-Johns (Table 2) will lead to an increased risk of mould growth; from 3.6 to 4.9 for maximum MoI, from 2.3 to 3.8 for average MoI and from 12035 to 20413 for the total number of hours with MoI values greater than 3. For this reason, different assumptions to mitigate the risk in the city of St-Johns were tested.

Table 3: Mould growth index statistics for historical (H) and future (F) timeline

Cladding	Mould index parameter	Ottawa H	Ottawa F	Vancouver H	Vancouver F	Calgary H	Calgary F	St-Johns H	St-Johns F	Winnipeg H	Winnipeg F
Fibreboard	Maximum	0.2	1.6	5.0	5.0	0.1	0.2	3.6	4.9	0.8	0.2
	Average	0.0	0.4	3.7	1.2	0.0	0.0	2.3	3.8	0.1	0.0
	Hours > 3[a]	0	0	17618	5770	0	0	12035	20413	0.0	0.0
Aluminum	Maximum	0.1	1.2	4.3	3.4	0.1	0.1	1.2	4.1	0.4	0.1
	Average	0.0	0.0	2.5	0.5	0.0	0.0	0.5	2.3	0.0	0.0
	Hours > 3	0.0	0.0	12851	3409	0	0	0	8700	0	0

[a]: Total number of hours during which the mould index was greater than 3

The original assumptions used for simulations comprised a drainage cavity of 19 mm, an air change per hour (ACH) of 10, a 30-minute asphalt saturated paper with a vapour permeance (VP) of 490 ng/m^{2}sPa and a water penetration rate of 1%WDR. Under these assumptions, the wall does not perform well in St-Johns under historical and future climate. The first solutions tested were to replace the 30-minute paper with a more breathable membrane such as 60-minute paper (VP = 2600 ng/m^{2}sPa) or spun bonded polyolefin (VP = 4080 ng/m^{2}sPa). As shown in Table 4, none of these solutions improved the performance. The air change was modified to 20, which supposes a more ventilated cavity, but the risks are still relatively high (Table 4). Doubling the depth of the drainage cavity to 38 mm whilst keeping the number of ACH to 10 did not also improve the performance. The only two options that can maintain the durability of the wall in the future are (Table 4): (1) using the original assumptions but with reduced water penetration to 0.5 and 0.25% WDR; and (2) increase the drainage cavity depth to 38 mm with an ACH of 20 and a more breathable spun bonded polyolefin. Option (1) supposes substantially reducing the water leakage of the wall, which can be difficult to achieve especially over the long term as the building ages. Option (2) is more relevant as it tolerates water penetration of 1%WDR and can be easily implemented.

Table 4: Results obtained using several assumptions to mitigate the risk of mould growth in St-Johns.

Assumptions tested	Mould index Max	Avg	Hours > 3
DC19 & ACH10 & 30M & WS1%	4.9	3.8	20413
DC19 & ACH10 & **60M** & WS1%	4.7	3.4	19058
DC19 & ACH10 & **SBP** & WS1%	4.8	3.2	16772
DC19 & **ACH20** & 30M & WS1%	4.8	3.5	17391
DC19 & **ACH20** & **60M** & WS1%	4.7	3.1	16452
DC19 & **ACH20** & **SBP** & WS1%	4.6	2.7	12549
DC19 & ACH10 & 30M & **WS0.5**%	3.7	1.6	2909
DC19 & ACH10 & 30M & **WS0.25%**	0.1	0.0	0
DC38 & ACH10 & 30M & WS1%	4.9	3.5	17393
DC38 & ACH10 & **60M** & WS1%	4.7	3.1	16516
DC38 & ACH10 & **SBP** & WS1%	4.6	2.8	12639
DC38 & **ACH20** & **30M** & WS1%	4.7	3.0	15689
DC38 & **ACH20** & **60M** & WS1%	4.4	2.4	12638
DC38 & **ACH20** & **SBP** & WS1%	2.0	1.3	0

DC19: Drainage cavity of 19 mm
DC38: Drainage cavity of 38 mm
ACH10: Air change per hour of 10
ACH20: Air change per hour of 20
WS1%: 1% of WDR applied as water source
WS0.5%: 0.5% of WDR applied as water source
WS0.25%: 0.25% of WDR applied as water source
30M: 30 minutes paper, vapour permeance = 490 ng/m^{2}sPa
60M: 60 minutes paper, vapour permeance = 2600 ng/m^{2}sPa
SBP: Spun bonded polyolefin, vapour permeance = 4080 ng/m^{2}sPa
In bold are modifications added to the original assumptions.

4. Conclusions and outlook

The objective of this study was to assess the impact of climate change on the moisture performance of massive timber walls in five cities having different climate characteristics: Ottawa (ON), Vancouver (BC), Calgary (AB), Winnipeg (MB) and St-Johns (NL). The configuration of the wall studied comprised aluminum or fibreboard cladding, drainage cavity of 19 mm, 30-minute asphalt saturated paper, mineral fibre insulation, 3-layer CLT panel, air cavity and gypsum board. Simulation results showed that the risk of mould growth will decrease or will not significantly change in Ottawa, Calgary, Vancouver and Winnipeg. Whereas it was determined that in St-Johns, the risk will increase, especially with a wall incorporating fibreboard cladding, replacing the 30-minute paper with a spun bonded polyolefin and increasing the depth of the drainage cavity can substantially minimize this risk.

Acknowledgements

This work was carried out by the National Research Council of Canada with funding from Infrastructure Canada in support of the Pan Canadian Framework on Clean Growth and Climate Change. The authors are very thankful for their support.

References

AlSayegh, G. (2012). *Hygrothermal properties of Cross-Laminated Timber and moisture response of wood at high realive humidity.* Carleton University, Civil and Environmental Engineering. Ottawa: Carleton University.

ANSI/ASHRAE. (2016). *ASHRAE Standard 160-2016. Criteria for Moisture-Control Design Analysis in Buildings.* Atlanta: ASHRAE.

Bizikova, L., Neale, T., & Burton, I. (2009). *Canadian communities' guidebook for adaptation to climate change.* Ottawa: Adaptation and Impacts Research Division, Environment Canada.

Cornick, S., Djebbar, R., & Dalgliesh, W. A. (2003). Selecting moisture reference years using a moisture index approach. *Building and Environment, 38*(12), 1367-1379.

Gagnon, S., & Pirvu, C. (2011). *Cross-Laminated Timber. Special Publication. SP-528E.* Pointe-Claire, QC: FPInnovations.

Gaur, A., Lacasse, M., & Armstrong, M. (2019). Climate data to undertake hygrothermal and whole building simulations under projected climate change influences for 11 Canadian cities. *Data, 4*(2), 72.

Hukka, A., & Viitanen, H. (1999). A mathematical model of mould growth on wooden material. *Wood science and Technology, 33*, 475-485.

Incropera, F. P., & DeWitt, D. P. (1996). *Fundamentals of heat andmass transfer* (4th ed.). New York: John Wiley and Sons.

ISO. (2017). ISO 6946 (Building components and building elements - Thermal resistance and thermal transmittance - Calculation methods). Switzerland.

Karacabeyli, E., & Lum, C. (2014). *Technical Guide for the Design and Construction of Tall Wood Building in Canada. 1st ed. Special Publication SP-55E.* Pointe-Claire, QC: FPInnovations.

Kumaran, M. K., Lackey, J. C., Normandin, N., Tariku, F., & van Reenen, D. (2002). *A termal and moisture transport property database for common building and insulation materials. ASHRAE Research Project 1018-RP, 229pp.*

NBCC. (2015). *National Building Code of Canada.* Ottawa: National Research Council of Canada.

NEBC. (2015). *National Energy Code of Canada for Buildings.* Ottawa: National Research Council of Canada.

Ojanen, T., Viitanen, H., Peuhkuri, R., Lâhdesmäki, K., Vinha, J., & Salminen, K. (2010). Mold growth modeling of building structures using sensitivity classes of materials. *Pro. Building XI.* Florida.

Straube, J. F., & Burnett, E. F. (2000). Simplified prediction of driven rain deposition. *Proceedings of the international building physics conference.* Eindhoven.

Assessment of summertime overheating conditions in vulnerable buildings in Montréal

Liangzhu (Leon) Wang [a,*], Chang Shu [a], Hua Ge [a], Radu Zmeureanu [a], Michael Lacasse [b], Sylvie Leroyer [c], Stephane Belair [c], Lili Ji [a], Xuechen Bai [a, d], Lin Wang [a], Mohammad Mortezazadeh [a], Ali Katal [a]

[a] Centre for Zero Energy Building Studies, Building, Civil and Environmental Engineering, Concordia University
[b] Construction Research Center, National Research Council Canada, Canada
[c] Meteorological Research Branch, Environmental Numerical Prediction, Environment and Climat Change Canada
[d] School of Economics and Finance, Xi'an Jiaotong University, Xi'an, China
* Corresponding author, Tel 514-848-2424 ext. 5766, email leon.wang@concordia.ca

Abstract:
In Montreal, following a heatwave in 2018, up to 53 deaths were reported with most being elderly, and who suffered from mental or chronic illness. Most of them lived in buildings without access to air-conditioning and vulnerable communities of the city center, where it is significantly hotter than rural areas. To ensure the resiliency of Canadian buildings against overheating, and protect Canadians' health from a changing climate, Concordia University is leading a national research project collaborating with the National Research Council, Environment Canada and Climate Change, and Health Canada on the assessment and mitigation of summertime overheating in vulnerable buildings of urban agglomerations. The research activities include 1). Field monitoring: Indoor thermal conditions of selected buildings and exterior climatic conditions will be monitored to assess risks of summertime overheating. 2). Simulations: Development of urban-scale microclimate model and building-scale overheating model. The urban-scale model will be developed to simulate the surrounding microclimate effects on specific buildings for the detailed whole building simulations to predict indoor thermal conditions under extreme heat events. 3). Mitigations: Development of mitigation strategies at building levels by considering urban-scale microclimate and climate change for different Canadian climatic zones. 4). Guidelines: Development of design guidelines to support the National Building Code of Canada and Canadian construction standards to address climate change. This paper reports the most recent progress of the field monitoring and simulation tasks with the focus on Montreal, Canada.
Keywords:
buildings, climate change, health effects, forecasting, modeling, summertime overheating, urban agglomerations, vulnerable population

1. Introduction

It is unequivocal that the global climate has been consistently warming over the past decades and is projected to worsen in the future [1]. Furthermore, extreme climate events such as heatwaves are projected to increase in frequency and intensity [2]. Overheating of building interior spaces as may arise from such climate change and extreme heat events have been identified as a major concern to the comfort and health of building occupants particularly of the vulnerable people such as the homeless, elderly, children, socially disadvantaged people, the physically challenged or the sick. Urban area centers that are subject to the urban heat island (UHI) effects may exacerbate the risk of the overheating events in that the indoor thermal conditions can reach excessive values over a prolonged period. In a recent heatwave of June 30 – July 7, 2018, up to 53 deaths were reported in Montreal with most of them being older residents, such as those people who suffered from mental or chronic illness and addiction more easily than the others, as they were left without access to air conditioning in vulnerable communities of the city center [3].

Buildings play a major role in limiting the risk of overheating events [4]. Buildings influence the indoor thermal conditions to which occupants are exposed most of the time, given the fact that Canadian spend approximately 80% to 90% of their time indoors [5]. Buildings that house vulnerable people and/or with poor management of indoor thermal conditions will suffer the most from the effects of overheating. The severity of the indoor conditions depends on many factors of buildings: types (houses, retirement homes, apartment buildings, schools, hospitals, etc.), internal space usage (occupant density, internal heat gains), construction characteristics (insulation levels, window proportions, solar shading, orientation of facades), and building operation (air-conditioning use, natural ventilation, etc.) [6].

However, studies on building indoor thermal conditions as relating to the outdoor conditions are still very limited in Canada to enable the health care and building code organizations to establish threshold exposure limit of temperature and relative humidity to protect the health of the vulnerable population, which could be attributed to the following limitations and challenges: 1). There is a major lack of field monitoring data of indoor thermal environments for different building types in Canada. As a result, no reliable benchmarking data are available to support the assessment of the resilience level of the existing building stocks against overheating, and the establishment of threshold overheating exposure limit criteria. 2). There are limited simulation studies for establishing correlations between indoor and outdoor conditions, and the development of climate-adaptive mitigation strategies for developing associated guidelines against overheating. Accurate whole building performance simulations require adequate validations against field monitoring data. In the previous simulation study by Symonds et al. [7], the simulation results were not in good agreement with the measurements due to the lack of dwelling data. In this study passive building mitigation strategies, including shading and natural ventilation, will be tested on the developed simulation models. 3). The whole building simulations also require accurate and detailed inputs of

surrounding ambient conditions, which were often based on global/regional-scale weather and climate change data in the previous studies without considering the impacts from local microclimate environment down to building scales [8]. A scientific challenge still remains to derive reliable climate change information at a spatial resolution that is relevant for building-scale impact assessments (e.g., < 1 m) as opposed to the resolution at which they are generated at a global scale (e.g.,>100 km) and downscaled to regional level also taking into account the uncertainty in projections as contributed due to the existence of multiple Global Climate Models (GCMs) and greenhouse gas emission scenarios. To tackle the challenges, we conduct a showcase study in Montreal to assess the overheating risks in buildings.

2. Field monitoring

2.1. Building selection and field monitoring

Typical buildings housing vulnerable populations, including hospital, school, senior home, and multi-unit residential social housing, will be selected and monitored over at least two years with a focus during the summertime and heatwave periods. A vast building database for all the hospital buildings and school buildings in Montreal is obtained from the official institutes. For the hospitals, Ministère de la santé et des services sociaux (MSSS), and five different Centre intégré universitaire de santé et de services sociaux (CIUSSSs) in Montreal provided a total of 200 hospitals. As well, for the school buildings, the Ministère de l'Éducation et de l'Enseignement supérieur (MEES) provided information on three different Montreal school boards with 396 school buildings in total The characteristics of existing building stocks including building age, size, types of construction, occupancy, and mechanical systems (with/without air conditioning) are then reviewed to narrow down the scope for detailed survey and site visiting (Figure 1).

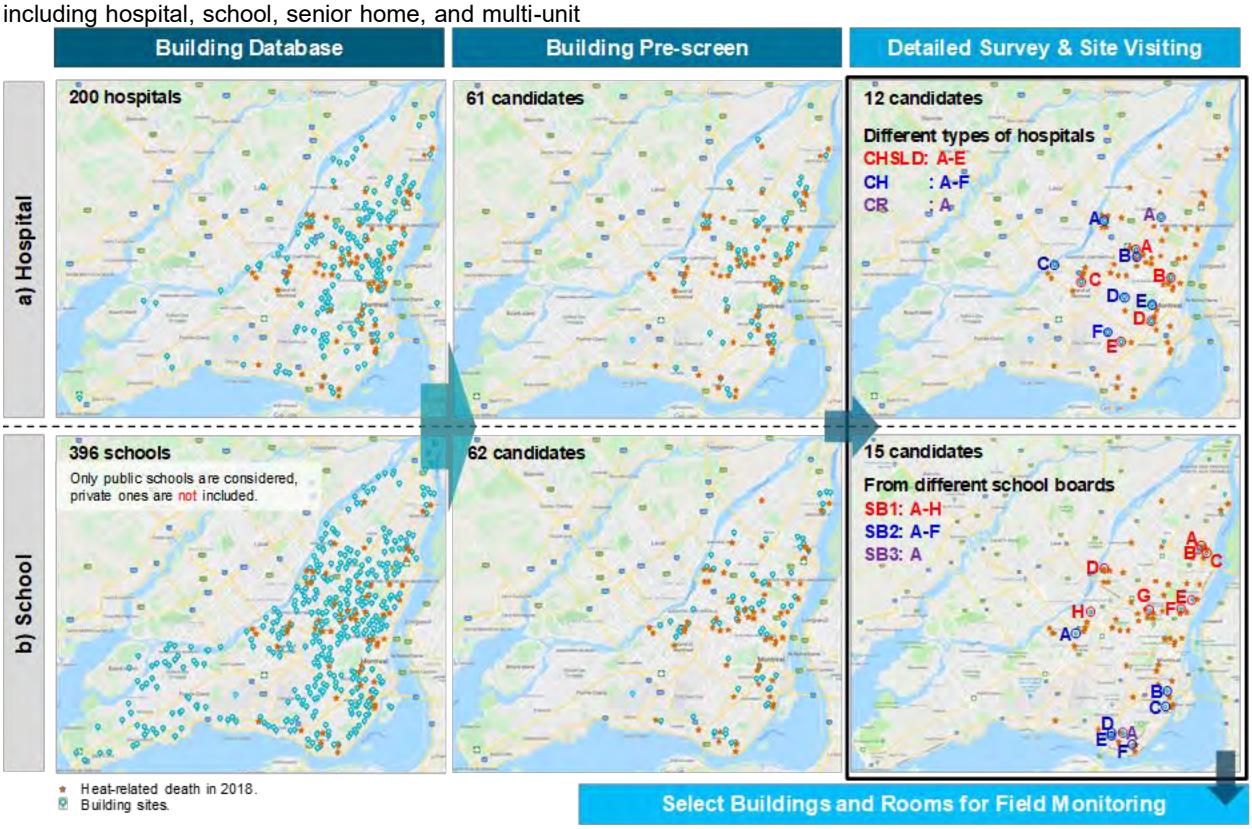

Figure 1. Distribution of a) hospital buildings and b) primary school buildings on Montreal Island and locations of heat-related death in 2018.
(CHSLD-Residential and long-term care centre, CH-Hospital centre, CR-Rehabilitation centre, SB-School board)

Site visitings can be a confirmation of the building information survey and an effective way to find more detailed information. The visits to the hospitals were in July and in September to schools. After several iterations of the site visiting practices, a team with four members was found to be the most effective and efficient way to complete the visiting tasks. Too many personnel for a visit might be distractive and can be undesirable to disturb the building occupants. At last, decisions can be made after a comprehensive analysis of all the information from the previous steps to evaluate the visited buildings. The distributions of the selected schools and hospitals can be found in Figure 2. Most of the selected buildings are well distributed over all of the central and eastern parts of Montreal thus capturing the city scale climate pattern; a few of

the building locations are close to one another, and the plan for these buildings is to share one weather station for the local weather conditions

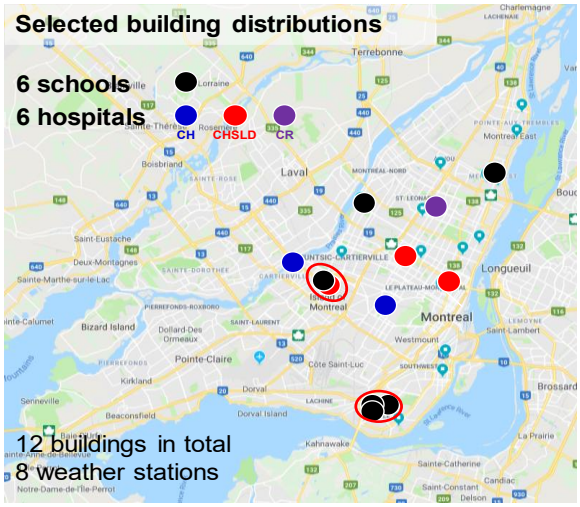

Figure 2 Distribution of selected school and hospital buildings.

For each test building, an on-site weather station will be installed to monitor outdoor conditions, including temperature, relative humidity (RH), solar radiation, wind speed, and direction. Several rooms in each building (an average of 4 sets per building) representing different orientations, floor levels, and occupancies will be instrumented to monitor indoor air temperature, mean radiant temperature, RH, airspeed, and CO_2 levels for indications of occupancy, which also have impacts on indoor temperature and RH levels. The indoor thermal conditions will be used to assess thermal comfort, overheating risks, and potential health risks to vulnerable occupants. The exterior surface temperatures of buildings will be scanned using infrared cameras to estimate building thermal responses and to validate simulations results. The field measurements provide benchmarking data and baselines of the existing vulnerabilities and overheating risks in these buildings.

3. Simulations

Urban microclimate information is often crucial for accurate building performance simulations. It was found that indoor temperature estimated with the microclimate information could be at least 5 °C different from that without it [9], which could be significant for the evaluations of overheating risks. Existing microclimate models, such as computational fluid dynamics, are computationally extensive and thus impractical for urban-scale problems. An integrated framework will be developed to generate the required microclimate data for the study of the long-term climate change impact, based on a cascade of mesoscale and microscale models starting from global climate model (GCMs) (global)→weather research and forecast model (WRF) or Global Environmental Multiscale Model (GEM) (regional,1-10 km) → City Fast Fluid Dynamics (CityFFD) (microclimate,1-1000 m) →EnergyPlus or City Building Energy Model (CityBEM) (building scale).

The urban microclimate model, CityFFD [9,10], is currently being integrated with WRF and urban building energy models [9] for the studies of the 2017 Montreal summer heatwave [9]. CityFFD is a 3D fast fluid dynamics solver [10–13] based on the GPU-CUDA [14] and high-order semi-Lagrangian algorithms, which is unconditionally stable, fast, and accurate to simulate urban microclimate. CityFFD will be further developed to provide accurate microclimate information for the whole building simulations. Meanwhile, CityFFD will also be integrated with the regional urban numerical weather prediction (UNWP) model for short-term forecasting of overheating and identifying vulnerable buildings on a city scale. The UNWP model will provide boundary conditions to CityFFD, which returns with higher-resolution data for its calibration. The forecasting simulations will also well inform the planning & scheduling of the field measurements.

In the following, three days heatwave 2018 is simulated by two-way interaction of CityFFD and CityBEM. Boundary conditions are provided from the Environment Canada GEM model. GEM provides transient boundary conditions, including velocity and temperatures. CityFFD simulates the urban microclimate and provides local airflow properties around the buildings for CityBEM. Then, CityBEM uses local data to simulate the indoor environment. In the next step, CityBEM provides building surface temperature as a boundary condition for CityFFD.

In this section, airflow is simulated at building levels by high resolution in the downtown of Montreal, around Concordia University Sir George Williams Campus. The computational domain is about 3.7 km by 3.7 km, and the grid size is 4 m. Fig. 3-a shows temperature contours simulated by GEM at two different times during the heatwave. Fig. 3-b shows CityFFD/CityBEM simulation data in the urban area.

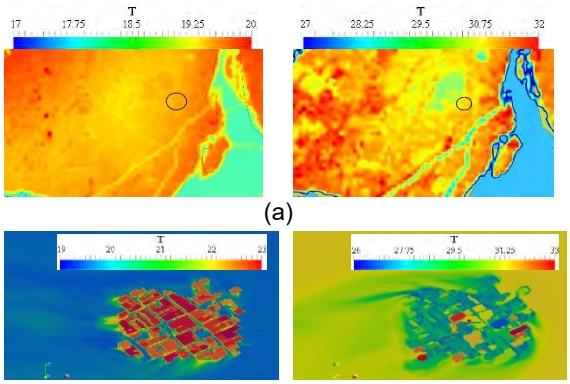

Figure 3. Temperature distribution in the downtown.

Figure 4 shows temperature variation over three days at the roof of EV building, and the results have a good agreement with the measurement data and also a GEM mesoscale model.

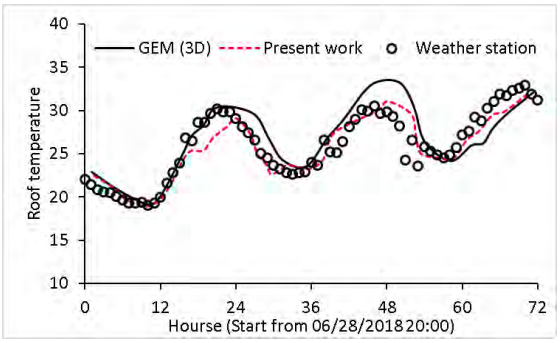

Figure 4 Comparison of temperature variation over three days.

4. Conclusions and outlook

To ensure the resiliency of Canadian buildings and protect Canadian's health from the changing climate. A series of field measurements and simulation studies are conducted to assess the overheating risks in buildings. The procedure to select buildings for measurement is elaborated in this paper. A global-regional-building scale simulation framework is introduced to study the interaction of indoor overheating with the outdoor microclimate and even the mesoscale meteorological conditions.

Acknowledgments

The authors would like to thank Ms. Chantal Saucier and their support from Ministère de la santé et des services sociaux (MSSS), Mr. Darius Tsé and their support from Ministère de l'Éducation et de l'Enseignement supérieur (MEES). We appreciate Mr. Jocelyn Poisson, Mr. Martin Massé, Mr. Pierre-Luc Roberge, Mr. Laure Pérès, Mr. Jairzinho Aburto, Mr. Bruno Cote, Mr. Yves Plourde, Mr. Akeen Kidder-Alexander and all those who helped us during the site visiting. The research is supported by the Natural Sciences and Engineering Research Council (NSERC) of Canada through the Discovery Grants Program and the Advancing Climate Change Science in Canada Program led by the corresponding author of the paper.

References

[1] IPCC, Climate Change 2014: Synthesis Report. Contribution of Working Groups I-III to the Fifth Assessment Report of the IPCC, 2014. doi:10.1016/S0022-0248(00)00575-3.

[2] IPCC, Summary for policymakers, in: Clim. Chang. 2014 Impacts, Adapt. Vulnerability. Part A Glob. Sect. Asp. Contrib. Work. Gr. II to Fifth Assess. Rep. Intergov. Panel Clim. Chang., 2013: p. 33. doi:10.1017/CBO9781107415324.

[3] K. Laframboise, Heat wave blamed for 53 deaths in Montreal, Glob. News. (2018). https://globalnews.ca/news/4338998/heat-wave-blamed-53-deaths-montreal/.

[4] M. Loughnan, M. Carroll, N.J. Tapper, The relationship between housing and heat wave resilience in older people, Int. J. Biometeorol. 59 (2015) 1291–1298. doi:10.1007/s00484-014-0939-9.

[5] IOM, Climate Change, the Indoor Environment, and Health, National Academies Press, D.C., 2011. doi:10.17226/13115.

[6] A. Quinn, J.D. Tamerius, M. Perzanowski, J.S. Jacobson, I. Goldstein, L. Acosta, J. Shaman, Predicting indoor heat exposure risk during extreme heat events, Sci. Total Environ. 490 (2014) 686–693. doi:10.1016/j.scitotenv.2014.05.039.

[7] P. Symonds, J. Taylor, A. Mavrogianni, M. Davies, C. Shrubsole, I. Hamilton, Z. Chalabi, Overheating in English dwellings: comparing modelled and monitored large-scale datasets, Build. Res. Inf. 45 (2017) 195–208. doi:10.1080/09613218.2016.1224675.

[8] S. Gracik, M. Heidarinejad, J. Liu, J. Srebric, Effect of urban neighborhoods on the performance of building cooling systems, Build. Environ. 90 (2015) 15–29. doi:10.1016/j.buildenv.2015.02.037.

[9] A. Katal, M. Mortezazadeh, L. (Leon) Wang, Modeling building resilience against extreme weather by integrated CityFFD and CityBEM simulations, Appl. Energy. 250 (2019) 1402–1417. doi:10.1016/j.apenergy.2019.04.192.

[10] M. Mortezazadeh, L. (Leon) Wang, Modelling urban airflows by a new parallel high-order semi-Lagrangian 3D fluid flow solver, in: COBEE 2018 4th Int. Conf. Build. Energy Environ., Melbourne,Australia, 2018.

[11] M. Mortezazadeh, L. (Leon) Wang, A high-order backward forward sweep interpolating algorithm for semi-Lagrangian method, Int. J. Numer. Methods Fluids. 84 (2017) 584–597. doi:10.1002/fld.4362.

[12] M. Mortezazadeh, L. (Leon) Wang, SLAC – A semi-Lagrangian artificial compressibility solver for steady-state incompressible flows, Int. J. Numer. Methods Heat Fluid Flow. Under Revi (2017).

[13] M. Mortezazadeh, A. Katal, L. (Leon) Wang, Numerical simulation of fire accident in the residential building's balcony by using the high-order backward forward sweep interpolating algorithm for semi-Lagrangian method, in: ESim 2018, Montreal, Canada, 2018.

[14] NVIDIA, NVIDIA CUDA C Programming Guide Version 4.1, NVIDIA Corporation, Santa Clara, 2011. http://developer.download.nvidia.com/compute/cuda/2_3/toolkit/docs/NVIDIA_CUDA_Programming_Guide_2.3.pdf.

COLD THERMAL ENERGY STORAGE FOR BUILDINGS: A FEASIBILITY STUDY

M. Ghobadi[a,*], A. Laouadi[a], A. Galasiu[a]

[a] National Research Council of Canada, Construction Research Centre
* Corresponding author, (613) 990-0921, mehdi.ghobadi@nrc-cnrc.gc.ca

Abstract:
In this study, we examined the feasibility of using cold ice as a medium to store the cold energy in the cold season and use it during the hot season in locations which experience both cold and hot seasons. We studied a cylindrical storage tank, two meters in diameter and two meters in length, wrapped with conventional insulation providing R-50. We assumed that the contained ice reaches -25 ℃ during the winter time and it was assumed to be exposed to the warm temperature of 18 ℃ for six months prior to being required for cooling. We used COMSOL Multiphysics to model the heat transfer in a three dimensional configuration. The results showed that 40 percent of the stored cold energy would be depleted during the six month period prior to the hot season. It would take 43 days for the ice in the tank to reach the melting point. after consuming the sensible stored cold, and the melting process begins after that. The remaining energy is able to provide the cooling energy for almost full 24 days for an R-2000 2-story detached house located in Ottawa, Ontario.

Keywords:
Cold storage, Cooling, Building, Climate change, Overheating, Feasibility study

1. Introduction

It is anticipated that in the coming 50 years, Canadian homes will be increasingly exposed to extreme overheating caused by global warming and urban heat island effects. Overheating of building interior spaces has been identified as a major concern to the comfort and health of vulnerable people, overloading of building HVAC systems, and straining the electric and water utility infrastructure. Prolonged exposure to extreme heat induces heat stress in people and may lead to severe health issues or even death. In urban settings, extreme heat events combined with air pollution were found to increase morbidity (sickness), mortality (loss of life), and insurance claims (particularly in North America). The extent of this effect varies from climate to climate, region to region, and city to city. In Canada and the USA, the number of excess mortalities due to extreme heat events is higher than any other natural hazard event such as storms and floods (ICLR, 2018; Bertko et al., 2014). Studies on climate change adaptations at a building (or individual) level have been, however, very limited in the Canadian context due to the lack of information on exposure to elevated indoor temperatures. Given the expected risk of Canadian homes overheating in the future as a result of the effects of climate change, there is a need to mitigate these effects by providing emergency cooling to homes when an overheating event occurs.

Since the occurrence of such events may require only a few days of additional cooling to prevent overheating in homes and thereby maintain a minimum level of comfort for its occupants, it is hypothesized that the cooling load may be provided from seasonally stored cooling energy located within the home. Seasonally stored cooling energy would be captured during the cold winter months through exchange of a storage fluid with the outdoor air. The cold storage would be maintained throughout the winter and subsequent summer months by means of a highly insulated storage tank.

As shown in Figure 1, thermal energy storage (TES) systems store energy using three types of technologies: (1) Sensible heat thermal energy storage (SHTES); (2) Latent heat thermal energy storage (LHTES); and (3) Chemical Reaction/Thermochemical storage (TCS).

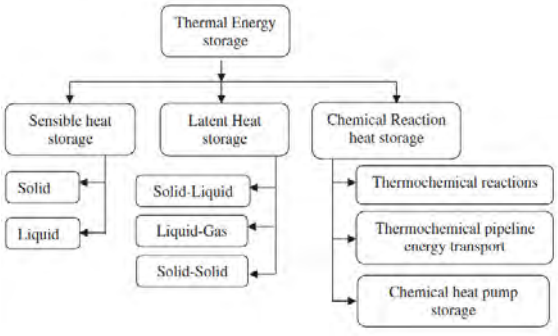

Figure 1: Classification of thermal energy storage (source: Raam Dheep & Sreekumar, 2014)

In latent heat thermal energy storage (LHTES) systems the energy is stored and released at a molecular level in a medium that has the capability to absorb and release heat during the phase change transformation (e.g. solid to liquid; liquid to gas; solid to gas; or solid to solid from one crystalline form to another). The term “Phase Change Material” (PCM) is commonly used in the literature to describe materials that absorb or release relatively large amounts of latent heat at a relatively constant temperature when solidifying or liquefying. The majority of PCMs used in TES systems are solid-liquid transition materials (Nazir et al., 2019). Energy enters or leaves the system without causing a temperature change in the system and the amount of heat stored depends on the mass and the capability of the PCM to absorb and release heat during its phase transition. The large amount of energy required to go through a change in phase between solids and liquids

(i.e., amount of energy needed to melt a given mass of a solid at its melting point temperature, or the amount of energy released when a given mass of liquid solidifies) is referred to as the latent heat of fusion, which for water at 0°C is ~334 joules/gram or ~80 calories/gram. Figure 2 shows the classification of PCMs used for cold thermal energy storage. Organic PCMs are carbon based compounds; Inorganic PCMs are usually metallic and hydrated salts; Eutectic PCMs are mixtures of two or more PCMs developed to achieve a certain melting point, which is a key criterion for cold storage applications. A comprehensive overview of PCMs for cold thermal energy storage (and their thermal characteristics) is available in the review article by Veerakumar & Sreekumar (2016). Recent PCM developments for TES are also available in Nazir et al. (2019), which lists 38 international organisations commercializing at present time PCMs for various TES applications. Lizana et al. (2017) found that at present time there are more than 250 commercially available organic and inorganic latent heat storage materials and provided a detailed review of their thermal properties and characteristics.

In this feasibility study we studied liquid-solid latent heat storage. A cylindrical tank of two meters in diameter and height was studied for storing ice. The tank was insulated using conventional insulation (e.g. EPS, XPS or fiberglass). COMSOL Multiphysics was employed to examine the cold storage depreciation through time.

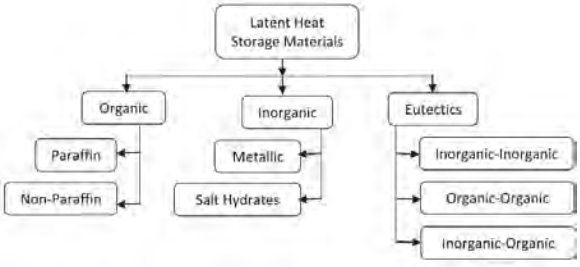

Figure 2: Classification of phase change materials (or latent heat storage materials) for cold thermal energy storage (source: Raam Dheep & Sreekumar, 2014).

2. Methodology

We studied liquid-solid latent heat storage. A cylindrical tank of two meters in diameter and height with flat ends was studied for storing ice. The tank was assumed to be insulated using conventional insulation (e.g. EPS, XPS or fiberglass). COMSOL Multiphysics was employed to examine the cold storage depreciation through time.

The following assumptions were made for the modeling of the cold storage tank in COMSOL Multiphysics:

- A two dimensional axisymmetric model was used to reduce the calculation time by taking advantage of the symmetry of the geometry.
- R-50 insulation around the tank was achieved using conventional insulation (340 mm of EPS). The temperature dependence of the insulation R-value was neglected.
- The initial ice temperature in the tank was set to -25 ℃ and the tank was placed in an indoor environment having a constant ambient temperature of 18 ℃.
- Convective heat transfer in the storage liquid was not considered.
- Time steps of 60 seconds, 30 seconds and 15 seconds were used to examine the time step dependency of the results. The sensitivity analysis showed that one minute time steps may predict the results properly thereby significantly reducing the computation time.
- The transient thermal behavior of the system was studied for 180 days (6 months).
- The tank shell was assumed to have negligible thermal mass and hence did not affect the storage capacity and transient behavior of the tank.

3. Results and discussions

Figure 3 shows the temperature and phase index contours after 45 days of being exposed to an ambient temperature of 18°C. The units in the graphs are adjusted according to the minimum and maximum values occurring in the system. Phase indicator shows the phase change of the ice. The phase indicator value of “0” as the minimum indicates full solid and “1” as the maximum value indicates full liquid. Values between the extremes indicate that the storage substance is undergoing the phase change and is in a mushy region. As it can be seen, after 45 days only the sensible cold in the system was used and no melting of the ice was observed.

Figure 4 depicts the temperature and phase indicator contours after 90 days (3 months). Melting at the surface of the ice has started and the latent heat portion of the stored energy is contributing to the heat transfer process; hence, the temperature remains constant at the edges. As it can be seen the minimum temperature in the system has risen to -1.38 ℃ from -6.16 ℃ on the 45th day.

Figure 5 shows the temperature and phase indicator contours after 135 days (4.5 months) of storage. The minimum temperature in the system has not changed since the 90th day which indicates that only the latent energy in the system has been used during this period. Also as it can be seen from the phase indicator graph more melting has happened especially around the corners.

Figure 6 illustrates the temperature and phase indicator contours after 180 days (6 months). There is still a significant amount of cold energy stored in the storage medium and the minimum temperature of the system has not changed, which means that the cold energy was only provided from the latent heat of fusion.

To better understand the heat transfer inside the tank, we also plotted the total heat flux magnitude (W) and the temperature (℃) on the tank wall and insulation wall, as shown in Figures 7 and 8, respectively. The heat fluxes begin at a very high rate (more than 100 Watts) when the temperature difference between the insulation surface and the ambient temperature is the largest, and then reaches an equilibrium when the

melting begins after 43 days. The total heat fluxes should be exactly the same at each time, due to the assumption of negligible thermal mass in the insulation; however, as it can be seen after the beginning of melting, the total heat.

We calculated the total energy available in the storage tank and how much energy remained after 180 days based on the simulation results. The total initial energy stored in the tank is expressed as follows.

$$Q = \left[\rho V C_{p,ice}\left(T_i - T_{phase\ change}\right) + \rho V L_{ice}\right]_{ice} = \\ = (58.277 + 1{,}929{,}718.4)\ kJ \\ = 1{,}929{,}777\ kJ$$

(Eq. 1)

where

ρ	=	Ice density
V	=	Ice volume
C_p	=	heat capacity
T_i	=	Initial temperature of ice
L_{ice}	=	Latent heat of ice

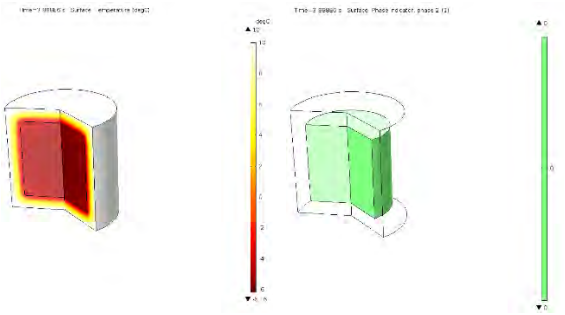

Figure 3. Temperature contours (left) and phase indicator contours (right) after 45 days of being exposed to the ambient temperature

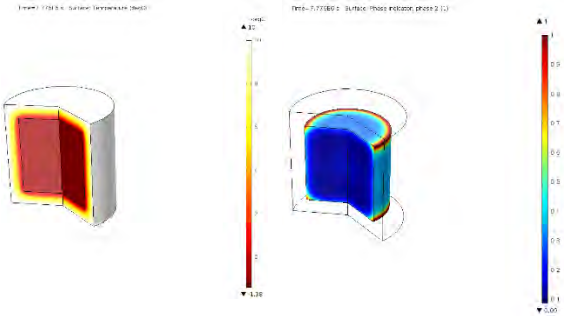

Figure 4. Temperature contours (left) and phase indicator contours (right) after 90 days of being exposed to the ambient temperature

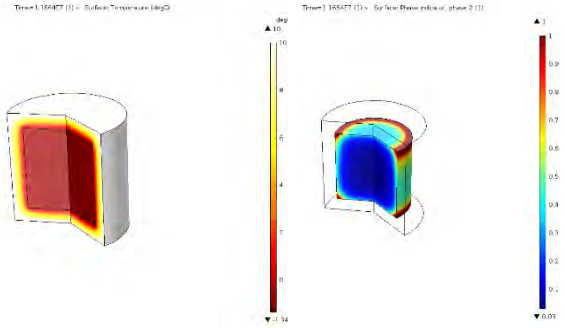

Figure 5. Temperature contours (left) and phase indicator contours (right) after 135 days of being exposed to the ambient temperature

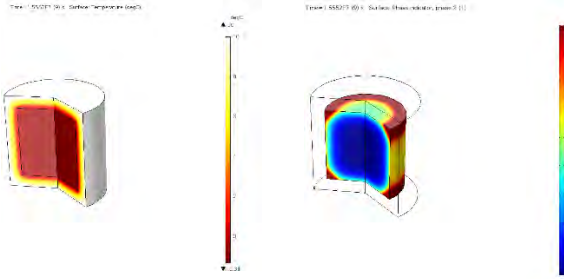

Figure 6. Temperature contours (left) and phase indicator contours (right) after 180 days of being exposed to the ambient temperature

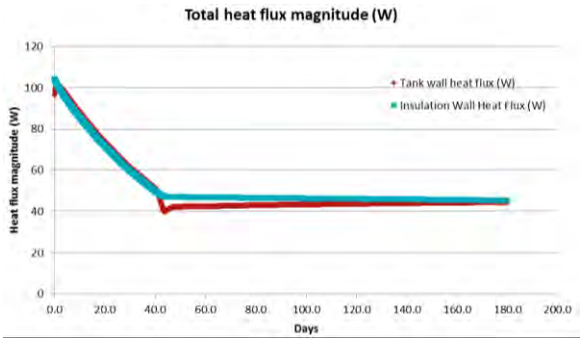

Figure 7. Total heat flux magnitude (W) on the tank wall surface and on the insulation surface

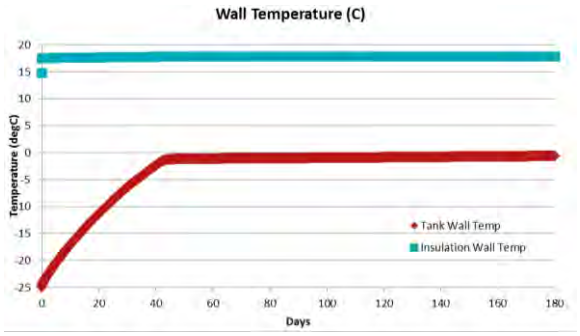

Figure 8. Wall temperature of tank and insulation

The first portion of the above equation shows the sensible heat of the ice, the second part is the latent

heat. It can be seen that the latent heat is the main part of the cold storage in the system and the sensible part is negligible (below 0.003%). The energy calculation for this cold storage system is summarized in Table 1. Also, using the values for total heat flux at each time step, as shown in Figure 6, we calculated the total heat lost by the system over 180 days. The remaining energy was assumed to be available to provide the required cold energy for space cooling of a typical residential 2-storey house. According to Laouadi (2010), the cooling energy used by a typical R-2000 house (including 250 m^2 of livable space; double-glazed low-e windows; interior venetian blinds) over the cooling season is 33,500 KJ, with a typical peak cooling demand of 1.5 kW. As such, the storage tank system proposed in this study could provide the cooling demand of the entire house for almost 23.5 days, or 35% of the cooling energy demand of the entire cooling season. Given that extreme heat waves may last a few days to a few weeks in the summer, the proposed storage system may easily fulfill the space cooling requirements of the house over an extreme heat wave event.

Table 1. The energy calculation of the cold storage system

Parameter	**Value**
Total cold energy stored	1,930,000 KJ
Heat loss to the surrounding environment	764,053 KJ
Net remaining energy for space cooling	1,165,947 KJ
Peak cooling demand of a typical R-2000 house in Ottawa	1.528 KW
Average daily cooling energy demand (at 9h/day)	49,507 KJ
Cooling energy use of a typical R-2000 house in Ottawa	3,358,800 KJ
Cold storage satisfies the cooling energy use of R-2000 house by	35%
Number of days provided by the cold energy tank	23.5 days

4. Conclusions and outlook

The feasibility of using ice as a medium for cold storage in the Canadian climate was investigated. A cylindrical tank, two (2) meters in diameter and height, wrapped with conventional insulation to provide R-50 of insulation to the cold storage tank was considered. The tank contained ice at -25 ℃ during the winter time and it was assumed to be exposed to warm interior temperatures of 18 ℃ for six months. COMSOL Multiphysics was employed to examine the amount of heat that transferred to the system and whether the sensible and latent cold energy stored in the ice could withstand the heat transfer process. It was found that 40 % of the stored cold energy was lost during the six months leading to the hot season, and the remaining 60% could provide the cooling energy of an R-2000 residential 2-storey house located in Ottawa for almost 24 days based on the required daily cooling energy demand of the building. The melting process begins after 43 days and the high value of latent heat capacity of ice maintains the ice temperature at 0 ℃.

Further studies on the topic are required to examine other dimensions of the storage tank and its insulation values, geometry and boundary conditions. The charging feasibility of the cold storage considering the dimensions and heat losses of the heat exchanger located inside the storage tank as well as outdoors, should also be investigated. Additionally, the convective heat transfer of the liquid should be considered in the COMSOL model. The tank size can also be further optimized based on the cold energy demand according to the cooling load of either residential or commercial buildings. Also other geometries can be studied to determine the optimum geometry to minimize heat transfer, energy storage and the type and installation of different insulation products. Different boundary conditions such as an isothermal situation (e.g. should the tank be stored beneath ground level or on the roof of a building) can be considered to establish the most suitable location to install the tank.

Acknowledgements

This work was carried out by the National Research Council of Canada with funding from Infrastructure Canada in support of the Pan Canadian Framework on Clean Growth and Climate Change. The authors are very thankful for their support.

References

Berkout, F., J. Hertin, D.M. Gann. 2006. Learning to Adapt: Organizational Adaptation to Climate Change Impacts. Climatic Change. 78: 135-156.

ICLR. 2018. Durham Region Climate Resilience Standard for New Houses. A Standard to improve the disaster resilience of new low-rise residential buildings in the Region of Durham. Institute for Catastrophic Loss Reduction.

Laouadi A., 2010. Guidelines for effective residential solar shading devices. Research Report B3243. National Research Council Canada, Ottawa, Ontario.

Lizana, J., et al., Advances in thermal energy storage materials and their applications towards zero energy buildings: A critical review. Applied Energy, 2017. 203: p. 219-239.

Nazir, H., et al., Recent developments in phase change materials for energy storage applications: A review. International Journal of Heat and Mass Transfer, 2019. 129: p. 491-523.

Raam Dheep, G. and A. Sreekumar, Influence of nanomaterials on properties of latent heat solar thermal energy storage materials – A review. Energy Conversion and Management, 2014. 83: p. 133-148.

Veerakumar, C. and A. Sreekumar, Phase change material based cold thermal energy storage: Materials, techniques and applications – A review. International Journal of Refrigeration, 2016. 67: p. 271-289.

BASIC STUDY ON DEVELOPMENT OF DECISION SUPPORT SYSTEM FOR EVACUATION INSTRUCTIONS

K. Kawano[a,*], K. Tsukahara[a], Y. Mitani[a], H. Taniguchi[a], T. Sato[a]

[a] Department of Civil Engineering at KYUSHU UNIVERSITY
* Corresponding author, Tel +8192-802-3397, email kawano@doc.kyushu-u.ac.jp

Abstract:
Japan is prone to disasters caused by floods and landslides caused by heavy rains such as typhoons and rainy seasons due to conditions such as topography and weather. Local governments that respond to disasters have to do many times the usual work with limited manpower. In the work at the time of disaster, it is necessary to respond appropriately to each inhabitant.
However, the current local government calls on all residents to evacuate if one part of the area is dangerous. This is a problem because the inhabitants who do not yet need to evacuate are instructed to evacuate, and the danger may not be correctly conveyed to those who need to evacuate. The biggest reason that local governments cannot judge appropriate evacuation instructions is that they cannot extract information necessary for judgment from a large amount of disaster information. In this study, a system that supports decision-making regarding evacuation instructions of local governments by calculating the risk of disaster and the necessity of evacuation for each small area such as a district or school district from the vulnerability of the region to the disaster and the predicted precipitation Develop.

Keywords:
Evacuation, Decision making, Hazard, Vulnerability, Support system.

1. Introduction

Japan is frequently damaged by typhoons and torrential rains. Many river floods caused damage because Typhoon No. 19 in 2019 is a record heavy rain. There are limits to measures taken by hardware such as embankments against floods caused by heavy rain. Therefore, software measures such as early evacuation guidance are also important.
The site itself has prepared hazard maps and disaster response manuals as software measures. There are quantitative standards and qualitative standards. An example of a quantitative standard is a standard that sets a specific threshold for the observation result. Qualitative criteria are based on vague risks such as “when heavy rain can be expected to last for a long time” and “when flooding can be expected”.
Therefore, in the case of qualitative standards, local governments tend to issue evacuation instructions at an early stage over a wide range compared to quantitative standards. However, many residents in the area misunderstand that they are not yet at risk compared to the situation at the time of announcement, and there are cases where evacuation is delayed.
Therefore, in this study, the basics for quantitative judgment even if qualitative criteria are used for the purpose of developing a decision support system for local governments to issue evacuation instructions within an appropriate range at an appropriate timing. Conduct research.

2. Overview of research

This study quantitatively evaluates and embodies the ambiguous danger that causes local governments to issue evacuation instructions early to a wide area. Specifically, the risk of flooding and landslide disasters that can secure time to evacuate to a safe place from the occurrence of heavy rain will be quantified. An existing method for calculating natural disaster risk is GNS (Gross National Safety for natural disasters) [1]. GNS is an index for decision-makers of disaster prevention and mitigation investments that quantitatively shows natural disaster risks. In this study, the risk is calculated using the following formulas (1) and (2) with reference to the GNS calculation method. H_{flood} and $H_{sediment}$ are the degree of flood and sediment disaster caused by heavy rain. EV is a vulnerability of residents exposed to disasters.

$$R_{flood}=H_{flood}\times EV \quad (1)$$
$$R_{sediment}=H_{sediment}\times EV \quad (2)$$

3. Flood disaster hazard

An existing approach to predicting the occurrence of flooding due to heavy rain is inundation simulation. In Japan, a simulation model is created for rivers managed by the country. However, many small and medium-sized rivers managed by local governments lack the river channel data necessary for creating simulation models. Therefore, in this study, the simulation model is applied to small and medium rivers using artificial intelligence.
The outline of the flood hazard assessment method in this study is shown in Figure 1 below. In this method, the terrain around rivers managed by the country and the results of inundation analysis simulation are

learned as teacher data by DNN (Deep Neural Network), and flood inundation hazards around terrain around small and medium rivers managed by local governments are divided into 50m2 areas. To evaluate. The flood analysis simulation results used as teacher data are evaluated using Nays2DFlood [2].

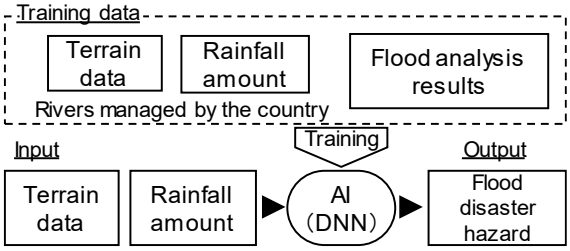

Fig 1: Flood disaster hazard assessment method

4. Sediment disaster hazard

As an existing effort to predict the occurrence of landslide disasters due to heavy rain, there is landslide disaster warning information issued by the Japan Meteorological Agency. Sediment disaster hazard information is evaluated in five stages based on rainfall per 1km^2 area based on the survey results of landslide disasters that occurred in the past. Local governments make decisions on evacuation decisions using both sediment disaster risk information for each 1km^2 or 5km^2 region, which summarizes the results of sediment disaster risk information and the results of surveys of places where damage may occur due to slope failures or debris flows. Is going. Therefore, in this study, we apply the evaluation of sediment-related disaster risk points to 50m^2 area using artificial intelligence.

The outline of the sediment disaster hazard assessment method in this study is shown in Figure 2 below. In this method, first, topographic map interpretation results and risk location estimation results by experts are learned as teacher data by DNN, and the presence or absence of danger is evaluated for each 50 m^2 area. Based on the soil rainfall index, the landslide disaster hazard in the area where there is a risk of landslide disaster is evaluated in five levels.

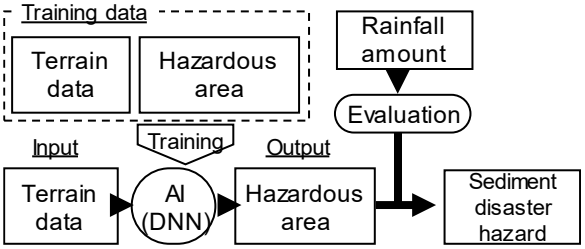

Fig 2: 4. Sediment disaster hazard assessment method

5. Vulnerability of people

This study refers to GNS. The GNS assesses the proportion of population exposed to disasters and the vulnerability of societies individually. GNS is characterized by 0 risk when there are no people in the area or there is no vulnerability in the area. Therefore, in this study, the target of vulnerability assessment is limited to buildings, and the index that should evacuate residents living in the building early is assessed as vulnerability.

The vulnerability of this method is evaluated by dividing into the vulnerability of residents and the vulnerability of evacuation routes. Vulnerability of inhabitant attributes evaluates the percentage of persons who should be especially considered in disaster prevention measures for the elderly and infants. For vulnerability of evacuation routes, the combination of the time required to evacuate to nearby evacuation centers and the gradient of the evacuation route is evaluated in five stages, and the smallest value is adopted as the evaluation value (Figure 3).

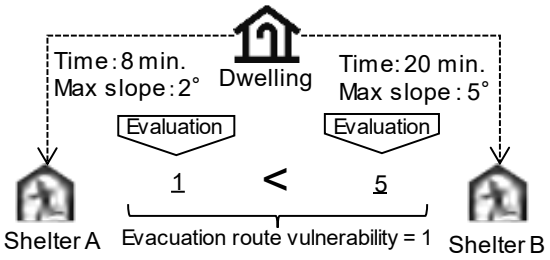

Fig 3: Evacuation route vulnerability

6. Conclusions and outlook

This study proposed a quantitative risk calculation method for flood inundation and landslide disasters for the purpose of developing a decision support system for local governments to issue evacuation instructions within an appropriate range at an appropriate time. In the future, we will first develop a decision support system for evacuation judgment that implements the risk calculation method proposed in this study. And, it is used to evaluate its usefulness by using it at actual disaster response sites.

Acknowledgements

This work was supported by Council for Science, Technology and Innovation(CSTI), Cross-ministerial Strategic Innovation Promotion Program (SIP), Enhancement of National Resilience against Natural Disasters (Funding agency:NIED).

References

[1] Geotechnical Society Kanto Branch, Risk index for natural disasters GNS (2017).
[2] International River Interface Cooperative, Nays2Dflood, https://i-ric.org/solvers/nays2dflood/.

Thermal Bridging: Methodologies, Tools, and Advancements in Mitigation

V. Gretka[a*], P. Roppel[b]

[a] Morrison Hershfield Ltd., Victoria, BC, Canada
[b] Morrison Hershfield Ltd., Vancouver, BC, Canada
* Corresponding author, 250.361.1215, vgretka@morrisonhershfield.com

Abstract:
Energy codes and standards in Canada are driving toward net-zero energy performance for all new construction by 2032. The building envelope performance required for net-zero construction requires more insulation and mitigation of thermal bridging than conventional practice.

When the *Building Envelope Thermal Bridging (BETB) Guide* was launched in 2014, the impact of thermal bridges was largely overlooked in practice, energy standards and energy calculations. Fast-forward to the present and a clearer understanding of the impact of thermal bridging has led to the introduction of comprehensive thermal bridging calculations as a requirement in new codes and standards such as National Energy Code for Buildings 2017, B.C. Energy Step Code, Vancouver Building Bylaw, and the Toronto Green Standard v3.

This paper will delve into three focus areas:

A. Methods and tools for assessing and characterizing thermal bridging, highlighting past and present research on the subject;
B. How to account for both thermal transmittance and dynamic response in energy modeling software, and how this body of work has been incorporated into energy standards, and;
C. Case studies on hygrothermal modeling of thermal bridging and durability analysis: how to use a combination of 3-D thermal, hygrothermal, and energy models to answer questions related to insulating existing buildings and durability.

Keywords:
Energy, modeling, thermal, bridging, hygrothermal

1. Introduction

The advent of the first energy requirements in building codes was largely due to oil price shocks in the 1970's, demanding a more concerted effort on energy efficiency by the industry. As our understanding of building materials and construction practices have evolved over decades, so too has the technology to model, measure, and analyze building energy performance. One of the biggest differences in modeled vs actual performance is in the thermal performance of the building envelope, where thermal transmittance calculations (effective R-values) have overlooked the full impact of thermal bridging.

Building energy codes are now in the midst of a renaissance as a result of government policies attempting to mitigate the impact of climate change. Notably, the BC Energy Step Code (ESC) [1], National Energy Code for Buildings (NECB) [2], ASHRAE 90.1 [3], Vancouver Building Bylaw (VBBL) [4], and the Toronto Green Standard (TGS) [5] are all aiming for net zero energy, low-GHG, or some performance combination thereof in the 2030-2040 timeframe.

Changes to thermal transmittance calculations have been introduced or are proposed for the ESC, NECB 2017, VBBL, ASHRAE 90.1 (2018 Addendum AV), and TGS v3.

To this end, the ESC, VBBL and TGS require compliance with a thermal energy demand intensity (TEDI) target – an annualized heating energy metric that accounts for envelope energy performance inclusive of thermal bridging, envelope air leakage, and heating of ventilation air. A TEDI target is important in a Canadian context since heating energy has historically represented a substantial fraction of end-use energy in buildings. Further, building envelopes typically have a service life much longer than that of lighting or mechanical systems since upgrades are significant undertakings and costly. A TEDI target effectively eliminates the common code-compliance strategy to trade off poor envelope performance with more efficient heating (ie heat pump) or lighting (ie. LEDs) systems to name a few.

2. ASHRAE Research Project 1365

Commissioned in 2009, *ASHRAE Research Project 1365* [6,7] involved using an extensively calibrated and validated 3D heat transfer model to explore the impact of thermal bridging. Completion of this project helped spark market transformation to better evaluate building envelope thermal performance, but only scratched the surface in terms of identifying how to effectively mitigate thermal bridging, and did not directly correlate the impact of thermal bridging on building energy consumption.

This formed the motivation for the *Building Envelope Thermal Bridging (BETB) Guide v1.0* [8] in 2014, a visually-aided reference catalog of thousands of assemblies and transitions that facilities streamlined thermal bridging calculations. The cost-benefit analysis completed for the guide made it clear that if reducing energy consumption in buildings is a real goal in society (and in codes) then thermal bridging at interface details cannot be ignored. As mentioned earlier, several codes now incorporate the methodology outlined in the *BETB Guide* to calculate envelope thermal performance, in part due to the availability of one centralized reference catalog for all practitioners which in turn also simplifies enforcement.

The *BETB Guide* continues to grow. The latest release Version 1.3 (2019) [9] marked the first of four major planned expansions of the *BETB Guide* for a multi-year project. The objective of this work is to extend the database to:

- provide data for all Canadian climate zones;
- apply to current Canadian construction practices and what is needed for net-zero ready buildings, and;
- apply to all construction types and buildings

Part of this project is the development of a web-application called *betb.ca* as is discussed below.

3. The Low TEDI Guide

The *Guide to Low Thermal Energy Demand for Large Buildings (Low TEDI Guide)* [10] was introduced in 2018 to provide design direction for large buildings required to meet higher levels of energy efficiency targets, including more rigorous expectations for mitigating thermal bridging. It compares and contrasts International Organization for Standardization (ISO) 10211, Passive House Institute (PHI), and *BETB Guide* approaches to evaluating thermal bridges.

It demonstrated that two-dimensional simplifications were sufficient for thermal analysis of moderately conductive structures with simple heat flow paths such as concrete structures with a single insulation layer; however, a three-dimensional analysis is recommended for thermal analysis of highly conductive and complex heat flow paths, such as intermittent cladding attachments, metal framing intersections with multidirectional conductive heat flow paths (ie. spandrel panels), and for estimating temperature at interface details for evaluating risk of condensation.

The approach outlined in the *BETB Guide* generally follows ISO 10211, but has additional requirements for accuracy and to accommodate North American standards such as NFRC for glazing. The research summarized in the *Low TEDI Guide* found that the biggest impact to realizing a low TEDI building is the quality of the interface details, challenging design teams to minimize thermal bridging.

4. betb.ca

The *BETB Guide* is migrating to a web-based platform (*betb.ca*). It will enhance the user experience by reducing the effort required to perform holistic assessment of thermal bridges, allowing users to search, sort, and compare details. The BETB database is connected to an integrated thermal calculator that reduces the effort to do overall thermal transmittance calculations and replaces the current spreadsheet method.

The online catalog's interface will facilitate better collaboration within design teams and raise the knowledge and awareness of thermal bridging in the industry. The custom report generation functionality will streamline preparation and review of compliance documentation by authorities having jurisdiction.

5. Dynamic Response of Thermal Bridging

Some industry stakeholders in North America have raised questions with the recent focus on mitigating the impact of thermal bridging by more comprehensive, and accurate, steady-state thermal transmittances, without explicit new methods for how thermal mass or the dynamic response of the building envelope is addressed. This section summarizes these questions and concerns, past research on simulating the dynamic response of the building envelope, and how steady-states U-values are a required input for dynamic whole building energy models.

Those raising concerns may appear to have two divergent viewpoints with regard to the impact:

- More accurate steady-state thermal transmittances may overstate the impact of thermal bridges, with mass, such as a concrete intermediate floor slab [11,12].
- Conventional approaches to accounting for dynamic thermal response understates the impact of thermal bridges, with volume, for the heating energy demand and overstates the impact for cooling energy demand compared to directly modeling thermal bridges in whole building energy simulations [13,14].

However, closer examination reveals that there is overlapping viewpoints for cooling for details where thermal bridges have volume and mass (thermal inertia), such as is the case with interior insulated concrete walls. The ultimate question that follows from these concerns is if the potential impact warrants changes to how the dynamic response of the building envelope is addressed in practice.

The first viewpoint is a concern or question that is sometimes raised in response to proposed changes to thermal transmittance calculations for energy codes and standards. However, questions are raised without specific research or analysis to support the concerns [11,12].

The second viewpoint follows from recent research at Concordia University [13,14] and in Europe [15-18] that primarily focuses on mass wall construction (reinforced concrete, concrete and clay masonry) where the intermediate floors and roof decks completely bypass the thermal insulation. The premise of the work is that U-values are adjusted in whole building energy models, but the dynamic thermal characteristics are typically not and the dynamic response is based on one dimensional correlations. This approach is called the equivalent U-value method.

The work done by Concordia compares the impact of thermal bridges on whole building energy-use for an archetype Canadian multi-unit-residential building, in climate zones 4 to 7, for three approaches for accounting for the impact of thermal bridges. The equivalent U-value method is compared to more advanced methods where the dynamic thermal response at interfaces, such as intermediate floors, are accounted by an equivalent wall [19,20] or directly modeled in a whole building energy model.

The results show that for interior insulated concrete walls or details where the concrete structure completely bypasses the thermal insulation underpredicts the heating energy demand by 13% and overpredicts the cooling energy demand by between 2.5% and 9.5% for the U-value method compared to a direct modelling approach. However, the difference is reduced to less than 3% for both heating and cooling for mitigated details and exterior insulation. A discussion in the ASHRAE Handbook of Fundamentals about deciding the level of detail required to make an adequate approximation for accounting dynamic effects is worth repeating and puts these findings into perspective: “remember that, for buildings with windows and internal heat gains, the conduction heat gains make up a relatively small part of the cooling load. For heating load calculations, the conduction heat loss may be more significant” [21]. In other words, focus on the heating energy demand for the opaque envelope in heating dominated climates where the energy demand might be underestimated. Further extension of these points is sufficient to address concerns raised to proposed changes to thermal transmittance calculations for energy codes and standards. The only question that remains is if more should be done to account for the negative impact of large thermal bridges, with thermal inertia, for simulating the dynamic response.

There is an intermediary approach between the equivalent U-value method and equivalent wall that is not discussed in the Concordia work called the homogenous layer method [22,23]. The homogeneous layer builds upon the U-value method by also adjusts each 1D layer to account for the 3D geometry of the thermal bridge based on the density and specific heat volume fractions that is discussed below.

The advanced methods, equivalent wall and direct model, rely on 2D or 3D finite difference or finite element analysis of the building interface. The drawback of both of these methods is they rely on assigning “effective” areas to the interface thermal bridge. Assigning standardized “effective” areas for complex thermal bridges with strong multi-directional lateral heat flow paths is problematic, as outlined in *ASHRAE Research Project 1365* and European studies that have evaluated the impact of thermal bridging for dynamic conditions [6,7,24,25]. Accurately applying these methods using detail specific “effective” areas is both time consuming and somewhat complicated.

Additional considerations for determining if directly modeling 3D thermal bridges in whole building models is worthwhile for simulating building energy use are:

- There are limited software options for directly modeling 3D thermal bridging in whole building models (WUFI Plus [26], ESP-r [27,28]).
- The most accurate software for energy analysis depends on how well all the building systems and loads are simulated as interdependent variables. Available software to model 3D thermal bridges directly are not necessarily the best options to accurately simulate other building systems, such as sophisticated HVAC and partial loads, or comply with energy codes and standards effectively.
- Three dimensional sections modeled in available whole building models must be simplified to accommodate mesh limitations (orthogonal), model size constrains (number of nodes and elements) and sensible computational solving time.
- Complex geometry with small components within insulated assemblies, such as is common with clip and rail systems for attaching cladding through exterior insulation, that do not have much thermal mass are better analyzed (time and accuracy) with specialized 3D finite element software that has more comprehensive meshing options and can accommodate larger models.
- The thermal transmittance for many thermal bridges, such as window to wall interfaces, can vary significantly by the window type (frame, glass, spacer), position within the thermal insulation, and other lightweight components (metal flashing), but without significantly changing the dynamic response functions.
- Whole building models that are capable of modeling some 3D thermal bridges (WUFI Plus) also allow for input of linear transmittances, with acknowledgement that not every detail interface will be modeled directly in 3D in the whole building model.
- Publically available database and catalogs of thermal transmittances with reliable and consistent data is advantageous not only for saving time, but also for peer reviews, enforcing

energy codes and standards, and leveling the playing field across industry.

- The drive towards net-zero ready construction in Canada is essentially phasing out interior insulated concrete or similar types of construction as a viable option due to the thermal inefficiency and attainable overall effective R-value. Therefore, the underestimation of the heating energy demand is quickly becoming a moot point for new construction. This type of construction maybe relevant for energy retrofits, but the majority of projects will explore exterior retrofits unless tasked with maintaining a historic façade.

The conduction transfer functions (CTF) used by EnergyPlus to model the dynamic response is convenient because the coefficients only need to be determined once for each construction type and do not rely on construction details [29,30].

Our viewpoint with all these considerations in mind is that direct modeling of 3D thermal bridges in whole building energy models to calculate energy demand is currently an academic pursuit and is not a viable alternative for general professional practice. All the uncertainties with whole building energy analysis overshadows any potential error with prevailing dynamic approximations for new construction. However, direct modeling of 3D thermal bridges using whole building or a room model for hygrothermal or thermal comfort studies does have practical applications [26,31,32].

Comparisons between the U-value, homogeneous layer, and direct 3D modeling approach follow. Figure 1 illustrates and provides an overview of these three methods for an interior insulated concrete wall at intermediate floor intersection.

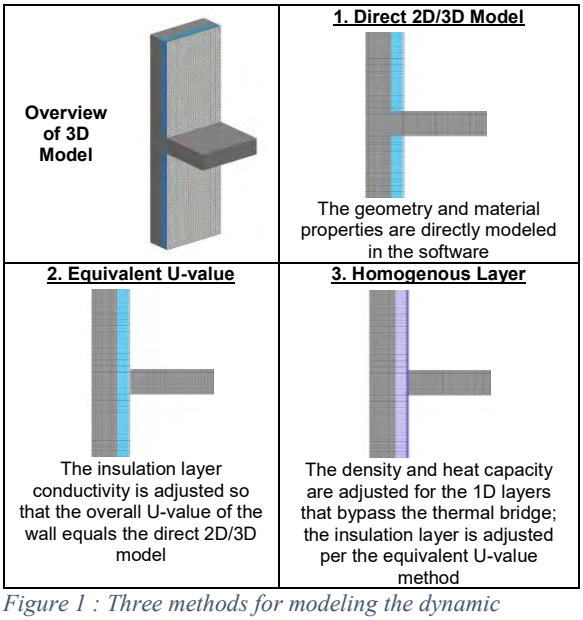

Figure 1 : Three methods for modeling the dynamic response of the building envelope in energy simulations

Simulations were performed with Nx, a 3D thermal modelling software from Siemens which is a general purpose computer aided design (CAD) and finite element analysis (FEA) package. The thermal solver and modelling procedures were extensively calibrated and validated to within ±5% of hotbox testing for both steady-state and dynamic conditions as part of *ASHRAE Research Project 1365* and the *BETB Guide*. Figure 2, Table 1, and Table 2 summarize the assumptions for the simulations.

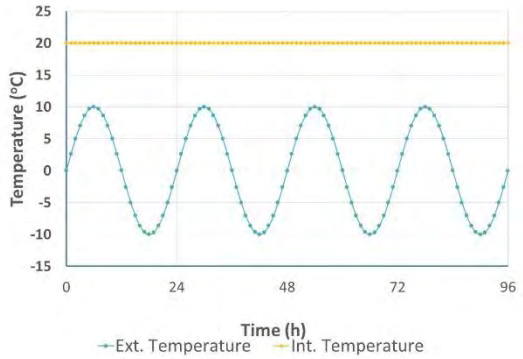

Figure 2 : Modeling conditions (convection coefficients: 8.3 W/m²K interior vertical, 9.3 W/m²K interior ceiling, 6.1 W/m²K interior floor, and 25 W/m²K exterior)

Table 1 : Material properties

Layer	Thk. (mm)	Cond. (W/mK)	Density (kg/m³)	Sp. Heat Cap. (J/kgK)	1-D R-Value (ft² °F hr/BTU)
Interior Film					0.68
Gypsum	16	0.16	800	1090	0.56
Insulation	90	0.046	19	960	11.0
Concrete	203	1.95	2240	900	0.59
Exterior Film					0.23
					R-13.1

Table 2 : Adjusted properties

Layer	Thk. (mm)	Cond. (W/mK)	Density (kg/m³)	Sp. Heat Cap. (J/kgK)	1-D R-Value (ft² °F hr/BTU)
Int. Film					0.68
Gypsum + Concrete	16	0.16	**909**	**1055**	0.56
Insulation + Concrete	90	0.046	**187**	**906**	**5.31**
Concrete	203	1.95	2240	900	0.59
Ext. Film					0.23
					R-7.4

Figure 3 compares the heat flow at the interior surface. There is good agreement between all three methods. There is maximum ±7% and ±5% difference at the peak between the direct 3D model and the equivalent U-value and homogenous layer methods, respectively.

This is the same wall assembly explored in the Concordia work. The difference here is that the impact is shown for one detail using the same software. Comparing the details in this manner eliminates questions related to potential errors as a result of differences in software, modeling procedures, and mesh and model size limitations. To put these findings in perspective, there is no agreement between the direct 3D model and steady-state response or the dynamic response ignoring the large thermal bridge at the intermediate floor as seen in Figure 4. There is between -110% to 51% difference with the steady-state response and between -36% to -46% for the dynamic response of the wall without the thermal bridge.

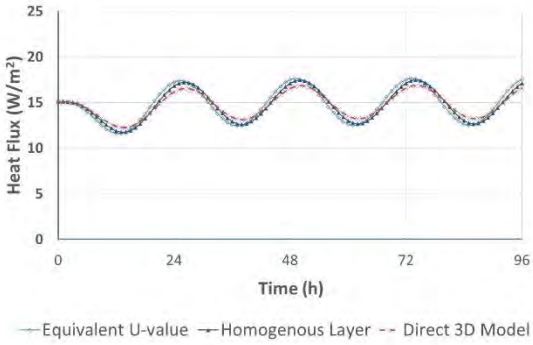

Figure 3 : Comparisons of direct 3D dynamic model to 1D dynamic approximations for an interior insulated concrete wall at an intermediate floor

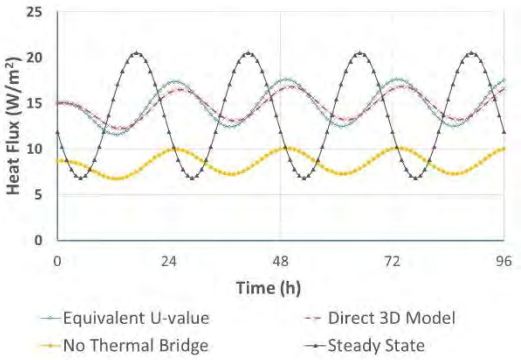

Figure 4 : Comparisons of dynamic response with thermal bridges to dynamic response without thermal bridges and steady-state response

The intermediate concrete floor bypassing interior insulated concrete walls is one example that there is a difference in the dynamic response and it is feasible to directly model the detail in some whole building energy models because the geometry is simple. However, there are many examples of thermal bridging where directly modeling the interface in a whole building energy model is not practical from a perspective of time, complexity, and attaining accurate thermal transmittances. For example, Chapter 2 in the *Low TEDI Guide* shows the possible variations in results for a detailed versus simplified geometry for the window to wall interface. The detailed FEA analysis demonstrated in this example is not practical to directly model in a whole building energy model as seen in Figure 5 due to the complexity of the geometry and meshing. Nevertheless, the difference between the direct 3D model and equivalent U-value is much less than the concrete intermediate floor in absolute terms as shown in Figure 6.

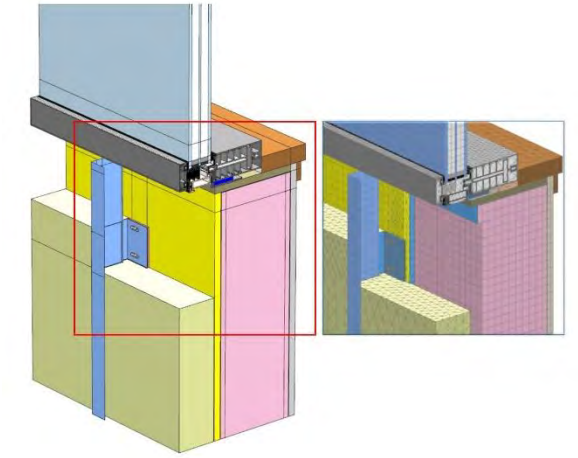

Figure 5: Example of a FEA model of a window to wall interface with complex geometry, meshing, and 3D heat flow

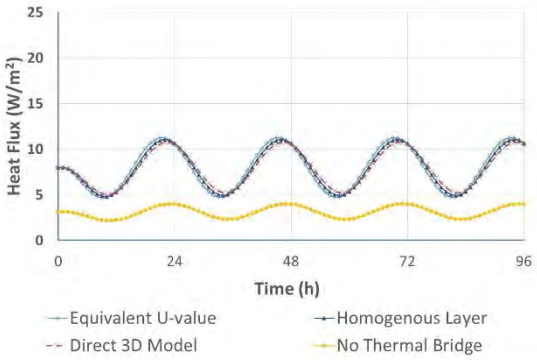

Figure 6 : Comparisons of direct 3D dynamic model to 1D dynamic approximations for a window to wall interface

6. Case Studies and Utilization

The key benefit of the BETB methodology and resources is that it facilitates comprehensive thermal transmittance calculations in practice. The BETB resources provide easy-to-use tools, access to accurate and reliable information that are important for design decisions, and provides incentives to mitigate the impact of thermal bridging. This section provides an overview of the process for a case study building.

The first step to performing overall thermal transmittance calculations is to perform quantity takeoffs as illustrated in Figure 7.

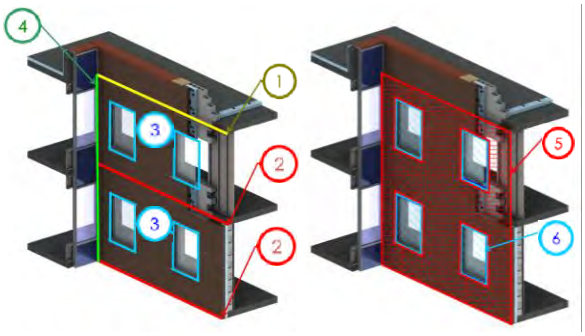

Figure 7 : Scope of quantity takeoffs for thermal bridging calculations; lengths: (1) parapet (2) slab (3) window-wall transition (4) corner, and areas: (5) opaque wall (6) glazing

Breaking down the calculation by interface or component losses helps target details where improvements can be realized.

For example, for the building shown in Figure 8 the clear field split insulated steel framed wall assembly only accounts for 45% of the total heat flow with conventional interface details. The rest of the heat flow is associated with the interface details for a breakdown as follows:

- 29% - Window to wall interface
- 10% - Balcony
- 8% - At-grade interface
- 8% - Roof to wall interface

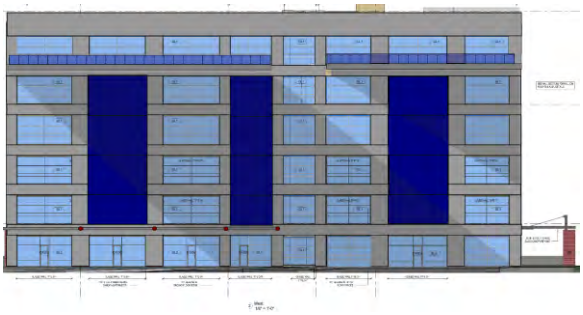

Figure 8: Overview of case study building façade

The clear wall effective R-value is R-23.5, while the overall effective R-value accounting for all the interface is R-9.9. There are clearly opportunities for mitigation of thermal bridging and to increase the overall effective R-value.

The first detail that makes the most sense to tackle is the window to wall interface because of its relative impact and does not require specialized manufactured products. Simply by orienting the glazing thermal break and glass in the plane of the exterior insulation reduces the window-wall interface contribution from 29% to 12%, and increases the effective R-value of the assembly to R-12.4.

Mitigating linear transmittance losses can similarly be achieved by introducing thermal breaks to balconies and parapets, as well as by introducing insulation outboard of foundation walls. Collectively implemented in this case study, the effective R-value increased to R-15.9. In this scenario, linear detail losses decreased to 32% of overall heat flow (as opposed to 55% per above). Table 3 summarizes this effect, and illustrates that while increasing insulation can increase the performance further, more efficient details are required to achieve above R-30 effective overall.

Table 3 : Contrasting opaque wall performance from different assemblies and details

Assembly	Interior and exterior insulated 6" steel stud; aluminum metal panel cladding supported by clip and rail system			
Cavity Insulation	R-20 fibreglass batts			
Exterior Insulation	4" mineral wool (R-16.8)		10" mineral wool (R-42)	
Clip System	Clips spaced @ 24" horizontal spacing		Fiber Reinforced Plastic @ 36" vertical and 16" horizontal spacing	
Details	Standard	Mitigated	Mitigated	Low TEDI Details
Clear Field R-Value	R-23.5	R-23.5	R-48.5	R-48.5
Effective R-Value	R-9.9	R-15.9	R-24.5	R-32.7
Clear Field Heat Flow	45%	68%	51%	69%
Linear Thermal Bridge Heat Flow	55%	32%	49%	31%

It is interesting to note that the impact of the interface details were reduced to approximately 30% for the conventional wall assembly, but increases to approximately 50% for the highly insulated wall. However, the impact of the interface details can be reduced to 30% for this wall assembly, but only with significantly more thermally efficient details.

More efficient details are similar to the ones outlined in the *Low TEDI Guide*. The expectations for the efficiency of interface details will continue to increase as building codes strive for net-zero energy ready performance. For example, Figure 9 highlights what was considered good or efficient when the version of the *BETB Guide* was released compared to what is required for net-zero ready or low TEDI buildings.

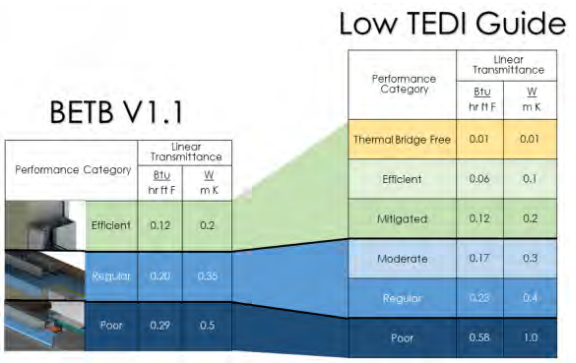

Figure 9: Expectations for conventional versus low TEDI buildings

On an annual basis, a typical multi-unit residential building in Vancouver, BC can curb total energy use intensity (TEUI) by ~3.3% as a result of improving the wall from R-9.9 to R-15.9. Using a visualization tool per Figure 10 can quickly communicate these and other performance impacts to design teams.

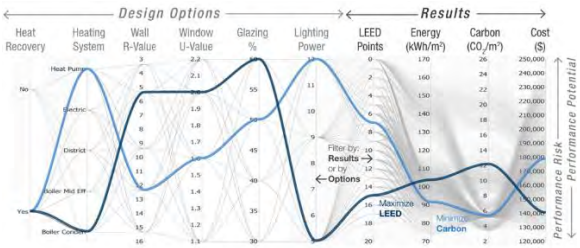

Figure 10: Mapping impacts of design options on energy performance metrics; the impacts of two designs are highlighted for an example project

Further, it should not be overlooked that thermal efficiency of components is not the only factor in the thermal bridging picture. How the cladding is attached to the building as a result of structural requirements and installation are also important considerations. The same proprietary clip at the same spacing can have two different clear field R-values as illustrated in Figure 11 and summarized in Table 4. This difference is larger than any of the differences in how the dynamic response is modeled in whole building energy simulations. Moreover, not only does the horizontal layout have a higher effective R-value, but also is more cost effective because the quantity of rails is reduced. Data provided in the BETB Guide allows practitioners to make these type of comparisons on projects.

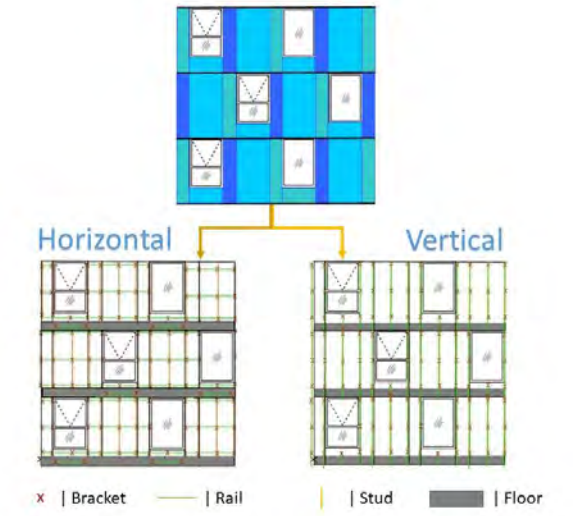

Figure 11 : Example of a wall façade with fibre cement panels that can have a significant difference in cost and performance depending on the sub-framing layout

Table 4 : Performance comparison of two possible configurations in Figure 11

	Vertical Layout	Horizontal Layout	% Increase
Total Rail Length (ft)	347	223	-36%
Number of Clips	105	111	7%
Clear Field R-value	R-18.5	R-21.5	16%

* ISO Clip with Rail, 6 inches of exterior mineral wool insulation; clips at spaced at 40" o.c. (insulation module)

Considering the impact of thermal bridges can also help to answer critical questions related to durability of existing building envelopes. Retrofitting older load-bearing multi-wythe clay brick masonry buildings is not straightforward, as in a case study building in Ottawa, ON [33] depicted in Figure 12.

Figure 12: Overall condition of building and brick masonry of a building in Ottawa, ON

Field investigation combined with lab testing of brick samples informed hygrothermal analysis, 3D thermal, and building energy analysis to evaluate feasible levels of insulation where energy savings and thermal comfort objectives could be met without increasing the risk of freeze-thaw damage and compromising the structural integrity of the existing buildings. By first evaluating risk of freeze-thaw damage (Figure 13), appropriate combinations of assemblies and components could be evaluated for overall energy and comfort impacts (Figure 14).

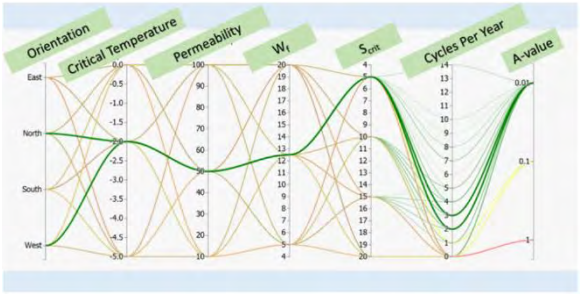

Figure 13: Mapping the effect of various material and climate conditions on freeze-thaw risk indicators

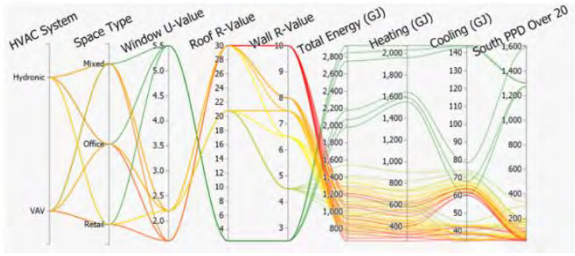

Figure 14: Mapping energy and comfort (PPD) impacts simultaneously

The study concluded that adding insulation beyond an R-21 roof or an R-6 effective wall is a frivolous endeavour due to diminishing energy benefits.

In the case of additional wall insulation, thermal bridging will remain at the intermediate floor and roof interfaces limiting its overall effectiveness. Moreover, it raises the question of what detailing is required at windows for this approach in the event of a retrofit. BETB calculations can help make these decisions more easily, while dynamic modeling helps with determine the energy and thermal comfort impacts. It is recommended to apply both methodologies in parallel for existing buildings.

7. Conclusions and Outlook

Canada's building energy policy is trending toward net zero ready energy & GHG buildings, where mitigating thermal bridging is essential. Holistic and accurate steady-state thermal transmittance calculations combined with dynamic whole building energy simulations is pivotal to calculating energy demand with the long term energy policy for buildings in mind. The *BETB Guide* and related work has helped push forward these energy efficiency initiatives forward. However, there is still work to be done. Examples are:

- Development of educational resources and delivery of training;
- Standardization of the BETB methodology in CSA Z5010;
- Expansion of the BETB database;
- Collaboration tools to share thermal transmittance data;
- Enhanced web application for the BETB database and integrated thermal calculator, and;
- Automated tools to streamline compliance documentation and review of thermal transmittance calculations.

Some researchers are encouraging direct 3D modeling of thermal bridges in whole building energy simulations to calculate energy demand, rather than relying on catalogs, such as the *BETB Guide*, for thermal transmittances and 1D approximations for dynamic response factors or conduction transfer functions (CTFs). The motivation is increased accuracy. However, direct 3D modeling in whole building energy simulations is problematic given the effort, limited opportunity for collaboration amongst the design team to focus on details to mitigate, software limitations, and difficultly of peer review. Moreover, the research done showing underestimation of heating energy demand is for a type of construction that is already being phased out in new construction due to thermal inefficiencies that are clearly evident by R-value calculations. Nevertheless, direct 3D modeling of thermal bridges in whole building energy simulations does have some potential applications, such as studies focused on interior insulation retrofits of historic facades or improving thermal comfort.

The bottom line is publically available thermal transmittance databases, such as the *BETB Guide*, with reliable and consistent data is advantageous not only for saving time, but also for peer review and collaboration, encouraging good practice, and leveling the playing field across industry. Moreover, it is critical to recognize that the underlying BETB methodology strikes the right balance between accuracy and practical utilization; without this work industry might still be overlooking the impact of thermal bridging because the alternatives are too complicated and difficult to implement.

Acknowledgements

The authors would like to thank the support of BC Hydro Power Smart, BC Housing, CMHC, Canadian Wood Council, FortisBC, FPInnovations, Manitoba Hydro, Natural Resources Canada, and Transition Energetique Quebec for their support of the *BETB Guide*.

References

[1] British Columbia Energy Step Code (2018). https://www2.gov.bc.ca/gov/content/industry/construction-industry/building-codes-standards/energy-efficiency/energy-step-code (retrieved January 2020).
[2] National Energy Code for Buildings (2017). Canadian Commission on Building and Fire Codes; National Research Council of Canada.
[3] ASHRAE. 2019. ASHRAE 90.1 Energy Standard for Buildings Except Low-Rise Residential Buildings. Atlanta: ASHRAE.
[4] Vancouver Building Bylaw (2019). https://vancouver.ca/your-government/vancouver-building-bylaw.aspx (retrieved January 2020).
[5] City of Toronto Green Standard (Version 3). https://www.toronto.ca/city-government/planning-development/official-plan-guidelines/toronto-green-standard/toronto-green-standard-version-3/ (retrieved January 2020).
[6] Roppel, P., and M. Lawton. 2011. Thermal Performance of Building Envelope Details for Mid- and High-Rise Buildings. ASHRAE Research Project RP-1365 Final Report.
[7] Roppel, P., Lawton, M., and N. Norris. 2012. Thermal Performance of Building Envelope

Details for Mid- and High-Rise Buildings. ASHARE Transactions 118 (2):569-584.
[8] Morrison Hershfield Limited. 2014. Building Envelope Thermal Bridging Guide Version 1.0. BC Hydro Powersmart. https://www.bchydro.com/powersmart/business/programs/new-construction.html#thermal (retrieved January 2020)
[9] Morrison Hershfield Limited. 2019. Building Envelope Thermal Bridging Guide Version 1.3. BC Hydro Powersmart. https://www.bchydro.com/powersmart/business/programs/new-construction.html#thermal (retrieved January 2020).
[10] Morrison Hershfield Limited. 2019. Guide to Low Thermal Energy Demand for Large Buildings (Low TEDI Guide). BC Housing. https://www.bchousing.org/research-centre/library/residential-design-construction/guide-low-energy-demand-large-buildings&sortType=sortByDate (retrieved January 2020).
[11] Van Geem, M. Challenges and Complexity of Proposal for Mitigating Thermal Bridges. Concrete International, September 2018. American Concrete Institute. http://www.vangeemconsulting.com/2_Challanges_and_Complexity_of_Proposal_for_Mitigating_Thermal_Bridges.pdf (retrieved January 2020).
[12] Challenges of Thermal Bridging Requirements - ASHRAE 90.1 Addendum av - AIA Codes Network Webinar. https://www.gotostage.com/channel/3148ae5284bf425ebfcfd898825c9c66/recording/6219b1c94ded4b308ff024dd140843f6/watch (retrieved January 2020).
[13] Baba, F, H. Ge. 2017. Dynamic Effect of Thermal Bridges on the Energy Demand of Residential Buildings in British Columbia. Proceedings of 15th Canadian Conference on Building Science and Technology.
[14] Baba, F. 2015. Dynamic Effect of Thermal Bridges on the Energy Demand of Residential Buildings. Master Thesis at Concordia University.
[15] Antretter, F, Radon, J., and M. Pazold. 2013. Coupling of Dynamic Thermal Bridge and Whole-Building Simulation. Proceedings of Thermal Performance of the Exterior Envelopes of Whole Buildings XII International Conference
[16] Van Nieuwenhove, S. 2014. Numerical analysis of thermal bridges under dynamic boundary conditions. Masters Thesis at Universiteit Gent.
[17] Piotr Narowski, P, Jacek Stasierski, J, and P. Wereszczyński. 2011. Modelling of Conduction Transfer Functions for Typical Thermal Bridges indentified in BIM Data. Proceedings of 12th Conference of International Building Performance Simulation Association.
[18] Ascione, F., Bianco, N., de Rossi, F., Turni, G., and G.P. Vanoli. 2012. Different methods for the modelling of thermal bridges into energy simulation programs: Comparisons of accuracy for flat heterogeneous roofs in Italian climates. Applied Energy 97: 405-418.
[19] Kossecka, E. and J. Kosny. 2004. Two-Step Procedure for Determining Three-Dimensional Conduction Z-Transfer Function Coefficients for Complex Building Envelope Assemblies. Proceedings of Thermal Performance of the Exterior Envelopes of Whole Buildings XII International Conference
[20] Enermodal Engineering Limited. 2001. Modeling Two- and Three-Dimensional Heat Transfer Through composite Wall and Roof Assemblies in Transient Energy Simulation Programs (1145-TRP). Part 1: Final Report. ASHRAE.
[21] ASHRAE. 2017. ASHRAE Handbook of Fundamentals. Atlanta: ASHRAE.
[22] Karambakkam, B.K. 2004. Transient Conduction Heat Transfer in Two-Dimensional and Heavy One-Dimensional Walls. Master Thesis at Oklahoma State University.
[23] Karambakkam, B.K., B. Nigusse, J., and D. Spitler. 2005. A One-dimensional Approximation for Transient Multi-dimensional Conduction Heat Transfer in Building Envelopes. Proceedings of the 7th Symposium on Building Physics in the Nordic Countries 1: 340-347.
[24] Martin, K., Erkoreka, A., Flores, I., Odriozola, M., and J.M. Sala. 2011. Problems in the calculation of thermal bridges in dynamic conditions. Energy and Buildings 43: 529-535.
[25] Martin, K., Escudero, C., Erkoreka, A., Flores, I., and J.M. Sala. 2012. Equivalent wall method for dynamic characterisation of thermal bridges. Energy and Buildings 55: 704-714.
[26] Antretter, F, Winkler, M, Fink, M, Pazold, M, Radon, J, S. Stadler. 2017. WUFI Plus 3.1 Manual. Fraunhofer IBP.
[27] Strachan, P., Nakhi, A., and C. Sanders. 1995. Thermal Bridge Assessments. Building Simulation 95: 563-570
[28] Ben-Nakhi, Abdullatif & Aasem, Essam. (2020). Conflation of Thermal Bridging Assessment and Building Thermal Simulation.
[29] Burch, D.M., Seem, J.E., Walton, G.N., and B.A. Licitra. 1992. Dynamic Evaluation of Thermal Bridges in a typical Office building. ASHARE Transactions 98:291-304.
[30] Iu, I. and D.E. Fisher. 2004. Application of Conduction Transfer Functions and Periodic Response Factors in Cooling Load Calculation Procedures. Proceedings of the 7th Symposium on Building Physics in the Nordic Countries 1: 340-347. ASHARE Transactions 109 (2):829-841
[31] Almeida, F., Lee, I., and Roppel P. Validation and Application of CFD for Condensation Risk Assessment. 2019 Buildings XIV International Conference. ASHRAE.
[32] Antretter, F, Klingenberg, K, and M. Pazold. 2013. All-in-One DesignTool Solution for Passive Houses and Buildings— Monthly Energy Balance and Hygrothermal Simulation. Proceedings of

Thermal Performance of the Exterior Envelopes of Whole Buildings XII International Conference.
[33] Lee, I. et al. Guiding Design Teams by Hygrothermal, Energy, and Thermal Comfort Analysis while Managing Uncertainty. 2016 Buildings XIII International Conference. ASHRAE.

National Energy Code of Canada reference thermal resistance calculation methods compared to a validated 3D heat transfer simulation for framed walls containing thermal bridges

H. Schreiber*, T. Moore, M. Ghobadi

National Research Council Canada, Construction Research, 1200 Montreal Rd, Ottawa, ON K1A 0R6, Canada
* Corresponding author, Tel +1 613 998 6804, email: heike.schreiber@nrc.ca

Abstract:
Construction of buildings in Canada requires adherence to the minimum requirements of the National Energy Code for Buildings (NECB) through one of three respective compliance paths: the prescriptive path, the trade-off path, or the performance path. The most straight forward path is the prescriptive path, which defines minimum performance levels for different components and assemblies of the building to meet for compliance. One prescriptive requirement is a minimum effective thermal resistance value for the wall assembly. Within the prescriptive path, methods are referenced for determining the effective thermal resistance of wall assemblies, as detailed in section 3.1.1.5(5) of the NECB. Specifically, the effective thermal resistance of a wall assembly can be determined through either testing a representative wall assembly in accordance with ASTM C1363, or, calculation using: ISO 14683, two-or three dimensional modelling, or the calculation methods described in the ASHRAE Handbook of Fundamentals. Additional guidance for the use of the calculation methods described in the ASHRAE Handbook of Fundamentals for calculating the effective thermal resistance of framed walls (i.e. wood and steel stud framed) in accordance with the NECB is provided in the NECB "Users Guide". This paper investigates the accuracy of using the methods described in the "User's Guide" on three representative steel stud framed wall assemblies with increasing thickness of exterior insulation: none, 25 mm and 50 mm of thickness. The accuracy of each calculation method is determined by comparing the results to ASTM C1363 guarded hot box tests. This paper will focus on the accuracy of these calculation methods and include some commentary on any restrictions that should be imposed on the use of these methods, especially in instances where the framing can significantly influence the effective thermal resistance of the wall assembly through thermal bridging.

Keywords:
Thermal Bridging, National Energy Code Canada, Steel Stud wall Assemblies, COMSOL Multiphysics

1. Introduction

The prescriptive path of the National Energy Code for Buildings (NECB) of Canada has requirements for the minimum effective thermal resistance of wall assemblies for each given climate zone. The accepted calculation methods are detailed in section 3.1.1.5(5) of the NECB and consist of, either: testing a representative wall assembly in accordance with ASTM C1363, calculating using ISO 14683, two-or three dimensional modelling, or using the calculation methods described in the ASHRAE Handbook of Fundamentals [1]. This paper compares the results of the ASHRAE calculation method, the NECB Users guide method, 2D and 3D simulations for accuracy in predicting the thermal resistance of a steel stud wall with varying exterior insulation layer thicknesses: none, 25 mm and 50 mm. The results are compared to the results from guarded hot box test according to ASTM C1363. The purpose of this work is to determine, for a steel stud wall, which calculation methods lead to acceptable results in predicting the effective thermal resistance of a steel stud wall with varying levels of exterior insulation.

2. Methods

We calculated the effective thermal resistance for three wall assemblies containing steel studs and different configurations of insulation. The thermal resistance was determined with four methods of different complexity (I-IV). We calculated the effective R-value based on simplified calculation methods and compared those results to numerical simulations in COMSOL Multiphysics and guarded hot box (GHB) measurements. The calculations were done according to (I) NECB [2] and (II) ASHRAE [1]. The methods for calculation are based on parallel path calculations defined in the AHSRAE Handbook. [1]. For comparison, we also developed a 2D model of each wall assembly (III) and compared all derived values to the most complex method (IV) based on numerical simulations with a 3D model in COMSOL Multiphysics [3]. The calculated and simulated effective thermal resistance values are then benchmarked to guarded hot box measurements of the same three wall assemblies according to ASTM C1363.

All three wall assemblies share a basic construction with wall assembly 1 (see Figure 1) consisting of interior gypsum drywall board, a 6mil polyethylene vapor barrier, 20 gauge steel studs spaced 406 mm (16 in) on center with R12 fiberglass batt insulation in between the studs and an exterior layer of OSB sheathing. Wall assemblies 2 and 3 have additional layers of XPS (Styrofoam) insulation on the exterior of the OSB sheathing (see Figure 2). The thicknesses of all wall assembly components is given in Table 1.

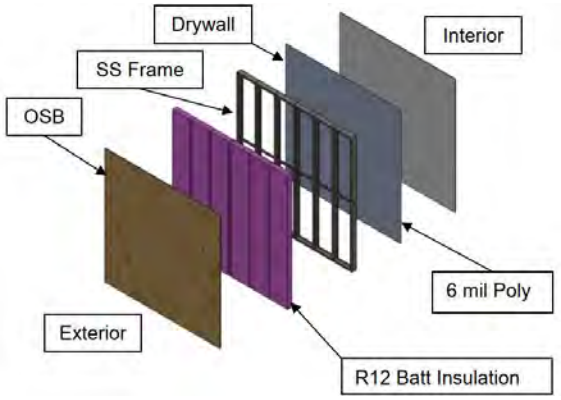

Figure 1: Schematic of Wall 1

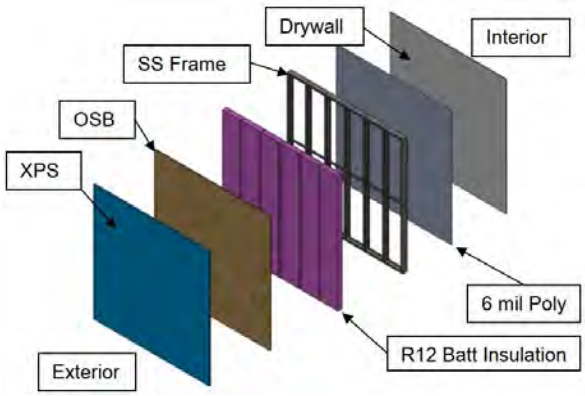

Figure 2: Schematic of Wall 2 and 3. The Styrofoam (XPS – Extruded Polystyrene) panel was 25 mm (1 in) thick for Wall 2 & 50 mm (2 in) thick for Wall 3.

Table 1: Wall assembly geometries

Property (in mm)	Wall 1	Wall 2	Wall 3
depth of wall	124	149	175
thickness gypsum board	13		
Polyethylene vapour barrier	0.15		
depth of studs	92		
stud spacing o.c.	406		
depth of cavity insulation	89		
thickness OSB sheathing	16		
thickness exterior insulation		25	50

To calculate the effective thermal resistance of the wall assemblies, thermal resistance or their reciprocal thermal conductivity values for all materials within the wall assemblies need to be known or estimated. The material properties used in this study were derived from measurements at the NRC's Heat Flow Meter in compliance to ASTM C1667-15 and described in Ref. [3]. The thermal resistance is a temperature dependent property. The detailed simulations allow for this effect to be taken into account. Thermal conductivity is given as a function of temperature within the COMSOL simulations. Simulations and GHB measurements were performed at 21 °C indoor and -5 °C outdoor temperature. Results are reported as effective thermal resistance from air to air.

3D simulations were performed in COMSOL with the geometries depicted in Figure 1 and 2. A thorough discussion of the 3D simulations and guarded hot box measurements of the three wall assemblies can be found in [3]. Temperature dependence of the assembly material properties and resulting effective resistances for different outdoor temperatures are also discussed there.

2D simulations were performed in COMSOL based on the geometry as shown in Figure 3. The same temperature dependent material properties were used as for the 3D calculations.

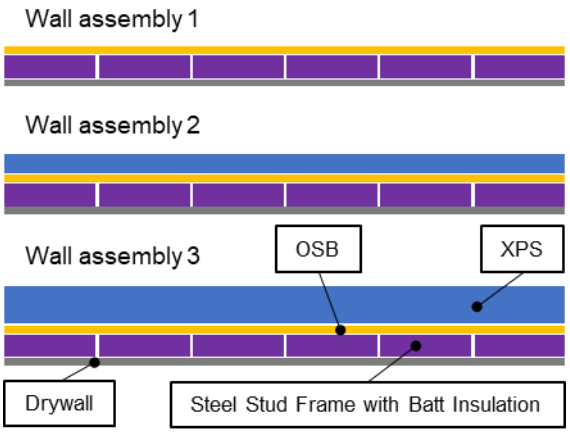

Figure 3: 2D geometry for COMSOL simulations

NECB specifies a variation on the Isothermal Planes Method [1] for the calculation of effective thermal resistance for metal-frame construction. A table provides values for the effective thermal resistance RSI of the insulation/framing layer in metal-frame wall assemblies depending on the cavity depth, insulation RSI and frame spacing. The RSI values for all parallel material layers are then added up to the effective thermal resistance of the assembly.

From the ASHRAE Handbook of Fundamentals, the Modified Zone Method for Metal Stud Walls with Insulated Cavities was used to calculate the effective thermal resistance of the three wall assemblies.

For the calculations according to ASHRAE and NECB, constant thermal conductivity values are used, derived from the Heat Flow Meter measurements at an average temperature of 8 °C (see Table 2). Please note that the tables in NECB and ASHRAE Handbook report material thermal resistance values at 24 °C.

Since the measured results from guarded hot box testing give the most accurate results, if air to air thermal resistance values are reported, air films were taken into account for calculations and simulations, with an interior air film RSI of 0.12 (m^2K)/W and an exterior air film RSI of 0.03 (m^2K)/W. These values were translated into convective heat transfer coefficients for the numerical simulations.

Table 2: Thermal conductivity k in W/m K and thermal resistance RSI per mm material thickness in (m^2K)/(W mm) of all materials in the wall assemblies at an average temperature of 8 °C

Material	k in W/mK	RSI/mm
Batt insulation	0.036	0.028
XPS	0.028	0.036
OSB	0.13	0.0077
Gypsum board	0.16	0.0063
Metal	40	2.5e-5

Results and discussions

The results from calculations based on ASHRAE and NECB are compared to modeling results from 2D and 3D simulations and benchmarked to GHB measurements. Figures 4 gives the results for the effective RSI-values air to air of 3 steel-stud wall assemblies with varying exterior insulation thickness (0, 25, 50 mm). The measurement uncertainty of 8 % is included in Figure 4, as reported for the guarded hot box test chamber at NRC. However, additional uncertainties from the manufacturing process of the wall assemblies could occur as well.

Figure 4 shows that the results from 2D and 3D simulations are within the measurement's uncertainty for all 3 wall assemblies, while ASHRAE and NECB underestimate the effective thermal resistance for the steel-stud wall assembly 1 which does not have a layer of exterior insulation. In particular, the modified zone method from the ASHRAE Handbook shows a large discrepancy from the measured results if the steel-stud wall assembly is built without exterior insulation.

The more insulation is added to the exterior, the closer the calculated results agree with the GHB measurements. For the wall with 25 mm exterior insulation, the ASHRAE methods predicts the thermal resistance as accurately as the 3D simulations. The NECB method, however, still yields results only close to the uncertainty band width of the GHB measurements.

For the third wall with 50 mm insulation, all four methods yield results within the uncertainty bandwidth of the measured effective thermal resistance.

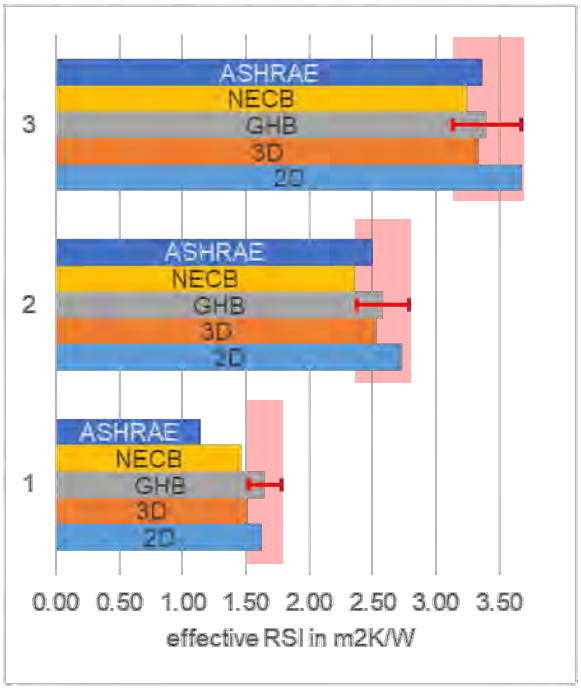

Figure 4: Effective RSI-values for wall 1 with 0 mm exterior insulation, wall 2 with 25 mm exterior insulation and wall 3 with 50 mm exterior insulation, calculated by 2D and 3D simulations, according to ASHRAE and NECB and compared to guarded hot box (GHB) measurements (with 8 % reported uncertainty, shown as error bars and red squares)

3. Conclusions and outlook

From the comparison of results, we can derive the following recommendations as to which method should be used when calculating thermal bridging effects for steel-stud walls: when measurements of the wall assembly are not an option, simulations should be performed if the steel-stud wall has no insulation on the exterior side. For wall assemblies with insulation on the exterior, the modified zone method from the ASHRAE Handbook yields as accurate results as 2D and 3D simulations. The results so far suggest that the method described in the NECB should only be used for insulation thicknesses reaching 50 mm.

For future work, we want to study further insulation thickness levels between 0 and 50 mm to be able to derive distinct recommendations as to how much exterior insulation will lead to accurate results when using simplified calculation methods.

Acknowledgements

The authors would like to thank for funding from the office of energy efficiency (OEE) Natural Resources Canada.

References

[1] ASHRAE, "ASHRAE Handbook of Fundamentals", ASHRAE, Atlanta, GA, USA, 2017.

[2] Canadian Commission on Building and Fire Codes, “User’s Guide – National Energy Code of Canada for Buildings 2015”, Ottawa, ON, Canada, 2015.

[3] M. Ghobadi, T. Moore, M. Lacasse, The Thermal Bridging Effects in Steel Stud Wall Assemblies, Thermal Buildings XIV, ASHRAE 2019

The Thermal Effects of Adding a window to a Wood Stud Wall Assembly

M. Ghobadi[a,*], J. Cingel[a], K. Kadzadej[a]

[a] National Research Council of Canada, Construction Research Centre
* Corresponding author, (613) 990-0921, mehdi.ghobadi@nrc-cnrc.gc.ca

Abstract:
Improving the thermal performance of buildings is an essential element when addressing issues related to the effects of climate change on the building envelope. Minimizing energy usage of and heat losses from buildings are important measures in achieving these associated goals. The thermal performance of a building envelope can highly impact the overall performance and energy efficiency of the building. It has been shown that the thermal resistance (R-value) of a building envelope can be affected by thermal bridging sources. Hence, it is important to accurately determine the R-value of building envelopes with thermal bridging components. In this study the thermal bridging effect of a window on wood stud wall assemblies was investigated both experimentally and numerically. A 2.4 m × 2.4 m wood-stud wall assembly, typical of North American wood-frame construction practice, was fabricated with an opening to accommodate a window. The opening in the wall assemblies was first filled with EPS and thereafter tested in the guarded hot box; following which, the EPS in the wall assembly, was replaced with a window. In this study Numerical simulation packages, THERM and WINDOW, were employed to calculate the thermal resistance of a window. The incremental effect of adding this window to a wood stud wall assembly was then investigated numerically and experimentally. COMSOL Multiphysics was employed to evaluate the effective thermal resistance of the wall and the results were benchmarked against the Guarded Hot Box (GHB) results collected in the NRC facility.

Keywords:
Window Walls, Thermal Bridge, THERM, WINDOW, COMSOL Multiphysics

1. Introduction

Adopting the Pan-Canadian Framework on clean growth and climate change in 2016, Government of Canada invested on investigations of mechanisms by which the National Model Codes (National Building Code of Canada (2015) and National Energy Code of Canada (2017)) be used to ensure building resilience and energy efficiency considering a changing climate. One specific area under investigation is in the best approaches to implement energy efficiency and clean energy technologies in Canadian building design as 17% of Canada's total GHG emissions are associated with the built environment (12% from direct emissions and 5% from electricity generation). The heating and cooling demand of a building is the result of heat loss due to heat transmission (conduction, convection and radiation), ventilation and infiltration. In this context, it is generally recognized that the thermal performance of building envelopes can be significantly affected by thermal bridging. Thermal bridges are localized areas of high heat flow through walls, roofs and other insulated building envelope components. These paths allow heat flow to bypass the insulating layer thereby reducing the overall effectiveness of the building envelope in limiting heat transfer between the building interior and the exterior environment. Some recognized examples of thermal bridges in the building envelope include repeating structural members, balcony edges, and window frames. Additionally, as the push towards increasingly insulated building envelopes continues, the effect of thermal bridges on the effective thermal resistance of the assembly becomes increasingly significant.

In this study the thermal bridging effect of a window on wood stud wall assemblies were investigated both experimentally and numerically. A 2.4 m × 2.4 m wood-stud wall assembly, typical of North American wood-frame construction practice, was fabricated with an opening to accommodate a window. The opening in the wall assemblies was first filled with EPS and thereafter tested in the guarded hot box; following which, the EPS in the wall assembly, was replaced either with a window. WINDOW and THERM were employed to model thee glazing system and the results were then used in COMSOL Multiphysics to model the whole wall assembly using the three dimensional simulation configuration of the wall. The numerical results were benchmarked against results obtained experimentally from completion of standard guarded hot box tests. The results were used to study the reduction in thermal resistance for each case.

2. Methodology

A typical 2.4 m × 2.4 m wood-stud wall assembly was fabricated with an opening to accommodate a window (Figure 1). The opening was first filled with EPS and was tested in the NRC Guarded Hot Box (GHB) facility. The EPS was then removed from the wall and replaced by a window (Figure 2).

Numerical simulations were completed on the wall assemblies in three dimensions. The modeling sequence for both series consisted of: (i) creating the geometry to be modelled; (ii) selecting the material properties; (iii) determining and applying the boundary conditions; (iv) performing a mesh verification; (v) conducting the numerical simulations, and; (vi) comparing the results to those obtained from laboratory tests.

The heat transfer in the walls was also simulated in COMSOL Multiphysics. Three dimensional simulations were chosen to capture the lateral heat transfer in the wall assemblies that occur due to the thermal bridging elements. The 3-D geometries for the wall assemblies

were created in Solidworks®. The geometries were imported in COMSOL Multiphysics and material properties were assigned to the corresponding domains. The temperature dependent thermal conductivity was used for fiberglass batt insulation and extruded polystyrene (XPS) as follow:

$$K_{Fibergalss} = 0.0355+0.0002T_{mean} \quad \text{Eq. 1}$$

$$K_{EPS} = 0.0388+0.0001T_{mean} \quad \text{Eq. 2}$$

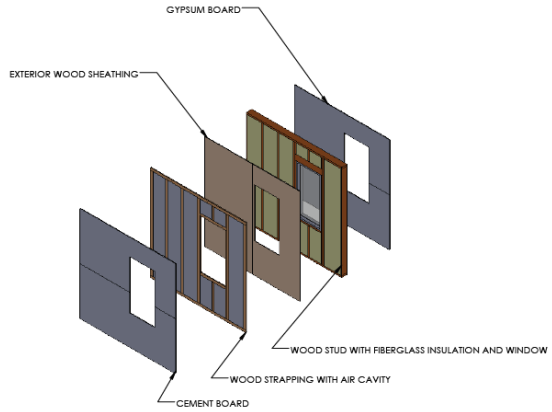

Figure 1. Exploded view of the window wall

Figure 2. Window wall which was tested in the GHB

Natural convection on the interior surface and forced convection on the exterior surface were used as the hot and cold boundary conditions. Convective heat transfer coefficients were derived from the GHB results and are shown in Table 1.The symmetry boundary condition was applied on the edges of the wall.

Figure 3 illustrates the window glazing system. In the WINDOW (v7.6) software, “6mm Clear Float Glass” from Guardian (WINDOW ID #3016) was used as the clear glass, and for the low-e glass, “ClimaGuard 70/36 LE on 6mm” glass from Guardian (WINDOW ID #3256) was used. The low-e coating was placed on the inner side of the glass (surface #2) to maximize thermal performance. The cavity between the glass lites (12.7 mm / 0.5-in.)) was filled with Argon gas. The glazing also had a spacer between the glass lites (which is later made in THERM). A generic spacer was chosen from a study completed on spacer and edge seals by the Berkley Lab; his same study was also used in the NFRC manual. The spacer consisted of butyl rubber separating a 0.015-in. thick steel stud from the glazing, as well as a layer of desiccant (Silica gel) inside the stud to improve performance. This 6 mm clear, Argon, filled, low-e glazing system is generic and considered to replicate the actual glazing reasonably well. After the glazing was created in the WINDOW (v7.6) software, the frame parts (head, sill, jambs) were then created separately in THERM. The drawing was imported to THERM, where predefined THERM materials were assigned to each part of the detail. The PVC frame was assigned the THERM material “Polyvinylchloride PVC / Vinyl – Rigid” whereas the frame cavities were modeled using THERM material “Frame Cavity NFRC 100”, which is the NFRC standard for frame cavities. The spacer materials were the same as those described above. After the material selection was complete, the glazing was imported from WINDOW (v7.6).

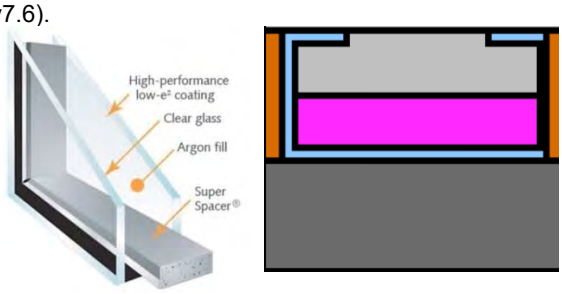

Figure 3. The Glazing system (left) the spacer (right)

Table 1. Exterior and interior boundary conditions

$T_{cold\ air}$ (°C)	$T_{hot\ air}$ (°C)	$T_{cold\ surface}$ (°C)	$T_{hot\ surface}$ (°C)	h_{cold} $(\frac{W}{m^2K})$	h_{hot} $(\frac{W}{m^2K})$
-5	21	-4.6818	19.824	32.7	9.2
-20	21	-19.513	19.19	34.0	8.9
-35	21	-34.355	18.589	34.0	8.9

The boundary conditions used for the calculations were:

- “NFRC 100 – 2010 Exterior” for the exterior edges of the frame and glazing
- “Interior Wood/Vinyl Frame (convection only)” for the interior edges of the frame
- “U-factor Inside Film” for the interior glazing
- “Adiabatic” for surfaces that are connected to the wall

Laboratory thermal tests were conducted on four wall assemblies in NRC’s GHB test facility following the test procedures given in ASTM C1363. The NRC GHB test facility is a test apparatus specifically designed to determine the thermal resistance of building envelope assemblies and components by subjecting a test specimen to a temperature difference and measuring the amount of energy required to maintain interior set point conditions. The tests were conducted at two different exterior temperatures; i.e.: -20 °C and -35 °C.

3. Results and discussions

The final THERM results are shown in Figure 4**Error! Reference source not found.**. As is evident, a thermal transmittance of 1.543 W/m^{2}K was obtained which is equivalent to a R value of 3.68 ft2.hr°F/Btu or 0.648 m^{2}K/W. The results were used to calculate the equivalent conductivity of the window in COMSOL. AS such, and instead of modeling the window, an artificial artifact was created as a proxy material that replicates the window in terms of its thermal performance. For this wall assembly, which has a thickness of 0.243 m, the equivalent thermal conductivity of 0.375 W/m.K was used for the proxy material. The window or EPS occupy 13.3 percent of the total surface area of the wall. Also, as stated before, the wall assembly had no exterior insulation.

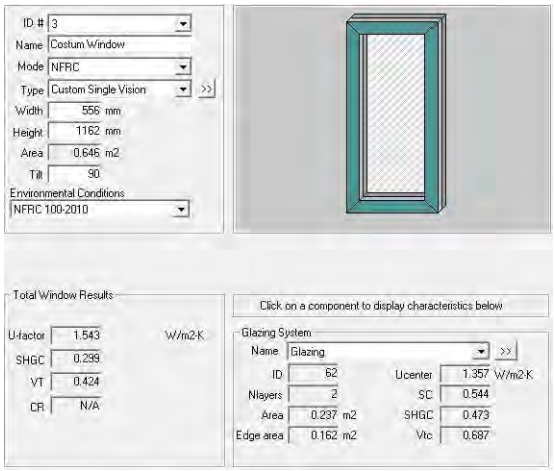

Figure 4. THEMR final results

Table 2 and Interior surface

4. Conclusions and outlook

The incremental effect of adding a window to a wood stud frame wall assembly was studied numerically employing COMSOL Multiphysics, THERM, WINDOW and experimentally using standard guarded hot box testing. First WINDOW and THERM were used to simulate the glazing part and the frame. The results were used to assign the thermal conductivity to an equivalent and proxy material in COMSOL Multiphysics.

It has been shown that the window wall thermal performance is significantly affected by the thermal transmittance of the window. The window only occupied 13 percent of the wall, but reduced the effective thermal resistance of the wall by more than 50 percent. It also decreased the minimum temperature index on the interior surface; this can lead to less comfortable thermal conditions for the occupants in proximity to the window and as well, increases the risk to condensation on the glazing.

This is an ongoing project and additional work on this topic will be reported in the future. Now that the numerical method has been benchmarked against experimental results, additional numerical work can now be conducted to extract more results. Since, numerical simulations are time consuming and given that access to appropriate numerical tools cannot be assumed, these results could be used to find simple correlations that thereafter, practitioners can employ to find the effective thermal resistance of window-walls.

Table *3* summarize the window-wall results for the cases where the openings were filled with EPS and a window at two exterior temperatures of -5 °C and -20 °C. For the case where the exterior temperature was set to -35 °C, the calorimeter heater could not generate sufficient heat to compensate for the heat flow passing through the window-wall. Hence, the warm side temperature could not reach the desired temperature. It can be seen that the R-values dropped 54 percent when the window was added to the wood-stud wall assembly. The differences between the COMSOL simulation and GHB test were also found to be less than three percent and well below the uncertainty of the NRC GHB.

Figure 5 and Figure 6 illustrate the temperature index on the interior and exterior surfaces of the wood-stud wall assembly with the opening filled with EPS. Figure 7 and Figure 8 show the same for the wall with window in the opening. It can be seen that for the case where the EPS was used to fill the opening, wood-studs are the main source of thermal bridging and the minimum temperature index occurs near the edge of the opening where double wood-studs were used in the assembly. The temperature index on the exterior is also very uniform. Whereas, for the case having a window installed in the wall, a maximum temperature index of 0.1228 on the exterior surface was obtained whereas, and a minimum temperature index of 0.67 was achieved on the interior surface. Hence, the window is the primary element of heat flow through the wall and that evidently significantly affects the thermal transmittance of the entire wall assembly.

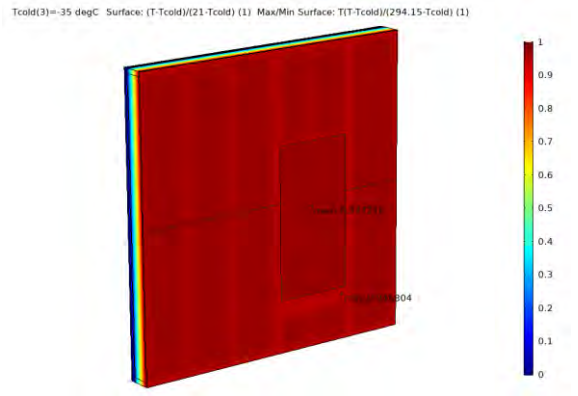

Figure 5. The window wood stud wall assembly with the hole filled with EPS- Values of temperature index on the Interior surface

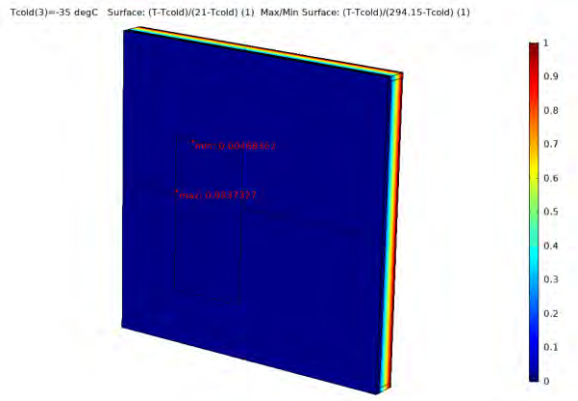

Figure 6. The window wood stud wall assembly with the hole filled with EPS- Values of temperature index on the exterior surface

Table 2. Window wall and clear field results calculation for the exterior temperature of -5°C

Study	R_o ft². hr. °F/Btu (m²K/W)	U_o Btu/ft². hr. °F (W/m²K)	R_{ww} ft². hr. °F/Btu (m²K/W)	U_{ww} Btu/ft². hr. °F (W/m²K)
COMSOL	R-22.40 (3.94)	0.0446 (0.2539)	R-10.17 (1.79)	0.0983 (0.5602)
Experiments	R-22.16 (3.90)	0.0451 (0.2564)	R-10.08 (1.77)	0.0992 (0.5650)
Difference	0.98%		0.86%	

Interior surface

5. Conclusions and outlook

The incremental effect of adding a window to a wood stud frame wall assembly was studied numerically employing COMSOL Multiphysics, THERM, WINDOW and experimentally using standard guarded hot box testing. First WINDOW and THERM were used to simulate the glazing part and the frame. The results were used to assign the thermal conductivity to an equivalent and proxy material in COMSOL Multiphysics.

It has been shown that the window wall thermal performance is significantly affected by the thermal transmittance of the window. The window only occupied 13 percent of the wall, but reduced the effective thermal resistance of the wall by more than 50 percent. It also decreased the minimum temperature index on the interior surface; this can lead to less comfortable thermal conditions for the occupants in proximity to the window and as well, increases the risk to condensation on the glazing.

This is an ongoing project and additional work on this topic will be reported in the future. Now that the numerical method has been benchmarked against experimental results, additional numerical work can now be conducted to extract more results. Since, numerical simulations are time consuming and given that access to appropriate numerical tools cannot be assumed, these results could be used to find simple correlations that thereafter, practitioners can employ to find the effective thermal resistance of window-walls.

Table 3. Window wall and clear field results calculation for the exterior temperature of -20°C

Study	R_o ft². hr. °F/Btu (m²K/W)	U_o Btu/ft². hr. °F (W/m²K)	R_{ww} ft². hr. °F/Btu (m²K/W)	U_{ww} Btu/ft². hr. °F (W/m²K)
COMSOL	R-22.51 (3.96)	0.0444 (0.2527)	R-10.20 (1.79)	0.0981 (0.5589)
Experiments	R-22.90 (4.03)	0.0437 (0.2481)	R-9.93 (1.75)	0.1007 (0.5714)
Difference	1.80%		2.23%	

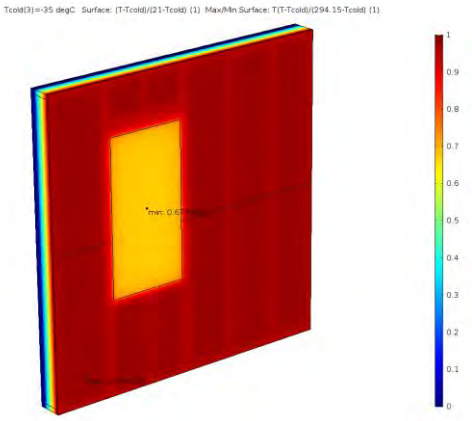

Figure 7. The window wood stud wall assembly with the window- Values of temperature index on the

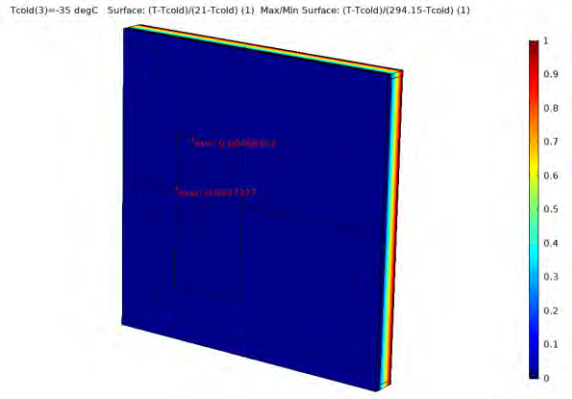

Figure 8. The window wood stud wall assembly with the window- Values of temperature index on the exterior surface

Acknowledgements

The authors acknowledge the financial support of NRCan to support this project.

References

ASTM C1363 – 11 Standard Test Method for Thermal Performance of Building Materials and Envelope Assemblies by Means of a Hot Box Apparatus

American Society of Heating, Refrigerating and Air-Conditioning Engineers. ASHRAE Standard : Energy Standard for Buildings Except Low-Rise Residential Buildings, 2016 ASHRAE ISSN 1041-2336

Natural Resource Canada, Energy Use Data Handbook, 2009, http://oee.nrcan.gc.ca/corporate/statistics/neud/dpa/handbook (retrieved 2013).

EN ISO 10211: Thermal Bridges in Building Construction – Heat Flows and Surface Temperatures – Detailed Calculations, 2007.

EN ISO 14683: Thermal Bridges in Building Construction – Linear Thermal Transmittance Simplified Methods and Default Values, 2007.

Lawrence Berkley National Laboratory, "THERM 6.3/WINDOW 6.3 NFRC Simulation Manual," Berkley Lab, 2011.

Pan-Canadian Framework on Clean Growth & Climate Change – Environment & Climate Change Canada, 2016.

S. Van Der Bergh, R. Hart, B. Petter Jelle and A. Gustavsen, "Window Spacers and Edge Seals in Insulating Glass Units: A State-of-the-Art Review and Future Perspectives," Energy and Buildings, 2013.

Research for Detecting Relationship Information Between Point Cloud Data and Plan of Completion Drawing

Y. Umehara[a*], K. Nakamura[b], Y. Tsukada[c], S. Tanaka[d], K. Nakahata[e]

[a] Organization for Research and Development of Innovative Science and Technology, Kansai University, 3-3-35 Yamate-cho, Suita-shi, Osaka, Japan
[b] Faculty of Information Technology and Social Sciences, Osaka University of Economics, 2-2-8 Osumi, Higashiyodogawa-ku, Osaka-shi, Osaka, Japan
[c] Faculty of Business Administration, Setsunan University, 17-8 Ikeda-nakamachi, Neyagawa-shi, Osaka, Japan
[d] Faculty of Informatics, Kansai University, 2-1-1 Ryozenji-cho, Takatsuki-shi, Osaka, Japan
[e] Graduate School of Informatics, Kansai University, 2-1-1 Ryozenji-cho, Takatsuki-shi, Osaka, Japan
* Yoshimasa Umehara, +81-6-6368-1121, y.umeha@kansai-u.ac.jp

Abstract:
In recent years, with the development of laser measurement technology, means for measuring three-dimensional shape of road features as point cloud data have been diversified. The Ministry of Land, Infrastructure, Transport and Tourism is promoting i-Construction as an effort to improve the productivity of construction sites by utilizing point cloud data. However, since that does not have information on road features indicated by points, it is difficult efficiently to operate according to the application. Therefore, the technology to extract road features from point cloud data is attracting attention. In existing research, a method of dividing point cloud data into road features by referring to outline information described in the plan of completion drawing has been proposed. However, there is a problem that the position is shifting between the point cloud data and the plan of completion drawing, or between the point cloud data for each trajectory. Thus, this research proposes a method to correct this positional shift.

Keywords:
road features, point cloud data, plan of completion drawing, registration

1. Introduction

In recent years, with the development of laser measurement technology, means for measuring three-dimensional shapes of road features as point cloud data have been diversified, including Mobile Mapping Systems (hereinafter “MMS”), ground-based laser scanners and UAVs. The Ministry of Land, Infrastructure, Transport and Tourism is promoting i-Construction[1] as an effort to improve the productivity of construction sites by utilizing three-dimensional information such as point cloud data, and utilization and application of point cloud data is being promoted in a variety of settings. With a focus on the field of roads, through analyzing point cloud data measured in road environments, efforts are being made to generate three-dimensional models of bridges as well as the road foundation map data necessary for self-driving technology, self-inspection of road-attached structures such as signs and lighting, and surveys of road conditions.

However, point cloud data measured in road environments combines various types of road features together, including traffic lanes, sidewalks, signs and lighting. In addition, point cloud data only expresses the shapes of the various road features through aggregation of vast numbers of points and does not have information on the road features that these points represent. Efficient application of this type of point cloud data in maintenance operations requires to select point cloud data of the road feature depending on purpose. However, the problems faced in these operations are that point cloud data processing software is essential and that it is necessary to conduct the operations manually.

Therefore, technology is required that is capable of automatically extracting point cloud data of each individual road feature seperately with the aim of promoting utilization and application of point cloud data. Against this background, by referencing plan of completion drawings based on Manual of Completion Drawing Production for Road Works[2], the authors have proposed a method[3] to extract road features from point cloud data. However, because MMS point cloud data, which is typically used in the field of roads, is generated by measuring multiple traffic lanes and using the measurement data for each lane separately, errors occur due to the measurement environment based on the trajectory of each vehicle, which causes positional shifts between point cloud data. In addition, positional shifts occur between the point cloud data measured and plan of completion drawings due to differences in how precisely each piece of data is retained, which becomes a factor that lowers precision when extracting features.

Therefore, this research contributes to increasing the precision of feature extraction technology[3] by revising point cloud data based on plan of completion drawings and examining methods to eliminate the aforementioned positional shifts.

2. Research outline

(1) Research contents

This research proposes a method to eliminate positional shifts occurring in point cloud data by revising point cloud data based on plan of completion drawings. In addition, this research targets MMS point cloud data typically used in road environment measurements.

(2) Problem of positional shifts

As a result of detailed analysis of problems in positional shifts of point cloud data that lower precision in existing methods[3], it was found that it is possible to classify the problems into the following two categories.

a. Positional shifts between point cloud data by each trajectory

Because it is difficult to measure an entire measurement location in a single pass, MMSs generate point cloud data for entire measurement locations by driving down multiple traffic lanes and overlapping the point cloud data measured by each trajectory. However, it was found that positional shifts occur between the point cloud data of each trajectory, because the surrounding environment differs by trajectory.

b. Positional shifts between plan of completion drawings and point cloud data

MMS point cloud data contains measurement errors as well as errors that occur when aligning points. Accordingly, when overlapping plan of completion drawings, which accurately recorded completion shapes, it was found that positional shifts of anywhere from tens of centimeters to one meter occur between plan of completion drawings and point cloud data.

(3) Countermeasures to these problems

This research solves the problems of “positional shifts between point cloud data” and “positional shifts between plan of completion drawings and point cloud data” by utilizing plan of completion drawings as the standard positions and overlapping the point cloud data of each trajectory onto these drawings. In addition, The road feature as the standard position is lane dividing lines which are a fundamental road feature and easy to extract using reflection intensity from point cloud data.

3. Revision algorithm for positional shifts

The process flow of the proposed method is shown in Fig 1. By inputting point cloud data and plan of completion drawings based on Manual of Completion Drawing Production for Road Works[2], the proposed method outputs point cloud data in which positions have been revised via three processes: extraction function for outline data, extraction function for lane dividing line and position revision function for point cloud data. The details of each function are as follows.

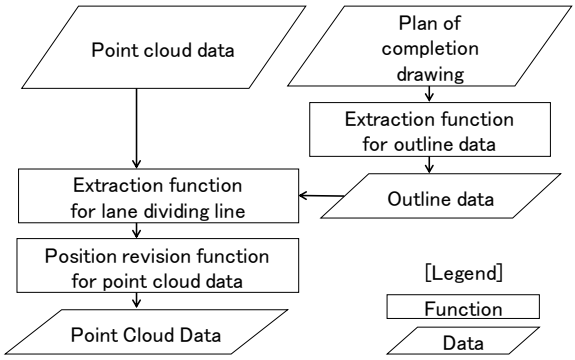

Fig 1: Process flow

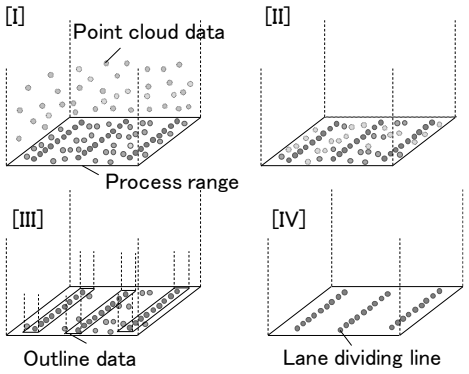

Fig 2: Extraction process for lane dividing line

(1) Extraction function for outline data

This function extracts outline data on lane dividing lines from plan of completion drawings. Manual of Completion Drawing Production for Road Works[2] define lane dividing lines as a line feature within the C-STR-STRZ-LINE layer, so in accordance with this definition, this function extracts line information on lane dividing lines from two-dimensional CAD data within the plan of completion drawings. Then it extracts those extracted line information as outline data on lane dividing lines.

(2) Extraction function for lane dividing line

This function extracts point cloud data on lane dividing lines from point cloud data. First, as shown in Item I inside Fig 2, with a focus on the fact that lane dividing lines always exist on the road surface, this function extracts point cloud data on road surfaces from point cloud data using the Cloth Simulation Algorithm[4]. The Cloth Simulation Algorithm is a method that inverts the height values of point cloud data and utilizes points that come into contact when covered with cloth of a fixed rigidity as road surface point cloud data. Next, as shown in Item II inside Fig 2, with a focus on the fact that lane dividing lines have high reflection intensity, this function extracts the lane dividing lines by removing points which the reflection intensity are at or lower than a set value from point

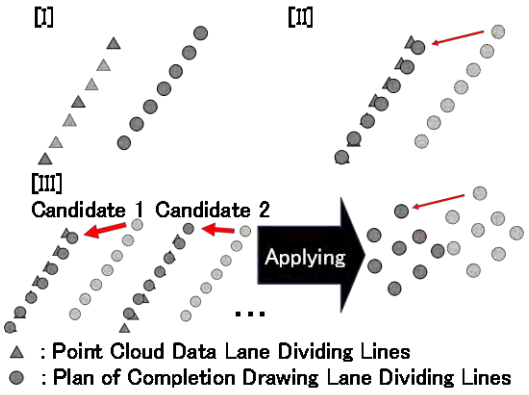

Fig 3: Position revision process for point cloud data

cloud data. Finally, as shown in Item III inside Fig 2, this function extracts points included in the range of outline data with a certain width as the lane dividing lines by overlapping outline data and point cloud data relating to lane dividing lines.

(3) Position revision function for point cloud data

This function utilizes outline data on lane dividing lines acquired from plan of completion drawings (hereinafter "Plan of Completion Drawing Lane Dividing Lines") as the standard positions and revises positional shifts throughout the point cloud data by overlapping lane dividing lines extracted from point cloud data (hereinafter "Point Cloud Data Lane Dividing Lines"). First, as shown in Item I inside Fig 3, because Plan of Completion Drawing Lane Dividing Lines have fewer endpoints than Point Cloud Data Lane Dividing Lines, points are inserted into Plan of Completion Drawing Lane Dividing Lines at fixed intervals. Next, as shown in Item II inside Fig 3, Plan of Completion Drawing Lane Dividing Lines and Point Cloud Data Lane Dividing Lines are overlapped using the Iterative Closest Point (ICP) Algorithm[5]. Finally, as shown in Item III inside Fig 3, this function revises positional shifts by acquiring the conversion parameter with the smallest amount of movement and in which the RMS value in comparison to the Plan of Completion Drawing Lane Dividing Lines and the Point Cloud Data Lane Dividing Lines that were aligned using ICP is at or lower than a fixed value. And this function applies these parameter to the point cloud data.

4. Demonstration experiments

These experiments evaluate the utility of the proposed method by applying the proposed method to MMS point cloud data and comparing positional shifts of pre/post-revision.

(1) Experimental conditions

The experiments utilize MMS point cloud data measured in the vicinity of Shukuinchonishi, Sakai Ward, Sakai City, Osaka. As shown in Fig 4, the data

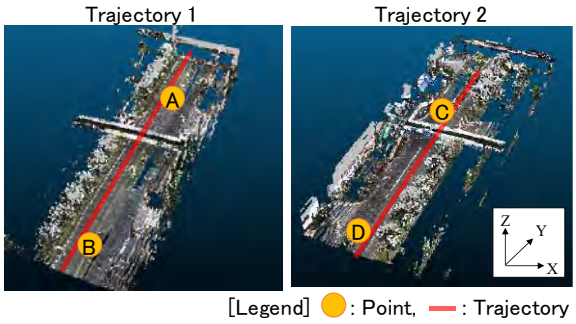

Fig 4: Point cloud data used in experiments

Table 1: Details of point cloud data

Trajectory	Number of points	Point cloud density (point/m²)	Name of construction project
1	365,303	94.1	National Route 26 Shukuin Area Pavement Repair Project
2	448,285	106.9	

Table 2: Experimental results

Trajectory	Point	Evaluation indicators (distance)	Pre-revision (cm)	Post-revision (cm)	Difference
1	A	X	50.0	28.1	-21.9
		Y	53.1	62.5	9.4
		Direct	72.9	68.5	-4.4
	B	X	50.0	14.0	-36.0
		Y	51.5	60.9	9.4
		Direct	71.7	62.4	-9.3
2	C	X	123.4	20.3	-103.1
		Y	67.1	85.9	18.8
		Direct	140.4	88.2	-52.2
	D	X	93.7	12.5	-81.2
		Y	90.6	100.0	9.4
		Direct	130.3	100.7	-29.6

contains point cloud data for two trajectories. Details of point cloud data are shown in Table 1.

(2) Experimental methodology

The experiments apply the proposed method to point cloud data and compare positional shifts of pre/post-revision with plan of completion drawings. As the measurement range of evaluation points differs by trajectory, the four locations shown in Fig 4 were selected. In addition, the degree of positional shifts with lane dividing lines was evaluated using three indicators: the vertical (hereinafter the "X component") and horizontal (hereinafter the "Y component") distances as well as the Euclidean distance (hereinafter "direct distance").

(3) Results and discussions

Experimental results are shown in Table 2. In addition, point cloud data of both pre/post-revision is

shown in Fig 5. Experimental results clarified the following two points.

a. Successful positional revision in X components

Looking at the X component distances in Table 2, it was found that it is possible to revise positional shifts in point cloud data of post-revision by an average of 60.6cm in comparison to the values of pre-revision. In addition, looking at Fig 5, it was visually identifiable that X component distances in point could data of post-revision had shortened in comparison to the values of pre-revision.

b. Unsuccessful positional revision in Y components

Looking at the Y component distances in Table 2, it was found that positional shifts had increase by an average of 11.8cm. This is thought to be due to the fact that RMS values converged at an incorrect horizontal position when the ICP Algorithm was applied because lane dividing lines are long Y-axis lines that extend along traffic lanes.

As a countermeasure to this problem, it is thought possible to deal with this by calculating the optimal parameters for both components through aligning Y components using long features that are vertical in comparison to lane dividing lines such as crosswalks after aligning X components using lane dividing lines.

5. Conclusions and outlook

This research examined a method to eliminate positional shifts occurring between plan of completion drawings and point cloud data by revising point cloud data with the aim of increasing the precision of existing research[3] in extracting road features using plan of completion drawings. Demonstration experiments showed that the proposed method is effective regarding positional shifts in X components. However, the problem was that revisions to Y components were unsuccessful. From now on, we aim to improve the precision of positional revisions by applying the ICP Algorithm while taking into consideration the positions and shapes of features used in conducting alignment. In addition, although this research targeted MMS point cloud data, it is thought that the proposed method could solve similar problems in ground-based laser scanners that measure multiple points and overlap point cloud data. So, we plan to implement additional experiments using ground-based laser scanners.

Acknowledgements

This research was financially supported by research grants from the Research Society for the Technological Fusion and Creation of New Urban Society relating to “Research on Utilization and Application of 3D Data in Road Works” as well as the Kansai University Fund for Domestic and Overseas Research, fiscal year 2018. The authors would like take this opportunity to express gratitude.

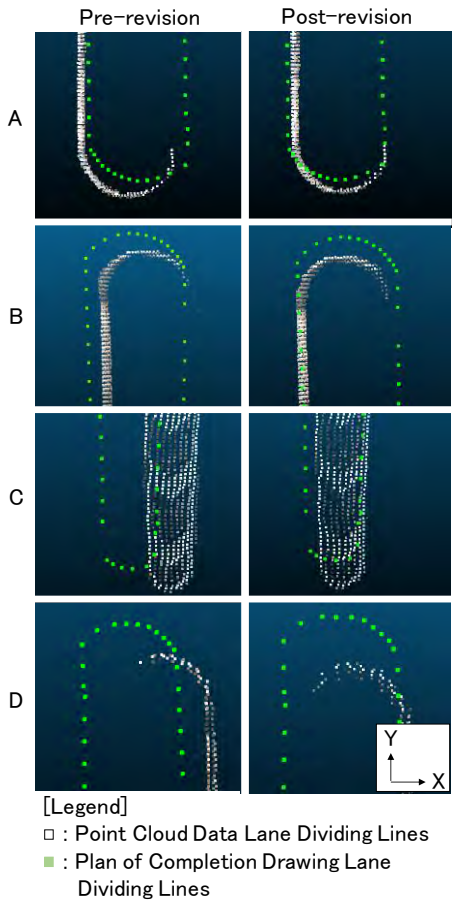

Fig 5: Results of overlapping lane dividing lines and point cloud data of pre/post-revision

References

[1] MLIT, i-Construction, <http://www.mlit.go.jp/tec/i-construction/index.html>, Accessed on Nov. 30, 2019.

[2] MLIT, Manual of Completion Drawing Production for Road Works, <http://www.nilim.go.jp/lab/bcg/siryou/tnn/tnn0493pdf/ks0493.pdf>, Accessed on Nov. 30, 2019.

[3] K. Nakamura, T. Teraguchi, Y. Umehara, S.Tanaka, Research Concerning Extracting Objects From Point Cloud Data Based on Road Completion Drawing, *Proceedings of JSCE F3 (Civil engineering informatics)*, JSCE 73 (2017) I_424-I_432.

[4] W. Zhang, J. Qi, P. Wan, H. Wang, D. Xie, X. Wang, G. Yan, An Easy-to-Use Airborne LiDAR Data Filtering Method Based on Cloth Simulation, *Remote Sensing*, MDPI 8 (2016) 501-509.

[5] R. Szymon, L. Marc, Efficient Variants of the ICP Algorithm, *Proceedings Third International Conference on 3D Digital Imaging and Modeling*, IEEE (2001) 145-152.

Identify the common challenges in the green building practices

Zahra Alaghehmandan[1*], Christiane Papineau[2], Gabriel Lefebvre[3]

[1*] Master of science Department of Project Management Engineering, ETS University, Montreal, Quebec, Canada (corresponding author), Tel: +1(514) 618-1802, Email: zahra.alaghehmandan.1@ens.etsmtl.ca
[2] Professor Department of Project Management Engineering, ETS University, Montreal, Quebec, Canada.
[3] Professor Department of Project Management Engineering, ETS University, Montreal, Quebec, Canada.

Abstract:
Global concerns like climate change and sustainability have raised the need for green construction. It is crucial to assure that green projects as a rising trend in the construction industry are thriving. One of the primary keys to success in a project is identifying issues and challenges and improve the process of construction by preventing identified challenges. This research is sought to investigate the issues and challenges of constructing green buildings (GBs) by conducting a comprehensive literature review. To do that, first, the research finds a list of recent surveys used in the construction industry attempting to identify the challenges of GBs. Then, focus group meetings are utilized to identify the overlapping of the challenges and develop the list of the most common challenges encountered by stakeholders. A data analysis method will be developed to rank the identified challenges. The results suggest the most common challenges inhibiting the adoption of GBs. The results can be used for future research, where developing a management risk tool is the primary problem of the research.
Keywords: Green Building, Issues and challenges, Contractor's guideline, Adoption of GBs

1. Introduction

Green building is a practice of developing structures and processes that are environmentally responsible and resource-efficient throughout a building life cycle from siting to design, construction, operation, maintenance, renovation and deconstruction [1]. Different terms of sustainable building, high-performance building and green building have often used interchangeably within the construction industry [2], [3]. A building is a green building when it assessed by a green ratio system and approved that the building can meet minimum levels of environmental performance set by the green ratio systems. The environmental performances include sustainable sites and transport, water efficiency, energy efficiency, indoor air quality improvement, and using environmentally friendly materials [4]–[7]. Green buildings proved to have economic benefits due to higher return on investment (ROI) regarding the lower rate of energy efficiency, which leads to lower cost of operation at the operation stage [8]–[10]. Empirical studies conclude that the adoption of the green building enables the building to reduce the rate of CO2 emission and other pollutants preventing global warming and climate change, which leads to protection of the ecosystem [11], [12]. Other benefits such as waste reduction through the lifecycle of the building, improvement of the health of occupants are other causes motivating industry to adopt green buildings [13], [14]. Despite these benefits, challenges are inhibiting the stakeholders from reaping the benefits. It is crucial to identify and address these barriers in order to ensure an efficient adoption of green buildings is achieved [15].

However, there are numerous studies attempted to analyze barriers to adoption of green buildings practices [16], most of the studies use questionnaire survey or case study analysis to identify the barriers which increase the subjectivity of the results. This subjectivity prevents to be able to accomplish overall results, which enables the researchers to use the results as input for developing the framework and management tools for owners and contractors involved in the green building practices. As a previous study suggests, there is a gap that needs to be bridged, mainly because the surveys rely on local experts' knowledge affecting the applicability of the outcomes to the other regions and countries [13]. Furthermore, some of the studies are only investigating the barriers from individuals such as owners or contractors and few studies endeavoured to develop barriers encountered by all the stakeholders in a project. The main objective of the study is to compare 15 surveys identified in the literature review to find the most common challenges in the green buildings. As such, this study aims to identify the barriers in the process of green building practices by analyzing various surveys conducted across the world. The results develop a set of ranked barriers based on multiple surveys, which increase the applicability of the results to be utilized for future practices.

2. Research Methodology

Figure 1 represents the proposed methodology conducted by the research. As it is illustrated, the research's approach can be described in the following steps:

1- Finding the Surveys

In order to find the recent surveys, a combination of keywords was searched in three different document categories using the search databases such as

"ASCE," "Science Direct," "Taylor & Francis Online," and "Emerald Insight" to find articles. The search was also limited to articles published after the year 2005. The study uses the combination of keywords "Green buildings," "Sustainable building," "Sustainable construction," "Challenges," "Barriers," "Adoption of green building" have been searched into the mentioned databases. The study seeks to find studies that contain a survey of the industry. The results of this step found 60 surveys.

2- Filtering the surveys

To use the data, all the relevant information should be consistent and be able to identify. As observed among the literature review, two primary elements are impacting the results of a survey in the construction industry [17], [18]: 1) No of respondents the study uses to identify the challenges; 2) The number of years of experience the respondents have. Coupled with the criteria mentioned above, the surveys that develop a ranking system for the challenges are selected for further investigation. Table 1 tabulates the studies selected for the next steps based on which the ranking of challenges is suggested.

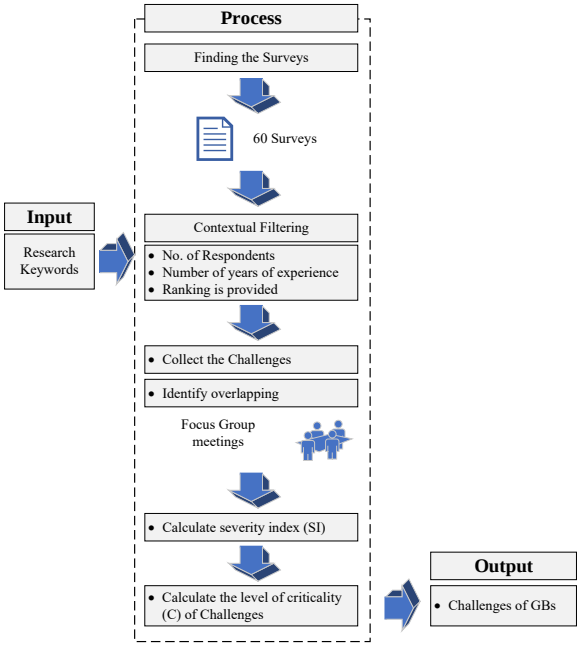

Figure 1: Proposed Methodology

1- Collect the challenges

A total of 232 of the challenges identified in the first step of filtering as is tabulated in Table 1. However, some of the challenges are meaningful and contextually, similar to each other. Therefore, different sets of focus group meetings conducted to identify the overlapping among the challenges.

2- Identify the overlapping among the challenges

The similarities between the challenges are identified during focus group meetings. As Morgan and Krueger (1998) suggest, the recommended number of participants of focus group meetings is 8–12. As such, the research invited eight researchers in the field of green construction. The meetings conclude 34 challenges as the critical challenges in the green construction, as illustrated in Table 2.

3- Calculate the level of importance (L_i)

Each survey uses different numbers of respondents as well as a different number of years of experience, which impacts the results of the research. In order to establish a proper measurement regarding this discrepancy, the following relationship is used:

$$CS_i = N \times \sum_{j=1}^{n} \frac{Avg.of\ years \times N_j}{N \times 100}; \qquad Equation\ 1$$

$$L_i = CS_i \times \frac{N - (RC_i - 1)}{N}; \qquad Equation\ 2$$

Where N is the total number of respondents to the survey, CS_i is the coefficient used to calculate the surveys, as presented in Table 1. The "i" presents the number of the survey, while j presents the number of categories of expertise respondents in the survey (S_i). The CS_i is used to calculate the level of importance (L_i) of each challenge, as illustrated in Equation 2. RC_i represents the ranking of each challenge presented in Table 3.

Table 1: Surveys found to be used in the research

No. of Survey	Source	No. of respondents	Coefficient	No. of challenges ranked
S1	(Yin et al. 2018)	16	1.11	12
S2	(HwangBon-Gang 2018)	52	6.97	34
S3	(Shi et al. 2013)	212	4	15
S4	(Lam et al. 2010)	100	12.5	5
S5	(Darko et al. 2018)	43	1.47	22
S6	(Alsanad 2015)	80	12.6	10
S7	(Albert P.C. Chan et al. 2017)	104	10.5	26
S8	(Djokoto, Dadzie, and Ohemeng-Ababio 2014)	62	3.85	20
S9	(Ayarkwa, Ayirebi-dansoh, and P.Amoah 2010)	37	1.4	9
S10	(Ayarkwa, Ayirebi-dansoh, and P.Amoah 2010)	21	1.3	9
S11	(Ayarkwa, Ayirebi-dansoh, and P.Amoah 2010)	19	1.2	9
S12	(Albert Ping Chuen Chan et al. 2018)	43	5.12	26
S13	(Boateng 2017)	68	4.99	15
S14	(B. G. Hwang and Tan 2012)	31	1.13	10
S15	(Ruparathna and Hewage 2015)	20	3.5	10
	Total	908		232

3. Results and discussions

Table 3 tabulates the ranking associated with each challenge where 'Count' is the number of recurrences of the challenge among the surveys. C1, C 10, C9 and C3 represents the most repeated challenges identified in the green building practices. 'Mean' and 'Max' represents the most criticality and least criticality of each challenge.

Table 2: Rank of the challenges among the surveys

	S1	S2	S3	S4	S5	S6	S7	S8	S9	S10	S11	S12	S13	S14	S15	Count	Mean	Max
C1	1	16	12		11	6	8	1	6	5	7	14	3	5	10	14	1	16
C2	1		5	5	6		18	10				23				7	1	23
C3	2	4			5	8	2	3	3	1	2	1	6	1		12	1	8
C4	3				3		3		7	9	6	13		6		8	3	13
C5	3	7	7	3	17										6	6	3	17
C6	4	18	14				10		8	8	9	24	9			9	4	24
C7	4	3	13													3	3	13
C8	5	5		2				6				25		2		6	2	25
C9	5	23			15	5	1	14	1	4	3	17		7	1	12	1	23
C10	6	25	6	1	2		4	18	4	3	1	6	12	8		13	1	25
C11	6	31	2													3	2	31
C12	7	19	8		9	2	6	5	5	6	8	2				11	2	19
C13		8						12								2	8	12
C14		1						13					14	9	5	5	1	14
C15		2											14			2	2	14
C16		6														1	6	6
C17		14							9	7	5					4	5	14
C18		15					24					26			5	4	5	26
C19		13	3		21		15	17	2	2	4	4	11			10	2	21
C20			1				12									2	1	12
C21			4	4												2	4	4
C22			9			7						18				3	7	18
C23		12			1	4	7					19	14			6	1	19
C24					7	1	4	4				11	8		8	7	1	11
C25		33			8	3	13	8				9	2	10	2	9	2	33
C26					10		14					5	7	4	3	6	3	14
C27					12		8					3	1			4	1	12
C28		27			16		20	2				6			2	6	2	27
C29					19	9	5	7				15	15			6	5	19
C30					20	4	9	11	2	2	4	6	12		2	10	2	20
C31						10		9	3	1		1	4	3	10	8	1	10
C32								16				8	10		7	4	7	16
C33								19					13		7	3	7	19
C34												22			4	2	4	22

Table 3 shows the results of the research indicating the challenges and the Li and rank associated with each challenge. The identified challenges can be categorized into six primary groups;

Market trend: As illustrated in Table 3, the market trend toward green practices is the most critical challenge against the adoption of green buildings. 'Market trend' refers to the challenges and barriers raised by the attitude that existed amongst the construction industry against practicing green construction. As Williams and Dair (2007) report the most commonly cited barriers to achieving sustainability is that sustainability measures are not being considered by stakeholders which are primarily due to the perceptions of the stakeholders from the risks and uncertainties associated with the green construction projects (C1, C29) [21], [22]. These risks should be further investigated during the feasibility analysis when the incorporation of sustainable principles into the project should be conducted, as Li-yin Shen et al. (2010) suggest.

Lack of knowledge about green practices (C10, C23) is another significant challenge to the adoption of green construction. This challenge may cause more difficulty during the procurement stage when the contractors are not willing to bid due to a lack of knowledge. Similarly, a construction enterprise may reject the proposed green material by the contractor in the procurement stage when they are unfamiliar with the particular product. Also, lack of knowledge about the performance and cost of the materials (C29), equipment and techniques may generate another constraint [18]. Li-yin Shen et al. (2010) asserted that contractors and suppliers should be engaged during the early stage of construction projects due to their knowledge of the environmental issues associated with construction activities, building materials and plants.

Financial-related challenges: The cost-effectiveness of the project is one of the most important considerations for making decisions in the construction industry [25]. The results show that 'high cost of green materials and technologies' (C3) is one of the critical challenges inhibiting owners from adopting green construction, which often is the top reason for the difference in the cost premiums between green and conventional construction projects. This cost can affect both the cost and productivity of the project when the design and construction of the project become more complicated due to the objective of the project [26], [27]. Also, green techniques such as high-performance insulation protection usually cost more in the production stage, which causes the additional cost for the project [3], [28], [29]. The high cost of research and development for green practices is another challenge contributing to the difference in the cost premium due to more effort required for testing and approving green products. Another cause of the higher cost of green practices could be the lack of required expertise in the green practices, which leads to an unnecessary increase in the cost of the project as the key players of the team are not able to utilize green practices efficiently [28]. Besides, due to lack of familiarity with green standards, the project often ends up with reworks and change orders, which lead the project to an increase in the cost of construction (C22) [30].

Technology-related challenges: As it is illustrated in Table 3, 'lack of green building regulations and codes' and 'lack of available experts and personnel' are two most significant challenges related to technology inhibiting implementation of green practices. Green materials and equipment are essential for achieving green construction [31]. Reduction of performance of the project in green construction may caused by uncertainitites of green materials and equipment. The limited certification bodies and materials available in the green construction market (C19, C25) can also contribute to the challenges of green practices, which limits the adoption of such green materials and technologies to be used. Using unclear context and requirements in the green specifications (C5) can cause misunderstanding between the contractor and the owner of the project which impacts both cost and time of the project. However, in a survey conducted by Shi et al. (2013), clients did not rank this challenge as the most critical ones, whereas both contractors and construction engineers ranked this barrier as the critical factor constraining participation in the green projects.

Time-related challenges: Time is a prime project objective for all stakeholders in most countries [27]. Delay is on of the critical factors of causing over cost in the project [32]. As it discussed in the above, lack of familiarity of the stakeholders in the construction industry with the green concepts may cause rework, which in turn impacts the schedule of the project.

Government-related challenges: While 'Lack of government incentives' is not a sign in developed countries where the governments extensively support the built industry [34], it is still the most critical challenge inhibiting the adoption of green construction

in the developing countries such as Ghana [36] which therefore suggests that the developing countries need to focus on issues that promote the reduction of taxes and levies on sustainable products (i.e. recyclable materials, etc.).

Construction-related challenges: Post-construction liability and construction insurance are two critical aspects of sustainable construction [38]. Practices such as involving professionals after the completion of the building, on the one hand, create a feedback loop for the project [39], on the other hand, introduces challenges to the contract management. As a result, the responsibility for a warranty for green construction is increased. Hence, the contractual and liability puzzles of green construction need to be resolved.

Table 3: Challenges per category

No.	Category	Challenge	Importance Level	Rank	Total
C1	Market trend	Lack of Interest and market demand	34.34	4	263.2
C4		Lack of management support and time management	16.42	16	
C6		Conflicts in benefits with competitors (i.e. competitors often uses materials which are less environmentally friendly and at a lower cost)	15.37	19	
C9		Resistance to change from conventional to green practices	32.25	6	
C8		Lack of communication among the stakeholders	21.19	11	
C10		Lack of knowledge on sustainable construction	38.08	2	
C17		Objective of the building project	5.56	31	
C22		Misunderstanding of green technologies	8.66	23	
C23		Limited experience with the use of non-traditional procurement methods (difficulty with the specifications and performances required)	25.30	9	
C24		Lack of awareness about the benefits	33.06	5	
C28		Lack of demonstration projects/ lack of technical procedures/ frameworks	15.87	18	
C29		Risks and uncertainties involved in adopting new technologies	17.05	14	
C2	Financial Risks	Complex building costs and regulations to evaluate the cost benefits	14.22	20	101.10
C3		Higher cost than budget/ higher cost of materials	38.94	1	
C20		Additional cost required due to longer time of construction	10.05	22	
C27		Lack of financing schemes (e.g., bank loans)	18.12	13	
C31		Higher investment cost/ long duration of ROI	16.32	17	
C34		Separation of capital and operational costs	3.43	33	
C5	Technology-related risks	Immature green technology specifications (lack of comprehending)	18.71	12	139.0
C7		Uncertainty in the performance of green materials and equipment	8.19	25	
C19		Availability of green material and equipment and suppliers	23.11	10	
C25		Lack of green building polices and regulations/ rating systems and labeling	31.09	7	
C26		Lack of local institutes for research and development	17.03	15	
C30		Lack of green building technological training for project staff	30.0	8	
C32		Lack of database and information	8.10	26	
C33		Lack of technology of GBs	2.78	34	
C11	Time- related risks	Incremental time caused by green construction due to approvals	5.20	32	24.3
C14		Longer time required during the pre-construction process	11.50	21	
C18		Meeting the schedule/ cause delay	7.60	27	
C12	Government	Insufficient incentives from government	36.33	3	36.33
C13	Construction Process-related	Planning of different construction sequence	7.26	29	28.84
C15		Difficulty in the selection of subcontractors in providing green construction service	7.43	28	
C16		More alteration and variation with the design during the construction process	5.94	30	
C21		Additional responsibilities for maintenance stage	8.2	24	

4. Conclusions and outlook

While the adoption of green construction practices is increasing, some challenges might impact the effectiveness of the benefits gained from green concepts. This research provides the most critical challenges faced by stakeholders in the construction industry. The perception of the industry from the challenges in green construction can be different based on the stakeholders. Some of the challenges may be more critical from the owner's perspective, while those challenges may not be a constraint from the contractor's perspective. As such, the research encompassed 15 surveys among the industry stakeholders to make sure a broader view is captured. The outcome of the result suggests 34 critical challenges based on six categories of market trend, technical-related challenges, financial-related challenges, government-related challenges and construction process-related challenges. The ranking and level of importance (L_i) of the challenges establish a better understanding of the challenges which can input the future research where developing a framework for the management of the risks is the main problem of the research. The results revealed that while the "Higher cost of green construction" is the most critical challenge amongst the surveys, the financial-related challenges is not the most critical group of the challenges encountered by stakeholders in the green construction industry. Furthermore, this challenge may be caused by different reasons which interrelate with other challenges, as discussed above.

The significant challenges in the industry are derived by a lack of knowledge about green practices and the benefits associated with this practice. To address these challenges, Governments should take initiatives and provide regulations, frameworks and financial incentives to encourage the industry implementing green concepts [42], [43]; however, some of the governments provide significant effort supporting green concepts, some developing countries are still lacking support from the government which impact the trend market in those regions. Therefore, developing guidelines to assist stakeholders in understanding the importance and value of utilizing green construction may be the first step in eliminating the negative perception of industry against green construction. The value of sustainability should be more investigated and presented in different aspects of economic, environmental and social rather than focusing more on economic benefits. Chu, Anguelovski, and Roberts (2017) and [41] similarly adopt such strategic messaging and actions as a means of realizing substantial benefits on urban environmental issues in situations of high environmental complexity.

Moreover, by improving the level of skills and experience with green construction among the team players of the project, both of project performance in terms of cost and time can be achieved, which is also agreed by [44] and [45]. The improvement of the cost performance of the project is due to the reduction of rework and change orders as the understanding of the team from the main objectives of the project is enhanced. Ong (2013) [46] suggests that governments can fund some educational programs such as green courses as one step to improve the skills of the industry with green construction.

Developing lessons learned from the current practice of green construction is a practical approach in order to find the opportunities and challenges associated with practicing green concepts in the construction industry. The lessons learned can provide feedbacks as input for management methods in green construction. It also pinpoints the challenges that should be improved in future projects. The identified opportunities should be documented in order to ensure that they repeat in future practices.

However, the research categorizes all the challenges into six groups; each group has interrelationships with each other as some of the challenges arise in the project; it might impact on other challenges as well.

The research endeavoured to use a large size of data to identify the challenges associated with practicing green construction. It is suggested that future research uses the results of the research to develop frameworks and management tools for future projects. Developing best practices from the current process of green construction by investigating the identified challenges in the research can be useful for improving the knowledge of the construction industry.

References

[1] EPA, "Sustainable Design and Green Building Toolkit," 2013.

[2] J. Zuo and Z. Y. Zhao, "Green building research-current status and future agenda: A review," *Renew. Sustain. Energy Rev.*, vol. 30, no. 71371072, pp. 271–281, 2014.

[3] Kibert C.J., *Sustenance: Green Building Design and Delivery*. Hoboken, NJ: Wiley, 2012.

[4] C. Say and A. Wood, "Sustainable rating systems around the world," *CTBUH J.*, vol. Volume 2, 2008.

[5] M. Braune, "Status of Green Building in South Africa," in *In NBI seminar, COP17, Durban.*, 2011.

[6] E. Mpakati-Gama, S. C. Wamuziri, and B. Sloan, "Green Building Challenges: Evaluating The Operation of Adopted Building Assessment Tools - Case Study," in *Procs 28th Annual ARCOM Conference (pp. 1257–1267). Edinburgh, UK.*

[7] P. C. Ozolins, H. Rodriguez-camilloni, L. S. Grossman, J. R. Jones, and J. S. Tlou, "Assessing Sustainability in Developing Country Contexts : The Applicability of Green Building Rating Systems to Building Design and Construction in Madagascar," 2010.

[8] R. Ries, M. M. Bilec, N. M. Gokhan, and K. L. Needy, *The economic benefits of green buildings: A comprehensive case study*, vol. 51, no. 3. 2006.

[9] Y. Liu, X. Guo, and F. Hu, "Cost-benefit analysis on green building energy efficiency technology application : A case in China," *Energy Build.*, vol. 82, pp. 37–46, 2014.

[10] Q. K. Qian, E. H. W. Chan, and A. G. Khalid, "Challenges in delivering green building projects: Unearthing the transaction costs (TCs)," *Sustain.*, vol. 7, no. 4, pp. 3615–3636, 2015.

[11] Y. H. Ahn, A. R. Pearce, Y. Wang, and G. Wang, "Drivers and barriers of sustainable design and construction : The perception of green building experience," *Int. J. Sustain. Build. Technol. Urban Dev.*, vol. 4, no. 1, pp. 35–45, 2013.

[12] UNEP, "Global Status Report," 2016.

[13] A. Darko and A. P. C. Chan, "Critical analysis of green building research trend in construction journals," *Habitat Int.*, vol. 57, pp. 53–63, 2016.

[14] A. Darko, A. P. C. Chan, Y. Yang, M. Shan, B. J. He, and Z. Gou, "Influences of barriers, drivers, and promotion strategies on green building technologies adoption in developing countries: The Ghanaian case," *J. Clean. Prod.*, vol. 200, pp. 687–703, 2018.

[15] C. Mao, Q. Shen, W. Pan, and K. Ye, "Major Barriers to Off-Site Construction: The Developer's Perspective in China," *J. Manag. Eng.*, vol. 31, no. 3, p. 04014043, 2013.

[16] L. Shen, Z. Zhang and Z. Long, "Significant barriers to green procurement in real estate development," *Resour. Conserv. Recycl.*, vol. 116, pp. 160–168, 2017.

[17] E. Brogan, W. McConnell, and C. M. Clevenger, "Emerging Patterns in Construction Defect Litigation: Survey of Construction Cases," *J. Leg. Aff. Disput. Resolut. Eng. Constr.*, vol. 10, no. 4, 2018.

[18] Q. Shi, J. Zuo, R. Huang, J. Huang, and S. Pullen, "Identifying the critical factors for green construction - An empirical study in China," *Habitat Int.*, vol. 40, pp. 1–8, 2013.

[19] D. Morgan and R. Krueger, *The focus group kit*. Thousand Oaks, CA: SAGE., 1998.

[20] K. Williams and C. Dair, "What is stopping sustainable building in England? Barriers experienced by stakeholders in delivering sustainable developments," *Sustain. Dev.*, vol. 15, no. 3, pp. 135–147, 2007.

[21] A. D. Rafindadi, M. Mikić, I. Kovačić, and Z. Cekić, "Global perception of sustainable construction project risks," *Procedia-Social Behav. Sci.*, vol. 119, pp. 456–465, 2014.

[22] B. Hwang, M. Shan, and N. N. B. Supa'at, "Green commercial building projects in Singapore: Critical risk factors and mitigation measures," *Sustain. cities Soc.*, vol. 30, pp. 237–247, 2017.

[23] L. Shen, V. W. Y. Tam, L. Tam, and Y. Ji, "Project feasibility study: the key to successful implementation of sustainable and socially responsible construction management practice," *J. Clean. Prod.*, vol. 18, no. 3, pp. 254–259, 2010.

[24] M. Bilec, R. Ries, and H. S. Matthews, "Sustainable development and green design—Who is leading the green initiative?," *J. Prof. Issues Eng. Educ. Pract.*, vol. 133, no. 4, pp. 265–269, 2007.

[25] H. Meryman and R. Silman, "Sustainable engineering–using specifications to make it happen," *Struct. Eng. Int.*, vol. 14, no. 3, pp. 216–219, 2004.

[26] P. T. I. Lam, E. H. W. Chan, C. S. Poon, C. K. Chau, and K. P. Chun, "Factors affecting the implementation of green specifications in construction," *J. Environ. Manage.*, vol. 91, no. 3, pp. 654–661, 2010.

[27] G. Ofori and H. L. Kien, "Translating Singapore architects' environmental awareness into decision making," *Build. Res. Inf.*, vol. 32, no. 1, pp. 27–37, 2004.

[28] N. Malin, “The cost of green materials,” *Build. Res. Inf.*, vol. 28, no. 5–6, pp. 408–412, 2000.
[29] J. Y. Liu, S. P. Low, and X. He, “Green practices in the Chinese building industry: drivers and impediments,” *J. Technol. Manag. China*, 2012.
[30] H. Bon-Gang, “Cost Premium, Performance and Improvement of Green Construction Projects,” *Perform. Improv. Green Constr. Proj.*, pp. 103–118, 2018.
[31] Q. Shi, J. Zuo, and G. Zillante, “Exploring the management of sustainable construction at the programme level: a Chinese case study,” *Constr. Manag. Econ.*, vol. 30, no. 6, pp. 425–440, 2012.
[32] D. Arditi and T. Pattanakitchamroon, “Selecting a delay analysis method in resolving construction claims,” *Int. J. Proj. Manag.*, vol. 24, no. 2, pp. 145–155, 2006.
[33] A. J. Hoffman and R. Henn, “Overcoming the social and psychological barriers to green building,” *Organ. Environ.*, vol. 21, no. 4, pp. 390–419, 2008.
[34] B. G. Hwang and J. S. Tan, “Green building project management: Obstacles and solutions for sustainable development,” *Sustain. Dev.*, vol. 20, no. 5, pp. 335–349, 2012.
[35] B.-G. Hwang and J. S. Tan, “Sustainable Project Management for Green Construction,” *Challenges, Impact Solut.*, no. June, p. 9, 2012.
[36] B. E. Boateng, “Factors affecting the implementation of sustainable construction in Ghana: The architect’s perspective,” *6th Int. Conf. Infrastruct. Dev. Africa*, no. April, pp. 377–386, 2017.
[37] B.-L. Oo and B. T. H. Lim, “A review of Singapore contractors’ attitudes to environmental sustainability,” *Archit. Sci. Rev.*, vol. 54, no. 4, pp. 335–343, 2011.
[38] C. Thormark, “A low energy building in a life cycle—its embodied energy, energy need for operation and recycling potential,” *Build. Environ.*, vol. 37, no. 4, pp. 429–435, 2002.
[39] A. Leaman, F. Stevenson, and B. Bordass, “Building evaluation: practice and principles,” *Build. Res. Inf.*, vol. 38, no. 5, pp. 564–577, 2010.
[40] E. Chu, I. Anguelovski, and D. Roberts, “Climate adaptation as strategic urbanism: assessing opportunities and uncertainties for equity and inclusive development in cities,” *Cities*, vol. 60, pp. 378–387, 2017.
[41] W.-Y. Shih and L. Mabon, “Land-use planning as a tool for balancing the scientific and the social in biodiversity and ecosystem services mainstreaming? The case of Durban, South Africa,” *J. Environ. Plan. Manag.*, vol. 61, no. 13, pp. 2338–2357, 2018.
[42] M. Bourgeois, K. Breaux, M. Chiasson, and S. Mauldin, “Tax Incentives of Going Green.,” *CPA J.*, vol. 80, no. 11, pp. 19–24, 2010.
[43] J. Popovec, “Incentives assuage investor fears over green premiums,” *Natl. Real Estate*, 2006.
[44] Y. Jiang, “Understanding the cost of green buildings: Evidence from Singapore,” *Master’s thesis, Natl. Univ. Singapore, Singapore*, 2010.
[45] S. D. Johnson, “The economic case for ‘High performance buildings,’” *Corp. Environ. Strateg.*, vol. 7, no. 4, pp. 350–361, 2000.
[46] Y. H. Ong, “Green building retrofit projects: Critical success factors, barriers and solutions,” *Undergraduate, Natl. Univ. Singapore, Singapore*, 2013.

Research on Improvement of Road Maintenance Using Point Cloud Data with Feature Information

Y. Tsukada[a*], K. Nakamura[b], R. Imai[c], S. Tanaka[d], Y. Umehara[e]

[a] Faculty of Business Administration, Setsunan University, 17-8 Ikeda-nakamachi, Neyagawa-shi, Osaka, Japan
[b] Faculty of Information Technology and Social Sciences, Osaka University of Economics, 2-2-8 Osumi, Higashiyodogawa-ku, Osaka-shi, Osaka, Japan
[c] Faculty of Engineering and Design, Hosei University, 2-33 Ichigayatamachi, Shinjuku-ku, Tokyo, Japan
[d] Faculty of Informatics, Kansai University, 2-1-1 Ryozenji-cho, Takatsuki-shi, Osaka, Japan
[e] Organization for Research and Development of Innovative Science and Technology, Kansai University, 3-3-35 Yamate-cho, Suita-shi, Osaka, Japan
* Yoshinori Tsukada, +81-7-2839-9247, yoshinori.tsukada@kjo.setsunan.ac.jp

Abstract:
In Japan, the Ministry of Land, Infrastructure, Transport and Tourism is promoting i-Construction, which improves construction-site productivity using Information and Communication Technology. As a result, opportunities to use point cloud data acquired from measuring instruments, such as airborne lasers, terrestrial laser scanners, mobile mapping systems, and unmanned aerial vehicles, have increased in recent years. However, point cloud data is only a huge set of points with three-dimensional positions, and each point does not have feature information. Therefore, it is difficult to search for specific features from point cloud data and confirm them quickly. In this research, we propose the specification of attribute management for road management using point cloud data and develop a point cloud browser based on this specification to improve the efficiency of road maintenance.

Keywords:
i-Construction, road, point cloud data, specification of attribute management, point cloud browser

1. Introduction

In Japan, the Ministry of Land, Infrastructure, Transport and Tourism (MLIT) is promoting i-Construction[1], which is an effort to improve productivity at construction sites using ICT (Information and Communication Technology). Along with this, in recent years, point cloud data acquired from measuring instruments, such as airborne lasers, TLS (terrestrial laser scanners), MMS (mobile mapping systems), and UAV (unmanned aerial vehicles), have been attracting attention. Point cloud data are useful as a means to understand the shape of actual conditions precisely, and are expected to be utilized in many ways, including maintenance support for infrastructure. In recent years, in particular, efforts have been made to promote the utilization of these data by releasing point cloud data to the public. Major examples of this include the “Shizuoka Point Cloud DB” (PCDB)[2] by Shizuoka Prefecture and "My City Construction"[3] by the Institute of Industrial Science of The University of Tokyo, CTI Engineering International Co., Ltd., and Association for Promotion of Infrastructure Geospatial Information Distribution. The PCDB releases point cloud data collected in public projects to the public. My City Construction focuses on the fact that it is difficult for the traditional electronic delivery system to utilize assets and allows point cloud data and image data to be delivered online.

Prompted by i-Construction in this way, the opportunities for utilizing point cloud data are surely increasing. However, since point cloud data are only a huge set of points that indicate spatial locations and do not store information about the features represented by the points or the relationships with other points, it is hard to use them in a way that meets the designed usage. Therefore, it is essential to define the data structure for utilizing the data effectively by associating “computer-readable data” including two- or three-dimensional CAD data and TS as-built management data with “point cloud data”, and to standardize the environments for utilizing them.

In this research, aiming at advanced maintenance using the point cloud data of road spaces, we formulated a specification for attribute management using point cloud data, and developed a point cloud browser for road administrators, which has functions in conformity with the specification.

2. Specification of Point Cloud Attribute Data for Road

We discussed how to manage the attributes of point cloud data in the “Subcommittee for Specification of Point Cloud Attribute Data for Road” under the Infrastructure Information Standardization Committee of JACIC[4], and released the outcome as “Specification of Point Cloud Attribute Data for Road (draft)” to the public[5]. This specification classifies point cloud data measured by airborne lasers, TLS, MMS, UAV, and so on, and adds what kind of features each of them represent as attribute information. Fig 1 shows an illustration of given

attributes of point cloud data. As shown in the figure, attribute information, such as lighting, road sign, and the road surface, are given to the point cloud data.

Attribute information is defined by a file of XML format, which is a different file from that of the point cloud data. Fig 2 shows the data structure of attribute information. The point cloud meta data in the figure preserves information such as the measurement date of the point cloud data, measuring instruments, and measuring procedures. The area data file is composed of multiple area data sets indicating the locations of features and the area meta data that manage detailed information about the area data. The following effects can be expected by managing the attribute information based on this specification.

- The data size does not swell because the measurement data (point cloud data) is not processed.
- Data exchange can be made easily because attribute information (the point cloud meta data and the area data file) is defined by separate files.
- It is easy to reuse the defined attribute information (the point cloud meta data and the area data file).
- The area data can be associated with external files such as registries and drawings.
- Since the area data file plays a role of a filter for extracting planimetric features from point cloud data, it is easy to retrieve and extract the necessary part of the point cloud data according to the usage.

Fig 3 shows an example of providing the area data to the point cloud data to the public at My City Construction[3]. As the figure shows, the area data defines the range of a feature that surrounds the point cloud data, such as a roadway, planting, or a bridge. This makes it possible to acquire the point cloud data of a particular feature automatically by computer processing.

3. Development of a point cloud browser for advanced road management

(1) Problems toward the utilization of point cloud data in road management

In this research, we conducted interviews with road administrators to find out their needs for utilizing point cloud data in road management. Most of their opinions concentrated on the problems below. In this research, we develop a point cloud browser that has solved these problems.

- Since massive point cloud data cannot be stored on a personal computer (PC), it is difficult to acquire the point cloud data of the target place.
- An environment for confirming point cloud data easily has not been achieved yet.
- It is impossible to grasp the change of state or time-series variations for every feature, such as a slope face or road surface.

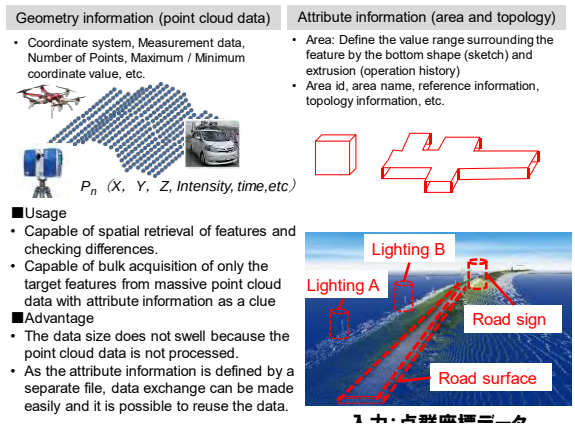

Fig 1: Overview of the specifications of point cloud attr ibute data for road

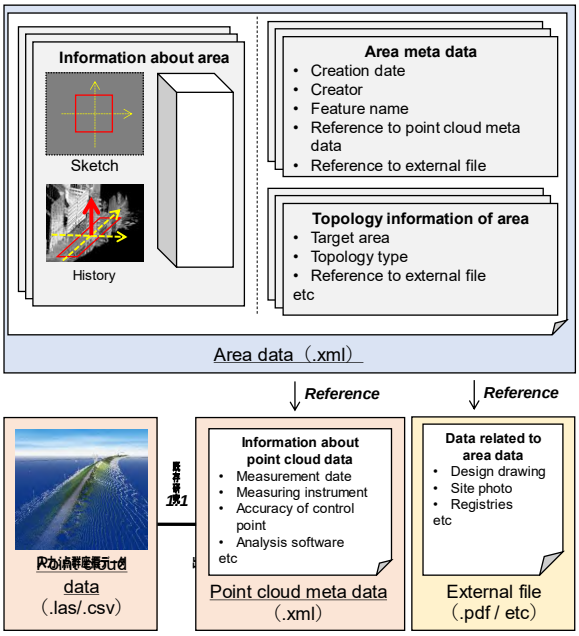

Fig 2: Data structure of the attribute information

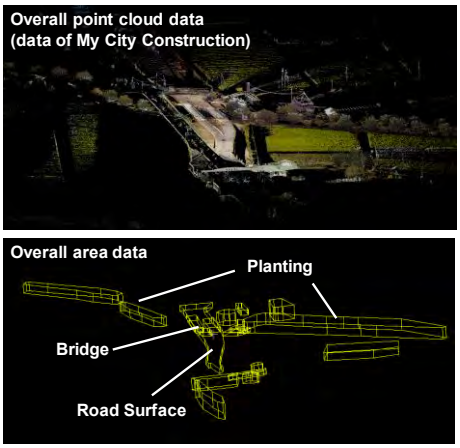

Fig 3: Definition example of the area data
(source of the point cloud data: My City Construction)

- When receiving complaints or inquiries from local residents, it is necessary to visit the sites, otherwise there is no means of understanding the situations of these sites.

(2) Building an environment for utilizing point cloud data

To solve the problems mentioned above, we developed a point cloud browser[6] that has the functions of point cloud data visualization, point cloud data management by road feature, and plug-ins using SDK. The details of these functions are shown below.

a. Function of visualizing point cloud data

This function has two modes: online and local (Fig 4). The point cloud browser can be used to confirm the overview of the point cloud data open to public on the Internet in the online mode. The point cloud data are divided into files of units of 1:250-level map border for the national base map for every measuring operation. Therefore, the terrain around the site can be confirmed immediately by specifying only the concerned map border to confirm (Fig 5). Then, after downloading the point cloud data to the user environment, detection of a change of state or data analysis are performed as needed. This makes it possible to confirm the overview without downloading and sharing information according to the user needs. Consequently, the distribution cost for sharing large-capacity point cloud data can be reduced significantly.

b. Function of managing point cloud data by road feature

This function is capable of managing point cloud data in units of road feature not by analyzing massive point cloud data as they are but by given attribute information that indicates the location and area of the road feature (hereinafter referred to as “area data”) to the point cloud data. To be specific, it is capable of retrieving and extracting particular features from point cloud data[7][8], detecting the difference between the sets of point cloud data from two different periods of time, and associating point cloud data with images, videos, and registries, etc. (Fig 6). The extraction speed of the road feature from the point cloud data depends on the total number of points and the shape of the area data. Using a notebook computer (CPU: Intel Core i7/GPU: GeForce GT560M/ memory: 16GB), the time taken to extract road features from the point cloud data containing 6,860,310 points acquired by MMS is approximately 0.31 seconds for the road sign (4,939 points), approximately 0.48 seconds for the lighting (910 points), and approximately 0.88 seconds for the sidewalk (78,630 points).

These functions lead to the promotion of utilizing point cloud data and increased the efficiency of information retrieval by associating point cloud data with existing materials. Consequently, it is considered that they can contribute to higher efficiency in daily management work, cost reduction, and an increase in quality.

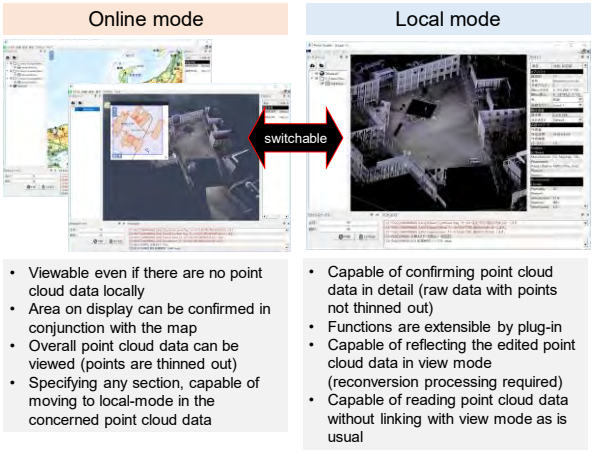

Fig 4: Point cloud browser for road administrators

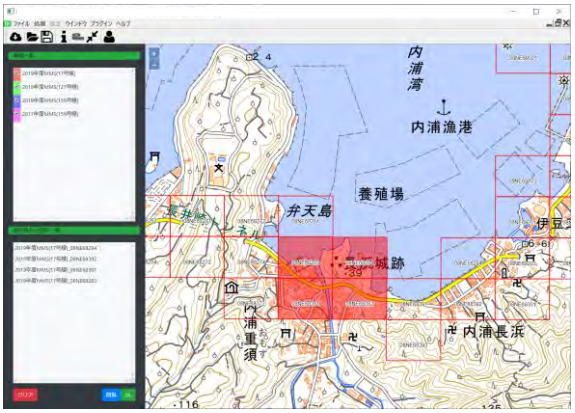

Fig 5: Redivision of the point cloud data based on the map border of the national base map

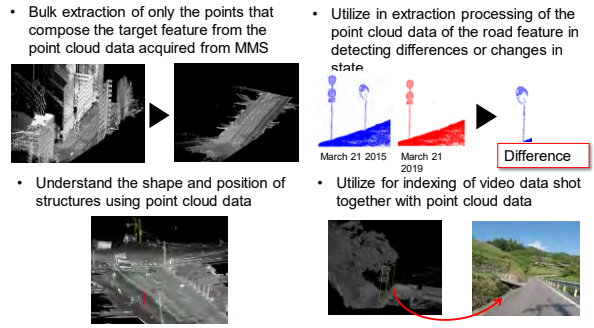

Fig 6: Utilization of point cloud data

c. Function of plug-ins using SDK

Functions of this browser related to processing point clouds are freely extensible by using SDK. For example, Fig 7 shows the plug-in for detecting differences between the point cloud data sets from two different periods of time and Fig 8 shows the plug-in for identifying features of point cloud data by machine learning.

The plug-in for detecting differences (Fig 7) automatically detects the presence or absence of vegetation as well as places where there may be a difference in levels and exfoliation by generating normal vectors in grid units from the point cloud data sets of the slope face for 2 different periods of time and comparing the normal vectors. The plug-in for identifying features (Fig 8) automatically generates area data by identifying road sign, lighting, tree, traffic lights and so on from point cloud data by machine learning[9] [10].

4. Conclusions

In this research, we developed a point cloud browser with functions for solving problems discovered through interviews with road administrators. The preparation of area data is indispensable for the realization of the proposed measures. We are also committed to research on feature recognition from point cloud data using deep learning or plan of completion drawing, and have achieved some results for the automatic generation of area data.
In the future, we are planning to release the research results to the public as well as make further improvements, aiming at the realization of more practical application, while at the same time taking in opinions from MLIT, local governments, and working sites.

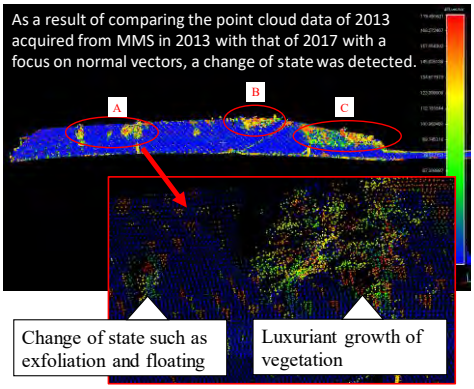

Fig 7: Plug-in for detecting differences

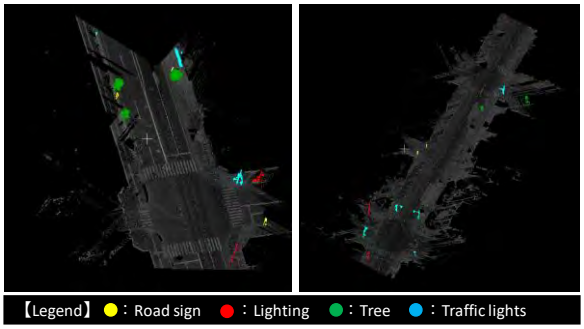

Fig 8: Plug-in for identifying features

Acknowledgements

Part of this research was financially supported by the Kansai University Fund for Domestic and Overseas Research, fiscal year 2018. The authors would like take this opportunity to express gratitude.

References

[1] MLIT, i-Construction, <http://www.mlit.go.jp/tec/i-construction/index.html>, Accessed on Nov. 30, 2019.
[2] Shizuoka Prefecture, Shizuoka Point Cloud DB, <https://pointcloud.pref.shizuoka.jp/>, Accessed on Nov. 30, 2019.
[3] Institute of Industrial Science of The University of Tokyo, CTI Engineering International Co., Ltd., and Association for Promotion of Infrastructure Geospatial Information Distribution, My City Construction, <https://mycityconstruction.jp/>, Accessed on Nov. 30, 2019.
[4] Infrastructure Information Standardization Committee of JACIC, InSubcommittee for Specification of Point Cloud Attribute Data for Road,<http://www.jacic.or.jp/hyojun/2017shouiinnkai-02.html>, Accessed on Nov. 30, 2019.
[5] Maintenance Information Technology Div, Research Center for Land and Construction Management of NLIM, Specification of Point Cloud Attribute Data for Road (draft) ver. 1.0, <http://www.nilim.go.jp/lab/qbg/standards/standards.html#zokuseikanri>, Accessed on Nov. 30, 2019.
[6] K. Nakamura, Y. Tsukada, R. Imai, S. Tanaka, Y. Umehara, and T. Hiwatashi, Development of Point Cloud Browser for Road Administrators, *33th Japan Road Conference*, Japan Road Association (2019).
[7] K. Nakamura, Y. Tsukada, S. Tanaka, Y. Umehara, and M. Nakahata, "Increasing High Accuracy Method of Extracting Road Features from Point Cloud Data Using Plan of Completion Drawing", *44th JSCE F3 (Civil engineering informatics) Symposium*, JSCE (2019) 253-256.
[8] K. Nakamura, T. Teraguchi, Y. Umehara, and S. Tanaka, Research Concerning Extracting Object From Point Cloud Data Based on Road Completion Drawing, *Proceedings of JSCE F3 (Civil engineering informatics)*, JSCE 73 (2017) I_424-I_432.
[9] Y. Umehara, Y. Tsukada, K. Nakamura, S. Tanaka, Y. Hirano, S. Otsuki, and Y. Kawamura, Basic Research for Recognizing Road Features Using Point Cloud Data by Machine Learning, *35th Fuzzy System Symposium*, Japan Society for Fuzzy Theory and Intelligent Informatics (2019) 493-494.
[10] Y. Tsukada, K. Nakamura, S. Tanaka, Y. Umehara, Y. Hirano, S. Otsuki, and Y. Kawamura, Basic Research for Recognizing Road Features Using Point Cloud Data by Deep Learning, *35th Fuzzy System Symposium*, Japan Society for Fuzzy Theory and Intelligent Informatics (2019) 491-492.

Research for Detection and Positional Analysis of People in Construction Fields using Multiple Cameras from a Single Viewpoint

W. Jiang[a,*], Y. Yamamoto[b], S. Tanaka[c], K. Nakamura[d], C. Tanaka[e]

[a] Organization for Research and Development of Innovative Science and Technology, Kansai University, 3-3-35 Yamate-cho, Suita-shi, Osaka, Japan
[b] Faculty of Information Science and Technology, Osaka Institute of Technology, 1-79-1 Kitayama, Hirakata-shi, Osaka, Japan
[c] Faculty of Informatics, Kansai University, 2-1-1 Ryozenji-cho, Takatsuki-shi, Osaka, Japan
[d] Faculty of Information Technology and Social Sciences, Osaka University of Economics, 2-2-8 Osumi, Higashiyodogawa-ku, Osaka-shi, Osaka, Japan
[e] Graduate School of Informatics, Kansai University, 2-1-1 Ryozenji-cho, Takatsuki-shi, Osaka, Japan
* Wenyuan Jiang, +81-07-2690-2151, b.kyo@kansai-u.ac.jp

Abstract:
With the development of information technology in recent years, several studies have been conducted on the use of information and communication technology (ICT) for construction field safety management, especially pertaining to the automatic management of workers. To realize it, techniques for detecting workers in the entire field of view by video and acquiring their positions and movements are a necessity. However, the problem with gathering many workers is that the accuracy of identifying each worker decreases because of occlusion. To solve this problem, deep learning methods that can detect occluded people have attracted attention. However, as the size of the workers in the video feed is small, it becomes difficult to identify them via deep learning. Therefore, in this research, we will use multiple cameras from a single viewpoint to detect workers with high accuracy, specify their positions by photographing occlusion points with a high zoom scale, and then apply deep learning with OpenPose.

Keywords:
People Identification, Positional Analysis, Construction Field, Occlusion, OpenPose.

1. Introduction

In recent years, onsite safety in the construction industry has become an urgent issue owing to aging, shortage of skilled workers, and other issues. To combat this, the Ministry of Land, Infrastructure, Transport and Tourism has been promoting digitized construction by actively introducing the use of information and communication technology (ICT) [1]. Studies [2] on the use of ICT in construction site safety management, especially with regard to the self-management of workers, are being conducted. As a base for these studies, there is a need for a technique that identifies workers from onsite images and acquires their positions and movement paths. This can be actualized by having the workers wear GNSS sensors and obtaining their positions. However, the accuracy of GNSS sensors varies greatly depending on the weather and environment, and there is a possibility of the sensors making errors in the range of several meters or more, especially while measuring heights. Therefore, onsite image analysis shall be the main technique for obtaining the positions of workers. However, in the case where many workers work together, images may get occluded, decreasing accuracy. In order to solve this problem, deep learning, which can identify each person even if the images are occluded, has attracted our attention. However, for a construction site that is captured with a wider photographic range, it is difficult to identify each worker even by deep learning because the size of each worker on the image is small. Thus, this research proposes an analytical model that overlaps the identification results of multiple images with different zoom scales, thereby aiming to improve the accuracy of identifying workers at construction sites.

2. Proposed Model

This research proposes an analytical model that overlaps the identification results of multiple images from different zoom scales. As shown in Fig 1, the image to be analyzed is captured from a construction site with multiple cameras installed on the same spot with different zoom scales.

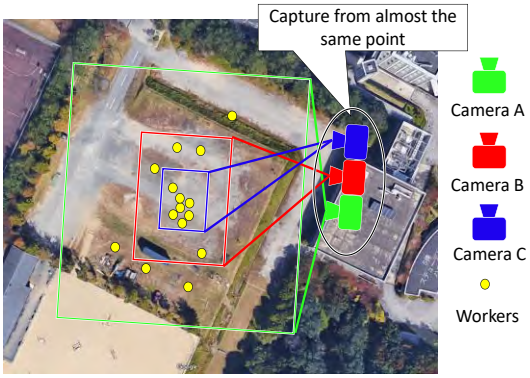

Fig 1: Capturing method

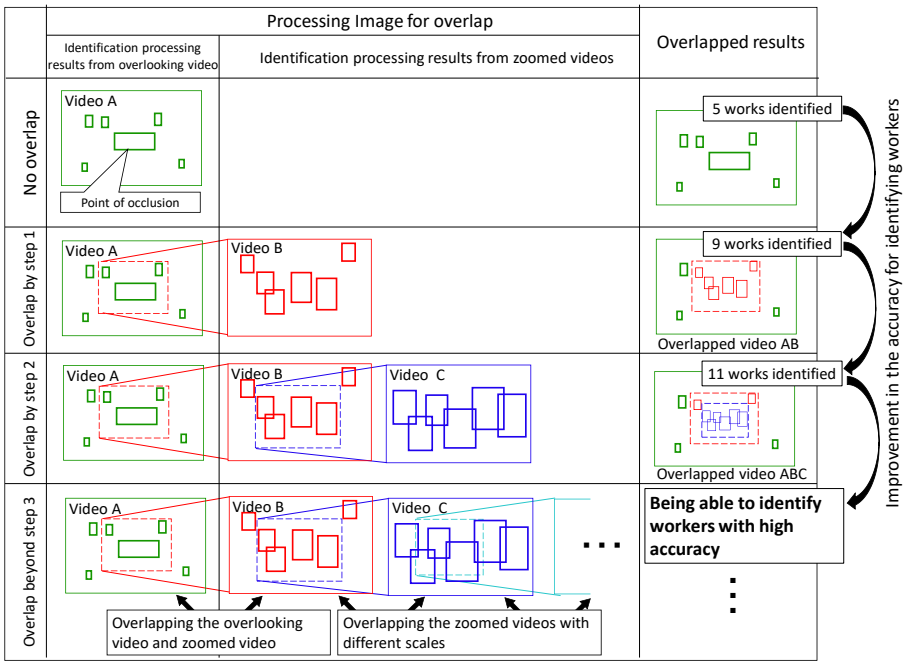

Fig 2: Proposed model

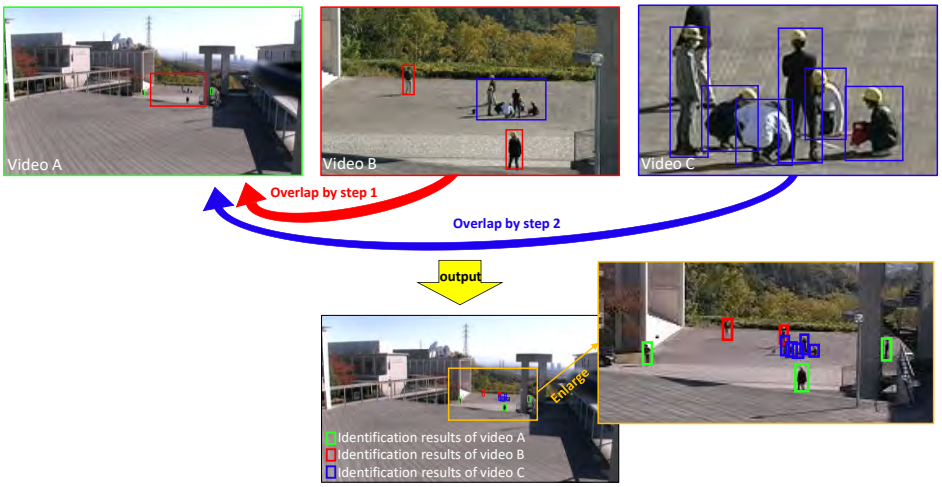

Fig 3: Image of output

As shown in Fig 2, the proposed model aims to improve the accuracy of identifying workers by analyzing each video step by step and overlapping the results . As shown in Fig 3, it is possible to gradually increase the identification count by taking overlooking video A (which captures the entire area) as the base, overlapping medium zoom scale video B over video A (creating overlapped video AB), followed by overlapping high zoom scale video C over that (creating overlapped video ABC). This research will explain in detail the first step of overlap (the overlooking video and zoomed video), which adds the medium zoom scale video over the overlooking video. Hereafter, an explanation of the second step of overlapping (the medium and high zoom scale videos), which mainly adds another high zoom scale video over the medium zoom scale video obtained from the overlapped results of the first step, will be discussed. Anything past the third step is carried out by repeating the second steps of overlapping.

3. Proposed System

In order to actualize the model that is described in section 2, a system is proposed as shown in Fig 4.
The system is composed of a worker identification function (overlooking video), worker identification function (zoomed video), video position determination function (overlooking video) and video position determination function (zoomed video).

The worker identification function (overlooking video) obtains the positions of the workers by identifying each individual worker in each frame of the

overlooking video. As it is difficult to apply deep learning here owing to the low resolution of the workers in the image, a background subtraction method is used to help identify the workers with a certain level of accuracy.

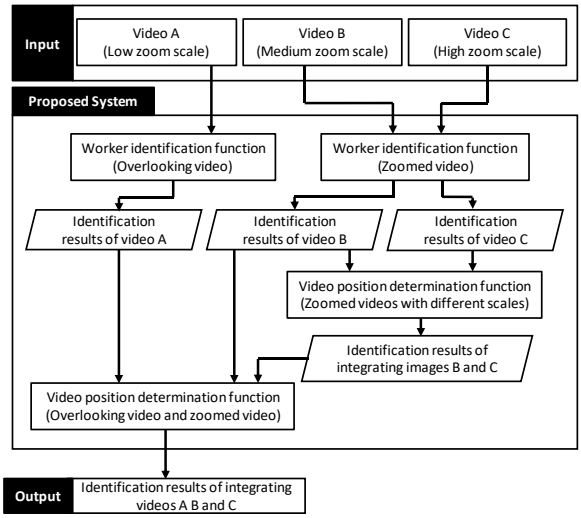

Fig 4: Proposed system

The worker identification function (zoomed video) obtains the positions of the workers by identifying all videos that are being occluded. It identifies the workers with high accuracy from the zoomed video of each frame. As the resolution is high on the workers in the zoomed video, it is possible to identify each worker with high accuracy by applying deep learning, even in the case of occlusion. Therefore, this function uses OpenPose [3].

The video position determination function (overlooking video and zoomed video) specifies the positions of the occluded workers by embedding the identification results obtained by OpenPose from video B into the identification results obtained by the background subtraction method from video A. All the workers have the same positional relationship in both the videos, when taken from a single viewpoint, with different zoom scales. As shown in Fig 5, this function extracts two persons from video A corresponding to the two persons on the left and right of video B and overlaps them by changing the position and scale. The position of other workers also gets overlapped at the same time. Thus, this function enables the embedding of images by using this overlapping method.

The video position determination function (zoomed videos with different scales) embeds the identification results by OpenPose from video C into the identification results by OpenPose from video B. In order to achieve this, we use the feature of workers having the same positional relationship in both the videos, similar to the video position determination function (overlooking video).

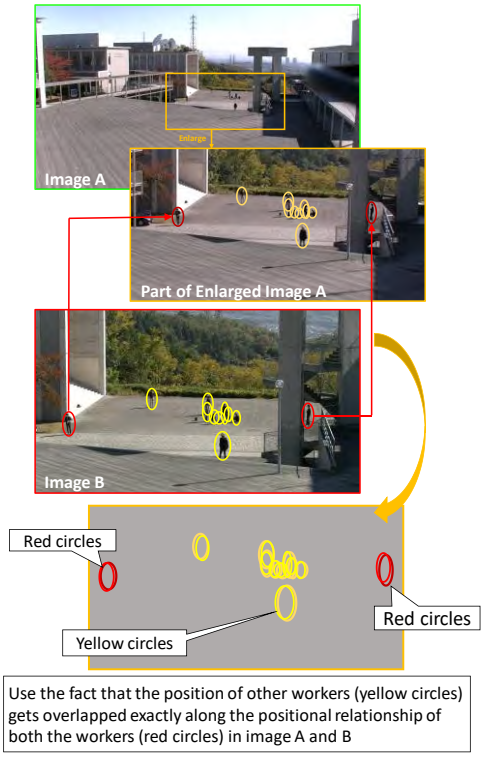

Fig 5: Overlapping method

However, as there are only a few isolated workers in the zoomed video, it is difficult to overlap using isolated workers. Therefore, this function overlaps videos by focusing on the fact that the identification results of OpenPose are individual workers. More specifically, the optimal positions and scales are calculated in such a way that all of the workers identified in the identification results by OpenPose in videos B and C will overlap. Thus, workers in video C obtain their positions in video B. Finally, the workers in video C obtain their positions in video A by overlapping the identification results overlapped on video B on video A, using the video position determination function (overlooking video).

4. Experiment

In this experiment, we use an open space corresponding to a construction site and capture the activity of multiple persons from a single viewpoint using multiple cameras. Next, we identify the workers from the captured videos and overlap the videos using this system. Finally, we confirm the usefulness of the proposed system and the model by extracting 10 frames and tabulate the success rate of the overlap and the identification rate of the workers at that time. The experiment was conducted with 11 people, with a maximum of 6 people during occlusion.
The experimental results are shown in Tables 1 and 2. Table 1 shows a high success rate of the overlapped

videos and confirms the usefulness of the proposed system.

Table 1: Success rate of overlap

	Average success rate
Overlap of overlooking video and zoomed video	90%
Overlap of zoomed video and zoomed video	90%

Table 2 shows that the average identification count in image A, overlapped image AB and overlapped image ABC were 5.1, 8.7, and 10.1 respectively, indicating that there was a gradual improvement in the identification rates of people. Therefore, the proposed model was found to be useful. In addition, the maximum and minimum identification rate after overlapping all three videos was 100% (Fig 6) and 81.8% respectively. In addition, even with the maximum number of occluded persons, it was still possible to identify all people. This accuracy is enough for tracking workers in real construction sites. Therefore, it is thought that this can be applied in the future for safety management, based on the movement history of onsite workers.

5. Summary

In this research, we proposed a model and a system for improving the accuracy of collecting the positional data of workers and identifying them, for ensuring safety of workers in construction sites. The results of the demonstration experiment confirmed the usefulness of the proposed model and system. The proposed method is highly versatile as it is not limited to 3 videos but can also be applied to 4 or more videos. In the future, we shall attempt to use it for the safety management of workers by tracking them using their positional data obtained from this system. Although the learning model of OpenPose used in this research can identify workers with high accuracy, there may be a decrease in this accuracy due to specific working postures. In the future, we will re-learn those specific postures and will aim to improve the accuracy by working on these identification errors.

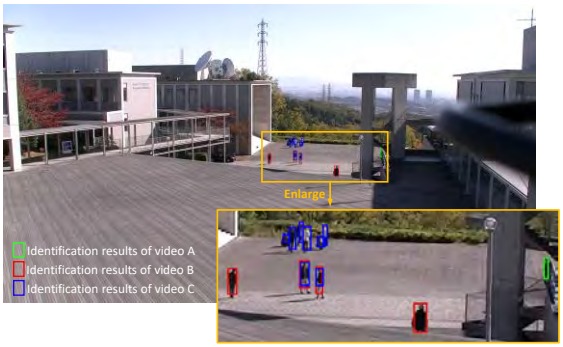

Fig 6: Sample output

Acknowledgements

This research was financially supported by the Kansai University Fund for Domestic and Overseas Research, fiscal year 2018.

References

[1] Ministry of Land, Infrastructure, Transport and Tourism, Regarding the overall use of ICT (ICT earthworks), <http://www.ktr.mlit.go.jp/ktr_content/content/000648822.pdf>, Accessed on Nov. 30, 2019.

[2] R. Imai, D. Kamiya, H. Inoue, S. Tanaka, K. Sakamoto, J. Fujii, E. Kikuchi, M. Ito, Research on accuracy verification of person identification when wearing bibs using deep learning，*Proceedings of the Symposium on Civil Engineering Informatics*, Japan Society of Civil Engineers 44 (2019) 165–168.

[3] Z. Cao, T. Simon, S. Wei, Y. Sheikh, Realtime multi-person 2d human pose estimation using part affinity fields, *Conference on Computer Vision and Pattern Recognition*, IEEE (2017) 1302–1310.

Tabel 2 Identification rate of people

	Number of people	Number of occluded people	Number of people identified (Image A)	Number of people identified (Overlapped Image AB)	Number of people identified (Overlapped Image ABC)	Identification rate
Frame 1	-	-	-	-	-	Overlap failed
Frame 2	11	6	4	8	11	100.0%
Frame 3	11	6	3	7	10	90.9%
Frame 4	11	5	4	7	9	81.8%
Frame 5	11	5	6	9	10	90.9%
Frame 6	11	5	6	11	11	100.0%
Frame 7	11	4	6	9	9	81.8%
Frame 8	11	6	5	8	11	100.0%
Frame 9	11	4	6	9	10	90.9%
Frame 10	11	6	6	10	10	90.9%
Average	11	5.2	5.1	8.7	10.1	91.9%

Fundamental Research concerning Personal Identification for Safety Management of Construction Sites Using Deep Learning

R. Imai[a], D. Kamiya[b], H. Inoue[c*], S. Tanaka[d]

[a] Faculty of Engineering and Design, Hosei University, 2-33 Ichigayatamachi, Shinjuku-ku, Tokyo, Japan
[b] Faculty of Engineering, University of the Ryukyus, 1 Senbaru, Nishihara-cho, Nakagami-gun, Okinawa, Japan
[c] Faculty of Information Technology and Social Sciences, Osaka University of Economics, 2-2-8 Osumi, Higashiyodogawa-ku, Osaka, Japan
[d] Faculty of Informatics, Kansai University, 2-1-1 Ryozenji-cho, Takatsuki-shi, Osaka, Japan
* Haruka Inoue, +81-6-6328-2431, h.inoue@osaka-ue.ac.jp

Abstract:
In order to eliminate labor accidents at construction sites, it is important to implement effective safety management measures. For example, there is a measure that warns a person when they enter a dangerous place or come into contact with construction machines, using cameras. In existing research, technology has been developed for identifying people using deep learning for surveillance cameras in towns. However, at construction sites it is necessary to identify workers with similar clothes and construction machines. Thus, there is a possibility that the existing technology could not be applied. Therefore, in this research, we tried to identify a person wearing a helmet using deep learning for the purpose of safety management in the construction fields.

Keywords:
Construction Sites, Workers, Person Identification, Camera, Deep Learning.

1. Introduction

There is always a potential risk at construction sites, where numerous workers and construction machinery coexist, operating based on their respective roles. The number of industrial accidents has been decreasing in recent years. However, as some accidents are still occurring, including falls and trips, and traffic accidents, as well as the flying and falling of materials [1], it is necessary to investigate more effective safety management and implement it thoroughly. As an on-site safety precaution, efforts are being made for creating hazard maps that report dangerous spots and make them known to every worker. Although this is effective in deterring accidents, the effect is rather small compared with warning from the outside. In addition, although there is a method of detecting obstacles by installing an ultrasonic sensor at the rear end of construction machines [3], its measuring range is limited. One way of solving these problems is to give warnings in real-time by monitoring the on-site conditions that vary hour by hour using video cameras to identify workers who are in danger of entering a dangerous place or touching construction machinery. In the existing study [4], the technology of identifying and tracking the same person across multiple cameras has been developed using deep learning, to apply to the monitor cameras in towns and commercial facilities. However, on construction sites, this technology may not be applied as it is, because the clothes of workers are similar to each other and it is necessary to identify individual construction machines.

In recent years, a form of artificial intelligence, deep learning, has been attracting attention. It is expected to achieve a more accurate result than conventional machine learning in areas such as image recognition and image classification. Thus, in this research, we verify the applicability of personal identification using deep learning as fundamental research aiming at the safety management of construction sites. In this paper, Chapter 2 proposes a method for identifying a person, and Chapter 3 summarizes the conditions of construction sites. Chapter 4 makes a trial of personal identification on a construction site.

2. Organizing the measurement environment of construction sites and conditions of workers

(1) Contents of organization

In personal identification using deep learning, images to use for learning greatly influence the identification accuracy. Especially on construction sites, since the measurement environment and workers' conditions vary from time to time, it is necessary to create images by taking these conditions into consideration. Thus, in this research, we organize the conditions that may influence the personal identification accuracy on construction sites. Table 1 shows a list of conditions. The details are described below.

(2) Measurement environment

The measurement environment can be divided into 4 kinds: time period, weather, place, and camera position. "Time period" can be classified into the daytime and nighttime periods. In the daytime, there are bright places illuminated by the sun and dark places hidden by buildings. In the nighttime, persons shot by cameras look different depending on the presence or absence of lighting devices.

"Weather" can be classified into sunny, cloudy, and rainy. When it is sunny, the entire image turns whitish due to sunshine. When it is raining, clothes get wet or puddles appear at the site, causing changes in the appearance of the person shot by the camera. "Place" can be classified into indoors and outdoors. Shots are influenced by the outdoor sunshine and weather or interior illumination.

For "Camera position", horizontal viewpoints and bird's eye viewpoints can be considered as the position of installing an on-site camera. For a horizontal viewpoint, a camera is installed at a height of about 1-2m, so that human faces are projected. This is considered to improve the identification accuracy of a person. However, it may be impossible to install a camera where it obstructs the progress of construction machines, etc. On the other hand, for a bird's-eye viewpoint, a camera must be installed on the upper floor of a building or on a pole to shoot from a height taller than 2m. Though human faces are not shot, this has an advantage of being able to be installed at various places.

(3) Conditions of workers

The conditions of workers can be classified into clothes, wearing articles on the head, wearing articles on the face, action, and carrying something. For "Clothes", it is usual for workers to wear working clothes on construction sites. Therefore, it is considered that all workers' clothes are similar to each other, though there are some differences in the color or patterns.

For "Wearing articles on the head", everyone wears a helmet in principle. For "Wearing articles on the face", it is considered that they may wear masks or protective glasses. It is necessary to note that it depends on the day or time period whether or not they are worn. "Action" can be roughly divided into 4 types: to walk, rest, squat down, and lie down. Differences in these actions make the conditions or parts of a person shot by the camera vary. "Carrying something" can be classified into empty hands and holding articles. On the construction site, it is necessary to consider scenes of holding articles under various conditions, since there are a great many opportunities for workers to carry materials.

3. Proposal for a method of personal identification using deep learning

(1) Overview of proposed method

In this research, we propose a method for identifying a person by classification of images using deep learning to investigate the influence of whether or not there is a background, among the conditions organized in Chapter 2. Fig 1 shows the process flow of the proposed method. In the flow of the learning part in the left part of Fig 1, first, the background difference and image extension are processed for the input data in the preprocessing part. Next, using the

Table 1: Organizing measurement environment of construction sites and conditions of workers

Classification	Condition	Pattern
Measurement environment	Time period	daytime, nighttime
	Weather	sunny, cloudy, rainy
	Place	outdoor, indoor
	Background	with/without
	Camera position	horizontal viewpoint, bird's-eye viewpoint
Condition of the worker	Clothes	working clothes
	Wearing articles on the head	helmet
	Wearing articles on the face	none, mask, sunglasses
	Action	walk, rest, squat down, and lie down
	Carrying something	empty hands, holding articles

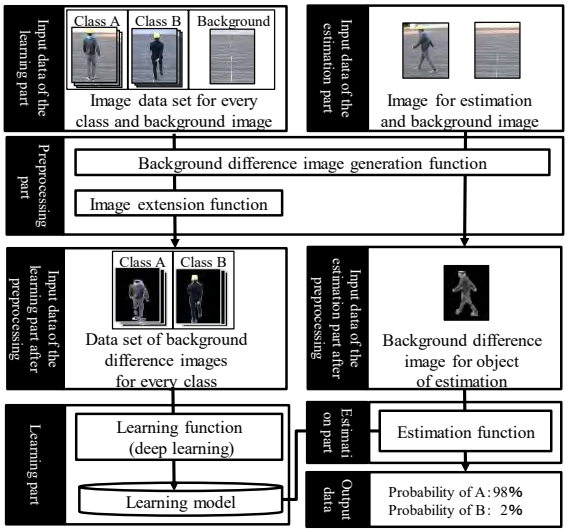

Fig 1: Process flow of proposed method

data, deep learning is performed in the learning part to generate a learning model. On the other hand, in the flow of the estimation part in the right part of Fig 1, background difference images are generated in the preprocessing part. Next, classes are estimated in the estimation part using the data and the learning model to output the probability of each class. Then the class with the highest probability is determined as the object person.

(2) Preprocessing part

The preprocessing part comprises the background difference image generation function and the image extension function. Here, taking into consideration that workers at the construction site move in free directions, it treats a moving image of a person walking while turning around for 10 seconds shot at the position where the worker's whole body is included within the shooting range. For the input data

of the learning part, frame images at 0.1-second intervals are extracted from the moving images to create 100 images of a person. Fig 2 shows an example of images of a person who is walking while turning around. The image size is adjusted to the size of the whole body of the person to be included.

The background difference image generation function learns only the characteristics of a person. In particular, using an image with a person and a background image without a person, luminance values are compared per pixel. From the compared difference, pixels with values equal to or higher than the threshold are extracted to generate an image with only a person. Fig 3 shows an example of images with and without a background.

The image extension function suppresses overlearning. Specifically, it helps extend the number of images by expansion, reduction, rotation, parallel translation, and shearing. Fig 4 shows an example of extended images. In the case of ones without a background, the image of only a person generated by the background difference image generation function is treated as an object. Here, although it is possible to increase the number of images by changing the conversion parameters to any number, it takes learning time. Therefore, in this research, image conversion shall be performed once for an image. From the above, the input data for the learning part after preprocessing shall be 100 original images and 100 converted images generated with the image extension function per person: 200 times the number of persons in total.

(3) Learning function

This function helps learning using the Convolutional Neural Network of deep learning. Its model structure uses VGG-16 comprising 16 layers in total, which include 13 convolutional layers that have gained high evaluation at ImageNet large scale visual recognition challenge (ILSVRC), a competition for classification using deep learning, and 3 fully-jointed layers. Input images are set to channel 3 in 224 x 224 pixel-size so that learning can be performed with specifications of general personal computers (PC). For other configuration elements, RelU and LeakyReLU are used for the activation function of the convolutional layers and fully-jointed layers, respectively. However, Softmax is used for the last fully-jointed layer. The stochastic gradient descent is used for weight updating, and cross entropy for loss function.

(4) Estimation function

This function helps with calculating the probability of each class for estimated images using a learning model generated with the learning function. Since dispersion occurs in the estimation result, estimation is performed 10 times per image and the average value is calculated.

Fig 2: Example of images of a person who is walking while turning around

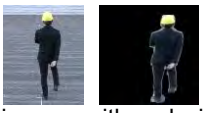

Fig 3: Example of images with and without background

Fig 4: Example of extended images

4. Experiment of personal identification using the proposed method

In this chapter, the accuracy of personal identification using the deep learning proposed in Chapter 3 is evaluated. Then its applicability to construction sites is verified.

(1) Research items

In this experiment, the influence caused by the difference in the presence and absence of a background is investigated. Nine people wearing helmets served as the test subjects (Table 2), considering its application to construction sites in the future. "With background" are images that show persons and a background. On the other hand, "Without background" are images that show only persons generated with the background difference image generation function. In this experiment, the threshold was determined as 30. However, for the part where the background was left partially, it was removed manually.

(2) Experimental environment

The experiment site was set as the outdoors within the grounds of Kansai University, where a video camera was installed horizontally at a height of 1.15m. As a measuring method, a test subject stood at a position of 5m horizontally from the camera, walked while turning around for 10 seconds, and then walked freely around the vicinity 5m from the camera.

(3) Learning method

At the time of learning, 200 images for each of the 9 test subjects with a rotating walk are created according to the method of creating input data for the learning part described in Chapter 3. Here, the number of epochs, which indicates the number of times of learning, is set at 500 times, taking practicability into account. In this environment, the process was completed in about 17.5 hours. It was verified that the correct answer rate, which is an evaluation index in learning, converged to about

100% for both image groups with and without a background.

(4) Estimated images and evaluation method

For Images to be estimated, the walking conditions in the four directions of right, left, backward, and forward during free walking are extracted. Four images are set per person. For the evaluation method, precision, recall, and F-measure are used. The precision refers to the rate of correct answers to the estimated number, the recall to the rate of correct answers to the total number, and F-measure to the value of harmonic average of the relevance and recall.

(5) Evaluation results

Table 3 shows the evaluation results of "With background" and "Without background". The total number in the table indicates the number of data for the object classes, the estimated number indicates the number of estimated results of object classes by the system, and the number of correct answers indicates the number of cases that the classes in the estimated results agreed to the total number. Focusing on F-measure of the total, that of "With background" is 0.86, while that of "Without background" is 0.97, showing that the identification accuracy of "Without background" was higher.

It can be considered that it was possible to learn the characteristics of persons, such as clothes and physical constitution, by removing the background, even when they were all wearing helmets. However, the clothes of persons C and F with their backs turned were similar, and the concerned image allowed erroneous identification. At the construction site, it is considered that the workers' clothes look similar because they put on working clothes. Therefore, it is necessary to improve accuracy by utilizing images of individual parts or a time series, for example. The above results suggest that even when the place to shoot a video is changed, it is possible to identify a specific person by taking pictures of him or her from different directions in advance.

Table 2: Test subjects

Person	With background / Without background	Person	With background / Without background
A	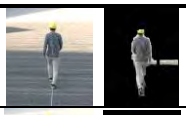	F	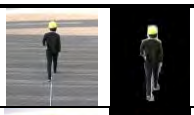
B		G	
C		H	
D		I	
E			

Table 3: Experimental results

Person	With background			Without background		
	Estimation	Correct answer	F-measure	Estimation	Correct answer	F-measure
A	4	4	1.00	4	4	1.00
B	2	2	0.67	4	4	1.00
C	6	4	0.80	3	3	0.86
D	4	4	1.00	4	4	1.00
E	4	4	1.00	4	4	1.00
F	4	4	1.00	5	4	0.89
G	7	4	0.73	4	4	1.00
H	1	1	0.40	4	4	1.00
I	4	4	1.00	4	4	1.00
Total	36	31	0.86	36	35	0.97

5. Conclusion

In this research, the applicability of personal identification using deep learning was verified as fundamental research aiming at the safety management of construction sites. As a result, it was verified that even when the image contains a background, it allows personal identification with an accuracy of about 86%. In the future, we will aim at improvement in the identification accuracy to realize its application to actual sites.

Acknowledgements

The authors would like to thank the member companies joining the Center for Socio-Spatial Information Science (CSSIS), Kansai University, who supported this research greatly. Part of this research was financially supported by the Kansai University Fund for Domestic and Overseas Research, fiscal year 2018.

References

[1] Ministry of Health, Labour and Welfare, Industrial Accidents Statistics, <http://anzeninfo.mhlw.go.jp/user/anzen/tok/anst00.htm>, Accessed on Nov. 30, 2019.

[2] Council for promotion of construction site safety precautions of the Kinki District, Casebook for precautions to prevent accidents in construction etc. (2015).

[3] Takenaka Engineering, Back censor for vehicle-type construction machines SSW-5M2, < https://www.takex-eng.co.jp/ja/products/saleend.php>, Accessed on Nov. 24, 2019.

[4] C. Su, F. Yang, S. Zhang, Q. Tian, L. S. Davis, W. Gao, Multi-Task Learning with Low Rank Attribute Embedding for Multi-Camera Person Re-Identification, *Transactions on Pattern Analysis and Machine Intelligence*, IEEE 40 (2018) 1167–1181.

Survey Research on Mobile Recognition Technologies using Deep Learning for Application to Traffic Census

R. Imai[a], D. Kamiya[b], Y. Yamamoto[c,*], S. Tanaka[d], M. Nakahara[e], K. Nakahata[e]

[a] Faculty of Engineering and Design, Hosei University, 2-33 Ichigayatamachi, Shinjuku-ku, Tokyo, Japan
[b] Faculty of Engineering, University of the Ryukyus, 1 Senbaru, Nishihara-cho, Nakagami-gun, Okinawa, Japan
[c] Faculty of Information Science and Technology, Osaka Institute of Technology, 1-79-1 Kitayama, Hirakata-shi, Osaka, Japan
[d] Faculty of Informatics, Kansai University, 2-1-1 Ryozenji-cho, Takatsuki-shi, Osaka, Japan
[e] Graduate School of Informatics, Kansai University, 2-1-1 Ryozenji-cho, Takatsuki-shi, Osaka, Japan
*Yuhei Yamamoto, +81-72-866-5373, yuhei.yamamoto@oit.ac.jp

Abstract:
With recent developments in ICT, mechanical surveys have been introduced as a method for efficiently conducting traffic censuses in the road sector. However, despite expectations to reduce human costs and human errors, the cost has not been drastically reduced compared to manual surveys. In addition, the traffic volume of motorcycles and bicycles cannot be investigated. Existing technologies that automatically recognize vehicles using deep learning have been proposed. These technologies use images from easily installable cameras. However, the possibility of application to the real environment has not yet been fully examined and has not reached the practical stage. Therefore, in this research, in order to investigate the applicability of existing technologies to the real environment, these technologies are applied to camera images taken of actual traffic conditions. And we will clarify the matters to be considered in order to develop the technology for automatic traffic censuses.

Keywords:
Traffic Census, Camera Image, Deep Learning, Object Detection

1. Introduction

In recent years, with the advancement of ICT (Information and Communication Technology), methods for efficiently collecting big data and utilizing them have been investigated in every field. Focusing on the field of road traffic, survey methods for traffic volume, including that of motorcycles and bicycles, have been studied. Conventional traffic censuses are accompanied by a huge amount of human cost and human error because they need surveyors to be placed on the spot to perform manual counting. Accordingly, mechanical surveys have been introduced using measuring equipment, such as traffic counters, in the expectation of reducing labor costs and human error. However, using these traffic counters requires traffic control at the time of installation and removal, as well as the personal expenses and operation expenses of traffic guides. Therefore, a drastic reduction in operation costs has not been achieved yet. Moreover, since the traffic counter is not capable of measuring motorcycles and bicycles, it is necessary to develop the technology for surveying traffic volume including these traffic modes.

Existing studies have proposed technologies to recognize vehicles, motorcycles, and bicycles automatically from images shot by commercial video cameras or monitoring cameras that are easy to install. Since these technologies are capable of recognizing vehicles broken down by traffic mode by employing deep learning, it may be possible to automatically investigate the number of vehicles that have passed particular roads by traffic mode in a simple and easy way. It can be expected that this will facilitate a reduction in human cost and error as well as a significant reduction in the operation costs for installment and removal. Although there are technologies expected to make traffic censuses efficient, which are attracting attention in the concerned field, no existing study can be found which has proven applicability to a real environment.

The purpose of this research was to study the applicability of existing technologies to real environments and clarify matters to be considered in developing the surveying technology of traffic volume irrespective of the traffic mode. In Section 2, we present the technology for recognizing the locations of objects such as motorcycles, bicycles, or automobiles. In Section 3, application experiments with a video of actual traffic situations are outlined. In Section 4, matters to consider in developing the technology for automatic surveys of traffic volume irrespective of traffic mode are described. Section 5 presents a summary of this study as well as future prospects.

2. Research on existing object recognition technologies

Using the existing technology for recognizing the location of objects from a camera using deep learning, methods are proposed using Object Detention[1][2], Semantic Segmentation[3], and Instance Segmentation[4].

The method using Object Detection[1][2] recognizes the location of an object in a rectangular form by obtaining multiple candidate areas of an object from the image and selecting only the area with which the estimated accuracy between the overlapping areas is the largest. Fig 1 shows an example of recognizing the results. This method is capable of recognizing vehicles by type by allowing it to learn trucks and buses as different labels. However, when recognizing an object with an image of a small size, a sufficient number of characteristics cannot be extracted, consequently causing the problem of a difficulty to recognize it.

The method using Semantic Segmentation[3] judges which type of object the pixel composes for every pixel in the image, and recognizes the contour line of the object and the area it surrounds. This method is capable of recognizing the location of an object more accurately than Object Detection. However, as Fig 2 shows, when objects of the same type overlap each other, it is impossible to judge the location of the boundary between the different objects, thus causing the problem that the number of objects cannot be recognized.

The method using Instance Segmentation[4] judges which object the pixel composes for every pixel in the image. As Fig 3 shows, even when objects of the same type are overlapping each other, it is possible to recognize them as different objects. Although this method allows for recognizing an object more accurately than the methods using Object Detection or Semantic Segmentation, it requires an enormous amount of calculation in comparison to Object Detection and Segmentation, causing the problem of a longer processing time.

Fig 1: Result example by Object Detection

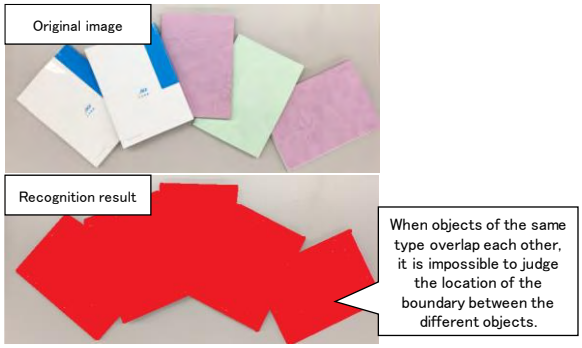

Fig 2: Result example by Semantic Segmentation

Fig 3: Result example by Instance Segmentation

3. Demonstration experiment

(1) Experimental design

Using video images of vehicles shot during an actual traffic census, the three existing methods studied in Chapter 2 are applied to images shot in the real environment to verify the applicability to the real environment. From these validation results, issues that are necessary to apply the existing technologies to the real environment are made clear.

(2) Experimental conditions

This experiment was conducted using video images of a prefectural road with one lane on each side, of which the traffic volume of 12 hours is about 11,000 vehicles, the congestion degree is 1.24, travel speed is 14.7km/h, and the heavy vehicle ratio is about 7% (hereinafter referred to as “Experimental site”). The video was shot of the lane of only one side by fixing a camera at a height of 3 meters on a telegraph pole installed on the sidewalk alongside the carriageway.

From this video, we randomly selected 5 different images for each of an ordinary car, a motorcycle, a bus, a truck, and a bicycle, which were placed in the center of the image at the point of time. To these images, we applied YOLO (You Only Look Once) as a method of using existing Object Detection[2], SegNet as a method of using Semantic Segmentation[3], and Mask R-CNN as a method of using Instance Segmentation[4], to evaluate the recognition accuracy of the existing technologies for vehicles including motorcycles and bicycles. For each method, we used existing learning models open to the public.

(3) Experiment description

In this experiment, we confirmed by visual inspection the results of recognizing vehicle location and identifying vehicle type by employing existing technologies, using frame images captured from a video of the experimental site. To confirm the difference in recognition accuracy by vehicle type, we used 5 different images for each of an ordinary car, a motorcycle, a bus, a truck, and a bicycle placed around the center of the image. The results were classified into 3 groups: if the estimated location of a vehicle is almost correct and its vehicle type is also correct, it is classified as “success in recognition and identification”; if there is an error only in the vehicle type, it is classified as “erroneous identification of vehicle type”, and if the area is not estimated, it is

Table 1: Evaluation of recognition result

Methods	Groups	Number of recognitions					
		Ordinary Car	Motor-cycle	Bus	Truck	Bicycle	Total
Object Detection	Success in recognition and identification	2	5	5	2	4	18
	Erroneous identification of vehicle type	3	0	0	2	1	6
	No recognition at all	0	0	0	1	0	1
Semantic Segmentation	Success in recognition and identification	5	4	5	1	4	19
	Erroneous identification of vehicle type	0	0	0	4	0	4
	No recognition at all	0	1	0	0	1	2
Instance Segmentation	Success in recognition and identification	5	5	5	4	5	24
	Erroneous identification of vehicle type	0	0	0	0	0	0
	No recognition at all	0	0	0	1	0	1

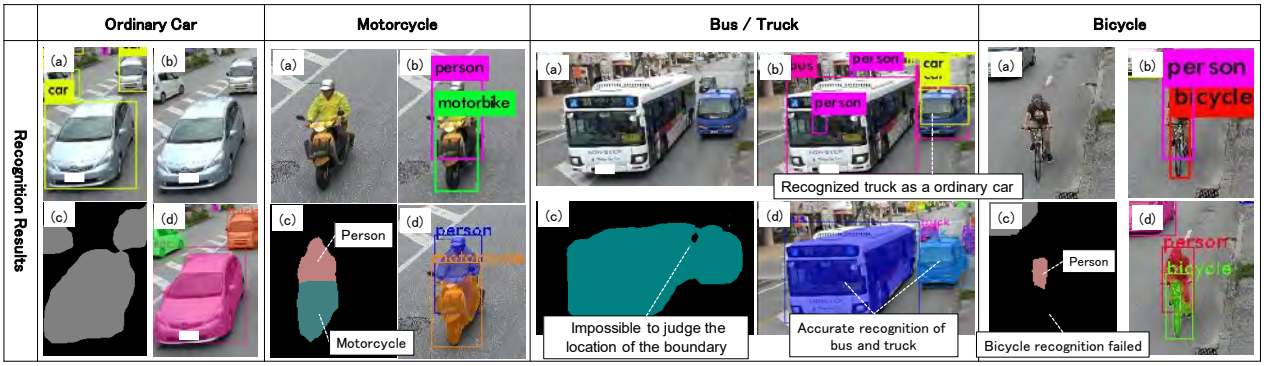

(a)Original image (b)Object Detection (c) Semantic Segmentation (d)Instance Segmentation

Fig 4: Examples of object recognition result

classified as “no recognition at all”. Then the number of vehicles for each group was evaluated.

(4) Experimental Results and Discussion

Table 1 shows the evaluation results for the recognition results by each existing technology, and Fig 4 shows an example of the visualization results. First, from the recognition results of Fig 4, any vehicle type can be recognized by existing technologies with a high accuracy. However, the recognition result of the bus and truck by Semantic Segmentation (Fig 4-c) indicates that when multiple vehicles overlap each other, it is impossible to judge the boundaries of the vehicles. This is because Semantic Segmentation outputs the recognition result as the same vehicle color even when different vehicles are recognized. Consequently, it is difficult to apply it as it is when a vehicle is changing lanes, when there is a stopped vehicle, or on a road where vehicles often overlap each other such as in traffic congestion. On the other hand, the results of recognition by Object Detection and Instance Segmentation indicate that even when different vehicles overlap each other, it is possible to recognize them as different vehicles. However, as shown in Fig 5, an ordinary car may be erroneously recognized as a truck. The cause of this is considered to be because Object Detection and Instance Segmentation are methods specialized for recognizing the locations and boundaries of objects and not specialized for classifying objects with similar characteristics. Thus, by combining these existing

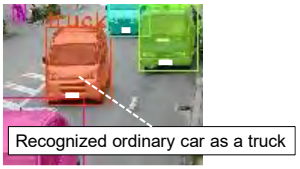

Fig 5: Example of erroneous identification of vehicle type

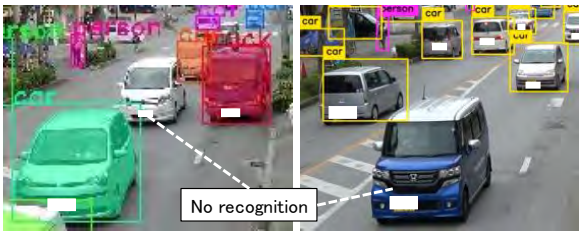

Instance Segmentation Object Detection

Fig 6: Examples of no recognition

technologies with a method specialized for classifying images, a higher accuracy of vehicle recognition and classification of vehicle types can be expected.

As far as the images used in the experimental results are concerned, both methods of Object Detection and Instance Segmentation are capable of recognizing vehicles with a high accuracy. However, there were also cases where they failed in recognizing vehicles in scenes other than the images evaluated in this experiment (Fig 6). The cause of this is considered to be that the diversity of the training data learned by

both methods as well as the number of times they were learned were insufficient. On the other hand, an excessive increase in the diversity or number of times of learning may cause overlearning and diverge the results. Therefore, by combining a method of predicting or interpolating the vehicle location using the recognition results for the point before or after failure in recognition, a practical application to traffic censuses can be expected. In addition, since the travel speed of the road used in this experiment was as low as 14.7km/h, there is a possibility that the recognition accuracy of these technologies may decrease if the target road is a road with a high travel speed. Therefore, verification with a target road with a travel speed equal to or higher than the one studied in this experiment is required.

4. Matters to be considered in order to develop the technology for automatic traffic censuses

In this section, in view of the results of the demonstration experiment in this research, developments of the technology required for applying existing object-recognition technology toward the development of technology for automatic traffic censuses are outlined below.

(1) Technology for predicting and interpolating the location at the time of passing a cross section

Traffic censuses investigate the number of vehicles passing a certain cross section on a road. However, if the existing technology is applied as it is, when it fails to recognize vehicles at the moment of passing a cross section, the measured number of passing vehicles will be smaller than the actual one. Therefore, it is considered necessary to develop a method for predicting or interpolating the location when an object passes there, using the recognition results from before and after the point of time.

(2) Technology for identifying the location recognized at different points of time

To measure the number of vehicles passing a certain cross section on a road automatically, it is necessary to trace the same vehicle by identifying it before and after it passes the cross section. However, as the existing technology recognizes the vehicle location by means of a static image, it is not capable of identifying vehicles in a proper time sequence. Therefore, it is necessary to develop the technology capable of judging the passage of a cross section using these recognition results and fixing the vehicles in a video image.

(3) Technology for identifying vehicle type accurately

From the experiment results, it was found that the existing technologies have the problem of erroneous identification of vehicle type. Consequently, it is necessary to improve the identification accuracy of vehicle type by developing technology specialized to the classification of images.

Moreover, in a traffic census, there may cases depending on the research content where the number of passing vehicles should be investigated by vehicle type including not only buses and trucks but also taxis and rental cars. However, since there may be cases where it is difficult to identify vehicles only by the form of the vehicle, such as ordinary cars and rental cars, it is necessary to develop an identification method that combines information on the number plate with that of the form.

5. Conclusions

In this research, we focused on deep learning as a method for realizing effective traffic censuses, investigated technologies capable of the automatic recognition of vehicles from their video images, and validated their practicability. Then, through the demonstration experiment, we organized element technologies required for realizing automatic surveys of traffic volume irrespective of the traffic mode. The results of the demonstration experiment indicate that among the technologies for recognizing the locations of objects using deep learning, object-recognition technologies, such as Object Detection and Instance Segmentation, can be utilized to recognize vehicles from videos of the real environment. On the other hand, in measuring the number of vehicles passing a cross section, there were cases of failure to recognize vehicles or of erroneous identification of the type of recognized vehicle. In the future, we aim for the realization of automatic traffic censuses without depending on the traffic mode, by developing technologies capable of solving these challenges and validating the applicability to the site.

Acknowledgements

We would like to thank Chuo Kensetu Consultants, Co., Ltd. for providing us with the video images used in this research. Part of this research was financially supported by the Kansai University Fund for Domestic and Overseas Research, fiscal year 2018.

References

[1] Computer Vision: Trace Blade AI Suite / Traffic Blade , <http://www.media-juggler.co.jp/doc/ComputerVision_roductinfo .pdf>, Accessed on Nov. 30, 2019.
[2] Joseph, R., Santosh, D., Ross, G. and Ali, F.: You Only Look Once: Unified, Real-Time Object Detection, (2016) arXiv:1506.02640.
[3] Badrinarayanan, V., Kendall, A. and Cipolla, R.: SegNet: A Deep Convolutional Encoder-Deconder Architecture for Image Segmentation, *Transactions on Pattern Analysis and Machine Intelligence*, IEEE 39 (2017) 2481-2495.
[4] Kaiming, H., Georgia, G., Piotr, D. and Ross, G.: Mask R-CNN, (2017) arXiv:1703.06870.

Field Survey on Indoor Overheating in School and Hospital Buildings in Montréal

Chang Shu [a], Lili Ji [a], Lin Wang [a], Xuechen Bai [a, c], Michael Lacasse [b], Hua Ge [a], Radu Zmeureanu [a]
Liangzhu (Leon) Wang [a,*]
[a] Centre for Zero Energy Building Studies, Department of Building, Civil and Environmental Engineering, Concordia University, Canada.
[b] Construction Research Center, National Research Council Canada, Canada
[c] School of Economics and Finance, Xi'an Jiaotong University, Xi'an, China
* Corresponding author, Tel 514-848-2424 ext. 5766, email leon.wang@concordia.ca

Abstract:
In 2018 Montreal experienced a severe heatwave (extreme heat event), causing 66 deaths, for which most of the deceased lived in buildings located in hot areas within the city and that had limited access to air-conditioning. To study the resiliency of buildings against extreme heat events (EHE), in particular within the context of the changing climate, a field study was conducted in the Montreal area on the thermal response of hospitals and primary schools to EHEs. Satellite thermal maps, historical distributions of heat-related-deaths and building construction years were used to identify the regions within the city and buildings most vulnerable to EHE. Overall, 14 hospitals and 15 schools were selected for site visits to obtain information on thermal comfort and occupant behaviour, envelope materials and the accessibility and operation of HVAC systems. The indoor temperature and relative humidity (RH) of typical rooms on different floors and orientations in six hospitals and six schools will be monitored continuously over the summer season at 5 minute intervals. On-site weather stations will be placed on the roofs of buildings to gather local weather data, including: air temperature, relative humidity, solar radiation, wind speed and direction, and precipitation. The dynamics of indoor conditions of the different types of buildings investigated may reveal their distinctive air movement patterns that are related to HVAC operations, building schedules and envelope components. A detailed description of the field study, including the rationale for building selection, is provided. From this study, it is anticipated that valuable field data of the response of building overheating will be obtained that can subsequently be used in the preparation of a best practice guideline for similar studies when high-quality field data are required and experimental resources are limited.
Keywords: Extreme heat event; field monitoring; overheating; survey; thermal comfort

1. Introduction

With the rapid progress of urbanization and global warming, extreme heat events (EHE) become more severe and frequent, imposing a threat to the wellbeing of urban dwellers. In the face of such challenges, the Canadian government has formulated a framework to mitigate and adapt to climate change across Canada [1], under which a better prediction on urban weather conditions is required for the resilient design, operation, and renovation of buildings and infrastructure assets. In recent years, two severe EHEs occurred in Montreal with recorded deaths of 106 in 2010, and 66 in 2018 [2]. Most of the deaths occurred in overheated buildings, whereas investigations of these deaths did not reveal building indoor thermal conditions over the EHE.

This paper focuses on the occurrence of overheating in a number of schools and hospital buildings as determined from results of field monitoring. Hospitals are expected to provide a shelter to heal those who are suffering from the heat during summer. The resilience of hospitals against EHEs may help to reduce the mortality and morbidity of vulnerable groups of people, e.g., the elderly, sick, and those having mental illness [3]. Results from existing field monitoring studies have shown that severe overheating problems occur in west-facing rooms [4]. Three different types of hospitals were considered in this study: hospital centres (CH), residential and long-term care centres (CHSLD), and rehabilitation centres (CR), having long-term care residents.

School children aged between 8-14 can also be vulnerable to EHEs, and high indoor temperatures may disrupt the academic performance of students [5]. Therefore, only pre-school and primary schools were considered in this study.

A long-term monitoring campaign for summertime building overheating is to be carried out in Montreal, Canada in this study. To overcome the limitation of the prohibitive costs of field studies, a systematic method to complete the studies was explored that included a building information survey and an on-site visit, to permit the selection of suitable buildings for completing a detailed summertime field monitoring program of indoor overheating. In the following section, the procedures used for the systematic method is elaborated step-by-step. Outcomes arsing from site visits are showcased by an example of a hospital building and another for a school building, both having with notable overheating problems in the summer. The overall decision for building selection and an outlook for field monitoring will also be provided.

2. Methodology

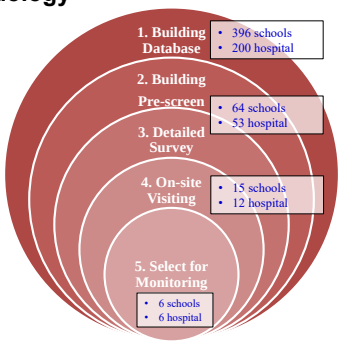

Fig. 1 Procedure for screening and selection of buildings for field monitoring.

In this study, the field monitoring will be carried out for a limited number of school and hospital buildings for three year period. Therefore, determining the best combination of buildings as regards the most vulnerable to EHEs, can be a significant challenge to ensur capturing both the EHE and indoor overheating problems during the long-term monitoring program.
A 5-step guideline for the screening and selection of buildings for field monitoring is given in Fig. 1. . A vast database for all the hospital buildings in Montreal was obtained from the: (i) Ministère de la santé et des services sociaux (MSSS), (ii) 5 different Centre intégré universitaire de santé et de services sociaux (CIUSSSs) in Montreal. As well, for selection of school buildings, the Ministère de l'Éducation et de l'Enseignement supérieur (MEES) provided information on 5 different Montreal school boards. Typically, the building database should have a significant number of buildings to permit covering more possibilities for potential cases.

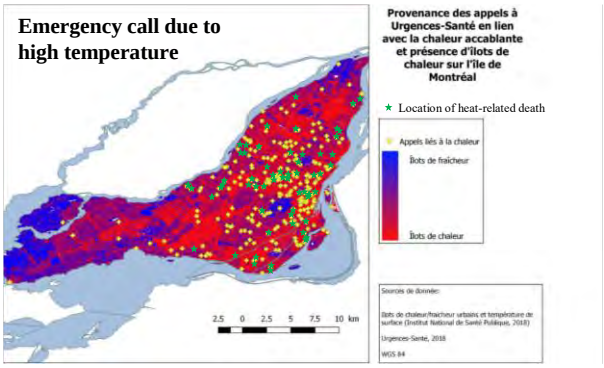

Fig. 2 Distribution of emergency calls due to EHEs in 2018 and death-related EHEs as provided in a heat island intensity map [2,6]

To further reduce the scope for building selection, a pre-screening of the building database was conducted. An investigation on previous heat-related deaths during EHEs showed the he location and distribution of emergency calls and the heat-related deaths attributed to EHEs; these are highly related to the urban heat island intensity as given in Fig. 2. As well, most of the health events (i.e. heat-related deaths and emergency calls) happened in areas with intensive heat island problems, indicating those dwelling in these areas may have had a higher exposure during the EHE, and the buildings in these areas may be more vulnerable to overheating issues. Thus, the location of the buildings become an essential criterion for the selection of appropriate buildings to study. Google maps and Google street views were found to be useful tools to inspect the location, orientation and the surrounding environment of the buildings. A graphic set of each of the buildings was created from the southern view on Google street maps, and the buildings were filtered using the following criteria:

1. Schools mainly with children aged 8 – 14;
2. Hospitals with long-term residents;
3. The building location is close to those sites where deaths had been previously noted;
4. Buildings with the longer façade facing the north-south direction
5. Buildings that were not close to green areas or parks
6. Buildings located in a high-density neighbourhood and close to major streets or parking lots having large areas of impervious land cover without any shading

For that reduced set of candidate buildings, a building information survey was prepared to permit gathering detailed information about this set of buildings. A building information survey form was distributed to the building owners and their material service managers to obtain information on construction details, building equipment, and related information. The survey sheet also contained information in which the study objectives were provided and that to explain the possibility for building managers to support the study. The building information survey form is organized in 5 sections:

1. General information of buildings: building name construction year, number of floors, number of occupants, etc.
2. Building performance and occupant behavior: thermal comfort and historical heat-related health events, building activities, overheating complaints, and relevant measures to mitigate impacts of overheating.
3. HVAC system: type of system, fresh air system, cooling system, ventilation, etc.
4. Building envelope: type of envelope construction, materials, window type, window-wall-ratio, etc.
5. Building plans.

After we received the survey forms, it was important to conduct on-site visits to gather more firsthand information about the building. The visits to hospital sites were conducted in July whereas this occurred in September for schools. Usually, it is optimal to have a team comprised of four members, each member assigned a corresponding task; these were:

1. Communicate with the building manager to know the function of the rooms, building system, and equipment, confirm important questions on the previous building information survey forms.
2. Communicate with people in the building, i.e., students and teachers in schools, patients, and doctors in the hospital, to know the general level of comfort in the building.
3. Take photos to keep a good record of the site; undertake thermal images of building surfaces for quantitative comparisons later.
4. Take notes of the communications and use a checklist for process control to ensure all tasks have been completed.

Along with the practice of visits to many different buildings, a team approach using assigned tasks provided a most effective and efficient way to collaborate with building managers and users. Too

many personnel for a visit may disturb the building occupants of which may be undesirable.
Decisions for the selection of buildings were made after completing the site visit. The overall distribution of selected buildings, the real condition of the building, and the attitude and intention for collaboration of the building owners should be considered comprehensively. The results of these major steps during the site studies are discussed in the next section.

3. Results and discussions

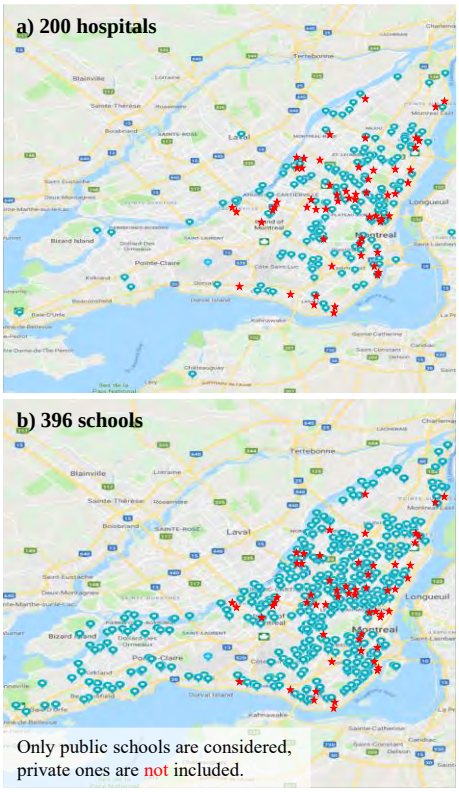

Fig. 3 Distribution of a) hospital buildings and b) primary school buildings on Montreal Island and locations of heat-related death in 2018

In the first step, a list of 200 hospitals and 396 schools was obtained for the Montreal area. The locations of the buildings were marked on Google maps, as in Fig. 3, so that the locations could be compared with those of the previous heat-related deaths (red stars). After that, the large database of buildings was filtered to 64 schools and 53 hospitals over the entire island. Some of the locations would not be able to participate in this project, given that for some, either they had no overheating problems evident in their buildings or, retrofitting activities were to take place in the near future. To determine these instances, the building survey form was used to investigate these candidate building and communicate with the respective building managers. A number of completed survey forms were received at the end of step 4: 12 hospitals and 15 schools. On-site visits are the most critical step for final decisions on selecting buildings. As examples, only one hospital building and one school building are each described.

- **Onsite visiting to a hospital building**

This hospital has seven floors in total with a building envelope composed of ceramic, brick and plaster without insulation. The window- wall-ratio is 40%-50%, and curtain and blinds are installed inside for shading. The plant coverage in proximity to the building is low, whereas building density is high in the surroundings.

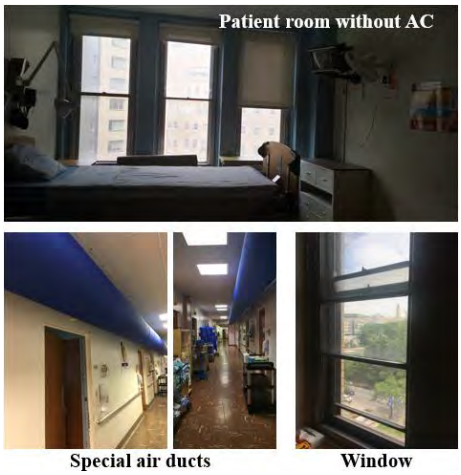

Fig. 4 On-site visiting of a hospital building

Although there exists a centralized air conditioning system, it does not cover the whole building. To deal with the overheating problem in summer, a temporary air conditioning system is temporarily installed in the corridor during the summertime (round air ducts; Fig. 4). In some rooms without centralized AC, window units are used. There is no AC system on the top floor (7th floor). The rooms facing south, including a family room, a clinic room, and a therapy room, have higher indoor temperatures than that of the corridor. There is also overheating problems on the 5th floor. On that floor it was found that apparent high temperature occur in a waiting room without operable windows; this room is often fully occupied. As such, these rooms, having obvious overheating complaints and problems, are potential candidates for monitoring later in the study.

- **Onsite visiting to a school building**

This selected school has two floors and one basement, was built in 1951, and in the 1990s, a gym and two classrooms were added. There is a fresh air system in the gym, but no cooling for the entire building and no fresh air system for the rest of the building.
Four typical classrooms were selected to be monitored. Two large classrooms next to the gym on the 1st floor are south facing and have received complaints of overheating. However, the thermal image in these two classrooms exhibited a noticeable difference because in one of them, a portable air conditioner had been added, whereas the other room is cooled passively through operation of the windows. These two classrooms can be used for completing comparisons and thus are an ideal pair for undertaking case studies.

For those classrooms located on the 2nd floor (top), the temperature in the morning could reach 47℃ in southwest facing rooms in June and August, whereas the classroom on the opposite side (facing Northeast) is much cooler. Therefore, these two classrooms have also been selected for comparative studies.

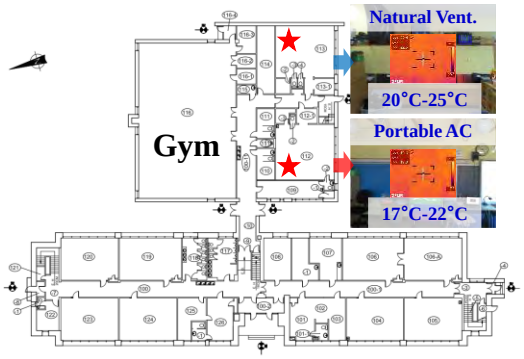

Fig. 5 Building plan, thermal images, and photos of 1st floor of the school building

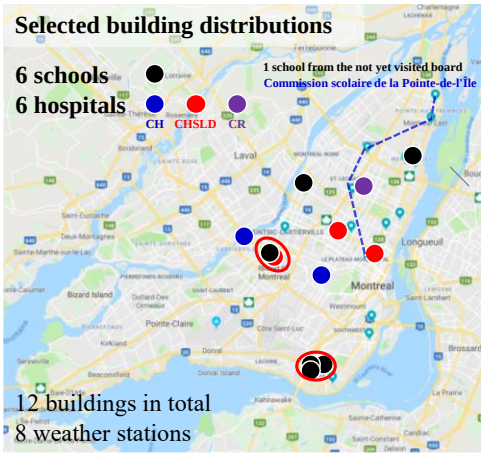

Fig. 6 Distribution of selected buildings

- **Building Selection Final Results**

A careful and comprehensive review of overheating problems in the selected buildings their distribution helps identify six schools and six hospitals for further field studies. Most of the selected buildings are well distributed over all of the central and eastern part of Montreal thus capturing the city scale climate pattern; a few of the building locations are close to one another and the plan for these buildings is to share one weather station for the local weather conditions.

4. Conclusions and outlook

A systematic guideline for the selection of buildings for the purpose of completing field monitoring of overheating events and interior building conditions has been postulated in this study. The methods in this guideline can be implemented for large-scale field monitoring studies having limited site options, and where both local weather data and indoor conditions are captured. The next step in the study is to install the sensors on-site and gather data over the research period. The data may reveal the relationship between the indoor and outdoor conditions and can then be used for the validation of mesoscale climate and building energy models.

Acknowledgments

The authors would like to thank Ms. Chantal Saucier and the support from Ministère de la santé et des services sociaux (MSSS), Mr. Darius Tsé and support from Ministère de l'Éducation et de l'Enseignement supérieur (MEES). We appreciate receiving support from Mr. Jocelyn Poisson, Mr. Martin Massé, Mr. Pierre-Luc Roberge, Mr. Laure Pérès, Mr. Jairzinho Aburto, Mr. Bruno Cote, Mr. Yves Plourde, Mr. Akeen Kidder-Alexander and all those who helped us during site visits. The research is supported by the Natural Sciences and Engineering Research Council (NSERC) of Canada through the Discovery Grants Program and the Advancing Climate Change Science in Canada Program led by the corresponding author of the paper.

References

[1] Government of Canada, Pan-Canadian Framework on Clean Growth and Climate Change: Canada's Plan to Address Climate Change and Grow the Economy, 2016. https://doi.org/https://www.canada.ca/content/dam/themes/environment/documents/weather1/20170113-1-en.pdf.

[2] F. Lamothe, M. Roy, S.-É. Racine-Hamel, Enquête épidémiologique - Vague de chaleur à l'été 2018 à Montréal, Montréal, Québec, 2019. https://doi.org/9782550840206.

[3] Z. Xu, J. Cheng, W. Hu, S. Tong, Heatwave, and health events: A systematic evaluation of different temperature indicators, heatwave intensities and durations, Sci. Total Environ. 630 (2018) 679–689. https://doi.org/10.1016/j.scitotenv.2018.02.268.

[4] L.J. Fifield, K.J. Lomas, R. Giridharan, D. Allinson, Hospital wards and modular construction: Summertime overheating and energy efficiency, Build. Environ. 141 (2018) 28–44. https://doi.org/10.1016/j.buildenv.2018.05.041.

[5] P. Barrett, F. Davies, Y. Zhang, L. Barrett, The impact of classroom design on pupils' learning: Final results of a holistic, multi-level analysis, Build. Environ. 89 (2015) 118–133. https://doi.org/10.1016/j.buildenv.2015.02.013.

[6] The Institut national de santé publique du Québec, Îlots de chaleur/fraicheur urbains et température de surface, INSPQ. (2018).

Performance of dynamic shading systems based on non-deterministic algorithm

V. Charpentier[a*], F. Meggers[b,c], S. Adriaenssens[a], O. Baverel[d]

[1] Department of Civil and Environmental Engineering, Princeton University, Princeton, New Jersey, United States
[2] School of Architecture, Princeton University, Princeton, New Jersey, United States
[3] Andlinger center for Energy and the Environment, Princeton University, Princeton, New Jersey, United States
[4] Laboratoire Navier, UMR 8205, École des Ponts, IFSTTAR, CNRS, UPE, Champs-sur-Marne, France
* Corresponding author, email :viccharp@gmail.com

Abstract:
Buildings account for about 40% of total U.S. energy consumption in 2018. The better design of building envelopes through the integration of external dynamic shades is critical for reducing this large energy consumption while at the same time improving the quality of indoor spaces for people. This paper elucidates the benefits of a novel control methodology for dynamic shading systems with a specific case study. A single degree-of-freedom (d.o.f.) actuation external fabric awning is evaluated against an unshaded baseline case over annual sun hours for east, south-east and south orientations. A perimeter office space with 65% window to wall ratio (WWR) is modeled. In agreement with results found in literature, our methodology confirms that there are tradeoffs in optimizing the cooling energy in terms of accessible daylight. When tested on a prototype design of dynamic awning shades, our methodology led to a 33% overall reduction of energy. The awning shades lead to a 45% decrease in annual cooling energy demand, but an 64% increase in lighting energy to maintain the constraint daylight levels.

Keywords:
Dynamic shading, cooling, energy efficiency, control, optimization

1. Introduction

The façade of a building is the interface between the outdoor and indoor spaces. The complexity of designing a façade comes from how different both are and from the strong psychological influence of the outdoor on the indoor space. This influence requires that the two spaces be mediated by the façade. The complexity of both mitigating dynamically changing environmental stimuli (i.e. continuous sun movement, evolving cloud coverage) and human comfort requirements (i.e. thermal comfort and daylight) can be tackled by external dynamic shading systems. Existing strategies for active control of dynamic shades are rule-based. These strategies are based on deterministic methods that always assign an action to mitigate threshold values of a controlling environmental parameter. Usually, these rules are based on measuring the beam illuminance or beam solar radiation on the window [1, 2], or illuminance levels on the work plane [3].

In this paper we depart from rule-based control and, we introduce a novel non-deterministic methodology for the control of dynamic shades based on the global optimization for best performance. We present a two-step methodology based on the interpolation of pre-calculated energy and daylight simulations and on the search for global energy minimum with strict conditions on occupant comfort. The main objective of this paper is to present representative results of the novel methodology introduced by the authors for shading control and analysis. The case of a fictitious building room is selected in Mercer County, New Jersey, USA for three orientations (east, south east and south). Energy demand for heating, cooling and electric lighting are calculated to maintain a fixed level of thermal comfort. Work plane illuminance (average and maximum) is calculated as principal metric for daylight quality. The performance of an external awning shading system (see Figure 1) is shown using the presented methodology.

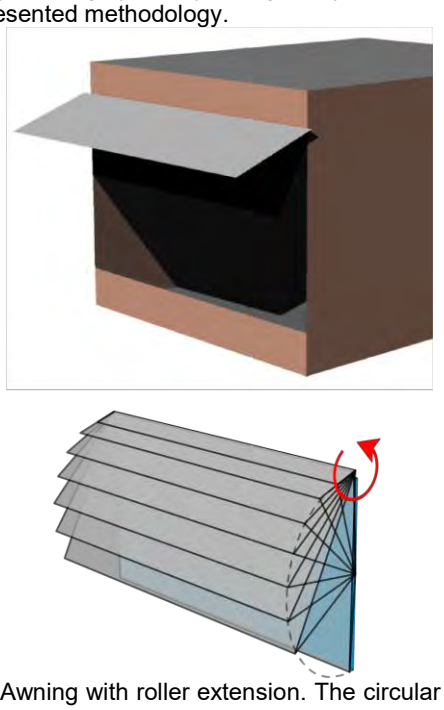

Fig 1: Awning with roller extension. The circular arrow denotes rotational actuators.

2. Methodology

The present paper focuses on mediating the energy (heating, cooling, and lighting) demand under daylighting requirements for one type of shading systems. The room is a typical (4.5 m x 5 m x 3.2 m high) perimeter office space in Mercer County NJ (USA, latitude 40.3573° N) and the window-to-wall-ratio is fixed by design at 65% (Figure 2). Weather data relative to Mercer County comes from the meteorological year (TMY3) dataset[4]. In the dataset 4306 hours of sunlight are recorded for this position. Three factors were selected to enter the optimization: (i) the heating and cooling energy demand, (ii) the lighting energy demand, and (iii) the average and maximum illuminance on an 80-cm high work plane.

The position of the shades is not based on a rule (e.g. the shades are oriented at time t, so that the projected shadow of the shades along the sun vector covers the glazing) but on the result of an optimization system that indicates the best position to satisfy all the daylighting constraints and minimize the operating energy. Rule based control strategies are specific to each shading system because they often relate to geometry. The proposed methodology is applicable in the exact same way to every shading system that can be modelled numerically.

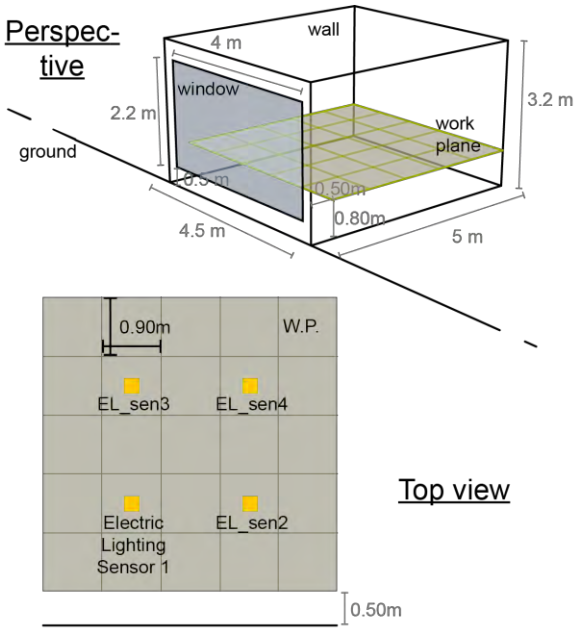

Fig.2: Perspective: perimeter office space – window in blue, work plane in yellow - exterior / interior ground, walls indicated – top view: daylighting grid with a daylight sensor per grey square, the four artificial lighting sensors determine when electric lighting is needed

The optimization system *S* is the same for both hot and cold periods since the objective function is the sum of the entire energy demand in the system at time t. Similarly, the constraints of comfort are identical for the users throughout the year. The optimization system must be solved for each orientation, and sun hour considered. In total, the optimization system is solved 12 918 (=3 orientations ×4306 sun hours) times. Each function used in the optimization system is a linear interpolation of the simulation results. Each of these gives the value at time t of one of the five parameters as a function of the position of the shades. For a given shading case, five of those interpolated functions are needed at each time step t since there are five parameters modeled. The functions need to be determined for each time step. The optimization interval is the interval of the possible position of the shades. The interpolation and optimization (Augmented Lagrangian Genetic Algorithm) are performed in MATLAB[5].

$$(S) \quad \begin{cases} \min\limits_{x \in I} \left(E_{heat,s}^{\alpha}(x) + E_{cool,s}^{\alpha}(x) + E_{light,s}^{\alpha}(x) \right) \\ \text{s. t.} \begin{cases} A_s^{\alpha}(x) = l_1 \\ M_s^{\alpha}(x) < l_2^{+} \end{cases} \end{cases}$$

(Eq. 1)

where

$\alpha \in$ [awning, venetian, tracker] as the shading system

s the sun vector

I the actuation interval

$E_{heat,s}^{\alpha}$ the interpolated heating energy for sun vector s and shade α

$E_{cool,s}^{\alpha}$ the interpolated cooling energy for sun vector s and shade α

$E_{light,s}^{\alpha}$ the interpolated lighting energy for sun vector s and shade α

A_s^{α} the average illuminance interpolated function

M_s^{α} the maximum illuminance interpolated function

l_1 the target value for the average work plane illuminance (500 lx)

l_2^{+} the upper limit for the maximum work plane illuminance (2000 lx).

The energy and daylighting simulations are performed with DIVA[6] in the program Rhino3D/Grasshopper[7]. The thermal state of the test room is simulated with EnergyPlus[8]. The daylighting and electric lighting analysis are performed by Radiance [9]. The goal of the thermal model is to produce energy demands for heating and cooling of the room. The simulation engine is EnergyPlus. It is interfaced by Archsim in Grasshopper3D/Rhino3D. The model takes the climate data from the epw weather file of Mercer County, NJ as weather input.

The heating setpoint is set at 20°C while the cooling setpoint is set at 26°C. The heat balance is performed with four timesteps per hour and implements the conduction transfer function method[10]. The computation of solar radiation is performed with the detailed timestep integration method. In this study, the thermal model in EnergyPlus is not set to integrate electric lighting and daylighting simulations. Both of those are run independently in daylighting program Radiance [9].

3. Results and discussions

For the three orientations, the annual energy demand for the baseline case of no shading is significantly decreased by the shading system (Figure 3). The optimization results show a decrease of annual cooling demand on the east of 26% for the awning. This decrease is more pronounced on the south-east (-35%) and south (-37%). The efficiency of the shading system on the east is about 10 percent lower than for the other orientations. This significant decrease in annual energy demand is due to a large reduction in cooling for all orientations. The lighting and heating energies both increase, but they remain small overall.

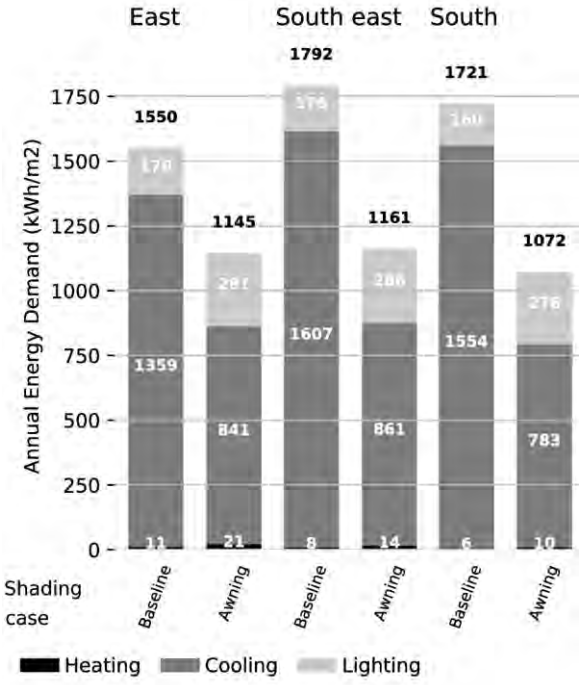

Fig. 3: Annual energy demand in kWh/m2 for east, south-east and south orientation and for the baseline and awning shades. Heating, cooling, and lighting energies are summed to make the total energy demand.

In terms of illuminance levels, the optimization satisfies for all annual sun hours the constraint of maximum illuminance. While for the baseline case, high illuminance values (>2000 lx) occur frequently in the morning on the east, between 10h00 and 15h00 on the south-east and at +/- 3 hours around the noon sun hour on the south. For three orientations, the baseline average is well beyond the 2000 lx comfort threshold. The average maximum work plane illuminance is reduced to ~1100 lux with the presence of the awning shades.

The second constraint in *S* on the average illuminance is well respected. As exemplified in Figure 4, the baseline case of the unshaded window provides many average illuminance values that would cause severe discomfort. More precisely, let us consider the baseline sun hours over the three orientations that provide over 500 lux of average illuminance. There are 3046 on the east, 3139 on the south east and 3233 on the south. The control strategy allows the awning shades to set the average work plane illuminance to 500 lux in 98.7% of those on the east, 84.0% on the south east and 97.5% on the south. This ratio of 500 lux shaded count over the >500 lux baseline count as the accuracy. A high accuracy means the shading system and algorithm are able to filter the high environmental illuminance to the level fixed by the occupant.

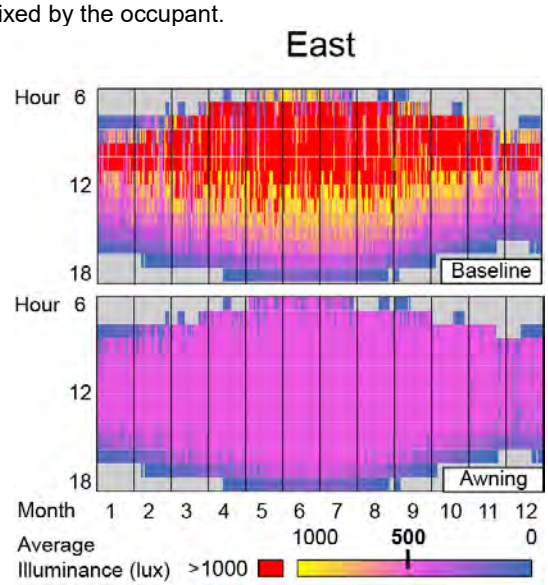

Fig. 4: Hourly average daylight illuminance resulting from the optimization for east, south-east and south orientation and for the baseline and awning shades. Average illuminances over 1000 lx are highlighted in red

These high accuracy values show that the awning shades are efficient for the parameters and are compatible with the chosen comfort constraints. They reduce the maximum illuminance and match very accurately the target average illuminance. While the east and south orientations have over 97% of accuracy each, the awning shades perform less well on the south east orientation with 84% of accuracy. 16% of the sun hours with a high baseline illuminance cannot meet the target average illuminance. The sun vectors often have large tangent angles with the south east oriented façade in the mornings and in the afternoons. Since the awning shade cannot rotate to

follow the azimuthal movements of the sun, the only solution available to the algorithm to prevent values of illuminance above 2000 lux is to reduce the average illuminance. This methodology therefore highlights the performance of the shading system but also provides supplemental evidence that this design of the shades could be improved.

Further studies of the shading systems can already use some of the results presented here. The choice of comfort criteria to be used as input in the optimization system influences the outcome of the analysis. To evaluate the performance of the shading system a sensitivity analysis on the values of the constraints should be performed. A consistent level of accuracy at different levels of work plane illuminance would ensure that the shading system is flexible enough to allow maximal range of operation for the occupant. Furthermore, the improvement of performance could come from a re-design of the kinematic design of the shading system. Such a revised kinematics should be analyzed and compared to the current shading system.
Setting adequate constraints for an optimization procedure will shape the type of shading that will perform best. Picking the right constraints is therefore essential. In this methodology, the constraints are based on human comfort, hence occupants are put at the center of the study, which promises to increase wellbeing and enjoyment in the building.

4. Conclusions and outlook

The governing assumption of the control strategy is that user comfort should be the controlling parameter in the dynamic shading system. For that purpose, the energy demand parameters (heating, cooling and lighting) are set as the objective to be minimized and the visual comfort as constraints to be met in the non-deterministic algorithm. This methodology is adaptable since the choice of criteria for the objective or the constraints is selected by the designer. The results presented in this study are specific to the case chosen at 40° latitude and east to south building orientations. They are representative of a design case one might encounter. The methodology, however, can be applied to many cases. It can be used in early design phases as well as for in-depth simulations and shading system design. The methodology can refine the design of a specific shading system by quantifying effects of parametric variations on the system's performance.

The critical path for the successful application of this methodology depends on choosing the correct performance and comfort metrics adapted to the environmental context of the building. A novel type of shades such as a two-axis spherical tracking shading system could have the potential to handle the highly tangential sun vector cases and increase the accuracy of the daylighting control system. The design of better shading systems can contribute to decreasing the tension between the conflicting goals of energy demand reduction and user comfort increase.

Acknowledgements

The authors would like to thank the National Science Foundation under the Grant No 1538330 and the Andlinger Center for Energy and the Environment at Princeton University for their support. Many thanks to Georgina Hall from INSEAD Decision Sciences Department for her advice on interpolation.

References

1. Tzempelikos, A. and A.K. Athienitis, *The impact of shading design and control on building cooling and lighting demand.* Solar Energy, 2007. **81**(3): p. 369-382.
2. Nielsen, M.V., S. Svendsen, and L.B. Jensen, *Quantifying the potential of automated dynamic solar shading in office buildings through integrated simulations of energy and daylight.* Solar Energy, 2011. **85**(5): p. 757-768.
3. Cziker, A., M. Chindris, and A. Miron. *Fuzzy controller for a shaded daylighting system*. in *2008 11th International Conference on Optimization of Electrical and Electronic Equipment*. 2008. IEEE.
4. Wilcox, S. and W. Marion, *Users manual for TMY3 data sets*. 2008: National Renewable Energy Laboratory Golden, CO.
5. Moore, H., *MATLAB for Engineers*. 2017: Pearson.
6. Jakubiec, J.A. and C.F. Reinhart. *DIVA 2.0: Integrating daylight and thermal simulations using Rhinoceros 3D, Daysim and EnergyPlus*. in *Proceedings of building simulation*. 2011.
7. McNeel, R., *Grasshopper for Rhino3D*. 2012, retrieved.
8. Crawley, D.B., et al., *EnergyPlus: creating a new-generation building energy simulation program.* Energy and buildings, 2001. **33**(4): p. 319-331.
9. Ward, G.J. *The RADIANCE lighting simulation and rendering system*. in *Proceedings of the 21st annual conference on Computer graphics and interactive techniques*. 1994. ACM.
10. Li, X.Q., et al., *Applicability of calculation methods for conduction transfer function of building constructions.* International Journal of Thermal Sciences, 2009. **48**(7): p. 1441-1451.

Mechanical behavior of a new type of flexible, pressurized storm surge barrier under hydrostatic loading

J. Goodglass[a], A. Niewiarowski[b], S. Adriaenssens[c]

[a,b,c] Department of Civil & Environmental Engineering, Princeton University
59 Olden Street, Princeton, NJ 08544, USA
josephhg@princeton.edu

Abstract:
Motivated by the need to combat future coastal flooding, this work explores alternatives to flood barriers based on the concept of pneumatic barriers. A pneumatic barrier, otherwise known as an inflatable barrier, comprises a flexible nylon coated vulcanized rubber membrane anchored to one or two linearly clamped supports attached to a ballast caisson foundation with skirt walls. Air inflated pneumatic barriers are quicker to employ during a storm surge but are accustomed to large displacements in both the horizontal and vertical direction. The internal pressure within the membrane must be sufficient to ensure no material failure in response to the applied loading, while maintaining adequate crest height. The research goal of this paper is to establish the engineering feasibility of an 8 m diameter air-inflated barrier subject to variable hydrostatic loading, using a finite-element analysis. This study establishes a novel paradigm for flood protection technology and promotes flexible civil structures as viable systems to channel extreme hazard loads.

Keywords:
Resilience, Urban Environment, Flooding, Pneumatic barrier, Fluid/Structure Interaction

Introduction

Demand for coastal flood protection infrastructure is projected to increase as sea levels rise and hurricane activity intensifies increases.[1] Inflatable temporary structures may confer economic and environmental advantages over conventional permanent seawalls or breakwaters. The most common type of inflatable structure consists of a single sheet of rubberized nylon fabric folded and clamped to a reinforced concrete foundation. This type of structure was originally utilized as an adjustable gate to control water levels in rivers and reservoirs.[2] A unique characteristic of the inflatable weir, in this regard, is its ability to adjust height, offering a control system which meets different needs. For example, during flood conditions in rivers, it can either be in the fully inflated or deflated position. This offers protection while reducing damming and allows sediment removal from the basin. It is hypothesized that certain U.S. coastal regions requiring additional coastal protection, such as the Rockaway Peninsula and Jamaica Bay (NY), can adopt inflatable barriers to mitigate storm surge flooding. Natural protection is minimal in these regions and traditional coastal defense solutions such as seawalls or dikes would disrupt beach access for people, animals and reduce real estate value. While pneumatic barriers are permanently installed, necessity will dictate time of deployment. After inflation, they can resist storm surge loads through tensile membrane action direction and carry such internal loading to the caisson foundation. Currently, the only inflatable storm surge barrier in operation is the Ramspol Barrier, located in the Netherlands.[3] The barrier consists of three identical inflatable rubber sheets, each of whose dimensions are 75 m long, 13 m wide and a design height of 8.35 m.[4]

Benchmark Study – Equilibrium Shaping

Analysis of an inflatable barrier involves the determination of the deformation and stress field due to external hydrostatic loads, i.e. a varied upstream and downstream head and internal pressure, where “upstream” and “downstream” refer to the left and right sides of the barrier, respectively. Harrison (1970)[5] proposed basic equations of the discretized equilibrium method with a trial and error solution process to analyze these barriers. In addition, Bonet et al.[6] addressed air supported membrane structures and considered the pressure/volume relation of the internal gas. The follow assumptions can be applied to our finite element (FE) model in this regard: (i) The behavior of a 2-dimensional transverse section of unit width is fully representative of a 3-dimensional structure. (ii) The static loads due to water and air pressures are acting on the elements themselves, not at the nodes, and are modeled as space-attached loads. (iii) The membrane’s constitutive behavior can be derived from a hyperelastic potential, given by the incompressible neo-Hookean material model. Specifically, the forces acting on the barrier under hydrostatic conditions include: internal air pressure, upstream and downstream hydrostatic water pressure, and self-weight of the membrane.

Finite Element Model Description

The pneumatic barrier is modelled as a thin, isotropic, elastic shell and the static response is analyzed using the finite element method (Abaqus/CAE, version 2019). It is supported by an internal uniform and constant pressure, which provides the stiffness to resist external loading. For unidirectional loads and constant cross section geometry, we assume a plane strain condition and a unit-width section of the barrier is modeled to save time on the analysis. The pressure field is given by $p_{stat} = \rho g d_{ave}$ where ρ is the density of water, g is the gravitational acceleration constant, and d_{ave} is the average depth at the nodes of each submerged element in the model. The four-node shell element (S4R)[7] is adopted under the assumption that the membrane will experience large deflections, large rotations, and small strains. The barrier is presumed to be clamped to a foundation (assumed rigid and not modelled). Therefore, zero displacement and zero rotation boundary conditions are prescribed as the degrees of freedom at the anchor line. The initial configuration of the barrier is a semicircle. The analysis is performed in two steps: first, the internal pressure is applied to the inside face of each element (step 1) and then external hydrostatic loads are applied (step 2). The hydrostatic loads are the result of an external pressure field acting normal to the membrane’s surface. Based on the Ramspol barrier’s dimensions, the elements of this model will have a uniform thickness of 16 mm and uniform material properties.[8] For all numerical examples, the

modulus of elasticity of the rubber-coated nylon fabric is 3.00 GPa, the density is 997 kg/m^2, and Poisson's ratio is 0.45. The initial model has a circumferential length of 24.3 m and a fully inflated height of 8.2 m.[9] The barrier is analyzed with internal air pressures ranging from 20 kPa to 40 kPa, in increments of 5 kPa. Each trial is carried out under various hydrostatic conditions to determine the vertical crest displacement and stresses in the membrane. The external loading conditions depend upon upstream head ranging from 1 m to 8 m, while the downstream head is set at four levels: 0 m, 2 m, 4 m and 8 m. Varying these conditions shows how the membrane responds, both in form and internal tensile loading, to various external hydrostatic conditions and at different levels of internal pressure. According to the Japanese Standard, based on experience with inflatable barriers in Japan, the initial design tensile strength should be 9 times the static loads calculated for two-dimensional cross-section.[10] This general safety factor covers all material aspects (e.g. creep and UV degradation) as well as additional loadings (e.g. hydrodynamic loads). The performance of the barrier can thus be verified in accordance with these guidelines.

Results

In the first stage (i.e. the inflation stage), the circular arc shape is representative of a nearly uniform stress throughout the membrane. Figure 1 illustrates this semicircular shape representative of the membrane's stresses and displacements for the five internal pressures (20, 25, 30, 35 and 40 kPa).

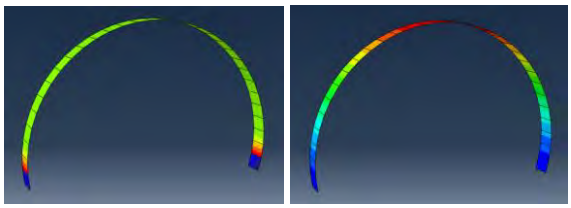

Figure 1: Equilibrium Stresses and Displacements After Inflation

While the initial step of applied internal pressure results in the same shape for all five scenarios, the maximum principal stress (m.p.s.) varies greatly between each trial. For an internal pressure (i.p.) of 20 kPa, the m.p.s. is 8,364 kPa. This pressure rises significantly to 12,560 for an i.p. of 30 kPa, and 16,780 for an i.p. of 40 kPa. The second step adds the hydrostatic forces in both the upstream and downstream direction. Twenty tests of varying upstream and downstream heads are carried out for each internal pressure; a total of a hundred different loading combinations. Table 1 displays the highest value of the max principal stress and the corresponding vertical crest displacement, as well as the lowest max principal stress and corresponding displacement. Table 1 also provides maximum and minimum positive and negative crest displacements. The results show that as the internal pressure increases, the overall max principal stress throughout the barrier increases, irrespective of the various hydrostatic forces acting on the membrane. In this regard, the greatest m.p.s. for all hundred loading combinations occurs when there is an i.p. of 40 kPa, an upstream head of 2 m head and zero downstream head. These conditions produce the greatest maximum stress in the membrane because the internal pressure is high and there is a relatively high variance between the upstream pressure and downstream pressure.

	Stress (kPa)	Displacement (cm)	Internal Pressure (kPa)	Upstream Head (m)	Downstream Head (m)
High Max Principal Stress	**16,790**	5.3	40	2	0
Low Max. Principal Stress	**7,769**	-13.4	20	8	2
Max Positive Displacement	13,660	**83**	40	8	8
Min. Positive Displac.	8,356	**2.4**	20	1	0
Max Negative Displac.	10,870	**-13.5**	30	8	0
Min Negative Displac.	10,840	**-11.7**	30	8	2

Table 1: Maximum and minimum values for principal stresses and displacements under various loading conditions.

On the other hand, the lowest maximum principal stress occurs under internal pressure of 20 kPa, an upstream head of 8 m and zero downstream head. The variance between the upstream and downstream head is still high, but the internal pressure is 20 kPa lower than the previous result. When the upstream and downstream heads are at their maximum value of 8 meters (78.24 kPa), the vertical crest displacement is greatest for all five internal pressure scenarios. The crest height falls however when there is significant upstream head and relatively small downstream head. This negative displacement is greatest when there is an internal pressure of 30 kPa, an upstream head of 8 m and zero downstream pressure.

Discussion

Depending on the internal pressure, in addition to the upstream and downstream forces, there are four distinct equilibrium shapes the membrane can adopt. When there is only internal pressure applied, the sheet will form an arc of a semi-circle, regardless of the magnitude (see Figure 2a). However, when an upstream pressure is applied, the membrane will begin to displace in the vertical and horizontal direction (see Figure 2b). As this external pressure reaches a maximum value of the initial crest height (8 m), the membrane forms an inverse curve (see Figure 2c). Lastly, if the downstream head rises to meet the upstream head, the equilibrium shape will gradually move toward a bell-shaped curve (see Figure 2d). These shapes match the ones described in Watson.[11] When there is a relatively small upstream pressure, the tension in the barrier gradually increases along the length of the membrane then decreases from one anchored point to the next (see Figure 3.a). The lowest stresses occur in the region where the upstream pressure is greatest because the hydrostatic forces counteract the uniform force of the internal air pressure. The downstream pressure in these cases vary from 2 m to 8 m, where the lowest stresses tend to occur when both upstream and downstream heads are relatively high. At the same time, the greatest vertical displacement occurs along the length of the membrane is exposed to internal pressure only. The new crest height is thus the sum of the initial crest height of 8.2 m and the vertical displacement of approximately 32 cm; a total height, h_{crest1}, of 8.52 m. (see Figure 3.b).

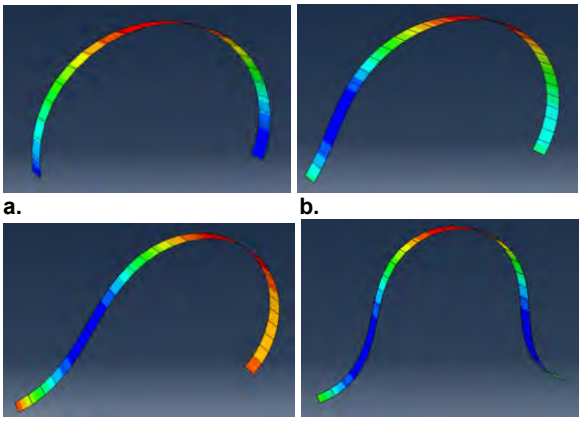

a. b. c. d.

Figure 2: Equilibrium Shapes: (a) Arc of a semi-circle, (b) Crest height displaced vertically and horizontally, (c) Inversion of curvature in membrane, (d) Bell shaped

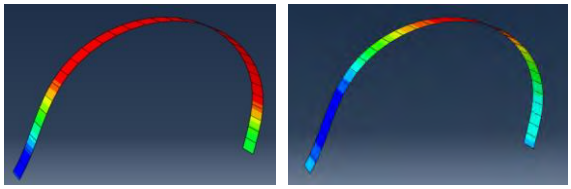

a. b.

Figure 3: (a) Stress plot of 30 kPa internal air-filled barrier membrane with 6 m upstream head and 4 m downstream head, (b) Vertical displacement plot. Principal stresses range from 4,350 kPa (Blue) to 1,180 kPa (red). Displacements range from -1 cm (blue) to 3.2 cm (red).

By increasing the upstream head from 6 m to 8 m (see Figure 4.a. and b), the maximum principal stress decreases along the length of the sheet as the greater external forces acting upon the membrane counterbalance the internal pressure. At the same time, the maximum vertical displacement increases from 32.68 cm to 38.43 cm (downstream).

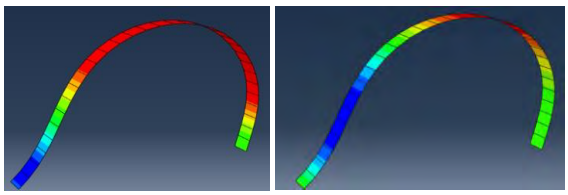

a. b.

Figure 4: (a) Stress plot of 30 kPa internal air-filled barrier membrane with 7 m upstream head and 4 m downstream head (b) Vertical displacement plot. Principal stresses range from 1,370 kPa (Blue) to 11,140 kPa (red). Displacements range from -4.4 cm (blue) to 3.8 cm (red)

By increasing the upstream head to 8 m, the maximum principal stress further decreases along the length of the sheet. However, because the internal pressure is not high enough, the max vertical displacement decreases from 38.3 cm to 31.4 cm, lower than the vertical displacement experienced by the 6 m upstream head and 4 m downstream head conditions. This is because there is a greater difference between the upstream and downstream heads. As this variance increases, there will be a greater horizontal displacement, and inversion will occur (see Figure 5), where there is an upstream head of 8 m and zero downstream head. In this case, the crest height significantly decreases, from a previous value of approximately 8.4 m to 8 m, 20 cm below initial height of the fully inflated membrane. If the static upstream head were to increase any further, it would exceed the crest height and spillover of the water would occur.

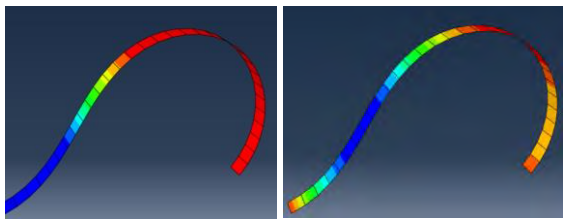

a. b.

Figure 5: (a) Stress plot of 20 kPa internal air-filled barrier membrane with 8 m upstream head and 0 m downstream head. (b) Vertical displacement plot. Principal stresses range from 0 kPa (Blue) to 7,800 kPa (red). Displacements range from -1.37 cm (blue) to 1.19 cm (red)

When the upstream and downstream heads are equal, the stress distribution is symmetrical and the greatest tension in the membrane is located at the crest, where the largest vertical displacement is taking place (see Figure 6). This bell-shaped curve is accentuated when the internal pressure is lower and the membrane stiffness is not as high, as evident by the steeper slope of the upstream and downstream sides for an internal pressure of 20 kPa (as compared to an internal pressure of 40 kPa).

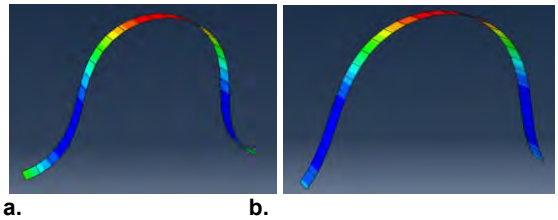

a. b.

Figure 6: (a) Displacement plot of 20 kPa and (b) Displacement plot of 40 kPa internal air-filled barriers with 8 m upstream head and 8 m downstream head.

When plotting the vertical displacements for internal pressures 20 kPa (light blue curve) and 25 kPa (orange curve) in Figure 7, the crest heights peak sooner (in regard to external upstream pressure) than those ranging from 30 kPa (grey curve) to 35 kPa (yellow curve). The vertical displacement for an internal pressure of 40 kPa (dark blue curve) exhibits a more gradual rise, as the membrane's stiffness has increased, (assuming there is no change in the external hydrodynamic conditions), thus minimizing both horizontal and vertical displacement. Spillover is also less likely to occur with a larger internal pressure; however, that condition correlates to greater maximum principal stresses in comparison to lower pressurized membranes (peak stress is approximately twice the magnitude for an internal pressure of 40 kPa in comparison to an internal pressure of 20 kPa). It can be observed that convergence occurs at an upstream head of approximately 5.25 m for the light blue and orange curves (internal pressures 20 and 25 kPa respectively), and at an upstream head of approximately 6.25 m for the grey and yellow curves (internal pressures 30 and 35 kPa respectively). Convergence of the grey and dark blue

curves (30 kPa and 40 kPa) also occurs at a lower upstream head than convergence of the yellow and dark blue curves (35 kPa and 40 kPa). This means that the crest height will begin to fall at lower upstream pressure heads for lower pressurized systems than higher pressurized systems.

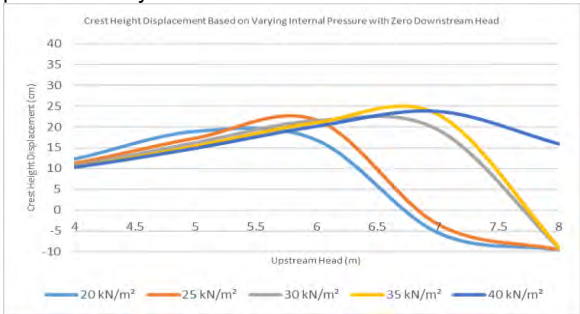

Figure 7: Crest height displacement based on varying internal pressures (air only) with a downstream head of 0 m.

The membrane exhibits a similar response for all five different internal pressures, but with a downstream head of 4 m, as shown in Figure 8. Convergence in this case occurs at an upstream head of approximately 6.25 m for the light blue and orange curves (internal pressures 20 and 25 kPa respectively), and at an upstream head of approximately 7 m for the grey and yellow curves (internal pressures 30 and 35 kPa respectively).

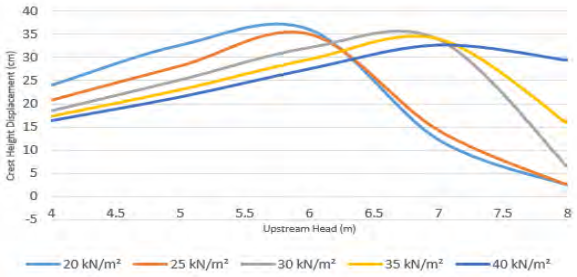

Figure 8: Crest height displacement based on varying internal pressures (air only) with a downstream head of 4 m.

This means that at a lower downstream head, the pressurized membrane tends to displace at a lower upstream head, regardless of the internal pressure. Furthermore, regardless of the upstream head, the membrane will exhibit an overall larger max principle stress.

Conclusion

This study yields insight to whether a large-scale inflatable barrier is suitable as a coastal defense technology for certain flood-prone areas in the U.S. Using numerical analysis, the following insights are gained. (i) The stresses in the membrane increase with internal pressure, regardless of the external upstream and downstream pressure loads. (ii) For internal pressures ranging 20 - 25 kPa, the vertical crest height displacement reaches its peak at lower upstream heads than for membranes with internal pressures ranging 30 – 40 kPa, regardless of the downstream head. (iii) Regardless of the internal pressure, the membrane will exhibit a larger positive crest height displacement when the downstream head rises and a larger negative crest height displacement at lower downstream heads when the upstream pressure rises.

From the numerical results, it can be determined that the optimal internal pressure lies between 30 and 35 kPa for the majority of upstream and downstream conditions because the membrane exhibits a relatively low stress without compromising a large negative crest height displacement at high upstream pressures. The reaction forces for these load combinations will provide input to verify the foundation design. Moreover, different barrier properties, such as thickness and width between anchoring lines, can also be tailored to optimize the barrier response to various loading conditions.

References

[1] Emanuel, K. A. (2013). Downscaling CMIP5 climate models shows increased tropical cyclone activity over the 21st century. Proceedings of the National Academy of Sciences,110(30),12219–12224. https://doi.org/10.1073/pnas.1301293110.
[2] Plaut R.H., Liapis S.I., and Telionis D.P. (1998). “When the levee inflates”. ASCE, Vol. 68, No. 1.
[3] Michael Gebhardt. Inflatable Structures in Hydraulic Engineering August 2013. Smart Rivers Conference.
[4] N.H. Rövekamp, Storm Surge Barrier Ramspol, Hollandsche Beton- en Waterbouw, Engineering Department, Gouda, The Netherlands.
[5] Breukelen, Marjolein van (2013). “Improvement and scale enlargement of the inflatable rubber barrier concept.” In: Maste Thesis, Delft University of Technology (cit. on p. 48).
[6] H.B. Harrison, (1970). The analysis and behavior of inflatable barriers under static loading. Proceedings of the Institution of Civil Engineers, 45:661-676.
[7] J. Bonet, R. D. Wood, J. Mahaney, P. Heywood, Finite element analysis of air supported membrane structures. Computer Methods in Applied Mechanics and Engineering, 190, 2000.
[8] ABAQUS 1994 *Theory Manual*, Vol. I, Version 5.4 Pawtucket, RI: Hibbitt, Karlsson & Sorensen, Inc.
[9] Mysore, Liapis and Plaut. Dynamic Analysis of Single-Anchor Inflatable Dams, March 1998. Journal of Sound and Vibration.
[10] Ryszard Daniel, Tim Paulus. Lock Gates and Other Closures in Hydraulic Projects, November 2018
[11] Bas Reedijk, Case study inflatable storm surge barrier Ramspol, August 1999. Conference: Post Academic Course Delft University.
[12] Abdullah Ali, Nasser Alhamati, et al. Behavior of Inflatable Barriers Under Hydrostatic Conditions, December 2004.
[13] Marjolein van Breukelen (2013). Improvement and scale enlargement of the inflatable rubber barrier concept: A case study applicable to the Bolivar Roads barrier, Texas, USA.
[14] Dorremans, (1997). Balgstuwen gevuld met lucht en/of water. Master's thesis, Technical University of Delft.
[15] Kaj van der Valk (2014). Life Cycle Costs: a comparison between inflatable and traditional barrier; Master thesis.
[16] Watson, R., 1985. A note on the shapes of flexible dams, Journal of Hydraulic Research, Vol. 23, No.2, 179-194.

Global bioretention cell guidelines: a review and recommendations to meet hydrological performance targets

M. Bacys[a], U. T. Khan[b,*], J. Sharma[c], T. R. Bentzen[d]

[a] MSc Water & Environment graduate, Dept. of Civil Engineering, Aalborg University, Thomas Manns Vej 23, 9220 Aalborg, Denmark.
[b] Assistant Professor & Graduate Program Director, Dept. of Civil Engineering, York University, Toronto, ON M3J 1P3, Canada
[c] Professor, Dept. of Civil Engineering, York University, Toronto, ON M3J 1P3, Canada
[d] Associate Professor & Head of Study Board, Dept. of Civil Engineering, Aalborg University, Thomas Manns Vej 23, 9220 Aalborg, Denmark
* Corresponding author, Tel 416-736-5890, email usman.khan@lassonde.yorku.ca

Extended Abstract:
With increasing urbanization and land development, more urban landscapes are being covered with impermeable surfaces, such as roofs, parking lots, roads, and pathways [1]. These surfaces restrict the natural flow of water and consequently impair processes, such as evapotranspiration (ET), infiltration, percolation, detention and retention of water, while at the same time generating overland flow that has not only increased volume, but also higher flow rates [1]. In order to reduce the negative environmental impacts many jurisdictions have adopted regulations in terms of reducing runoff quantity and improving runoff quality. Some of the more popular global initiatives established for easing the effects of urbanization have been termed low-impact development (LID) in North America and Canada, water-sensitive urban design (WSUD) in Australia, and sustainable drainage systems (SuDS) in the UK [2]. Many of these practices are similar or have the same objective, primarily, to try to mimic the natural hydrology of a site for stormwater management (SWM) purposes. Bioretention cells (BRCs also called bioretention, bioinfiltration, or rain gardens) are a type of stormwater control measure (SCM) frequently used as LID practices.

Figure 1 shows a cross-sectional area of a typical BRC configuration, highlighting the different design parameters. BRCs are densely-planted depressions on a ground, typically comprising a ponding layer, a mulch layer, bioretention soil media (BSM) layer, and storage layer. Some of the optional or site-specific components include: underdrains, internal water storage layer, transitional layer between BSM, and storage, geotextiles or impermeable liners. Finally, additional design specifications that affect the performance of the cells are BRC-to-impervious surface area ratio, drawdown time of the ponded water, BSM's texture, BSM's saturated hydraulic conductivity, and the depth from the bottom of the BRC to the seasonal high-water table (SHWT).

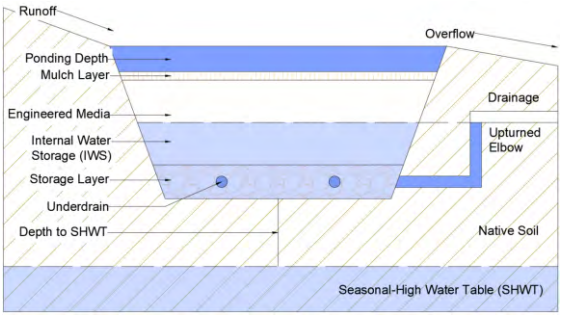

Fig 1: Schematic cross-section of a typical bioretention cell.

As BRC practices become more popular for urban stormwater management purposes, many jurisdictions are dedicating more time and effort on developing their own BRC design guidelines. However, as the number of these guidelines increases, it is imperative to know if they meet hydrological performance targets and whether they account for local climatic conditions and other variations.

In this research, twenty-four global bioretention cell design guidelines from four different continents were reviewed, compared, and classified based on their main climate (using the Köppen-Geiger climate classification), temperature, and precipitation. Nine key BRC design parameters were selected, including: (i) minimum BRC area as a percentage of the upstream impervious catchment area; (ii) maximum ponding depth; (iii) maximum drawdown time; (iv) maximum thickness of the mulch layer; (v) minimum thickness of the BSM; (vi) minimum thickness of the storage

layer; (vii) minimum saturated hydraulic conductivity of the media; (viii) BSM's texture; and lastly, (ix) minimum depth from the bottom of the BRC to the SHWT. These parameters were chosen for the comparison because most of the guidelines provide specifications for these aspects of the BRC design.

The review and comparison of the guidelines showed no categorical (e.g. precipitation- or temperature-based) trend of the recommended BRC design parameters across the different regions. Most of the guidelines recommend similar criteria for different BRC design aspects regardless of the location of the jurisdictions that prepared them. For example, Figure 2 shows a summary of the minimum BRC area recommended by all the guidelines for different climatic categories. The majority of guidelines, regardless of climatic category, recommend sizing the BRC to 2% to 10% (with some exceptions that recommend an upper limit of 20%) of the upstream drainage area. These recommendations are consistent despite widely different precipitation patterns and native soil types in the jurisdictions reviewed.

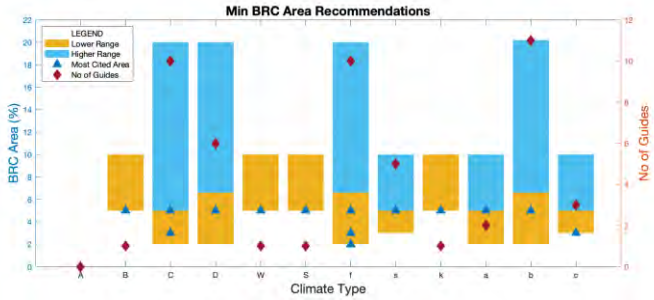

Fig 2: A summary of bioretention cell (BRC) area as a percentage of the upstream drainage area for all twenty-four jurisdictions

This example and the broader review suggest that these design guidelines have not adequately considered the local climatic conditions. They appear to adopt a more generic approach based on recommendations from other jurisdictions that have carried out more research in to the design and performance of BRCs. While this is a good starting point when little to no information is available on BRC performance in a given climate, it is not a sustainable practice in the longer term as BRC's performance is also climate dependent [3-4]. Specifically, climatic conditions affect plant types and their health, soil media type availability, portion and type of pollutants, rain intensities and durations, safety concerns, humidity, etc., all of which are important design parameters that influence BRC performance. Thus, while it might be a good idea to extend cooperation between jurisdictions located in close proximity to one another and containing similar conditions (as that would also save some costs associated with preparation of these reports), it is not advisable to use the guidelines from locations with obvious climatic differences. Hence, the creation of climate-specific design guidelines is recommended through a combination of extensive lab and field-testing and numerical modelling and simulations.

Following this review, a numerical analysis was performed to determine the optimum BRC design parameters to meet hydrological performance targets for one jurisdiction (Toronto, Ontario, Canada). For this analysis, first a numerical model of a BRC using PC Storm Water Management Model (PCSWMM) and local hydrological parameters for a residential area in the North York region of the city was developed. Following this, local sensitivity analysis (LSA) (with one-factor-at-a-time method) and global sensitivity analysis (GSA) (with factorial design) was performed on the nine BRC design parameters highlighted above to optimize BRC design recommendations to meet hydrological performance targets (i.e., capture 27 mm of precipitation) for Toronto, Ontario, Canada. The model was driven using both event-based (several return periods) and continuous precipitation data. The LSA found the BRC surface area, the saturated hydraulic conductivity of the soil media, and the ponding depth to be the most dominant design parameters in ensuring adequate runoff reduction. The GSA found that simultaneous increase of BRC surface area, saturated hydraulic conductivity, and storage depth leads to the highest performance in BRC. The key conclusions from LSA and GSA are: BRC overflow can be reduced by increasing BRC surface area, BRC ponding depth, or media hydraulic conductivity; and, the media hydraulic conductivity should be increased along with storage depth.

The minimal recommendations of Ontario's BRC design guidelines can capture and treat close to 100% of the annual North York runoff even when the BRC is installed in loamy soils; and BRCs designed to the minimal Ontario design guidelines are not capable of managing the 27 mm hydrological targets in Toronto. However, this requirement can be met by minimal design perturbations of, for example, 0.4% increase in BRC surface area, 5 cm addition to ponding depth, or 3 cm/h increase in BRC media hydraulic conductivity [5].

The proposed numerical modelling approach along with the LSA and GSA can be used in other jurisdictions to check whether the published design guidelines meet the local hydrological targets, and can highlight which design parameters need to be adjusted to find the optimum BRC design

Keywords:
bioretention cells, stormwater management, low impact development, sensitivity analysis, design

Acknowledgements

The authors would also like to thank CHI Inc. for granting the license for the student version of the PCSWMM model for this research.

References

[1] Davis, A.P. Green Engineering Principles Promote Low-Impact Development. Environ. Sci. Technol. 39 (2005), 338A–344A.

[2] Fletcher, T.D., Shuster, W., Hunt, W.F., Ashley, R., Butler, D., Arthur, S., Trowsdale, S.A., Barraud, S., Semadeni-Davies, A., Bertrand-Krajewski, J.L., Mikkelsen, P.S., Rivard, G., Uhl, M., Dagenais, D., Viklander, M.. SUDS, LID, BMPs, WSUD and more – The evolution and application of terminology surrounding urban drainage. Urban Water J. 12 (2015), 525–542.

[3] Khan, U.T., Valeo, C., Chu, A., van Duin, B. Bioretention cell efficacy in cold climates: Part 1 — hydrologic performance. Can. J. Civ. Eng. 39 (2012a), 1210–1221.

[4] Khan, U.T., Valeo, C., Chu, A., van Duin, B. Bioretention cell efficacy in cold climates: Part 2—water quality performance. Can. J. Civ. Eng. 39 (2012b), 1222–1233.

[5] Bacys, M., Khan, U. T., Sharma, J., & Bentzen, T. R. Hydrological Efficacy of Ontario's Bioretention Cell Design Recommendations: A Case Study from North York, Ontario. Journal of Water Management Modeling 27 (2019).

The Low Impact Development Demand Index: a geospatial framework to identify LID demand for three Canadian cities

S. Kaykhosravi[a], K. Abogadil[b], U. T. Khan[c,*], A. Jadidi[d]

[a] PhD candidate, Dept. of Civil Engineering, York University, Toronto, ON M3J 1P3, Canada
[b] Research assistant, Dept. of Civil Engineering, York University, Toronto, ON M3J 1P3, Canada
[c] Assistant Professor & Graduate Program Director, Dept. of Civil Engineering, York University, ON M3J 1P3, Canada
[d] Assistant Professor, Geomatics Engineering, Department of Earth & Space Science & Engineering, York University, Toronto, ON M3J 1P3, Canada

* Corresponding author, Tel 416-736-5890, email usman.khan@lassonde.yorku.ca

Extended Abstract:
Increased urbanization has led to a significant increase of impervious surfaces. This has led to higher levels of stormwater runoff, resulting in higher flood risks, overflowing sewer systems, and damage to existing stormwater infrastructure [1]. Low impact development (LID) has become one of the most popular methods for managing urban stormwater [2-3], and examples include bioretention cells, green roofs, detention tanks, and permeable pavement systems. LID are primarily used for stormwater management (i.e., to reduce the volume of runoff, reduce peak flow, and reduce the overall risk of urban floods); however, there are several indirect environmental and socioeconomic benefits, such as improved public health and enhanced air quality that result from implementing LID in urban areas. In identifying feasible sites for LID, previous research has only considered the hydrological benefits, while largely ignoring the significant secondary or "co-benefits" of LID. In order to maximize all the benefits of LID, sites must be identified with consideration of hydrological, environmental and socioeconomic benefits. This research aims to solve this spatial decision-making problem through a geospatial framework that is based on publicly available data, hydrological-hydraulic principles, and an analytic hierarchy process (AHP) model. This framework is then applied to three Canadian cities (Vancouver, Toronto and Montreal) to determine both the current and future LIDDI. The future LIDDI scenarios use future climate change scenarios (using precipitation data from global circulation models) and project urban growth trends in each city to determine how the demand for LID may change in the future.

The LID demand was determined by developing and combining three indices: (1) hydrological and hydraulic index (HHI), (2) socioeconomic index (SEI), and (3) environmental index (ENI). A heuristic model based on hydrological-hydraulic principles was used to develop the HHI: it included the spatially distributed data of the study region where the LID are to be installed, specifically the rainfall intensity, the hydraulic conductivity of the native soils, the water storage capacity of the soils (based on the average porosity), and the catchment slope. The SEI combined the population density, the existing green infrastructure, and important socioeconomic institutions (e.g., hospitals and schools) as indicators of socioeconomic benefits of LID. Lastly, the ENI combined indicators for air and water quality, and biodiversity to represent the environmental benefits of LID. Using the AHP model, SEI and ENI are integrated into HHI, resulting in the low impact development index (LIDDI) that determines the demand or need for LID within a region.

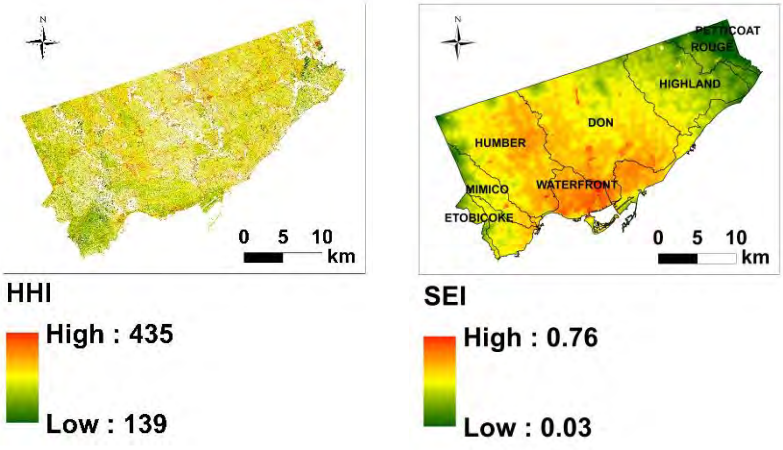

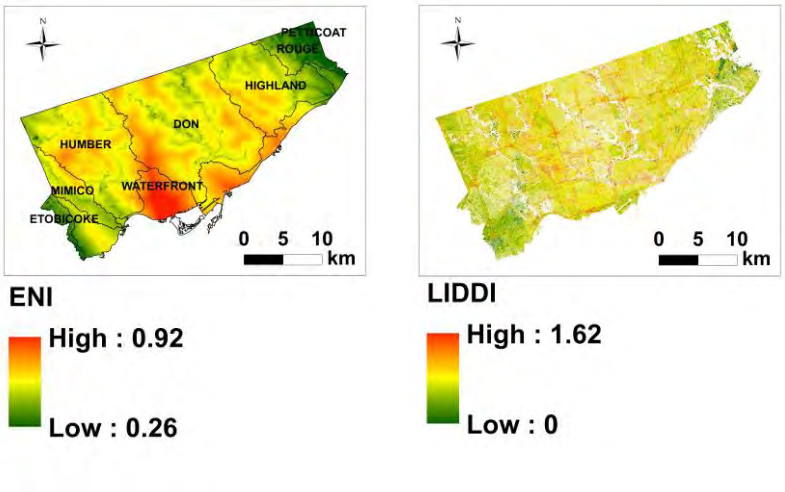

Figure 1: The spatial distribution of the hydrological-hydraulic index (HHI), the socioeconomic index (SEI), the environmental index (ENI), and the integrated Low Impact Development Demand Index (LIDDI) for Toronto, Canada.

Fig 1 demonstrates the application of the proposed LIDDI for the City of Toronto, in Ontario, Canada. Data from open source data portals was used to create each index, which were then combined to generate the LIDDI. Higher values of LIDDI (in red) are areas that have a relatively higher "demand" or "need" for LID within the city, and vice versa for areas with a lower values of LIDDI (in green) [4]. It is important to note that these results not only consider the hydrological and hydraulic function of different types of LID and their role in reducing urban runoff generation, but also considers the secondary benefits. Thus, this analysis can help city planners and stormwater management professionals to systematically decide where LID need to be installed within a city.

Following this, future climate change data, specifically intensity-duration-frequency curves from [5] were used to update the rainfall intensity data used within the LIDDI framework. Future scenarios included the three commonly used Representative Concentration Pathways (RCP, 2.6, 4.5, and 8.5) for three future periods (2030s, 2050s and 2090s). Several rainfall stations were used for each city to determine the spatial distribution of rainfall for future conditions for the HHI calculations. Project population data for each city to coincide with the three future periods of analysis were collected from several sources [6-8]. A heuristic method to relate the population, population density, land-cover type (pervious or impervious) was developed to determine the future urbanization levels for each city. Analysis of the data shows a near-uniform increase of rainfall intensity for each city, highlighting a higher demand for LID within each city. Urban growth projections result in much higher degree of urbanization for each city (as shown in Fig 2); while Vancouver and Toronto will still have a significant portion of pervious areas, Montreal land cover is projected to be mostly impervious. This represents a combination of the current level of impervious areas, and the expected change in population (and hence degree of urbanization) in the future.

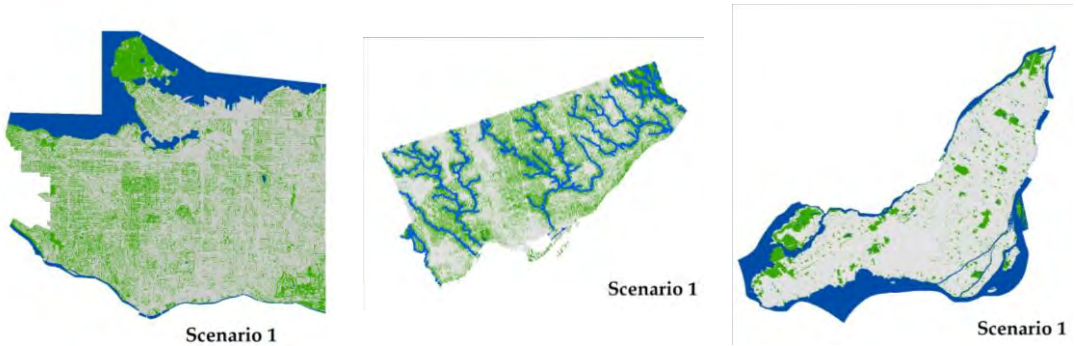

Figure 2: Degree of urbanization in Vancouver, Toronto, and Montreal, for future climate scenarios

Preliminary results suggest that the change in rainfall intensity due to climate change in each city will have a comparatively lower impact on runoff generation, and hence need for LID within the cities, as compared to the degree of urbanization due to increasing population. Given that Canada's population is projected to increase by approximately 50% [9] by 2068, and with the majority of the increase in urban areas [10], the runoff generation potential, and hence, the demand for LID will increase significantly. The

effects of climate change may exacerbate this phenomenon. This research shows that the need for LID to manage stormwater will also increase significantly in Canadian cities, and a systematic approach (as proposed in this research) to determine where to install LID to achieve hydrological and hydraulic benefits, as well as the socioeconomic and environmental benefits should be used.

Keywords:
low impact development, sustainable urban drainage systems, stormwater modelling, urbanization, climate change

Acknowledgements

The authors would like to thank Natural Sciences and Engineering Research Council of Canada for funding this research.

References

[1] Frantzeskaki, N.; Kabisch, N.; McPhearson, T. Advancing urban environmental governance: Understanding theories, practices and processes shaping urban sustainability and resilience. Environ. Sci. Policy, 62 (2016), 1–6.

[2] Coffman, L.; Clar, M.; Weinstein, N. Overview of low impact development for stormwater management. In Proceedings of the 25th Annual Conference on Water Resources Planning and Management, Chicago, IL, USA, 7–10 June 1998; pp. 16–21.

[3] Fletcher, T.D.; Shuster, W.; Hunt, W.F.; Ashley, R.; Butler, D.; Arthur, S.; Trowsdale, S.; Barraud, S.; Semadeni-Davies, A.; Bertrand-Krajewski, J.-L.; et al. SUDS, LID, BMPs, WSUD and more—The Evolution and Application of Terminology Surrounding Urban Drainage. Urban Water J. 12 (2015), 525–542.

[4] Kaykhosravi, S., Abogadil, K., Khan, U. T., & Jadidi, M. A. The Low-Impact Development Demand Index: A New Approach to Identifying Locations for LID. Water, 11(2019), 2341.

[5] Institute for Catastrophic Loss Reduction; Western University Computerized Tool for the Development of Intensity-Duration-Frequency Curves under Climate Change – Version 4.0, IDF_CC Tool 4.0.

[6] Ontario Ministry of Finance Ontario Population Projections, 2018–2046: Based on the 2016 Census, for Ontario and its 49 Census Divisions. (2019).

[7] QUÉBEC, I.D.L.S. DU Perspectives démographiques des MRC du Québec, 2016-2041; (2019).

[8] MetroVancouver. Metro Vancouver Growth Projections – A Backgrounder (2018).

[9] Statistics Canada. Population projects: Canada, provinces and territories (2018 to 2068). Statistics Canada (2019).

[10] Editorial. Canada's cities are about to add millions of new residents. They can't all drive to work. The Globe and Mail (2020, January 6).

Assessment of Feasibility of Hollow Core Slabs in Building Construction Considering Cost, Energy, and Carbon Imprint

A. Noman[a], A. Bagchi[b], A. Athienitis[c]

[a] PhD student, BCEE Dept. Concordia University, Montreal, QC, Canada. Email: asnoman71@gmail.com
[b] Chair and Professor, BCEE Dept. Concordia University, Montreal, Canada. Email: ashutosh.bagchi@concordia.ca
[c] Professor, BCEE Dept. Concordia University, Montreal, QC, Canada. Email: aathieni@encs.concordia.ca

Abstract:
Building energy can be categorized into two parts: operational energy and non-operation-stage energy, commonly known as embodied energy. While operational energy is mostly utilized in temperature control and electrical appliances and machinery, embodied energy is associated with a building from cradle to grave: construction materiel production, transportation, disposal, and recycling of materials, and during their construction and demolition. Recently, ventilated hollow core slabs (VHCS) are being considered a viable option for improved thermal energy performance of floors. Also, the reduction in slab concrete due to the presence of hollow cores and prestressing can have a cumulative weight reduction from top to foundation. Such reduction has a benefit of reduced seismic design forces for the building situated in high earthquake-areas. This study is an attempt to quantify the changes in cost, embodied energy, and carbon footprint for adopting VHCS instead of more commonly used flat slabs and slabs-on-beams floor systems. A set of case-studies were explored for rectangular buildings with 5 and 15 storeys in Montreal for all three slab types in consideration. The changes in structural cost, embodied energy, and carbon imprint were calculated and discussed. It has been found that a reduction in embodied energy and embodied carbon emission is possible by adopting a VHCS floor system instead of the other two types, while the frames with slabs-on-beams have been found to have the least structural costs.

Keywords:
Hollow-core slab, VHCS, flat-slab, embodied energy, carbon emission

1. Introduction

For a sustainable future, a building systems should be energy efficient for its entire life cycle. Hence, building materials, for both load-bearing components and environmental envelops, should consume less energy and have minimal impact on carbon imprint during production, construction, operation, demolition, disposal, and recycling. To optimize the load-bearing system for reduced embodied energy and environmental impact, an integrated engineering design approach is needed.

A building-integrated thermal energy storage system (BITES), consisting mostly of the structural skeleton, envelop, and partition walls, can absorb and release a significant amount of thermal energy from and to the spaces for temperature modulation [1–3]. For moderate amplitude of space-conditioning loading, the BITES with exposed surfaces of walls and slabs can form sufficient thermal coupling [4–6]. For high conditioning amplitude load, as in cold weather, a stronger thermal coupling is required [7–9]. As an alternative, active BITES with hollow-core (HC) slabs and walls have attracted significant research interest [7, 10–14]. Also, the hollow cores in slabs are likely to result in reduced weight of a building and thereby reduce the earthquake loading on the structure. This can benefit the buildings more in the areas of high seismic hazard.

This study investigates the feasibility of the building structural frames with Hollow Core Slabs (HCS) systems compared to those with flat slabs and slabs-on-beams.

A common aspect of all three structural forms considered in this study is that they are all made of reinforced concrete (RC), which is the most widely used construction material for buildings worldwide. The total amount of embodied energy and associated carbon emission in reinforced concrete structures is considered to be much higher than those built with steel and timber. A comparative study among the buildings with RC, steel, steel-timber composite, and steel-concrete composite structural frames shows that the RC building has the largest embodied energy [15]. The cement production consists of 5% of the global CO_2 emissions due to human activities [16]. Also, concrete structures are found to induce 73% of environmental impacts in the construction industry [17]. Hence, the minimization of both embodied and carbon emission in addition to the cost reduction should be considered in designing structures. Accordingly, three constraints—cost, embodied energy, and carbon imprint, were explored in this study.

2. The case study

This is a parametric design study for combined minimization and/or optimization of cost, embodied energy, and CO_2 emission of a group of RC residential buildings with HCS, flat slabs, and slabs-on-beams floor systems of 5 and 15 storeys, located in Montreal, Canada. The building has a plan area of 1974 m^2. The plan of the prototype buildings is shown in Fig. 1. An

RC shear wall core is located in the middle of the building.

The thickness of the walls was kept constant for the building with the same number of stories. For 5- and 15-storey variants, 3 and 9 different square column types were considered. The dimension of a column type was varied with the reinforcement ratio. In the design analysis, the maximum reinforcement of columns was varied approximately from 2 to 5%. Hence, a large array of column cross-sectional dimensions was used in the analysis

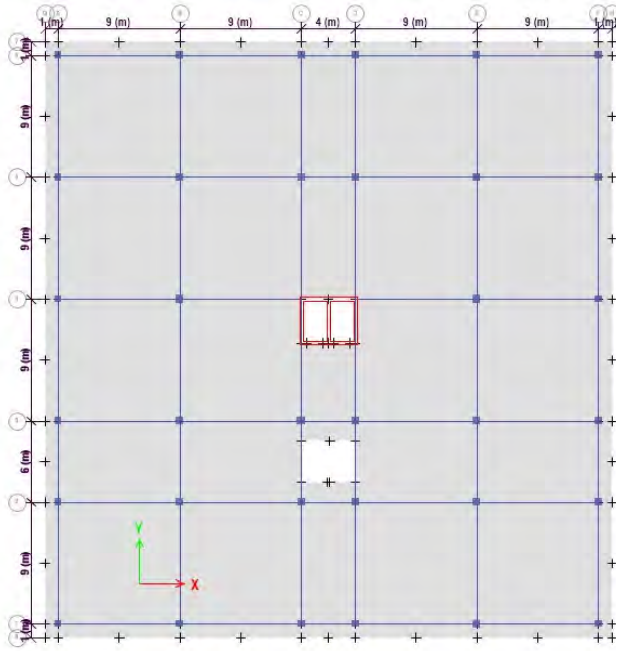

Fig. 1: The Typical Grid Plan

For the slabs-on-beams systems, RC beams of web width of 300 mm and depth of 650 mm for all span were assumed. A slab thickness of 205 mm, as calculated by the Code equation, was assumed. The slab thickness for flat slabs was taken as 285 mm, as calculated from the Code equation. A 1 m × 1 m drop panel of 150 mm thickness was assumed for all columns. For the HCS systems, the typical module designed was 1.22 m wide and 203 mm deep. A 50 mm topping was assumed. The net cross-sectional area is 139, 700 mm^2. Each module has 5 nos. 12.7 mm dia. prestressing strands. For the slab supports, 600 mm deep T-beams with a 300 mm wide web and 1000 mm wide and 200 mm thick flange were assumed. A typical cross-section of an HCS module is shown in Fig. 2. The design parameters are shown in Table 1

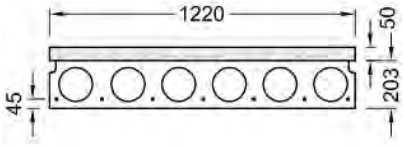

Fig. 2: Cross-section of a hollow-core slab module

In the case of the 5-storey building, no cross-sectional reduction of columns and walls over height was made. The sectional reduction was done for column and wall at a 5-storey interval over height for 15-storey variants. The design optimization of the shear walls is beyond the scope of the study.

Table 1: Design parameters

Name	Value
f'_c (column concrete)	35 MPa
f'_c (HCS concrete)	40 MPa
f'_c (other slab concrete)	25 MPa
f_y (mild steel)	400 MPa
f_{pu} (prestressing steel)	1860 MPa
Floor load:	
Live load	1.9 kPa
Partitioning + floor finish (dead load)	3.0 kPa
Wind analysis:	
Velocity pressure	0.42 kPa
Gust effect factor, C_g	2.0
Importance factor, I_W	1.0
Terrain Type	Rough
Dynamic Earthquake Analysis:	
Peak ground acceleration	0.377
Site class	C
Importance factor, I_E	1.0

National Building Code of Canada, 2015 (NBCC 2015) was followed for load analysis [26-27], and the design of components was performed according to the Canadian concrete structure design standard CSA 23.3-14. The structural programs ETABS, spSlab, and spBeam were used for analysis and design.

3. Objective Functions

For a single rectangular RC beam, Yeo and Gabbai 2011 [18] developed an objective function for the embodied energy. Also, for an RC square column, Yoon et al. 2018 [19] defined the objective functions of cost and CO_2 emission. In practice, continuity of members and the detailing consideration makes it difficult to implement the objective functions stated above accurately. Moreover, optimization of individual members separately does not lead to overall optimization of entire structure because design input and output for structural elements such as slabs,

beams, columns, and shear walls, etc. are interrelated. Therefore, a combined approach is required for overall optimization or minimization of the cost, embodied energy, and carbon imprint. Hence, the objective functions for the entire frame were developed by Noman et al. 2019 [20], as shown in Eq. 1a, 1b &1c.

$$f_c\,(V, M_s) = C^c\left[M_s\left(\frac{R}{100} - \frac{1}{\rho_s}\right) + V\right] \qquad \text{(Eq 1a)}$$

$$f_{ee}\,(V, M_s) = M_s E_e^s + \left(V - \frac{M_s}{\rho_s}\right) E_e^c \qquad \text{(Eq 1b)}$$

$$f_{ec}\,(V, M_s) = M_s E_c^s + \left(V - \frac{M_s}{\rho_s}\right) E_c^c \qquad \text{(Eq. 1c)}$$

where

f_c, f_{ee} & f_{ec} *are* cost, embodied energy, CO_2 emission objective functions respectively.

V = gross concrete volume, m^3

M_s = steel mass, kg

C_C = cost of 1 m^3 concrete

R = cost ratio between 100 kg steel and 1 m^3 concrete.

E_e^c = embodied energy (MJ) per 1 m^3 of concrete

E_e^s = embodied energy (MJ) per 1 kg of the steel

E_c^s = embodied CO_2 emissions (kg-CO_2) per 1 kg of steel

E_c^c = denotes the CO_2 emissions (kg-CO_2) per 1 m^3 of concrete

The value of *R* falls between 0.80 and 1.1 [21 – 23]. The costs for 25, 35, and 40 MPa concretes were taken as CA $165, $186, and $203 per m^3 [24]. The value of *R* is taken as 0.95 for mild steel and 3.0 for prestressing strands. For the values of embodied energy and CO_2 emission coefficients, the table given by Hammond and Jones 2008 [25] was consulted. The embodied energy coefficients for concrete were taken as 1.39 for compressive strength of 35 MPa and 40 MPa, and 1.11 MJ/kg for compressive strength of 25 MPa concrete. By unit conversion, these two values were calculated as 3336 MJ/m^3 and 2664 MJ/m^3, respectively. The embodied energy coefficient for recycled steel was taken as 8.8 MJ/kg and for virgin wires as 36 MJ/kg. The carbon emission coefficients were taken as 0.239 kg-CO_2/kg for 35 MPa and 40 MPa concrete, and 0.159 kg-CO_2/kg for 25 MPa concrete. These two values were then converted to 502 and 382 kg-CO_2/m^3, respectively. The value of the carbon emission coefficient was taken as 0.42 kg-CO_2/kg for recycled steel bars and 2.83 kg-CO_2/kg for virgin wires.

4. Results and discussions

There is a distinct correlation between column steel ratio and column construction cost, as seen in Fig. 3 below for 5-storey frames.

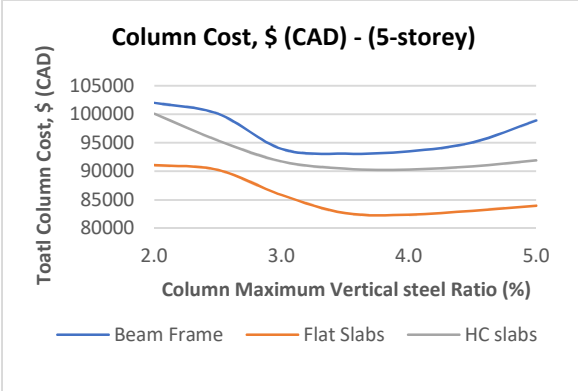

Fig. 3: Column cost for different frames and maximum column steel ratio.

The column cost for HCS frames is in-between other two types. There is a cost-minimum corresponding to the 4% maximum steel ratio. A 10% decrease in cost can be achieved for adopting a maximum steel ratio of 4% instead of 2%. The embodied energy for column in HCS frames is in-between other types, while it has the lowest for carbon emission. In both cases, the values decrease as steel ratios increase.

Total frame cost mostly depends on the floor systems for both 5- and 15-storey variants. Fig. 4 shows this trend for 15-storey frames. Despite being the lightest of all, the HCS frame has been found to be the most expensive, primarily due to a high cost involving pre-stressing on high strength concrete. At a 4% maximum column steel ratio, the HCS frame is 19 & 4.3 % costlier than the slabs-on-beams and flat-slab frames, respectively.

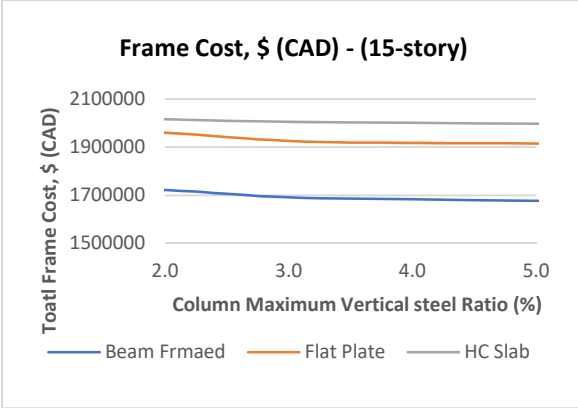

Fig. 4: Total frame cost for column steel ratio and different floor types for 15-storey-frames

On the other hand, in terms of both embodied energy and carbon imprint, the HCS frame has been found to perform the best, as seen in Fig. 5 & 6. This can be attributed to a more effective use of materials in the HCS system. While flat-slab floor system is generally a preferred choice by most users in the North American context, it corresponds to a higher embodied energy than that for a HCS system. In the case of the 15-story

building studied here, the embodied energy for the flat slab system is found to be 16% higher than that of the HCS frame.

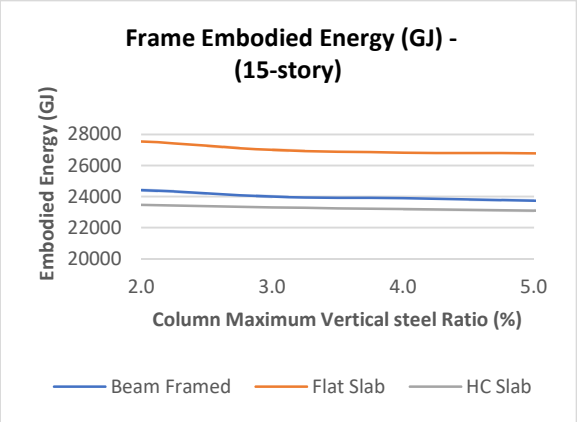

Fig. 5: Total frame embodied energy for column steel ratio and different floor types for 15-storey-frames

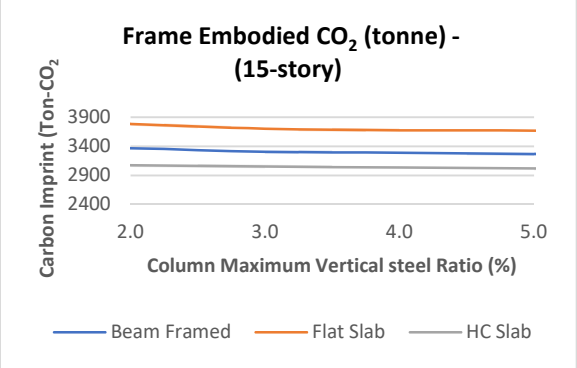

Fig. 6: Total frame carbon imprint for column steel ratio and different floor types for 15-storey-frames

Again, corresponding to the 4% maximum column steel ratio, it has been found that carbon imprint can be reduced by 17.7% and 7.5% if HCS floor is used instead of flat-slab and beam-framed structures, respectively.

The embodied energy per m^2 also tends to increase with building height. At the 4% maximum column steel ratio, cost, embodied energy, and CO_2 emission per m^2 are CA $68.80, 782 kJ and 101 kg-CO_2, respectively for the 5-storey buildings. The corresponding figures per m^2 for the 15-storey buildings are CA $71.6, 828 kJ, and 108 kg respectively. The differences are 4.1%, 5.9% and 6.9% for the cost, embodied energy, and CO_2 emission per m^2, respectively.

5. Conclusions and outlook

From the results presented here, it is evident that the major factor affecting the three constraints (cost, embodied energy, and CO_2 emission) is the type of the floor system. While the HCS system is found to be the most expensive one, it has the least embodied energy and CO_2 emission. If the cost is the priority, one may adopt the slabs-on-beams floor system with the expense of increased values for the other two constraints. If the HCS system is used instead of the flat-slab system, significant decreases in the other two constraints are possible with a small increase in the cost. Therefore, for environmental benefits, the HCS floor is better than the flat-slab floor while availing most of the service benefits of the latter one. The favorable values of the constraints for the HCS system is expected to get better for longer span slabs.

Though the column design optimization accounts for small variation in the three constraints for the entire structures, the designer should consider the maximum column steel ratio around 4%, as it will optimize/minimize not only the column cost but also minimize the other two constraints. It is recommended for a tall building that the ground floor columns be designed for 4% steel ratio and decreased gradually to 2% upwards and then column cross-section should be slightly reduced to increase the steel ratio again. The process can be repeated if the number of storeys is 10 or more. A significant reduction, however, in cross-section is not encouraged, as it may result is stress concentration and increased slenderness.

The trends outlined from this case study should not be considered in general term since there are other factors such as location, site condition, span lengths, material costs, which can show a different trend. Despite this limitation, it can be assumed that smaller cross-sectional areas are better for reduced embodied energy and CO_2 emission. Constructability, however, is an important criterion to be considered since smaller dimensions may result in reinforcement congestion for high steel ratio.

Acknowledgements

The authors would like to thank IC-IMPTCS Research Network for supporting the research.

References

[1} G. Guldentops, A. M. Nejad, C. Vuye, W. Van den bergh, N. Rahbar, 2016. Performance of a pavement solar energy collector: Model development and validation. *Applied Energy*, 163 (2016) 180–189

[2] E. Heymsfield, A. Osweiler, P. Selvam, M. Kuss, 2014. Developing Anti-Icing Airfield Runways Using Conductive Concrete with Renewable Energy. *ASCE Journal of Cold Regions Engineering*, (2014), 28(2): 04014001

[3] A. Hassanieh, H. R. Valipour, M. A. Bradford, 2017. Experimental and numerical investigation of short-term behavior of CLT-steel composite beams, *Eng. Struct.* 144 (2017) 43–57, doi: 10.1016/ j.engstruct. 2017. 04. 052.

[4] C. Loss. B. Davison, 2017. Innovative composite steel-timber floors with prefabricated modular

components, *Eng. Struct.* 132 (2017) 695–713, doi: 10.1016/j.engstruct. 2016.11.062.
[5] A. A. Chiniforush, H. Valipour, A. Akbarnezhad, M. Bradford, 2017. Steel-timber composite (STC) beams: numerical simulation of long-term behavior, Ce/papers 1 (2017) 2051–2059, doi: 10. 1002 /cepa. 250.
[6] A. A. Chiniforush, A. Akbarnezhad, H. Valipour, U. Dackermann, 2017. Dynamic response of steel-timber composite (STC) beams, *24th Int Congr Sound Vib, 2017*.
[7] S. Schoenwald, B. Zeitler, I. Sabourin, F. King, 2013. Sound insulation performance of Cross Laminated Timber. *Building Systems* (2013) 247: 4337–46.
[8] M. A. Bezabeh, S. Tesfamariam, M. Popovski, K. Goda, S. F. Stiemer, 2017. Seismic base shear modification factors for timber-steel hybrid structure: collapse risk assessment approach, *J. Struct. Eng.* 143 (2017) 4017136, doi:10.1061/(ASCE)ST. 1943-541X.0001869.
[9] S. Tesfamariam, S. F. Stiemer, C. Dickof, M. A. Bezabeh, 2014. Seismic vulnerability assessment of hybrid steel-timber structure: steel moment-resisting frames with CLT Infill, *J. Earthq. Eng.* 18 (2014) 929–944, doi:10.1080/13632469.2014.916240.
[10] A. Hashemi, R. Masoudnia, P. Quenneville, 2016. Seismic performance of hybrid self-centering steel-timber rocking core walls with slip friction connections, *J. Con- str. Steel Res.* 126 (2016) 201–213, doi: 10.1016/j.jcsr.2016.07.022.
[11] Australian Building Codes Board, BCA 2015: Building Code of Australia, National Construction Code Series, 2015.
[12] L. Gustavsson. R. Sathre, 2006. Variability in energy and carbon dioxide balances of wood and concrete building materials, *Build. Environ* 41 (2006) 940–951, doi: 10.1016/j.buildenv.2005.04.008.
[13] J. D. Balcomb, Passive Solar Buildings. Cambridge, MIT Press, MA, USA, 1992.
[14] J. Heier, C. Bales, V. Martin, 2015. Combining thermal energy storage with buildings - a review, Renew. *Sustain. Energy Rev.* 42 (2015) 1305–1325.
[15] A. A. Chiniforush, A. Akbarnezhad, H. Valipour, J. Xiao,. 2018. Energy implications of using steel-timber composite (STC) elements in buildings. *Energy & Buildings,* 176: 203–215
[16] E. Worrell, L. Price, N. Martin, C. Hendriks, L. O. Meida, 2001. Carbon dioxide emissions from the global cement industry 1. *Annu. Rev. Energ Env*., 26: 303–329
[17] C. L. Thiel, N. Campion, A. E. Landis, A. K. Jones, L. A. Schaefer, M. M. Bilec. 2013. A materials life cycle assessment of a net-zero energy building, *Energies* 6 (2): 1125–1141
[18] D. Yeo. R. D. Gabbai. 2011. Sustainable design of reinforced concrete structures through embodied energy optimization. *Energy and Buildings* 43: 2028–2033
[19] Y. C. Yoon, K. H. Kim, S. H. Lee, D. Yeo, 2018. Sustainable design for reinforced concrete columns through embodied energy and CO_2 emission optimization. *Energy & Buildings,* 174: 44–53
[20] A. Noman, A. Bagchi, A. Athienitis, 2019. Sustainable Design of Reinforced Concrete Flat-Plate Buildings Based on Cost, Embodied Energy, and Carbon Footprint. *CSCE Annual Conference*, Canadian Society of Civil Engineering, Laval, QC.
[21] J. P. Zaforteza, V. Yepes, A. Hospitaler, F. G. Vidosa, 2009. CO_2 optimization of reinforced concrete frames by simulated annealing. *Eng. Struct.*, 31 (7): 1501–1508
[22] M. G. Sahab, A. F. Ashour, V. V. Toropov, 2006. Cost optimization of reinforced flat slab buildings *Eng. Struct.*, 27: 313–322.
[23] A. Guerra, A. M. Newman, S. Leyffer. 2011. Concrete structure design using mixed-integer nonlinear programming with complementarity constraints. SIAM J. Optim., 21 (3): 833–863.
Habitat Journal, 3: 50–51.
[24] CBM-GCPL 2019. General Contractors; Price List. Eastern Region. 2300 Carp Rd, Carp, ON. http:// www.canadabuildingmaterials.com
[25] G. P. Hammond. C. I. Jones. 2008. Embodied energy and carbon in construction materials, Proceedings of the Institution of Civil Engineers - Energy, 161 (2) https:// doi.org/1 0.1680/ ener. 2008.161.2.87.
[26] Yousuf, M. and Bagchi, A., (2010), "Seismic performance of a 20-story steel-frame building in Canada", The Structural Design of Tall and Special Buildings 19 (8), 901-921.
[27] Yousuf, M. and Bagchi, A., (2009), Seismic design and performance evaluation of steel-frame buildings designed using the 2005 *National building code of Canada*, Canadian Journal of Civil Engineering 36 (2), 280-294.

Post Occupancy Evaluation in Canada: Challenges, Potential Improvements and New Frontiers

I. Tripathi[a*], T. Froese[b]

[a] Graduate Student, Department of Civil Engineering, University of Victoria
[b] Professor, Department of Civil Engineering, University of Victoria
* Corresponding & Presenting author: Ishan Tripathi, 6473910693, itripathi@uvic.ca

Abstract:
Canada's Build Smart strategy has a goal to build high-performance buildings by integrating occupant comfort with energy efficiency. Despite having established best practices to design high-performance buildings, there is a considerable gap between sustainable design and the actual performance of the building. Building performance evaluation provides tools and methods to investigate and analyze performance gaps in the buildings. Pre-occupancy and post-occupancy evaluations can be used to assess the way buildings function and establish a better understanding of sustainable performance. First, this study discusses the background and evolution of post-occupancy evaluation techniques in Canada. Second, the paper summarizes the methods and findings of a 2014 study by the International Institute of Sustainable Built Environment Canada that conducted post-occupancy evaluations of several green buildings across Canada, and it identifies the limitations of this study's protocol. Third, the paper discusses potential improvements to refine and prepare the protocol for a new iteration of studies in 2020, including foundations for a more rigorous and specific level of post-occupancy evaluations.

Keywords:
Post-occupancy Evaluations, Building Performance Evaluations, Performance Gap, Building Information Modeling

1. Introduction

The building sector accounted for almost 1/3 of the total energy consumption and Green House Gas (GHG) emissions in Canada in 2016 according to a Natural Resources of Canada's survey [4]. Moreover, according to the World Green Building Council's report in 2015, people spend a significant amount of time indoors (almost 90%). Therefore, indoor environment plays a vital role in occupants' health, well-being and productivity [1].

Efforts to address buildings' impact on the environment while still addressing the occupants' experience have inspired several sustainable agendas and policies in Canada such as the Energy Step Code in British Columbia and the Build Smart strategy at the federal level. Despite these initiatives, there is a lack of effort in evaluating these green building relative to their expected performance criteria. When these evaluations are conducted, there are often gaps between the expected and actual performance [2], which is regarded as 'the performance gap' in the industry. Therefore, there is a need to measure the performance of the buildings after they are occupied to understand the performance of the implemented strategies, to investigate the performance decay over time and to inform decision making to improve facilities management.

Building Performance Evaluation (BPE) is a systematic and rigorous approach encompassing a number of activities including research, measurement, comparison, evaluation, and feedback that take place through every phase of a building's lifecycle, including: planning, briefing/programming, design, construction, occupancy and recycling [2]. Apart from the technical aspects, it also helps to establish the effects of human behaviour, needs and desires.

Post-Occupancy Evaluation (POE) is a part of BPE that can be used to obtain feedback about various parameters such as energy performance, indoor environmental quality (IEQ), occupant satisfaction, productivity, etc. [1]. Based on the collected data, Key Performance Indicators (KPIs) can be derived to establish a better understanding of the performance gap and to provide potential solutions.

The primary aim of this paper is to determine the current state of and potential improvements for POE in Canada.

First, the paper provides background of POE and discussion the findings from a 2014 POE study by the International Institute of Sustainable Built Environment Canada (iiSBE). Second, the discussion section describes the POE protocol developed by iiSBE. Third, the limitations of the 2014 iiSBE protocol are discussed. Fourth, potential improvements and suggestions are proposed for a new series of POE studies that iiSBE is planning to conduct in 2020.

2. Points of Departure

This section summarizes reviews of POE by Li et al. [1] and Mallory-Hill et al. [2], [3].

2.1. The Background and Evolution of POE

The roots of POE date to the 1960s. Since then, POE has evolved to include a variety of practices. Simultaneously, the building sector's shift towards achieving energy efficiency and minimal environmental impact has driven the industry towards the adoption of the green certification systems [2]. There are at least 150 different green certifications around the world such as LEED, Green Globe, ASHRAE etc. However, their ability to provide the expected performance is comprehensively debated in the literature.

Li et al. [1] argues that even though POE is gaining popularity, it is still an underdeveloped concept. The analysis of 146 POE studies in the paper concludes that residential buildings are the primary research targets, and occupant comfort is the most common focus among all the studies, which results in occupant surveys being the most frequently used method. Ultimately the paper gives five topics as a future direction of POE: from one-off to continuing, from high-level to detailed, from researchers-oriented to owners/occupants oriented, from academia to industry, and from independent to integrated.

The nature of POE studies varies according to their purpose. Also, it is difficult to link POE studies back to original root causes and project phases [2]. Despite decent efforts from the industry, POE studies are difficult to generalize, which makes standardizing POE protocol a challenge [1].

2.2. POE in Canada – iiSBE Studies 2014

The 2014 iiSBE study was initiated as a Canada-wide study of a total 9 different green buildings across different regions. The main objective of the study was to create a standardized POE protocol suited to the Canadian Industry.

Despite the limitations, the team was successful in identifying crucial performance gaps in all nine buildings. Analyses of these gaps helped the team conclude key issues, potential areas of improvement in design, construction, commissioning & operations phases, and evolution of POE as a process. Below are the key takeaways from the 2014 iiSBE POE study [3].

- More emphasis on communication and commissioning stage rather than primarily on the design stage.
- Benchmarking is difficult except for energy.
- Without recalibrated models, it is difficult to determine the performance gap
- Commissioning is often overlooked and should be one of the key process for improving the performance.
- Without submetering, collecting desired data is challenging.
- Three building underperformed in the modeled and actual energy performance. Some of the factors are inconsistency in occupancy modeling, unregulated occupant behaviour and lack of building systems commissioning.
- Water use is depended on the occupancy.

3. Methodology

A literature review has been conducted to identify the BPE & POE concepts. Moreover, a thorough study of the 2014 iiSBE project is conducted to describe the findings and limitations of the project. These findings have been used as a base to suggest improvement and to determine next steps for POE in Canada. Also, these suggestions will be used as a part of the second iteration of iiSBE project in 2020.

4. Discussions

4.1. POE - Concepts and Definitions

POE has a very wide range of definitions and scope according to various literature [1]. Pre-Occupancy Evaluations (Pre-OE) and Post-Occupancy Evaluations (POE) forms a part of systematic BPE approach. In this section, concepts of Pre-OE and POE in the context of the iiSBE Canada project have been summarized.

Post-Occupancy Evaluation (POE):
POE is a process of evaluating building performance after it has been occupied for at least 2 years. It is usually a measure of how well the design objectives are met without compromising the occupant comfort [3].

Pre-Occupancy Evaluation (Pre-OE):
Pre-OE evaluates the existing building before retrofits and addition of green features. Moreover, it can be used to assess the current conditions of occupants who will occupy a greener building. It uses techniques that are similar to POE [3].

4.2. The 2014 iiSBE Protocol

The protocol formed by iiSBE was intended to help standardize the gathering and processing of information for the KPIs.

The protocol's objective is to use a series of indicators to compare simulated performance at the design stage with actual performance achieved after at least 2 years of occupancy. Moreover, it can also be used to provide reference values for typical performance for similar buildings in the same region.

4.2.1. Key Performance Indicators

Below are the KPIs chosen by the research team for the assessment of nine buildings across Canada.

- Energy
- Water
- Materials & Waste
- Indoor Environmental Quality
    - Lighting
    - Thermal Comfort
    - Acoustics
    - Co2
    - Particulates
    - TVOC
- Economic Factors
- Occupancy Factors

4.2.2. Methodology

- Onsite building observation,
- Collection of design documentation regarding building type, spatial allocation, floor plans, green building rating systems, etc.,
- Collection of metered data for water and energy use,
- Spot measurements for IEQ with the use of an IEQ measurement cart,
- A standard survey of occupant comfort,
- Interview with design team, building owner/manager and when possible, occupants,
- Data Analysis & KPI determination, and
- Findings & Conclusion.

4.3. Challenges in the 2014 iiSBE Protocol

Observed limitations in the 2014 iiSBE protocol are as follows:

- The definition of the performance gap is very holistic.
- Data collection and management procedures need to be more structured.
- There needs to be a standardized benchmarking for equipment used for spot measurement and its data collection.
- New buildings have started to integrate sensors as a part of Building Management Systems (BMS), however, there are no provisions regarding using BMS data along with spot measurements.
- There is not an efficient way to measure occupancy with high accuracy.
- Better visualization required to communicate the performance gap at a non-technical level.

4.4. Proposed Improvements in the iiSBE Protocol

Based on the literature review and identified gaps, potential improvements are proposed to generalize the POE process and make it more robust.

4.4.1. Levels of Evaluations

The BPE process should be divided in three levels for better data collection and analysis purposes.

Level 0: Pre-Occupancy Evaluations (Pre-OE)
Evaluations for existing buildings using the same KPIs from the 2014 iiSBE protocol.

Level 1: Post Occupancy Evaluations (POE)
Preliminary evaluations using the 2014 iiSBE protocol after the new green building has been occupied for at least 2 years.

Level 2: Post Occupancy Evaluations (POE)
Detailed Investigation after conducting preliminary Level 1 evaluations.

4.4.2. Data Collection & Management

- Standardize the equipment with specifications and tolerance for consistency,
- Integration of the data from BMS systems and other sensors along with the spot measurements,
- Pilot and implement efficient ways for occupancy tracking,
- Cloud based and structured database for the effective data management and collaboration, and
- An interactive occupant survey to encourage more engagement.

4.4.3. Data Analyses and Visualization

- Visualization of POE through Building Information Models (BIM),
- Spatial models of occupant satisfaction for effective communication at a non-technical level, and
- Analyses of the occupant survey databases is a very crucial topic and subjected to further research

5. Next Steps

- Revisit and refine level 1 iiSBE protocol developed in 2014,
- POE studies will be conducted on several new green buildings across Canada in 2020, and
- An attempt will be made for visualizing POE and occupant comfort data through BIM models.

6. Conclusions

- POE is a vital component of the design – construction – operations life cycles of the building. Although, it's still underdeveloped in Canada, it should be integrated as a part of sustainable agendas and green building certifications.
- Due to the unique nature of POE studies, it is difficult to generalize the protocol, however, it is possible to develop a protocol that can be easily customized according to the nature and location of the building and purpose of POE.
- Despite of the limitations, the 2014 iiSBE protocol lays a solid foundation for 2020 POE studies.
- The current iiSBE protocol can be improved by linking BMS into data collection, utilizing cloud for better organization and collaboration, efficient occupancy tracking and effective visualization of spatial comfort and performance gaps through BIM

References

[1] P. Li, T. M. Froese, and G. Brager, "Post-occupancy evaluation: State-of-the-art analysis and state-of-the-practice review," *Build. Environ.*, vol. 133, pp. 187–202, Apr. 2018, doi: 10.1016/j.buildenv.2018.02.024.

[2] S. Mallory-hill, W. F. E. Preiser, and C. Watson, *1 Introduction to Building Performance Evaluation: Milestones in Evolution*.

[3] S. Mallory-Hill and M. Gorgolewski, "Mind the Gap: Studying Actual Versus Predicted Performance of Green Buildings in Canada," in *Building Performance Evaluation*, W. F. E. Preiser, A. E. Hardy, and U. Schramm, Eds. Cham: Springer International Publishing, 2018, pp. 261–274.

[4] https://www.nrcan.gc.ca/energy-efficiency/energy-efficiency-buildings/energy-efficiency-existing-buildings/20682

[5] ASHRAE (2010). Performance Measurement Protocols for Commercial Buildings. Atlanta, GA: ASHRAE.

[6] Preiser, W.F.E. (2005) Building performance assessment—From POE to BPE, a personal perspective, *Architectural Science Review*, 48:3, 201-204.

[7] K. Bartlett et. al. 'Do our green buildings perform as intended?', Conference paper, SB 14.

[8] http://iisbecanada.ca/sb-14/

[9] KPI Guidebook, 2014 iiSBE protocol for POE

Stormwater Management by Bioretention Mesocosms – the Dynamic Role of Vegetation and Media in the Performance

A. Skorobogatov*[a], J. He[a], A. Chu[a], C. Valeo[b], and B. van Duin[c]

[a] Civil Engineering, Schulich School of Engineering, University of Calgary, Canada
[b] Mechanical Engineering, Faculty of Engineering, University of Victoria, Canada
[c] Water Resources, City of Calgary, Canada
* Corresponding author, Tel 587-896-4074, email askorobo@ucalgary.ca

Abstract:
Low Impact Development (LID), also known as Sustainable Urban Drainage, is a promising approach to stormwater management, which aims to mitigate as well as prevent the negative impacts of urbanization on the hydrology and water quality of the affected water bodies. Bioretention systems are some of the most commonly utilized LID systems that offer various benefits, including reduction of peak runoff, attenuation of excess runoff volume, retention of various pollutants, as well as aesthetic and habitat benefits. One of the challenges of bioretention systems is balancing the often-conflicting objectives of the overall performance. A recurring conflict is one between optimizing bioretention systems from a water resources management perspective and an urban parks perspective. The functional as well as perceived role of vegetation and bioretention media is pivotal to this matter. To date, very few studies have had the opportunity to investigate the roles of various media and vegetation within the same experimental setup, and no studies had the opportunity to analyze the dynamic impacts of growing and maturing vegetation on the performance. This research project investigated the change in the performance of twenty-four bioretention mesocosms with different media and vegetation over the period of 3 growing seasons since establishment. The mesocosms were constructed using three different bioretention media and planted with three different kinds of vegetation in the summer of 2016 in the Town of Okotoks, Alberta. The multi-year investigation showed that vegetation type had a significant effect on the hydrological and water quality performance of the mesocosms. Contrasting performance was observed between mesocosms containing larger woody species and mesocosms containing turfgrass, with the latter having inferior impact on the water and nutrient retention over the years. The practical outcomes of the research can facilitate future optimization and implementation of bioretention systems and LID in general.

Keywords:
Water Resources, Stormwater Management, Low Impact Development, Green Infrastructure, Bioretention.

1. Introduction

In recent decades, stormwater management has evolved from being exclusively focused on addressing the issues of urban drainage and flooding to recognizing the negative impacts of land development and urbanization on the downstream environments and attempting to address some of these impacts with the aid of natural processes. Low Impact Development (LID) is an approach to stormwater management, which acknowledges natural processes and offers a variety of tools that can lessen the negative impacts of urbanization and increasing imperviousness. One of the main issues with urbanization and imperviousness is that much greater runoff peak flows and volumes are generated in response to a storm event as compared to a pre-development condition. The excess runoff can lead to flooding and erosion, as well as water quality impairment in the receiving water bodies since urban contaminants become mobilized by the runoff. Some of the common LID systems are bioretention, bioswale, green roof, absorbent landscape, and permeable pavement. These practices can reduce peak flows and overall runoff volumes, as well as retain urban contaminants. Bioretention systems are likely the most common LID practices due to flexibility of their design, and the multiple hydrological, water quality, aesthetic, and ecological benefits that these systems offer [1]. Bioretention systems are essentially vegetated depressions with specially designed media in place of soil and a drainage layer with an underdrain beneath the media (Figure 1).

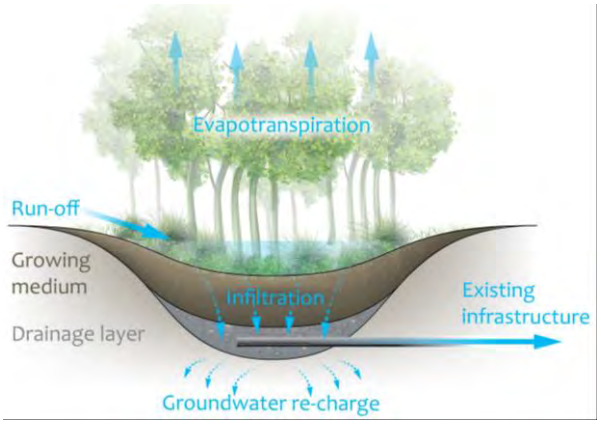

Fig 1: Bioretention cell schematic.

Bioretention systems are designed to collect and treat runoff from a proportionately larger contributing area

and to allow for infiltration, contaminant breakdown and retention, groundwater recharge, and evapotranspiration (ET) to take place, which ultimately improves the urban condition. Bioretention media make-up is regarded by many as being the key factor that simultaneously controls multiple aspects of the performance, which is why numerous studies focus predominantly on the media. A potential shift in the perception and research focus is underway, as several recent studies argued that the role of the living components, such as bioretention vegetation and microorganisms, may be critical in the performance [2], which calls for a different approach to bioretention design and performance optimization.

Very few studies to date had the opportunity to investigate the change in the performance of bioretention systems as they mature and evolve. Many assume that the performance can be predicted based on the initial design parameters combined with safety factors to account for deteriorating performance over time. This approach is potentially flawed as it underutilizes the benefits of the living components of bioretention systems. Some of the potential benefits are improved nutrient retention and contaminant breakdown, long-term maintenance of hydraulic conductivity, and increased volumetric capture due to ET. A related consideration that needs to be addressed is a desire to create bioretention systems that are aesthetically pleasing and can support healthy vegetation, which is not always easy with the media that were only optimized for hydrological and treatment purposes.

This project aims to analyze the combined effects of media and vegetation on bioretention performance by comparing the hydrological and water quality parameters of different media and plant combinations at a mesocosm scale. This project is also aimed to investigate the changes in the effects of media and vegetation on the performance as bioretention systems mature.

2. Materials and Methods

The research was conducted at a newly constructed field research facility in 2016 in the Town of Okotoks, Alberta, Canada. The facility contains a total of 24 mesocosms with three different types of media and three different types of vegetation (Figure 2). Each mesocosm is sized to 2x2x1.2 m (WxLxH) and is fully lined to be able to assess the water balance. Each mesocosm contains 300 mm deep drainage layer at the bottom, which consists of 3 sublayers – a 100 mm of coarse gravel at the base, followed by a 100 mm of pea gravel, and a 100 mm of coarse sand at the top. The drainage layer is overlaid by 600 mm of specially designed media. Above the media, there is 300 mm of freeboard, which allows ponding to be accommodated within the mesocosm cells during the simulated runoff events.

Fig 2: Bioretention mesocosms in July of 2019.

Among the three media types, two of them are based on the local guidelines (70 mm/hr mix and 40 mm/hr mix as per the City of Calgary LID guidelines). The third media contains amended clay loam soil, which is abundant in the area and is typically considered as not suitable for bioretention systems due to the low permeability associated with clay. The clay loam soil was amended with 40% wood chips (by volume) in order to support adequate infiltration. The mesocosms were planted in 2017 with three kinds of vegetation - turfgrass as a control, herbaceous mix of native grasses and forbs, and a woody mix of native shrubs.

Each type of media and vegetation were subjected to two hydrological loadings based on the size of a hypothetical impervious catchment that they would be managing the runoff from. One of the hydrological loadings was based on a catchment 15 times larger than the area of the bioretention cell, and the other was based on a catchment 30 times larger. Simulated runoff from a total of 25 storm events was applied to the mesocosm cells during the growing season of 2018 (May to October) and 24 events during 2019. The simulated events were designed to ensure that the magnitude, the frequency, and the total applied volume of runoff are representative of local conditions. Each simulated event involved applying a specific quantity of stormwater that was sourced from a local pond and mixed with street sweeping materials to simulate sediments. The concentration of sediments used in the experiments was 400 mg/L, which is considered to be representative of northern climates, where a considerable amount of grit is applied to the roads during the winter months. The stormwater was applied to the cells at a constant rate of 2 L/s using garden hoses and submersible pumps. The simulated events were of 4 different magnitudes (4 mm, 9 mm, 14 mm, and 24 mm), allowing to analyze the effects of event magnitude on the performance. Two hydrological metrics, namely volumetric retention and infiltration rate, were analyzed for assessing the hydrological performance. The water quality performance focused on analyzing the retention of different forms of nutrients and dissolved organics.

3. Results and discussions

The data collected during 2018 and 2019 showed substantial inter-event variability, and indicated that there were significant impacts of media, vegetation, and their interaction on the hydrological and water quality performance. A key finding was that the mesocosms were leaching nutrients rather than providing retention and the extent of leaching varied across the different media types (Figure 3).

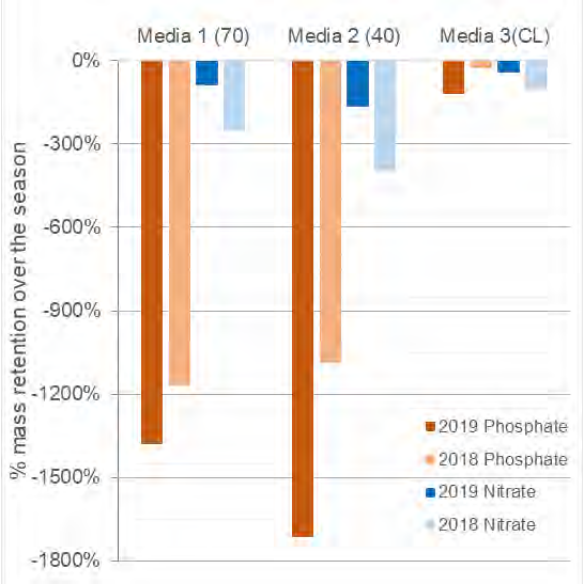

Fig 3: Nutrient retention by the three media, shown as % of total mass loading over the growing season.

The difference in leaching between the CL and the other two media was dramatic with the CL media leaching an order of magnitude less phosphate and several-fold less nitrate. However, due to the high percentage of wood chips, CL media cells had very high infiltration rates, which could lead to very short retention times and result in minimal leaching but also potentially minimal treatment if the inflow contaminant concentrations were higher.

Overall, there was a key difference between the leaching of nitrate and phosphate across the mesocosms. Namely, nitrate leaching generally decreased over the course of the season (7-fold in 2018 and 5-fold in 2019) and was 2.5 times less in 2019 than in 2018, whereas phosphate leaching was actually greater in 2019 than in 2018. The flushing-out pattern of nitrate leaching and lack thereof for phosphate leaching can also be observed in Figure 4, which shows the average retention of nutrients averaged across the mesocosms over the two seasons. It is interesting that phosphate leaching was particularly pronounced at the very end of the 2019 season, which could be due to the nutrients being released from the plants as they fall dormant and contribute additional nutrients and organic matter to the system.

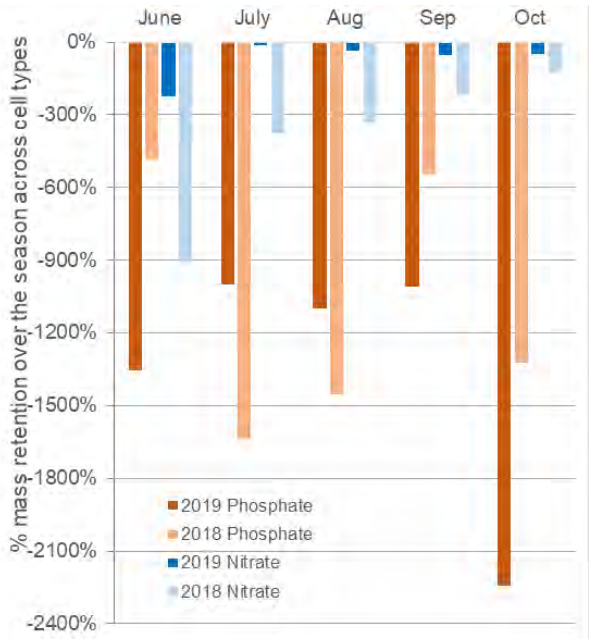

Fig 4: Nutrient retention shown as % of mass loading over the months of 2018 and 2019; the values are average across cell types.

The effect of vegetation type on the nutrient retention as well as the difference in the vegetation role between the 2018 and 2019 seasons were observed. (Figure 5).

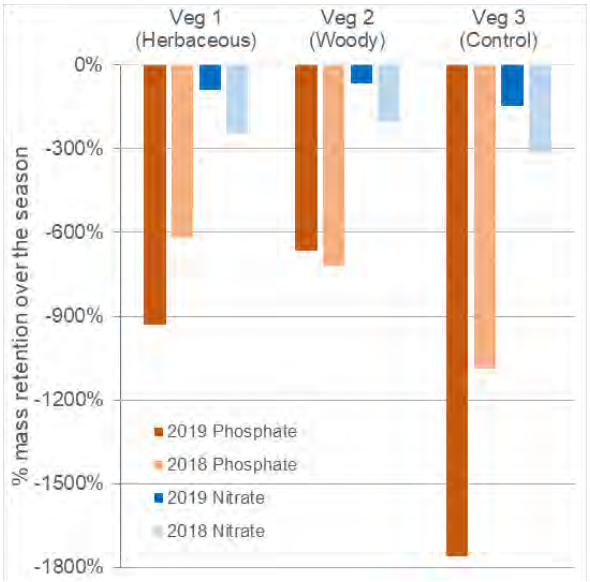

Fig 5: Nutrient retention by the three vegetation types, shown as % of total mass loading over the growing season.

Across the vegetation types, less nitrate was released in 2019 than in 2018 with the woody vegetation showing the greatest reduction in leaching compared to the other two (3.1 times less as compared to 2.7 and 2.2 for herbaceous and woody vegetation, respectively). As for phosphate, woody cells were the

only ones that appeared to cause a slight reduction in leaching in 2019 as compared to 2018. The other two vegetation types released more phosphate in 2019, and the turfgrass control appeared to be the most prone to leaching phosphate or nitrate.

The water quality performance was assessed using the percent reduction of mass of contaminant, not the concentration. Thus, the effect of the volumetric reduction on water quality performance can be taken into account. Volumetric reduction depends on several factors, including the magnitude of inflow, media storage, and drainage and ET during the inter-event periods. Vegetation could have a significant impact on the storage available within the cell prior to an event due to ET and the associated media drying. When looking at the overall amount of simulated runoff that was retained during the 2019 and 2018 seasons, there was a clear increase in the amount of water retained during the 2019 as compared to the 2018 season, which could be associated with the increased vegetation growth and establishment (Figure 6).

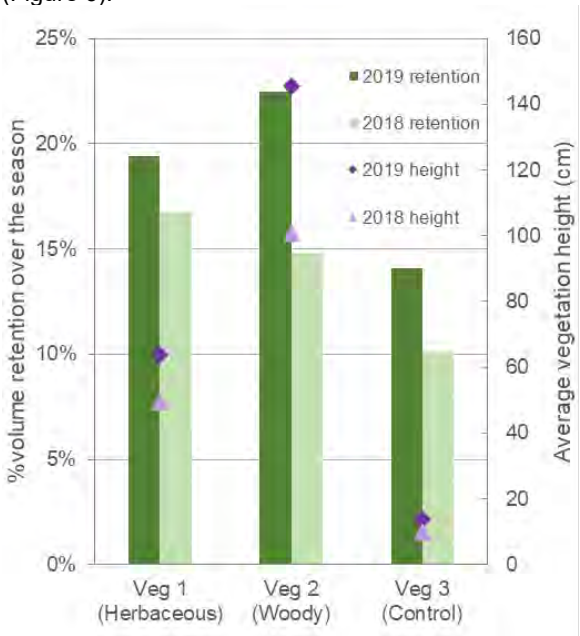

Fig 6: Volume retention by the three vegetation types and the corresponding average vegetation height over the growing seasons.

The cells with woody vegetation had the greatest increase in height between the two seasons and the greatest increase in water retention. However, only a modest increase in average height was observed for the control cells, yet the increase in water retention was still substantial (about 4% more of total inflow volume retained in 2019) over the two years. This suggests that mechanisms other than vegetation growth and increased uptake have contributed to the enhanced water retention in 2019. The increased water retention in 2019 for the cells can be possibly attributed to the increased residence time with the increase of the filled media voids by the input of sediments and the increased root growth in 2019, which enhances utilization of media moisture by the plants. In either case, if the observed effect is due to vegetation, it will change further as plants mature, and especially as woody species grow to a larger size. It is the intent of this project to continue to monitor the evolution of the performance of the mesocosms and to attempt to quantify the relationship between the relatively inert components of the bioretention systems, such as the media, and the ever-changing living components of the system.

4. Conclusions and outlook

Overall, both media and vegetation type had a significant impact on the amount of runoff retained and the nutrients released over the seasons. The more traditional bioretention media that were based on the local guidelines resulted in substantially more nutrient leaching as compared to the clay loam media. In addition, the effects of media type were apparent immediately after the construction, which supports the notion of bioretention media being critical in the performance. After two seasons of data collection, vegetation effects were starting to become more apparent. In terms of the vegetation, turfgrass appeared to be the least effective at volumetric and nutrient retention despite the considerable increase in volumetric retention between the two seasons, whereas the herbaceous and woody vegetation performed in a generally similar manner during their first season, and woody cells performed better in the second season. As the degree of maturity of the living components of bioretention systems appeared to impact the performance, long-term studies that assess such impacts are recommended.

Acknowledgements

The authors would like to thank the multiple sponsors and partners that contributed to this project – Bow River Basin Council, Alberta Environment and Parks, University of Calgary, City of Calgary Water Resources, Source2Source Inc., Alberta Low Impact Development Partnership, Environment Canada EcoAction, Natural Sciences and Engineering Research Council, MITACS, TD Bank Friends of Environment Foundation, and FortisAlberta.

References

[1] Li, H., Davis, A.P. (2009) Water Quality Improvement through Reductions of Pollutant Loads Using Bioretention. Journal of Environmental Engineering 135, 567-576.

[2] Funai, J.T., Kupec, P. (2017) Exploring Planting and Filter Media in Stormwater Bioremediating Landscapes: a Review. Water, Air, & Soil Pollution 228.

Thermal behaviour of an extensive green roof in a cold and semi-arid climate

M. Akther [a,*], J. He[a], A. Chu[a], B. van Duin [b]

[a] Civil Engineering, Schulich School of Engineering, University of Calgary, 2500 University Drive NW, Calgary, AB, Canada
[b] The City of Calgary, Calgary, AB, Canada
* Corresponding author, Tel. 587-718-0496, email msakther@ucalgary.ca

Abstract:

Green roofs (GRs) have been shown to have numerous environmental benefits, one of which is the reduction of building energy consumption. The quantification of this benefit, however, is still needed owning to their regional and climate-specific nature. The objectives of this research are to assess the thermal performance of an extensive GR situated in Calgary, Alberta (of a cold and semi-arid climate) relative to a near-by reference roof (RR), and to investigate the linkage of the thermal performance to its moisture content. The data collected in January 2017-December 2018 were used in the study. In general, in the summers, the GR temperatures were lower than those of the RR; whereas in the winters they were higher than those of the RR. These demonstrated that the GR is beneficial in reducing energy consumption for both summer cooling and winter heating. In particular, the role of the GR in energy reduction appeared to be most prominent in summers among all the four seasons. In addition, the potential relationship between the GR temperature and moisture suggested that further energy reduction in particular in summers can be achieved by adjusting the soil moisture conditions such as through irrigation.

Keywords:
Green roof; Energy consumption; Temperature profile; Volumetric water content.

1. Introduction

Green roofs (GRs) have received considerable attention in recent years, because they have been shown to have a variety of benefits, including relieving the urban head island effect [1,2], decreasing stormwater runoff [3], and reducing carbon emissions [4,5]. Therefore, many places across the world have promoted the implementation of GRs [1–3]. Besides, GRs are also beneficial in reducing the energy consumption of buildings in different climate zones [6,7,8,9], as they can reduce the thermal fluctuation of the outer surface of roofs, contribute to the cooling of the spaces below the roof during the summer, and increase their heating during the winter. However, this benefit of GRs is believed to vary from a place to another, as it is largely dependent on their environmental exposure.

The GR implementation in the arid and semi-arid climate zones is not as prevalent as in other climate zones. The assessment of the benefit of GRs in the energy consumption reduction in these zones is thus limited. Therefore, the objective of this research are to examine and assess the thermal performance of an extensive GR, situated in a semi-arid climate zone, relative to a near-by reference roof (RR).

2. Methodology

2.1 Study site

The City of Calgary is situated about 80 km east of the front ranges of the Canadian Rockies in the transition zone between the Canadian Rockies foothills and the Canadian Prairies and has more than one million people. The total annual expenditure on energy is $2.6 billion, which equates to 3% of its gross domestic product. Calgary's climate is characterized as semi-arid with long and cold winters. The temperature in winters is usually below 0°C; however, Calgary's cold winter is interspersed with brief warm periods, known as Chinooks, several times in a year, which quickly bring the air temperature above 0°C resulting in repeated freeze-thaw cycles. Calgary's average low temperature in the coldest month is -15.1° C, while the average high temperature in the warmest month is 22.9°C. The average annual rainfall and snowfall over the past 30 years (1981-2010) are 326.4 mm and 128.8 cm, respectively. There are four seasons, namely spring (March - May), summer (June - August), and fall (September - November) and winter (December - February).

The field-scale extensive GR and the RR, which are same in size, are situated on the fifth and fourth floors of the Calgary's Municipal Building in the downtown core (Fig.1). The construction and instrumentation of roofs were completed in the summer of 2014. The GR and the RR consist of the same base layers including a root barrier, 12 mm drainage mat c/w filter fabric, 100 mm/ 4" rigid insulation, and a diffusion membrane. On the top of the base layer, the GR has a FD-25 drainage board (with holes facing up) c/w filter fabric (separate) and engineered growing media; while the RR has a DBV 12 drainage board c/w filter fabric and 75 mm/ 3" concrete pavers. The growing media of the GR is 150 mm in depth and planted with nine different native plant species, which covers approximately 50% of the 335 m^2 rooftop.

Fig 1: The full-scale extensive green roof (left) and the reference roof (right).

2.2 Monitoring and data collection

Both the GR and the RR were divided into four equal quadrants (namely, SW, NW, NE and SE), each of which was instrumented to monitor the temperature profile, heat flux and moisture content. The locations of the sensors in the GR and the RR are shown in Fig. 2. The thermocouples were installed in the layers (from bottom to top) including one on the underside of concrete roof slab (TCIUS), two on top of the concrete roof slab (TCM1 and TCM2), one below the lower drainage board (TCTDB), and one on the top of the insulation (TCTOI). A heat flux transducer (HFT) was embedded on the top surface of the thermal insulation. For the GR, three additional thermocouples were placed at the bottom (TCBGM), middle (TCMGM) and on top (TCTGM) of the growing media; and one granular matrix soil moisture sensor (placed approximately in the middle of the media layer).

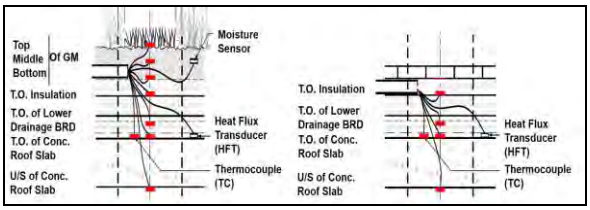

Fig 2: Location of sensors for the green roof (left) and the reference roof (right).

In addition, a meteorological station was deployed to each roof to record meteorological data including air temperature (T_a), relative humidity, rainfall, solar radiation, wind at a 5-minute interval. On each roof, an infrared radiometer of electromagnetic radiation was also used to measure the surface temperature (T_s). The data collected in January 2017-December 2018 were used in the study.

3. Results and discussions

3.1 Temperature profile of the roofs

Fig. 3 illustrates the boxplots of the daily average temperatures in different layers of the GR and the RR. The temperatures in the bottom layers (TCM and TCIUS) displayed much less fluctuations compared to those in the other layers, T_a and T_s for both roofs. The medians of the TCM and TCIUS of the GR are significantly higher than those of the RR. This suggests that overall, the GR keeps its bottom layers warm in average (over a year) than the RR. However, no obvious differences between the roofs were observed for TCTDB, TCTOI, T_a and T_s in their annual averages. Furthermore, the significant differences among the GM temperatures (TCBGM, TCMGM and TCPGM) were absent as they varied in a similar range from -3°C to 24°C.

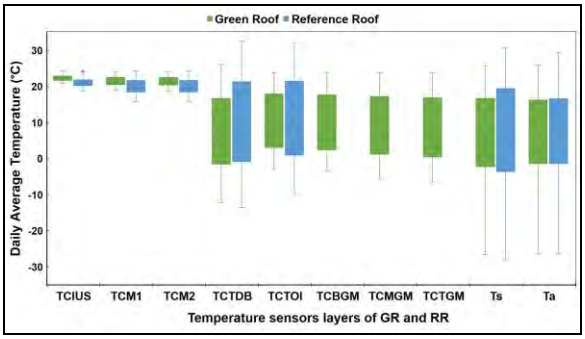

Fig 3: The boxplots of the temperatures at different layers of the green roof and the reference roof.

3.2 Comparison between the GR and the RR

When comparing the temperature between the RR and the GR at same layers, the largest difference was observed for TCTOI. Figure 4 shows the daily average temperature differences between the RR and the GR for T_s and TCTOI of the GR, respectively. In general, in the months (April – September), both the TCTOI and T_s of the GR were lower than those of the RR; and the maximum difference was up to 13°C in both T_s and TCTOI. In contrast, in other months the temperature of the GR was generally higher than those of the RR; and the maximum differences were up to -11°C and -4°C, for the TCTOI and T_s, respectively. These results illustrate that the roof temperature of the GR is lower in warm months and higher in cold months compared to the RR and imply that the GR is beneficial in reducing energy consumption for both summer cooling and winter heating.

3.3 Seasonal temperature regime

In this section, the collected temperature data were grouped into four seasons, namely spring, summer, fall and winter, to qualitatively assess the benefit of the GR in different seasons. Figure 5 shows the average surface temperature in a randomly selected day of each season for both the GR and the RR. This figure further confirms that T_s of the GR is in general lower and higher than that of RR in the summer and the spring/winter, respectively. Note that the

temperature difference in the fall appears to be absent/or minor. Thus, the role of the GR on reducing of energy consumption is prominent in the spring, summer and winter. In different climate regions, the prominent role of the GR was found in summers in the tropical areas [10] and the temperate zone [11].

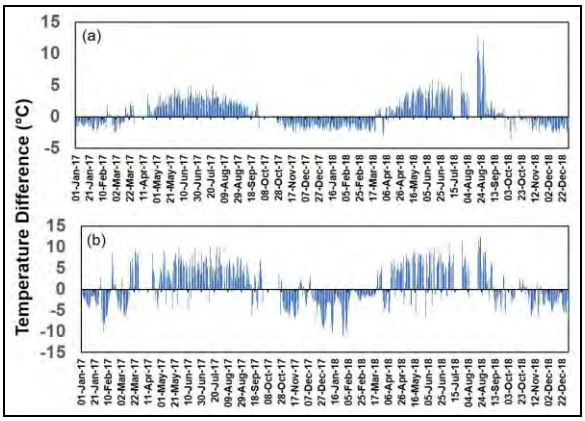

Fig 4: Daily average temperature differences between the reference roof and the green roof of (a) surface temperature (T_s) and (b) TCTOI.

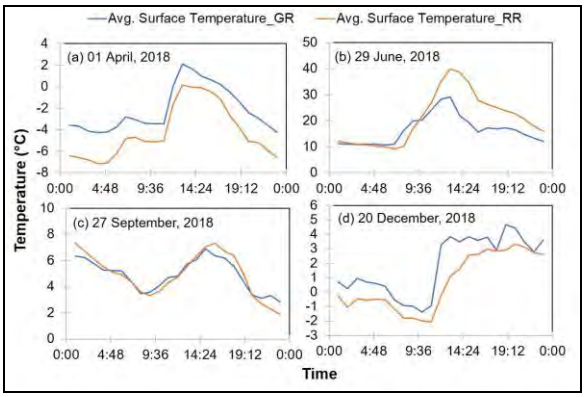

Fig 5: Surface temperature (T_s) of the green roof and the reference roof in a selected day in (a) spring, (b) summer, (c) fall and (d) winter.

In the summers, the daily average T_s is 18.79°C and 22.02°C for the GR and the RR, receptively. In addition, in average the temperature differences between the RR and the GR were 4.80°C and 3.24°C for T_s and TCTOI, respectively. During the study period, there were number of days on which the hourly T_s exceeds 42°C for GR and 52°C for the RR. These illustrate that the GR can effectively reduce the temperature of the roofs at the different layers, but at different degrees.

In the falls, T_s is similar between the GR and the RR as illustrated in Fig. 5(c). In addition, in average the temperature differences between the RR and the GR were -1.00°C and -0.10°C for T_s and TCTOI, respectively. The small to negligible role of the GR in the season might be due to cool and cloudy weather in general.

In contrast to the summers, in the winters the temperature of the GR is higher than that of the RR at all layers including the roof surface. In average the temperature differences between the RR and the GR were -3.00°C and -1.50°C for T_s and TCTOI, respectively. On winter days, the insulating effect of the snow is apparent. However, the temperature difference between the RR and the GR supports that the GR provides additional thermal insulation and thus is effective in increasing the roof temperature.

In the early springs, similar to the winters, the temperature of the GR is higher compared to the RR. It was also observed that T_s of the RR fluctuated considerably over a day compared to that of the GR. Throughout the springs, the temperatures of growing media (TCBGM, TCMGM and TCTGM) shifted from the more or less stable winter–spring (frozen) regime into the regime with a big fluctuation when the roof surface heats up in the daytime and freezes at night. Although the temperature of the GR is higher compared to the RR in the early springs, in average the temperature differences between the RR and the GR were 2.00°C and 1.00°C for T_s and TCTOI, respectively, over the seasons in the study period.

Considering the magnitudes of the temperature differences between the RR and the GR for T_s and TCTOI in the four seasons, the highest differences were found in summer, followed by winter, spring/fall. Thus, the GR appears to be more efficient in reducing energy consumption for cooling. Overall, the GR helps reducing energy consumption in summer for cooling, and winter for heating.

Assuming a constant temperature inside the room/building, the energy demand can be estimated by summing the heat entering and leaving through the roof. Fig. 6 shows the roof heat flux for the study time period. The RR is shown to have the largest fluctuation in heat gain during daytime and heat loss during nighttime. In contrast, the GR substantially helps in reducing the heat entering and leaving the roof. This further confirms that the extensive GR could improve the energy efficiency of the roofing system, particularly is effective in reducing heat gain in the summers when the significant reduction (compared to the RR) in the head gain was observed.

3.4 Temperature and moisture of growing media

Fig. 7 illustrates the temperature measured within the growing media of the GR. Overall, the average TCBGM (9.44°C) is higher than the averages of TCTGM (8.07°C) and TCMGM (8.63°C) over the study period. The increases of these temperatures in the cold months and similar or slightly lower in the warm months indicate that the growing media of the GR acts as a layer of insulation.

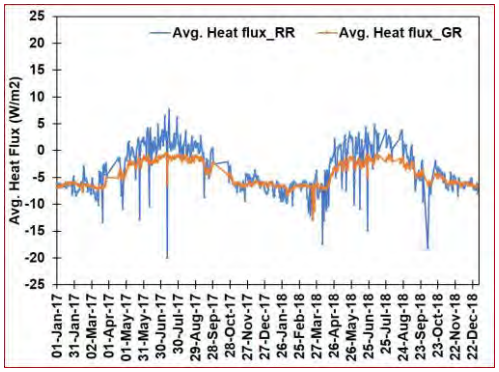

Fig 6: Time series of the heat flux through the green roof and the reference roof.

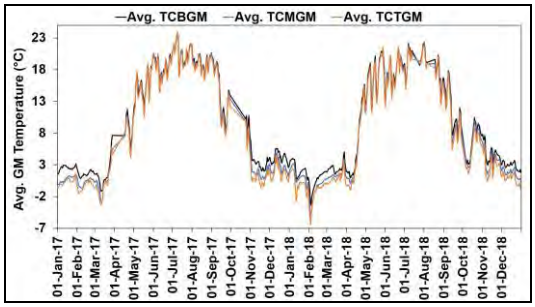

Fig 7: Time series of the temperatures of the green roof measured within the growing media.

Furthermore, to understand the influence of the soil moisture on temperature, the relationship between the average growing media temperature and the volumetric moisture content (VMC, in %) was investigated. Only the data collected in the summer months (June - August) were used in this analysis. It was found that in general the media temperature decreases with the increase of VMC in both 2017 and 2018 years. In average, the growing media temperature is approximately 1.35°C lower when VWC >15% than that when VWC < 15%. All the results demonstrated that the increase of VMC would lead to the decrease of the growing media temperatures of the GR.

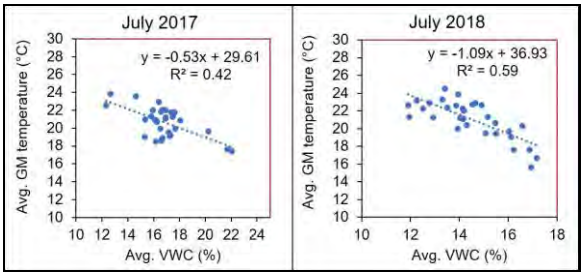

Fig 8: Relationship between the average growing media (avg. GM) temperature and the volumetric moisture content (VMC) of the GR in July of 2017 (left) and 2018 (right).

Further observation from the monthly analysis found that, similarly, the growing media temperature declines with the increase of VMC in all the summer months in each year. However, their significant dependence was only detected in July of both 2017 and 2018 (Fig.8), when the temperature is highest, and the GR is well covered by the vegetation among the summer months. Thus, in summer months further energy reduction can be achieved by optimizing the moisture content of the GR, such as through irrigation.

4. Conclusions

The extensive GR was capable of reducing energy consumption in cooling in summers and in heating in winters and springs, as the temperature of the GR was lower and higher than that of the RR in the seasons, respectively. In particular, the role of the GR in energy reduction appeared to be most prominent in summers among all the four seasons. Overall, GRs are beneficial in reducing energy consumption in the semi-arid region; while the comparison of their role with other climatic regions is of great interest. In addition, the potential relationship between the growing media temperature and moisture of the GR suggested that further energy reduction in particular in summers can be achieved by adjusting the soil moisture conditions such as through irrigation.

Acknowledgements

The authors would like to acknowledge the Natural Sciences and Engineering Research Council of Canada (NSERC) and the City of Calgary for the financial support, and the valuable contributions of personnel of the City of Calgary, who have been involved with the project.

References

[1] M. Razzaghmanesh et al. Urban Forestry & Urban Greening 15 (2016) 89-102.
[2] J. Yang et al. Solar Energy 173(2018) 597-609.
[3] A.W. Sims et al. Journal of Hydrology 542 (2016) 115-124.
[4] K.L.Getter et al. Environ Sci Technol. 43(2009) 7564-7570.
[5] D. Chemisana and C.Lamnatou. Appl Energy 119 (2014) 246–256.
[6] A. Gagliano et al. Building and Environment 90 (2015) 71-81.
[7] A.H. Refahi and H.Talkhabi. Renewable Energy 80 (2015) 595-603.
[8] A.Mahmoud et al. Buildings 7(2) (2017), p.30.
[9] S.M. dos Santos et al. Journal of cleaner production 219 (2019) 639-648.
[10] N.H. Wong et al. Building and Environment 38 (2003) 261-270.
[11] T.G. Theodosiou Energy and Buildings 35 (2003) p.909-917.

Municipal Natural Asset Management as a Climate Resiliency Strategy

Al Strang, P. Eng. [a], Emanuel Machado [b]

[a] Senior Environmental Planner, Morison Hershfield Limited
[b] Chief Administrative Officer, Town of Gibsons

Abstract:
Natural assets, and the ecosystem services they provide are, a fundamental part of local government infrastructure systems. Natural assets such as forests, wetlands, aquifers and green spaces provide key services to communities such as water storage, filtration and conveyance. They are cheaper to operate and maintain, if not degraded; may provide "free" ecosystem services; do not depreciate, if properly managed; and are carbon neutral, or even carbon-*positive*.

The Town of Gibsons was the first North American municipality to manage natural assets, using asset management, financial management and ecology principles that are systematically applied to managing engineered assets. The rationale is that the services provided by these systems, in the form of rainwater management, flood control and water purification, have tangible value, and play a vital role in a community's ability to withstand the impacts of an already changed climate.

In this paper we will share Gibsons' experience in integrating

- The economic, social and environmental benefits of including natural assets in climate resiliency planning;
- The use of principles of asset management, financial planning and ecology to maintain the ecosystems services nature provides; and
- The operational changes required to accommodate the expanded focus on natural assets.

Keywords:
Municipal natural assets, Asset management, Municipal infrastructure, Climate resiliency

1. Introduction

Local governments across Canada are faced with significant challenges when managing assets. Many of the services they provide—including water and wastewater, waste removal, transportation, and environmental services—incorporate engineered infrastructure that is in need of renewal. At the same time, the effects of climate change are putting additional strain on these assets and on local government budgets.

To provide community services in a cost effective and sustainable manner, now and in the future, local governments are looking for ways to improve management of the assets that supply these services. Asset management—the process of inventorying a community's existing assets, determining the current state of those assets, and preparing and implementing a plan to maintain or replace those assets—allows municipalities to make informed decisions regarding a community's assets and finances.

Unfortunately, many local governments lack policies to measure and manage one important class of assets: Natural Assets - the ecosystem features that provide, or could be restored to provide, services just like the other engineered assets, but historically have not been considered on equal footing or included in asset management plans.

As municipal infrastructure asset management processes evolve, it will be critical to ensure that all community assets that may provide municipal services - lakes, wetlands, green spaces and trees as well as water and sewer lines, bridges and buildings - are appropriately identified and managed.

2. What are Municipal Natural Assets

Although the term natural asset, or natural capital, is relatively well known in environmental research and policy, applying it in a municipal context is a new and emerging concept.

Nature provides many services that our communities rely on for our long-term health and well-being. Vegetation and soil soak up rainwater and recharge the aquifers, rivers, and lakes that provide many of us our drinking water sources. Wetlands store excess rainwater that is slowly released over time; pollutants are removed from the water and peak flood volumes are decreased. Forests cool our urban areas and remove air pollutants, helping us breathe better and reducing our energy consumption. At the local level, we all rely heavily on nature's services for our day-to-day well-being.

From a local government perspective, the term asset typically refers to engineered infrastructure that provides municipal services, such as roads, bridges, water treatment plants and drainage pipes. Yet nature also provides many services that fall within the realm

of municipal services, such as water storage and filtration or rainwater management. In this capacity, from a service perspective, natural assets are a municipal asset no different from other forms of infrastructure.

Table 1 provides an example of the types of municipal water services typically provided by engineered infrastructure that can also be provided by natural assets. This can conversely be viewed as natural infrastructure that, if lost, would need to be replaced by engineered infrastructure.

Municipal Water Services	Ecosystem Service	Natural Asset	Engineered Replacement
Drinking Water Supply	Aquifer recharge Lake recharge	Aquifer and source water area Lake watershed	Water supply pipes Water treatment plant
Drinking Water Treatment	Water purification Water filtration	Wetlands Forests Vegetation	Water treatment plant
Stormwater Management	Rainwater absorption Rainwater filtration	Wetlands Forests Vegetation	Water treatment plant
Flood Mitigation	Rainwater absorption	Wetlands Forests Vegetation	Dams Retaining walls Embankments

Table 1: Water specific municipal services that can be provided by natural assets and ecosystem services

3. Shared Management of Natural Assets

Unlike traditional infrastructure, such as roads and sewers, which can easily be divided along jurisdictional lines, natural assets often extend beyond the boundaries of a single jurisdiction and may require collaboration between municipal departments, private property owners, and with adjacent municipalities and other levels of government.

A creek can flow through two adjacent municipalities, providing services to each, but if the management of that creek is disjointed, the whole system will be affected. For example, if the downstream municipality protects the creek by maintaining vegetated buffers and controlling the amount of pollutants but the up-stream municipality does not protect the stream, the whole system will be impaired to the detriment of both municipalities. In these cases, shared responsibility for the asset will be required.

A good example of shared management of a natural asset is Still Creek, which flows through Vancouver and Burnaby, eventually draining into the Fraser River. Still Creek provides a cooling effect to the highly urbanized area through which it flows, habitat for a number of species, and stormwater management. Jurisdiction over the creek includes the Government of Canada (Fisheries Act), the Province of British Columbia (Water Sustainability Act, Environmental Management Act, and Riparian Areas Protection Act), Metro Vancouver (Liquid Waste Management Plans), and finally the Cities of Vancouver and Burnaby (land-use bylaws, zoning, and integrated stormwater management plans). In 2007, an Integrated Stormwater Management Plan (ISMP) was created for the Still Creek watershed, based on collaboration and joint decision-making. The cities of Vancouver and Burnaby both officially adopted their own version of the ISMP for implementation matters that are within their individual jurisdictions and the Metro Vancouver works with both cities on issues that are overarching. In 2012, spawning salmon returned to the creek, something that had not happened in almost 80 years.

4. Gibsons' Natural Asset Management Strategy

Gibsons is a town of about 4,500 people on British Columbia's Sunshine Coast. As a coastal community, Gibsons is blessed with a natural shoreline, as well as a healthy natural environment. Consistent with the practice of effective asset management practices, the Town is moving away from reactively maintaining individual assets to managing all assets over their entire lifecycle.

An asset inventory revealed that Gibsons owns approximately $60 million in assets. This value reflects the historical costs of the assets as required by financial reporting. Current replacement cost can be significantly higher depending on the age of the asset. Each asset requires upkeep, repair and maintenance, which in turn requires corresponding financial plans.

The Town established that to maintain assets properly they must spend or put aside, as a rough guide, up to 3 - 4% of asset value, or about $1.8 million to $2.4 million, each year for asset replacement. This was an uncomfortable realization for the Town given that the Town's annual revenue for operating, maintaining and replacing assets as well as constructing new assets is only about $6.6 million. Town administration realized that a major change would be required to ensure long term financial sustainability. Gibsons needed to reduce the number and value of the assets they owned and operated, and reduce the maintenance costs for those assets they retained – all while meeting community expectations for services.

Part of the solution lay, quite literally, at their feet.

4.1 Gibsons Aquifer

The Gibsons Aquifer is a confined aquifer underneath the Town that holds water and provides it to the Town's wells and springs.

Gibsons conducted an extensive study of the aquifer between 2009 and 2013 to determine its properties. One finding was that the aquifer filters and stores enough water to supply the present and projected future populations of the Town.

Simply recognizing the services provided by the Gibsons Aquifer gave the Town a basis for more informed decisions and better risk management. The Town's research helped staff determine that if the aquifer became degraded, then engineered assets would be required to provide the same services, at a cost that could be calculated based on costs in other municipalities. Conversely, a well-managed aquifer provides clean drinking water in perpetuity and reduces the risk of liabilities for new water storage and purification infrastructure. Gibsons also invests $28,000 annually in monitoring the aquifer, a small fraction of the operating costs of an engineered facility. These insights have given Gibsons the basis for determining the actions, timelines and costs needed to maintain aquifer health and officially include them in the Asset Management Plan in order to ensure sufficient funds are in place to do so.

4.2 Gibsons' Creeks and Woodlands

Gibsons has identified Goosebird, Charman and Gibsons Creeks as providing the vital services of conveying and treating rain water run-off, although more analysis on their properties are required before they are formally entered into the asset management strategy. The headwaters of Charman Creek are located in a forested recreation area in Upper Gibsons. Stormwater run-off from development in Upper Gibsons flows into the creeks, through natural settling ponds that clean and filter it, and finally, into the ocean as a naturally treated product. This means that Upper Gibsons has less engineered drainage infrastructure than if the creeks did not exist.

If these creeks and ponds ceased to perform their current functions then flooding would result and either development in Upper Gibsons would need to slow or stop, or engineered infrastructure would need to be constructed and maintained, again, at a cost that can be determined based on similar structures elsewhere in the Town and in other municipalities.

Engineered asset replacement for the woodland would, in almost any scenario, be far more expensive than simply keeping the woodland healthy, which requires only general maintenance and pond dredging every three to four years at a cost of approximately $10,000 per dredging. Additional analysis is required to determine the optimal number and type of trees in the woodland, as well as best practices for dredging, maintenance and associated costs, to maximize the ecosystem services provided by the creeks and woodland.

4.3 Gibsons' Foreshore

The Town has another important natural asset in the foreshore of Lower Gibsons, where much of the commerce is located. The foreshore provides a vital seawall to protect the waterfront from more storm surges and sea level rise, both of which are the ongoing consequences of climate change.

Engineered alternatives would be required if the foreshore became degraded, with associated capital and operating costs that likely far exceed what is required to keep the foreshore in good health. A foreshore condition assessment, completed in August 2014 by an engineering firm, provides a basis for a long-term master plan for the redevelopment of the foreshore to ensure the shoreline, associated infrastructure, and adjoining development is properly protected from an anticipated sea level rise of about one metre around the Town of Gibsons by the year 2100. This analysis will also provide a basis for long-term stewardship and for formally deeming the foreshore to be an asset within the Town management framework.

4.4 Rethinking Gibsons' Asset Management Process

Gibsons has made other changes to properly manage its assets over their entire lifecycle, reduce the number of assets managed and reduce operating costs.

1. Moving to an evidence-based approach

Gibsons recently invested in sophisticated asset management software to help the Town analyze its assets and calibrate its efforts.

This revealed that:

• A large amount of asset management effort was spent addressing crises and breakdowns instead of on preventive work

• Gibsons spent the majority of asset management budgets on a minority of engineered assets

These insights have given Gibsons a stronger basis for both strategic and operational decisions that will help prevent potentially costly and disruptive breakdowns and infrastructure crises.

2. Developing a natural asset policy

In July 2014, Gibsons became the first municipality in North America – and possibly anywhere – to pass a municipal asset management policy that:

• Explicitly defines and recognizes natural assets as an asset class

• Creates specific obligations to operate, maintain and replace natural assets alongside traditional capital

assets, including having natural asset management strategies and financial resources to maintain them

With this move, Gibsons moved natural assets from the periphery of municipal decision-making to its core and together with the natural asset policy, provided a framework for the Town's future asset management actions.

3. Adapting financial statements

Following extensive discussion with its auditors, the Town of Gibsons also included the following text in its financial statements:

"The Town is fortunate to have many natural assets that reduce the need for man-made infrastructure that would otherwise be required. This includes the Gibsons Aquifer (water storage and filtration), creeks, ditches and wetlands (rain water management) and the foreshore area (natural seawall). Canadian public sector accounting standards do not allow for the valuation and recording of such assets into the financial statements of the Town. As such, these natural assets are not reported in these financial statements. Nevertheless, the Town acknowledges the importance of these assets and the need to manage them in conjunction with man-made infrastructure."

This statement sends an important message about the Town's focus on natural assets and creates an opportunity to set future standards for their management.

4. Team-based management and training

Repairs to engineered assets such as stormwater drains have well-known solutions that can typically be handled by a single Town department. Gibsons' increasing focus on preventive measures, by contrast, requires team-based, collaborative approaches across Town departments and disciplines.

The natural asset strategy is also prompting changes in how the Town works. For example, Town departments have traditionally addressed different aspects of the foreshore in isolation; Public Works would address storm outfall related issues, and Parks would address recreation or horticultural matters. The result was piecemeal management that often did not support the integrity of the natural asset.

In some instances, the team-based approaches require additional knowledge and training. That training will be identified as needed. For example, Town crews may require additional training to ensure that they maintain woodland ponds in a way that maintains ecosystem integrity.

5. Developing partnerships

The Town does not have all the required resources in-house to implement a natural asset strategy and as a pioneer, cannot emulate what others have done. As a result, they are exploring partnership opportunities with academia, granting organizations and others that can help them further the natural assets strategy.

6. Long-term financial planning

The Town is developing financial plans for all assets within the Asset Management Plan to ensure sufficient resources to manage them over their lifecycle. This task has led to challenges such as determining the Annual Cost for Asset Replacement (ACFAR), which has direct bearing on recommended rate increases for taxpayers.

The ACFAR can represent a significant percentage of the overall annual cost of each engineered asset category; if natural assets are maintained appropriately ACFAR does not need to be considered, as the proper management of these assets means that they will last in perpetuity. This is a significant financial advantage to incorporating natural assets into an overall asset management plan.

5. Conclusions and Outlook

Gibsons' aquifer, creeks, foreshore and other natural assets provide vital services that the Town would otherwise have to provide through engineered solutions. The assets can, in theory, last indefinitely and they never depreciate. They can also typically be maintained at a fraction of the cost of an engineered alternative.

The Gibsons Aquifer is already formally listed as an asset within the Town asset management framework, and analysis is underway that could allow the other natural assets to also be included. Also noteworthy is that the Town is calculating the value of these natural assets relative to the cost of an engineered substitute; each of these assets provides additional ecosystem services that can also be calculated, such as recreation opportunities. Moreover, all of the assets may play an increasingly important role in climate change adaptation. As has been conducted on the Gibsons Aquifer, research is also needed in other classes of natural assets to understand more fully the civil services that each natural asset provides, and how best to maintain them.

Acknowledgements

The authors would like to thank The Town of Gibsons and Morrison Hershfield for their support in preparing this presentation.

References

[1] E. Machado et al, Toward an Eco-Asset Strategy in the Town of Gibsons (2015).

Metro Vancouver's Application of the Envision Sustainable Infrastructure Framework

Al Strang, P. Eng. [a], Marcel Pitre [b], Don McCallum, P. Eng. [c]

[a] Senior Environmental Planner, Morison Hershfield Limited
[b] Division Manager, Policy & Facility Development, Solid Waste Services, Metro Vancouver
[c] Vice President, Environment, Morison Hershfield Limited

Abstract:
Metro Vancouver provides essential services, including managing the region's solid waste, for over two million residents in British Columbia's lower mainland. In partnership with the City of Surrey, Metro Vancouver is currently building a recycling and waste drop off facility for residents and small businesses in an industrial business park in the East Newton area of Surrey BC. Metro Vancouver has implemented a Sustainable Infrastructure and Buildings Policy that establishes standards for sustainable design and construction of Metro Vancouver infrastructure and buildings.

The Envision Sustainable Infrastructure Framework provides industry-wide sustainability metrics for all types and sizes of infrastructure to help users assess and measure the extent to which a project contributes to conditions of sustainability across the full range of social, economic, and environmental indicators. Envision helps users optimize project resilience for both short-term and long-term effects. For infrastructure, including transfer stations, Metro Vancouver's Policy requires an Envision Gold performance level.

In this paper we will share Metro Vancouver's experience with the Envision Framework on the Surrey recycling and waste drop-off facility, including how community and stakeholder feedback was incorporated into the facility design, and reporting requirements included in project specifications to facilitate Envision scoring.

Keywords:
Sustainable infrastructure, Sustainability, Envision

1. Introduction

Metro Vancouver is a federation of 21 municipalities, a Treaty First Nation and an electoral area, representing a regional population of about 2.5 million people. This entity is responsible for core regional services including drinking water, wastewater treatment and solid waste management. Included in its responsibilities are planning, operating, maintaining and renewing assets representing billions of dollars in investment. Metro Vancouver is committed to reducing the environmental effects and increasing the social and environmental benefits of its infrastructure and buildings in a fiscally responsible manner, and has implemented a Sustainable Infrastructure and Buildings Policy. The policy directs the region to use the "Envision" rating system to guide and document the design and construction of this infrastructure. This paper illustrates the application of this rating system with a case study from Metro Vancouver's solid waste management system.

Metro Vancouver is responsible for long term planning and disposal of the solid waste generated by residents and businesses in the region. The region's solid waste management system consists of six transfer stations, a waste to energy facility, and a landfill. Within the region there are also private facilities which manage recycling and construction and demolition waste.

In 2001, as a condition of rezoning the Surrey Transfer Station, Metro Vancouver committed to build a recycling and waste drop-off facility (RWDF) in Surrey. In partnership with the City of Surrey, Metro Vancouver proceeded to select, purchase and rezone a property specifically as the Surrey RWDF for residents and small businesses in an industrial business park in the East Newton area of Surrey.

The Envision Sustainable Infrastructure Framework provides industry-wide sustainability metrics for all types and sizes of infrastructure to help users assess and measure the extent to which a project contributes to conditions of sustainability across the full range of social, economic, and environmental indicators. Envision helps users optimize project resilience for both short-term and long-term effects. For infrastructure, including transfer stations, the target specified in Metro Vancouver's Sustainable Infrastructure and Buildings Policy is Envision Gold performance level.

In this paper we discuss how Envision has been applied at the Surrey RWDF.

2. Surrey Recycling and Waste Drop-Off Facility

The facility will be located on a 1.7 ha lot, located at 67th Avenue and 154th Street in Surrey. It will have the capacity for 20,000 tonnes per year of solid waste and recyclables, and is expected to service about 125,000 customers annually (an average of 345 customers per day), with a peak design capacity of 600 customers per day. Design includes open and covered areas for the

drop-off of free recyclables (materials accepted in Surrey's curbside collection program and by Product Stewardship Agencies), and a 3,000 m^2 enclosed transfer building for paid recycling (green waste, gypsum, clean wood, mattresses) and garbage drop-off. Budget for the project is $62 million, including land acquisition, design and construction.

The site was cleared in 2019, and construction of the facility is expected to begin in the second quarter of 2020, and be complete by mid-2021. The facility is expected to be open seven days per week, 363 days per year.

The location of the project is shown in Figure 1, and a rendering of the facility is shown in Figure 2.

Figure 1. Location of Surrey RWDF

Figure 2. Surrey RWDF Rendering

A number of sustainable features are included in the building design, including:

- Translucent wall panels on the transfer building to increase natural light and reduce energy consumption;
- Recycled steel;
- Low CO_2 concrete;
- Energy efficient lighting;
- Use of recovered materials where practical; and
- Electric vehicle charging infrastructure.

The facility is designed to fit into the neighbourhood. The site is surrounded by other industrial properties, with the nearest residents more than 200 m away.

Project benefits include increased recycling and reduced waste; decreased illegal dumping; reduced traffic congestion; and reduced greenhouse gas emissions.

3. Envision Framework Overview

The Envision Sustainable Infrastructure Framework provides industry-wide sustainability metrics for all types and sizes of infrastructure to help users assess and measure the extent to which a project contributes to conditions of sustainability across the full range of social, economic, and environmental indicators. Envision helps users optimize project resilience for both short-term and long-term effects.

Envision is a framework that includes 64 sustainability and resilience indicators, called 'credits', organized into five categories:

- Quality of Life (14 credits);
- Leadership (12 credits);
- Resource Allocation (14 credits);
- Natural World (14 credits); and
- Climate and Resilience (10 credits).

These collectively address areas of human wellbeing, mobility, community development, collaboration, planning, economy, materials, energy, water, siting, conservation, ecology, emissions, and resilience. These indicators collectively become the foundation of what constitutes sustainability in infrastructure.

Each of the 64 credits has five potential levels of achievement representing the spectrum of possible performance goals from slightly improving beyond conventional practice, to conserving and restoring communities and environments.

Improved: Performance that is above conventional. Slightly exceeds regulatory requirements.

Enhanced: Sustainable performance that is on the right track. There are indications that superior performance is within reach.

Superior: Sustainable performance at a very high level.

Conserving: Performance that has achieved essentially zero negative effect.

Restorative: Performance that restores natural or social systems. Such performance receives the highest award possible and is celebrated as such.

By assessing achievement in each of the credits, project teams establish how well the project addresses the full range of sustainability indicators, and are challenged to pursue higher performance.

To receive recognition, projects must achieve a minimum percentage of the total applicable Envision points. Projects can be recognized at four award levels: Verified: 20%; Silver: 30%; Gold: 40%; and Platinum: 50%.

4. Application of Envision to Surrey RWDF

Metro Vancouver has implemented a Sustainable Infrastructure and Buildings Policy that establishes standards for sustainable design and construction of Metro Vancouver infrastructure and buildings. For infrastructure, including transfer stations, the target specified in Metro Vancouver's Sustainable Infrastructure and Buildings Policy is Envision Gold performance level.

Some Envision credits can be evaluated now based on the pre-construction consultation activities and site selection process. Other credits assess performance during construction and scoring cannot be determined until after completion. The final performance level of the project will be assessed following construction.

Some of the various ways that the Envision framework has been applied to the Surrey RWDF are described below.

Credit QL1.4 Minimize noise and vibration

Intent: Minimize noise and vibrations during operations to maintain and improve community livability.

Metric: The extent that operational noise and vibration is assessed and mitigated, and target levels achieved.

A technical review of anticipated noise from the facility was completed. Based on in situ measurements at an existing facility to determine design levels, noise mitigation has been integrated into the facility design – the building will be enclosed and a landscaped berm will be built. Other noise mitigation such as rubber mats to reduce bin drop noise and alternative back-up alarm systems for operations vehicles are currently under consideration.

Expected rating: Improved

Credit RA 1.2 Use recycled materials

Intent: Reduce the use of virgin natural resources and avoid sending useful materials to landfills by specifying reused materials, including structures, and material with recycled content.

Metric: Percentage of project materials that are reused or recycled. Plants, soil, rock, and water are not included in this credit.

Through the contract specifications, the construction contractor will be required to submit information showing the percentage of post-consumer and pre-consumer recycled content of materials used with recycled content. This will facilitate calculation of the quantity of recycled materials used post-construction. Recycled steel and low CO_2 concrete (limestone cement) are specified.

Expected rating: Improved or Enhanced

Credit RA 1.4 Reduce construction waste

Intent: Divert construction and demolition waste streams from disposal to recycling and reuse.

Metric: Percentage of total waste diverted from disposal.

Also through specifications, the construction contractor will be required to prepare and implement a Waste Management Plan for handling and disposal of waste, including trash, recyclables, and materials for reuse/salvage. The plan must include the handling, return and disposal of packaging waste, such as pallets crates, padding and packaging materials. Methodologies to be used to reduce waste generated during construction must also be indicated in the plan. Trees harvested from the site were recycled into engineered fuel.

Expected rating: Improved or Enhanced

Credit RA 1.5 Balance earthwork on site

Intent: Minimize the movement of soils and other excavated materials off site to reduce transportation and environmental impacts.

Metric: Percentage of excavated material retained on site or nearby.

The specifications require the construction contractor to report monthly, for each source of imported engineered fill, the address of the source and the approximate volume of material imported from that source. Excavated soils may be beneficially used on site if acceptable, otherwise, they will be sent to local landfill for use as daily cover and road construction. Following construction, this information will be used to calculate the maximum distance to the site from which material is sourced.

Expected rating: Improved

Credit 2.2 Reduce construction energy consumption

Intent: Conserve resources and reduce greenhouse gases and air pollutant emissions by reducing energy consumption during construction.

Metric: The number of strategies implemented on the project during construction that reduce energy consumption and emissions.

Through the contract specifications, the construction contractor will be required to submit an Energy Review Report before start of work. The report must identify energy uses during construction, major activities that consume fuel, energy-intensive activities, and energy efficient methods that will be implemented to minimize energy consumption. Metro Vancouver also requires that non-road diesel engine equipment be registered and maintained to higher emission standards.

Expected rating: Improved or Enhanced

Credit RA 2.3 Use renewable energy

Intent: Meet operational energy needs through renewable energy sources.

Metric: Extent to which renewable energy sources are incorporated.

Through the contract specifications, the construction contractor will be required to submit documentation identifying the quantities of electricity and fuels used at the site on a monthly basis throughout construction. This information will allow the calculation of the percentage of energy obtained from renewable sources during construction.

Expected rating: Superior

Credit CR 2.6 Improve infrastructure integration

Intent: Enhance the operational relationships and strengthen the functional integration of the project into connected, efficient, and diverse infrastructure systems.

Metric: The degree to which the project is integrated into other connected systems, where beneficial and appropriate, in order to increase resilience and systems performance.

The Surrey RWDF will add to Metro Vancouver's current solid waste infrastructure of six transfer stations, one waste-to-energy facility and one landfill.

The City of Surrey is one of the fastest growing municipalities in the Metro Vancouver region, with a 1.8% increase in population in the last five years. By providing a convenient drop-off location in Surrey Metro Vancouver expects to:

- Increase recycling and reduce waste;
- Reduce illegal dumping;
- Reduce traffic congestion, greenhouse gas emissions, and travel distances for residents and small businesses.

The facility also builds on the popularity of Surrey's existing Pop Up Junk Drop, a program that allows residents to dispose of a pick-up load of materials that are not allowed in the regular waste collection services.

Expected rating: Improved

5. Summary

Metro Vancouver expects to complete construction of the Surrey Recycling and Waste Drop-Off Facility in 2021. Once completed, the facility will fulfil a commitment made by Metro Vancouver to the City of Surrey as a condition of rezoning the Surrey Transfer Station.

Sustainability considerations have been incorporated into facility design through several features. Requirements have also been included in the contract specifications in order to facilitate calculation of various sustainability factors post-construction.

Following construction, the contribution of the facility to conditions of sustainability across the full range of social, economic, and environmental indicators will be assessed using the Envision Sustainable Infrastructure Framework.

Acknowledgements

The authors would like to thank Metro Vancouver and Morrison Hershfield for their support in preparing this presentation.

References

[1] Metro Vancouver, Sustainable Infrastructure and Buildings Policy (2018).

[2] Institute for Sustainable Infrastructure, Envision Sustainable Infrastructure Framework Version 3 (2018).

[3] Maclean's Magazine, Fastest growing communities in Canada (2019) https://www.macleans.ca/economy/fastest-growing-communities-in-canada-2019/

Kalman Filtering Applied to Sensor Fused Data to Deliver Accurate and Rapid Environmental Feedback of an Occupied Space

G. Mustapha [a], D. De Vaz [b], K. Batdorf [c]

[a] Delta Controls Inc. gmustapha@deltacontrols.com, [b] Delta Controls Inc.. ddevaz@deltacontrols.com
[c] Delta Controls Inc. kbatdorf@deltacontrols.com

Abstract:
Building occupants control the environment of their space or facility based on discomfort or a specific need at the time. In this manner, the correction occurs after the occupant is already uncomfortable or has been adversely impacted. Often, the actions taken by the occupant are seldom recorded or acknowledged for future reference, so that the same uncomfortable conditions perpetuate.

A device to sense environmental conditions at the occupant's height and location was designed so that increased comfort and productivity are achieved before the occupants' discomfort is realized. Additionally, a fast acting control system will provide the exact heating and cooling necessary resulting in significant energy savings.

The concept to move indoor environmental temperature sensing from the wall to the ceiling and scan the occupied space was investigated. This concept, coupled with machine learning techniques applied to multiple sensors proved capable of providing more accurate, faster and smarter feedback of the conditions of a monitored space. Temperature measurements with a 0.5°C level of accuracy are capable at 1m above the floor with the sensing device mounted at a maximum ceiling height of 5m. This was accomplished by using a combination of integrated thermistors and infrared sensing.

Additionally, a natural requirement is to accommodate and compensate for to the effects of internal heating from the device electronics itself as well as the heating and cooling effects from HVAC equipment in the room.

Keywords:
Temperature, HVAC, sensors, controls, infrared sensing, sensor hub, building automation

1. Introduction

The sensing methodology discussed in this paper makes real-time environmental adjustments possible by providing accurate and immediate feedback to the building automation system. The methods explored track environment changes based on a model synthesized from a large amount of collected data and by using sensors that react to the source of environmental changes.

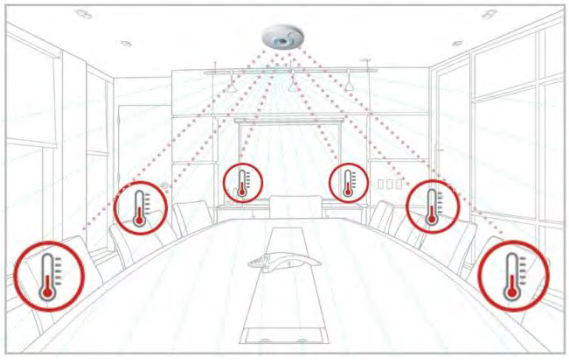

Figure 1. Sensor Hub Mounting

The ceiling-mounted sensing unit as shown in Figure 1 is typically mounted in the center of the room. The IR temperature sensor has a controlled field-of-view pointed downward toward the floor. A model that tracks the air temperature and the temperature detected by the IR sensor based on radiant energy estimates room temperature at occupant-height. [1]

2. Background

The Sensor Hub is typically mounted on the ceiling at a height between 3m to 5m. Despite the Sensor Hub mounted on the ceiling, optimal temperature measurements should be acquired at a height of 1m from the floor as well as closer to the center of the room where people typically occupy the space. Using a combination of local air temperature sensors and infrared temperature sensing, a series of techniques were applied to determine how to reliably calculate temperature 4m away from the device in the surrounding area below the hub.

The effect of internal heating from the device electronics and the effects of heating and cooling from HVAC equipment must also be taken into account. Figure 2 illustrates this the effects of these sources. The red plot shows the internal temperature measured within the device. The plot labeled *0 in 2* shows the temperature measured 10cm away from the device, to

demonstrate the localized heating from the electronics. Each plot line below that shows the stratification of the air temperature as you move further down towards 1m from the floor. Lastly, the bottom plotline shows the air temperature of the supply air coming from the HVAC system.

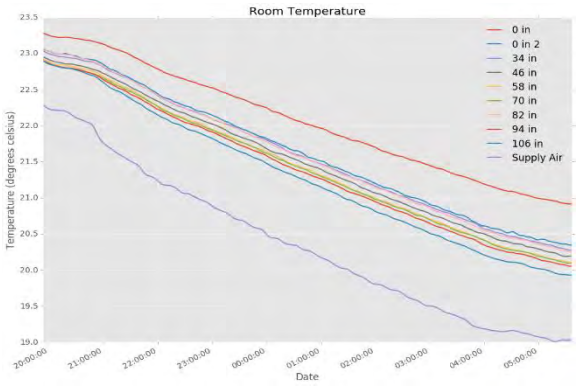

Figure 2. Temperature Influences in an Occupied Space

3. Kalman Filter Solution

A number of different techniques were investigated including simple averaging of the ambient temperature at the ceiling and IR temperature sensors as well as using a Complementary Filter where relative weightings are applied to the sensors. [2] This model did not account for changes in the environment such as ceiling height, cooling or heating rates as well as air circulation.

Linear quadratic estimation, also known as Kalman filtering [3] was investigated to model temperature readings over the area of influence. Kalman filtering is an algorithm that uses a series of measurements observed over time, containing statistical noise and other inaccuracies to produce estimates of unknown variables that are typically more accurate than those based on a single measurement alone, by estimating a joint probability distribution over the variables for each timeframe. [4] In a typical thermostat, the temperature is sampled and reported as the most recent measurement. In the next iteration, the previous result is discarded and the new sensor measurement is reported. Instead of discarding the previous sample, the Kalman filter incorporates the historical information to improve the next temperature estimate.

For example, suppose the previous output of the Kalman filter was 23 °C. Since sensors are subject to noise the next reading could be far from the current value, say 27°C. Since the Kalman filter has learned the dynamics of the system, it would recognize that the current measurement is likely an outlier and would down-weight its effect. This would cause the output to be between 23°C and 27°C much like a simple moving average.

However the difference is that the Kalman filter adjusts its parameters every time step in order to produce an optimal estimate. In addition to using historical data, the Kalman filter tracks the correlation between every signal (sensor) in the system and incorporates this into the estimate. Once the correlation between multiple sensors has been learned (the filter has converged) then the weighting given to any new measurement will be determined by looking at measurements from the other sensors in comparison to the newly sampled sensor. The Kalman filter tries to extract as much information from each signal as possible in order to produce an optimal state estimate.

Prediction Step

Predict using (noisy) process model: [3]

$$\hat{\mathbf{x}}_{k|k-1} = \mathbf{F}_k \hat{\mathbf{x}}_{k-1|k-1}$$

Update covariance (correlation): [3]

$$\mathbf{P}_{k|k-1} = \mathbf{F}_k \mathbf{P}_{k-1|k-1} \mathbf{F}_k^{\mathrm{T}} + \mathbf{Q}_k$$

Table 1. Update Step [3]

Name	Equation
Residual	$\tilde{\mathbf{y}}_k = \mathbf{z}_k - \mathbf{H}_k \hat{\mathbf{x}}_{k\|k-1}$
Residual covariance	$\mathbf{S}_k = \mathbf{R}_k + \mathbf{H}_k \mathbf{P}_{k\|k-1} \mathbf{H}_k^{\mathrm{T}}$
Kalman gain	$\mathbf{K}_k = \mathbf{P}_{k\|k-1} \mathbf{H}_k^{\mathrm{T}} \mathbf{S}_k^{-1}$
Updated state estimate	$\hat{\mathbf{x}}_{k\|k} = \hat{\mathbf{x}}_{k\|k-1} + \mathbf{K}_k$
Updated estimate covariance	$\mathbf{P}_{k\|k} = (\mathbf{I} - \mathbf{K}_k \mathbf{H}_k) \mathbf{P}_{k\|k-1} (\mathbf{I} - \mathbf{K}_k \mathbf{H}_k)^T + \mathbf{K}_k \mathbf{R}_k \mathbf{K}_k^T$
Measurement post-fit	$\tilde{\mathbf{y}}_{k\|k} = \mathbf{z}_k - \mathbf{H}_k \hat{\mathbf{x}}_{k\|k}$ $\tilde{\mathbf{y}}_{k\|k} = \mathbf{z}_k - \mathbf{H}_k \hat{\mathbf{x}}_{k\|k}$

Where **F** is the state-transition model, **H** is the observation model, **Q** is the covariance of the process noise and **R** is the covariance of the observation noise.

For the desired application, the room temperature and its time derivative (rate of change) are tracked. The time derivative is included so that the filter will track temperature trends correctly. If the rate of change is not included, then long temperature trends would be treated as process and/or measurement noise in the filter, causing noticeable lag.

$$\mathbf{x} = \begin{bmatrix} T \\ \dot{T} \end{bmatrix}$$

A simple kinematic model is used to track changes in temperature: $T_{k+1} = T_k + \Delta t * \dot{T}_k$

The process model, $\mathbf{F}$ describes this in matrix form with respect to the chosen state variables $\mathbf{x}$.

$$\mathbf{F} = \begin{bmatrix} 1 & \Delta t \\ 0 & 1 \end{bmatrix}$$

$$\mathbf{P} = \begin{bmatrix} 1 & 0 \\ 0 & 1 \end{bmatrix}$$

$$\mathbf{Q} = \begin{bmatrix} \sigma_p^2 & 0 \\ 0 & \sigma_p^2 \end{bmatrix}$$

Since temperature is measured directly, the coefficients for the $\dot{T}$ terms are set to zero.

$$\mathbf{H} = \begin{bmatrix} 1 & 0 \\ 1 & 0 \end{bmatrix}$$

$$\mathbf{R} = \begin{bmatrix} \sigma_m^2 & 0 \\ 0 & \sigma_m^2 \end{bmatrix}$$

The initial state estimate, T (room temperature) and $\dot{T}$, are set to the mean of the temperature signals and the initial sample-to-sample difference respectively. Filter performance is highly dependent on parameters listed in Table 1, parameters were selected through experimentation.

Once the filter reliably converged, the Kalman filter was plotted against a high precision temperature reference as well as the simple average as shown in Figure 4.

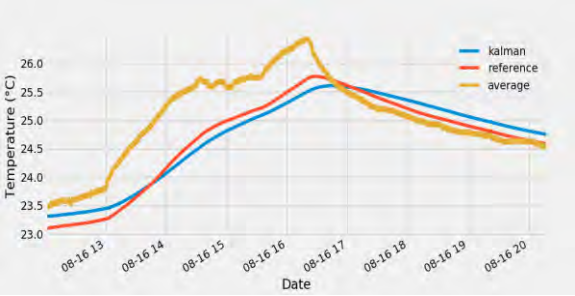

Figure 4. Kalman filter performance

Calibration

A single calibration point is required to tune the temperature sensor to measure 1m from the ground as well as to negate effects of airflow, floor material and other temperature influencing room parameters.

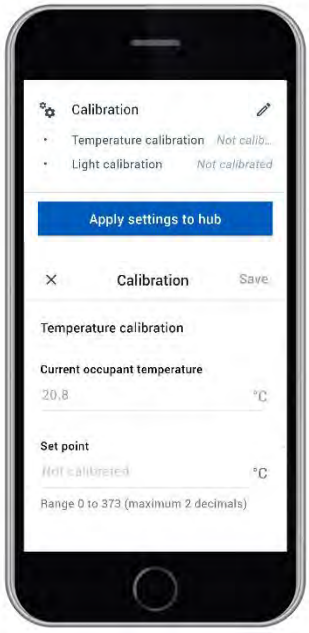

Figure 3. Calibration Tool

A simple mechanism to calibrate the sensor hub was created using a Smartphone app as shown in **Error! Reference source not found.** and high precision thermometer. The user simply needs to sample temperature at the appropriate height under the sensor hub and input the data into the app. The app then synchronizes this data over a direct Bluetooth connection to the Sensor Hub and applies the calibration value to the equation.

4. Results and discussions

Lab testing and field deployments have proven the Sensor Hubs temperature sensing method to function superior to any traditional thermostat. Results are shown in Figure 5.

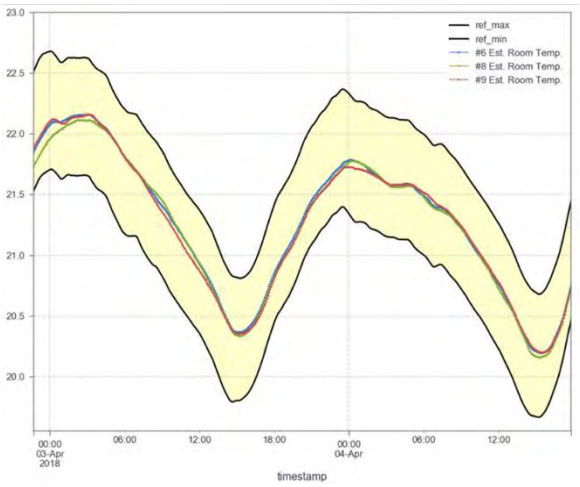

Figure 5. Temperature Measurement Results

Measurements from six high precision temperature sensors recorded temperature in the field of view of the Sensor Hub. The variance of these measurements is indicated by the yellow shaded area in Figure 5.

After calibration, three Sensors Hubs recorded temperature over time, measurements were recorded in the middle of the variance recorded by the high precision sensors. All three Sensor Hubs tracked each other very well.

Energy Savings

Sensor Hub Mounting Height is 4.6m

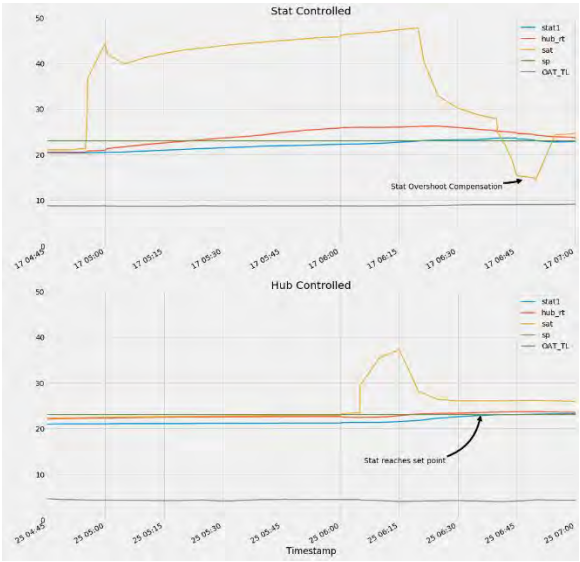

Figure 6. Energy Savings

As shown in Figure 6 the yellow plot shows the supply air temperature used to control the temperature in a large open office space. The red plot is the temperature measured by the sensor hub in the space. The blue plot is the temperature measured by a traditional thermostat in the same space.

Both graphs show a pre-heat in the early morning and how the system responds. The top graph is controlled by the thermostat, the bottom by the sensor hub.

As you can see, the system is active for much less time using the sensor hub, and the total energy savings are significant.

5. Conclusions and outlook

The Sensor Hub has been accepted by building control integrators, engineers and architects as a more aesthetic and functional device due to its diverse sensor suite and optimal installation location on the ceiling directly above the space that is actually being utilized. The integration of various sensors in a single device and ability to provide visual and audible interaction with the building occupants has positioned the device as a conduit for sensor data for every space throughout an entire building.

The accurate and fast temperature response using the Kalman filter design achieves the requirement for both occupant comfort and energy savings.

Using a high resolution thermal IR sensor an even more accurate representation of the occupied space can be achieved. Additional value added features can be incorporated such as people counting and equipment failure detection.

Acknowledgements

We gratefully acknowledge the contributions from all member of the Sensor Hub development team at Delta Controls Inc.

References

[1] Delta Controls Inc. 2018, March 16. Chris Kwong et al. Building Automation System Patent 16354007.

[2] Sensor Fusuion. 2020, March 2. Wikipedia. Available at https://en.wikipedia.org/wiki/Sensor_fusion

[3] Kalman Filter. 2020, March 2. Wikipedia. Available at https://en.wikipedia.org/wiki/Kalman_filter

[4] Kalman, R. E. (1960). "A New Approach to Linear Filtering and Prediction Problems". Journal of Basic Engineering. 82: 35–45. doi:10.1115/1.3662552

About the Editor

Phalguni Mukhopadhyaya, Ph.D., P.Eng.
Professor
Department of Civil Engineering, University of Victoria, BC, Canada.
Tel: (250) 472-4546, E-mail: phalguni@uvic.ca

After doing PhD in Civil Engineering from the University of Sheffield (UK) and postdoctoral research assignments in UK, Germany and Canada, Phalguni's professional career started with the National Research Council of Canada (NRCC), Ottawa, Ontario in 1999. During last two decades, his research activities have attracted significant research funding from industry and government partnerships, and his research outputs have influenced many changes in building construction practices over the years. He has received several awards/recognitions (ASCE Best Application Paper Award-2002; NRC Industrial Partnership Award-2002; ASTM Honor and Appreciation Awards - 2008,2013,2017, etc.) from the stakeholders of the construction industry in Canada and abroad. In 2015, Phalguni moved to the University of Victoria (UVic) to be a Professor in the newly established Civil Engineering Department. Phalguni's current research focus is on high performance thermal insulations, energy efficient buildings, moisture management, green buildings, and novel structures and construction materials.